

**Copyright**

**By**

**John Mark Howard Puryear**

**2007**

**Passive, Wireless Corrosion Sensors for  
Reinforced Concrete Structures**

by

**John Mark Howard Puryear, B.S.M.**

**Thesis**

Presented to the Faculty of the Graduate School of

The University of Texas at Austin

in Partial Fulfillment

of the Requirements

for the Degree of

**Master of Science in Engineering**

**The University of Texas at Austin**

**August 2007**

**Passive, Wireless Corrosion Sensors for  
Reinforced Concrete Structures**

**APPROVED BY  
SUPERVISING COMMITTEE:**

---

**Sharon L. Wood**

---

**Dean P. Neikirk**

## **Dedication**

*To my wife, Mary, without whom not.*

## **Acknowledgements**

A hearty thanks to Dr. Sharon L. Wood for her leadership over the course of this research. Her uncanny insights and indefatigable commitment to empirical verification greatly strengthened conclusions that could be drawn from the research. Dr. Wood was also very generous in supporting my attendance at the SPIE conference in San Diego, CA.

Thanks to the National Science Foundation as well for funding the research and my education through a grant to the University of Texas at Austin.

Dr. Dean P. Neikirk and Matthew Andringa are to be thanked for their assistance with the electrical aspects of the research. Matthew Andringa's curve-fitting algorithm was a great asset to the research. Thanks also to Dr. Harovel G. Wheat for generously providing insight into the theory of corrosion.

Randy Poston and Justin Norvell of WPD & Associates are to be thanked for kindly allowing me to use of their linear polarization device and resistivity meter. Randy Poston also made fruitful suggestions for the research. A thanks to Dr. Karl H. Frank for his advice on the chemistry of steels and for use of his excellent camera. Thanks also to Housatonic Wire of Seymour, CT, which generously donated steel wire to the research.

A general thanks to my colleagues at Ferguson Structural Engineering Laboratory and the Construction Materials Research Group. These colleagues helped me in far more ways than I can list.

August 2007

# **Passive, Wireless Corrosion Sensors for Reinforced Concrete Structures**

John Mark Howard Puryear, M.S.E.

The University of Texas at Austin, 2007

SUPERVISOR: Sharon L. Wood

Corrosion of steel in reinforced concrete structures is a costly problem. Effective planning is required to raise the considerable capital expended annually on the repair and replacement of structures damaged by corrosion. Essential to this planning is knowledge that corrosion has initiated in a given structure. The passive, wireless corrosion sensor is a technology that could potentially provide this knowledge of initiation of corrosion, both economically and reliably. The sensor, which consists of two resistor-inductor-capacitor circuits, requires no onboard power supply or wires to send a signal. The signal of the sensor is obtained by magnetic coupling with a reader coil. As a threshold sensor, the

sensor has a binary output with one signal indicating that corrosion has not initiated and another signal indicating that corrosion has initiated. Multiple designs of the sensor have been tested in concrete and reinforced concrete structures, some full-scale, subjected to extreme environmental conditions over long durations. Certain designs have proved highly reliably at indicating the initiation of corrosion, verifying the concept of the passive, wireless corrosion sensor.

## Table of Contents

<b>LIST OF TABLES</b> .....	<b>xiv</b>
<b>LIST OF FIGURES</b> .....	<b>xvi</b>
<b>CHAPTER 1 INTRODUCTION</b> .....	<b>1</b>
1.1 Introduction .....	1
1.2 Required Attributes .....	2
1.2.1 Economy .....	3
1.2.2 Reliability .....	4
1.2.3 Durability .....	4
1.3 Scope of Research .....	5
<b>CHAPTER 2 THE CONCEPT OF THE PASSIVE, WIRELESS CORROSION SENSOR</b> .....	<b>8</b>
2.1 Introduction .....	8
2.2 Theoretical Basis of Threshold Corrosion Sensor.....	8
2.3 Geometries of the Sensor .....	13
2.3.1 Concentric Sensor .....	14
2.3.2 Coplanar Sensor .....	18
2.3.3 Sensor Interrogation .....	21
2.4 Types of Sensors .....	21
2.4.1 Isolated Sensor .....	22
2.4.2 Coupled Sensor .....	25
2.4.3 Anodic Sensor .....	28
2.5 Characterization of Sensor Response.....	34
2.5.1 Characterization of Corrosion Threshold.....	34



2.5.2	Characterization of Variability in Sensor Response .....	36
2.6	Baseline Shift .....	40
2.7	Conclusion.....	44
<b>CHAPTER 3 ENVIRONMENTAL TESTS OF ISOLATED SENSORS EMBEDDED IN CONCRETE PRISMS.....</b>		<b>46</b>
3.1	Introduction .....	46
3.2	Design of Experiment.....	46
3.3	Measured Response.....	51
3.3.1	Control Conditions .....	52
3.3.2	Varying Moisture Conditions.....	53
3.3.3	Varying Thermal Conditions.....	56
3.3.4	Varying Moisture and Thermal Conditions .....	58
3.3.5	Comparison of Response of Concentric and Coplanar Sensors .....	62
3.3.6	Summary of Measured Response.....	64
3.4	Results from Autopsies of Prisms .....	69
3.4.1	Control Conditions .....	71
3.4.2	Varying Moisture Conditions.....	71
3.4.3	Varying Thermal Conditions.....	73
3.4.4	Varying Moisture and Thermal Conditions .....	74
3.4.5	Differential Thermal Expansion.....	75
3.4.6	Sensor Rotation .....	76
3.5	Conclusions .....	77
<b>CHAPTER 4 TESTING OF ISOLATED SENSORS IN REINFORCED CONCRETE SLAB SECTIONS.....</b>		<b>80</b>
4.1	Introduction .....	80
4.2	Design of Experiment.....	80

4.3	Measured Response of Sensors .....	89
4.3.1	Detected State of Sensing Wires at the Conclusion of Testing.....	90
4.3.2	Summary of the Measured Response of Sensors .....	93
4.3.3	Comparison of the Variability of the Response of Sensors Tested in Slabs 1 and 2 to the Variability of the Response of Sensors Tested in Prisms .....	99
4.3.4	Effect of Displacement and Rotation of Sensors on the Variability of the Response of the Sensors .....	101
4.3.5	Effect of Gage of Sensing Wire on Variability of Sensor Response .....	110
4.4	Comparison of Sensor Response with Other Indicators of Corrosion .....	111
4.4.1	Observed Condition of Reinforcement .....	112
4.4.2	Half-Cell Potentials .....	118
4.4.3	Chloride Concentration .....	124
4.4.4	Influence of Crack Path.....	128
4.4.5	Accelerated Corrosion of Transverse Reinforcement .....	133
4.5	Conclusions .....	135
<b>CHAPTER 5 TESTING OF COUPLED SENSORS IN REINFORCED CONCRETE SLAB SECTIONS .....</b>		<b>138</b>
5.1	Introduction .....	138
5.2	Design of the Experiment.....	138
5.3	Measured Response of the Sensors .....	152
5.3.1	Detected State of the Sensing Wires after 12 Months of Testing .....	153
5.3.2	Summary of the Measured Response of the Sensors .....	155
5.3.3	Effect of Moisture Content of the Concrete on the Response of Sensors with Fractured Sensing Wires.....	161
5.3.4	Possible Instances of Uniform Corrosion of the Sensing Wire.....	168
5.3.5	Deterioration of the Reference Circuit due to Black Corrosion within the Epoxy Housing.....	171

5.3.6	Dependence of the Response of the Sensors on the Internal Temperature of the Concrete.....	174
5.4	Comparison of Sensor Response with Other Indicators of Corrosion .....	178
5.4.1	Observed Condition of Steel Reinforcement .....	180
5.4.2	Half-Cell Potentials.....	185
5.4.3	Chloride Concentration .....	191
5.4.4	Influence of Crack Path.....	196
5.5	Conclusion.....	198
<b>CHAPTER 6 BLACK CORROSION WITHIN EPOXY HOUSING OF SENSOR.....</b>		<b>202</b>
6.1	Introduction .....	202
6.2	Development of Black Corrosion.....	202
6.3	Causes of Black Corrosion of the Sensing Wire .....	206
6.3.1	Mixed Potential Theory.....	207
6.3.2	Differential Aeration .....	211
6.4	Conclusion.....	215
<b>CHAPTER 7 TESTING OF ANODIC SENSORS IN REINFORCED CONCRETE SLAB SECTIONS.....</b>		<b>217</b>
7.1	Introduction .....	217
7.2	Design of the Experiment.....	217
7.3	Measured Response of Sensors .....	234
7.3.1	State of the Sensing Wires after 14 Weeks of Testing.....	235
7.3.2	Summary of the Measured Response of the Sensors .....	237
7.3.3	Effect of Moisture on the Surface of the Sensor Inductors .....	242
7.3.4	Causes of the General Decrease in the Phase Dip and Pseudo-Quality Factors of the Reference Circuits .....	250

7.4	Sensor Response, Half-Cell Potentials, and Corrosion Current.....	257
7.4.1	Half-Cell Potentials.....	258
7.4.2	Current Circulation in Slabs 5 and 6.....	265
7.5	Conclusion.....	268
<b>CHAPTER 8 SUSCEPTIBILITY OF ANODIC SENSORS TO FALSE POSITIVE READINGS.....</b>		<b>271</b>
8.1	Introduction.....	271
8.2	Anodic Sensors Tested in A Large Area of Bridge Deck.....	272
8.2.1	Design of the Experiment.....	272
8.2.2	Measured Response of the Sensors.....	275
8.2.3	Effect of the Embedded Sensor on the Durability of the Structure.....	279
8.3	Galvanic Corrosion Experiment.....	280
8.3.1	Design of the Galvanic Experiment.....	281
8.3.2	Results from the Galvanic Experiment.....	285
8.4	Conclusion.....	290
<b>CHAPTER 9 CONCLUSIONS.....</b>		<b>292</b>
9.1	Summary.....	292
9.2	Recommendations.....	295
<b>APPENDIX A CONCRETE PRISM SENSOR MONITORING RESULTS.....</b>		<b>298</b>
<b>APPENDIX B MONITORING RESULTS FOR SLABS 1 AND 2.....</b>		<b>310</b>
<b>APPENDIX C MONITORING RESULTS FOR SLABS 3 AND 4.....</b>		<b>330</b>
<b>APPENDIX D MONITORING RESULTS FOR SLABS 5 AND 6.....</b>		<b>344</b>

<b>APPENDIX E FIBER-REINFORCED CEMENT PASTE SENSOR HOUSING .....</b>	<b>364</b>
<b>APPENDIX F RESPONSES OF SENSORS EMBEDDED IN A FULL-SCALE BRIDGE DECK .....</b>	<b>372</b>
<b>APPENDIX G GALVANIC CORROSION TEST RESULTS.....</b>	<b>376</b>
<b>REFERENCES .....</b>	<b>380</b>
<b>VITA .....</b>	<b>382</b>

## List of Tables

Table 3-1 Environmental Cycles for Prisms .....	50
Table 3-2 Statistical Summary of Sensors with Intact Sensing Wires .....	65
Table 3-3 Mean Resonant Frequencies of Sensors with Fractured Sensing Wires .....	66
Table 3-4 Mean Phase Dips of Sensors with Fractured Sensing Wires .....	67
Table 3-5 Mean Pseudo-Quality Factors of Sensors with Fractured Sensing Wires .....	68
Table 3-6 Observed Condition of Concentric Sensors at Conclusion of Testing .....	69
Table 3-7 Observed Condition of Coplanar Sensors at Conclusion of Testing .....	70
Table 4-1 Chemical Composition of AISI-ASE 1005 and 1006 Steel.....	83
Table 4-2 Moisture Conditions of Sensors.....	88
Table 4-3 Statistical Summary of Sensors with Intact Sensing Wires .....	95
Table 4-4 Mean Resonant Frequencies for Sensors with Fractured Sensing Wires .....	96
Table 4-5 Mean Phase Dips for Sensors with Fractured Sensing Wire.....	97
Table 4-6 Mean Pseudo-Quality Factors for Sensors with Fractured Sensing Wires .....	98
Table 4-7 Displacement, Rotation, and Cover of Sensors Embedded in Slab 1.....	104
Table 4-8 Displacement, Rotation, and Cover of Sensors Embedded in Slab 2.....	105
Table 4-9 Distribution of Signals of Concentric Sensors by Category .....	115
Table 4-10 Distribution of Signals of Coplanar Sensors by Category .....	116
Table 4-11 Distribution of Signals of Concentric Sensors with 26-gage Sensing Wire .....	117
Table 4-12 Distribution of Signals of Concentric Sensors with 21-gage Sensing Wire .....	118
Table 5-1 Chemical Composition of Sensing Wire, W5 Wire, and #5 Bar .....	145
Table 5-2 Moisture Conditions of Sensors.....	151
Table 5-3 Statistical Summary of Sensors with Intact Sensing Wires Tested in Slab 3 .....	157

Table 5-4 Statistical Summary of Sensors with Intact Sensing Wires Tested in Slab 4 and Control .....	158
Table 5-5 Mean Resonant Frequency of Sensors with Fractured Sensing Wires Tested in Slabs 3 and 4 .....	159
Table 5-6 Mean Phase Dip of Sensors with Fractured Sensing Wires Tested in Slabs 3 and 4 .....	159
Table 5-7 Mean Pseudo-Quality Factor of Sensors with Fractured Sensing Wires Tested in Slabs 3 and 4 .....	160
Table 5-8 R <sup>2</sup> Values for the Response Parameters of Control Sensors with Respect to Temperature .....	177
Table 5-9 Reliability of Sensors Tested in Slab 4 with respect to the Observed Condition of the Steel Reinforcement .....	184
Table 7-1 Chemical Composition of Zinc and Aluminum Sensing Wire .....	220
Table 7-2 Moisture and Chloride Conditions of Sensors .....	233
Table 7-3 Statistical Summary of Sensors Tested in Slab 5 and Control .....	239
Table 7-4 Statistical Summary of Sensors with Intact Sensing Wires Tested in Slab 6 and Control .....	240
Table 7-5 Mean Resonant Frequency of Sensors with Fractured Sensing Wires Tested in Slab 6 .....	241
Table 7-6 Mean Phase Dip of Sensors with Fractured Sensing Wires Tested in Slab 6 .....	241
Table 7-7 Mean Pseudo-Quality Factor of Sensors with Fractured Sensing Wires Tested in Slab 6 .....	241
Table 7-8 Change in Reference Pseudo-Quality Factor of Sensors Tested in Slabs 5 and 6 .....	251
Table 8-1 Statistical Summary of Response of D19 and E19 .....	278
Table A-1 Initial Weights of Concrete Prisms .....	298
Table A-2 Change in Moisture Content of Concrete Prisms with Time (17 Jan to 09 May 2005) .....	299
Table A-3 Change in Moisture Content of Concrete Prisms with Time (09 May to 12 Jul 2005) .....	300
Table B-1 Elevation of Contour Lines for Contour Plots of Concentric Sensors .....	313
Table C-1 Elevation of Contour Lines for Contour Plots .....	331
Table D-1 Elevation of Contour Lines for Contour Plots .....	346
Table E-1 Amounts of Components Combined to Make Fiber-Reinforced Cement Paste Housing .....	365

## List of Figures

Figure 1-1 Damage to a Reinforced Concrete Structure .....	2
Figure 1-2 EAS Tag .....	4
Figure 2-1 Circuit Diagram of an RLC Circuit .....	9
Figure 2-2 Response of RLC Circuit to an Applied Alternating Current of Variable Frequency .....	9
Figure 2-3 RLC Circuit Magnetically Coupled to an Alternating Current Source .....	10
Figure 2-4 RLC Circuit Used to Detect Corrosion Initiation .....	12
Figure 2-5 Response of Sensor with Fractured Sensing Wire .....	14
Figure 2-6 Diagram of Concentric Sensor .....	15
Figure 2-7 Photograph of Concentric Sensor .....	15
Figure 2-8 Response of Concentric Sensor with Intact Sensing Wire .....	16
Figure 2-9 Response of Concentric Sensor with Fractured Sensing Wire .....	17
Figure 2-10 Mutual Inductance in the Concentric Sensor .....	18
Figure 2-11 Diagram of Coplanar Sensor .....	19
Figure 2-12 Photograph of Coplanar Sensor .....	19
Figure 2-13 Response of Coplanar Sensor with Intact Sensing Wire .....	20
Figure 2-14 Response of Coplanar Sensor with Fractured Sensing Wire .....	20
Figure 2-15 Magnetic Coupling of Corrosion Sensor and Reader Coil .....	21
Figure 2-16 Isolated Corrosion Sensor Embedded in Reinforced Concrete Structure .....	23
Figure 2-17 Crack Formation and the Isolated Sensor .....	23
Figure 2-18 Relationship between the Resistance and Sensing Wire Length of a Sensor .....	24
Figure 2-19 Corrosion Initiation in Reinforced Concrete .....	26
Figure 2-20 Potential of Sensing Wire Relative to the Anode in Case of Crack .....	27
Figure 2-21 Idealized Behavior of Coupled Sensor .....	28
Figure 2-22 Galvanic Cell of Iron and Zinc .....	29
Figure 2-23 Length of Steel Embedded in Concrete .....	30
Figure 2-24 Model of Length of Steel Embedded in Concrete .....	30
Figure 2-25 Chloride Penetration into Region B .....	31
Figure 2-26 Model of Chloride Penetration into Region B .....	32
Figure 2-27 Model of Chloride Penetration into Region A .....	33
Figure 2-28 Response of Concentric Sensor as Contour Plot .....	35
Figure 2-29 Response of Coplanar Sensor as Contour Plot .....	36
Figure 2-30 Parameters $\omega_{\theta_{\min}}$ and $\Delta\omega$ which Define the Pseudo-Quality Factor .....	38



Figure 2-31 Displacement of Reader Coil from Corrosion Sensor .....	39
Figure 2-32 Amplitude of Phase Dip and Pseudo-Quality Factor with Respect to Displacement .....	39
Figure 2-33 Baseline Shift of Reader Coil .....	41
Figure 2-34 Baseline Shift of Sensor B51: Phase Angle vs. Frequency .....	42
Figure 2-35 Baseline Shift of Sensor B51: Contour Plot .....	42
Figure 2-36 Effect of Baseline Shift on Curve Fit of Sensor B51 .....	43
Figure 3-1 Deformation of Prism Containing Coplanar Sensor .....	47
Figure 3-2 Concentric Sensor in Concrete Prism .....	48
Figure 3-3 Coplanar Sensor in Concrete Prism .....	48
Figure 3-4 Response of Sensor B22 .....	53
Figure 3-5 Response of Sensor B27 .....	54
Figure 3-6 Lack of Correlation between Moisture Content of the Concrete Prism and Phase Dip and Pseudo-Quality Factor .....	56
Figure 3-7 Response of Sensor B19 .....	57
Figure 3-8 Response of Sensor B24 .....	59
Figure 3-9 Lack of Correlation between Moisture Content of Concrete and Phase Dip and Pseudo-Quality Factor .....	60
Figure 3-10 Temperature Dependence of Phase Dip and Pseudo-Quality Factor in Sensing Circuit of B24 .....	61
Figure 3-11 Reversal of Sensor B23 Response .....	62
Figure 3-12 Response of A27 .....	63
Figure 3-13 Exhumed Sensor B22 .....	71
Figure 3-14 Autopsy of Prism Containing B27 .....	72
Figure 3-15 Discolorization of Sensor B19 .....	73
Figure 3-16 Autopsy of Prism Containing Sensor B24 .....	75
Figure 3-17 Cracks due to Differential Thermal Expansion .....	75
Figure 3-18 Corrosion Products from Sensing Wire of B23 .....	76
Figure 3-19 Rotation of Sensor A22 .....	77
Figure 4-1 Plan View of Slab 1 .....	81
Figure 4-2 Plan View of Slab 2 .....	81
Figure 4-3 Cross-Section of Concrete Slab Section .....	82
Figure 4-4 Layout of Sensors and Steel Reinforcement .....	82
Figure 4-5 Position of the Sensing Wire of Isolated Sensors .....	84
Figure 4-6 Loaded Slab with Water Reservoir .....	85
Figure 4-7 Crack Map of Slab 1 Immediately After Loading .....	85
Figure 4-8 Crack Map of Slab 2 Immediately After Loading .....	86
Figure 4-9 Half-Cell Potential Points .....	89
Figure 4-10 Concentric Sensors with Fractured Sensing Wires .....	91
Figure 4-11 Coplanar Sensors with Fractured Sensing Wires .....	91
Figure 4-12 Observed State of Sensing Wires at Autopsy .....	92

Figure 4-13 Response of Sensor B05 .....	93
Figure 4-14 Response of B01 .....	100
Figure 4-15 Baseline Shift in Sensor B59 .....	101
Figure 4-16 Parameters Defining the Position of a Sensor Relative the Reader Coil .....	103
Figure 4-17 Displacement from Design Position and Rotation Relative Slab Surface of Sensors Embedded in Slabs 1 and 2 .....	106
Figure 4-18 Coefficients of Variation of Response Parameters of Coplanar Sensing Circuits Embedded in Slab 1 with Respect to Displacement and Rotation .....	108
Figure 4-19 Coefficients of Variation of Response Parameters of Coplanar Reference Circuits Embedded in Slab 1 with Respect to Displacement and Rotation .....	108
Figure 4-20 Coefficients of Variation of Response Parameters of Concentric Sensing Circuits Embedded in Slab 1 with Respect to Displacement and Rotation .....	109
Figure 4-21 Coefficients of Variation of Response Parameters of Concentric Reference Circuits Embedded in Slab 1 with Respect to Displacement and Rotation .....	109
Figure 4-22 Response of B57 .....	110
Figure 4-23 Extent of Corrosion on Reinforcement Adjacent to Sensors .....	114
Figure 4-24 Half-Cell Potentials of Slab 1 with Respect to Time .....	119
Figure 4-25 Half-Cell Potential of Slab 2 with Respect to Time .....	119
Figure 4-26 Slab 1 Half-Cell Potential Distribution at the End of Final Wet Cycle .....	122
Figure 4-27 Slab 1 Half-Cell Potential Distribution at the End of Final Dry Cycle .....	122
Figure 4-28 Slab 2 Half-Cell Potential Distribution at the End of Final Wet Cycle .....	123
Figure 4-29 Slab 2 Half-Cell Potential Distribution at the End of Final Dry Cycle .....	123
Figure 4-30 Chloride Concentration of Slab 1 .....	125
Figure 4-31 Chloride Concentration of Slab 2 .....	125
Figure 4-32 Locations at which Chloride Concentration Determined in Specimens, Relative Cracks in Concrete Cover .....	127
Figure 4-33 Paths of Cracks in Specimens Superimposed on the Measured Position of the Sensors .....	130
Figure 4-34 Crack Path Intersecting Sensing Wire of B53 and Reinforcement, Causing Corrosion of Both .....	132
Figure 4-35 Crack Path Failing to Intersect Sensing Wire of B55 but Causing Corrosion of Reinforcement .....	132

Figure 4-36 Bottoms of Sensors with Concentric and Coplanar Geometries .....	134
Figure 4-37 Air Voids beneath Concentric and Coplanar Sensors .....	135
Figure 5-1 Top Plan View Slab 3 .....	139
Figure 5-2 Bottom Plan View of Slab 3 .....	139
Figure 5-3 Top Plan View of Slab 4 .....	140
Figure 5-4 Bottom Plan View of Slab 4 .....	140
Figure 5-5 Typical Section of Slab 3 and Slab 4.....	141
Figure 5-6 Resistor Connecting Top and Bottom Reinforcement.....	142
Figure 5-7 Sealed End of Transverse Reinforcement .....	142
Figure 5-8 Plan View of Top and Bottom of Control Specimen .....	143
Figure 5-9 Layout of Sensors and Steel Reinforcement .....	146
Figure 5-10 Sensing Wire Placed in the Expected Path of the Crack .....	146
Figure 5-11 Sensing Wire Positioned out of the Expected Path of the Crack .....	147
Figure 5-12 Crack Map of Slab 3 Immediately after Loading.....	148
Figure 5-13 Crack Map of Slab 4 Immediately after Loading.....	149
Figure 5-14 Locations at which Half-Cell Potentials Taken in Slabs 3 and 4 .....	152
Figure 5-15 Sensors with Fractured Sensing Wires after 12 Months of Testing .....	153
Figure 5-16 Detected State of Sensing Wires after 12 Months of Testing .....	154
Figure 5-17 Response of Sensor B155 .....	162
Figure 5-18 Detail of Response of Sensor B155.....	162
Figure 5-19 Experiment Showing Effect of Fractured Sensing Circuit on Reference Circuit.....	164
Figure 5-20 Response of Sensor B124 in Dry and Wet Conditions.....	164
Figure 5-21 Fracture in the Sensing Wire of B155 .....	166
Figure 5-22 Response of Sensor B154.....	167
Figure 5-23 Response of Sensor B154 in Plane of Phase Angle and Frequency .....	167
Figure 5-24 Response of Sensor B134 .....	169
Figure 5-25 Response of Sensor B148.....	170
Figure 5-26 Uniform Corrosion on a Segment of the Sensing Wire of B148.....	170
Figure 5-27 Response of Sensor B152 .....	172
Figure 5-28 Cracking of Epoxy Housing of B152 .....	173
Figure 5-29 Response of Sensor B135 .....	174
Figure 5-30 Resonant Frequency of B159 with Respect to Temperature.....	175

Figure 5-31 Phase Dip of B159 with Respect to Temperature.....	176
Figure 5-32 Pseudo-Quality Factor of B159 with Respect to Temperature.....	176
Figure 5-33 Internal Temperature of the Concrete and Air Temperature .....	178
Figure 5-34 External Corrosion on the North Face of Slab 4 .....	179
Figure 5-35 Extent of Corrosion on Reinforcement on the Top Layer of Steel of Slab 4 .....	181
Figure 5-36 Pits on Transverse and Longitudinal Reinforcement .....	182
Figure 5-37 Tensile Test of W5 Wire Transverse Reinforcement .....	183
Figure 5-38 Half-Cell Potentials of Slab 3 with Respect to Time .....	185
Figure 5-39 Half-Cell Potentials of Slab 4 with Respect to Time .....	186
Figure 5-40 Current in Slab 3 with Respect to Time .....	188
Figure 5-41 Current in Slab 4 with Respect to Time .....	189
Figure 5-42 Slab 3 Half-Cell Potential Distribution at the End of 12 Months of Testing .....	190
Figure 5-43 Slab 4 Half-Cell Potential Distribution at the End of 12 Months of Testing .....	190
Figure 5-44 Locations at which Chloride Concentration of Concrete Cover of Slab 4 Determined .....	192
Figure 5-45 Chloride Concentration of Slab 4 .....	193
Figure 5-46 Chloride Concentration of the Concrete Cover of Slab 4 at the End of 12 Months of Testing .....	195
Figure 5-47 Paths of Cracks in Specimens Superimposed on the Positions of the Sensors.....	197
Figure 6-1 Black Corrosion in the Housing of Sensor B52 .....	203
Figure 6-2 Trace of Black Corrosion in the Housing of Sensor A57.....	204
Figure 6-3 Instances of Internal Black Corrosion in Slab 1 .....	204
Figure 6-4 Instances of Internal Black Corrosion in Slab 2 .....	205
Figure 6-5 Instances of Internal Black Corrosion in Slab 4 .....	205
Figure 6-6 Development of Cavity along Sensing Wire .....	207
Figure 6-7 Polarization Curve of Reaction $Fe \rightarrow Fe^{2+} + 2e^{-}$ .....	209
Figure 6-8 Polarization Curve of Reaction $O_2 + 2H_2O + 4e^{-} \rightarrow 4OH^{-}$ .....	210
Figure 6-9 Corrosion Potential and Current Defined by Anodic and Cathodic Polarization Curves .....	211
Figure 6-10 Effect of Aeration on Corrosion Potential and Current.....	212
Figure 6-11 Differential Aeration Cell.....	213
Figure 6-12 Differential Aeration Cell on Sensing Wire .....	214
Figure 6-13 Black Corrosion in B04 .....	214

Figure 6-14 Crack in the Housing of Sensor B23 .....	215
Figure 7-1 Top Plan View of Slab 5 .....	218
Figure 7-2 Bottom Plan View of Slab 5 .....	218
Figure 7-3 Top Plan View of Slab 6 .....	218
Figure 7-4 Bottom Plan View of Slab 6 .....	219
Figure 7-5 Typical Section of Slabs 5 and 6 .....	219
Figure 7-6 Illustration of Sensor with Fiber-Reinforced Cement Paste Housing .....	221
Figure 7-7 Sensor with Fiber-Reinforced Cement Paste Housing .....	221
Figure 7-8 Illustration of Sensor with Fiber-Reinforced Cement Paste Housing with Epoxy Core .....	223
Figure 7-9 Sensor with Fiber-Reinforced Cement Paste Housing with Epoxy Core .....	223
Figure 7-10 Layout of Sensors and Steel Reinforcement .....	224
Figure 7-11 Sensing Wire Placed in the Expected Path of the Crack .....	225
Figure 7-12 Sensing Wire Placed out of the Expected Path of the Crack .....	225
Figure 7-13 Top and Bottom Plan Views of Slab 5 Control Specimen .....	227
Figure 7-14 Top and Bottom Plan Views of Slab 6 Control Specimen .....	228
Figure 7-15 Loaded Slab with Water Reservoir .....	229
Figure 7-16 Crack Map of Slab 5 Immediately after Loading .....	230
Figure 7-17 Crack Map of Slab 6 Immediately after Loading .....	231
Figure 7-18 Locations at which Half-Cell Potentials Taken in Slabs 5 and 6 .....	234
Figure 7-19 Sensors with Fractured Sensing Wires after 14 Weeks of Testing .....	235
Figure 7-20 Detected State of the Sensing Wires in Slab 6 after 14 Weeks of Testing .....	236
Figure 7-21 Response of D18 over First 14 Weeks of Testing .....	237
Figure 7-22 Response of Sensor D11 .....	243
Figure 7-23 Plastic Shrinkage Cracks in the Housing of E08 .....	244
Figure 7-24 Experiment Indicating Effect of Parasitic Inductance .....	246
Figure 7-25 Parasitic Inductance due to Moisture .....	247
Figure 7-26 Effect of Sensor Housing on Value and Variability of Reference Phase Dip .....	248
Figure 7-27 Effect of Sensor Housing on Value and Variability of Reference Pseudo-Quality Factor .....	248
Figure 7-28 Response of Sensor E07 .....	249
Figure 7-29 Response of Sensor E12 .....	254
Figure 7-30 Response of D06 .....	256
Figure 7-31 Half-Cell Potentials of Slab 5 with Respect to Time .....	259
Figure 7-32 Half-Cell Potentials of Slab 6 with Respect to Time .....	259

Figure 7-33 Slab 5 Half-Cell Potential Distribution at 14 Weeks: End of Wet Cycle .....	262
Figure 7-34 Slab 5 Half-Cell Potential Distribution at 12 Weeks: End of Dry Cycle.....	262
Figure 7-35 Slab 6 Half-Cell Potential Distribution at 14 Weeks: End of Wet Cycle .....	263
Figure 7-36 Slab 6 Half-Cell Potential Distribution at 12 Weeks: End of Dry Cycle.....	263
Figure 7-37 Slab 6 Half-Cell Potential Distribution at 13 days: End of Wet Cycle .....	264
Figure 7-38 Current in Slab 5 with Respect to Time .....	265
Figure 7-39 Current in Slab 6 with Respect to time.....	266
Figure 7-40 Total Current in Specimens with Steel, Aluminum, and Zinc Sensing Wires .....	267
Figure 8-1 Plan View of Tributary Area of Bridge Deck .....	273
Figure 8-2 Sensor D19 .....	274
Figure 8-3 Sensor E19.....	274
Figure 8-4 Placing of Concrete .....	275
Figure 8-5 Response of Sensor D19.....	276
Figure 8-6 Response of Sensor E19 .....	277
Figure 8-7 Sensors Embedded in Full-Scale Bridge Deck.....	280
Figure 8-8 Plan View of Full-Scale Bridge Deck and Position of Sensors .....	280
Figure 8-9 Galvanic Corrosion Experiment for Sensing Wire and Bar .....	282
Figure 8-10 Steel Mats with Eight and Seventeen Bars.....	282
Figure 8-11 Connection of Magnet Wire to Sensing Wire and Steel Mat.....	283
Figure 8-12 Connection of Magnet Wire to Bar and Steel Mat.....	284
Figure 8-13 Current and pH in the Case of Aluminum Bar .....	286
Figure 8-14 Passive Layer on Surface of Aluminum Bar .....	287
Figure 8-15 Initial and Fractured Condition of Aluminum Sensing Wire.....	287
Figure 8-16 pH of Solution Containing Aluminum Wire .....	287
Figure 8-17 Current and pH in the Case of Zinc Bar .....	288
Figure 8-18 Passive Layer on Surface of Zinc Bar .....	289
Figure 8-19 pH of Solution Containing Zinc Wire .....	289
Figure 8-20 Intact Zinc Sensing Wire Initially and after 124 Days of Testing .....	290
Figure A-1 Response of Sensor A21 .....	301
Figure A-2 Response of Sensor A22.....	301

Figure A-3 Response of Sensor A23.....	302
Figure A-4 Response of Sensor A24.....	302
Figure A-5 Response of Sensor A25.....	303
Figure A-6 Response of Sensor A26.....	303
Figure A-7 Response of Sensor A28.....	304
Figure A-8 Response of Sensor A29.....	304
Figure A-9 Response of Sensor A30.....	305
Figure A-10 Response of Sensor B20.....	305
Figure A-11 Response of Sensor B21.....	306
Figure A-12 Response of Sensor B24.....	306
Figure A-13 Response of Sensor B25.....	307
Figure A-14 Response of Sensor B26.....	307
Figure A-15 Response of Sensor B28.....	308
Figure A-16 Response of Sensor B29.....	308
Figure A-17 Response of Sensor B30.....	309
Figure B-1 Temperature of Air in which Slabs 1 and 2 Stored.....	310
Figure B-2 Fictitious Phase Dip in Response of B08.....	311
Figure B-3 Unreported Value of Reference Pseudo-Quality Factor of B54.....	312
Figure B-4 Baseline Shift in the Response of B54.....	312
Figure B-5 Response of Sensor A01.....	314
Figure B-6 Response of Sensor A02.....	314
Figure B-7 Response of Sensor A03.....	315
Figure B-8 Response of Sensor A04.....	315
Figure B-9 Response of Sensor A05.....	316
Figure B-10 Response of Sensor A06.....	316
Figure B-11 Response of Sensor A07.....	317
Figure B-12 Response of Sensor A08.....	317
Figure B-13 Response of Sensor A51.....	318
Figure B-14 Response of Sensor A52.....	318
Figure B-15 Response of Sensor A53.....	319
Figure B-16 Response of Sensor A54.....	319
Figure B-17 Response of Sensor A55.....	320
Figure B-18 Response of Sensor A56.....	320
Figure B-19 Response of Sensor A57.....	321
Figure B-20 Response of Sensor A58.....	321
Figure B-21 Response of Sensor B02.....	322
Figure B-22 Response of Sensor B03.....	322
Figure B-23 Response of Sensor B04.....	323
Figure B-24 Response of Sensor B06.....	323
Figure B-25 Response of Sensor B07.....	324
Figure B-26 Response of Sensor B08.....	324

Figure B-27 Response of Sensor B09 .....	325
Figure B-28 Response of Sensor B51 .....	325
Figure B-29 Response of Sensor B52 .....	326
Figure B-30 Response of Sensor B53 .....	326
Figure B-31 Response of Sensor B54 .....	327
Figure B-32 Response of Sensor B55 .....	327
Figure B-33 Response of Sensor B56 .....	328
Figure B-34 Response of Sensor B58 .....	328
Figure B-35 Response of Sensor B59 .....	329
Figure C-1 Relative Humidity of Air .....	330
Figure C-2 Response of Sensor B125 .....	332
Figure C-3 Response of Sensor B126 .....	332
Figure C-4 Response of Sensor B127 .....	333
Figure C-5 Response of Sensor B128 .....	333
Figure C-6 Response of Sensor B136 .....	334
Figure C-7 Response of Sensor B137 .....	334
Figure C-8 Response of Sensor B138 .....	335
Figure C-9 Response of Sensor B139 .....	335
Figure C-10 Response of Sensor B140 .....	336
Figure C-11 Response of Sensor B141 .....	336
Figure C-12 Response of Sensor B142 .....	337
Figure C-13 Response of Sensor B143 .....	337
Figure C-14 Response of Sensor B146 .....	338
Figure C-15 Response of Sensor B147 .....	338
Figure C-16 Response of Sensor B149 .....	339
Figure C-17 Response of Sensor B150 .....	339
Figure C-18 Response of Sensor B151 .....	340
Figure C-19 Response of Sensor B153 .....	340
Figure C-20 Response of Sensor B156 .....	341
Figure C-21 Response of Sensor B157 .....	341
Figure C-22 Response of Sensor B158 .....	342
Figure C-23 Response of Sensor B159 .....	342
Figure C-24 Response of Sensor B144 (Control Specimen).....	343
Figure D-1 Temperature Measured by Thermocouples Compared with Air Temperature .....	344
Figure D-2 Relative Humidity of Air .....	345
Figure D-3 Response of Sensor D01 .....	347
Figure D-4 Response of Sensor D02 .....	347
Figure D-5 Response of Sensor D03 .....	348
Figure D-6 Response of Sensor D04 .....	348
Figure D-7 Response of Sensor D05 .....	349
Figure D-8 Response of Sensor D07 .....	349



Figure D-9 Response of Sensor D08.....	350
Figure D-10 Response of Sensor D09.....	350
Figure D-11 Response of Sensor D10.....	351
Figure D-12 Response of Sensor D12.....	351
Figure D-13 Response of Sensor D13.....	352
Figure D-14 Response of Sensor D14.....	352
Figure D-15 Response of Sensor D15.....	353
Figure D-16 Response of Sensor D16.....	353
Figure D-17 Response of Sensor D17.....	354
Figure D-18 Response of Sensor D18.....	354
Figure D-19 Response of Sensor E01.....	355
Figure D-20 Response of Sensor E02.....	355
Figure D-21 Response of Sensor E03.....	356
Figure D-22 Response of Sensor E04.....	356
Figure D-23 Response of Sensor E05.....	357
Figure D-24 Response of Sensor E06.....	357
Figure D-25 Response of Sensor E08.....	358
Figure D-26 Response of Sensor E09.....	358
Figure D-27 Response of Sensor E10.....	359
Figure D-28 Response of Sensor E11.....	359
Figure D-29 Response of Sensor E13.....	360
Figure D-30 Response of Sensor E14.....	360
Figure D-31 Response of Sensor E15.....	361
Figure D-32 Response of Sensor E16.....	361
Figure D-33 Response of Sensor E17.....	362
Figure D-34 Response of Sensor E18.....	362
Figure D-35 Response of Sensor D20 (Control Specimen).....	363
Figure D-36 Response of Sensor E20 (Control Specimen).....	363
Figure E-1 Components of Fiber-Reinforced Cement Paste Housing.....	365
Figure E-2 Mortar Paddle Used to Stir the Mixture.....	366
Figure E-3 Mold with Convex Bottom.....	366
Figure E-4 Mixture Poured into Mold Containing Sensor.....	367
Figure E-5 Moist Curing of Sensor Housing.....	367
Figure E-6 PVC Slice of Reference Inductor Extending beyond Top of Sensing Inductor.....	368
Figure E-7 Bead of Hot Glue around Reference Inductor.....	369
Figure E-8 Epoxy Poured through Bottom of Reference Inductor.....	369
Figure E-9 Epoxy Core Visible on Top of Sensor.....	369
Figure E-10 Fiber-Reinforced Cement Paste Discs.....	370
Figure E-11 Concrete Prism.....	371
Figure F-1 Response of B160.....	372
Figure F-2 Response of B161.....	373

Figure F-3	Response of B162.....	373
Figure F-4	Response of B163.....	374
Figure F-5	Response of B164.....	374
Figure F-6	Response of B165.....	375
Figure G-1	Weight of Aluminum Wire.....	376
Figure G-2	Weight of Aluminum Bar.....	377
Figure G-3	Weight of Zinc Wire.....	377
Figure G-4	Weight of Zinc Bar.....	378
Figure G-5	Temperature of Simulated Pore Solutions.....	378
Figure G-6	Dissolved Oxygen Content of Simulated Pore Solutions.....	379
Figure G-7	Half-Cell Potentials of Steel Mats Coupled with Bars.....	379

# CHAPTER 1

## Introduction

### 1.1 INTRODUCTION

Corrosion of steel in concrete, shown in Figure 1-1, is a costly problem. The Transportation Research Board (1991) has estimated that deicing and sea salts have caused \$150 billion worth of corrosion damage to interstate highway bridges. In addition, the Transportation Research Board (1991) has calculated the annual cost of corrosion damage to American bridges and car parks to be as much as \$450 million. Raising the large amount of capital required to build and maintain infrastructure requires long-range planning. However, planning for the replacement of a structure cannot begin until the structure is known to be damaged. Conventional techniques for assessing the health of a reinforced concrete structure — half-cell potentials, chloride concentration of concrete, concrete resistivity, electrochemical impedance spectroscopy, and linear polarization — involve considerable uncertainty and expense. The result is that, in the case of many structures, outward indications of structural damage, such as pitting and spalling, are the first indications that corrosion has initiated. By that time, the structure may be near failure and require immediate replacement. Time spent planning and raising capital to replace the structure can have high economic costs, especially if the structure is a key component of infrastructure. What is needed to avoid this economic loss is a technique for determining the initiation of corrosion that is both economical and reliable.



***Figure 1-1 Damage to a Reinforced Concrete Structure  
([www.corrosion-club.com](http://www.corrosion-club.com))***

The passive, wireless corrosion sensor discussed in this thesis is a technology that can potentially detect the initiation of corrosion both economically and reliably. The sensor is intended to be installed in a reinforced concrete structure at the time of construction. Thereafter, the sensor provides information about the health of the structure by being monitored at regular time intervals. The information provided by the sensor is then used develop a plan for maintaining the structure. Information provided by the sensor is meant to complement information from conventional assessment techniques.

## **1.2 REQUIRED ATTRIBUTES**

For the corrosion sensor to monitor the health of a reinforced concrete structure effectively, it must have certain attributes. These required attributes — economy, reliability, and durability — are discussed in this section.

### **1.2.1 Economy**

Because the sensor is embedded in large civil infrastructure, many sensors are needed to monitor any given structure effectively. Therefore, the sensor must be economical to produce, maintain, and install. Highly economical production of the sensors is likely possible because the concept of the passive, wireless sensor is modeled on the concept of the electronic article surveillance (EAS) tag, which is produced at a cost of \$0.10. The EAS tag, shown in Figure 1-2, is used in retail stores to prevent shoplifting. The fact that the sensors are passive — they have no onboard power supply — affords economical maintenance of the sensors. Once they are embedded within a given structure, there is no additional cost to maintain them. Rather, the only cost remaining once the sensors are installed is the cost of monitoring. However, because the sensor lacks a power source, the amount of information that the sensor provides is limited compared with sensors that carry on onboard power supply. Finally, because the wireless sensor can be installed modularly, no wires need to be routed through the reinforced concrete structure during installation of the sensor. Consequently, the sensors are economical to install as well.

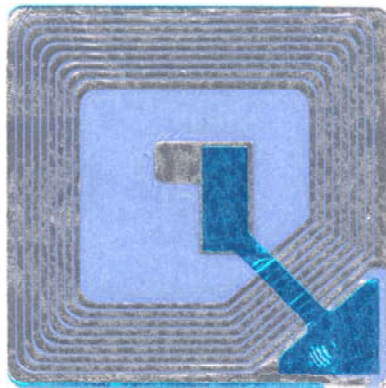


*Figure 1-2 EAS Tag*

### **1.2.2 Reliability**

To be effective in service conditions, the sensor must reliably detect the initiation of corrosion within a structure. When corrosion has initiated within the structure, the sensor must signal that corrosion has initiated. In practice, information would be obtained from the sensor only periodically. As a result, there would likely be a time interval between the initiation of corrosion and knowledge of initiation of corrosion. That said, because data from a large number of sensors would likely need to be processed for any given structure, the signal of the sensor should be unambiguous. That is, the sensor would ideally provide binary information: corrosion has or has not initiated. Therefore, the signal of the sensor would ideally be insensitive to changes in the environment in which it is embedded. Changes in temperature and the moisture content of the concrete, for example, should not significantly influence the signal of the sensor.

### **1.2.3 Durability**

The sensor must be durable enough to withstand construction of the structure in which it is placed. In addition, the sensor must continue functioning

throughout the design life of the structure, which can be as long as 100 years in the case of civil infrastructure. The sensor must have no negative impact on the reinforced concrete structure that the sensor is monitoring. The fact that the sensor is wireless is again advantageous in that wires entering a reinforced concrete structure provide a path of ingress for corrosive agents into the structure. Wireless technology denies corrosive agents a path of ingress in the structure.

### **1.3 SCOPE OF RESEARCH**

The objective of this research was to design improved passive, wireless corrosion sensors and to test the sensors in a variety of environmental conditions. Chapter 2 describes the concept of the sensor. Two geometries of the sensor — concentric and coplanar — and three types of sensor — isolated, coupled, and anodic — are described. Finally, the effect of environmental moisture on the process of obtaining information from the sensor is assessed.

Two sets of isolated sensors, one set with a concentric geometry and one set with a coplanar geometry, were embedded in concrete prisms and subjected to extreme variations in moisture and temperature. The sensitivity of the response of the sensors to these extreme environmental conditions was assessed. In addition, the responses of the sensors were compared with the physical states of their sensing wires. Chapter 3 presents the design and results of this experiment.

Chapter 4 describes the experimental design and results of testing isolated sensors in two sections of a reinforced concrete bridge slab. Portions of the reinforced concrete specimens were subjected to regular moisture cycles of salt-water over an 18-month period. Both concentric and coplanar geometries were tested. At the end of testing, the specimens were autopsied, and the signals of the sensors were compared with the condition of the steel reinforcement, half-cell potentials of the specimens, and the chloride concentration of the specimens.

Coupled sensors with concentric geometries were tested in two additional sections of a reinforced concrete bridge slab. Portions of the specimens were subjected to moisture cycles of salt-water over a 12-month period. At the end of that period, one of the specimens was autopsied, while testing of the other specimen is ongoing. Chapter 5 describes the design of this experiment and results after 12 months of testing. Conclusions drawn from the signals of sensors tested in the autopsied specimen were compared with the condition of the steel reinforcement in that specimen. The signals of the sensors were also compared with the chloride concentration of the autopsied specimen. In addition, the half-cell potentials of both specimens were compared with the signals of the sensors. Finally, exposed transverse reinforcement allowed for the amount of corrosion current circulating in the specimens to be measured and assessed.

The epoxy housings used for the sensors in the tests described in Chapters 3, 4, and 5 facilitated the development of black corrosion within the housing. Chapter 6 describes observed instances of black corrosion. Two possible causes of the black corrosion, lack of a passive layer on the segment of steel sensing wire within the epoxy housing and the development of a differential aeration cell on the sensing wire, are also discussed.

Chapter 7 describes an experiment for testing anodic sensors in two sections of a reinforced concrete bridge slab. One reinforced concrete specimen contained sensors with aluminum sensing wires, while the other contained sensors with zinc sensing wires. The housings of the sensors were composed of fiber-reinforced cement paste, instead of epoxy. Testing of both reinforced concrete specimens is ongoing, and the first 14 weeks of testing are discussed in Chapter 7. The signals of the sensors were compared with the half-cell potentials of the specimens. Finally, the corrosion current circulating in the specimens was determined using the same technique as in Chapter 5.



One possible deficiency of the anodic sensor was a susceptibility to false positive readings, signaling the initiation of corrosion when corrosion has not initiated. Chapter 8 assesses the susceptibility of the anodic sensor to false positive readings with two experiments. First, anodic sensors were placed in a large section of a bridge deck. Because the bridge deck was not exposed to corrosive agents, its reinforcing steel was assumed to be passive. The sensors were periodically interrogated to determine whether their sensing wires would fracture, despite the absence of corrosive agents. In the second experiment, a zinc sensing wire and bar and an aluminum sensing wire and bar were each coupled to mats of steel in a simulated pore solution. The condition of the wires and bars were observed, and trends in the corrosion rates of the bars were assessed.

Finally, Chapter 9 summarizes conclusions from the research and makes recommendations for future research.

## **CHAPTER 2**

# **The Concept of the Passive, Wireless Corrosion Sensor**

### **2.1 INTRODUCTION**

The concept of the passive wireless corrosion sensor is presented in this chapter. Section 2.2 provides the theoretical basis of how the sensor functions. The two geometries of sensor tested as part of this research are described in Section 2.3. Section 2.4 explains the three types of sensors: isolated, coupled, and anodic. Characterization of the response of the sensors is discussed in Section 2.5. Finally, Section 2.6 assesses the influence of the measured baseline shift on the response of the sensors.

### **2.2 THEORETICAL BASIS OF THRESHOLD CORROSION SENSOR**

The prototype corrosion sensor comprises two, separate, resistor-inductor-capacitor (RLC) circuits. In this section, the sensor is idealized as single RLC circuit for the sake of clarity. A circuit diagram of an RLC circuit is given in Figure 2-1. If alternating current of varying frequency is applied to an RLC circuit and the phase angle of the measured complex impedance is plotted with respect to frequency, the result is Figure 2-2. The critical feature of the response is a phase dip of a certain amplitude at a resonant frequency. The phase dip, as shown in Figure 2-2, is simply a change in impedance phase angle from an initial baseline, which is close to  $90^\circ$ . The resonant frequency is the frequency at which the minimum phase angle occurs, and it is unique for a given RLC circuit.

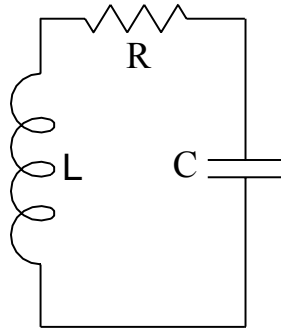


**Figure 2-1 Circuit Diagram of an RLC Circuit**

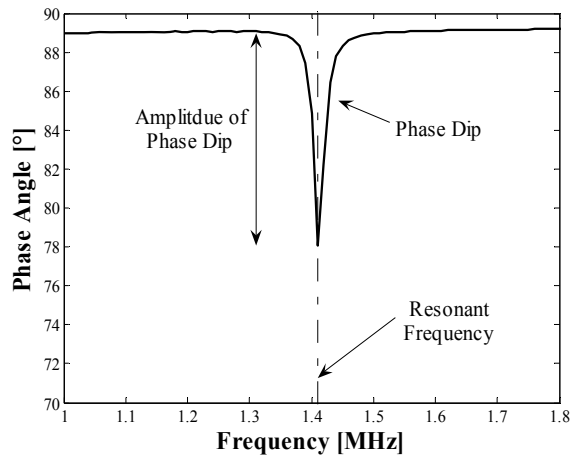


**Figure 2-2 Response of RLC Circuit to an Applied Alternating Current of Variable Frequency**

The amplitude of the phase dip and the value of the resonant frequency are determined by the physical parameters of the circuit. The amplitude of the phase dip is inversely proportional to the resistance of the circuit in cases of practical interest. As the resistance decreases toward zero, the amplitude of the phase dip increases, eventually approaching  $180^\circ$ . In contrast, as the resistance increases toward infinity, the amplitude approaches  $0^\circ$ . An infinite resistance corresponds to an open circuit. Furthermore, the resonant frequency,  $f_0$ , is determined by the inductance and capacitance of the circuit. Specifically,

$$f_0 = \frac{1}{2\pi\sqrt{LC}} \quad (2.1)$$

Therefore, response parameters — phase dip amplitude and resonant frequency — can be measured and used to calculate the physical parameters of an RLC circuit — resistance, inductance, and capacitance.

In addition, the response parameters of an RLC circuit can be measured passively and wirelessly. For the purposes of this thesis, a passive circuit is one that responds only to external stimuli and consequently does not require an onboard power supply. That said, because an RLC circuit contains an inductor, current can be induced in the circuit without actually hardwiring a current source into the circuit. Rather, as shown in Figure 2-3, an alternating current can be induced in an RLC circuit by magnetic coupling.

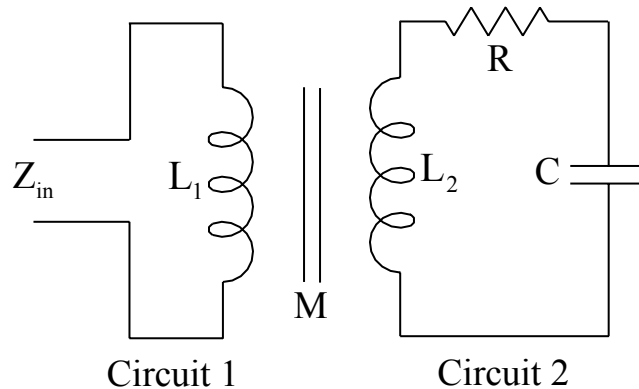


***Figure 2-3 RLC Circuit Magnetically Coupled to an Alternating Current Source***

The physical explanation for the magnetic coupling is the following. Alternating current at variable frequency is applied to circuit 1 and passes through inductor 1. The alternating current causes a change in magnetic flux in both inductor 1 and inductor 2. As the change in magnetic flux in inductor 2 approaches the resonant frequency of circuit 2, current flows through that circuit, while at frequencies far from the resonant frequency, there is no current flow.

The current that flows through inductor 2 at and around the resonant frequency of circuit 2 in turn changes the magnetic flux of inductor 1 and thus the current flowing through inductor 1. This change is measured as change in voltage over the circuit 1. Therefore, both the current applied to circuit 1 and the change in voltage over the circuit 1 are known. The impedance of the coupled circuit, characterized by its magnitude  $Z_m$  and phase angle  $\varphi$ , is expressed in phasor notation as  $Z = Z_m e^{j\varphi}$ . Similarly, the voltage measured over circuit 1 is expressed  $V = V_m e^{j\theta}$ , and the current applied to circuit 1 as  $I = I_m e^{j\beta}$ . Therefore, by the definition of impedance,

$$Z = \frac{V}{I} \quad (2.2)$$

From elementary operations with complex numbers,  $\varphi$  is the difference of  $\beta$  from  $\theta$ . Again, when the phase angle of the impedance is plotted with respect to frequency, the result is Figure 2-2.

Since the physical parameters of the circuit can be determined from the response parameters and the response parameters can be measured passively and wirelessly, the physical state of an RLC circuit can be ascertained without having direct access it. That is, if an interrogation is performed on an RLC circuit and the amplitude of its phase dip is zero, it can be inferred that the circuit is open because its resistance is essentially infinite. In contrast, if the amplitude of the phase dip is nonzero, it can be inferred that because the resistance is a finite value the circuit is closed. In short, whether an RLC circuit is open or closed can be determined simply from the response of the circuit to applied current.

This property of an RLC circuit can be exploited to determine the initiation of corrosion in a reinforced concrete structure. Suppose that the resistor of a given RLC circuit is a steel wire of small diameter. If the circuit is embedded in a reinforced concrete structure with only the resistor of the circuit exposed to the

environment within the concrete, as shown in Figure 2-4, any change in the resistance is due to a change in the dimensions of the resistor. Because the resistor is embedded in concrete, any change in the dimensions of the resistor is due to a change in the internal environment of the concrete. That is, if the environment within the concrete becomes corrosive, the resistor corrodes, and its resistance increases, ultimately becoming infinite due to loss of cross section. This change in the physical state of the circuit manifests itself as a change in sensor response, which can be measured passively and wirelessly. In contrast, if the internal environment of the concrete remains noncorrosive, the resistor remains intact and circuit signals as much. Since the resistor is placed in the same environment as nearby reinforcement, loss of reinforcement cross section can be inferred from the RLC circuit becoming open. Because the diameter of the resistor is small relative that of the reinforcement, corrosion initiation can be identified with fracture of the resistor, signaled as a phase dip of  $0^\circ$ . That is, if the resistor and reinforcement are corroding at the same rate, the reinforcement would lose a negligible percentage of cross section prior to the resistor fracturing and the circuit signaling that fracture.

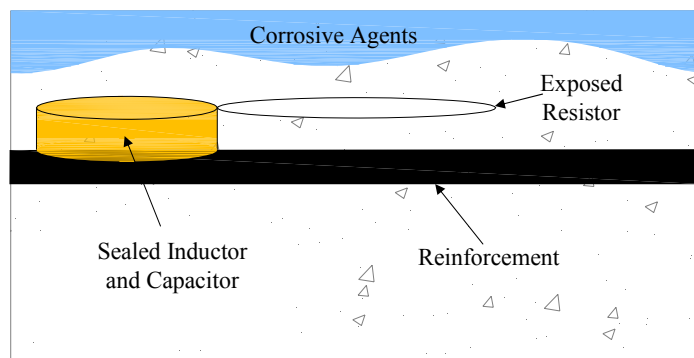


**Figure 2-4 RLC Circuit Used to Detect Corrosion Initiation**

If the corrosion sensor functions as a threshold sensor, the actual resistance of the circuit need not be determined. What is of interest is whether or

not the RLC circuit is intact, two distinct physical states that correspond respectively to whether or not a phase dip exists at the resonant frequency. The fact that the resistance of the circuit does not need to be determined greatly simplifies interpretation of the information obtained from the sensor. That is, the threshold sensor provides binary information (intact or fractured) about the state of the exposed resistor.

### **2.3 GEOMETRIES OF THE SENSOR**

Thus far, the corrosion sensor has been idealized as a single RLC circuit with an exposed steel resistor, or sensing wire. However, there is a practical difficulty with the sensor being a single circuit. If the location of a given sensor is known and the sensing wire is intact, the sensor will respond to applied current as in Figure 2-2. However, if the sensing wire has fractured, the response of the sensor will be as in Figure 2-5 corresponding to phase dip of  $0^\circ$ . Such a response is simply the phase angle of the impedance of circuit 1 in Figure 2-3. In application, circuit 1 is called the reader coil. Any measurement of the impedance of the reader coil in the absence of an intact RLC circuit, whether the measurement is performed in empty space or near a sensor with fractured sensing wire, will have the form of Figure 2-5. Thus, this response is the same regardless of position. If the measurement of the impedance of a circuit with a fractured sensing wire is performed, there is no confirmation that the reader coil was placed in the correct location. To prevent that difficulty, a second RLC circuit, called the reference circuit, was added to the corrosion sensor. The original circuit with the sensing wire is called the sensing circuit. The reference circuit is sealed from the external environment and remains intact throughout the service life of the sensor. Therefore, regardless of whether the sensing circuit is intact, the reference circuit confirms that the reader coil is placed in the proper location.

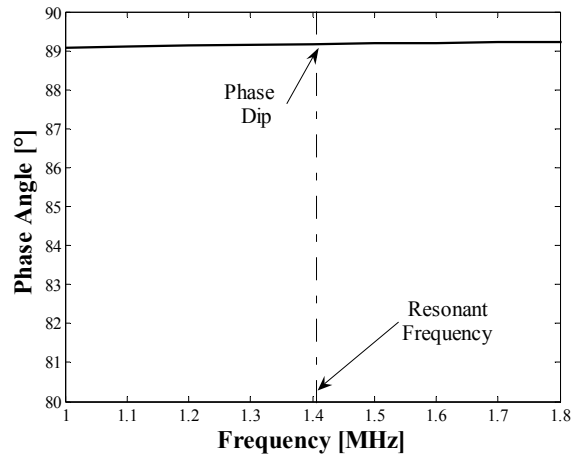


**Figure 2-5 Response of Sensor with Fractured Sensing Wire**

Two possible arrangements of the sensing and reference circuits were considered over the course of this research. In the case of the concentric sensor, the inductors of the sensing and reference circuits were placed concentric to one another, with the reference inductor inside the sensing inductor. In the case of the coplanar sensor, the inductors of the two circuits were placed beside one another. Both geometries are described below.

### 2.3.1 Concentric Sensor

A diagram and photograph of the concentric sensor are shown, respectively, in Figure 2-6 and Figure 2-7. The reference circuit, placed entirely within the inductor of the sensing circuit, is theoretically sealed from the outside environment by marine epoxy, which serves as the sensor housing. Thus, the reference circuit always exhibits a phase dip at its resonant frequency, confirming that the sensor has actually been located. In contrast to the reference circuit, a portion of the sensing circuit extends outside the epoxy housing of the sensor. This exposed portion of the circuit is the sensing wire, modeled as the resistor of the RLC circuit in Section 2.2.



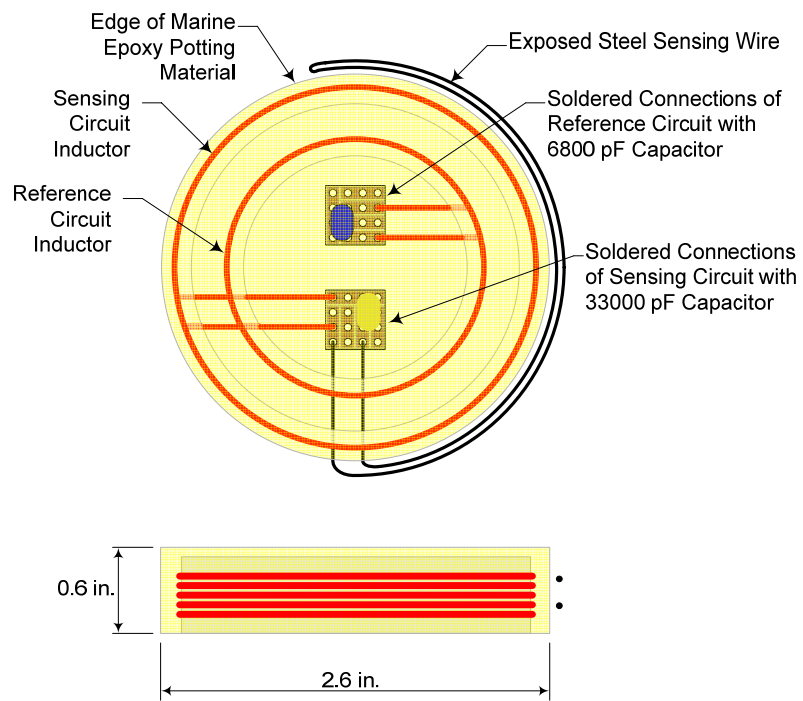


**Figure 2-6 Diagram of Concentric Sensor (Dickerson 2005)**

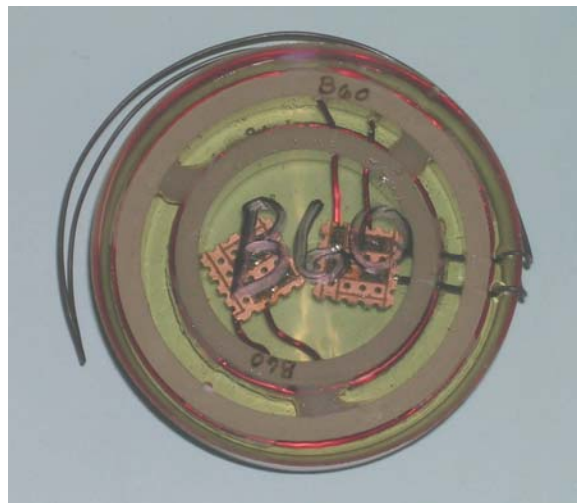
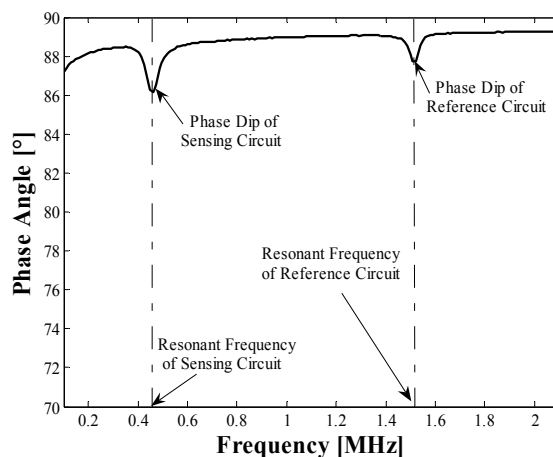


**Figure 2-7 Photograph of Concentric Sensor (Dickerson 2005)**

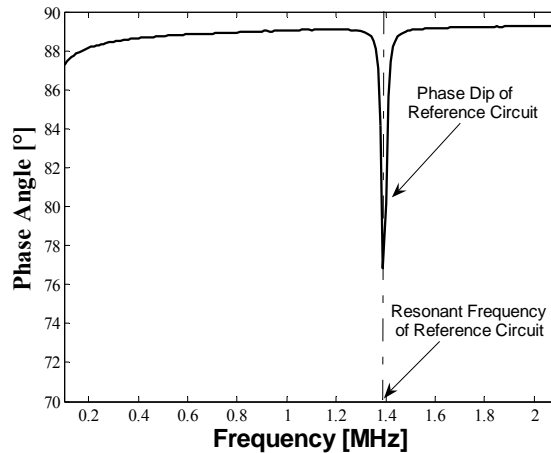
Because the resonant frequency of an RLC circuit depends only on the capacitance and inductance of the circuit, the frequencies of the sensing and

reference circuits can be conveniently set to any value within a physically practical range. For example, a given sensor could have a unique frequency assigned to its reference circuit. Then, that sensor could be identified in the field by its reference frequency. For the purposes of this research, all sensors of the same geometry — whether concentric or coplanar — were designed to have common sensing frequencies and common reference frequencies. The sensing and reference frequencies were set to conveniently distinct values. Despite that fact, the sensors have the intrinsic potential to be more uniquely defined.

The typical response of a concentric sensor with an intact sensing wire is given in Figure 2-8. Because the sensing wire is intact, there is a phase dip at both the sensing and reference frequencies. In contrast, once the sensing wire has fractured, the amplitude of the phase dip at the sensing frequency becomes zero. In that case, there is only a phase dip at the reference frequency, as shown in Figure 2-9.



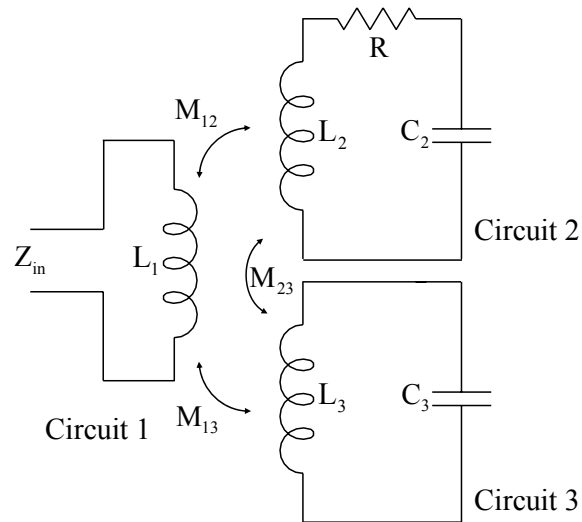
**Figure 2-8 Response of Concentric Sensor with Intact Sensing Wire**



**Figure 2-9 Response of Concentric Sensor with Fractured Sensing Wire**

Of interest is that the amplitude of the phase dip at the reference frequency increases significantly once the sensing wire has fractured. Furthermore, the reference frequency decreases somewhat, shifting to a lower value. This change in the reference circuit response is due to a change in the mutual inductance of the entire sensor. Because the two circuits are concentric, in the presence of a magnetic field, the inductance of the one influences the inductance of the other. Fracture of the sensing wire, however, eliminates the influence of the sensing circuit on the reference circuit. The consequence is an increase in the amplitude of the reference phase dip and a shift in the resonant frequency.

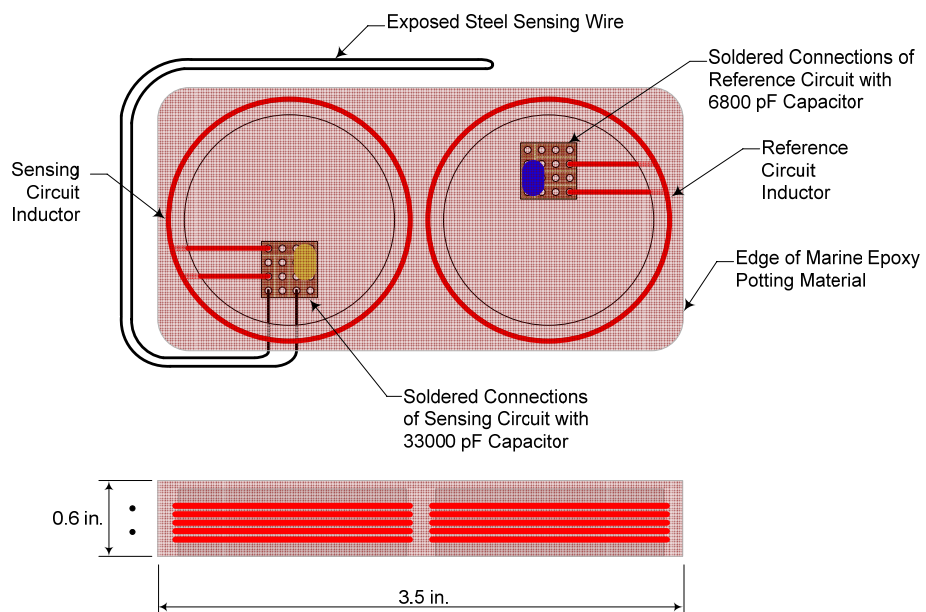
A circuit diagram illustrating the mutual inductance between the sensing and reference circuits is given in Figure 2-10. In the presence of the reader coil, circuit 1, a mutual inductance,  $M_{23}$ , develops between the sensing circuit, circuit 2, and the reference circuit, circuit 3. Because the reference inductor is entirely inside the sensing inductor, the sensing inductor masks the response of the reference circuit. Once the sensing wire has fractured, the response of the reference circuit is no longer masked, a fact expressed by the change in amplitude of the phase dip and shift of the resonant frequency.



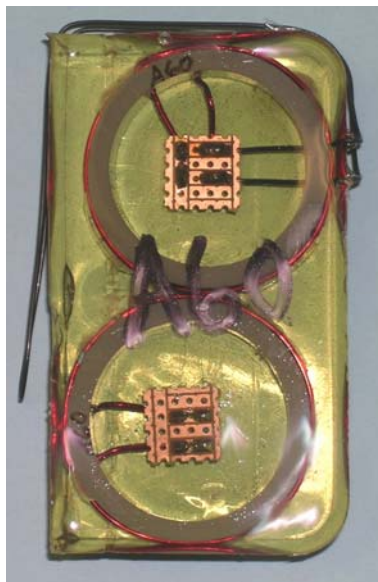
**Figure 2-10 Mutual Inductance in the Concentric Sensor**

### 2.3.2 Coplanar Sensor

As was mentioned above, the coplanar sensor comprises two side-by-side RLC circuits, as shown in Figure 2-11 and Figure 2-12. The primary differences between the coplanar and concentric sensors are the position and diameter of the sensing circuit inductor relative the reference circuit inductor. The objective in placing the two circuits side-by-side is to minimize their mutual inductance. Minimal mutual inductance renders the two circuits almost entirely independent, enabling the reference circuit to respond similarly, regardless of whether the sensing circuit is intact. Therefore, any signal processing of the reference circuit can be readily accomplished without speculation of the effect of the sensing circuit on the signal.



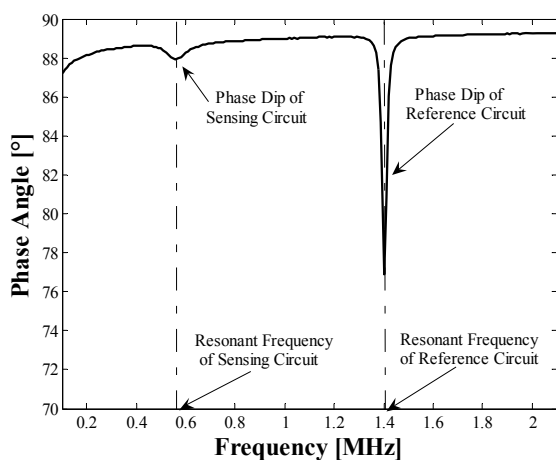
**Figure 2-11 Diagram of Coplanar Sensor (Dickerson 2005)**



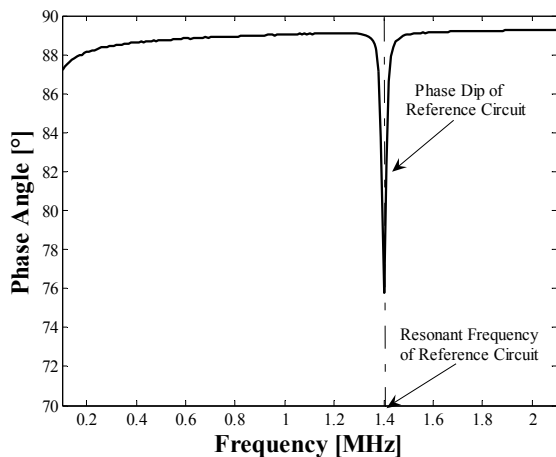
**Figure 2-12 Photograph of Coplanar Sensor (Dickerson 2005)**

Figure 2-13 and Figure 2-14 illustrate the independence of the responses of the sensing and reference circuits. The plots show the response of a sensor

with an intact and with a fractured sensing wire, respectively. The phase dip and frequency of the reference circuit are similar in both cases, though not identical, whether or not the sensing circuit is intact. In comparison to the concentric sensor, the phase dip at the sensing frequency of the coplanar sensor is small, causing it to be difficult to detect once the coplanar sensor is embedded in a reinforced concrete structure.



**Figure 2-13 Response of Coplanar Sensor with Intact Sensing Wire**



**Figure 2-14 Response of Coplanar Sensor with Fractured Sensing Wire**

### 2.3.3 Sensor Interrogation

The signal of the corrosion sensor, whether concentric or coplanar, is determined by an impedance/gain-phase analyzer with a reader coil. This determination of the response of the sensor to current applied by the reader coil is called interrogation. The impedance analyzer applies current of varying frequency to the corrosion sensor by magnetic coupling of the sensor and reader coil and measures the resulting impedance. That set of measurements is used to generate curves like those in Figure 2-8, Figure 2-9, Figure 2-13, and Figure 2-14. A diagram of the magnetic coupling through concrete is shown Figure 2-15. The distance between the reader coil and sensor is the read distance. Because the reader coil must be able to magnetically couple with the sensor in order to interrogate it, there is a limit on how large the read distance can be for any given reader coil and sensor.

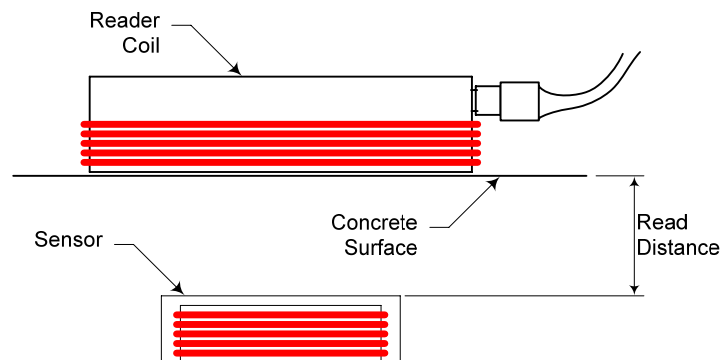


*Figure 2-15 Magnetic Coupling of Corrosion Sensor and Reader Coil (Dickerson 2005)*

## 2.4 TYPES OF SENSORS

In Section 2.2 and 2.3, the sensing wire was described as extending into the concrete in which it is embedded, fully exposed to the internal environment of the concrete. Then, if the environment around the sensor becomes corrosive, the sensing wire eventually fractures due to corrosion, and the sensor signals as much.

This is one possible type of sensor, and a sensor that is used in this way is called an isolated sensor. However, other types of sensors have been developed in which the sensing wire is attached directly to the steel reinforcement within the reinforced concrete structure, achieving an electrical connection between the two. If the sensing wire is galvanically neutral compared to the steel reinforcement, the sensor is called a coupled sensor. However, if the sensing wire is galvanically active compared to the steel, the sensor is called an anodic sensor. These three types of sensors are discussed below.

#### **2.4.1 Isolated Sensor**

Figure 2-16 depicts an isolated sensor embedded in a reinforced concrete structure. The sensing wire shown in the figure is above the reinforcement to emphasize the differences among the types of sensors. In practice, the wire should be located at the same elevation as the reinforcement. That said, corrosive agents ideally penetrate the concrete cover uniformly, reaching the elevation of the sensing wire and reinforcement simultaneously. Time of corrosion initiation is identified with the time at which the sensing wire fractures. Because the sensing wire has a much smaller diameter than the reinforcement, the reinforcement corrodes negligibly prior to the signaling of corrosion initiation. To ensure that the sensing wire and reinforcement corrode at a similar rate, the chemistry of the sensing wire should be similar to that of the reinforcement.



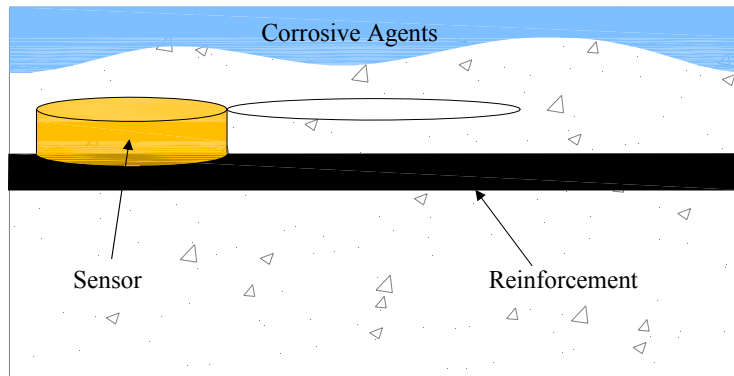


**Figure 2-16 Isolated Corrosion Sensor Embedded in Reinforced Concrete Structure**

A limitation of this design is the fact that crack formation in the concrete cover allows for nonuniform penetration of corrosive agents. As shown in Figure 2-17, it is possible for a crack to form in the concrete cover but fail to intersect the sensing wire. Corrosive agents are able to penetrate to the reinforcement rapidly without causing fracture of the sensing wire. In this way, the isolated sensor is strictly a point sensor: it detects corrosion initiation at the point where its sensing wire is exposed the internal environment of the concrete.

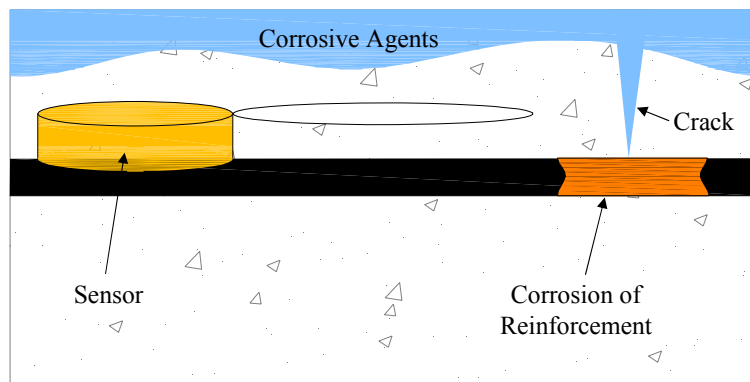


**Figure 2-17 Crack Formation and the Isolated Sensor**

One way to increase the area over which the sensor detects corrosion initiation, its tributary area, is to increase the length of the sensing wire.

However, there are two factors that limit the length of the sensing wire. First, the longer the sensing wire is, the less durable the sensor. That is, a long sensing wire is more likely to be damaged during installation and casting of the concrete, rendering it useless for detecting corrosion initiation. Furthermore, the longer wire can readily be shorted on the surrounding steel. In that case, no current flows through the sensing wire beyond the short, excluding the additional length from the circuit. Second, because the amplitude of the phase dip is inversely proportional to the resistance in the circuit, there is a critical value for the resistance beyond which the phase dip of the circuit is undetectable. This critical value depends on several factors, but for any given sensor it exists. Because the resistance of the circuit is theoretically proportional to the length of the sensing wire, there is also a critical wire length. Tests conducted on a set of sensors found the relationship between resistance and wire length to be governed by the line in Figure 2-18, verifying a linear relationship. Therefore, in order to maximize the tributary area of the sensor, some approach other than increasing the length of the sensing wire is necessary.

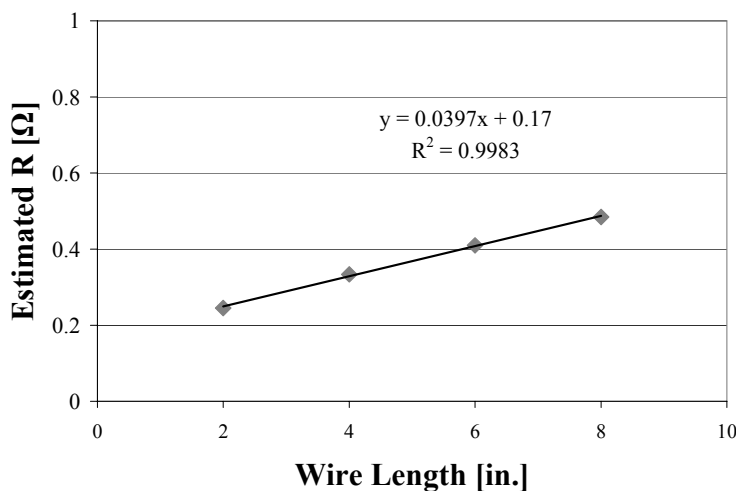


**Figure 2-18 Relationship between the Resistance and Sensing Wire Length of a Sensor (Andringa 2005)**

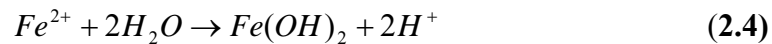
### 2.4.2 Coupled Sensor

In the case of the coupled sensor, an attempt is made to increase the tributary area of the sensor by electrically connecting the sensor to the steel reinforcement. To explain the underlying concept of the coupled sensor, it is first necessary to consider the basic theory of corrosion in reinforced concrete. The following discussion draws from treatments found in Broomfield (1997) and Bertolini et al. (2004). For the purposes of this discussion, the corrosive agents are assumed to be chlorides since their role in corrosion of reinforcement is thoroughly understood. This discussion, however, can potentially be generalized to take account of other types of corrosive agents.

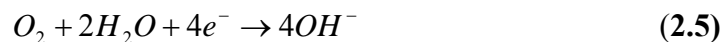
In the absence of external chemical influences, the pore solution of concrete remains at or above a pH of 12.5. At such a high pH, the pore solution contains a high concentration of hydroxyls, which support formation of a passive layer on the surface of steel. However, if chlorides penetrate through the concrete cover, they displace hydroxyls from the surface of the steel. As a result, the pore solution can no longer support a passive layer. In that event, the steel becomes active. The chlorides thereby catalyze the following anodic reaction:



Hydrolysis of the steel cation, in turn, produces acidity:



Because electrons are liberated in the anodic reaction, a cathodic reaction develops in which the electrons are consumed, producing alkalinity:



The anodic and cathodic reactions cause electrons to flow from the anode, region of negative charge because it is a source of electrons, to the cathode, region of positive charge relative the anode. This flow of electrons is the corrosion current.

Furthermore, the pore solution of the concrete sustains the cathodic reaction by supplying it with oxygen. In this way, the presence of moisture in the pore structure of the concrete is essential for the development of corrosion within the structure. The steps of the corrosion reaction are illustrated in Figure 2-19.

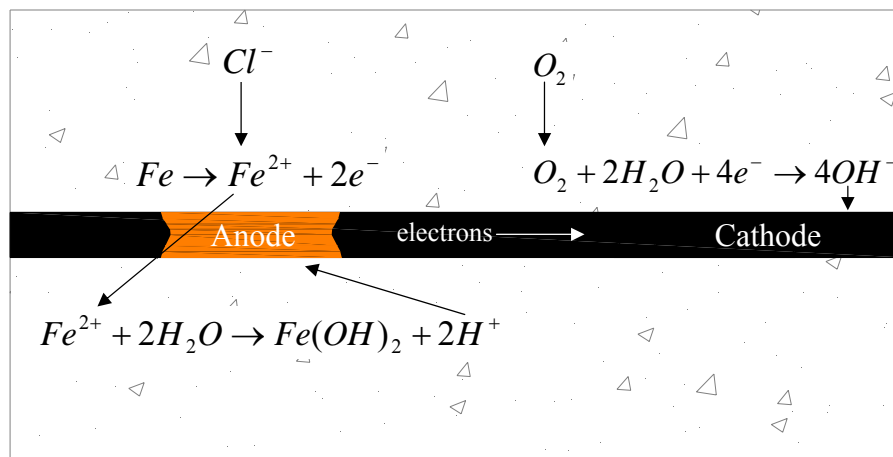


**Figure 2-19 Corrosion Initiation in Reinforced Concrete**

Of critical importance is that the anodic and cathodic reactions reinforce themselves. That is, the anodic reaction, by producing acidity, causes additional oxidation of iron. Similarly, the cathodic reaction strengthens the passive layer on the steel in its vicinity by producing alkalinity. The result is that a potential difference develops between the two regions of the reinforcement and sustains itself. Because the anode develops where chlorides penetrate the concrete cover to the surface of the steel, it tends to be a more defined region, especially if the chlorides penetrate by means of cracks. In contrast, the cathode is the indistinct remainder of the structure which is exposed to lower levels of chlorides.

Electrical connection of the sensing wire of a coupled sensor to the steel reinforcement is intended to extend the area over which the sensor can detect corrosion initiation. In the case of the isolated sensor, the potential of the sensing wire could be a wide range of values because no source of charges determines or

even influences its potential. If a crack forms in the concrete cover that fails to intersect the sensing wire, the potential at nearby reinforcement where the crack intersects the reinforcement will be more negative than that of the sensing wire. In fact, as part of the rest of the structure, the sensing wire becomes part of the cathode, having a positive potential relative to the anode. In terms of Figure 2-20,  $E_s$ , the potential of the sensing wire, is greater than  $E_a$ , the potential of the anode.

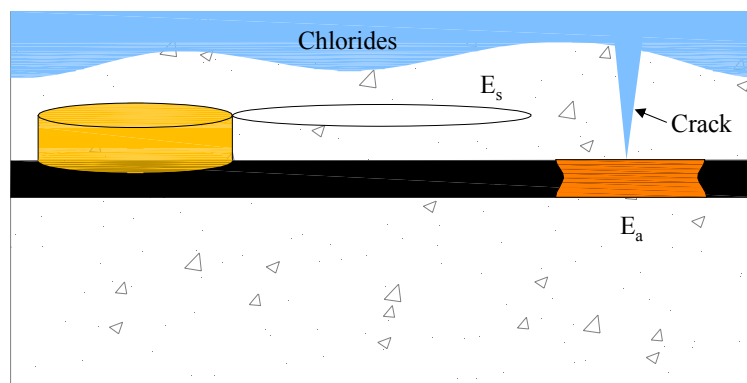


**Figure 2-20 Potential of Sensing Wire Relative to the Anode in Case of Crack**

In contrast, if the sensing wire is electrically connected to the steel reinforcement, its potential could be influenced by the potential of nearby corroding reinforcement. Ideally, the potential  $E_s$  would be equal to that of  $E_a$  such that the sensing wire becomes part of the anode. In that case, the sensing wire, by supplying electrons to the rest of the structure, would corrode at a comparable rate to nearby reinforcement and fracture prior to significant damage being done to the reinforcement. This idealization of the relationship between  $E_s$  and  $E_a$  is illustrated in Figure 2-21.

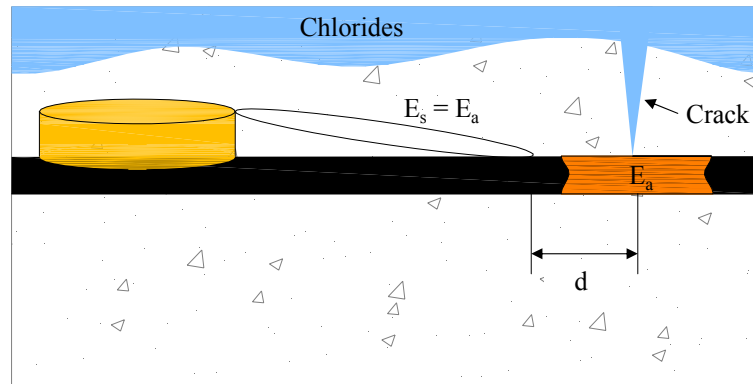


**Figure 2-21 Idealized Behavior of Coupled Sensor**

For the purposes of application, the critical parameter for the coupled sensor is  $d$ , illustrated in Figure 2-21. The parameter  $d$  is the maximum distance from the anode that the sensing wire can be attached and its potential still be equal to the potential of the anode such that the sensing wires is part of the anode. Because as part of the anode the sensing wire corrodes with the steel reinforcement, the parameter  $d$  defines the tributary area over which the sensor detects corrosion initiation. Given the many variables in corrosion of steel in concrete, any attempt to establish the value of  $d$  must be empirical. An empirical attempt to establish  $d$  is discussed in Chapter 5. What distinguishes the isolated and coupled sensors is that there is no parameter  $d$  associated with the isolated sensor because it functions as a point sensor. That is, the isolated sensor only provides time of corrosion initiation at the point where it is placed in the structure. In contrast, the coupled sensor is designed to detect corrosion initiation over a tributary area.

### 2.4.3 Anodic Sensor

In the case of both the isolated sensor and coupled sensor, the chemistry of the sensing wire is similar to that of the reinforcement. While similar chemistry is imperative to the proper functioning of the isolated sensor, it may limit the

tributary area of the coupled sensor. That is, use of a sensing wire that is galvanically active compared with steel, such as zinc or aluminum, has the possibility of increasing the tributary area of the sensor. The increased area would result from the sensing wire electrochemically coupling to the steel reinforcement, not simply connecting electrically as with the coupled sensor. To elaborate upon this approach, some of the basic features of galvanic corrosion must first be considered. In the following discussion, the sensing wire is assumed to be zinc. However, it is possible to use any metal that is galvanically active compared to steel as the sensing wire.

It is commonly known that when iron and a more galvanically active metal are immersed in an acidic aqueous solution, a potential difference develops between the two metals. Specifically, zinc develops a potential that is negative relative the potential of the iron, causing a net electron flow away from the zinc. That is, the zinc becomes the anode, and the steel becomes the cathode. In this way, the zinc is consumed in the resulting galvanic cell, shown in Figure 2-22.

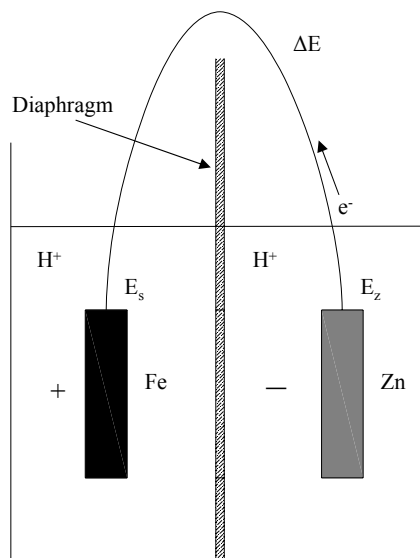


**Figure 2-22 Galvanic Cell of Iron and Zinc**

This property of iron and zinc could possibly be used to increase the tributary area of a coupled sensor. Figure 2-23 through Figure 2-27 illustrate this concept. The length of steel embedded in concrete in Figure 2-23 is electrochemically modeled in Figure 2-24. Although the pore solution of concrete contains numerous ions, it is modeled in Figure 2-24 as containing only hydroxyls because of their definitive role in formation of the passive layer.

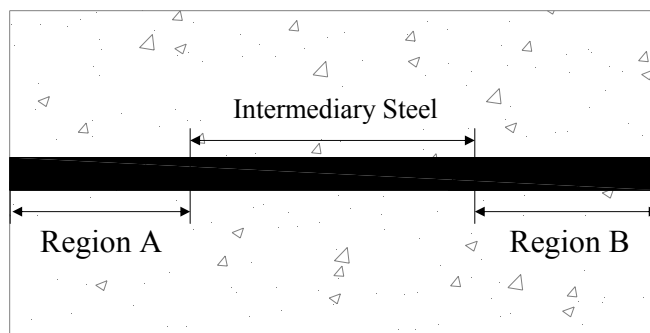


**Figure 2-23 Length of Steel Embedded in Concrete**

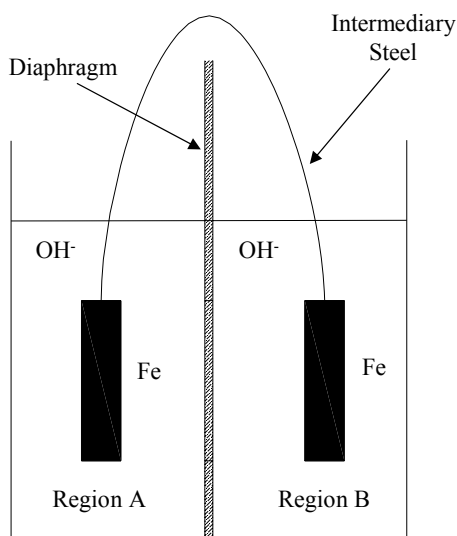


**Figure 2-24 Model of Length of Steel Embedded in Concrete**



An anodic sensor, having a zinc sensing wire, is embedded in the concrete in Figure 2-25 such that the sensing wire is attached to the steel in Region B. Two distinct cases for corrosion initiation are chloride penetration in region B but not region A and chloride penetration in region A but not region B. First, if chlorides penetrate the concrete cover in region B but not in region A, as shown in Figure 2-25, the resulting electrochemical model is Figure 2-26. Because the chlorides are a catalyst for the production of acid, region B is equivalent to the model in Figure 2-22. Therefore, the zinc sensing wire serves as a sacrificial anode for the steel in region B, fracturing even more readily than a steel sensing wire due to the development of a galvanic cell.

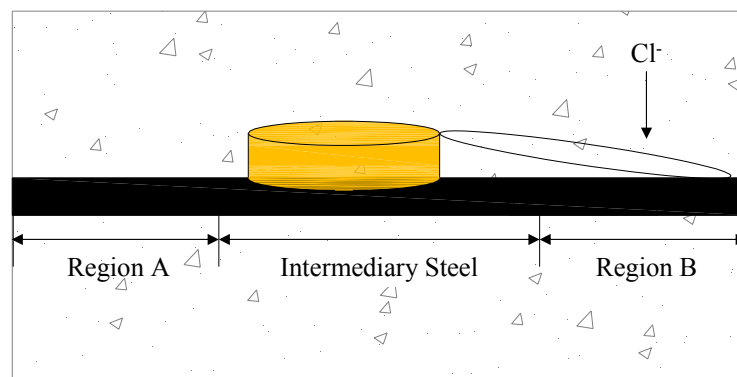


**Figure 2-25 Chloride Penetration into Region B**

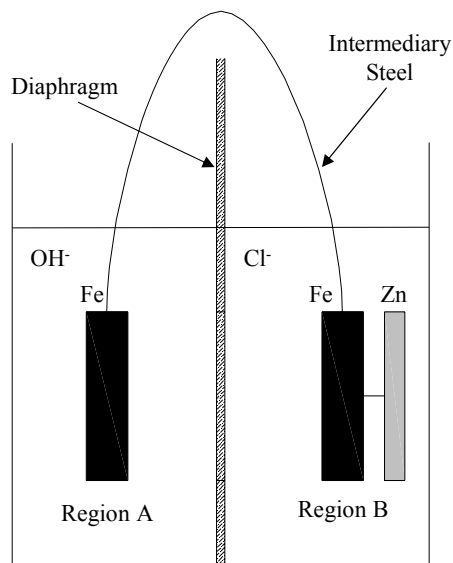


**Figure 2-26 Model of Chloride Penetration into Region B**

The sensing wires of both the isolated and coupled sensors would fracture nearly as readily as that of the anodic sensor in this first case because the sensing wire is directly exposed to the chlorides. Of greater interest is the second case in which the chlorides penetrate to the reinforcement in Region A, but not in Region B. This case is illustrated in Figure 2-27. The question of whether the zinc in this case will serve as a sacrificial anode can only be settled empirically. Ongoing experiments described in Chapter 7 address this very issue. Bertolini et al. (2002) have shown that an aluminum-zinc alloy serves as a sacrificial anode for passive steel up to 1 m from a salt water splash zone. However, in that study, the alloy was immersed in the salt water. In terms of Figure 2-26, an aluminum-zinc alloy in Region B served as the sacrificial anode for the steel in Region A, where the length of the intermediary steel was 1 m. Thus, Bertolini et al. (2001) have shown that a galvanic cell forms in reinforced concrete over significant distances for this first case of chloride penetration. However, the question of whether zinc

embedded in concrete unexposed to chlorides will serve as a sacrificial anode to steel exposed to chlorides remains open.

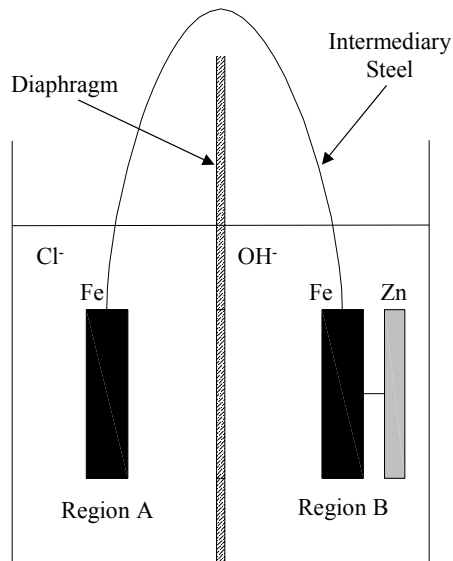


**Figure 2-27 Model of Chloride Penetration into Region A**

Another open question is at what rate a metal active compared to steel, such as zinc or aluminum, corrodes when coupled with an entirely passive tributary area of steel. Although the corrosion rate of passive steel is orders of magnitude less than that of active steel, the corrosion rate of passive steel is nonzero and could drive corrosion of a more active metal. Any practical application of the anodic sensor would involve the sensing wire being coupled to a large tributary area of steel. The result would be a large cathode to anode area ratio which would increase the corrosion rate of the anodic sensing wire. It is also possible, especially in the case of aluminum, that the sensing wire would corrode simply because it is embedded in the alkaline environment of the concrete. If the rate of corrosion is large enough to cause the sensing wire to fracture even in the absence of chloride penetration, the sensor would erroneously signal that corrosion had initiated when in fact it had not. Bertolini et al. (2002) have

measured the corrosion rate of the zinc-aluminum alloy coupled to an area of steel having both active and passive regions. Yet, the corrosion rate of a metal active compared to steel coupled to an entirely passive area of steel has not been determined. An experiment developed to determine trends in this corrosion rate is discussed in Chapter 8.

## **2.5 CHARACTERIZATION OF SENSOR RESPONSE**

The response of a threshold sensor, regardless of geometry or type, is primarily characterized by whether a phase dip exists at the sensing frequency. If the phase dip at the sensing frequency exists, corrosion has not initiated. If the phase dip at the sensing frequency does not exist, corrosion has initiated. Depiction of the existence of the phase dip at the sensing frequency over time is discussed in Section 2.5.1. A secondary feature of characterizing sensor response is determining the variability of the response. Section 2.5.2 addresses quantification of variability in sensor response.

### **2.5.1 Characterization of Corrosion Threshold**

A contour plot can readily depict, over time, whether a phase dip exists. In this way, the contour plot indicates whether a corrosion threshold has been exceeded. Depending on the type of sensor, the corrosion threshold could be environmental (isolated sensor) or in terms of corrosion current (coupled and anodic sensors). If the sensing wire is intact, the threshold has not been reached. In contrast, if the sensing wire is fractured, the threshold has been reached.

Figure 2-28 illustrates the essential features of a concentric sensor response. In Figure 2-28, the phase dip is directed into the page and is quantified by shades from white to black. From day 0 to 100, the phase dip at the sensing frequency exists and its amplitude is constant; the same is the case for the phase

dip at the reference frequency. After day 100, there is no longer a phase dip at the sensing frequency. In addition, the phase dip at the reference frequency increases in amplitude, and the reference frequency itself shifts to a lower value. The conclusion from this plot is that the sensing wire fractured before approximately day 100 of testing but after the time of the interrogation prior the interrogation in which the fracture was detected.

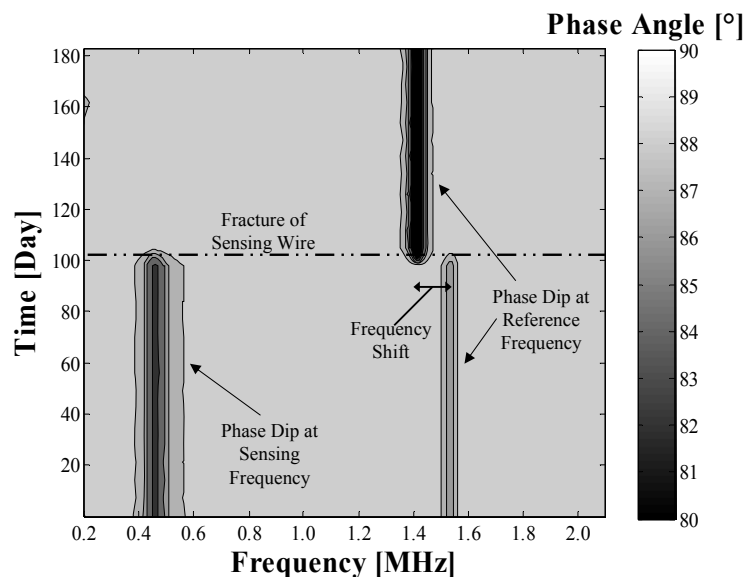


**Figure 2-28 Response of Concentric Sensor as Contour Plot**

Figure 2-29 illustrates the response of a coplanar sensor as a contour plot. As in the case of the concentric sensor, phase dips of constant amplitude exist at both the sensing and reference frequencies initially. At approximately day 150, the sensing phase dip disappears, indicating that the sensing wire has fractured. Notably, however, there is no discernible change in the amplitude of the phase dip at the reference frequency or in the reference frequency itself. Again, this independence is due to a lack of mutual inductance between the sensing and reference inductors.

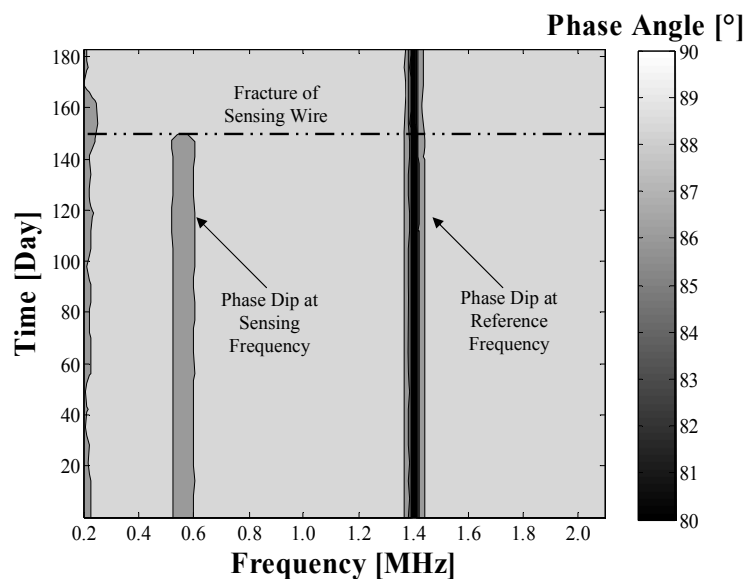


*Figure 2-29 Response of Coplanar Sensor as Contour Plot*

### 2.5.2 Characterization of Variability in Sensor Response

Because the contour plot provides primarily qualitative information about the response of a sensor, an algorithm was developed to extract parameters used to characterize the measured response of a sensor. The algorithm was developed by Andringa (2006) is described in Dickerson (2005). The algorithm was used to quantify the response of all sensors discussed in this thesis. The measured response of a sensor is a combination of the responses of the reader coil and circuits composing the sensor. The algorithm separates the baseline response (response of the reader coil) from the sensor response using a curve-fit approach. Some limitations with this approach have been observed in this research, as discussed in Section 2.6.

Once determined by the algorithm, the response parameters — resonant frequency, amplitude of phase dip, and pseudo-quality factor — were used to assess the variability of sensor response over time. Two of the parameters,

resonant frequency and the phase dip, have already been discussed in Section 2.4. The third parameter, the pseudo-quality factor, is briefly discussed here. For a detailed discussion the pseudo-quality factor see Andringa (2003) and (2006), whose treatment is the basis of the one below.

In general, the quality factor ( $Q$ ) of an RLC circuit is the ratio of the amount of energy stored in the circuit to the amount of energy dissipated by the circuit. In general, if  $\omega_0 = \frac{1}{\sqrt{LC}}$  is the circular resonant frequency,

$$Q = \frac{\omega_0 L}{R} \quad (2.6)$$

It can be shown from analysis of the impedance of an RLC circuit in the frequency domain that if  $\Delta\omega$  is the width of the curve at half the amplitude of the phase dip,

$$Q = \frac{\omega_0}{\Delta\omega} \quad (2.7)$$

Because the quality factor is a useful parameter for characterizing the response of an RLC circuit, a similar parameter was postulated to characterize the magnetically coupled circuit of the reader coil and each circuit of the corrosion sensor. A circuit diagram of the reader coil magnetically coupled to one of the circuits of the corrosion sensor, whether the sensing or reference circuit, is illustrated in Figure 2-3. This parameter for characterizing the coupled circuit was denoted as the pseudo-quality factor ( $\bar{Q}$ ). There is, therefore, a pseudo-quality factor of the sensing circuit and a pseudo-quality factor of the reference circuit. The similarity of the response between the coupled circuit and a single RLC circuit suggested the following definition of the pseudo-quality factor:

$$\bar{Q} \equiv \frac{\omega_{\theta\min}}{\Delta\omega} \quad (2.8)$$

The value  $\Delta\omega$  is the width of the phase dip at half of its amplitude, and  $\omega_{\theta\min}$  is the circular resonant frequency. These parameters are shown in Figure 2-30 and can be obtained from the measured impedance data using the curve-fitting algorithm.

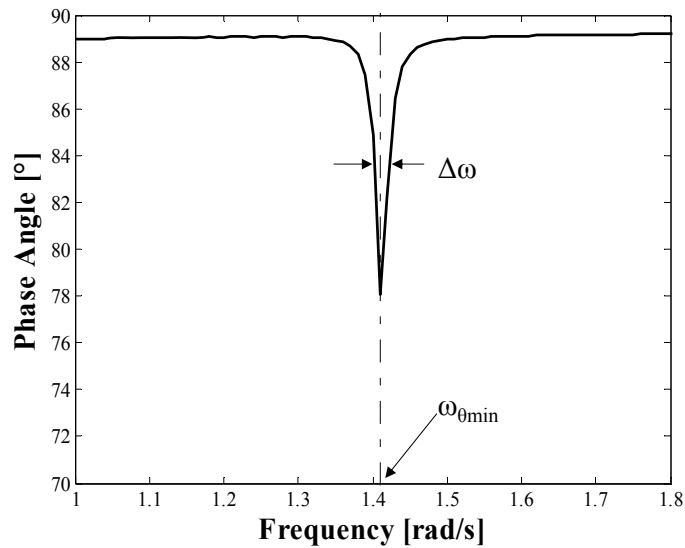


**Figure 2-30 Parameters  $\omega_{\theta\min}$  and  $\Delta\omega$  which Define the Pseudo-Quality Factor (Andringa 2006)**

Because there is not an explicit theoretical basis for using the pseudo-quality factor to characterize the response of the coupled circuit, the usefulness of the parameter was established empirically. The advantage of using the pseudo-quality factor to characterize variability in sensor response has been shown to be twofold. First, the pseudo-quality factor is less dependent on the relative position of the reader coil and sensor than the amplitude of the phase dip. That is, changes in position of the reader coil from one interrogation to another introduce less variability into the value of the pseudo-quality factor than into the amplitude of the phase dip. For example, if the reader coil is displaced by some relatively



small distance  $a$  from the centroid of the corrosion sensor, the change in the pseudo-quality factor is smaller than the change in the amplitude of the phase dip of the sensor. The displacement  $a$  and the effect of the displacement on the amplitude of the phased dip and pseudo-quality factor are shown in Figure 2-31 and Figure 2-32.

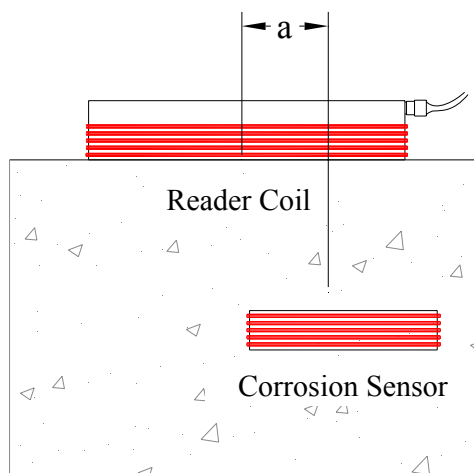


**Figure 2-31 Displacement of Reader Coil from Corrosion Sensor**

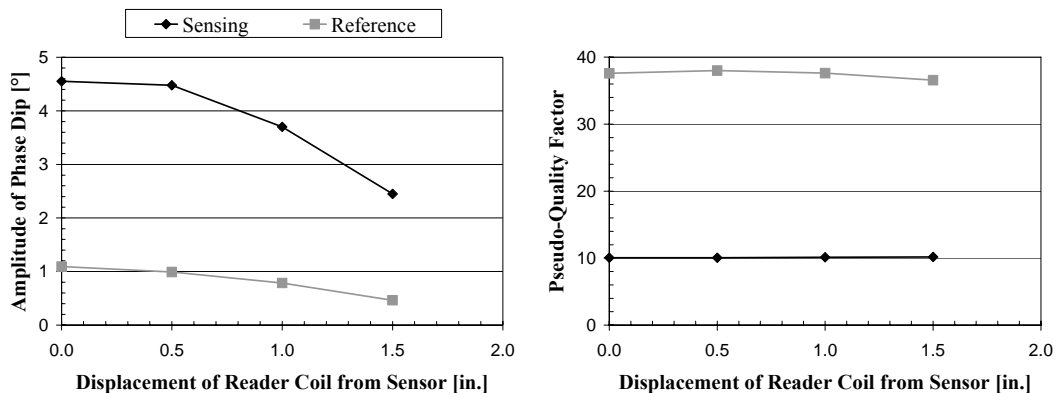


**Figure 2-32 Amplitude of Phase Dip and Pseudo-Quality Factor with Respect to Displacement**

Second, the pseudo-quality factor could potentially be used to extract analog information from the sensor. For instance, just as is the case with the

quality factor, the pseudo-quality factor has been found to be related to the resistance of the circuit. Therefore, changes in the resistance of the sensing circuit can be identified over time and potentially be related to changes in the cross section of the sensing wire. This and other analog applications are discussed in Andringa (2006) but receive no additional treatment in this thesis. What has bearing here, and in following chapters, is that the pseudo-quality factor is a parameter of sensor response that is less dependent of the relative position of the reader coil and sensor than is the amplitude of the phase dip. Therefore, the pseudo-quality factor is considered to be a more robust index for characterizing the variability in sensor response.

## **2.6 BASELINE SHIFT**

The primary source of variability in the response parameters of sensors subjected to large-scale testing was baseline shift. Baseline shift was observed in the responses of sensors discussed in Chapters 4 and 5 and is described here because baseline shift broadly influenced the responses of the sensors.

The baseline of a reader coil is the response of the reader coil to applied alternating current in the absence of a sensor. Since no RLC circuits are present in the magnetic field of the reader coil, baseline shift is simply a measurement of the impedance of the reader coil. In practice, the phase angle of the impedance gradually approaches  $90^\circ$ . Baseline shift is a gradual decrease in the value of the phase angle with respect to frequency. Figure 2-33 show different magnitudes of baseline shift that occurred over a three-hour period.

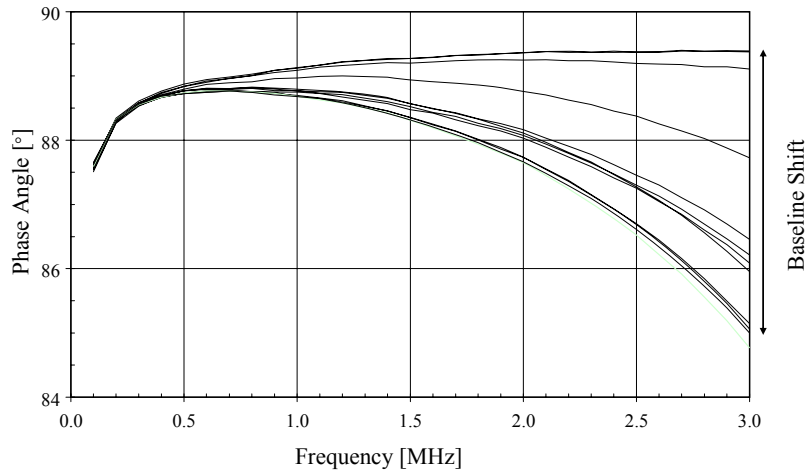


**Figure 2-33 Baseline Shift of Reader Coil**

Baseline shifts were observed in the interrogation histories of nearly all the sensors discussed in Chapter 4 and many of the sensors discussed in Chapter 5. For example, the baseline shift over an 18-month period of sensor B51, tested in Slab 2, is shown in Figure 2-34. The shifting of the baseline is manifest in the contour plot of B51, provided in Figure 2-35, between days 400 and 450 of testing, at frequencies from 1.5 to 2.0 MHz. In order to articulate the response of sensor B51, contour lines were placed with unequal spacing at the following values of phase angle: 80°, 84°, 85°, 87°, 88.5°, and 90°.

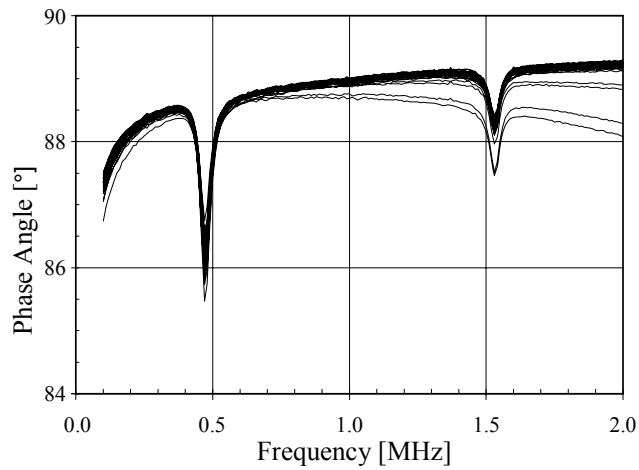


**Figure 2-34 Baseline Shift of Sensor B51: Phase Angle vs. Frequency**

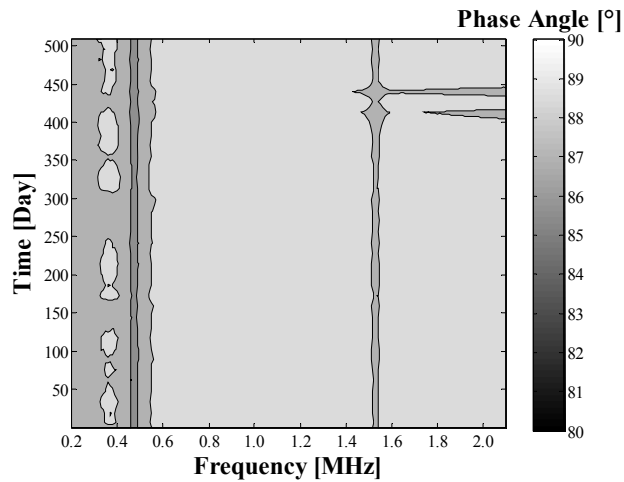


**Figure 2-35 Baseline Shift of Sensor B51: Contour Plot**

The presence of a baseline shift greatly complicated, and in some cases prevented, determination of the amplitudes of the phase dips and calculation of the pseudo-quality factors of certain sensors. When it was possible to obtain these parameters, the baseline shift added to the variability to the values obtained. Figure 2-36 illustrates the effect of baseline shift on the curve-fitting algorithm used to determine the resonant frequencies, amplitudes of phase dips, and pseudo-quality factors. Figure 2-36 shows the fit of a curve developed by the algorithm

to the response of sensor B51 on day 6 and day 441 of testing. On day 6, the baseline is undistorted, whereas on day 441 the baseline is distorted. Such distortion introduced error in determination of the response parameters.

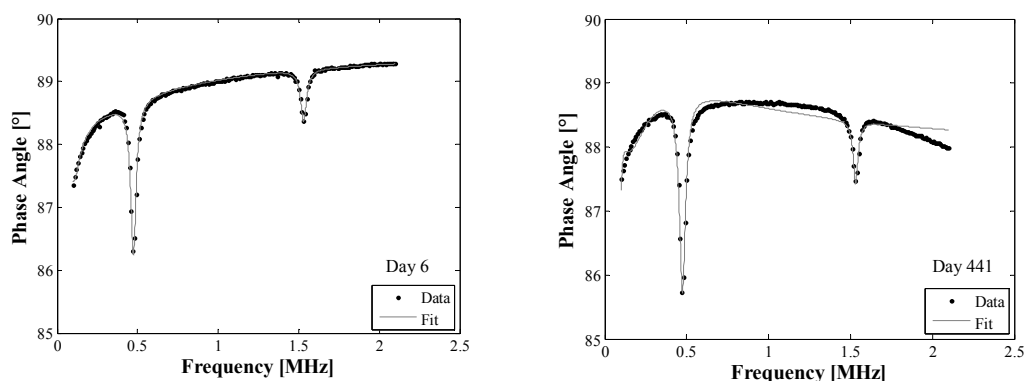


**Figure 2-36 Effect of Baseline Shift on Curve Fit of Sensor B51**

Subsequent examination of the reader coil linked the baseline shift to moisture on the surface of the reader coil. That is, when the surface of the reader coil was wet, its baseline tended to shift downward. When the surface was dry, the baseline approached 90°. Interrogations were performed at the same time as half-cell measurements, which required spraying the surface of the concrete with water to achieve an electrical connection with the steel reinforcement. This moisture adhered to the surface of the reader coil, causing baselines to shift downward. The shift was due to the moisture's increasing the capacitance of the reader coil, which caused gradual self-resonance of the reader coil. The conclusion is that in order to minimize noise due to shifting baselines, the surface of the reader coil must be kept dry.

Although the development of baseline shift complicated the extraction of analog information from the sensors, baseline shift did not prevent the sensors from functioning reliably as threshold sensors. That is, distortion of the baseline did not obscure whether the sensing wire was intact or fractured. Rather, baseline

shift revealed that the algorithm used to calculate the response parameters of the sensor was not sufficiently robust to overcome variability in the data from large-scale testing.

## 2.7 CONCLUSION

In summary, the passive wireless corrosion sensor comprises two RLC circuits. This design allows of the sensor to send a signal whether corrosion has initiated in a reinforced concrete structure without an onboard power supply or external wiring. This application of the sensor requires that it be economical, reliable, and durable.

Two possible geometries of the sensor are the concentric geometry and the coplanar geometry. In the case of the concentric sensor, the inductor of the reference circuit is located within that of the sensing, concentric to it. For the coplanar sensor, the two inductors are side-by-side. The former geometry allows for mutual inductance between the two circuits, while the latter nearly eliminates it. As a result, the responses of sensors with different geometries are distinct. Despite that fact, both geometries include an exposed sensing wire, and fracture of that sensing wire is signaled by the sensor.

The three types of sensors — isolated, coupled, and anodic — are distinguished by whether their sensing wire is connected to the steel reinforcement and by the metal used for the sensing wire. The steel sensing wire of the isolated sensor is simply exposed to the internal environment of the concrete, limiting the sensor to detecting corrosion initiation at a point. In contrast, the steel sensing wire of the coupled sensor is electrically connected to the reinforcement. The electrical connection is intended to allow the sensing wire to become part of an anode removed from the point of connection of the sensing wire by some distance. Lastly, like the coupled sensor, the sensing wire of the

anodic sensor is connected to the steel reinforcement. However, the sensing wire, instead of being steel, is a metal galvanically active compared to steel, such as zinc or aluminum. In this way, the sensing wire of an anodic sensor is intended to serve as the sacrificial anode of corroding steel a distance away from the sensing wire.

Whether the sensing wire of a sensor is intact, and thus whether corrosion has initiated in the structure, can readily be depicted as a contour plot. In that way, the contour plot shows when the corrosion threshold has been reached. Because the contour plot only depicts qualitative information, the variability of the response of a sensor is characterized by the resonant frequency, amplitude of the phase dip, and pseudo-quality factor of the circuit. Because the pseudo-quality factor is less dependent on relative position of the reader coil and sensor than the amplitude phase dip, it is the more robust parameter for determining variability in sensor response.

Finally, the primary source of variability in the response parameters of the sensors was baseline shift. Baseline shift is a gradual decrease in the phase angle of the baseline with respect to frequency due to moisture adhering to the surface of the reader coil. Although it complicated extraction of analog information from the responses of the sensors, it did not prevent the sensors from signaling that the corrosion threshold had been reached. Other sources of variability were variation in the moisture content of the concrete, discussed in Sections 3.3.2, 5.3.3, and 7.3.3; variation in temperature, described in Section 3.3.3 and 5.3.6; and the development of black corrosion within the epoxy housing, discussed in Chapter 6.

## **CHAPTER 3**

### **Environmental Tests of Isolated Sensors Embedded in Concrete Prisms**

#### **3.1 INTRODUCTION**

In order to test the sensitivity of sensor response to a variety of environmental conditions, two sets of isolated sensors were fabricated and cast in concrete prisms. The dimensions of the prisms were on the order of inches, and therefore constitute small-scale tests. Although small-scale testing cannot entirely replicate service conditions in civil engineering structures, it allows for much greater control of environmental conditions than does large-scale testing. Section 3.2 describes this experiment. The measured response of the sensors is assessed in Section 3.3. Finally, Section 3.4 discusses the results of autopsying the specimens. The isolated sensors were also embedded in large-scale slabs, and these results will be discussed in Chapter 4.

#### **3.2 DESIGN OF EXPERIMENT**

Though a complete description of this experiment appears in Dickerson (2005), a summary of its design is given below. Twenty-two sensors — twelve concentric (B19-B30) and ten coplanar (A21-A30) — were fabricated using 26-gage (0.0159-in. diameter) steel sensing wire. Subsequent chemical analysis of the wire indicated that it was alloy type AISI-ASE 1005. The chemical composition of the 1005 wire is given in Section 4.2. Each sensor was cast in a 4-in. diameter cylindrical mold with a height of 3 in. The dimensions of the coplanar sensors required some deformation of the cylindrical mold for the sensor to fit inside. The effect on the shape of the prism is shown in Figure 3-1, where a prism containing a coplanar sensor is compared with a prism containing a



concentric sensor. Despite this deformation, the dimensions of the prisms afforded 1 in. concrete cover over the sensing wire in all cases.



(a) Coplanar Sensor A27

(b) Concentric Sensor B21

***Figure 3-1 Deformation of Prism Containing Coplanar Sensor***

Illustrations of the two types of sensors embedded in prisms are shown in Figure 3-2 and Figure 3-3, respectively. The sensors were zip-tied to a plastic chair which was secured to the bottom of the mold by a screw. The screw was removed once the concrete had cured. Concrete with a 28-day compressive strength of 3,600 psi was specified, and the maximum aggregate size was  $\frac{3}{8}$  in. The prisms were cast on 16 December 2004 and cured for almost four weeks before beginning the environmental cycles.

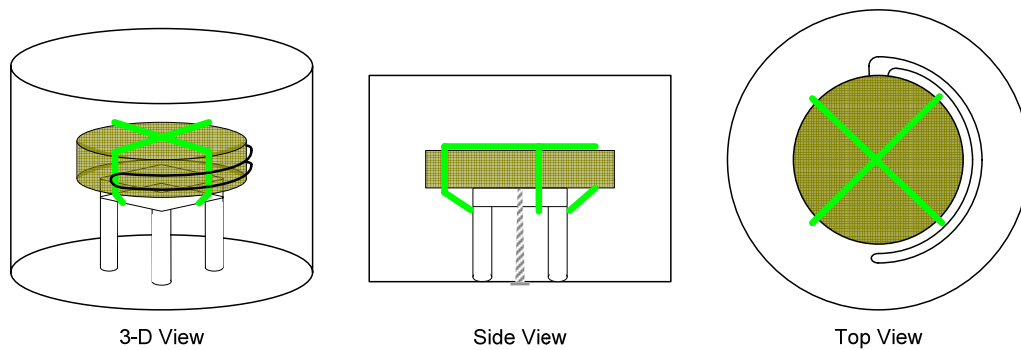


**Figure 3-2 Concentric Sensor in Concrete Prism (Dickerson 2005)**

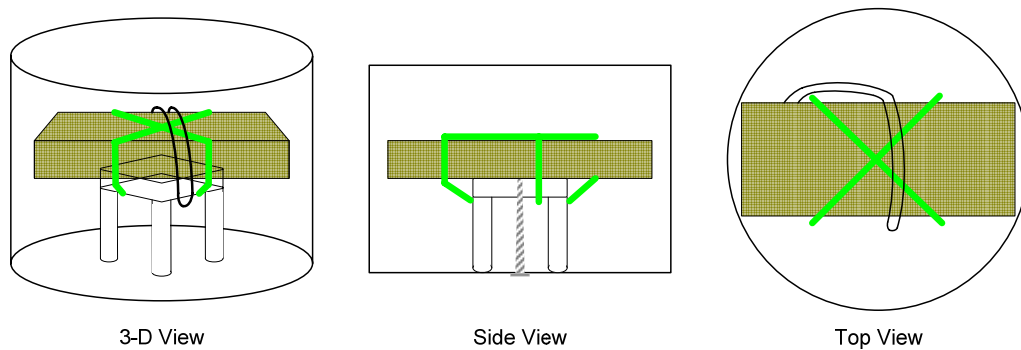


**Figure 3-3 Coplanar Sensor in Concrete Prism (Dickerson 2005)**

The environmental conditions to which the prisms were subjected were the following: (a) control, (b) varying moisture, (c) varying thermal, and (d) varying moisture and thermal. Each environmental cycle had duration of two weeks and consisted of two one-week stages. The second week of the combined moisture and thermal cycles was further divided into two distinct temperature stages. The environmental cycles are described below and summarized in Table 3-1.

- (a) Control conditions: prisms stored in air at 68-72 °F for the entire two-week cycle.
- (b) Varying moisture conditions: prisms submerged in either salt water or tap water at 68-72 °F for the first week and in air at 68-72 °F for the second

week. The salt water was 3.5% NaCl content by weight. Moisture variation within the concrete prisms was achieved by prisms being either submerged in water or stored in air.

- (c) Varying thermal conditions: prisms stored in air at 68-72 °F for the first week and either in an oven at 230 °F or in a freezer at -15 °F for the second week.
- (d) Varying moisture and thermal conditions: prisms submerged in either salt or tap water at 68-72 °F for the first week and either in the oven for seven days or in the oven for four days and in the freezer for three days during the second week.

*Table 3-1 Environmental Cycles for Prisms*

	<b>Concentric Sensors</b>	<b>Coplanar Sensors</b>	<b>First Week</b>	<b>Second Week</b>
<b>Control</b>	B21 B22	A21 A22	Air / 68–72°F / 7 days	Air / 68–72°F / days
<b>Varying Moisture Conditions</b>	B27 B28	A27 A28	Tap Water / 68–72°F / 7 days	Air / 68–72°F / days
	B29 B30	A29 A30	Salt Water / 68–72°F / 7 days	Air / 68–72°F / days
<b>Varying Thermal Conditions</b>	B19	-	Air / 68–72°F / days	Oven / 230 °F / 7 days
	B20	-	Air / 68–72°F / days	Freezer / -15°F / 7 days
<b>Varying Moisture and Thermal Conditions</b>	B23	A23	Salt Water / 68–72°F / 7 days	Oven / 230 °F / 4 days Freezer / -15°F / 3 days
	B24	A24	Tap Water / 68–72°F / 7 days	Oven / 230 °F / 4 days Freezer / -15°F / 3 days
	B25 B26	A25 A26	Salt Water / 68–72°F / 7 days	Oven / 230 °F / 7 days

The environmental tests began on 10 January 2005 and concluded on 12 July 2005. The sensors were interrogated at the end of each environmental cycle during the 183-day test period. Most of the sensors were interrogated once a week for a total of 28 readings. However, four of the sensors that experienced varying moisture and thermal conditions (A23, A24, B23, and B24) were interrogated three times during each two-week cycle, for a total of 38 readings.

A Solartron SI 1260 Impedance/Gain-Phase Analyzer was used to interrogate the sensors. The reader coil was 4 in. in diameter, with five turns of 18-gage copper magnet wire and was connected to the analyzer using a 3-ft cable. Furthermore, the prisms were weighed at the end of each environmental stage to evaluate changes in relative moisture content. These weights are reported in Appendix A.

### **3.3 MEASURED RESPONSE**

The measured responses of representative concentric sensors from each type of environmental cycle are discussed in Sections 3.3.1 through 3.3.4. In Section 3.3.5, the general response of the concentric sensors is compared with that of the coplanar sensors. The responses of sensors not discussed in this chapter are presented in Appendix A. Finally, Section 3.3.6 presents a statistical summary of measured response for the entire set of sensors. The coplanar sensors are not discussed in detail because their responses were considerably less reliable during subsequent testing than that of the concentric sensors. As a result, the coplanar sensor design was not included in subsequent tests.

Each figure depicting sensor response contains a contour plot and plots of resonant frequency, phase dip, and pseudo-quality factor with respect to time. All of these types of plots are discussed in detail in Chapter 2. Furthermore, in Chapter 2, a distinction was maintained between the phase dip and its amplitude.

Hereafter, for ease of expression, the term phase dip is used to refer either to the phase dip itself or the amplitude of the phase dip. It should be noted that the contour lines on the plots were not equally spaced over the interval  $80^\circ$  to  $90^\circ$ . Equally-spaced contour lines would have failed to articulate small values of phase dip. Therefore, the spacing of the contour lines was modified to display the response of the sensor clearly. For the concentric sensors, contour lines were placed at the elevations  $80^\circ$ ,  $82^\circ$ ,  $84^\circ$ ,  $86^\circ$ ,  $87^\circ$ ,  $88.1^\circ$ , and  $90^\circ$ , and for the coplanar sensors, lines were placed at the elevations  $80^\circ$ ,  $82^\circ$ ,  $84^\circ$ ,  $86^\circ$ ,  $88.3^\circ$ , and  $90^\circ$ .

### **3.3.1 Control Conditions**

Figure 3-4 shows that the response of sensor B22 remained constant throughout the testing period. The mean value of the sensing frequency was 0.46 MHz, while that of the reference frequency was 1.54 MHz, both with coefficients of variation less than 0.05%. The mean value of the sensing phase dip was  $2.4^\circ$  with a coefficient of variation of 1.3%, and the mean value of the reference phase dip was  $1.4^\circ$  with a coefficient of variation of 1.2%. Finally, the pseudo-quality factors of the sensing and reference circuits, respectively, were 7.8 and 34.4. Both factors had coefficients of variation less than 1%. All of these trends indicate that the state of the sensor did not change during the testing period, implying an intact sensing wire.

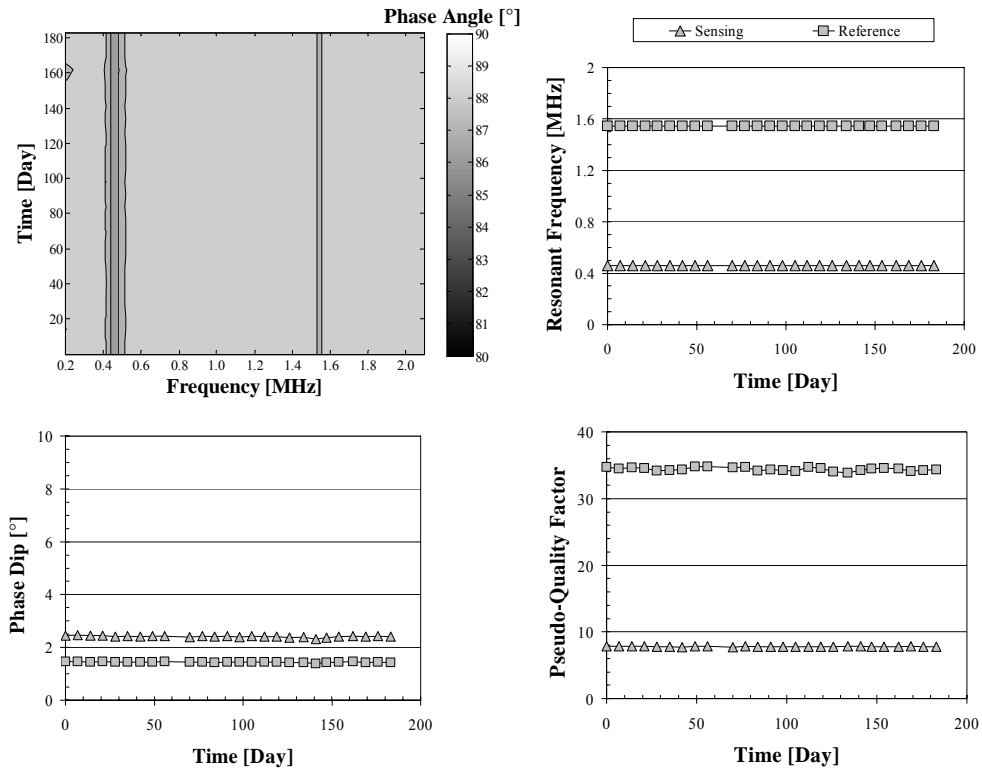


**Figure 3-4 Response of Sensor B22**

### 3.3.2 Varying Moisture Conditions

The response of sensor B27, given in Figure 3-5, had two distinct domains of response. The first domain extended from day 0 until day 105 and was comparable to the entire response of sensor B22. That is, there were negligible variations in the resonant frequencies, phase dips, and pseudo-quality factors of the sensing and reference circuits. However, after day 105, a second domain of response developed in which the resonant frequency and phase dip of the sensing circuit became undetectable, indicated on the plots as having values of zero. In addition, because the phase dip of the sensing circuit could not be detected, the

pseudo-quality factor was inferred to be zero for the sensing circuit. This condition is identical to the sensing circuit being an open circuit, having an infinite resistance. All of these indicated that the sensing wire fractured during the environmental cycle ending on day 105.

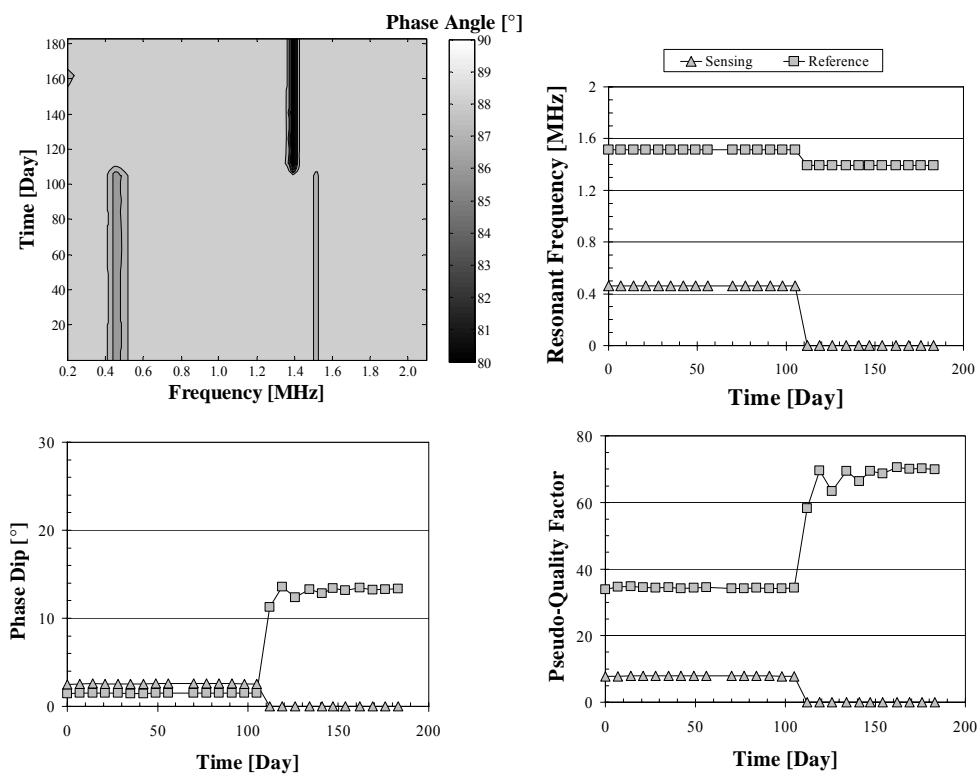


**Figure 3-5 Response of Sensor B27**

The fact that the response of the reference circuit also changed after day 105 reinforces the conclusion that the sensing wire fractured. Specifically, the reference frequency shifted from a mean value of 1.51 MHz to 1.39 MHz, but the coefficient of variation remained less than 1% before and after the shift. The phase dip and pseudo-quality factor of the reference circuit both increased significantly from respective means of 1.47 to 13.0 and 34.3 to 67.8. In both



cases after the shift, the coefficient of variation reached nearly 6.0%. This change in response of the reference circuit was due to the mutual inductance between the sensing and reference circuits. Because the inductors of the circuits are concentric, with the sensing coil surrounding the reference coil, their magnetic fields intersect such that the sensing circuit masks or suppresses the response of the reference circuit. Therefore, in the absence of the sensing circuit, the reference circuit has a larger phase dip and pseudo-quality factor.

Comparable variability in the responses of B27 in the first domain of response and B22 throughout testing establishes the independence of intact sensor response from the moisture content of the concrete. That is, because B27, while intact, exhibited no more variability in response than B22, despite changes in the moisture content of the concrete surrounding it, the response of B21 was independent of moisture content. Furthermore, the coefficient of variation of the reference frequency remained less than 1% even in the second domain, implying its independence from the moisture content of the concrete.

However, the variability of both the phase dip and pseudo-quality factor of the reference circuit increased in the second domain of the response of sensor B27. This increased variability was likely not due to a direct dependence of the phase dip and pseudo-quality factor on the moisture content of the concrete. To support this claim, both the phase dip and pseudo-quality factor were plotted with respect to the moisture content of the concrete, relative the initial weight of the prism. It should be noted that this initial weight was not the oven dry weight but simply the weight of the prism prior to its undergoing wet and dry cycles. Obtaining the oven dry weight was not possible because placing the prism in the oven would have introduced a thermal cycle into the testing regime. The plots are shown in Figure 3-6. The low  $R^2$  (Pearson product moment correlation coefficient) value in both cases indicates that there was little linear correlation

between the moisture content of the concrete and the phase dip and pseudo-quality factor of the reference circuit. Other curves applied to the data exhibited similarly poor fit, indicative of the parameters being independent.

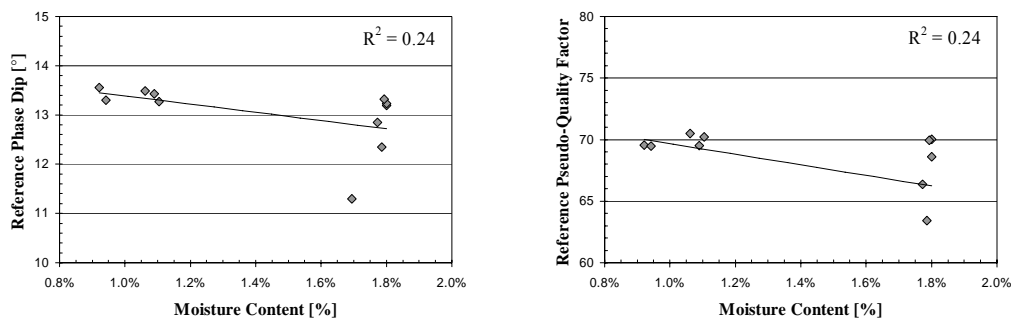


**Figure 3-6 Lack of Correlation between Moisture Content of the Concrete Prism and Phase Dip and Pseudo-Quality Factor**

Exclusion of a direct dependence of the phase dip and pseudo-quality factor on the moisture content of the concrete implies that the increased variability of those parameters has more diffuse causes. After the sensing wire fractures, the remains of the sensing circuit tend to participate in the external environment. For example, moisture may partially complete the sensing circuit, enabling the circuit to influence the reference circuit. The effect is slight, undetectable in the frequency response of the sensor, but it seems to have an effect, though indistinct, on the variability of the reference phase dip and pseudo-quality factor.

### 3.3.3 Varying Thermal Conditions

The response of sensor B19 is shown in Figure 3-7. The sensing and reference frequencies of B19 varied more than those of B22 in that their coefficients of variation were 0.6% and 0.2% respectively, but these values were low enough to establish the practical independence of the resonant frequencies from temperature. It should be noted that the resonant frequencies are not

absolutely independent of temperature. Rather, for this application, the variation in frequency was so small that it can be regarded as negligible. For an extended discussion of the effect of temperature on sensor response, see Andringa (2006).

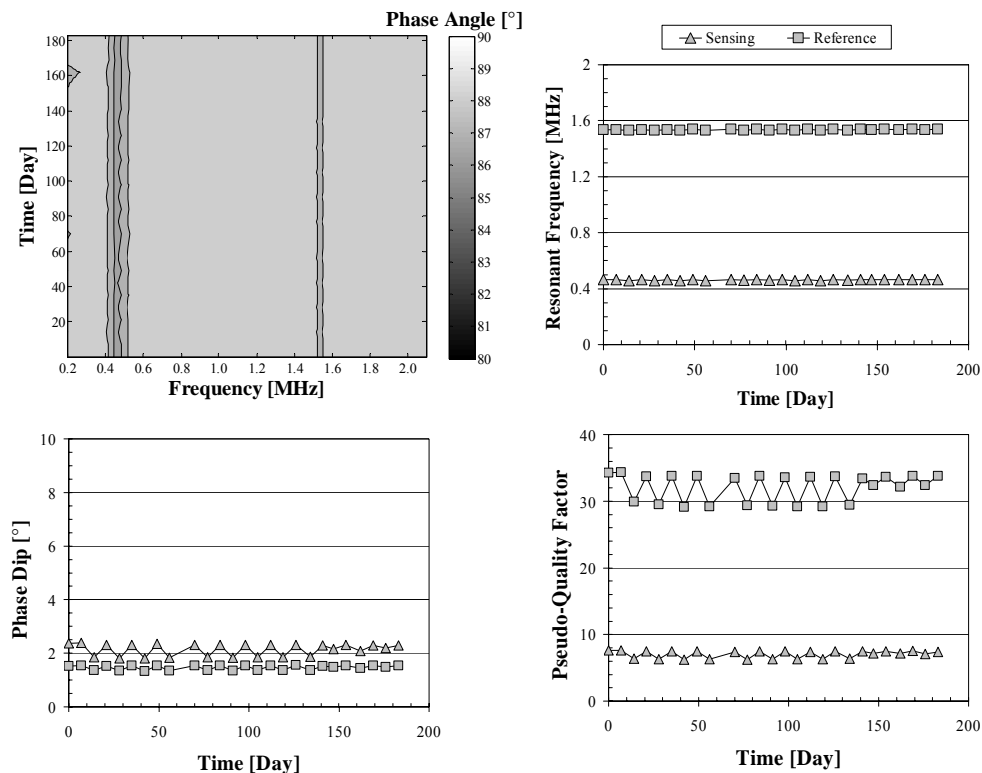


**Figure 3-7 Response of Sensor B19**

In contrast to the resonant frequencies, both the phase dips and pseudo-quality factors of the circuits exhibited a dependence on temperature. This dependence was largely due to the influence that temperature has on circuit resistance. That is, at higher temperatures, the resistance in the circuit is larger, causing a decrease in the phase dip and pseudo-quality factor of the circuit. This effect, evident in the plots of phase dip and pseudo-quality factor in Figure 3-7, resulted in much greater variability for those parameters. In the case of B19, the

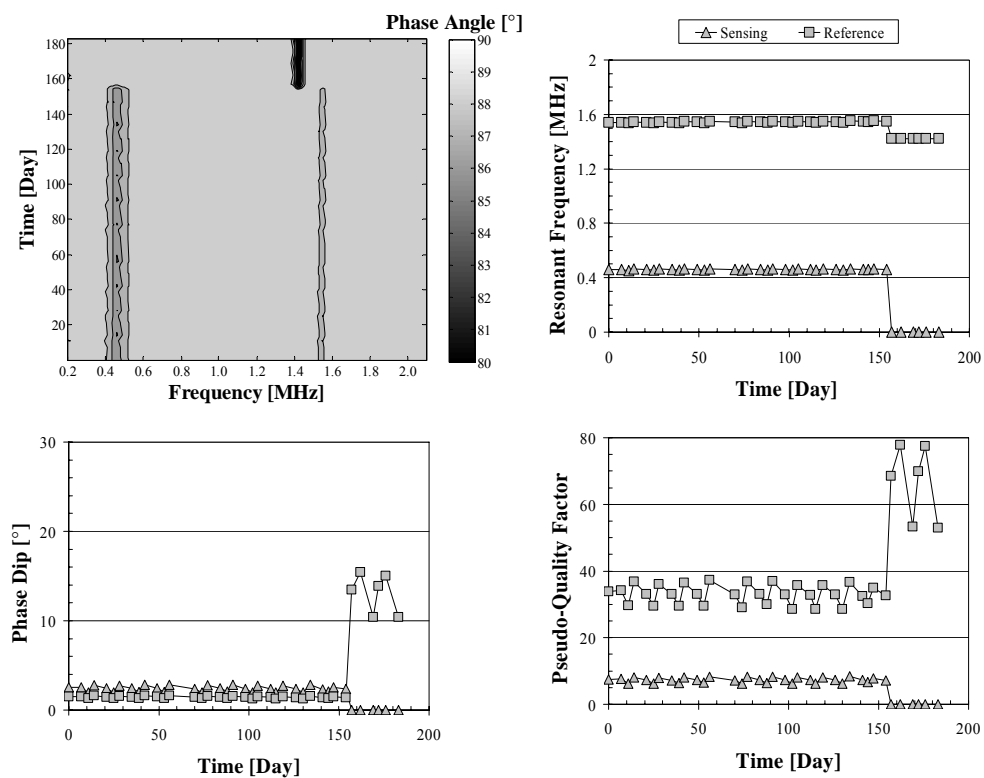
coefficients of variation of the sensing phase dip and pseudo-quality factor were 10.6% and 7.9%, respectively. It should be noted that beginning on day 147 the variability due to temperature decreases because of a change in how interrogations were conducted. In order to avoid damage to the reader coil, the prisms taken from the oven were allowed to cool for a longer period of time than was used during previous interrogations. The result was that the specimens were interrogated at lower temperatures than before, which in turn decreased the effect of temperature on the response.

Despite some dependence of response on temperature, the fact that the sensing wire remained intact throughout testing was clear from the contour plot. There was consistently a phase dip at the sensing frequency, and neither the reference frequency nor reference phase dip change in value significantly. The temperature fluctuations manifested themselves as noise in the contour plot, but that noise did not prevent, fundamentally, determination of the state of the sensing wire. In this way, the temperature dependence of the response in no way impaired the reliability of the sensor when used as a threshold corrosion sensor.

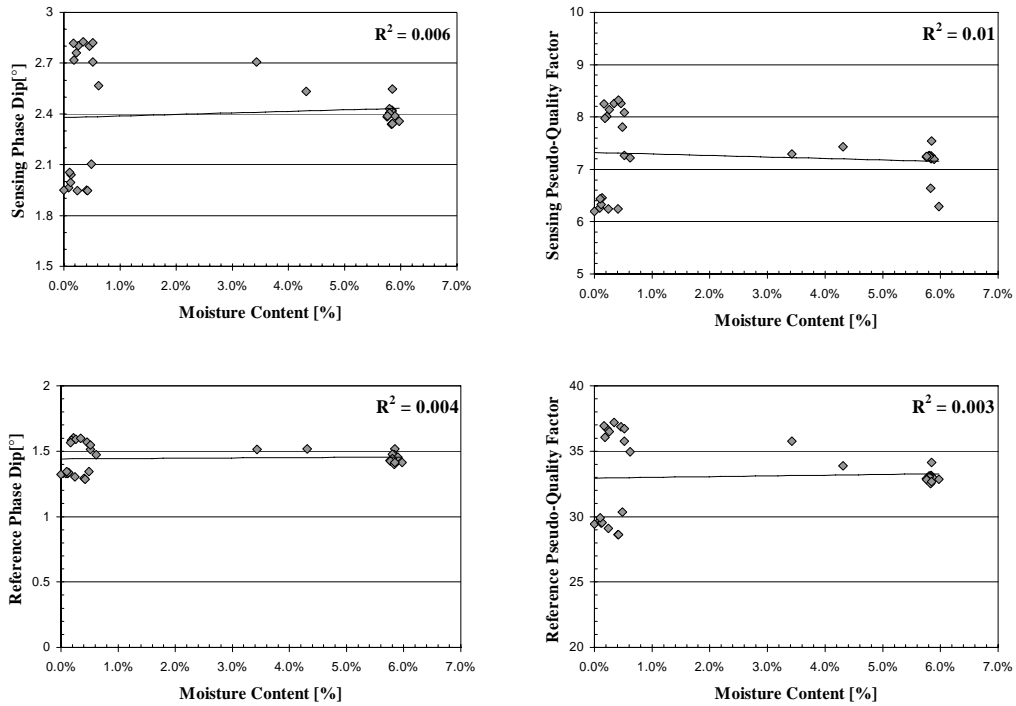
#### **3.3.4 Varying Moisture and Thermal Conditions**

Figure 3-8 presents the response of sensor B24. As in the case of B19, the response of the B24 is more variable than B22, and the variability is cyclical. With coefficients of variation less than 1%, the sensing and reference frequencies are practically independent of the environmental cycles. However, the possible causes of the variability in the phase dips and pseudo-quality factors are variation in temperature and variation in moisture content of the concrete. Figure 3-9 contains plots of the phase dips and pseudo-quality factors at the sensing and reference frequencies with respect to moisture content of the concrete, for the period in which the sensing wire was intact. In the case of B19, the moisture

content was calculated with respect to the oven-dry weight. Figure 3-9 shows that, just as with B19, there was no linear correlation between moisture content of the concrete and the phase dip and pseudo-quality factor at either the sensing or reference frequencies. A lack of correlation holds for numerous other curves that were fitted to the data.



**Figure 3-8 Response of Sensor B24**



**Figure 3-9 Lack of Correlation between Moisture Content of Concrete and Phase Dip and Pseudo-Quality Factor**

With variation in moisture excluded as a cause, variation in temperature was likely the cause of the fluctuation seen in Figure 3-8. In fact, there were distinct values of phase dip and pseudo-quality factor for each thermal cycle temperature — approximately 230 °F, 70 °F, and -15 °F — at which interrogations were taken. These distinct values are shown in Figure 3-10 for the sensing circuit of B24. Figure 3-10 is simply a detail of the phase dip and pseudo-quality factor plots shown in Figure 3-8.

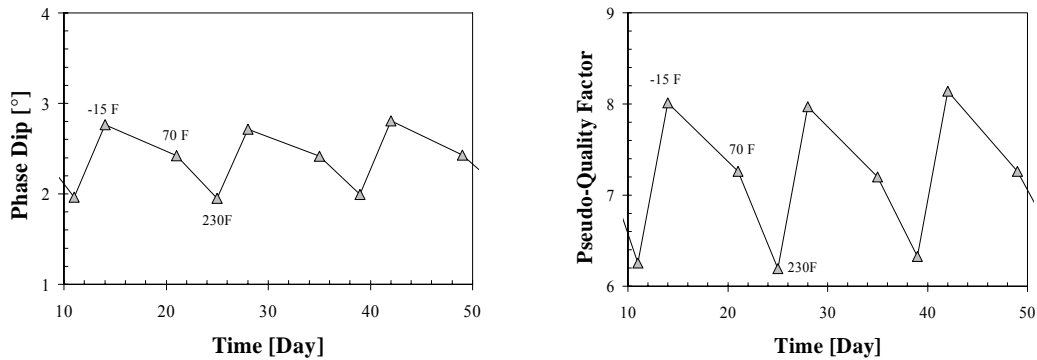


**Figure 3-10 Temperature Dependence of Phase Dip and Pseudo-Quality Factor in Sensing Circuit of B24**

It should be emphasized that, as with B19, despite fluctuations due to temperature, the B24 has two domains of response, corresponding to the sensor being intact and fractured. Therefore, at the time of autopsy, the sensing wire of B24 was expected to be fractured.

As was noted by Dickerson (2005), the only sensor to have its sensing phase dip reappear after the phase dip had disappeared was sensor B23. Otherwise, B23 behaved similarly to B24 because both were subjected to combined moisture and thermal cycles. Figure 3-11 presents measured response of B23, identified as reversal of response. From the contour plot, the sensing phase dip disappeared on day 11, reappeared on day 14, and then disappeared permanently thereafter. The sensing wires seems to have fractured due to differential thermal expansion during the oven cycle, only for the two parts of the fractured wire to come in contact during the freezer cycle, briefly completing the circuit. Fractures due to differential thermal expansion will be discussed thoroughly in the Section 3.4, but what is of interest here is that reversal in response took place at all. However, because B23 was the only instance of reversal and its reversal only lasted one cycle, its behavior does not diminish the reliability of the sensors in general.

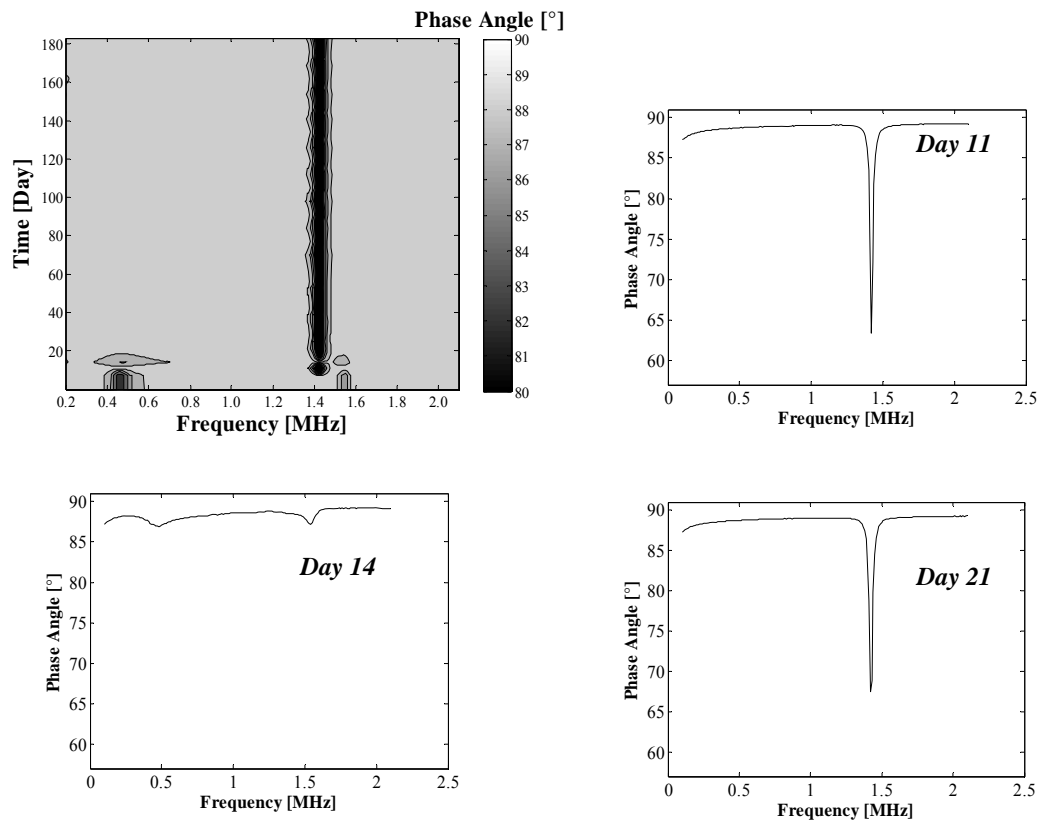


**Figure 3-11 Reversal of Sensor B23 Response**

### 3.3.5 Comparison of Response of Concentric and Coplanar Sensors

As was mentioned at the beginning of Section 3.3, the coplanar sensors proved to be less reliable than the concentric sensors in subsequent testing. Therefore, in this section, the response of the coplanar sensors is compared with that of the concentric sensors, but detailed information is not presented.

The response of the coplanar sensors during prism tests was no more variable, on the whole, than the response of the concentric sensors. However, the small phase dip of the sensing circuit –  $0.7^\circ$  on average compared to  $3.7^\circ$  for the concentric sensors – became undetectable in large-scale test specimens.



The smaller sensing phase dip of the coplanar sensors is a consequence of the geometry of the sensor itself. In Chapter 2, it was discussed that the sensing and reference circuits were placed beside one another in order to minimize their mutual inductance. Minimal mutual inductance would allow the circuits to respond independently. That is, whether or not the sensing circuit is intact, the reference circuit would have a more or less constant response. As can be seen in Figure 3-12, the design was successful in that respect. Fracture of the sensing wire had minimal effect on the response of the reference circuit, much in contrast to the behavior of the concentric sensors.

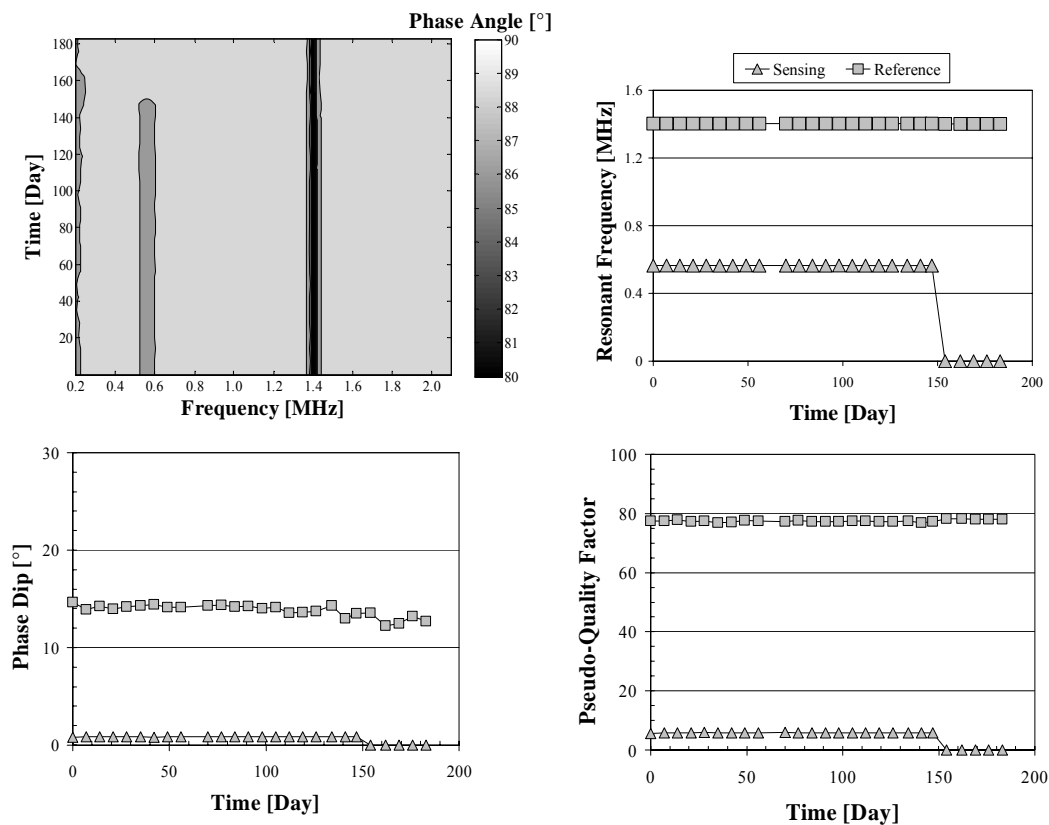


**Figure 3-12** Response of A27

Placing the two inductors beside one another had the additional effect of decreasing the phase dip at the sensing frequency. The coplanar geometry required that the diameter of the sensing inductor be less than the diameter of the sensing inductor in the concentric sensor –  $1 \frac{5}{8}$  in. compared to  $2 \frac{3}{8}$  in. The result for the coplanar sensing circuit was less overlapping area through which the magnetic field of the reader coil passes, causing a smaller phase dip.

Ironically, it is the very independence of the reference circuit from the sensing that increases the unreliability of the coplanar sensor. It was noted in Section 3.3.2 in the case of B27 that a change in response of the reference circuit signaled the fracture of the sensing wire. Thus, in the case of the concentric sensor, a fracture in the sensing wire could be detected even if the sensing circuit itself could not be detected. The independence of the coplanar reference sensor renders this approach impossible. Therefore, even intermittent inability to detect the sensing circuit of a coplanar sensor renders it inadmissibly unreliable.

### **3.3.6 Summary of Measured Response**

The response of the sensors is summarized in Table 3-2 through Table 3-5. In the tables, the resonant frequency is denoted as  $f_0$ , phase dip as  $\phi$ , pseudo-quality factor as  $\bar{Q}$ , and coefficient of variation corresponding with any given parameter as COV. Sensors for which a coefficient of variation is not listed were removed from their prisms immediately after fracture of the sensing wire was detected. Consequently, there was only one interrogation after the sensing wire fractured, rendering report of a coefficient of variation meaningless.

*Table 3-2 Statistical Summary of Sensors with Intact Sensing Wires*

Sensor	Sensing Circuit						Reference Circuit					
	$f_0$ [MHz]	COV [%]	$\phi$ [°]	COV [%]	$\bar{Q}$	COV [%]	$f_0$ [MHz]	COV [%]	$\phi$ [°]	COV [%]	$\bar{Q}$	COV [%]
<b>B19</b>	0.46	0.6	2.1	10.6	7.0	7.9	1.54	0.2	1.5	6.0	32.1	6.5
<b>B20</b>	0.46	0.4	2.8	6.6	7.9	5.3	1.55	0.2	1.4	3.4	34.8	4.5
<b>B21</b>	0.46	0.0	2.8	0.7	7.6	0.5	1.53	0.0	1.5	0.5	33.6	0.6
<b>B22</b>	0.46	0.0	2.4	1.3	7.8	0.6	1.54	0.0	1.4	1.2	34.4	0.7
<b>B28</b>	0.46	0.0	2.5	1.3	7.7	1.3	1.54	0.0	1.5	0.9	34.5	0.6
<b>A21</b>	0.57	0.1	0.8	3.0	5.4	1.6	1.41	0.0	16.9	1.8	76.3	0.2
<b>A22</b>	0.56	0.1	0.9	2.6	5.3	1.0	1.41	0.0	11.6	1.6	75.8	0.3
<b>A28</b>	0.57	0.1	0.7	3.3	5.7	1.8	1.42	0.0	13.0	4.5	75.2	0.3

**Table 3-3 Mean Resonant Frequencies of Sensors with Fractured Sensing Wires**

Sensor	Day of Fracture	Sensing Circuit		Reference Circuit			
		<i>Intact</i>		<i>Intact</i>		<i>Fractured</i>	
		$f_0$ [MHz]	COV [%]	$f_0$ [MHz]	COV [%]	$f_0$ [MHz]	COV [%]
<b>B23</b>	11	0.46	0.0	1.55	0.0	1.43	1.3
<b>B24</b>	157	0.46	0.8	1.54	0.3	1.42	0.1
<b>B25</b>	84	0.46	0.7	1.54	0.2	1.42	-*
<b>B26</b>	141	0.46	0.6	1.52	0.2	1.40	0.0
<b>B27</b>	112	0.46	0.0	1.51	0.0	1.39	0.0
<b>B29</b>	105	0.46	0.0	1.54	0.0	1.41	0.0
<b>B30</b>	84	0.46	0.1	1.54	0.0	1.41	-*
<b>A23</b>	11	0.56	0.0	1.40	0.0	1.41	0.4
<b>A24</b>	11	0.56	0.0	1.38	0.0	1.39	0.4
<b>A25</b>	28	0.56	0.6	1.41	0.1	1.41	0.1
<b>A26</b>	77	0.56	0.7	1.41	0.1	1.41	0.1
<b>A27</b>	154	0.56	0.1	1.40	0.0	1.40	0.0
<b>A29</b>	56	0.56	0.1	1.41	0.0	1.41	0.0
<b>A30</b>	77	0.56	0.1	1.41	0.0	1.40	-*

\*Testing of prism ended immediately after fracture of sensing wire detected.

**Table 3-4 Mean Phase Dips of Sensors with Fractured Sensing Wires**

<b>Sensor</b>	Day of Fracture	<b>Sensing Circuit</b>		<b>Reference Circuit</b>			
		<i>Intact</i>		<i>Intact</i>		<i>Fractured</i>	
		$\phi$ [°]	COV [%]	$\phi$ [°]	COV [%]	$\phi$ [°]	COV [%]
<b>B23</b>	11	6.1	0.1	2.9	0.3	25.8	22.9
<b>B24</b>	157	2.4	13.1	1.4	7.1	13.1	16.9
<b>B25</b>	84	5.5	13.2	3.0	5.5	24.4	-*
<b>B26</b>	141	4.6	11.3	2.4	5.0	20.7	21.2
<b>B27</b>	112	2.6	1.0	1.5	0.5	13.0	5.1
<b>B29</b>	105	5.3	1.9	2.8	0.9	21.0	8.9
<b>B30</b>	84	5.6	1.5	2.8	0.7	18.4	-*
<b>A23</b>	11	0.6	1.0	17.2	0.6	15.1	7.9
<b>A24</b>	11	0.5	1.3	10.5	1.4	9.6	8.0
<b>A25</b>	28	0.6	13.2	13.0	4.6	11.3	5.0
<b>A26</b>	77	0.6	11.6	15.7	6.0	13.7	2.8
<b>A27</b>	154	0.9	2.3	14.1	2.7	12.8	4.2
<b>A29</b>	56	0.7	2.5	14.8	1.1	13.5	0.3
<b>A30</b>	77	0.6	1.8	31.3	0.7	30.4	-*

\*Testing of prism ended immediately after fracture of sensing wire detected.

**Table 3-5 Mean Pseudo-Quality Factors of Sensors with Fractured Sensing Wires**

Sensor	Day of Fracture	Sensing Circuit		Reference Circuit			
		<i>Intact</i>		<i>Intact</i>		<i>Fractured</i>	
		$\bar{Q}$	COV [%]	$\bar{Q}$	COV [%]	$\bar{Q}$	COV [%]
<b>B23</b>	11	7.6	0.9	34.1	0.4	61.3	19.5
<b>B24</b>	157	7.2	10.0	32.9	8.7	66.7	16.8
<b>B25</b>	84	6.8	9.9	32.2	7.4	52.9	-*
<b>B26</b>	141	7.0	9.2	31.9	7.1	55.4	21.7
<b>B27</b>	112	7.9	0.9	34.3	0.6	67.8	5.6
<b>B29</b>	105	7.5	1.9	34.2	0.8	53.0	9.3
<b>B30</b>	84	7.9	1.3	34.8	0.8	46.1	-*
<b>A23</b>	11	5.4	1.6	74.4	0.1	75.7	7.5
<b>A24</b>	11	5.4	2.7	73.9	0.1	77.0	6.6
<b>A25</b>	28	5.2	9.9	74.2	3.7	74.8	2.9
<b>A26</b>	77	4.9	11.3	72.4	4.5	70.8	0.2
<b>A27</b>	154	5.8	1.2	77.3	0.3	78.1	0.1
<b>A29</b>	56	5.5	1.8	77.1	0.3	77.5	0.8
<b>A30</b>	77	4.9	1.1	71.2	0.2	76.0	-*

\*Testing of prism ended immediately after fracture of sensing wire detected.

### 3.4 RESULTS FROM AUTOPSIES OF PRISMS

At the end of six months of testing, the prisms were broken apart and the sensors examined. The results of each autopsy are summarized in Table 3-6 and Table 3-7. The condition of the prism was categorized by extent of cracking. In Table 3-6 and Table 3-7, a prism that had no visible cracking was identified as “none.” Prisms with cracks were identified according to the width of the cracks, with the crack width being identified as “small,” “medium,” and “large.” Furthermore, sensing wires were categorized as being either intact or fractured. An intact wire had no visible severing of its cross-section along its length, whereas for a fractured wire there existed at least one severed section.

**Table 3-6 Observed Condition of Concentric Sensors at Conclusion of Testing**

Environmental Conditions	Sensor	State of Wire		Day Fracture Detected	Width of Cracks
		<i>Detected</i>	<i>Observed</i>		
<i>Varying Thermal Conditions</i>	B19	Intact	Intact		Medium
	B20	Intact	Intact		None
<i>Control Conditions</i>	B21	Intact	Intact		None
	B22	Intact	Intact		None
<i>Varying Moisture and Thermal Conditions</i>	B23	Fractured	Fractured	11	Large
	B24	Fractured	Fractured	157	Medium
	B25	Fractured	Fractured	84	Medium
	B26	Fractured	Fractured	141	Medium
<i>Varying Moisture Conditions</i>	B27	Fractured	Fractured	112	Small
	B28	Intact	Intact		Small
	B29	Fractured	Fractured	105	Small
	B30	Fractured	Fractured	84	Small

**Table 3-7 Observed Condition of Coplanar Sensors at Conclusion of Testing**

Environmental Conditions	Sensor	State of Wire		Day Fracture Detected	Width of Cracks
		<i>Detected</i>	<i>Observed</i>		
<b>Control Conditions</b>	A21	Intact	Intact		None
	A22	Intact	Intact		None
<b>Varying Moisture and Thermal Conditions</b>	A23	Fractured	Fractured	11	Large
	A24	Fractured	Fractured	11	Medium
	A25	Fractured	Fractured	28	Medium
	A26	Fractured	Fractured	77	Medium
<b>Varying Moisture Conditions</b>	A27	Fractured	Fractured	154	Small
	A28	Intact	Intact		None
	A29	Fractured	Fractured	56	Small
	A30	Fractured	Fractured	77	Small

Results from the autopsies of B25, B30, A26, A29, and A30 were discussed in Dickerson (2005) and, therefore, are not repeated here. The remainder of this chapter discusses the observed conditions of the sensors that were presented in Section 3.3. In addition, the autopsy results for sensor A22 are presented in Section 3.4.6 in order to illustrate the influence of the relative position between the sensor and reader coil on the response of the sensor. Sensors discussed here collectively represent the essential features of behavior observed during the environmental tests.



### 3.4.1 Control Conditions

At the time of autopsy, the sensing wire of B22 was found to be intact and free of corrosion. Furthermore, no corrosion products were found in the concrete in the vicinity of the steel sensing wire. This result was consistent with the response of the sensor during the tests. The exhumed sensor is shown in Figure 3-13.

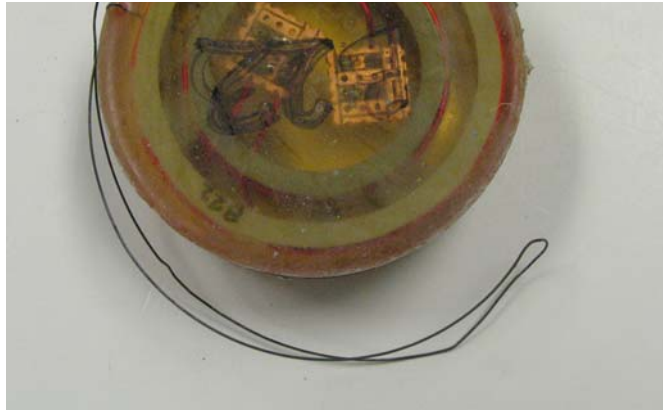


*Figure 3-13 Exhumed Sensor B22*

### 3.4.2 Varying Moisture Conditions

Photographs of sensor B27 after it was exhumed from the prism and the surrounding concrete are shown in Figure 3-14. As is evident in the photograph, the wire was highly corroded at the point where it entered the epoxy. This corrosion fractured the sensing wire, a state again consistent with the measured response of the sensor. In fact, the corrosion was extensive enough to stain the concrete adjacent to this entry point.



***Figure 3-14 Autopsy of Prism Containing B27***

The wire corroded preferentially at its entry point into the epoxy because of how the sensor was fabricated. During fabrication, the sensing wire is necessarily cold-worked at the 180° bend and at its entry point into the epoxy, making those points more vulnerable to corrosion. Over the course of the testing, most of the length of the sensing wire was likely exposed to moisture. In fact, traces of corrosion were present along the length of the wire, indicating that a small cavity had developed between the interior of the concrete prism and the sensor housing. This small cavity, a result of the epoxy housing debonding from the concrete, likely allowed moisture to travel along much the length of the wire through capillary action. Under such uniform exposure of the sensing wire to moisture, a cold-worked point corroded preferentially.

Fracture of the sensing wire in the case of B27 was somewhat unexpected because B27 was only exposed to tap water — essentially chemically neutral — in the wet cycle. The likely cause of the sensing wire of B27 fracturing was that a crack in the cover of the prism containing B27 intersected the sensing wire. In that event, neutral moisture likely functioned as a corrosive agent because the moisture had direct access to the steel wire. The pH of the moisture was too low to facilitate formation of a passive layer on the steel, and corrosion thereby

developed. In contrast, moisture that must pass through the concrete cover increases in pH as it does so, due to interaction with the pore solution. By the time the moisture reaches the steel, its pH is sufficiently high to support a passive layer. The sensing wire of B28 likely did not fracture because the cracks in the cover of the prism containing B28 likely did not intersect the sensing wire. Consequently, the pore solution supported a passive layer on the sensing wire of B28.

### **3.4.3 Varying Thermal Conditions**

Examination of the sensing wire of B19 confirmed that it was intact, at the conclusion of testing, as the response of the sensor indicated. No evidence of corrosion found on the wire or on the concrete in which the wire was embedded. There was, however, discolorization of the epoxy housing that occurred during testing, shown in Figure 3-15. This discolorization was due to the epoxy being placed in the oven at 230 °F. At such high temperatures, the marine epoxy tended to become discolored, though its structure remained intact.



***Figure 3-15 Discolorization of Sensor B19***

#### **3.4.4 Varying Moisture and Thermal Conditions**

Autopsy of the prism containing sensor B24 verified that its sensing wire had fractured due to corrosion. As shown in Figure 3-16, the sensing wire corroded to the point of fracture. The break was in the middle of the sensing wire, equidistant from the 180° bend and the point where the sensing wire enters the epoxy, even though the middle of the sensing wire had not been cold-worked during fabrication. This result was due to a crack forming near where the fracture in the wire took place. The crack allowed moisture and oxygen to penetrate to the wire directly, accelerating corrosion at that point. Penetration of carbon dioxide likely increased the acidity of moisture near the surface of the sensing wire as well. However, moisture apparently did not directly reach either the 180° bend or the point where the sensing wire enters the epoxy, since those points remained encased in concrete. Consequently, a passive layer likely remained on the surface of the sensing wire at those points. During casting, the sensing wire happened to be slightly removed from the surface of the epoxy housing. As a result, the debonding of the epoxy from the concrete likely did not directly expose the 180° bend of the sensing wire to moisture. In this case, then, proximity to a crack in the concrete cover, rather than cold-working of the wire, determined the location of the fracture. This trend held for nearly all the sensors with fractured sensing wires subjected to moisture cycles. That is, fracture of the sensing wire took place where cracks formed, but if the sensing wire was uniformly exposed to the corrosive agents due to debonding, the fracture took place where the sensing wire had been cold-worked.

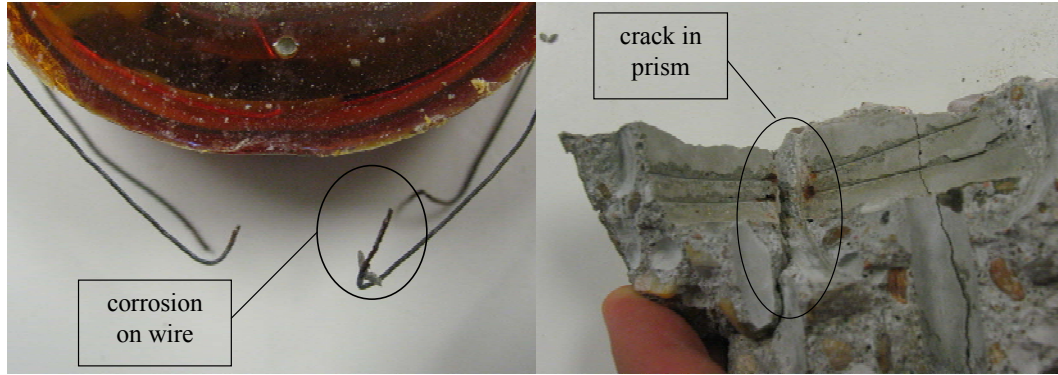


***Figure 3-16 Autopsy of Prism Containing Sensor B24***

### **3.4.5 Differential Thermal Expansion**

It was noted in Section 3.3 that the sensing wire of B23 fractured earlier than would have been expected had corrosion been the cause. Instead, the early fracture was due to differential thermal expansion between the epoxy and steel and concrete. That is, the epoxy had a much greater coefficient of thermal expansion than both the concrete and steel. Consequently, the first time the prism was placed in the oven, large cracks developed, and the steel wire, which spanned one of the cracks, fractured. Figure 3-17 shows the large-width cracks that developed in the prisms due to the thermal cycles.



***Figure 3-17 Cracks due to Differential Thermal Expansion***

Despite early fracture of the wire, the prism continued to undergo environmental cycles and interrogations in order to determine whether the sensing phase dip would reappear due to the sensing circuit being completed by moisture or some other means. As discussed in Section 3.3, the phase dip did briefly reappear. Because the prism continued to undergo testing, it was not possible to confirm the conjecture that the sensing wire was fractured due to differential thermal expansion. By the time of autopsy, there was a significant amount of corrosion on the sensing wire adjacent to where the cracks in the prism had formed and where the sensing wire enters the epoxy. This corrosion presumably took place in the weeks of testing, following the initial fracture of the sensing wire. Figure 3-18 shows corrosion on the sensor housing and concrete cover adjacent to the sensing wire.

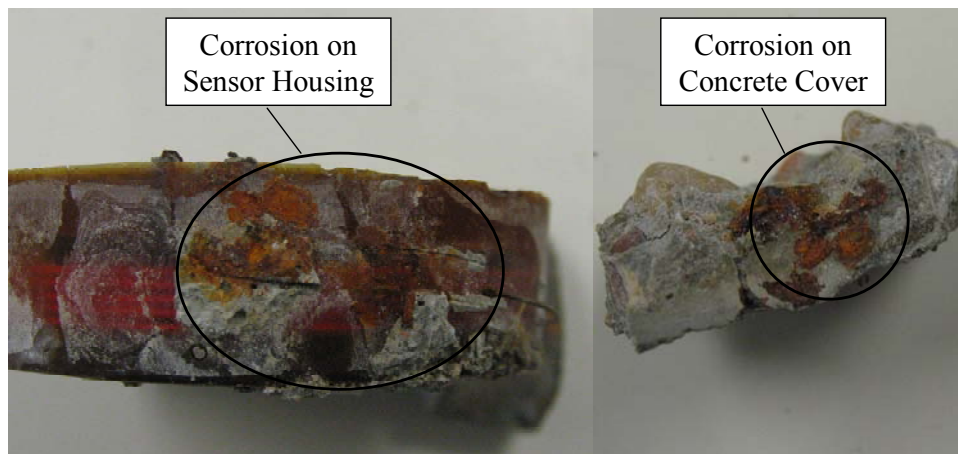


*Figure 3-18 Corrosion Products from Sensing Wire of B23*

#### **3.4.6 Sensor Rotation**

At the time of autopsy, it was found that two of the sensors — B23 and A22 — rotated in their concrete prisms during casting. Because A22 rotated more, the effect of its rotation on the measured response will be examined in this

subsection. Figure 3-19 depicts the rotation of sensor A22. From the illustration, the sensor rotated upward about its extreme corner. This rotation was due to the sensor having lower density than the fresh concrete, resulting in a net buoyant force being exerted on it. The angle of rotation, as shown, was approximately 27°.

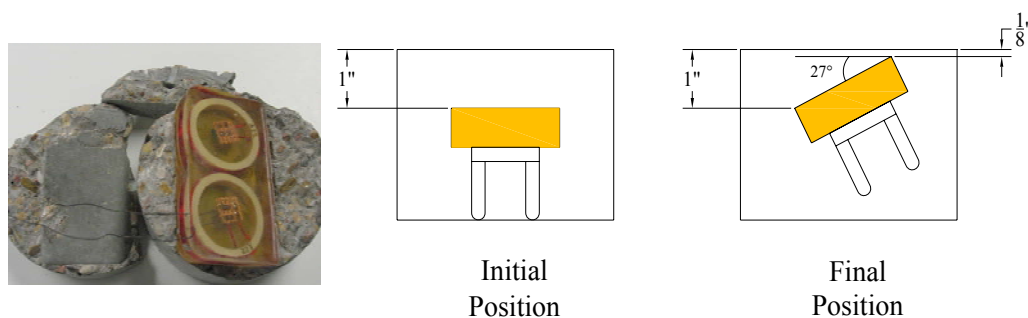


**Figure 3-19** *Rotation of Sensor A22*

As shown in Table 3-2, the rotation of A22 had a negligible effect on the response of the sensor. That is, the coefficients of variation of parameters characterizing the response of A22 were no larger than those of sensors that had not rotated. Because relative rotation of the reader coil and sensor attenuates their magnetic coupling, such a result was not expected. In this case the attenuation of the coupling due to rotation was likely offset by the sensor moving upward, decreasing read distance. The net effect of the two motions on sensor response was minimal since they more or less cancelled each other out.

### **3.5 CONCLUSIONS**

Several conclusions can be drawn from the concrete prism tests. First, the response of a given sensor can be readily be evaluated in small-scale testing. Regardless of the environmental cycle to which the sensor was subjected, it was possible to detect a phase dip at the sensing and reference frequencies and to

quantify those frequencies, phase dips, and the pseudo-quality factors of the circuits. Except for B23, the responses of the sensors were entirely consistent. That is, when the sensing phase dip disappeared for a given sensor, it did not reappear. Furthermore, the measured frequencies, phase dips, and calculated pseudo-quality factors of the circuits were independent of the moisture content in the concrete. While the frequencies were practically independent of temperature, the phase dip and pseudo-quality factors of the circuits exhibited a marked dependence on the temperature. Despite that dependence, the sensors functioned reliably as threshold sensors.

Second, the sensors accurately predicted the presence of corrosive agents when embedded in concrete, in highly variable environmental conditions. In control conditions, there were no corrosive agents, whether chlorides or chemically neutral moisture. The sensing wires remained intact, and the sensors signaled this fact. Significant amounts of chlorides and/or moisture were present in the prisms, especially along crack paths, subjected to varying moisture conditions. In all cases, other than A28 and B28, the sensing wires fractured. The response of the sensors was consistent with this result as well. In varying thermal conditions, the sensing wires remained intact, and the sensors signaled as much. This result corresponded with the physical situation because heat is not a corrosive agent, though its presence or absence can influence the rate of corrosion. Finally, excluding the sensing wires that fractured due to differential thermal expansion, the response of the sensors predicted the presence of either chlorides or moisture when varying moisture and thermal conditions were combined.

Third, detection of corrosive agents by the sensor apparently was influenced significantly by the paths of cracks in the concrete cover. If cracks intersected the sensing wire, allowing direct ingress of corrosive agents through



the concrete, sensing wire fractured readily. In contrast, if cracks failed to intersect the sensing wire, the sensing wire remained intact.

Finally, properties of the epoxy used for potting render that material unfit to serve as a sensor housing in concrete. In extreme cases, the epoxy can cause cracking of the concrete cover due to differential thermal expansion. In less extreme cases, the epoxy debonds from the concrete, leaving a cavity that can collect corrosive agents. Because the sensor does accurately signal the presence of corrosive agents in this case, this situation is not necessarily problematic for the sensor itself. However, a cavity, even a small one, collecting corrosive agents could accelerate damage to nearby steel reinforcement. Therefore, an alternative to the epoxy housing must be developed.

## **CHAPTER 4**

### **Testing of Isolated Sensors in Reinforced Concrete Slab Sections**

#### **4.1 INTRODUCTION**

Although the small-scale prism tests allowed for greater control of environmental conditions than large-scale tests, the small-scale tests could not entirely replicate service conditions within a reinforced concrete structure. Therefore, an additional set of isolated sensors was embedded in two specimens that were designed to represent sections of a reinforced concrete bridge slab. The specimens were exposed to salt water in wet and dry cycles over an 18-month period. The design of the experiment is described in Section 4.2. Section 4.3 discusses the response of the sensors during testing. Because the specimens contained steel reinforcement, it was possible to correlate the response of the sensors with the condition of the adjacent reinforcement. Section 4.4 assesses the reliability of the sensors at detecting the initiation of corrosion in the steel reinforcement and compares the signals of the sensors to conclusions drawn from the distribution of half-cell potentials in the specimens.

#### **4.2 DESIGN OF EXPERIMENT**

The design of the experiment is discussed in Dickerson (2005). Section 4.2 is a summary of that discussion, with some commentary on essential points. The slab sections were 10-ft long, 18-in. wide, and 8-in. deep. Plan views of the two specimens are shown in Figure 4-1 and Figure 4-2, while the cross-section of both specimens is given in Figure 4-3. Seventeen isolated sensors were embedded in each slab, nine of concentric geometry and eight of coplanar geometry. Sensors B01 through B09 and A01 through A08 were embedded in

Slab 1, and sensors B51 through B59 and A51 through A58 were embedded in Slab 2.

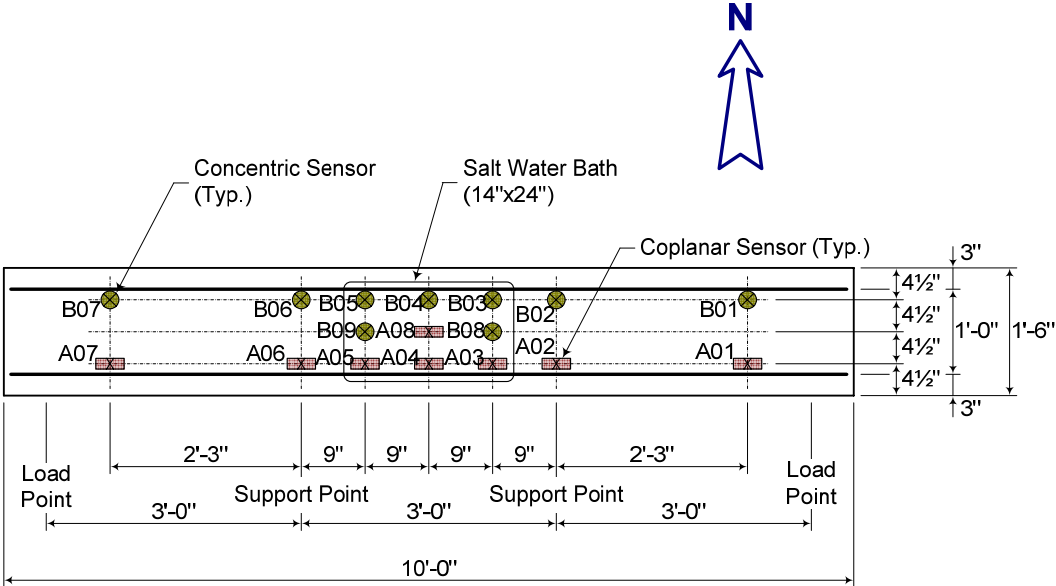


Figure 4-1 Plan View of Slab 1 (Dickerson 2005)

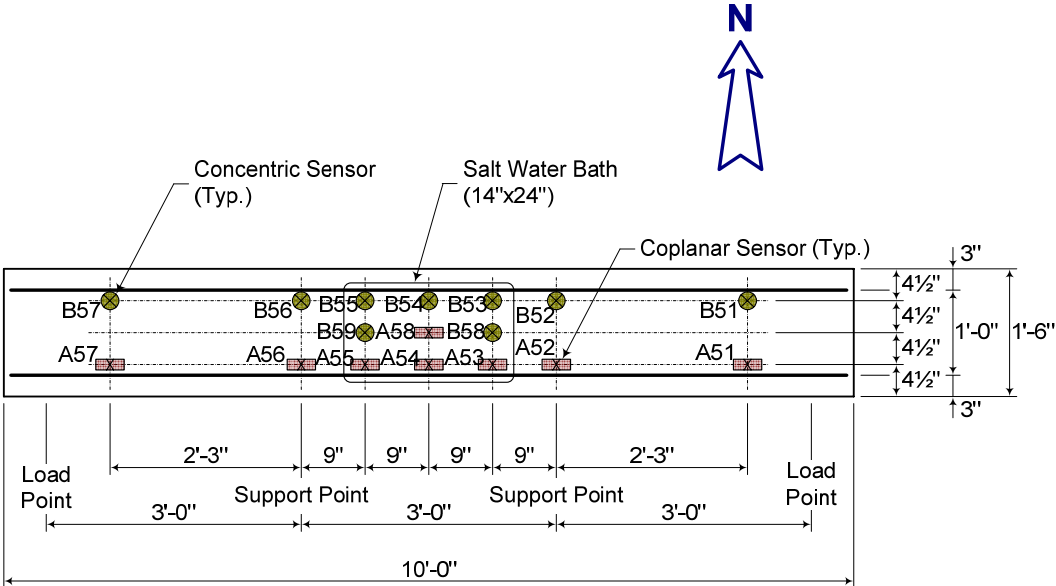
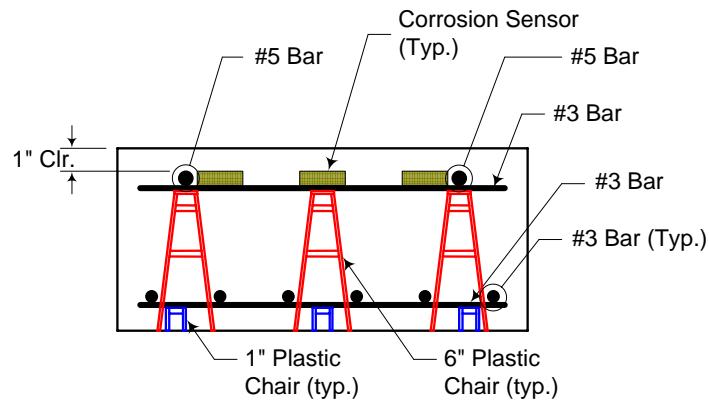


Figure 4-2 Plan View of Slab 2 (Dickerson 2005)



**Figure 4-3 Cross-Section of Concrete Slab Section (Dickerson 2005)**

The top and bottom reinforcement were electrically isolated from one another — no steel connected the two layers — in order to prevent the development of macrocell corrosion. To minimize the time to initiation of corrosion, both the sensors and top reinforcement had a nominal clear cover of 1 in. A photograph of the sensor and reinforcement is provided in Figure 4-4.



**Figure 4-4 Layout of Sensors and Steel Reinforcement**

The reinforcement layouts of the two slabs were identical; what distinguished them was the diameter of the sensing wire used. That is, the sensing

wire for Slab 1 was 26 gage, whereas that of Slab 2 was 21 gage. Chemical analysis found the 26-gage wire (0.0159-in. diameter) to be AISI-ASE 1005 and the 21-gage wire (0.0285-in. diameter) to be AISI-ASE 1006. Table 4-1 lists the nonferric chemical components of the two grades of steel by percent weight.

**Table 4-1 Chemical Composition of AISI-ASE 1005 and 1006 Steel**

<b>Chemical Element</b>	<b>1005</b>	<b>1006</b>
	[% ]	[% ]
<i>Carbon</i>	0.04	0.05
<i>Manganese</i>	0.22	0.38
<i>Phosphorus</i>	0.005	0.015
<i>Sulfur</i>	0.019	0.024
<i>Silicon</i>	<0.01	0.04
<i>Nickel</i>	0.04	0.04
<i>Chromium</i>	<0.01	0.01
<i>Molybdenum</i>	<0.01	<0.01
<i>Copper</i>	0.02	0.01

Different gages of sensing wires were used in order to optimize sensor reliability. A sensing wire with an excessively small diameter would be insufficiently durable to withstand concrete placement. In contrast, a sensing wire with too large a diameter would fracture only after nontrivial damage occurred in adjacent reinforcement. Such a large diameter wire would prevent the sensor from functioning as a threshold sensor, which is intended to signal initiation of corrosion, not extensive damage due to corrosion.

The sensors were secured with zip ties to transverse reinforcement spanning between the top two longitudinal bars. Because the sensing wires were a mild steel, they could simply be wrapped around the housing of the sensor, as

shown in Figure 4-5. In this way, the position of the sensing wire and the position of the edge of the sensor were identical.

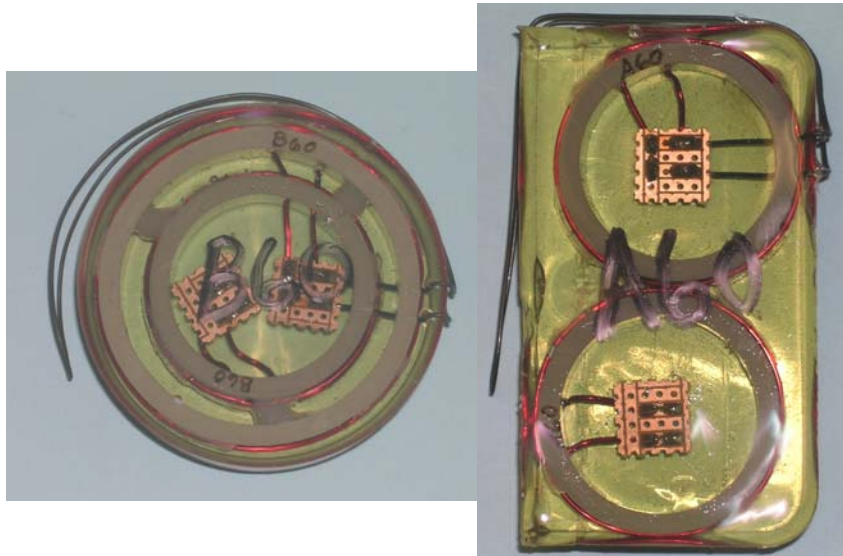


***Figure 4-5 Position of the Sensing Wire of Isolated Sensors***

The concrete was placed on 16 December 2004, and the specimens were allowed to cure for three weeks. The specimens were draped in plastic to facilitate moist curing. The slabs were then loaded at both ends with concentrated loads. Flexural cracks formed on the top surface of the specimens and were most pronounced in the constant moment region at the center of the specimens. Measured crack widths — 0.02 in. on average — were deemed sufficient to accelerate corrosion of the reinforcement. A salt-water reservoir was fixed at the middle of both slabs with an epoxy. The salt water was 3.5 % NaCl by weight. A plan view of the reservoirs is shown in Figure 4-1 and Figure 4-2. Figure 4-6 provides an elevation view of the loaded slab with the reservoir in place. Maps of cracks on the surface of Slabs 1 and 2, 24 hours after loading, are shown in Figure 4-7 and Figure 4-8, respectively.

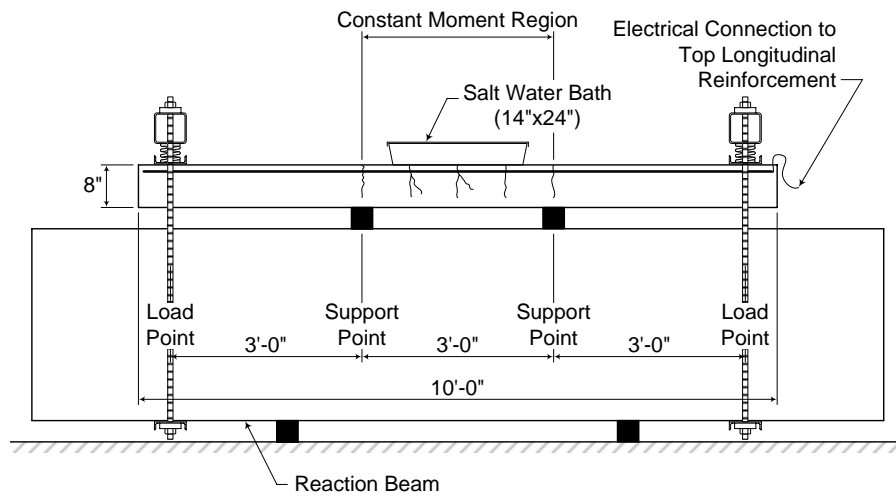


**Figure 4-6 Loaded Slab with Water Reservoir (Dickerson 2005)**

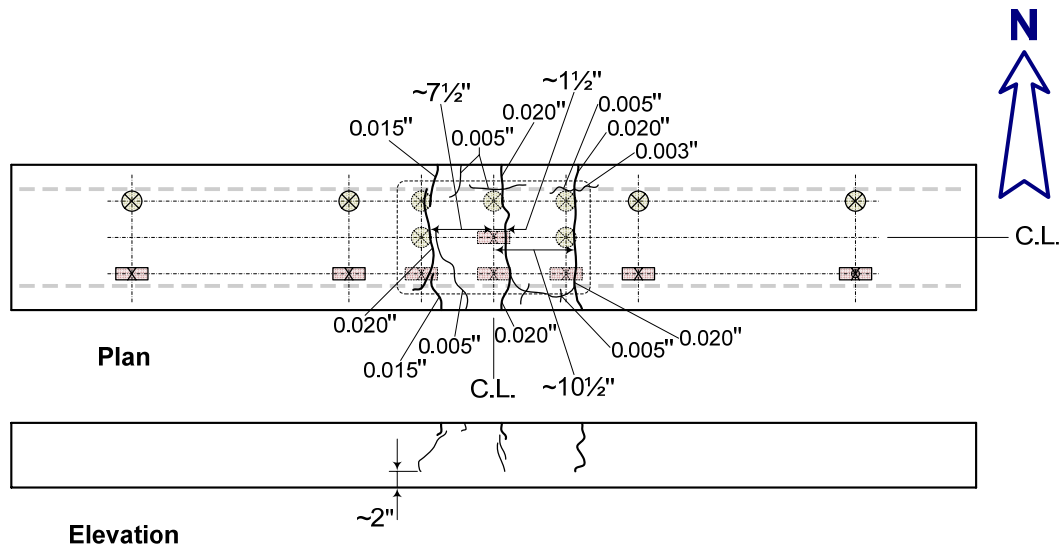


**Figure 4-7 Crack Map of Slab 1 Immediately After Loading (Dickerson 2005)**

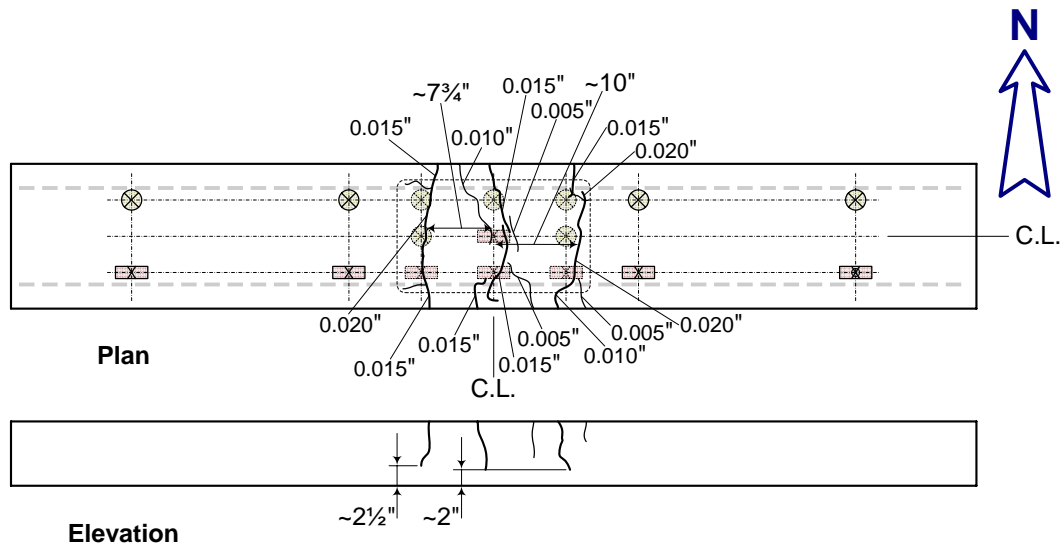


**Figure 4-8 Crack Map of Slab 2 Immediately After Loading (Dickerson 2005)**

Testing began 13 January 2005. Dickerson (2005) interrogated the sensors from the beginning of testing until 1 June 2005. The slabs were subjected to a two-week wet cycle in which the reservoir was filled with salt water, followed by a two-week dry cycle in which all moisture was removed from the reservoir. The wet and dry cycles continued throughout testing, simulating extreme service conditions for a bridge deck. The loaded slabs were stored indoors throughout the testing period to control their exposure to moisture and chlorides. The building in which they were stored was unheated such the slabs were subjected to temperature variation of approximately 50 °F.

As shown in Figure 4-1 and Figure 4-2, the sensors were distributed along the entire length of the specimens, while the salt water exposure was restricted to the midspan of the specimens. Therefore, three distinct environments were established within each specimen. They are summarized in Table 4-2.

- (a) The ends of the slabs were sufficiently removed from the salt water reservoir that the moisture levels did not vary. In addition, no



chlorides were present. Therefore, the risk of corrosion was considered to be low in this region. Four sensors in each slab were subjected to these dry conditions.

- (b) Directly below the salt-water reservoir, the concrete was subjected to regular variations in moisture and high levels of chlorides. Therefore, the risk of corrosion was considered to be high to severe in this region. Nine sensors in each slab were subjected to these conditions.
- (c) The environmental conditions in the regions of the specimens between the salt-water reservoir and the ends of the slabs were more variable than those at the ends of the slabs or below the salt-water reservoir. The moisture levels varied due to differences in the permeability of the concrete, but chloride levels were expected to be less than those below the salt-water reservoir. Therefore, the corrosion risk was assumed to be intermediate to high in these transition regions. Four sensors in each slab were subjected to these conditions.

**Table 4-2 Moisture Conditions of Sensors**

	SLAB 1		SLAB 2	
	Concentric	Coplanar	Concentric	Coplanar
<b>Ends of Slab</b> <i>(Dry Conditions)</i>	B01	A01	B51	A51
	B07	A07	B57	A57
<b>Beneath Salt-Water Reservoir</b> <i>(Controlled Moisture Conditions)</i>	B03	A03	B53	A53
	B04	A04	B54	A54
	B05	A05	B55	A55
	B08	A08	B58	A58
	B09	-	B59	-
<b>Transition Regions</b> <i>(Varying Moisture Conditions)</i>	B02	A02	B52	A52
	B06	A06	B56	A56

The sensors were interrogated at the end of each wet cycle and at the end of each dry cycle. As in the case of the prisms, the sensors were interrogated using a Solartron SI 1260 Impedance/Gain-Phase Analyzer connected to the reader coil with a 3-ft coaxial cable. The reader coil had a diameter of 4 in. and was fabricated using five turns of 18-gage copper magnet wire. In addition to interrogating the sensors, the static half-cell potential was taken in accord with ASTM C876 at the 31 locations illustrated in Figure 4-9, on the top surface of the slabs. The temperature of the air in which the specimens were stored was recorded immediately before the half-cell potentials were taken. Finally, the acid-soluble chloride concentration by weight of the concrete cover was determined at locations along the length of the slabs after approximately nine months of testing and at the conclusion of testing.

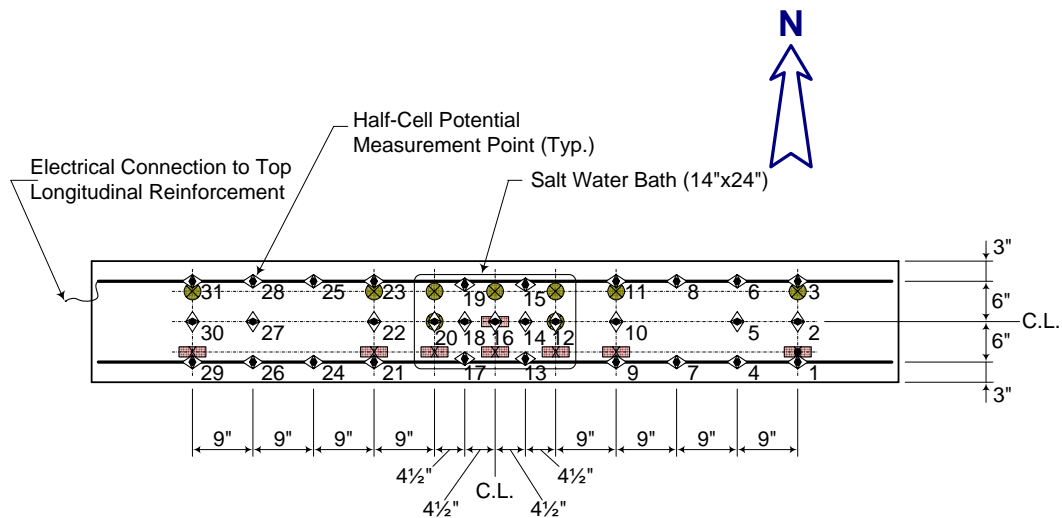


**Figure 4-9 Half-Cell Potential Points (Dickerson 2005)**

### 4.3 MEASURED RESPONSE OF SENSORS

The measured response of the sensors over 511 days of testing, approximately eighteen months, is presented in this section. Fourteen of the thirty-four sensors fractured during testing. The detected state of the sensors, whether having intact or fractured sensing wires, is presented in Section 4.3.1. In no case did the phase dip at the sensing frequency reappear once it had disappeared. That is, there were no reversals as in the case of sensor B23, which was tested in a prism and discussed in Section 3.3.4. Section 4.3.2 compares the responses of the concentric and coplanar sensors in general through a statistical summary of measured response for all sensors tested in Slabs 1 and 2. The measured responses of sensors not discussed in this chapter are presented in Appendix B. The response of sensors tested in the slabs exhibited greater variability in general than those tested in the prisms. To illustrate this fact, the response of a control concentric sensor tested in a slab is compared in Section 4.3.3 to the response of a control concentric sensor tested in a prism. Although

minor fluctuations in temperature contributed to variability in the response of the sensors, the primary cause of variability was baseline shift, discussed in Section 2.6. An additional cause of variability, attenuation of magnetic coupling between the reader coil and sensor due to displacement and rotation of the sensor during casting, is discussed in Section 4.3.4. The greater variability observed in large-scale testing did not limit the applicability of the sensors to detection of corrosion threshold, though it did complicate the extraction of quantifiable information — resonant frequency, phase dip, and pseudo-quality factor — from the sensors. Finally, the effect of differences in the diameter of the sensing wire on the response of the sensors is discussed in Section 4.3.5.

#### **4.3.1 Detected State of Sensing Wires at the Conclusion of Testing**

The concentric and coplanar sensors with sensing wires detected to be fractured at the conclusion of testing and the day of testing on which the fracture was detected are shown in Figure 4-10 and Figure 4-11. The detected state of the sensing wire was consistent in all cases with the observed state of the sensing wire, at the time of autopsy. Figure 4-12 illustrates in a plan view the sensors that were observed to have fractured sensing wires at the time of autopsy. Sensors with fractured sensing wires are colored red, while those with intact sensing wires are colored yellow.

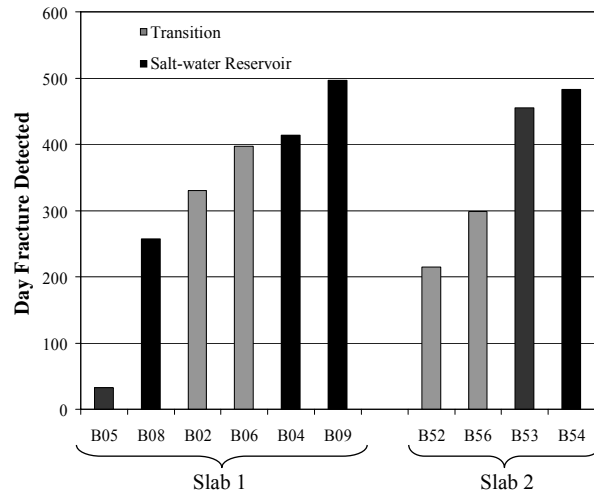


**Figure 4-10 Concentric Sensors with Fractured Sensing Wires**

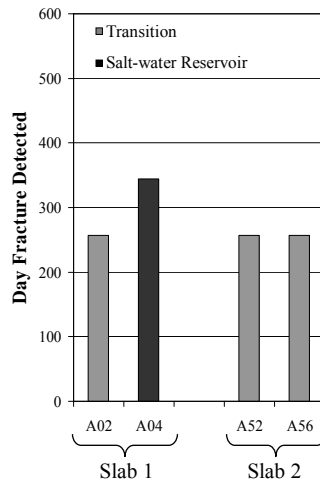


**Figure 4-11 Coplanar Sensors with Fractured Sensing Wires**

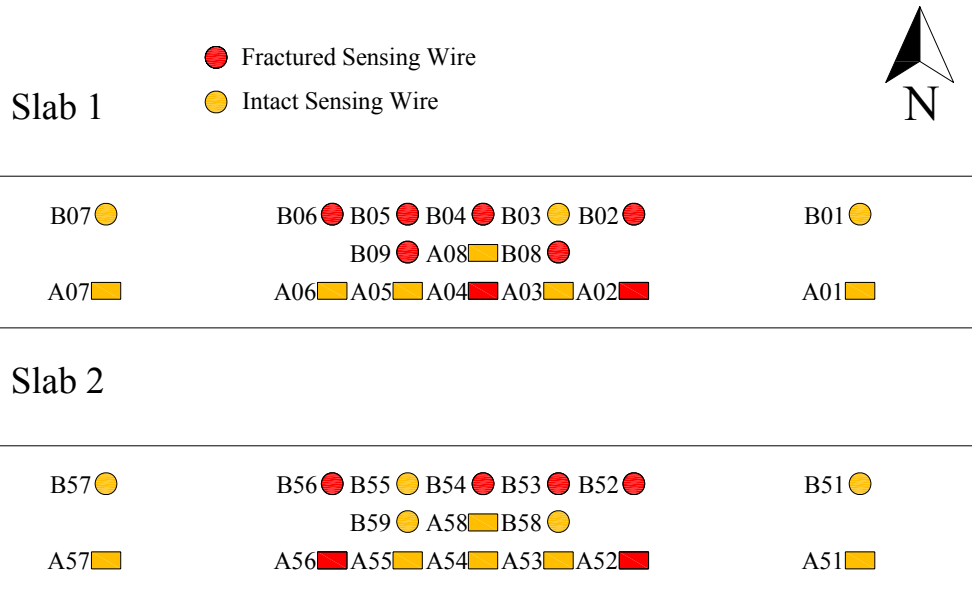


**Figure 4-12 Observed State of Sensing Wires at Autopsy**

Figure 4-10 and Figure 4-11 demonstrate that the sensing wires of sensors in the transition regions tended to corrode more readily than those beneath the salt-water reservoir. The regular exposure of the concrete beneath the reservoir to moisture caused its pore structure to become deaerated. The likely result was a slower rate of corrosion in that region relative the transition regions, which were not as deaerated. The role of deaeration in corrosion of steel is discussed in Chapter 6.

Of note in Figure 4-10 is that sensor B05 fractured after only 33 days of testing which is considered to be an insufficient amount of time for the sensing wire to have corroded. Therefore, the fracture was likely due to some other cause, such as the sensing wire being damaged during casting. Despite the fact that the sensing wire fractured prematurely, the reference circuit continued to respond at its resonant frequency, as shown in Figure 4-13. To highlight the response of

B05, the contour lines were placed at 80°, 82°, 84°, 86°, 88.1°, 88.9°, and 90°. Spurious values for the response parameters returned by the curve-fitting algorithm were not reported and were replaced with inferred values, colored white in Figure 4-13. A detailed discussion of spurious values and conventions for reporting replacement values is given in Appendix B.

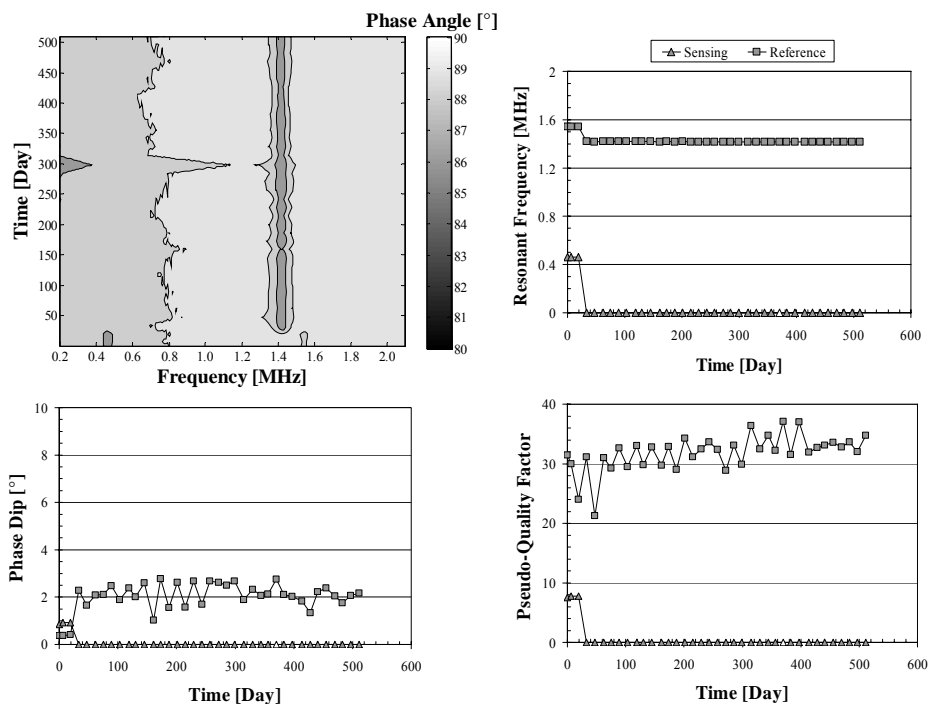


**Figure 4-13 Response of Sensor B05**

### 4.3.2 Summary of the Measured Response of Sensors

As was discussed in Section 3.3.5, the coplanar sensors signaled with less reliability than the concentric sensors. The geometry of the coplanar sensor afforded a smaller phase dip at the sensing frequency than the geometry of concentric sensor, causing the coplanar phase dip to be more difficult to detect.

Furthermore, the lack of mutual inductance between the sensing and reference circuits in the case of the coplanar sensor rendered inferences about the state of the sensing circuit from the state of the reference circuit impossible.

Table 4-3 through Table 4-6, which summarize the responses of all sensors tested in Slabs 1 and 2, show that the coplanar sensors responded with greater variability than did the concentric sensors. Results for sensor A06 could not be obtained at the sensing frequency because the sensor displaced and rotated significantly during casting, making the signal of the sensing circuit undetectable. This movement during casting of the sensors is discussed in Section 4.3.4. As was the case in Section 3.3.6, the resonant frequency in Table 4-3 through Table 4-6 is denoted as  $f_0$ , the phase dip as  $\phi$ , and the pseudo-quality factor as  $\bar{Q}$ .



*Table 4-3 Statistical Summary of Sensors with Intact Sensing Wires*

Sensor	Sensing Circuit						Reference Circuit					
	$f_0$ [MHz]	COV [%]	$\phi$ [°]	COV [%]	$\bar{Q}$	COV [%]	$f_0$ [MHz]	COV [%]	$\phi$ [°]	COV [%]	$\bar{Q}$	COV [%]
<b>B01</b>	0.46	0.1	1.5	14.6	7.1	5.1	1.54	0.1	0.8	14.8	30.4	9.8
<b>B03</b>	0.46	0.2	1.0	15.6	7.1	7.5	1.52	0.1	0.5	16.5	32.1	32.2
<b>B07</b>	0.47	0.1	1.5	9.1	6.9	2.2	1.56	0.0	0.8	7.1	28.1	3.6
<b>B51</b>	0.47	0.1	2.6	10.5	11.5	2.4	1.53	0.0	0.9	9.1	35.2	6.7
<b>B55</b>	0.48	0.1	2.8	9.9	11.1	4.3	1.54	0.1	0.8	9.3	35.3	11.8
<b>B57</b>	0.47	0.1	2.4	7.2	11.1	3.6	1.53	0.0	0.7	7.4	34.9	8.9
<b>B58</b>	0.48	0.1	3.0	13.3	11.5	4.4	1.53	0.1	0.7	7.9	34.6	10.9
<b>B59</b>	0.48	0.1	6.0	4.9	12.0	2.5	1.53	0.0	1.6	5.3	40.4	6.2
<b>A01</b>	0.56	1.9	0.2	39.0	4.3	28.4	1.43	0.0	9.8	7.1	33.8	1.3
<b>A03</b>	0.56	4.0	0.2	89.9	4.6	43.3	1.43	0.1	2.6	26.3	33.4	3.6
<b>A05</b>	0.56	1.1	0.2	25.8	5.5	17.3	1.43	0.1	2.7	20.8	35.0	2.0
<b>A06</b>	-	-	-	-	-	-	1.42	0.1	0.5	31.0	41.5	9.1
<b>A07</b>	0.57	1.2	0.1	35.7	5.8	14.7	1.43	0.0	3.1	17.8	33.9	1.5
<b>A08</b>	0.56	0.9	0.2	31.5	4.7	27.6	1.44	0.1	3.3	15.7	39.3	5.1
<b>A51</b>	0.59	4.0	0.3	28.4	8.6	8.9	1.41	0.0	2.8	19.9	34.2	4.0
<b>A53</b>	0.59	0.7	0.3	43.0	8.6	18.5	1.39	0.0	2.2	16.0	34.5	4.6
<b>A54</b>	0.59	1.0	0.3	41.1	8.0	18.3	1.42	0.0	3.4	24.3	33.2	5.0
<b>A55</b>	0.58	1.5	0.3	39.0	8.5	19.8	1.43	0.1	4.0	20.6	32.7	0.7
<b>A57</b>	0.59	0.6	0.3	23.5	8.2	18.5	1.42	0.0	4.4	8.5	32.5	2.8
<b>A58</b>	0.59	0.3	0.6	17.5	8.0	19.0	1.42	0.0	5.4	9.6	39.5	2.9

**Table 4-4 Mean Resonant Frequencies for Sensors with Fractured Sensing Wires**

Sensor	Day of Fracture	Sensing Circuit		Reference Circuit			
		<i>Intact</i>		<i>Intact</i>		<i>Fractured</i>	
		$f_0$ [MHz]	COV [%]	$f_0$ [MHz]	COV [%]	$f_0$ [MHz]	COV [%]
<b>B02</b>	330	0.46	0.2	1.51	0.1	1.39	0.0
<b>B04</b>	414	0.46	0.2	1.54	0.1	1.41	0.0
<b>B05</b>	33	0.46	0.1	1.54	0.1	1.42	0.1
<b>B06</b>	397	0.46	0.1	1.54	0.1	1.42	0.0
<b>B08</b>	257	0.46	0.1	1.55	0.1	1.43	0.1
<b>B09</b>	497	0.46	0.2	1.54	0.2	1.42	0.0
<b>B52</b>	215	0.47	0.1	1.53	0.1	1.41	0.1
<b>B53</b>	455	0.49	0.1	1.55	0.1	1.41	0.1
<b>B54</b>	483	0.47	0.1	1.52	0.1	1.39	0.2
<b>B56</b>	299	0.47	0.4	1.52	0.1	1.39	0.1
<b>A02</b>	257	0.55	2.5	1.40	0.0	1.40	0.0
<b>A04</b>	344	0.56	0.5	1.44	0.1	1.43	0.0
<b>A52</b>	257	0.59	0.3	1.39	0.0	1.39	0.0
<b>A56</b>	257	0.59	0.7	1.41	0.0	1.41	0.0

*Table 4-5 Mean Phase Dips for Sensors with Fractured Sensing Wire*

Sensor	Day of Fracture	Sensing Circuit		Reference Circuit			
		<i>Intact</i>		<i>Intact</i>		<i>Fractured</i>	
		$\phi$ [°]	COV [%]	$\phi$ [°]	COV [%]	$\phi$ [°]	COV [%]
<b>B02</b>	330	1.5	13.4	0.8	4.6	5.3	5.3
<b>B04</b>	414	0.9	18.9	0.4	18.6	2.0	10.7
<b>B05</b>	33	0.9	5.6	0.4	4.4	2.1	19.9
<b>B06</b>	397	1.1	17.7	0.6	18.7	3.2	19.0
<b>B08</b>	257	1.2	19.4	0.6	19.1	3.6	28.6
<b>B09</b>	497	0.8	27.5	0.4	31.4	2.1	6.0
<b>B52</b>	215	3.6	6.8	1.2	5.7	4.9	15.2
<b>B53</b>	455	3.2	12.3	0.8	9.9	3.9	25.4
<b>B54</b>	483	3.1	14.3	0.9	18.3	2.9	21.6
<b>B56</b>	299	2.8	22.9	1.1	13.7	6.0	10.6
<b>A02</b>	257	0.2	26.8	6.6	21.7	7.2	19.9
<b>A04</b>	344	0.2	25.0	3.0	17.7	3.3	11.5
<b>A52</b>	257	0.3	43.9	5.9	13.8	5.4	14.7
<b>A56</b>	257	0.2	29.4	6.8	8.6	6.3	10.0

**Table 4-6 Mean Pseudo-Quality Factors for Sensors with Fractured Sensing Wires**

Sensor	Day of Fracture	Sensing Circuit		Reference Circuit			
		<i>Intact</i>		<i>Intact</i>		<i>Fractured</i>	
		$\bar{Q}$	COV [%]	$\bar{Q}$	COV [%]	$\bar{Q}$	COV [%]
<b>B02</b>	330	7.0	10.0	29.2	5.4	43.8	5.7
<b>B04</b>	414	7.5	5.0	29.5	22.4	28.8	13.1
<b>B05</b>	33	7.7	1.7	28.5	13.8	32.1	8.8
<b>B06</b>	397	7.8	4.2	30.9	4.4	37.5	5.8
<b>B08</b>	257	7.4	3.7	27.7	8.3	34.5	19.4
<b>B09</b>	497	7.3	5.9	29.0	20.9	33.7	11.3
<b>B52</b>	215	11.8	1.5	36.8	4.2	30.0	15.1
<b>B53</b>	455	11.1	2.9	34.9	7.5	29.8	21.1
<b>B54</b>	483	11.5	3.4	33.2	9.3	20.1	22.0
<b>B56</b>	299	11.2	17.6	35.7	8.9	41.2	9.1
<b>A02</b>	257	5.3	16.5	46.9	1.2	48.8	2.5
<b>A04</b>	344	5.3	14.6	34.7	3.6	36.0	2.4
<b>A52</b>	257	9.4	6.5	44.5	1.2	46.4	3.6
<b>A56</b>	257	9.3	24.3	42.2	1.5	44.1	6.9

### **4.3.3 Comparison of the Variability of the Response of Sensors Tested in Slabs 1 and 2 to the Variability of the Response of Sensors Tested in Prisms**

In order to compare the variability of the response of sensors tested in the Slabs 1 and 2 to that of sensors tested in the prisms, the responses of control sensors from both types of test were compared. The measured response of sensor B01, tested at the eastern end of Slab 1, is given in Figure 4-14. In the contour plot, contour lines were placed at 80°, 82°, 84°, 86°, 87.9°, 88.7°, and 90°. The mean value of the sensing frequency was 0.46 MHz, while that of the reference frequency was 1.54 MHz. Both frequencies had a coefficient of variation of 0.1%. The phase dip of the sensing circuit had a mean value of 0.8° with a coefficient of variation of 14.8%. Similarly, the phase dip of the reference circuit had a mean value of 1.5° with a coefficient of variation of 14.6%. The pseudo-quality factor of the sensing circuit was 7.1 on average, and that of the reference circuit was a mean 30.4. The coefficient of variation of the former was 5.1% and of the latter 9.8%. Because there was not significant change in the response of the sensor, the sensing wire was concluded to be intact.

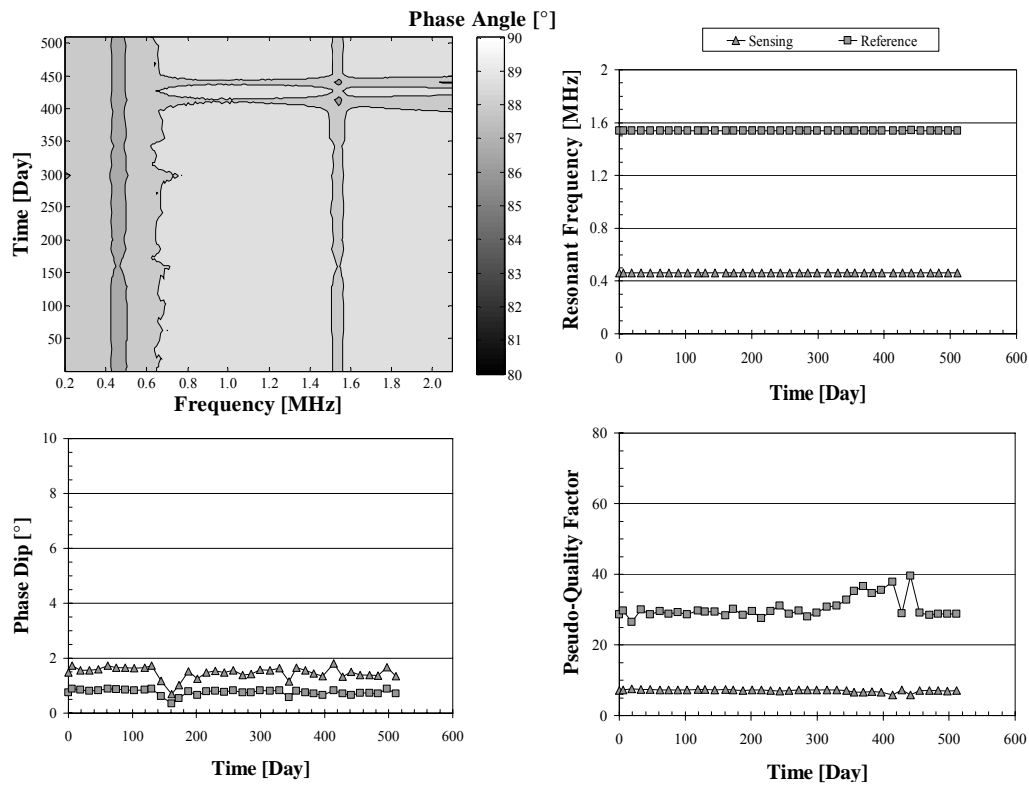


**Figure 4-14 Response of B01**

Figure 4-14 illustrates that B01 exhibited greater variability in phase dips and pseudo-quality factors than the control concentric sensors tested in the concrete prisms. For example, sensor B22, the response of which is shown in Figure 3-4, had coefficients of variation for the phase dip at the sensing frequency and reference frequency of 1.3% and 1.4% respectively. Similarly, the coefficients of variation for the pseudo-quality factors at the sensing frequency and reference frequencies were 0.6% and 0.7% respectively. For each of these parameters, therefore, the control sensor embedded in the slab exhibited variability an order of magnitude greater than the control sensors embedded in the prisms.

The trends observed in this comparison of control sensors held generally. That is, the sensors tested in the slabs exhibited greater variability in their phase dips and pseudo-quality factors than did the sensors tested in the prisms. There are two possible causes of the greater variability observed in the large-scale testing. The first of these, baseline shift, was discussed in Section 2.6. Figure 4-15, the response of sensor B59 in the plane of phase angle and frequency, is an example of the significant baseline shift that was observed in the response of sensors tested in Slabs 1 and 2. The second possible cause, attenuation of the magnetic coupling between the reader coil and sensor due to displacement and rotation of the sensor relative the reader coil, is discussed in Section 4.3.4.

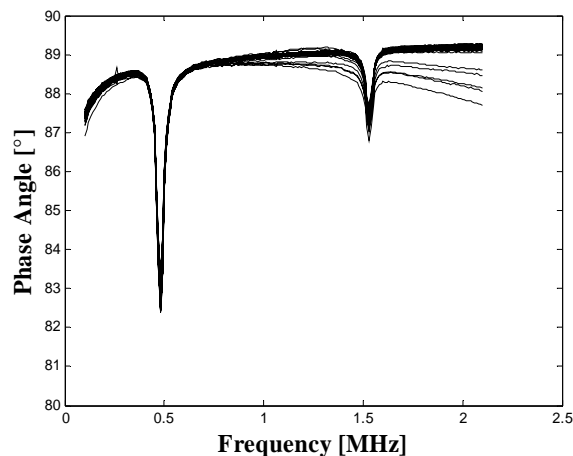


*Figure 4-15 Baseline Shift in Sensor B59*

#### **4.3.4 Effect of Displacement and Rotation of Sensors on the Variability of the Response of the Sensors**

When the Slabs 1 and 2 were autopsied, most of the sensors were observed to have displaced from their design positions during casting. The design positions of the sensors are given in Figure 4-1 and Figure 4-2. In addition, some of the sensors rotated relative the surface of the slabs during casting. Finally, the

measured concrete cover varied significantly from the design value of 1 in. This movement was possible because the top layer of reinforcement was supported on stacks of plastic rebar chairs, and these plastic chairs shifted during placement of the concrete.

Over the course of testing, the sensors were assumed to be in their design positions for the purposes of interrogation, such that the reader coil was placed on the surface of the slab at the design position. Therefore, displacement of the sensor from its design position resulted in the centroid of the sensor being displaced from the center of the reader coil. Furthermore, rotation of the sensor relative the surface of the slab was equivalent to rotation of the sensor relative the reader coil. Lastly, the read distance varied from one sensor to another because of differences in the clear cover of the concrete. All of these parameters — displacement of the centroid of the sensor from the center of the reader coil, angle of sensor relative reader coil, and read distance, shown respectively as  $a$ ,  $b$ , and  $c$  in Figure 4-16 — theoretically affect the magnetic coupling between the sensor and reader coil. Specifically, as  $a$ ,  $b$ , and  $c$  increase, the quality of the magnetic coupling between the reader coil and sensors decreases. Or, an increase in  $a$ ,  $b$ , and  $c$  attenuates the magnetic coupling between the reader coil and sensor. For a theoretical treatment of the relationship between the response of a sensor and its position relative to the reader coil, see Andringa (2006). The objective here is to determine empirically the effect of position of the sensor relative the reader coil on variability of the response of the sensor.



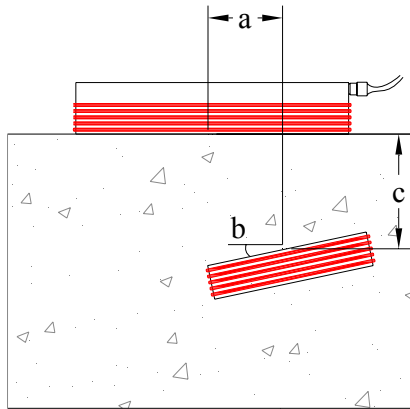


***Figure 4-16 Parameters Defining the Position of a Sensor Relative the Reader Coil***

The displacement of a given sensor from its design position, its rotation relative the surface of the slab, and its clear concrete cover are provided for each sensor in Slabs 1 and 2 in Table 4-7 and Table 4-8, respectively, and illustrated in Figure 4-17. The sensors that rotated are colored green in Figure 4-17 and their angle of rotation is recorded on the sensor itself.

**Table 4-7 Displacement, Rotation, and Cover of  
Sensors Embedded in Slab 1**

<b>Sensor</b>	<b>Displacement from Design Position [in.]</b>	<b>Rotation Relative to Surface of Slab [°]</b>	<b>Measured Clear Concrete Cover [in.]</b>
<b>B01</b>	1.5	0	1.1
<b>B02</b>	0.6	32	1.2
<b>B03</b>	1.1	0	1.3
<b>B04</b>	1.3	4	1.3
<b>B05</b>	1.1	0	1.3
<b>B06</b>	1.0	0	1.3
<b>B07</b>	1.4	0	1.1
<b>B08</b>	1.1	8	1.1
<b>B09</b>	1.4	0	1.3
<b>A01</b>	1.5	15	0.9
<b>A02</b>	1.3	0	0.9
<b>A03</b>	1.5	0	1.0
<b>A04</b>	1.1	5	1.2
<b>A05</b>	1.3	4	1.2
<b>A06</b>	1.6	22	1.3
<b>A07</b>	1.3	0	1.3
<b>A08</b>	1.1	0	1.5

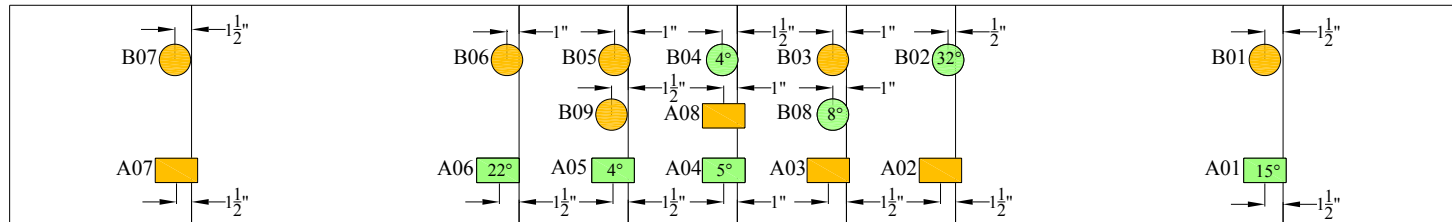
**Table 4-8 Displacement, Rotation, and Cover of  
Sensors Embedded in Slab 2**

<b>Sensor</b>	<b>Displacement from Design Position [in.]</b>	<b>Rotation Relative to Surface of Slab [°]</b>	<b>Measured Clear Concrete Cover [in.]</b>
<b>B51</b>	1.0	0	1.3
<b>B52</b>	0.9	0	1.1
<b>B53</b>	0.6	14	1.3
<b>B54</b>	0.6	0	0.9
<b>B55</b>	0.8	0	1.2
<b>B56</b>	0.8	0	1.0
<b>B57</b>	0.8	7	1.3
<b>B58</b>	0.6	18	1.1
<b>B59</b>	0.3	9	0.7
<b>A51</b>	1.3	0	1.1
<b>A52</b>	1.1	0	1.0
<b>A53</b>	1.1	0	1.3
<b>A54</b>	0.8	0	1.0
<b>A55</b>	0.9	0	1.2
<b>A56</b>	1.0	7	1.1
<b>A57</b>	1.1	0	1.3
<b>A58</b>	0.6	0	1.1



● Sensor Rotated and Displaced  
● Sensor Displaced

## Slab 1



## Slab 2

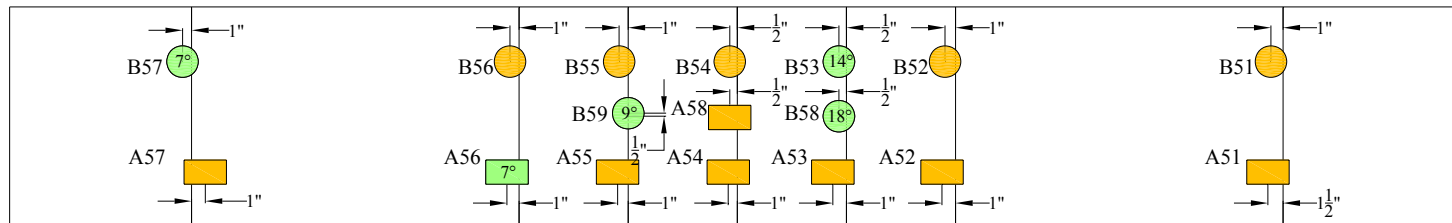


**Figure 4-17 Displacement from Design Position and Rotation Relative Slab Surface of Sensors Embedded in Slabs 1 and 2**

The effect of sensor displacement, rotation, and concrete cover on the variability of sensor response was characterized by plotting the coefficients of variation of the parameters of sensor response — resonant frequency, phase dip, and pseudo-quality factor — with respect to displacement, rotation, and concrete cover. As will be discussed in Section 4.3.5, the gage of the sensing wire influences the variability of sensor response. Therefore, because Slabs 1 and 2 contain sensors with sensing wires of different gages, a set of the above plots was developed for each slab. That is, the coefficients of variation of the resonant frequency, phase dip, and pseudo-quality factor of sensing circuits in Slab 1 were plotted with respect to displacement, rotation, and cover of the sensors. Because the variability of the sensors also depended on their geometry, the plots for Slab 1 were distinguished by coplanar and concentric geometry. The same was done for the coefficients of variation of response parameters of the reference circuits in Slab 1. Finally, this entire process was repeated for Slab 2.

As is shown in Figure 4-18 and Figure 4-19, the variability of the coplanar sensors with small-gage (26-gage) sensing wire exhibited a dependence on both the displacement and rotation of the sensor. However, the dependence of the variability of the coplanar reference circuits on rotation was weak. The plot with respect to cover was not included because no dependence existed. Incidentally, there is one fewer data point in the plot with respect rotation for the sensing circuit because response parameters could not be calculated for sensor A06, which was one of the sensors that rotated. No dependence of variability on displacement, rotation, or cover was observed in any of the other cases of sensors. That is, in no case did the variability of the concentric sensors depend on changes in their position relative the reader coil. The variability of coplanar sensors with large-gage (21-gage) sensing wires exhibited no dependence as well. For example, the lack of correlation between variability of the response of the

concentric sensors tested in Slab 1 on position is shown in Figure 4-20 and Figure 4-21. As was mentioned above, sensors with large-gage sensing wires exhibited less variability than those with small-gage sensing wires. This greater intrinsic variability of coplanar sensors with small-gage sensing wires most likely made the sensors more sensitive to displacement and rotation.

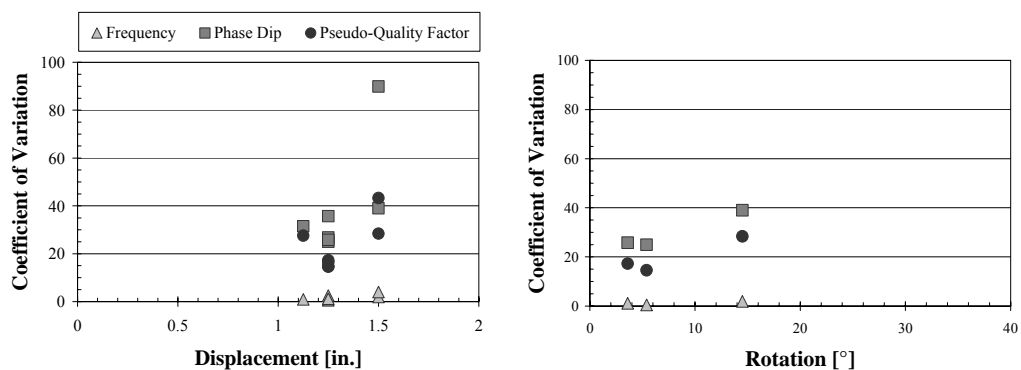


**Figure 4-18** *Coefficients of Variation of Response Parameters of Coplanar Sensing Circuits Embedded in Slab 1 with Respect to Displacement and Rotation*

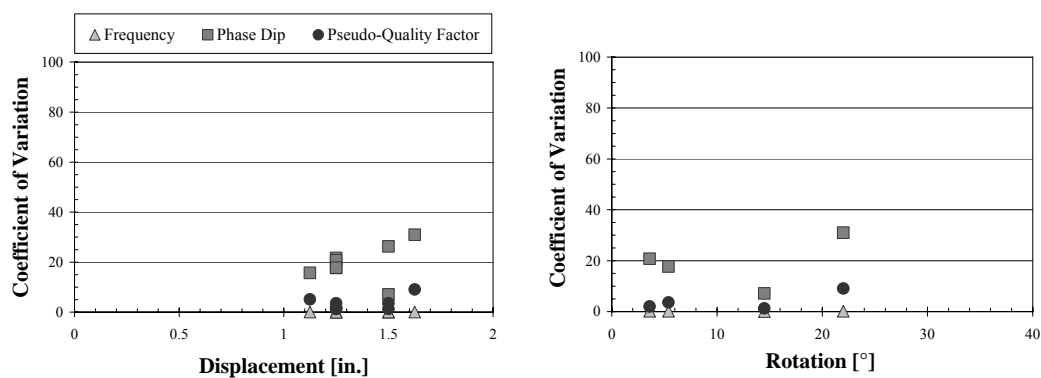


**Figure 4-19** *Coefficients of Variation of Response Parameters of Coplanar Reference Circuits Embedded in Slab 1 with Respect to Displacement and Rotation*

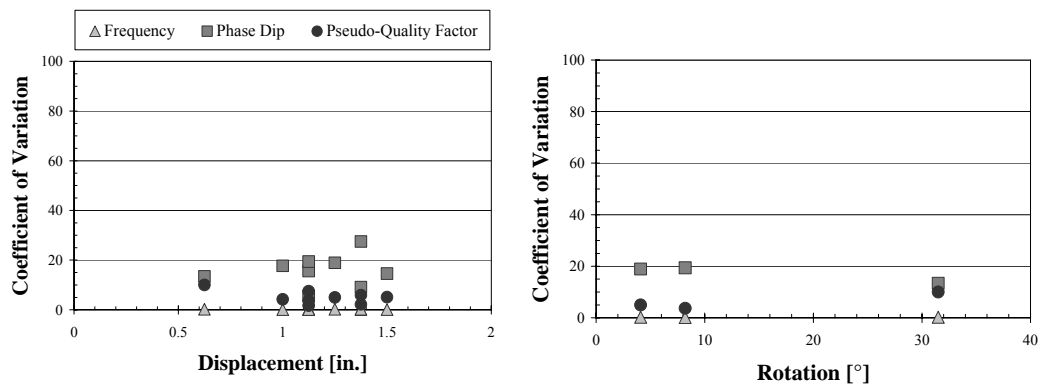


**Figure 4-20** *Coefficients of Variation of Response Parameters of Concentric Sensing Circuits Embedded in Slab 1 with Respect to Displacement and Rotation*

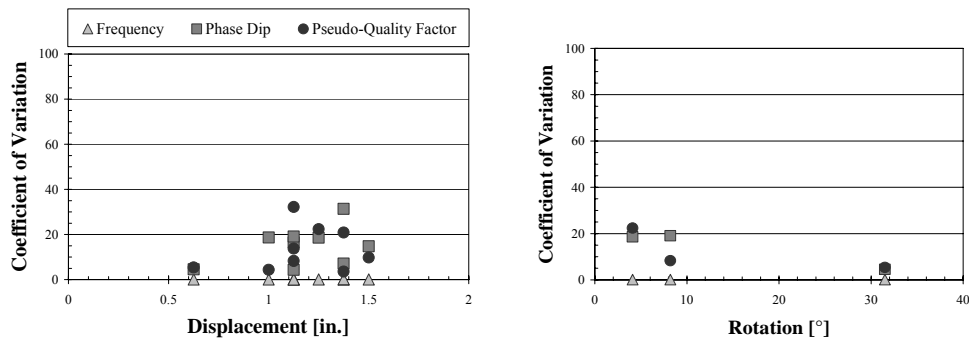


**Figure 4-21** *Coefficients of Variation of Response Parameters of Concentric Reference Circuits Embedded in Slab 1 with Respect to Displacement and Rotation*

The conclusion that can be drawn from this discussion is that in all cases, except coplanar sensors with small-gage sensing wires, the variability of the response of the sensor is independent of slight changes in position relative the reader coil. It must be emphasized that the magnitudes of the displacements, rotations, and changes in read distance considered here were relatively small. That is, there are physical limits to the displacement, rotation, and changes in read

distance that a sensor can be subjected while remaining detectable by the reader coil. However, for the relatively small displacements, rotations, and changes in read distance that a sensor might be subjected to during casting, the concentric sensors and coplanar sensors with large-gage sensing wires can be interrogated without an increase in variability of sensor response.

**4.3.5 Effect of Gage of Sensing Wire on Variability of Sensor Response**

As was noted in Section 4.2, two gages of wire were tested in Slabs 1 and 2 in order to optimize detection of corrosion threshold. Sensor B01, the response of which was discussed in Section 4.3.3, had a 26-gage sensing wire. By way of comparison, the response of sensor B57, which had a 21-gage sensing wire, is given in Figure 4-22. The contour lines in the plot of B57 were placed at the same values of phase angle as for B01.

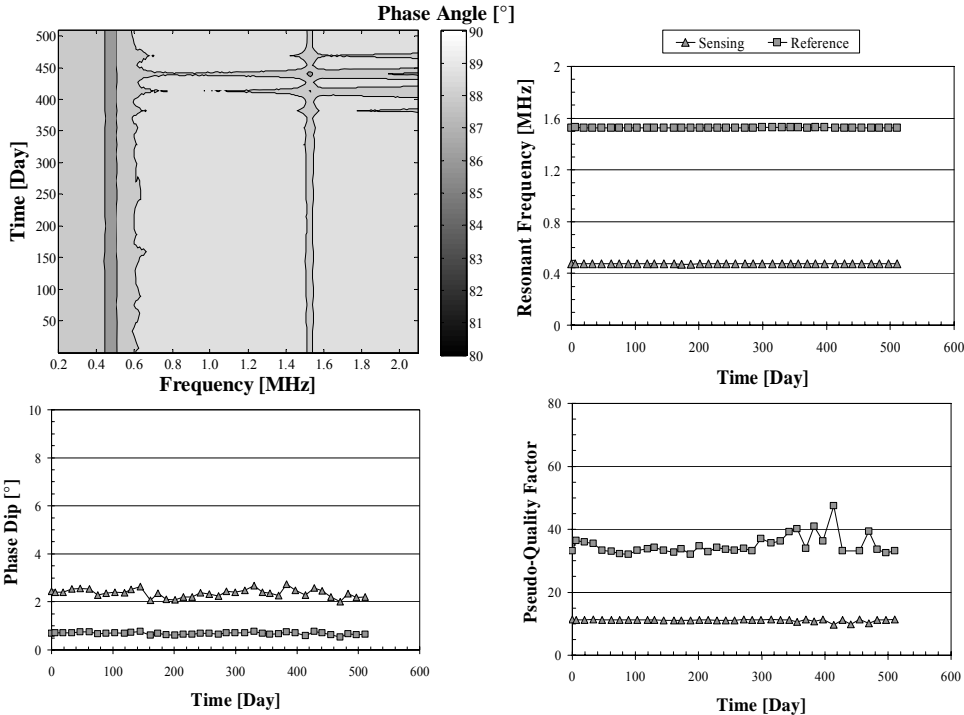


*Figure 4-22 Response of B57*



The most significant effect that the larger gage of sensing wire had on sensor response was an increase in the phase dip at the sensing frequency. B01 had a mean phase dip of  $1.5^\circ$  with a coefficient of variation of 14.6%. In contrast, B57 had a significantly larger mean phase dip of  $2.4^\circ$  with a lower coefficient of variation of 7.2%. Due to the larger gage of its sensing wire, the sensing circuit of B57 had less internal resistance than B01. Because the phase dip is inversely proportional to the resistance of the circuit, B57 had a larger phase dip. This larger phase dip contributed to a lower coefficient of variation because the curve-fitting algorithm more accurately determined large values of phase dip. The lower resistance of the sensing circuit of B57 also caused its mean pseudo-quality factor to be larger, 11.1 compared to 7.1 for B01. The variabilities of the pseudo-quality factors were comparable: 3.6% for B57 compared to 5.1% for B01.

The greater variability observed in the response of the sensor with small-gage sensing wire renders the signal of the sensor less reliable. In addition to contributing uncertainty to determination of the phase dip at the sensing frequency, the smaller phase dip causes the contour plot of the sensor to be less distinct, as is evident in a comparison of Figure 4-14 and Figure 4-22. Because the contour plot characterizes corrosion initiation, the small gage of the sensing wire mitigates the reliability of its signal even for threshold detection. Therefore, from the standpoint of signal detection, a larger gage of sensing wire increases the reliability of the sensor signal.

#### **4.4 COMPARISON OF SENSOR RESPONSE WITH OTHER INDICATORS OF CORROSION**

At the conclusion of testing, the slabs were autopsied and the state of the sensing wires of the sensors documented. Furthermore, the extent of corrosion on steel reinforcement adjacent to each sensor was recorded. In all cases, the

observed state of the sensing wire — whether intact or fractured — corresponded with the detected state during testing. In that respect, the sensors were reliable: in every case their signal corresponded with the physical state of the sensing wire. Of additional importance, however, is whether the sensors were reliable in detecting the initiation of corrosion on adjacent steel reinforcement. Such reliability was established by visual inspection of the steel reinforcement at the time of autopsy. If the sensors were reliable, the signals of the sensor would correspond with the condition of the adjacent steel reinforcement. Section 4.4.1 compares the signals of the sensors and the condition of adjacent reinforcement.

The signals of the sensors were also compared with the half-cell potentials of the specimens and the chloride concentration of the concrete cover, two measurements commonly taken to ascertain whether corrosion has initiated in a reinforced concrete structure. Section 4.4.2 addresses whether the signals of the sensors were consistent with the conclusions drawn from the half-cell potential measurements. Agreement between conclusions drawn from chloride concentrations of the specimens and the signals of the sensors is examined in Section 4.4.3.

An obstacle to reliable functioning of the isolated sensors was the formation of cracks in the concrete cover of the specimens, as discussed in Section 4.4.4. Section 4.4.5 describes how the shape of the epoxy housing accelerated corrosion of the transverse reinforcement in the specimens.

#### **4.4.1 Observed Condition of Reinforcement**

At the conclusion of testing, Slabs 1 and 2 were autopsied and the extent of corrosion on reinforcement near the sensors was documented. Figure 4-23 illustrates the extent of corrosion on the reinforcement near the sensors, with the design position of the sensors superimposed over a plan view of the specimens.

Corrosion on the reinforcement is depicted on the surface of the steel in orange, though corrosion on steel below the salt-water reservoir tended to be darker in color due to deaeration of the concrete. Sensors with fractured sensing wires at the conclusion of testing are labeled with red text, whereas those with intact sensing wires are labeled in black text.



**Figure 4-23** *Extent of Corrosion on Reinforcement Adjacent to Sensors*

As is evident from Figure 4-23, the concentric sensors were more reliable at detecting the initiation of corrosion on nearby reinforcement than were the coplanar sensors. Therefore, the reliability of the sensors was first assessed by geometry of the sensor. The two categories of erroneous signals that the sensors can send are the false negative and the false positive. In the former, the sensor fails to signal corrosion initiation when in fact corrosion has initiated in the structure. In the case of the latter, the sensors signal that corrosion has initiated when it, in fact, has not. The two other cases — signaling corrosion initiation when corrosion has initiated and not signaling corrosion initiation when it has not initiated — constitute reliable signaling. The instances of erroneous and reliable signaling for the concentric and coplanar sensors in Slabs 1 and 2 are shown in Table 4-9 and Table 4-10, respectively. From Table 4-9 and 4-10, it is evident that the concentric sensors functioned with greater reliability than the coplanar, yet another indication that the concentric design is superior.

***Table 4-9 Distribution of Signals of Concentric Sensors by Category***

		Observed State of Reinforcement	
		No Corrosion	Corrosion
Detected State of Reinforcement	Corrosion	0 (False Positive)	9
	No Corrosion	4	4 (False Negative)

**Table 4-10 Distribution of Signals of Coplanar Sensors by Category**

		Observed State of Reinforcement	
		No Corrosion	Corrosion
Detected State of Reinforcement	Corrosion	0 (False Positive)	4
	No Corrosion	4	8 (False Negative)

Another point of distinction for assessing the reliability of the sensors was the gage of their sensing wires. Because the concentric sensors functioned with greater reliability overall and will likely be used in future research, concentric sensors with sensing wires of different gages were compared. The results are shown in Table 4-11 and Table 4-12. The sensors with small-gage sensing wire functioned with greater reliability than those with large-gage sensing wire. This result complicates choice of an optimal gage for the sensing wire. It was found in Section 4.3.5 that the sensors having 26-gage sensing wire responded with greater variability than those having 21-gage sensing wire. Though the signals of the sensors with 26-gage sensing wire could be detected, the greater variability of the signal is problematic. It should be noted that the duration of testing was a rather arbitrary 18 months. In a longer test, the sensors having 21-gage sensing wire may have fractured such that the number of false negatives decreased. In that event, the 21-gage sensing wire would be the better choice of the two. In

addition, the data obtained from the sensors is intended to be weighed along with data obtained from conventional corrosion assessment techniques. Such measurements include half-cell potentials, chloride concentration of the concrete, concrete resistivity, electrochemical impedance spectroscopy, and perhaps linear polarization, though not all of these measurements are typically taken from a given structure. That said, the probability of false negatives remains nonzero but is tolerably low for concentric sensors with 26-gage sensing wires.

**Table 4-11 Distribution of Signals of Concentric Sensors with 26-gage Sensing Wire**

		Observed State of Reinforcement	
		No Corrosion	Corrosion
Detected State of Reinforcement	Corrosion	0 (False Positive)	5
	No Corrosion	2	1 (False Negative)

**Table 4-12 Distribution of Signals of Concentric Sensors with 21-gage Sensing Wire**

		Observed State of Reinforcement	
		No Corrosion	Corrosion
Detected State of Reinforcement	Corrosion	0 (False Positive)	4
	No Corrosion	2	3 (False Negative)

#### 4.4.2 Half-Cell Potentials

The half-cell potentials were taken with a standard calomel electrode (SCE), in units of millivolts, and were converted to the copper-copper-sulfate electrode (CSE) scale. The results were plotted with respect to time in Figure 4-24 and Figure 4-25. Because the primary factor in determining the half-cell potential at a point was the distance of that point from the center of the salt-water reservoir, data taken from points equidistant from the center were averaged and are presented here as a single value. For example, in Figure 4-9, half-cell points 1, 2, 3, 29, 30, and 31 were all 45 in. from the center of the reservoir. Therefore, the half-cell potentials taken at those points were averaged and plotted as the data series '45'. Ranges of risk of corrosion — low (less in magnitude than -200 mV), intermediate (-200 to -350 mV), high (-350 to -500 mV), and severe (greater in magnitude than -500 mV) — are included in Figure 4-24 and Figure 4-25. The



estimates of corrosion risk were obtained from ASTM C876 and are discussed in Broomfield (1997).

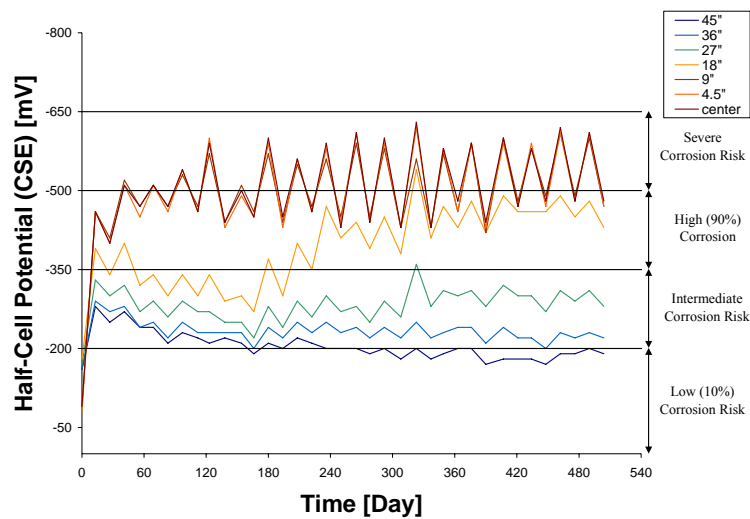


*Figure 4-24 Half-Cell Potentials of Slab 1 with Respect to Time*

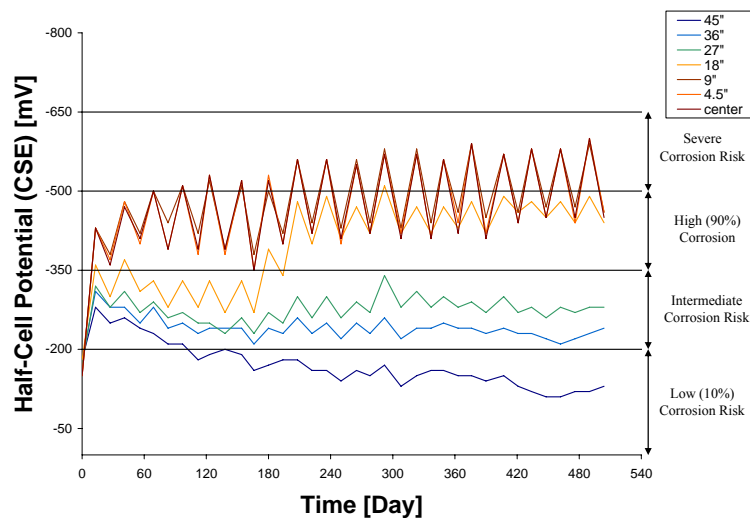


*Figure 4-25 Half-Cell Potential of Slab 2 with Respect to Time*

The areas of severe corrosion risk were inside the salt-water reservoir: at its center, 4.5 in. from the center, and 9 in. from the center. After approximately 180 days of testing, the potentials 18 in. from the center increased significantly. This increase corresponded with moisture from the salt-water reservoir leaking through the epoxy joining the reservoir to the slab and reaching points 18 in. from the center of the salt-water reservoir. Thereafter, the corrosion risk at those locations remained high. Finally, potentials taken 27 in. and 36 in. from the center of the reservoir remained in the medium corrosion risk range, while those taken 45 in. from the center of the reservoir tended to the low corrosion risk range.

As shown in Figure 4-24 and Figure 4-25, the half-cell potentials of both Slabs 1 and 2 converged to two distinct values associated with the environmental cycle to which the specimen had been subjected. That is, at the end of the wet cycle, the half-cell potentials, especially in the salt-water reservoir, were a distinct, relatively more negative value. In contrast, at the end of the dry cycle, the half-cell potentials were a distinct, relatively less negative value. Contour plots were developed by linearly interpolating among the measured values. The contour plots, shown in Figure 4-26 through Figure 4-29, present the half-cell potentials at the end of the final wet and final dry cycle. The gridlines on the plots are spaced 3 in. apart. Sensors colored black had intact sensing wires at the conclusion of testing, and sensors colored gray had fractured sensing wires at the conclusion of testing.

The signals of the concentric sensors were more consistent with the half-cell potentials than those of the coplanar sensors. Specifically, the signals of concentric sensors with 26-gage sensing wire, tested in Slab 1, correlated well with the half-cell potentials in that all concentric sensors except one signaled initiation of corrosion in areas of high to severe risk of corrosion. The signals of

concentric sensors with 21-gage sensing wire, tested in Slab 2, were less consistent with the half-cell potentials: three sensors in regions of high to severe corrosion risk failed to signal initiation of corrosion. The coplanar sensors corresponded with the half-cell potentials less than either case of the concentric sensors. A total of eight coplanar sensors located in regions of high to severe risk of corrosion failed to signal the initiation of corrosion.

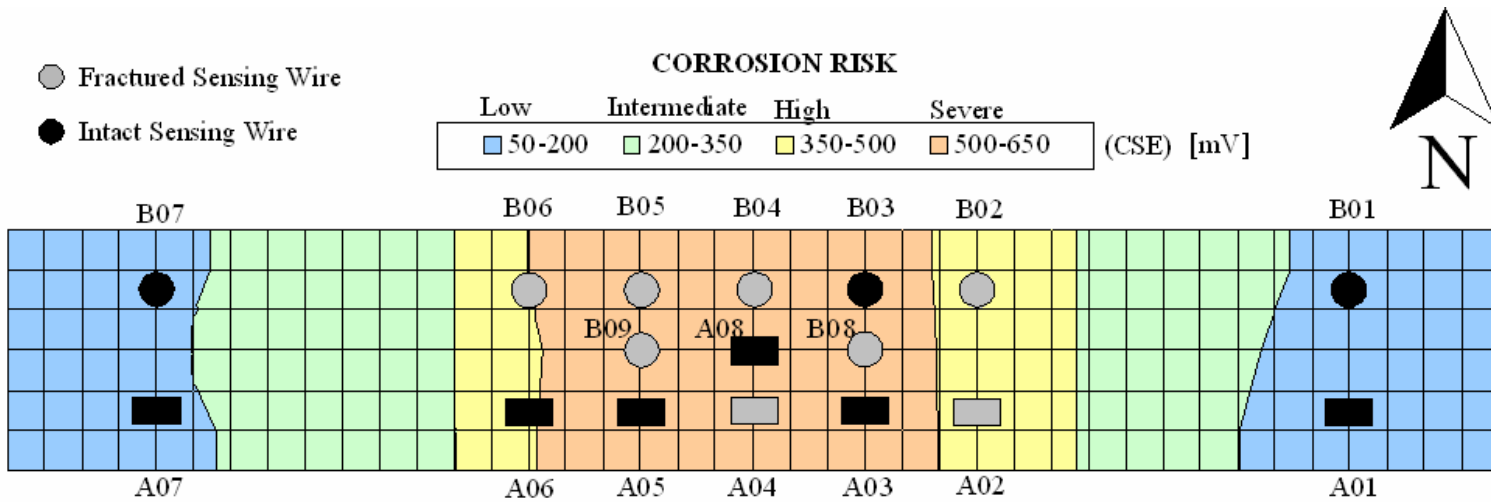


*Figure 4-26 Slab 1 Half-Cell Potential Distribution at the End of Final Wet Cycle*

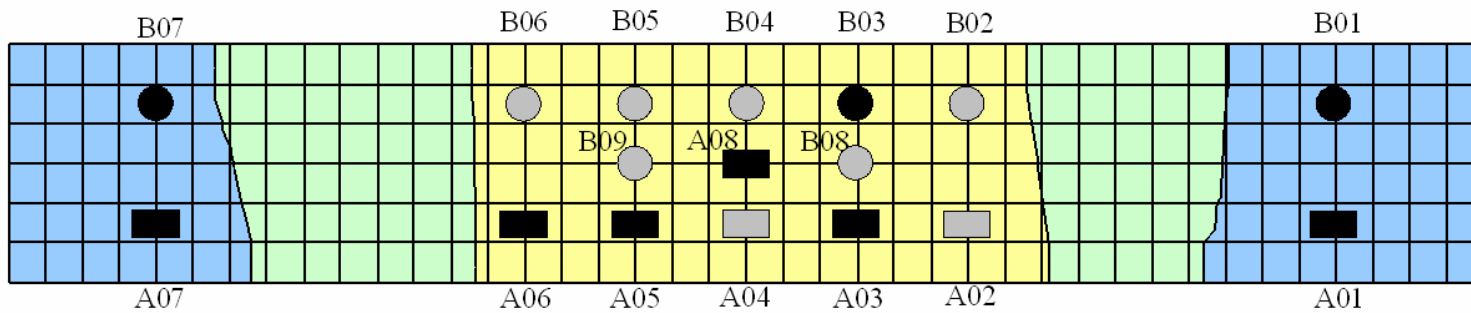


*Figure 4-27 Slab 1 Half-Cell Potential Distribution at the End of Final Dry Cycle*

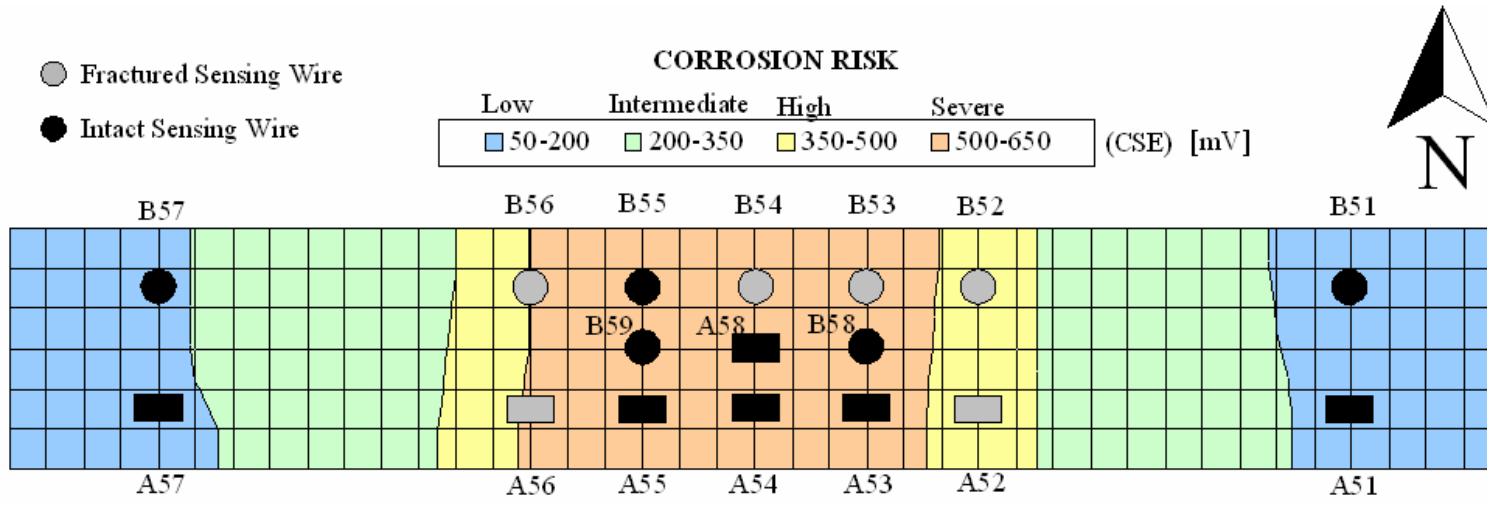


Figure 4-28 Slab 2 Half-Cell Potential Distribution at the End of Final Wet Cycle

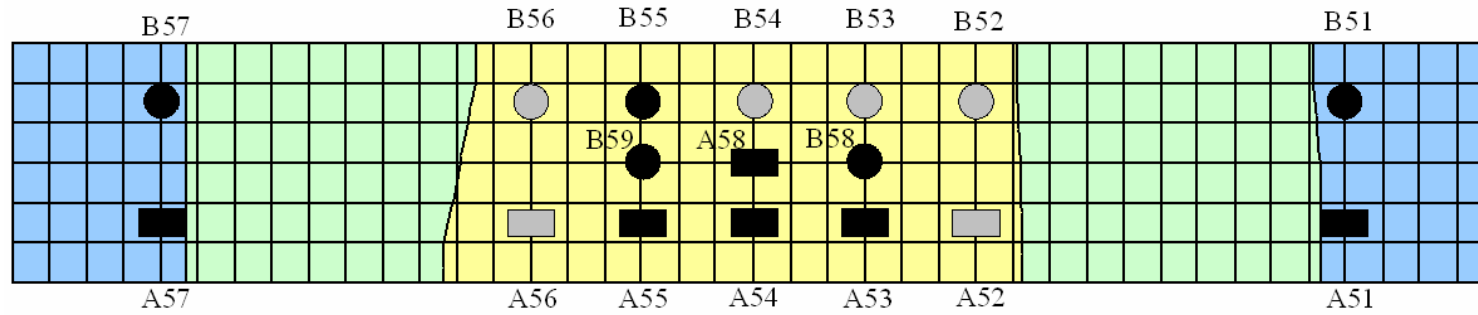
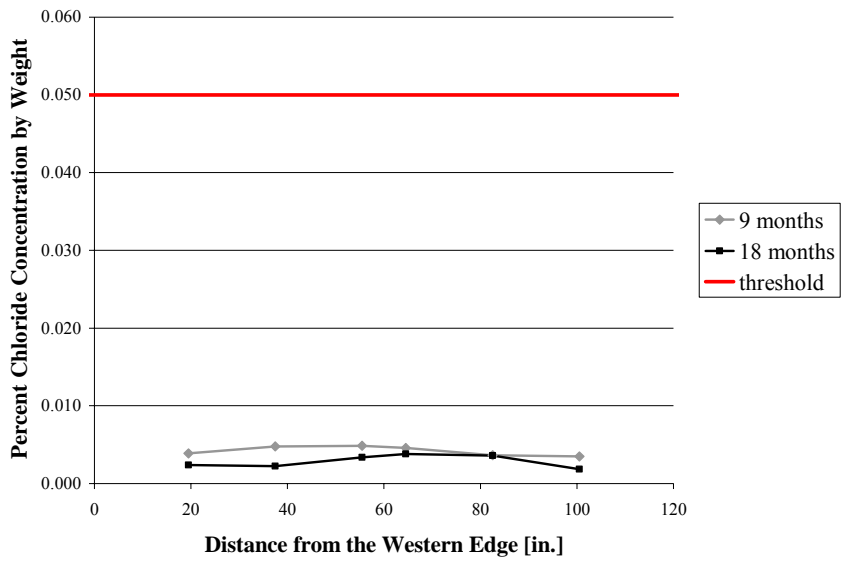


Figure 4-29 Slab 2 Half-Cell Potential Distribution at the End of Final Dry Cycle

#### **4.4.3 Chloride Concentration**

In order to determine the extent to which chlorides had penetrated into the concrete cover of the slab sections, samples of the concrete cover were taken after 9 months of testing and at 18 months of testing, immediately before autopsy of the specimens. Samples were taken 4.5 in., 22.5 in., and 40.5 in. from the center of the salt-water reservoir, on either side of it. As discussed below, none of these locations corresponded with the path of a crack in the concrete cover. The samples were taken from a depth of cover of 1 in., the nominal cover of the sensors. The acid-soluble chloride concentration by weight was determined by the James Instruments, Inc. chloride test system, which conforms to AASHTO T-260-94.

Figure 4-30 and Figure 4-31 are plots of chloride concentration with respect to position on the slab. In terms of Figure 4-1 and Figure 4-2, the coordinate 0 in Figure 4-30 and Figure 4-31 corresponds to the western edge of the slab, and coordinate 120 corresponds with the eastern edge of the slab. A chloride threshold value of 0.05% by weight of pulverized concrete is plotted along with the data. This value, specified by Comité Euro-Internationale du Béton (CEB), is a commonly used as the threshold for initiation of corrosion but is by no means the only proposed value. For an extended literature review of research into chloride threshold values, see West (1999).



**Figure 4-30 Chloride Concentration of Slab 1**

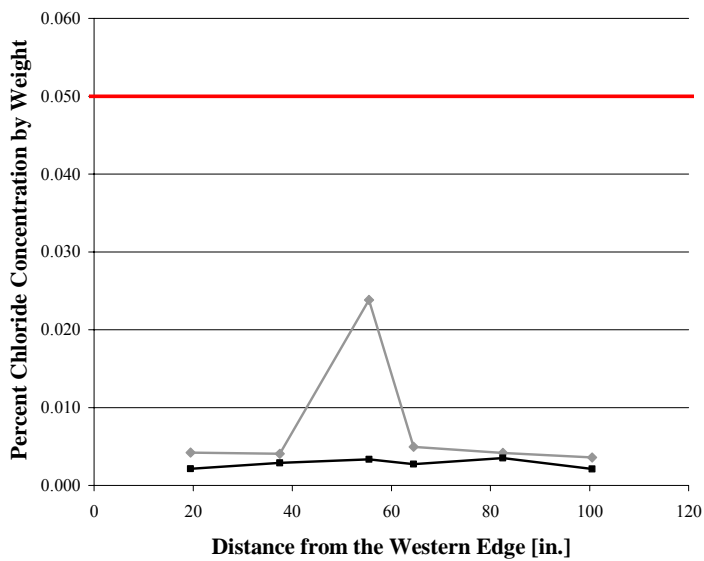
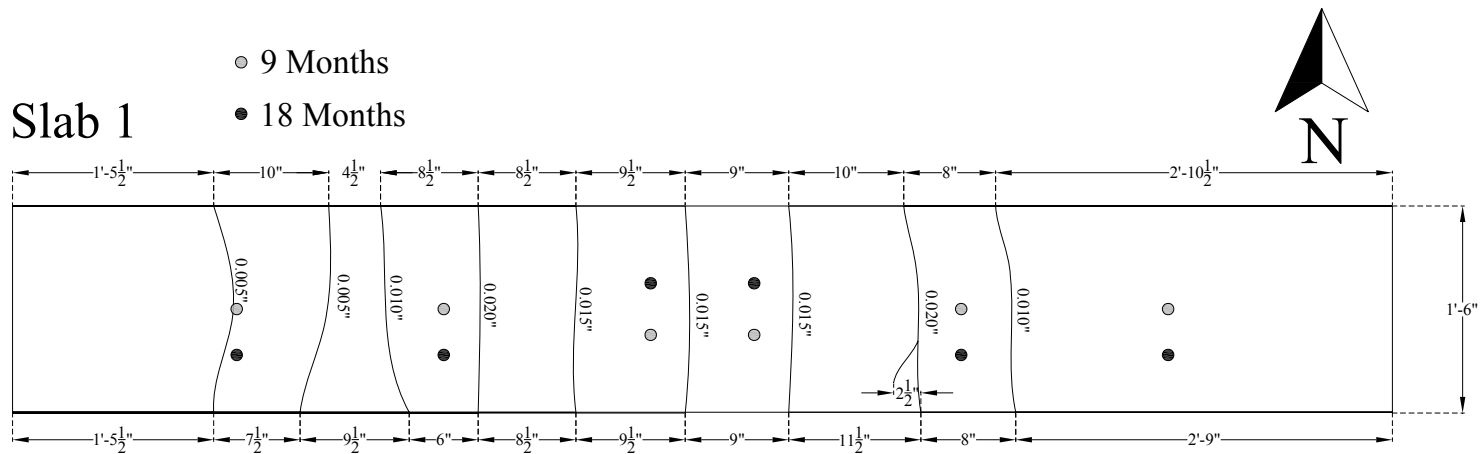


**Figure 4-31 Chloride Concentration of Slab 2**

As shown Figure 4-30 and Figure 4-31, the chloride concentration of the concrete cover remained below the threshold value by an order of magnitude,

except for in the case of Slab 2 near the center of the salt-water reservoir. Even though this value remained below the threshold value, it was well above all the other values. Multiple flexural cracks developed within the salt-water reservoir due to the sustained loading, but the elevated chloride concentration at that point was not due to part of the concrete sample being taken from a crack with elevated concentration of chlorides. As is shown in Figure 4-32, the samples of concrete taken from the salt-water reservoir did not coincide with the paths of any cracks in the reservoir. In Figure 4-32, the locations of samples taken after 9 months of testing are colored gray, while those taken after 18 months are colored black. The position and widths of the cracks are also labeled in Figure 4-32.





127

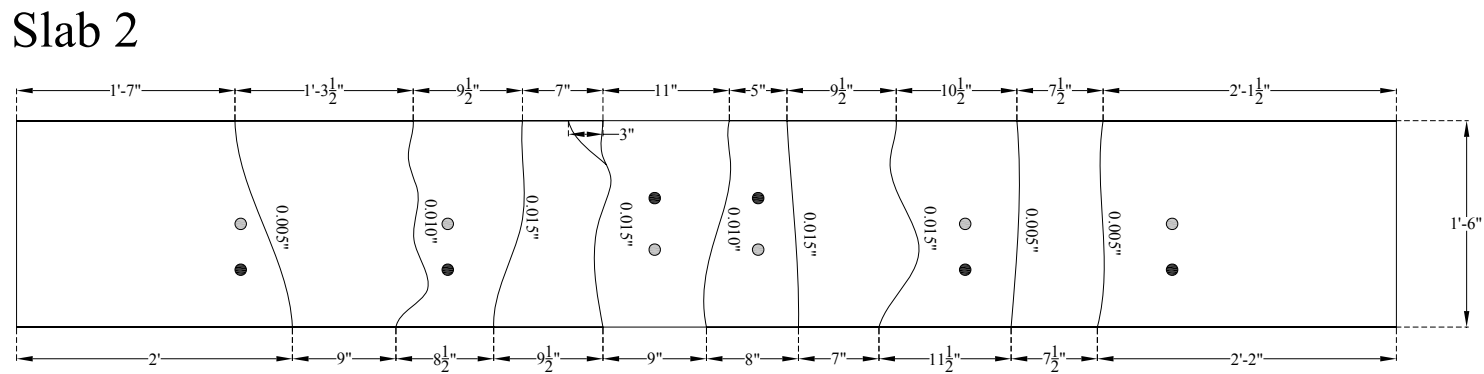


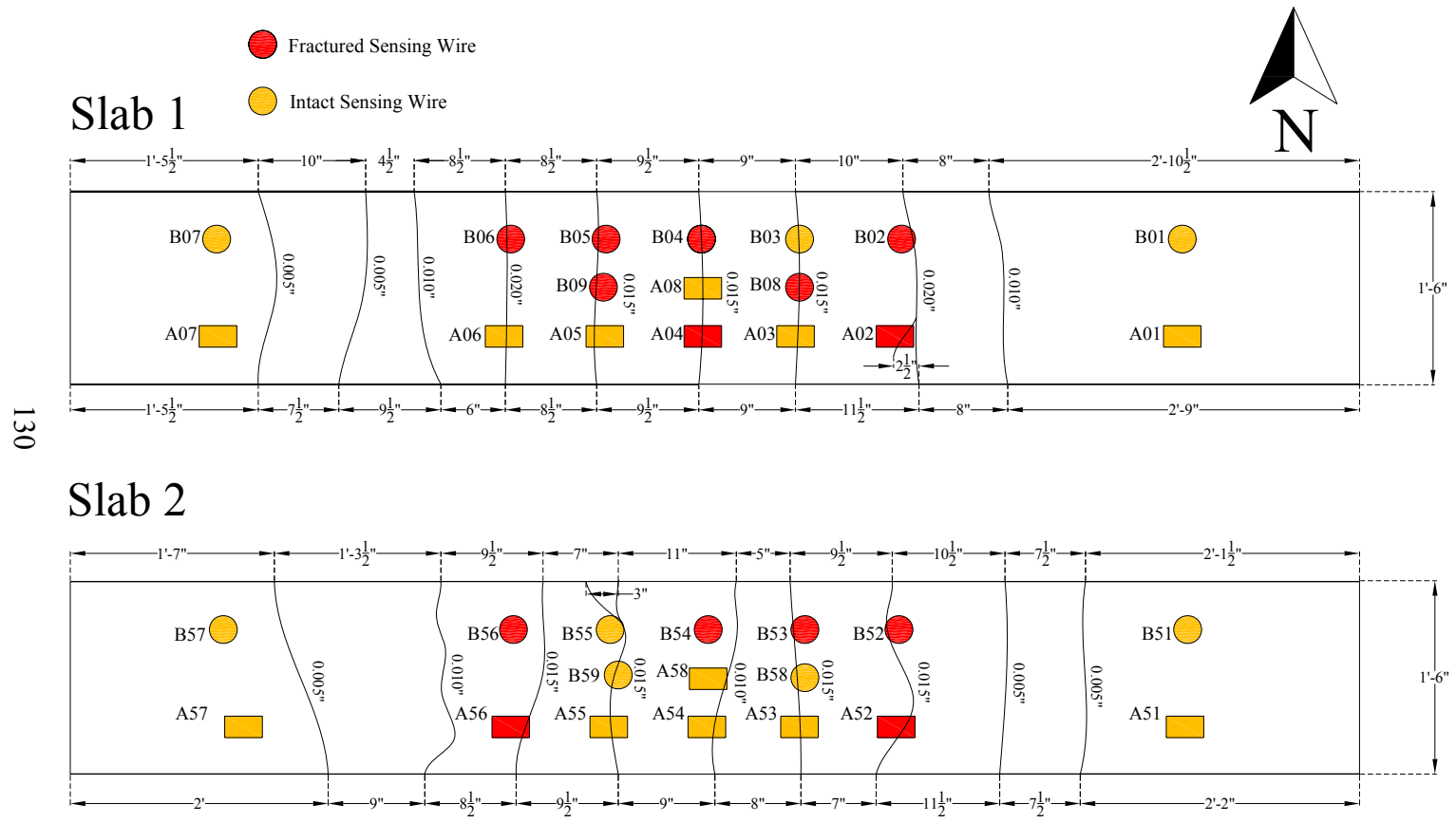
**Figure 4-32** Locations at which Chloride Concentration Determined in Specimens, Relative Cracks in Concrete Cover

The chloride concentration measurements indicated that initiation of corrosion was not likely in the specimens, but this indication was inconsistent with both the observed condition of the reinforcement and the half-cell potentials. Therefore, the signals of the sensors did not correlate with indications of the chloride concentration of the concrete cover because a limitation in the chloride test itself. That is, the rate at which chlorides penetrated the concrete cover was highly influenced by crack formation in the concrete cover. Because the locations at which chloride concentrations were determined in the salt-water reservoir happened to not coincide with the path of cracks, the chloride concentration test gave no indication that corrosion had initiated, though it clearly had. To overcome this difficulty, samples of concrete cover coinciding with the paths of cracks and not coinciding with the paths of a cracks were taken in tests of subsequent specimens.

#### **4.4.4 Influence of Crack Path**

In addition to affecting the reliability of the chloride concentration test, the paths of cracks affected the reliability of the sensors as well. In Chapter 3, it was shown that the paths of cracks in the prism cover were the dominant factor in determining whether a given sensing wire corroded. Cracks in the cover of the concrete prism that intersected the sensing wire provided a pathway for rapid ingress of chlorides, thereby causing corrosion of the sensing wire. Crack path was similarly important in determining which sensing wires fractured in Slabs 1 and 2. Figure 4-33 superimposes the width and position of cracks measured on the surface of the Slabs 1 and 2 immediately prior to the slabs being autopsied, after the slabs had been unloaded. Cracks smaller than 0.005” were not included in Figure 4-33. Sensors with fractured sensing wires are colored red, while those with intact sensing wires are colored yellow. The sensors are depicted in their

measured positions, as Figure 4-17, not their design positions because the actual relation between the sensor and the paths of cracks was critical.



130

*Figure 4-33 Paths of Cracks in Specimens Superimposed on the Measured Position of the Sensors*

From Figure 4-33, it is evident that cracks tended to form along the transverse reinforcement which supported the sensors. Consequently, cracks formed in the concrete cover above most of the sensors.

However, not all the sensing wires of the sensors fractured. The critical condition determining whether a sensing wire fractured was not whether a crack simply passed over a given sensor. Rather, whether the path of a crack actually intersected the sensing wire strongly influenced whether the wire fractured due to corrosion. If the crack intersected the sensing wire, allowing for rapid ingress of chlorides, the sensing wire fractured, and the sensor signaled initiation of corrosion. If the crack failed to intersect the sensing wire, the sensing wire usually failed to fracture, signaling a false negative.

A likely example of a path of a crack intersecting a sensing wire and causing the sensor to signal corrosion initiation was B53. Because of the loading, a transverse crack developed over the sensor B53, allowing chlorides conveyed by the salt water to penetrate through the concrete cover. Because the crack likely passed over the sensing wire, the wire fractured due to corrosion. Corrosion was also observed on the reinforcement near the sensor, along the path of the crack, as shown in Figure 4-34.



***Figure 4-34 Crack Path Intersecting Sensing Wire of B53 and Reinforcement, Causing Corrosion of Both***

In other cases, as was mentioned in Section 4.4.1, corrosion developed near a sensor without the sensor signaling corrosion initiation. For example, a transverse crack likely developed over sensor B55 in such a way that the transverse reinforcement corroded but the sensing wire did not. Figure 4-35 shows this outcome.



***Figure 4-35 Crack Path Failing to Intersect Sensing Wire of B55 but Causing Corrosion of Reinforcement***

The cases of B53 and B55 are representative of how the sensors functioned generally. That is, the reliability of a given sensor at detecting initiation of corrosion was significantly influenced by the path of cracks in the concrete cover. The possibility of false negatives, discussed in Section 4.4.1, is largely due to the possibility of a crack path failing to intersect the sensing wire of a sensor. However, as is shown in Figure 4-33, sensors B54 and B56 signaled the initiation of corrosion despite the fact that no measurable cracks intersected their sensing wires. Therefore, while the path of cracks is important to the reliability of the sensors, it does not determine their reliability.

#### **4.4.5 Accelerated Corrosion of Transverse Reinforcement**

Two complications with the sensor housing compromised the performance of the sensors: development of black corrosion within the epoxy housing and accelerated corrosion of the transverse reinforcement. Black corrosion was also observed in Slabs 3 and 4 and is discussed in Chapter 6. Accelerated corrosion of the transverse reinforcement due to the shape of the sensor housing is discussed in this section.

The sensor housing accelerated corrosion of the transverse reinforcement by collecting corrosive agents beneath the sensor. The epoxy of the sensors was nonpermeable, facilitating the collection of such corrosive agents. These corrosive agents were thereby in continual contact with the transverse reinforcement supporting the sensor and caused accelerated corrosion of that reinforcement. Although most transverse reinforcement on which the sensors were placed exhibited accelerated corrosion, the concentric sensors caused the greater acceleration because of the concave bottom of their sensor housing. This concave bottom facilitated the formation of an air void under the sensor that was in general larger than the voids found beneath coplanar sensors. This larger air void

increased the volume of corrosive agents continually in contact with the transverse reinforcement, causing greater acceleration of the corrosion. Figure 4-34 and Figure 4-35 show the results of this accelerated corrosion.

The bottoms of sensors having concentric and coplanar geometries are shown in Figure 4-36. Figure 4-37 shows the differences in air voids that typically formed beneath the two geometries of sensors. Because the shape of the sensor housing, regardless of geometry, diminished the durability of the reinforced concrete structure in which the sensors were embedded, some other mold must be developed to prevent corrosive agents from collecting beneath the sensors.

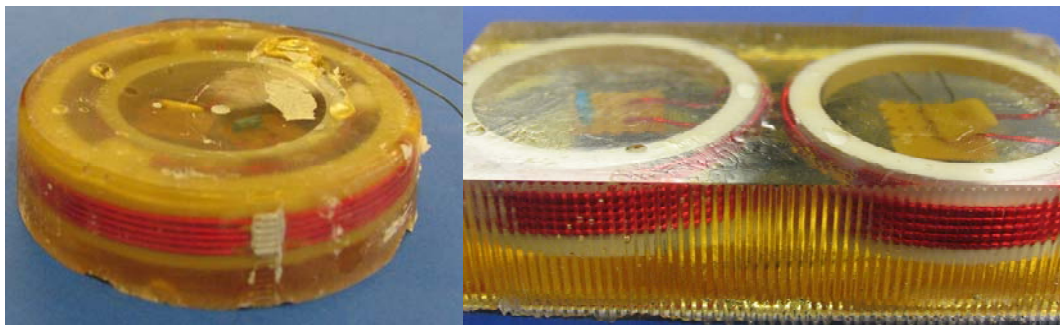


***Figure 4-36 Bottoms of Sensors with Concentric and Coplanar Geometries***



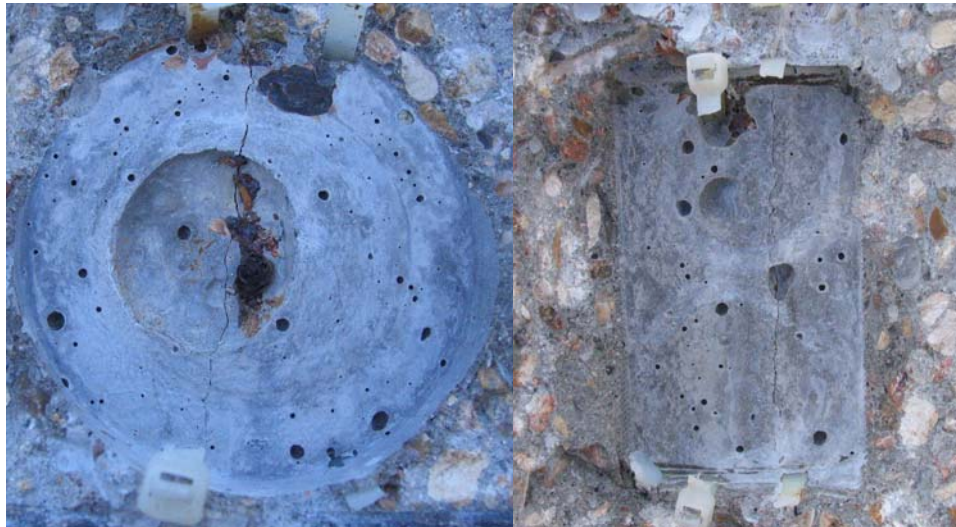


*Figure 4-37 Air Voids beneath Concentric and Coplanar Sensors*

#### **4.5 CONCLUSIONS**

Several conclusions can be drawn from the measured response of isolated sensors embedded in Slabs 1 and 2. First, isolated sensors subjected to large-scale testing reliably signaled the state of their sensing wires, whether intact or fractured. In every case the signal of the sensor was consistent with the physical state of the sensing wire, and in no case did the phase dip at the sensing frequency reappear after disappearing. In this way, the sensors signaled reliably as threshold sensors.

Second, sensors subjected to large-scale testing responded with greater variability than those subjected to small-scale testing. The primary cause of this increase in variability was the presence of baseline shift in the response of the sensors. A secondary cause in the case of coplanar sensors with small-gage sensing wires was change in position during casting relative where the reader coil was placed for interrogations. In contrast to these coplanar sensors, the variability in the response of the concentric sensors exhibited no dependence on change in

position during casting. Coplanar sensors with large-gage sensing wires also showed no such dependence. Although this increase in variability complicated the calculation of the response parameters — resonant frequency, phase dip, and pseudo-quality factor — the increased variability in no way prevented the sensors from functioning as threshold sensors. Differences in geometry and gage of sensing wire among the sensors resulted in differences in variability of sensor response. The coplanar sensors responded with greater variability than the concentric sensors. Furthermore, sensors with small-gage sensing wire responded with greater variability than sensors with large-gage sensing wire.

Third, the reliability of the sensors for detecting initiation of corrosion on steel reinforcement adjacent to the sensors was assessed on the basis of the observed condition of the reinforcement. Furthermore, the signals of the sensors were compared with the half-cell potentials and chloride concentration of the concrete cover of the specimens. With respect to the observed condition of the reinforcement, the concentric sensors were more reliable than the coplanar sensors. Furthermore, the concentric sensors with small-gage sensing wire were more reliable in this respect than those with large-gage sensing wire. In fact, the former concentric sensors signaled only a single erroneous signal, a false negative. In that respect, the concentric sensors with small-gage sensing wire were quite reliable at detecting initiation of corrosion and therefore may be regarded as a success. However, because sensors with small-gage sensing wires exhibited greater variability in response than those with large-gage sensing wires, small-gage sensing wire is not unequivocally the better choice.

The signals of the concentric sensors were significantly more consistent with the half-cell potentials of the specimens than were the signals of the coplanar sensors. However, measurements of the chloride concentration of the concrete indicated that corrosion had not initiated, a condition inconsistent with other data

taken from the specimens. The importance of the path of cracks in the concrete cover was not taken into account when the chloride concentration tests were performed, leading to erroneous conclusions regarding the initiation of corrosion in the specimens.

Fourth, the path of cracks also influenced the reliability of the sensors. By providing a direct path of ingress for chlorides, cracks in the concrete cover highly influenced where corrosion developed. In some cases, a crack intersected steel reinforcement near a sensor but failed to intersect the sensing wire of that sensor. Then, the reinforcement corroded, but the sensing wire failed to fracture, preventing the sensor from signaling initiation of corrosion. Although some sensors signaled the initiation of corrosion despite a crack failing to intersect their sensing wire, most sensors that signaled false negatives did so because a crack failed to intersect their sensing wires.

Finally, the epoxy housing of the sensors decreased the durability of the specimens in which the sensors were embedded. The impermeable epoxy housing accelerated corrosion of the transverse reinforcement on which it was placed by allowing corrosive agents to collect beneath the housing. Although both the concentric and coplanar sensors caused such accelerated corrosion, the concave bottom of the concentric sensors particularly facilitated the accelerated corrosion. The concave bottom formed a large air void beneath the sensor that collected corrosive agents above the transverse reinforcement. Thus, as discussed in Chapter 7, a substitute for the epoxy and molds used to pot the sensors was developed.

## **CHAPTER 5**

# **Testing of Coupled Sensors in Reinforced Concrete Slab Sections**

### **5.1 INTRODUCTION**

The concept of the coupled sensor is based on an electrical connection between the sensing wire of the sensor and the steel reinforcement. Therefore, because the design of the prisms used for small-scale testing did not accommodate steel reinforcement, the coupled sensors were only tested in reinforced concrete slabs. A set of coupled sensors was embedded in two such specimens, and the specimens were exposed to salt water in wet and dry cycles over a 12-month period. At the end of that period, one of the specimens was autopsied; the other specimen continues to undergo testing. Section 5.2 describes the design of the specimens used to test the coupled sensors and the environmental conditions to which they were exposed. The measured response of the coupled sensors is discussed in Section 5.3. Finally, Section 5.4 assesses the reliability of the coupled sensors at detecting the initiation of corrosion of the steel reinforcement and compares the signals of the sensors with conclusions drawn from the half-cell potentials and chloride concentration of the concrete.

### **5.2 DESIGN OF THE EXPERIMENT**

The slab sections fabricated to test the coupled sensors were 10-ft long, 18-in. wide, and 8-in. deep. Top and bottom plan views of the two specimens and a typical section of the specimens are shown in Figure 5-1 through Figure 5-5. Fourteen sensors were embedded in each specimen: sensors B125 through B128 and B134 through B143 in Slab 3 and sensors B146 through B159 in Slab 4.

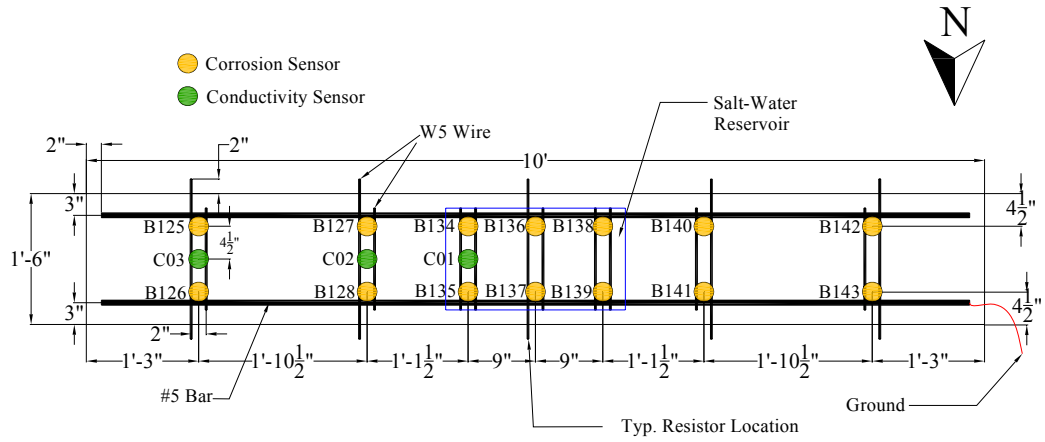


**Figure 5-1 Top Plan View Slab 3**

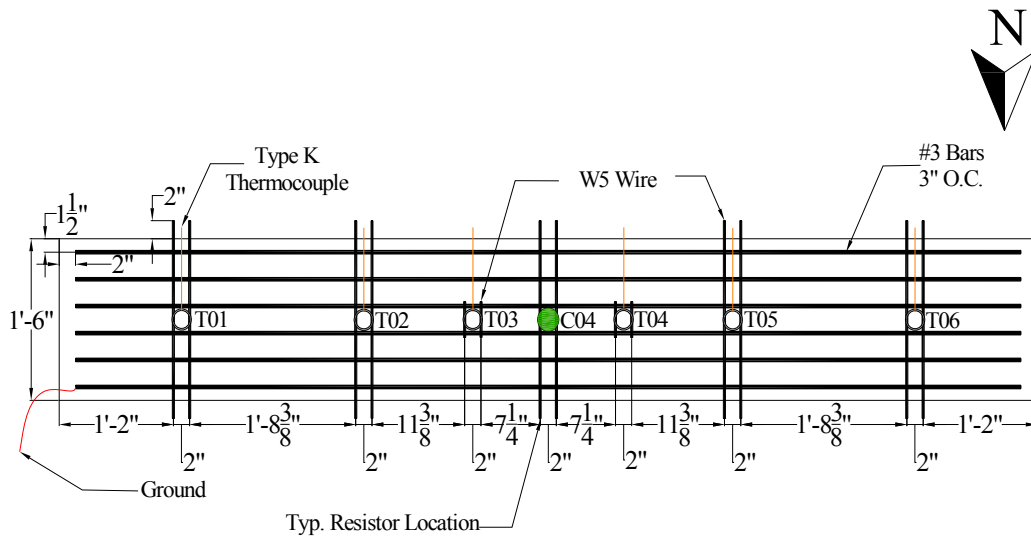


**Figure 5-2 Bottom Plan View of Slab 3**

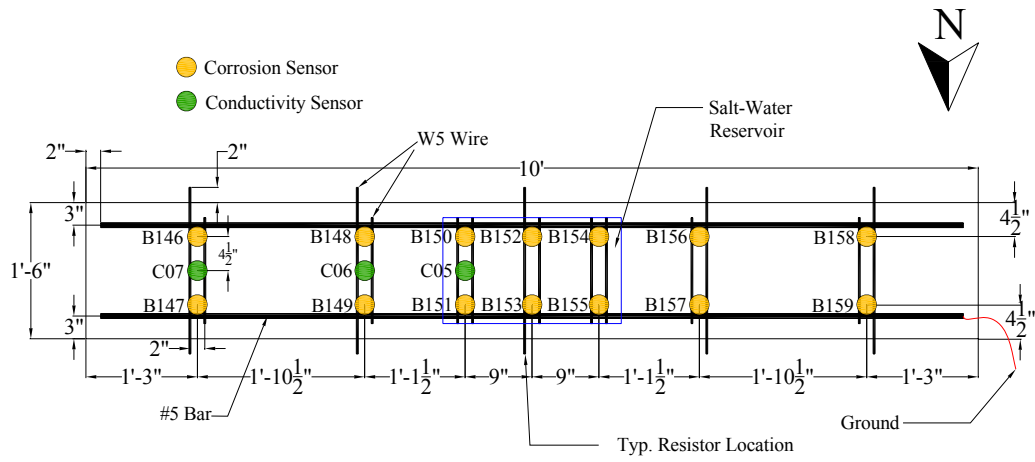


**Figure 5-3 Top Plan View of Slab 4**

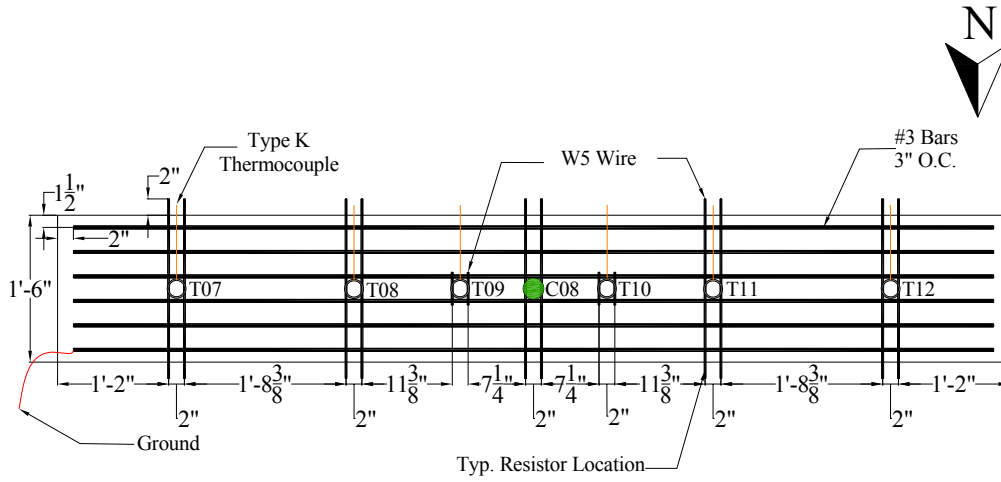


**Figure 5-4 Bottom Plan View of Slab 4**

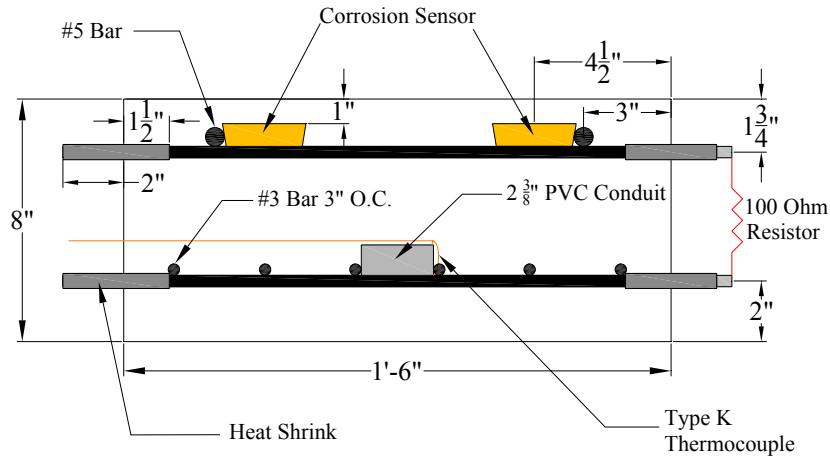


**Figure 5-5 Typical Section of Slab 3 and Slab 4**

Conductivity sensors — C01 through C04 in Slab 3 and C05 through C08 in Slab 4 — were also tested in the specimens. For a discussion of the conductivity sensors, see Andringa (2006).

In contrast to the reinforcement of Slabs 1 and 2, the top and bottom layers of Slabs 3 and 4 were electrically connected in order to facilitate the development of macrocell corrosion. As shown in Figure 5-1 and Figure 5-2, at five locations along the length of the specimens, a single length of W5 wire extended beyond the edge of the concrete on the top, and two lengths of W5 wire extended beyond the edge of the concrete on the bottom. On one side of the specimen, the ends of the bars were threaded, and stainless steel couplings were attached to the bars. The remainder of the exposed bar, including a 1 1/2-in. segment extending into the concrete, was wrapped with electroplating tape and covered with heat shrink in order to prevent atmospheric corrosion from developing and influencing the internal corrosion of the specimen. A 100-Ohm resistor, as shown in Figure 5-5 and Figure 5-6, was connected to the top transverse reinforcement extending from the slab to the bottom transverse reinforcement extending from the slab, using 18-

gage copper magnet wire. The amount of corrosion current flowing from the anode on the top of the specimen to the cathode on the bottom was determined by measuring the voltage over the 100-Ohm resistor. The segments of W5 wire extending from the specimens on the side opposite the resistors were wrapped in electroplating tape and completely covered with heat shrink, as shown in Figure 5-7, to prevent corrosion due to the atmosphere.



*Figure 5-6 Resistor Connecting Top and Bottom Reinforcement*



*Figure 5-7 Sealed End of Transverse Reinforcement*



In order to determine the degree to which the atmosphere caused internal corrosion of the specimens, a control specimen was fabricated and stored with Slabs 3 and 4. Top and bottom plan views of the control specimen are shown in Figure 5-8. The section of the control specimen was identical to the section of Slabs 3 and 4. Corrosion current circulating through the control specimen was determined by measuring the potential difference over the resistor. This value was deemed to be a reasonable approximation of the amount of corrosion current caused by the atmosphere in Slabs 3 and 4 because the control specimen was not exposed to chlorides through wet and dry cycles. Conductivity sensor C09 was also tested in the control specimen, and the results are discussed in Andringa (2006).

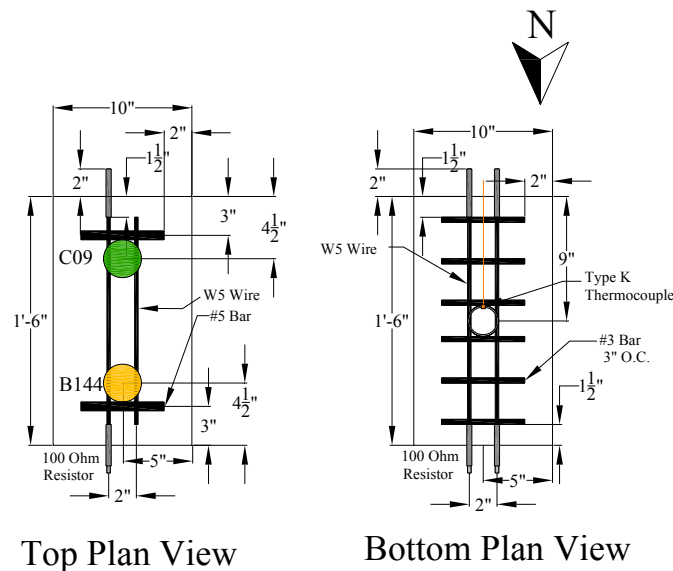


**Figure 5-8 Plan View of Top and Bottom of Control Specimen**

The only difference between Slab 3 and Slab 4 was how the top and bottom transverse reinforcement of each specimen were electrically connected. In

the case of Slab 3, only the set of top and bottom reinforcement at the center of the specimen was connected with a 100-Ohm resistor. This arrangement was maintained until day 238 of testing. Thereafter, all the sets of top and bottom reinforcement were connected. In contrast, all the sets of the top and bottom transverse reinforcement in Slab 4 were connected using 100-Ohm resistors throughout testing. The difference between the two specimens, then, is that for a portion of the testing, current flowing from the top reinforcement to the bottom reinforcement of Slab 3 had only one pathway. After day 238 of testing, the current had five pathways. The current flowing from the top reinforcement to the bottom reinforcement in Slab 4 had five pathways throughout testing.

As shown in Figure 5-2 and Figure 5-4, type K thermocouples were embedded along the lengths of both Slab 3 and Slab 4 to measure the internal temperature of the specimens. The thermocouples were attached to the bottom layer of reinforcement by being wrapped around a 1-in. slice of 2 <sup>3</sup>/<sub>8</sub>-in. PVC conduit. The PVC slices were secured to the reinforcement using zip ties. The distance between the end of the thermocouples, which sense the change in temperature, and the bottom surface of the specimens was 2 in.

The sensors embedded in Slabs 3 and 4 were nominally identical. They had a concentric geometry and were tested as coupled sensors. Therefore, their sensing wires were electrically connected to the top layer of the steel reinforcement. Because the connection of the sensors to the top reinforcement was intended to be only an electrical connection, not galvanic, the chemistry of the sensing wire was chosen to be similar to the chemistry of the reinforcement. The sensing wire selected was 21-gage (0.0285-in. diameter) annealed steel with no finish. Chemical analysis of the wire found it to be AISI-ASE 1060. Table 5-1 lists the nonferric chemical components of the 1060 sensing wire, the W5 wire used for transverse reinforcement, and the deformed #5 bars used for longitudinal

reinforcement. To increase the rate of corrosion, the longitudinal bars of the specimens were sprayed with salt-water prior to their being placed in the formwork.

**Table 5-1 Chemical Composition of Sensing Wire, W5 Wire, and #5 Bar**

<b>Chemical Element</b>	<b>1060 Wire</b>	<b>W5 Wire</b>	<b>Deformed #5 Bar</b>
	[% ]	[% ]	[% ]
<i>Carbon</i>	0.60	0.11	0.38
<i>Manganese</i>	0.78	0.60	0.89
<i>Phosphorus</i>	0.018	0.015	0.021
<i>Sulfur</i>	<0.005	0.040	0.036
<i>Silicon</i>	0.23	0.15	0.26
<i>Nickel</i>	0.06	0.05	0.13
<i>Chromium</i>	0.06	0.01	0.16
<i>Molybdenum</i>	<0.01	0.01	0.04
<i>Copper</i>	0.09	0.03	0.33
<i>Aluminum</i>	0.009	-	-

The sensors were zip-tied to platforms composed of two lengths of W5 wire. The second length of W5 wire, as shown in Figure 5-1 and Figure 5-3, did not extend beyond the edge of the concrete. Rather, it was attached to the longitudinal steel simply to serve as a platform for the sensors. The sensing wires were secured to the steel reinforcement using zip-ties in such a way that the sensing wire was in electrical contact with the reinforcement. Figure 5-9 shows the sensors zip-tied to the transverse reinforcement and their sensing wires connected to the upper layer of reinforcement. As was observed in Section 4.4.4, the path of cracks significantly influenced which sensing wires corroded, and cracks tended to develop where the transverse reinforcement was placed. Therefore, in the case of half of the sensors, their sensing wires were placed along

the expected path of the cracks, in the same section as the sensor. In the case of the other half of the sensors, the sensing wire was placed out of the expected path of the cracks. Figure 5-10 shows a sensor with sensing wire placed in the expected path of the cracks. Figure 5-11 shows a sensor with sensing wire placed out of the expected path of the cracks.



***Figure 5-9 Layout of Sensors and Steel Reinforcement***



***Figure 5-10 Sensing Wire Placed in the Expected Path of the Crack***

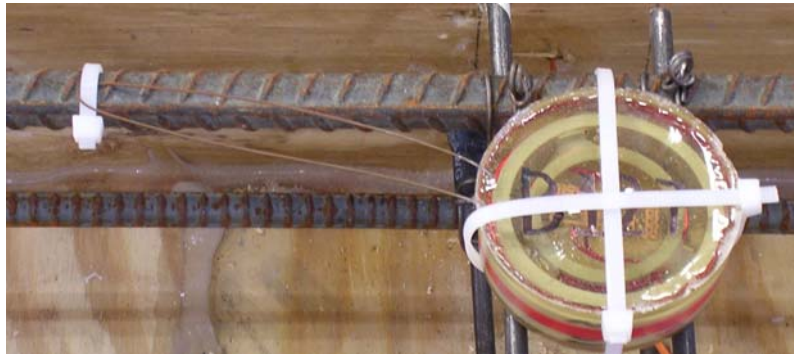


***Figure 5-11 Sensing Wire Positioned out of the Expected Path of the Crack***

The concrete was placed on 10 March 2006, and the specimens were allowed to cure for four weeks. The specimens were intentionally subjected to poor curing conditions. That is, they were not draped in plastic to facilitate moist curing. In addition, high-speed fans were directed at the surface of the specimens for the first week of curing in order to accelerate evaporation of moisture from the surface of the concrete. Prior to the specimens being moved from the casting bed, their compressive strength was determined. The 20-day strength of the concrete was 4,000 psi.

On 6 April 2006, the specimens were loaded at both end points with concentrated loads. The positions at which the loads were applied and the positions of the supports were identical to those positions in the case of Slabs 1 and 2, as shown in Figure 4-5. The specimens were loaded until the maximum width of flexural cracks on the top surface of the slabs was on the order of 0.01 in. Crack maps for Slabs 3 and 4, recorded immediately after the specimens were loaded, are shown in Figure 5-12 and Figure 5-13, respectively. This maximum width of cracks was significantly smaller than in the case of Slabs 1 and 2, which had crack widths with an average value of 0.02 in. The objective in restricting the maximum width of cracks in Slabs 3 and 4 was to reduce the influence of cracks on which sensing wires fractured due to corrosion. On day 317 of testing, the

specimens were unloaded, but otherwise testing of the specimens continued. Both Slabs 3 and 4 exhibited residual deformation after unloading, with the width of cracks remaining on the order of 0.01 in. As shown in Figure 4-5, Figure 5-1, and Figure 5-3, a salt-water reservoir was fixed at the middle of both specimens. Instead of an epoxy, which tended to crack over time, Sika 11FC, a waterproof adhesive, was used to attach the reservoir to the surface of the specimens.

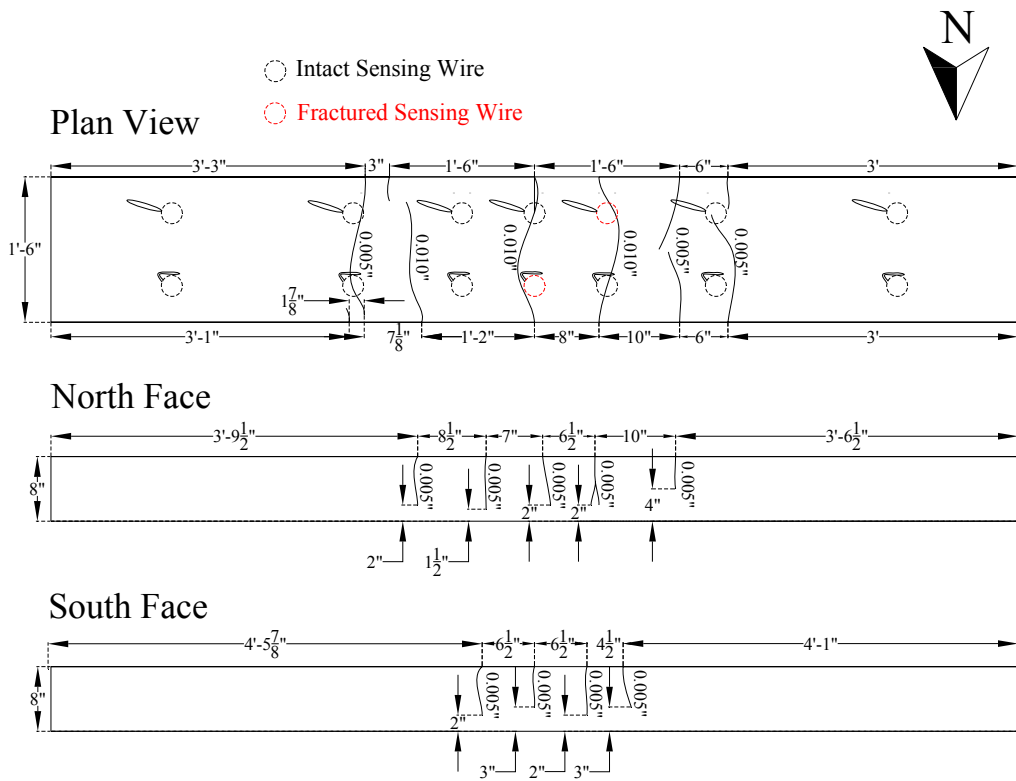


**Figure 5-12 Crack Map of Slab 3 Immediately after Loading**

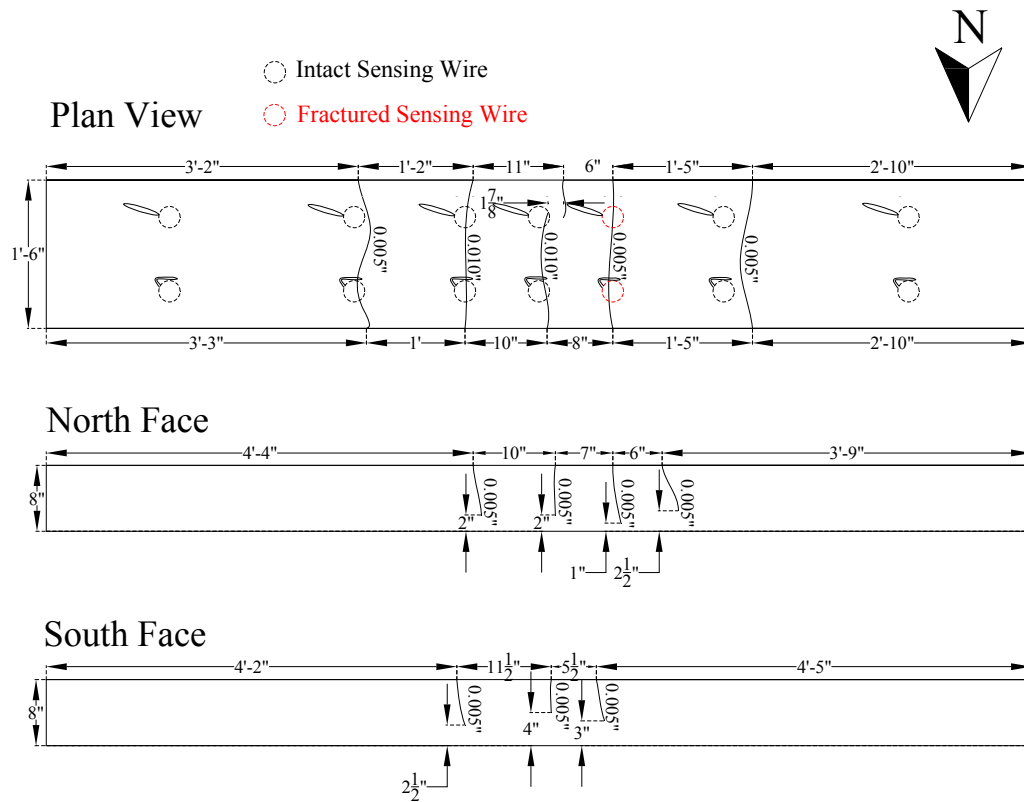


**Figure 5-13 Crack Map of Slab 4 Immediately after Loading**

Testing began 6 April 2006. On that date, the sensors were interrogated, and after interrogation, the salt-water reservoirs were filled, initiating a two-week wet cycle. Salt water, 3.5% NaCl by weight, was used for all wet cycles. All moisture was removed from the reservoir during the two-week dry cycles, which immediately followed the wet cycles. The wet and dry cycles continued throughout testing to simulate extreme service conditions for a bridge deck. The specimens were stored indoors throughout testing to control their exposure to moisture and chlorides. The building in which the specimens were stored was

heated irregularly such that the specimens were exposed to temperature fluctuations of nearly 60 °F.

As shown in Figure 5-1 and Figure 5-3, the sensors were placed along the length of the specimens, while salt-water exposure was restricted to the midspan of the specimens. Consequently, three distinct environments were established within each specimen: dry conditions, controlled moisture conditions, and varying moisture conditions. Corresponding with these environments were respective levels of corrosion risk: low, high to severe, and intermediate to high. Because sensors were embedded in each of these environments, some of the sensors were placed a distance from the likely locations of corrosion. The conditions to which the sensors were subjected are summarized in Table 5-2. To ensure that the risk of corrosion in the transition regions was distinct from the risk of corrosion within the salt-water reservoir, sensors in the transition regions of Slabs 3 and 4 were located 22 ½ in. from the center of the salt-water reservoir. In Slabs 1 and 2, the sensors in the transition regions were 18 in. from the center of the salt-water reservoir. Sensors placed a distance from the locations of corrosion were intended to lend insight into the tributary area of the coupled sensor, defined by parameter  $d$ , as described in Section 2.4.2. Specifically, if the sensing wire of a sensor is attached some distance  $d_1$  from a point of corrosion in the specimen and the sensor signals initiation of corrosion, then parameter  $d$  is greater than  $d_1$ . In contrast, if the sensing wire of a sensor is attached some distance  $d_2$  from a point of corrosion in the specimen and the sensor fails to signal initiation of corrosion, the parameter  $d$  is less than  $d_2$ . In this way,  $d$  was established empirically by the tests in Slabs 3 and 4.



**Table 5-2 Moisture Conditions of Sensors**

	<b>SLAB 3</b>	<b>SLAB 4</b>
<b>Ends of Slab</b> <i>(Dry Conditions)</i>	B125	B146
	B126	B147
	B142	B158
	B143	B159
<b>Beneath Salt-Water Reservoir</b> <i>(Controlled Moisture Conditions)</i>	B134	B150
	B135	B151
	B136	B152
	B137	B153
	B138	B154
	B139	B155
<b>Transition Regions</b> <i>(Varying Moisture Conditions)</i>	B127	B148
	B128	B149
	B140	B156
	B141	B157

The sensors were interrogated at the end of each wet cycle and at the end of each dry cycle. A Solartron SI 1260 Impedance/Gain-Phase Analyzer was used to interrogate the specimens. The reader coil was 4 in. in diameter and had 5 turns of 18-gage copper magnet wire to serve as the inductor. The reader coil was connected to the analyzer using a 3-ft coaxial cable. The static half-cell potentials of both specimens were taken at the end of each environmental cycle, in accordance with ASTM C876. The locations at which the half-cell potentials were taken are shown in Figure 5-14. In addition, the voltages over the connected resistors in each specimen and the control were measured at the end of each environmental cycle. That voltage was used to determine the amount of corrosion current circulating in the specimens. The internal temperature of each specimen and the control was measured at the locations shown in Figure 5-2 and Figure 5-4 and Figure 5-8. The temperature of the air in which the specimens were stored

was recorded prior to half-cell potentials being taken. Finally, after 12 months of testing, Slab 4 was autopsied. Prior to the autopsy, the acid-soluble chloride concentration by weight in the concrete cover of Slab 4 was determined. Slab 3 was not autopsied, and its testing is ongoing.

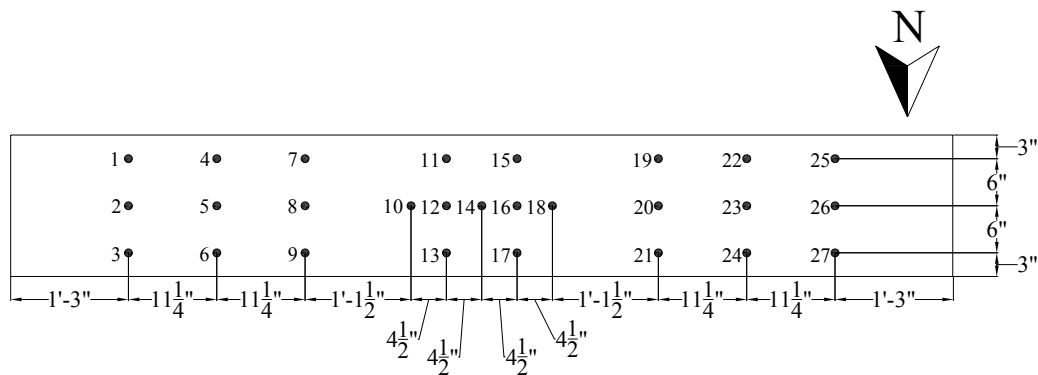


**Figure 5-14 Locations at which Half-Cell Potentials Taken in Slabs 3 and 4**

### 5.3 MEASURED RESPONSE OF THE SENSORS

The measured response of the sensors over 371 days is presented in this section. Two of the fourteen sensors in Slab 3 and two of the fourteen sensors in Slab 4 signaled that their sensing wires fractured during this period. The detected state of the sensors, whether having intact or fractured sensing wires, is discussed in Section 5.3.1. A statistical summary of the measured response of all the sensors tested in Slabs 3 and 4 is given in Section 5.3.2. As was the case with Slabs 1 and 2, in no case did the phase dip at the sensing frequency reappear after it had disappeared. Despite that fact, there was evidence in the response of the sensors with fractured sensing wires that the internal environment of the specimens was influencing the response of the reference circuits. Section 5.3.3 discusses possible causes of this influence. In addition, the internal environment

of Slabs 3 and 4 was such that the response of some sensors indicated that their sensing wires were corroding uniformly. Section 5.3.4 describes likely instances of uniform corrosion of the sensing wire. In the case of two of the intact sensors, one in each specimen, the reference circuit ceased to respond at its reference frequency. The response of these sensors and the cause of deterioration of the reference circuit, black corrosion, are discussed in Section 5.3.5. Finally, the dependence of the response of the sensors on temperature is assessed in Section 5.3.6. The response of sensors tested in Slabs 3 and 4 and not discussed in this chapter are given in Appendix C.

### 5.3.1 Detected State of the Sensing Wires after 12 Months of Testing

The coupled sensors with sensing wires detected to be fractured in the first 12 months of testing and the day of testing on which the fracture was detected are shown in Figure 5-15. Figure 5-16 provides a plan view of sensors the sensing wires of which fractured during testing. Sensors with intact sensing wires are colored yellow, while those with fractured sensing wires are colored red.

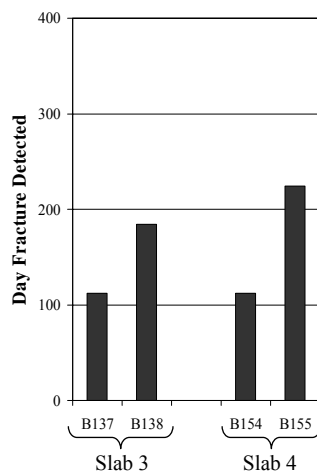


**Figure 5-15 Sensors with Fractured Sensing Wires after 12 Months of Testing**

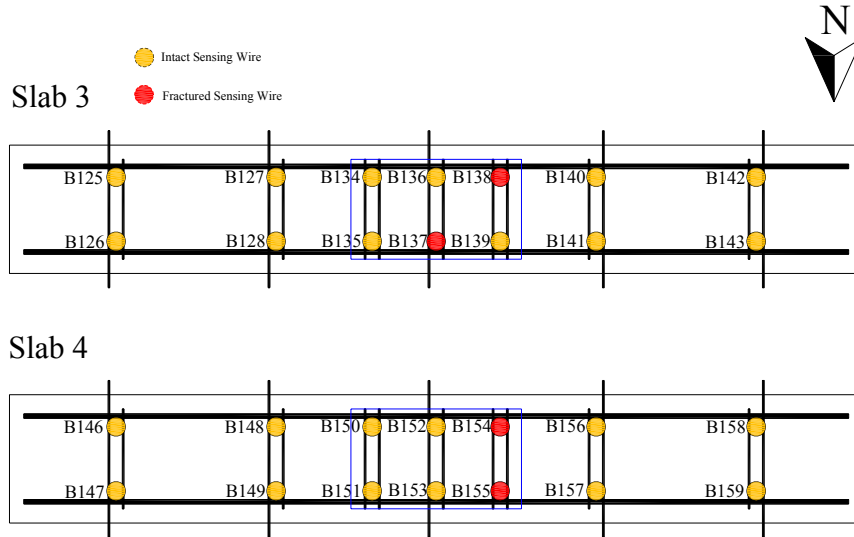


**Figure 5-16** *Detected State of Sensing Wires after 12 Months of Testing*

From Figure 5-16, all the sensors with fractured sensing wires were embedded beneath the salt-water reservoir. This result was in contrast to Slabs 1 and 2. In that case, the sensors in the transition region fractured more readily than sensors beneath the salt-water reservoir. Sensors embedded in the transition region of Slab 4 were less likely to fracture because less moisture and thus chlorides reached the transition areas in Slab 4 than in Slabs 1 and 2. The adhesive used for the salt-water reservoir in Slab 4 happened to form a bond with the concrete of sufficient quality to prevent a significant amount of moisture from reaching the transition areas over the surface of the specimens. Although moisture likely migrated to the transition region through the concrete, the effect of this moisture was likely in general small compared with the effect of moisture traveling along the top surface of the specimen.

In contrast, as in the case of Slabs 1 and 2, moisture from the salt-water reservoir was able to reach the transition areas of the specimen. The adhesive

bond in the case of Slab 3 happened to be of lower quality than in the case of Slab 4, allowing more moisture to reach the transition regions, as in the case of Slabs 1 and 2. Therefore, there is not a readily apparent reason why in Slab 3 the sensing wires in the transition regions fractured less readily. As is discussed in Section 5.3.3, the permeability of Slabs 3 and 4 was likely higher than that of Slabs 1 and 2. Higher permeability, therefore, may have reduced the effect of deaeration on the corrosion rate of steel embedded beneath the salt-water reservoir. That is, higher permeability of Slab 3 allowed oxygen to penetrate the pore structure of the specimen more readily during dry cycles than in the case of Slabs 1 and 2. Therefore, the rate of corrosion beneath the salt-water reservoir was not suppressed compared to the transition region as it likely was in Slabs 1 and 2. The effect of deaeration on corrosion of steel is discussed in Chapter 6.

### **5.3.2 Summary of the Measured Response of the Sensors**

The responses of sensors tested in Slabs 3 and 4 are statistically summarized in Table 5-3 through Table 5-7. In the tables, the resonant frequency is reported as  $f_0$ , the phase dip as  $\phi$ , and the pseudo-quality factor as  $\bar{Q}$ . Two observations can be made about the responses of sensors tested in Slabs 3 and 4. First, the variability of the response of sensors with intact sensing wires was relatively low. The primary cause of this lower variability was likely a decrease in the number of baseline shifts in the data. Greater quality control of the reader coil reduced the number of baseline shifts. Consequently, the curve-fitting algorithm was able to extract the response parameters — resonant frequency, phase dip, and pseudo-quality factor — with less variability.

Second, variability in the response of sensors with fractured sensing wires was relatively high. One possible cause of this result, influence of the internal

environment of the concrete on the response of the sensor, is discussed in Section 5.3.3.

*Table 5-3 Statistical Summary of Sensors with Intact Sensing Wires Tested in Slab 3*

Sensor	Sensing Circuit						Reference Circuit					
	$f_0$ [MHz]	COV [%]	$\phi$ [°]	COV [%]	$\bar{Q}$	COV [%]	$f_0$ [MHz]	COV [%]	$\phi$ [°]	COV [%]	$\bar{Q}$	COV [%]
<b>B125</b>	0.49	0.1	2.4	12.5	8.1	1.1	1.55	0.0	0.9	13.6	38.1	1.6
<b>B126</b>	0.48	0.1	4.3	4.9	9.5	1.4	1.56	0.0	1.0	4.8	37.3	2.4
<b>B127</b>	0.49	0.3	2.5	4.7	8.5	2.4	1.55	0.1	0.7	3.6	36.4	3.3
<b>B128</b>	0.48	0.1	4.6	4.7	10.4	1.5	1.54	0.0	1.1	5.0	37.5	1.9
<b>B134</b>	0.47	0.2	2.9	14.3	8.8	15.3	1.54	0.1	1.0	6.6	35.6	6.7
<b>B135</b>	0.47	0.1	4.3	8.9	10.5	2.1	1.55	0.1	0.9	7.9	36.9	7.7
<b>B136</b>	0.48	0.1	3.3	8.1	9.9	3.3	1.55	0.0	1.1	7.2	37.8	2.9
<b>B139</b>	0.48	0.1	3.1	7.3	9.3	6.2	1.57	0.0	1.1	6.2	37.4	2.5
<b>B140</b>	0.48	0.1	4.1	12.8	9.9	3.7	1.54	0.0	1.4	12.0	40.0	2.2
<b>B141</b>	0.48	0.1	4.0	3.8	10.4	4.0	1.56	0.0	1.2	3.2	39.4	2.8
<b>B142</b>	0.47	0.1	3.8	5.0	9.7	4.1	1.55	0.0	1.1	5.4	36.2	2.6
<b>B143</b>	0.47	0.1	4.1	5.1	10.0	4.0	1.54	0.0	1.0	4.7	38.5	3.1

*Table 5-4 Statistical Summary of Sensors with Intact Sensing Wires Tested in Slab 4 and Control*

Sensor	Sensing Circuit						Reference Circuit					
	$f_0$ [MHz]	COV [%]	$\phi$ [°]	COV [%]	$\bar{Q}$	COV [%]	$f_0$ [MHz]	COV [%]	$\phi$ [°]	COV [%]	$\bar{Q}$	COV [%]
<b>B146</b>	0.49	0.3	3.2	5.0	8.1	3.2	1.54	0.0	1.1	4.3	37.4	2.6
<b>B147</b>	0.48	0.1	4.6	4.0	9.8	1.2	1.55	0.0	1.0	5.3	38.4	2.5
<b>B148</b>	0.47	0.4	4.4	14.5	9.1	9.5	1.55	0.1	1.3	15.0	38.4	6.1
<b>B149</b>	0.48	0.1	3.5	6.6	9.7	1.4	1.56	0.0	1.1	4.7	37.9	2.3
<b>B150</b>	0.47	0.4	3.4	14.6	9.6	5.4	1.56	0.1	1.0	13.3	36.8	4.9
<b>B151</b>	0.48	0.1	3.0	9.0	10.3	3.5	1.56	0.0	1.0	8.1	39.4	3.8
<b>B152</b>	0.47	0.1	3.5	6.9	9.9	1.7	1.55	0.2	1.1	10.7	36.7	12.0
<b>B153</b>	0.47	0.1	2.8	7.9	9.8	2.2	1.56	0.0	0.9	7.4	38.6	4.1
<b>B156</b>	0.48	0.1	4.1	4.9	10.3	1.4	1.55	0.0	1.3	4.9	40.0	2.5
<b>B157</b>	0.47	0.1	3.7	4.3	10.5	1.6	1.52	0.0	1.8	5.7	41.2	2.7
<b>B158</b>	0.48	0.1	3.8	3.9	9.3	1.5	1.56	0.0	1.4	3.4	39.2	2.8
<b>B159</b>	0.48	0.1	3.8	4.8	9.2	1.6	1.53	0.0	1.4	4.3	39.8	2.7
<b>B144</b>	0.48	0.1	3.4	3.7	10.5	1.8	1.56	0.0	1.2	3.3	40.3	2.4



**Table 5-5 Mean Resonant Frequency of Sensors with Fractured Sensing Wires Tested in Slabs 3 and 4**

Sensor	Day of Fracture	Sensing Circuit		Reference Circuit			
		<i>Intact</i>		<i>Intact</i>		<i>Fractured</i>	
		$f_0$ [MHz]	COV [%]	$f_0$ [MHz]	COV [%]	$f_0$ [MHz]	COV [%]
<b>B137</b>	112	0.48	0.1	1.57	0.0	1.42	0.3
<b>B138</b>	184	0.47	0.1	1.56	0.0	1.42	0.2
<b>B154</b>	112	0.48	1.1	1.55	0.3	1.42	0.7
<b>B155</b>	224	0.48	0.1	1.56	0.0	1.43	0.0

**Table 5-6 Mean Phase Dip of Sensors with Fractured Sensing Wires Tested in Slabs 3 and 4**

Sensor	Day of Fracture	Sensing Circuit		Reference Circuit			
		<i>Intact</i>		<i>Intact</i>		<i>Fractured</i>	
		$\phi$ [°]	COV [%]	$\phi$ [°]	COV [%]	$\phi$ [°]	COV [%]
<b>B137</b>	112	3.9	2.5	0.9	3.5	2.9	24.3
<b>B138</b>	184	3.1	5.7	1.1	2.7	2.6	23.1
<b>B154</b>	112	1.4	65.7	0.9	21.6	4.7	59.4
<b>B155</b>	224	3.0	7.9	1.0	1.7	7.0	14.6

**Table 5-7 Mean Pseudo-Quality Factor of Sensors with Fractured Sensing Wires Tested in Slabs 3 and 4**

Sensor	Day of Fracture	Sensing Circuit		Reference Circuit			
		<i>Intact</i>		<i>Intact</i>		<i>Fractured</i>	
		$\bar{Q}$	COV [%]	$\bar{Q}$	COV [%]	$\bar{Q}$	COV [%]
<b>B137</b>	112	10.0	4.4	37.8	2.3	15.9	21.3
<b>B138</b>	184	9.9	4.9	37.4	2.6	15.1	26.3
<b>B154</b>	112	5.3	53.9	29.3	25.1	28.9	61.9
<b>B155</b>	224	10.0	7.0	38.9	2.8	42.1	11.5

### **5.3.3 Effect of Moisture Content of the Concrete on the Response of Sensors with Fractured Sensing Wires**

The response of sensor B155, given in Figure 5-17, illustrates that the internal environment of the concrete likely participated in the response of the sensor. Contour lines were placed at 80°, 82°, 84°, 86°, 87.4°, 88.6°, and 90°. As mentioned in Section 4.3.1, spurious values for the response parameters returned by the curve-fitting algorithm were replaced with inferred values, colored white in the following figures. The conventions for redacting the response of the sensors are discussed in Appendix B. The change in the response of the sensor on day 224 of testing signaled that the sensing wire fractured on that day or a day shortly before it. After the response of the sensor changed, the phase dip and pseudo-quality factor at the reference frequency cycled between higher and lower values. As shown in Figure 5-18, a detail of the response of B155, these cycles correspond with the wet and dry cycles to which the specimen was subjected. Therefore, changes in the response of the reference circuit of the sensor, after the sensing wire had fractured, correlated with changes in the moisture content of the concrete.

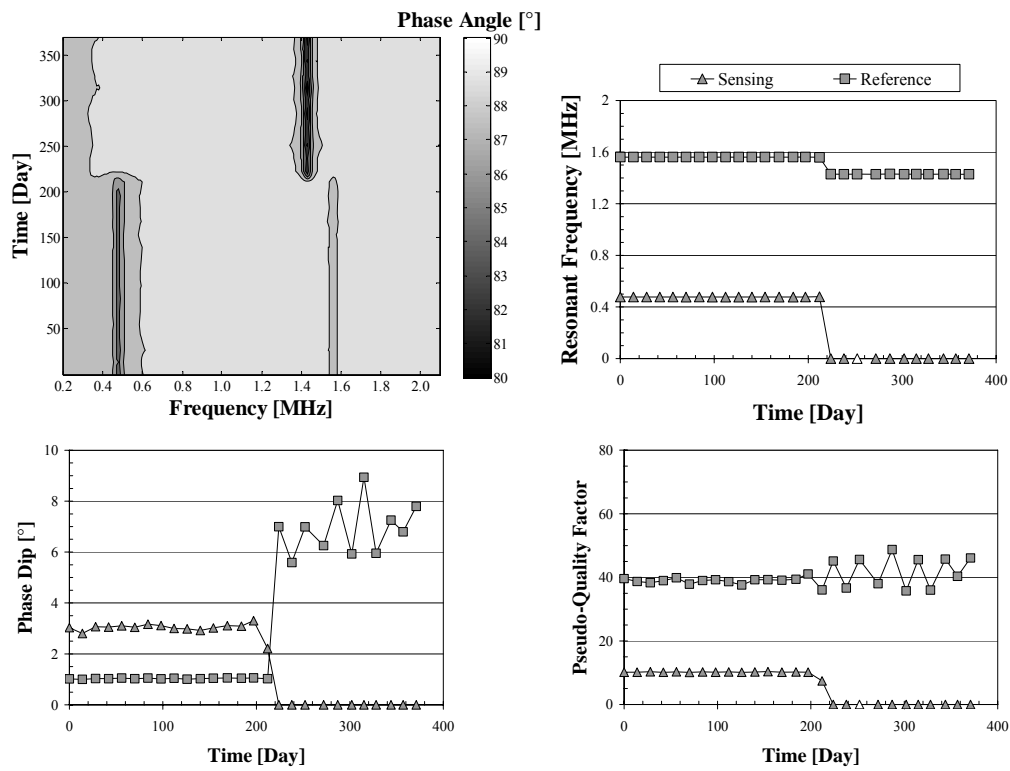


**Figure 5-17 Response of Sensor B155**

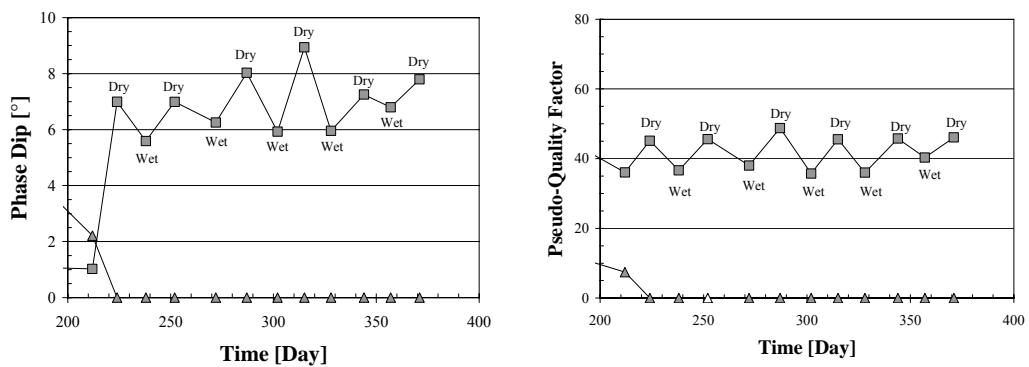


**Figure 5-18 Detail of Response of Sensor B155**

There were two possible causes of the correlation between the response of the reference circuit and the moisture content of Slabs 3 and 4. First, the epoxy housing may have cracked, allowing moisture to reach the surface of the reference

inductor. The amount of moisture on the reference inductor then fluctuated with moisture cycles. This possible cause is discussed thoroughly in Section 7.3.3.

A second possible cause of the correlation between the response of the reference circuit and moisture cycles was moisture in the concrete completing the sensing circuit. However, because water has low conductivity, the completed sensing circuit remained undetectable — there was no discernible phase dip at the sensing frequency — but the completed sensing circuit influenced the reference circuit through mutual inductance. That is, the moisture-completed sensing circuit added to the resistance of the reference circuit by mutual inductance. As a result, when the moisture content of the concrete was higher, after a wet cycle, the phase dip and pseudo-quality factor of the reference circuit were lower. When the moisture content of the concrete was lower, after a dry cycle, the phase dip and pseudo-quality factor of the reference circuit were higher.

The second explanation was supported with the following experiment. The sensing wire of sensor B124, which was not tested in a concrete specimen, was cut. The sensor was interrogated with the fractured sensing wire in air, as shown in the photograph labeled “Dry” in Figure 5-19. The sensors was also interrogated with the end of the fractured sensing wire immersed in a simulated pore solution contaminated by chlorides, as shown in the photograph labeled “Wet” in Figure 5-19. The solution was tap water containing 1% calcium hydroxide and 1 % sodium chloride by weight. The read distance was 1 in., and the results of the interrogations are shown in Figure 5-20. The phase dip and pseudo-quality factor of the reference circuit in the wet conditions were an order of magnitude lower than the values of those parameters in the dry conditions. Therefore, the conditions to which the fractured sensing wire is exposed significantly influence in the response of the reference circuit. The likely means

of this influence is mutual inductance between the inductors of the sensing and reference circuits.

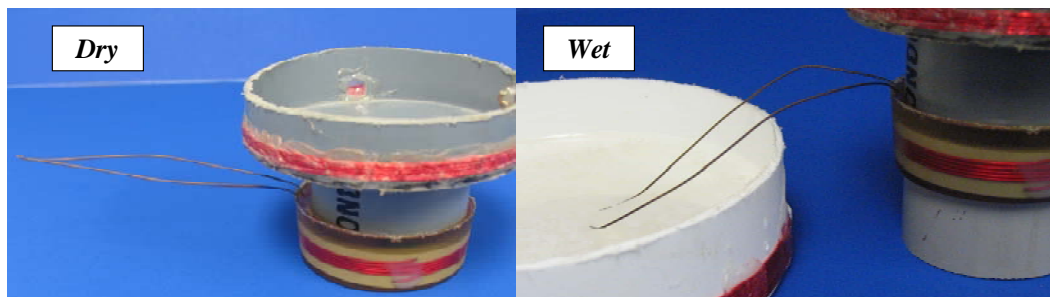


**Figure 5-19 Experiment Showing Effect of Fractured Sensing Circuit on Reference Circuit**

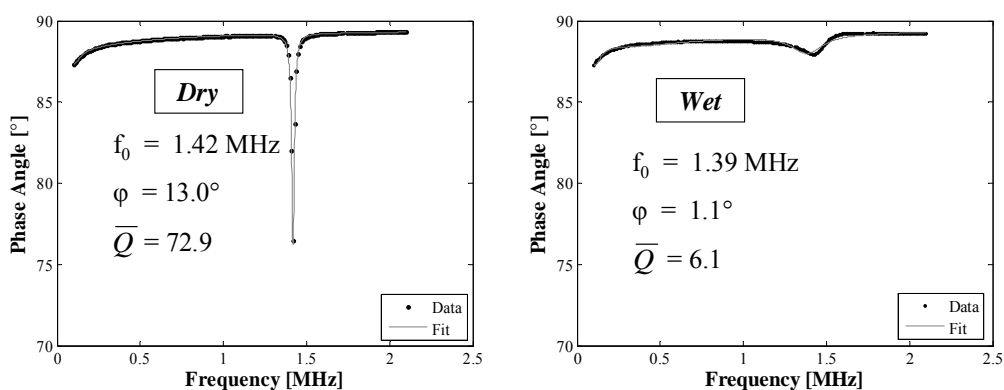


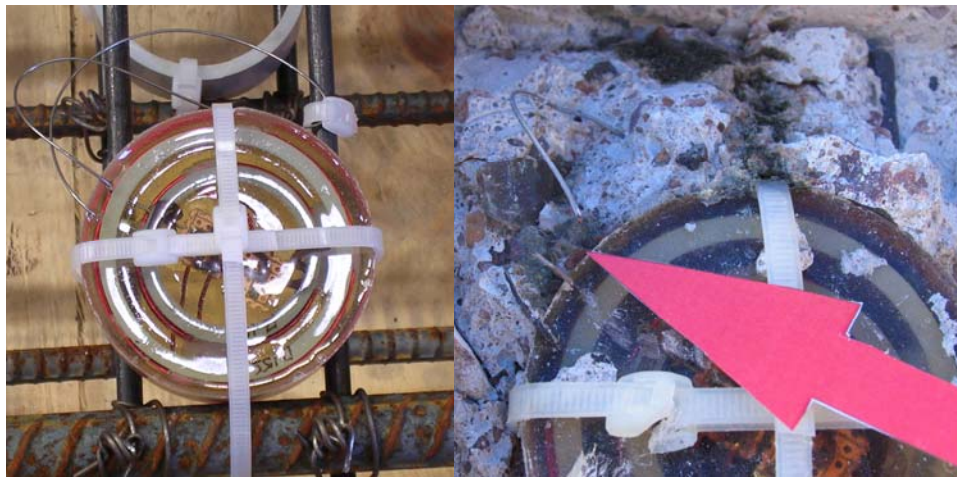
**Figure 5-20 Response of Sensor B124 in Dry and Wet Conditions**

As discussed in Section 3.3.2, the internal environment of the concrete prisms did seem to indirectly influence the response of the sensors. This influence was more pronounced in sensors with fractured sensing wires tested in the reinforced concrete slabs. However, though some correlation between the response of the reference circuit and the moisture cycles of the concrete was observed and in Slabs 1 and 2, the correlation was not as pronounced as in Slabs 3 and 4. In fact, three of the four sensors with fractured sensing wires tested in Slabs 3 and 4 exhibited such a correlation. The cause of this difference between

the response of sensors with fractured sensing wires in Slabs 1 and 2 and Slabs 3 and 4 was likely a difference in the permeability of the concrete.

The permeability of Slabs 3 and 4 was concluded to be higher than that of Slabs 1 and 2 for two reasons. First, Slabs 3 and 4 were subjected to poor curing, which is known from experience to increase the permeability of concrete. In contrast, Slabs 1 and 2 were subjected to moist curing. Second, as is discussed in Section 5.4.3, the rate of chloride penetration into the concrete cover of Slab 4 was high. In fact, much of the concrete cover near and beneath the salt-water reservoir was well above the threshold value for corrosion initiation, after only 12 months of testing. In contrast, the chloride concentration in the concrete covers for Slabs 1 and 2 was well below the threshold value for corrosion initiation, even after 18 months of testing, indicative of a lower permeability. The higher permeability of Slabs 3 and 4 increased the possible volume of moisture per unit volume of concrete in contact with the sensing wires of the sensors. Therefore, the effect of moisture cycles on the response of fractured sensors was more evident in the case of the Slabs 3 and 4 than in the case of Slabs 1 and 2.

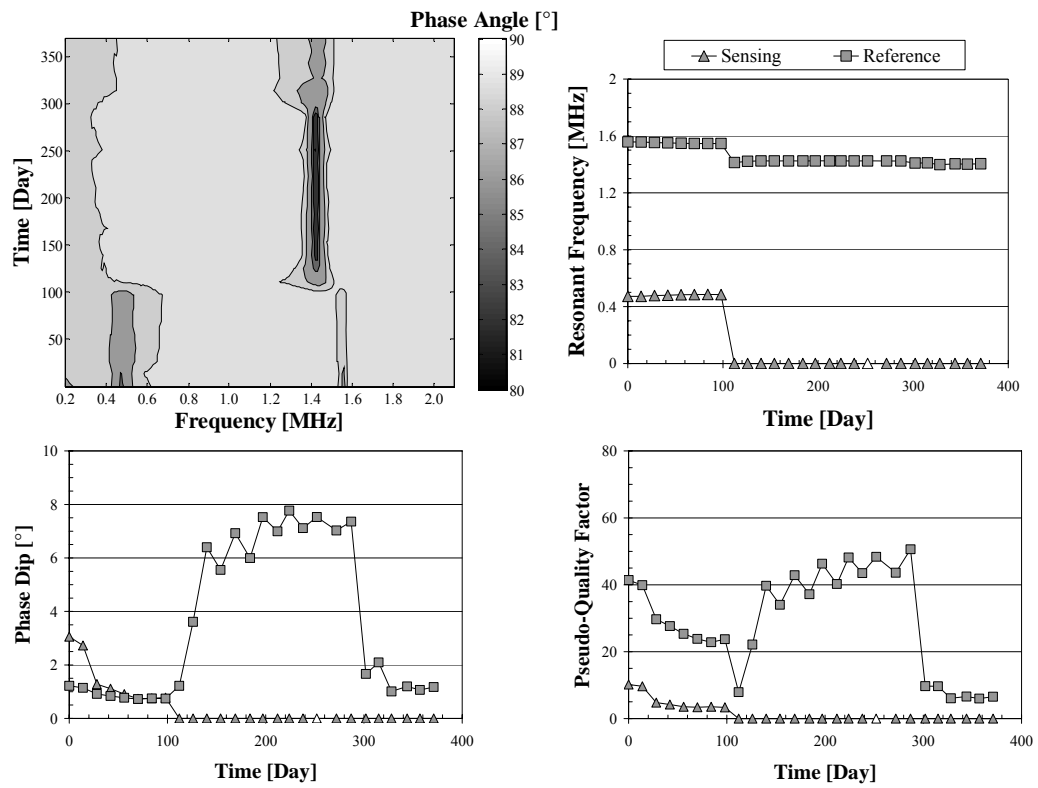
Influence of the internal environment of the concrete on the response of the sensor once its sensing wire had fractured was not more likely for coupled sensors. That is, connecting the sensing wire of sensor to the steel reinforcement did not appear to render the response of the sensor more dependent on the internal environment of the concrete. For example, at the time of autopsy of Slab 4, the portion of the sensing wire of B155 that was connected to the steel reinforcement showed no evidence of corrosion. Rather, the fracture in the sensing wire occurred elsewhere along its length. Therefore, the reinforcement was not completing the sensing circuit; moisture elsewhere along the length of the sensing wire likely was. Figure 5-21 shows how the sensing wire of B155 was secured to the reinforcement and where the sensing wire fractured.



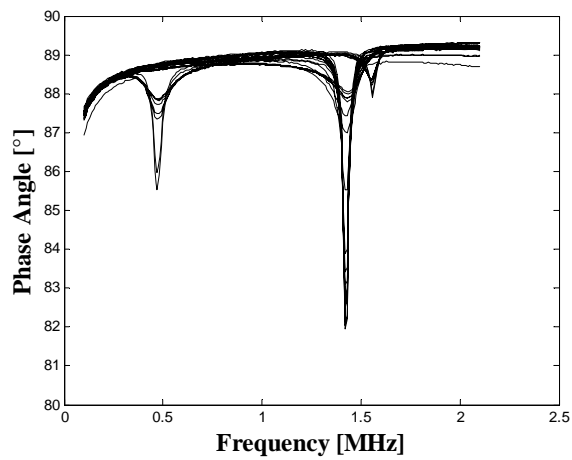
***Figure 5-21 Fracture in the Sensing Wire of B155***

The response of sensor B154 exhibited the same environmental dependence as sensor B155, but eventually the response of the reference circuit became constant. This result is shown in Figure 5-22. Contour lines were placed at  $80^\circ$ ,  $82^\circ$ ,  $84^\circ$ ,  $86^\circ$ ,  $88.1^\circ$ ,  $88.6^\circ$ , and  $90^\circ$ . The cause of this development cannot be known with certainty. However, one possible cause was that the concrete around B154 became saturated such that the effect of the wet and dry cycles ceased to influence the response of the reference circuit. Thereafter, the phase dip and pseudo-quality factor of the reference circuit remained small because the response of the reference circuit was masked by the moisture-completed sensing circuit. Another possibility is that the reference circuit decayed due to internal black corrosion, which is discussed in Chapter 6. The response of sensor B154 in the plane of phase angle and frequency is shown in Figure 5-23.





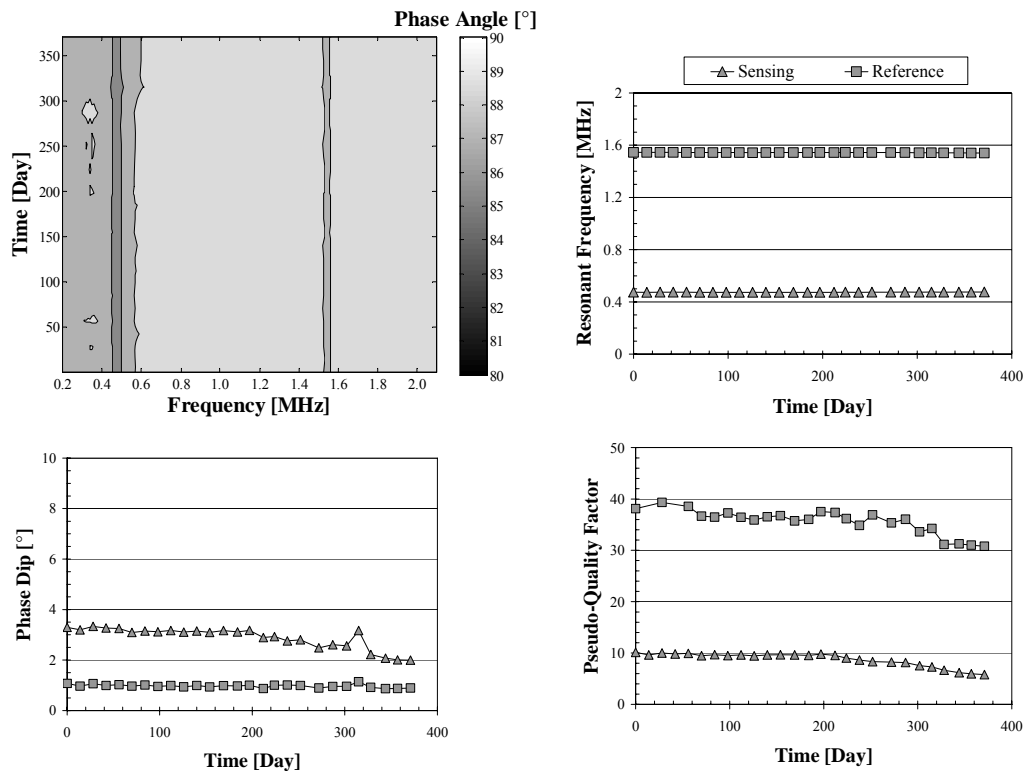
**Figure 5-22 Response of Sensor B154**



**Figure 5-23 Response of Sensor B154 in Plane of Phase Angle and Frequency**

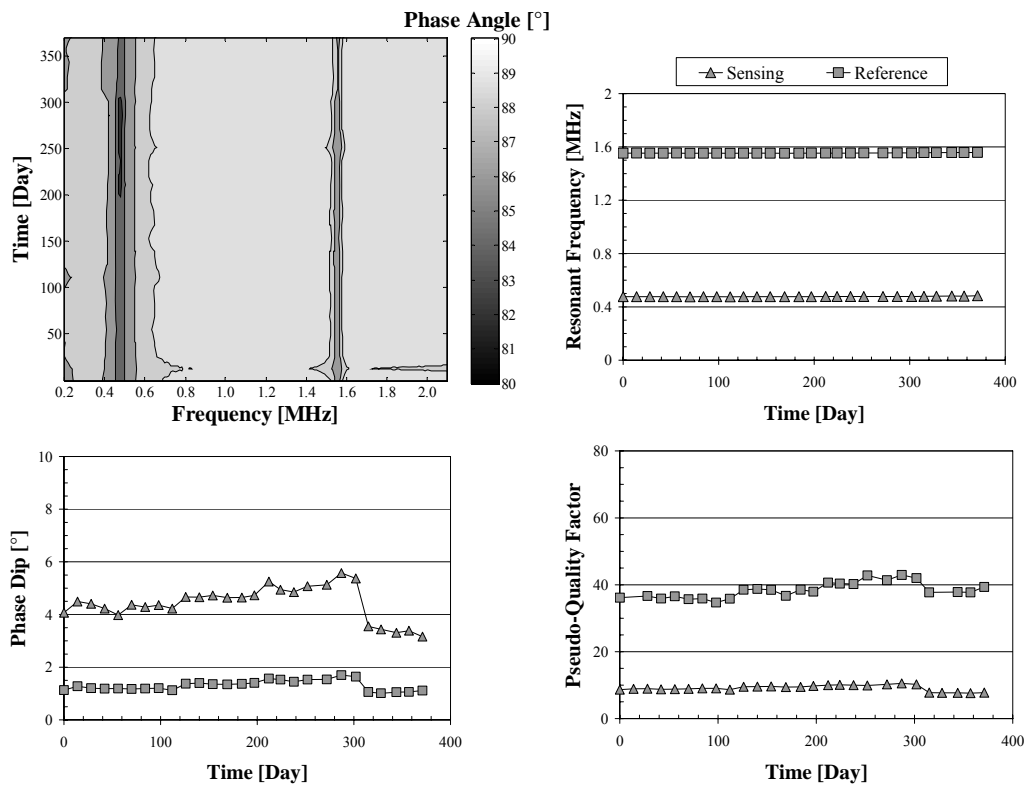
### **5.3.4 Possible Instances of Uniform Corrosion of the Sensing Wire**

Figure 5-17 shows that prior to the sensing wire of B155 fracturing, the phase dip and the pseudo-quality factor of the sensing circuit decreased gradually. Through mutual inductance of the sensing and reference circuits, the phase dip and pseudo-quality factor of the reference circuit decreased gradually in a similar way. The response of sensor B134, shown in Figure 5-24, exhibited a more lengthy gradual decrease in its phase dips and pseudo-quality factors. The lines of the contour plot were placed at  $80^\circ$ ,  $84^\circ$ ,  $85^\circ$ ,  $87^\circ$ ,  $88.5^\circ$ , and  $90^\circ$ . This gradual decrease in phase dip and pseudo-quality factor is possibly a result of uniform corrosion of the sensing wire. Specifically, if uniform corrosion is taking place, the sensing wire gradually loses cross section, increasing the resistance of the sensing circuit. This increase in resistance causes a decrease in the phase dip and pseudo-quality factor of the sensing circuit. Through mutual inductance, there is an accompanying decrease in the phase dip and pseudo-quality factor of the reference circuit. A shift in the resonant frequency of the reference circuit does not take place until the sensing wire fully fractures.



**Figure 5-24 Response of Sensor B134**

Because Slab 3 has yet to be autopsied and B134 was cast in Slab 3, it was not possible to confirm uniform corrosion along the sensing wire of B134. The response of sensor B148 also exhibited a decrease in phase dips and pseudo-quality factors without the sensing wire fracturing, although the decrease was less gradual than in the case of B134. The response of sensor B148 is shown in Figure 5-25. Contour lines were placed at the same values of phase angle as in the case of B154. After day 300 of testing, there is a decrease in the phase dips and pseudo-quality factors of both the circuits composing B148. At the time of autopsy, a segment of fairly uniform corrosion was observed on the sensing wire of B148, as shown in Figure 5-26. Therefore, the response of sensor B148, which includes a change in the phase dips and pseudo-quality factors of the circuits, corresponded with somewhat uniform corrosion of the sensing wire.



**Figure 5-25 Response of Sensor B148**

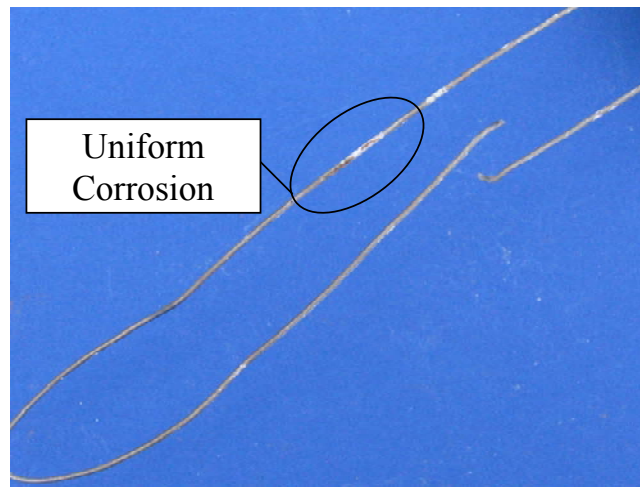


**Figure 5-26 Uniform Corrosion on a Segment of the Sensing Wire of B148**

The possibility of uniform corrosion of sensing wires in high-permeability concrete introduces the possibility of extracting information about the rate of corrosion within a reinforced concrete structure. It is theoretically possible to relate the gradual reduction in the pseudo-quality factor of a circuit, observed in the case of B134, to the resistance and thereby cross section of the sensing wire. In that case, a penetration rate of corrosion into the sensing wire might be obtained. However, because uniform corrosion was rare even in Slabs 3 and 4, which had likely had concrete with relatively high permeability, general applicability of such a procedure is likely impractical. An additional complication to extracting analog information from the sensors is the fact that temperature, moisture content of the concrete, and misalignment of the reader coil can introduce variability into the response of the sensor. However, the most significant difficulty is that interrogation of the sensor would, in practice, be infrequent. Consequently, slight changes in the response of the sensors would likely be undetected.

### **5.3.5 Deterioration of the Reference Circuit due to Black Corrosion within the Epoxy Housing**

Figure 5-27 is the response of sensor B152. Contour lines were placed at the same values of phase angle as in the case of B154 above. What is apparent from the response of B152 is that the phase dip at the reference frequency decreased over time. The decay of the reference circuit is especially evident in the plot of the pseudo-quality factor with respect to time. In contrast to the situation in Section 5.3.4, this decrease in the phase dip at the reference frequency was not accompanied with significant change in the phase dip at the sensing frequency. Rather, the quality of the reference circuit was decaying independently of the sensing circuit.

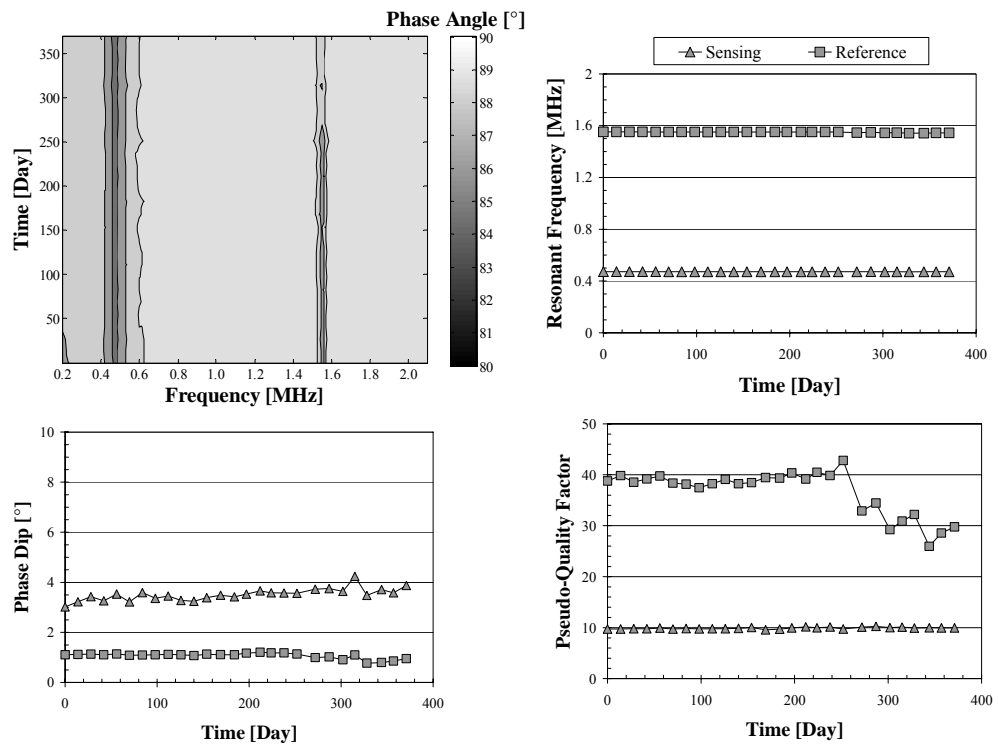


**Figure 5-27 Response of Sensor B152**

When Slab 4 was autopsied, large amounts of black corrosion were observed within the epoxy housing of B152. As shown in Figure 5-28, cracks developed in the epoxy housing of the sensor, likely exposing the circuitry to corrosive agents. This exposure lead to a decay of the circuitry, which was reflected in the response of the sensor.



***Figure 5-28 Cracking of Epoxy Housing of B152***

The development of black corrosion is likely the cause of the phase dip at the reference frequency disappearing in the case of other sensors. For example, as shown in Figure 5-29, the phase dip at the reference frequency of B135 nearly ceased to exist. Contour lines were placed at phase angle values of 80°, 82°, 84°, 86°, 88°, 88.5°, and 90°. Data were included in the response of B135 that has been taken since the end of 12 months of testing because deterioration of the reference circuit became noticeable after 12 months of testing. From Figure 5-29, the phase dip at the reference frequency has nearly disappeared; there is, however, little change in the response of the sensing circuit. That the cause was internal black corrosion within the epoxy housing cannot be confirmed because Slab 3 was not autopsied.

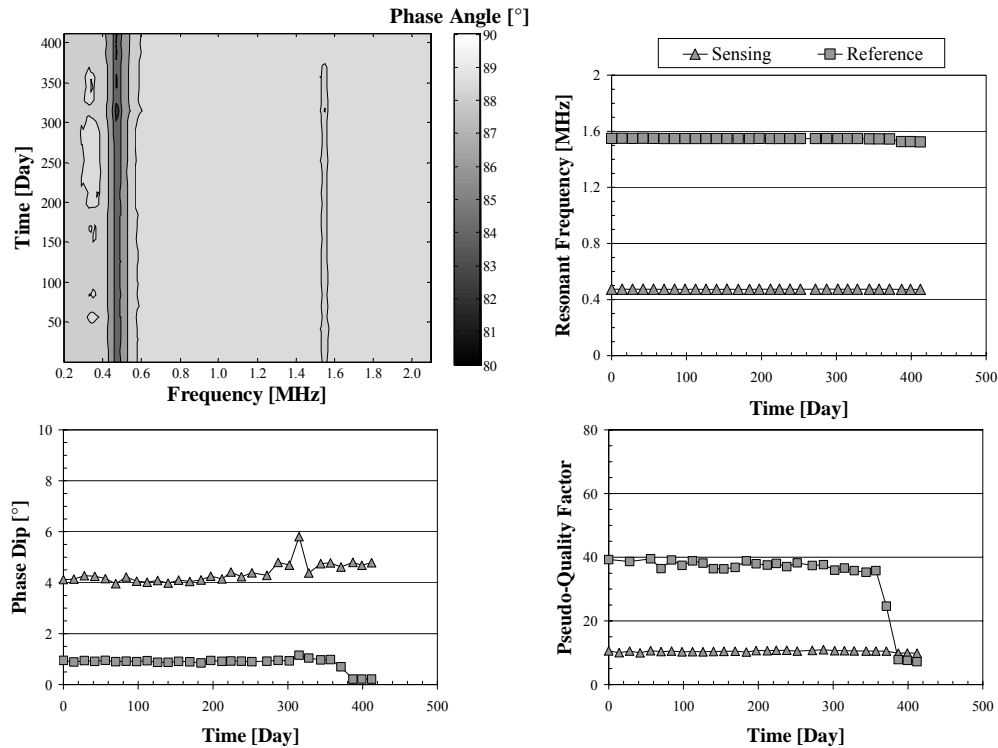


*Figure 5-29 Response of Sensor B135*

### 5.3.6 Dependence of the Response of the Sensors on the Internal Temperature of the Concrete

Another source of variability in the response of the sensors was the internal temperature of the concrete. This dependence was expected because the resistance, inductance, and capacitance of the RLC circuits composing the corrosion sensors are dependent on temperature. Therefore, a change in temperature causes a change in the physical parameters of the circuits, which is manifested as a change in the response of the circuits.



The dependence of the sensors on the internal temperature of the concrete was assessed by plotting the response parameters — resonant frequency, phase dip, and pseudo-quality factor — of sensors subjected to control conditions with respect to time. The response parameters of both the sensing and reference circuits were examined. Sensors subjected to control conditions were those embedded at either end of both slabs — B125, B126, B142, B143, B146, B147, B158, B159 — and the sensor embedded in the control specimen, B144. The temperature of each sensor was taken to be the temperature measured by the thermocouple nearest the sensor. A linear relationship between the response parameters and temperature was assumed and the square of the Pearson product moment correlation coefficient,  $R^2$ , was calculated for both the sensing and reference circuits of each control sensor. Figure 5-30 through Figure 5-32 show the response parameters of B159 plotted with respect to temperature and the corresponding  $R^2$  values as an example. The resulting  $R^2$  values for all the control sensors are shown in Table 5-8, where  $f_0$  refers to the resonant frequency,  $\phi$  refers to the phase dip, and  $\bar{Q}$  refers to the pseudo-quality factor.

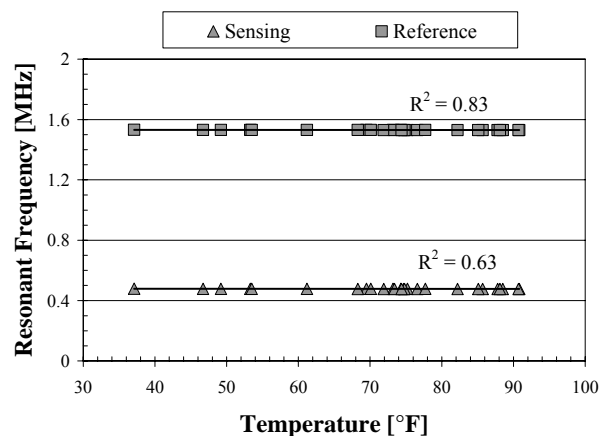


**Figure 5-30 Resonant Frequency of B159 with Respect to Temperature**

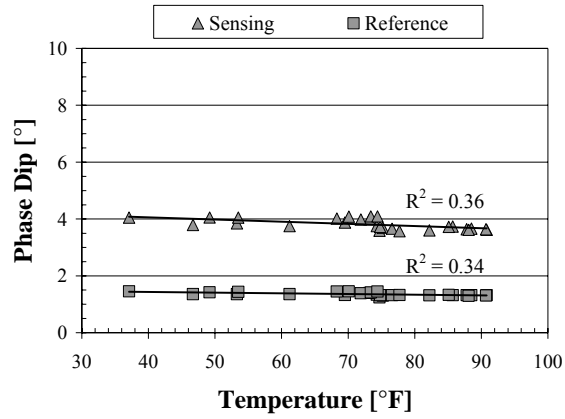


**Figure 5-31 Phase Dip of B159 with Respect to Temperature**

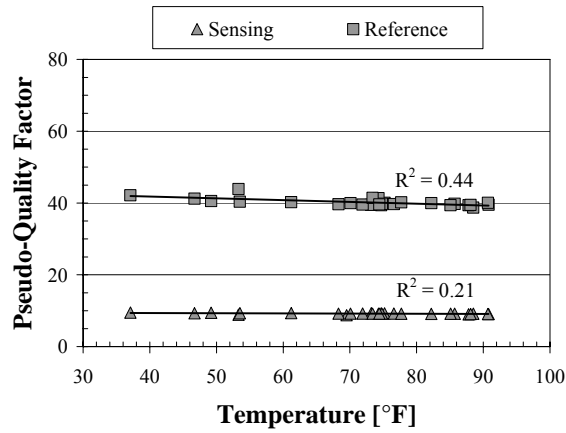


**Figure 5-32 Pseudo-Quality Factor of B159 with Respect to Temperature**

**Table 5-8  $R^2$  Values for the Response Parameters of Control Sensors with Respect to Temperature**

Sensor	Sensing Circuit			Reference Circuit		
	$f_0$	$\varphi$	$\bar{Q}$	$f_0$	$\varphi$	$\bar{Q}$
<b>B125</b>	0.50	0.02	0.47	0.79	0.02	0.08
<b>B126</b>	0.78	0.36	0.94	0.39	0.44	0.01
<b>B142</b>	0.87	0.31	0.20	0.40	0.35	0.25
<b>B143</b>	0.87	0.31	0.24	0.30	0.40	0.13
<b>B144</b>	0.86	0.35	0.76	0.79	0.39	0.17
<b>B146</b>	0.00	0.10	0.03	0.19	0.17	0.22
<b>B147</b>	0.43	0.35	0.27	0.37	0.22	0.23
<b>B158</b>	0.56	0.50	0.35	0.75	0.40	0.38
<b>B159</b>	0.63	0.36	0.21	0.83	0.34	0.44

Except for the case of sensor B146, there seems to be some correlation between resonant frequency and temperature. The correlations between phase dip and temperature and pseudo-quality factor and temperature are less pronounced. Despite the fact that there is some correlation between the response parameters and temperature, the dependence of the response parameters on temperature is weak. That is, for any given change in temperature, the change in the response parameters is small. Therefore, the effect of temperature on the response a given corrosion sensors can be neglected in practice. The property that the response parameters change with temperature could potentially be exploited for other applications. For a discussion of such applications, see Andringa (2006).

As shown in Figure 5-33, the internal temperature of Slabs 3 and 4, at all points where thermocouples were embedded, correlated closely with the

temperature of the air in which the specimens were stored. On a given day, there was a 2 to 3 degree variation in thermocouple readings. Therefore, determination of the dependence of sensor response on air temperature would have provided a reasonable approximation of the dependence of sensor response on the internal temperature of the concrete.

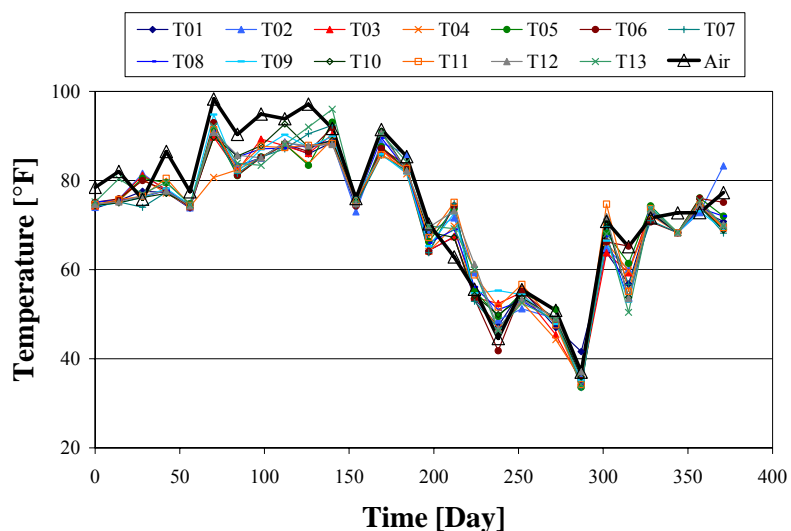


*Figure 5-33 Internal Temperature of the Concrete and Air Temperature*

#### 5.4 COMPARISON OF SENSOR RESPONSE WITH OTHER INDICATORS OF CORROSION

After 371 days of testing, Slab 4 was autopsied and the state of the sensors and condition of the steel reinforcement were documented. Slab 4 was presumed to be in an advanced state of corrosion because corrosion products were visible on the surface of the concrete. Figure 5-34 is a photograph of the north face of Slab 4, beneath the salt-water reservoir. In all cases for sensors embedded in Slab 4, the observed state of the sensing wire was consistent with the state of the sensing wire detected during testing. That is, B154 and B155 signaled that their sensing

wires had fractured, and the wires had fractured. The remaining sensors signaled that their sensing wires were intact, and their wires were observed to be intact. Therefore, the sensors reliably signaled the state of their sensing wires.

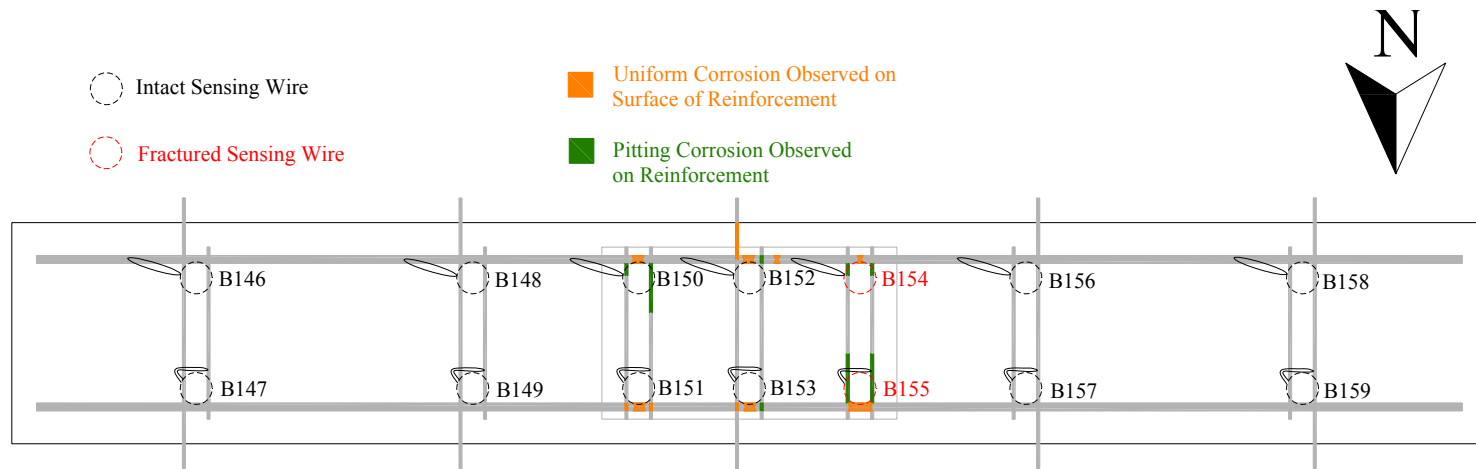


***Figure 5-34 External Corrosion on the North Face of Slab 4***

Because Slab 4 was autopsied, the reliability of its sensors at detecting the initiation of corrosion of the steel reinforcement could be assessed relative the condition of the reinforcement itself. The reliability of sensors tested in Slab 4 in this respect is discussed in Section 5.4.1. Measurements of half-cell potentials and chloride concentration of the concrete cover of Slab 4 provided a secondary basis for assessment of the signals of the sensors. The signals of sensors tested in Slab 3 could only be compared to half-cell potentials because the testing of Slab 3 is ongoing. Section 5.4.2 compares the signals of the sensors to the half-cell potentials of the specimens. Section 5.4.3 assesses the degree of consistency between the conclusions drawn from the signals of sensors tested in Slab 4 and the chloride concentration of the concrete cover of Slab 4. Finally, the effect of crack path on the reliability of the sensors at detecting the initiation of corrosion is discussed in Section 5.4.4.

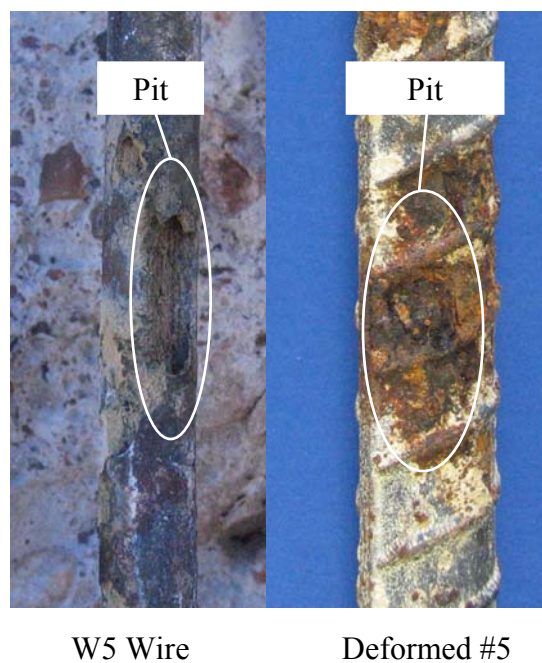
#### **5.4.1 Observed Condition of Steel Reinforcement**

Figure 5-35 illustrates the extent of corrosion on the steel reinforcement of Slab 4. The positions of the sensors, and their sensing wires, are superimposed over a plan view of the specimens. In Figure 5-35, sensors with fractured sensing wires at the conclusion of testing are labeled in red, while those with intact sensing wires are labeled in black. Relatively uniform corrosion is colored orange, while pitting corrosion is colored green. Despite this color scheme for the corrosion, the corrosion tended to be darker in color due to deaeration of the concrete beneath the salt-water reservoir. The effect of deaeration on corroding steel is discussed in Chapter 6.



**Figure 5-35 Extent of Corrosion on Reinforcement on the Top Layer of Steel of Slab 4**

Most corrosion was observed to be on the transverse reinforcement. Pitting corrosion in particular was observed almost solely on the transverse reinforcement, where the transverse reinforcement was in contact with the longitudinal reinforcement. A few pits were observed on the longitudinal reinforcement, where it contacted the transverse reinforcement. A photograph of pitting corrosion on the transverse reinforcement (W5 wire) and longitudinal reinforcement (deformed #5 bar) is shown in Figure 5-36. The transverse reinforcement corroded preferentially because it was cold-drawn. The results of a tensile test of the transverse reinforcement are shown in Figure 5-37. Three characteristics of the response — yield strength between 60 and 70 ksi, lack of a yield plateau, and little strain hardening — are characteristic of cold-drawn steel.



***Figure 5-36 Pits on Transverse and Longitudinal Reinforcement***



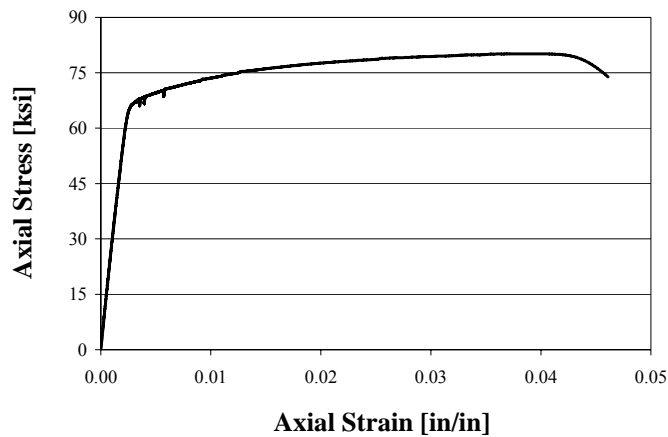


***Figure 5-37 Tensile Test of W5 Wire Transverse Reinforcement***

The condition of the reinforcement was compared to the signals of the sensors. The distribution of signals is shown in Table 5-9. The existence of false negatives was due to chlorides reaching the reinforcement adjacent to the sensor without reaching the sensing wire of the sensor. Indeed, the sensing wires of B151, B152, and B153 were positioned in such a way that reinforcement immediately adjacent to the sensor corroded without the sensing wires corroding. The implication is that the tributary area of the reinforcement over which the coupled sensors detect initiation of corrosion is small. That is, the parameter  $d$ , illustrated in Figure 2-21 and discussed in Section 2.4.2, is less than a few inches for the coupled sensors. In fact, the coupled sensors functioned similarly to isolated sensors: they detected corrosion only at the location of their sensing wires. Had the testing of Slab 4 continued for a longer period of time, several of the sensors that signaled false negatives likely would have begun signaling the initiation of corrosion. However, the fact remains that connecting the steel sensing wire of the sensors to the steel reinforcement fails to increase the area over which initiation of corrosion is detected.

**Table 5-9 Reliability of Sensors Tested in Slab 4 with respect to the Observed Condition of the Steel Reinforcement**

		Observed State of Reinforcement	
		No Corrosion	Corrosion
Detected State of Reinforcement	Corrosion	0 (False Positive)	2
	No Corrosion	8	4 (False Negative)

The presence of cold-worked steel in the specimens did not prevent the sensing wires of the sensors from corroding. By corroding preferentially to hot-rolled steel, the transverse reinforcement likely did serve as a sacrificial anode to the longitudinal steel. However, the sensing wire itself is cold-drawn. Furthermore, the sensing wire is subjected to cold-working during fabrication of the sensor. Therefore, the transverse reinforcement could not have corroded preferentially to the sensing wire. It is possible that the cold-worked transverse reinforcement decreased the tributary area of the coupled sensors. By restricting the anode of the specimen to smaller area than would have become anodic had the transverse reinforcement not been embedded in the specimen, the transverse reinforcement could have made participation of the sensing wire in the anode less likely. This effect, however, is arguably small. Therefore, the small tributary area of the coupled sensors was intrinsic to their design. This tributary area was essentially zero because the distance over which the sensing wire electrically participated in the anode of the structure was essentially zero.

### 5.4.2 Half-Cell Potentials

The half-cell potentials of Slabs 3 and 4 were obtained with a standard calomel electrode (SCE), in millivolts, and were converted to the scale of the copper-copper-sulfate electrode (CSE) to assess the risk of corrosion in terms of ASTM C876. The primary factor in determining the potential at a given point on the surface of the specimens was the distance from the salt-water reservoir. Therefore, the half-cell potential at points equidistant from the center of the salt-water reservoir were averaged and presented as a single data series, plotted with respect to time. In terms of Figure 5-14, half-cell potentials at locations 1, 2, 3, 25, 26, and 27, when plotted with respect to time, were the data series 45". Ranges of corrosion risk, mentioned in Section 4.4.2, are included in the plots. These plots of the half-cell potential of Slabs 3 and 4 are given in Figure 5-38 and Figure 5-39. The days for which only the center resistor of Slab 3 and the days for which all the resistors of Slab 3 were attached are identified in Figure 5-38.

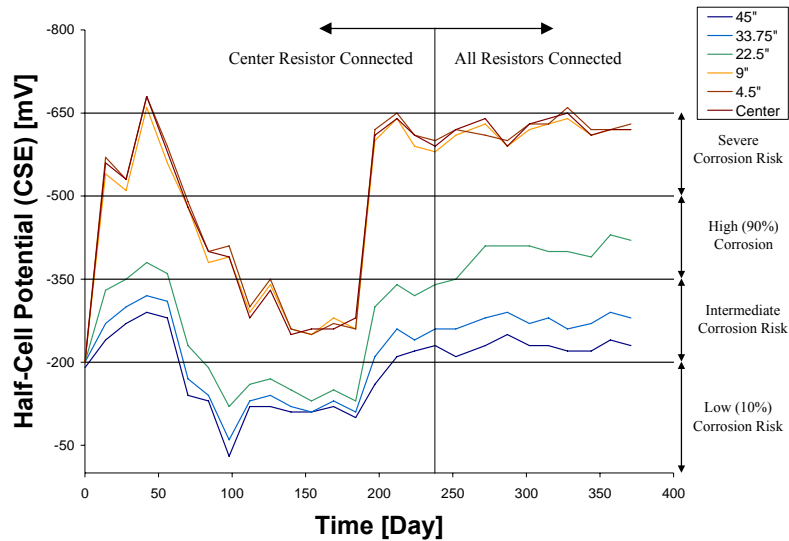
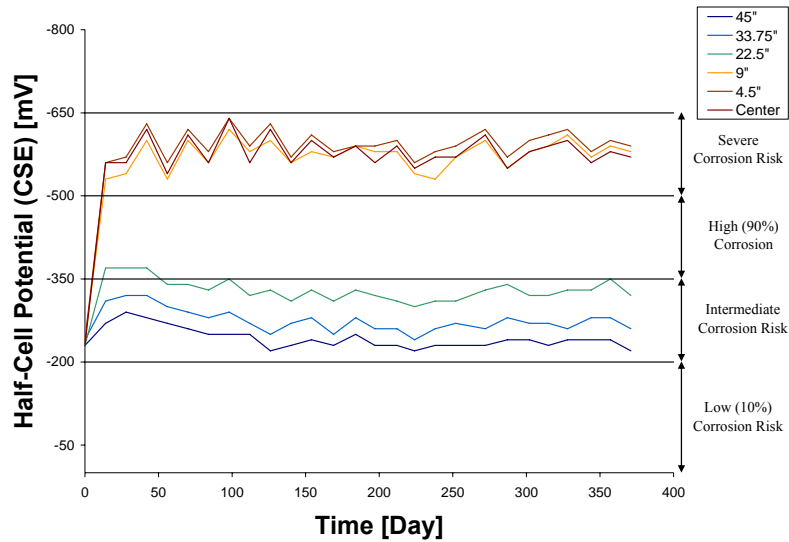


Figure 5-38 Half-Cell Potentials of Slab 3 with Respect to Time



**Figure 5-39 Half-Cell Potentials of Slab 4 with Respect to Time**

The half-cell potentials of Slab 4 were similar to those of Slabs 1 and 2, discussed in Section 4.4.2. Potentials in the salt-water reservoir were quite negative, indicative of severe risk of corrosion, while potentials outside the reservoir, including the transition regions, indicated intermediate risk of corrosion. In Slabs 1 and 2, the transition areas did eventually reach a high risk of corrosion.

The half-cell potentials of Slab 3 were more irregular. The area within the salt-water reservoir reached values of severe corrosion risk initially but soon decreased to values of intermediate corrosion risk, only to return to values of severe corrosion risk. The areas outside of the salt-water reservoir exhibited similar behavior, changing from values of intermediate to low to intermediate corrosion risk. The transition areas of Slab 3, data series 22.5", did reach values of high corrosion risk, in contrast to Slab 4. This wide variation in potentials is

apparently independent of the number of resistors connected because the potential returned to the higher values of corrosion risk prior to all five of the resistors being connected.

The cause of the wide variation in the potentials of Slab 3 is unclear. The facts that the longitudinal steel reinforcement was pre-corroded and that the exact paths of cracks were unpredictable contributed uncertainty to any conclusions that could be drawn about the causes of variability in the half-cell potentials of Slab 3. One suggested cause was that a transient anode developed on the bottom layer of the reinforcement. When Slab 4 was autopsied, corrosion was observed on the bottom layer of the reinforcement, indicating that chlorides were able to reach the bottom layer of steel. There is a possibility, therefore, that an anode developed early in testing on the bottom layer of reinforcement of Slab 3. However, current measurements did indicate that negatively-charged ions flowed from the top layer of reinforcement to the bottom throughout testing. That is, the top layer of reinforcement remained the anode throughout testing. The current measured over the resistors in Slab 3 with respect to time is shown in Figure 5-40. The current varied in magnitude, but at no point did it change direction.

The current circulating in Slabs 3 and 4, shown respectively in Figure 5-40 and Figure 5-41, was characterized in three data series — current 45” from the center of the salt-water reservoir, 22.5” from the center, and at the center. As in the case of half-cell potentials, these data series were obtained by averaging values of current equidistant from the center of the salt-water reservoir. However, only one line is distinctly visible in Figure 5-40 and Figure 5-41. This result was due to the fact that current passing through the five resistors was equal. The direction of the current remained the same throughout testing in the case of both specimens. Specifically, negatively-charged ions flowed from the top of the specimens to the bottom of the specimens throughout testing, indicative of the top

being anodic to the bottom. The current passing between the top and bottom layers of the control specimen is also included in Figure 5-40 and Figure 5-41. The values of current in the control were so small that they were almost undetectable. Therefore, the contribution of the atmosphere to the internal corrosion of Slabs 3 and 4 was likely negligible.

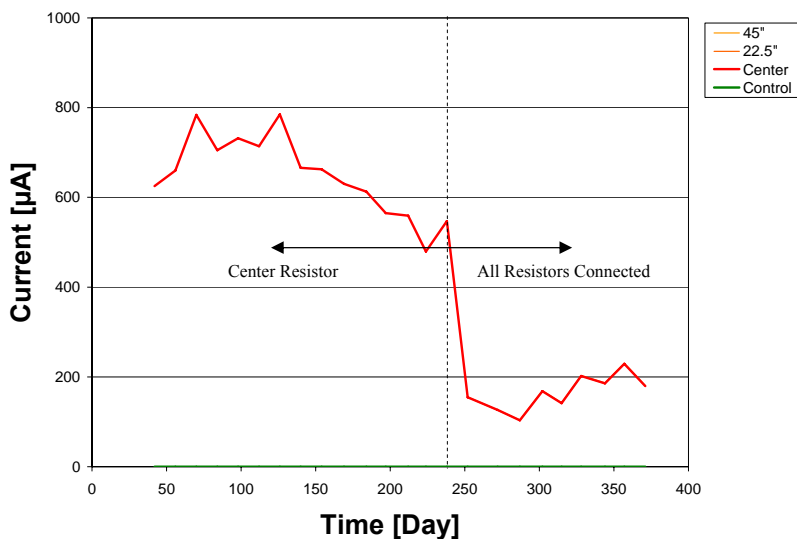


**Figure 5-40** *Current in Slab 3 with Respect to Time*

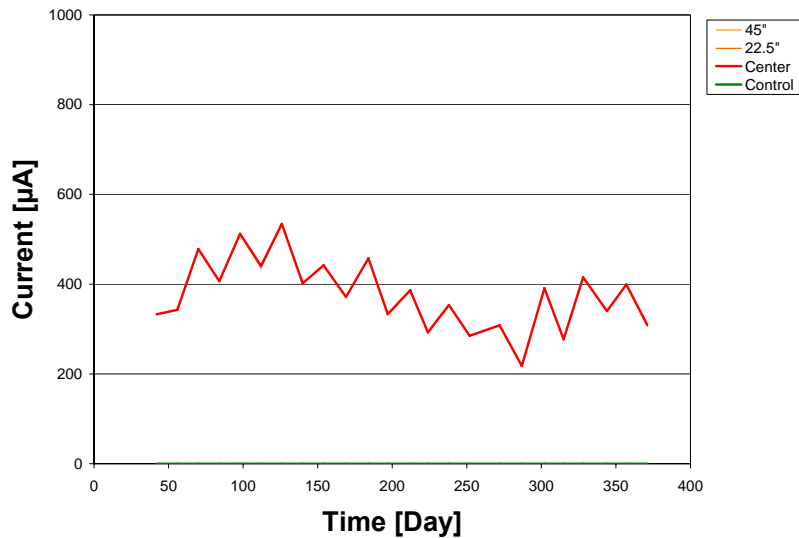


**Figure 5-41 Current in Slab 4 with Respect to Time**

Figure 5-38 and Figure 5-39 show that the half-cell potentials of Slabs 3 and 4 converged to distinct values with time. In contrast to Slabs 1 and 2, the distinct values were not distinctly associated with the wet and dry environmental cycles. Therefore, the signals of the sensors were only compared with the final values of half-cell potential. Figure 5-42 and Figure 5-43 show the distribution of half-cell potentials in Slabs 3 and 4, respectively, as contour plots. The contour plots were developed by linearly interpolating among the measured values of half-cell potential. In order for positions at which measurements were taken to correspond with an equal spacing of the gridlines, the initial gridline in the longitudinal direction at either end was placed 1.5 in. from the end, while all interior gridlines were spaced a regular 2.25 in. apart. In the transverse direction, the spacing of the gridlines was 3 in.

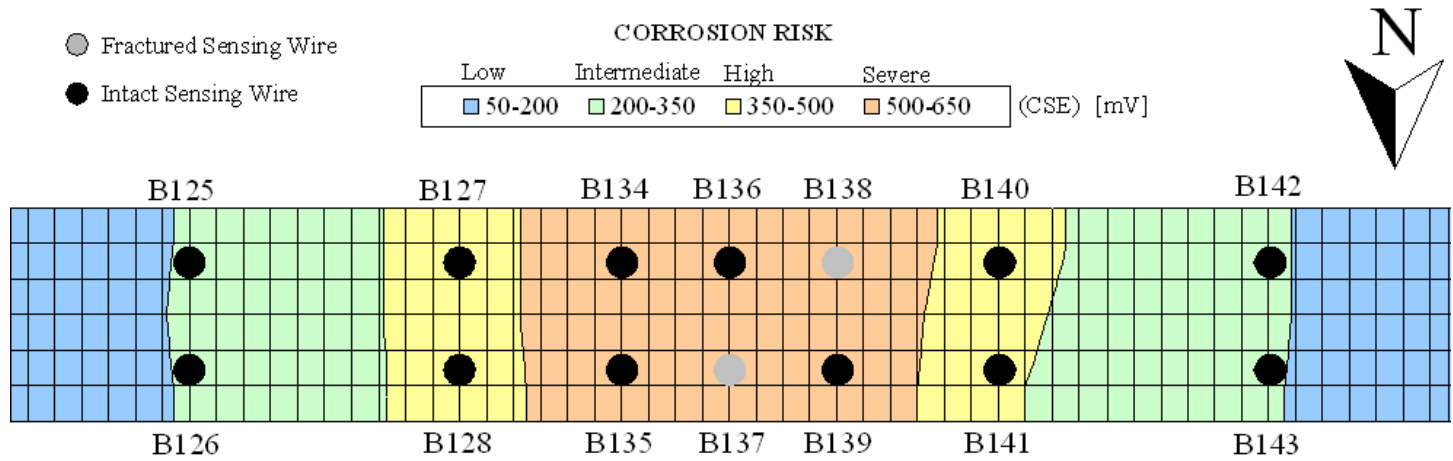


*Figure 5-42 Slab 3 Half-Cell Potential Distribution at the End of 12 Months of Testing*

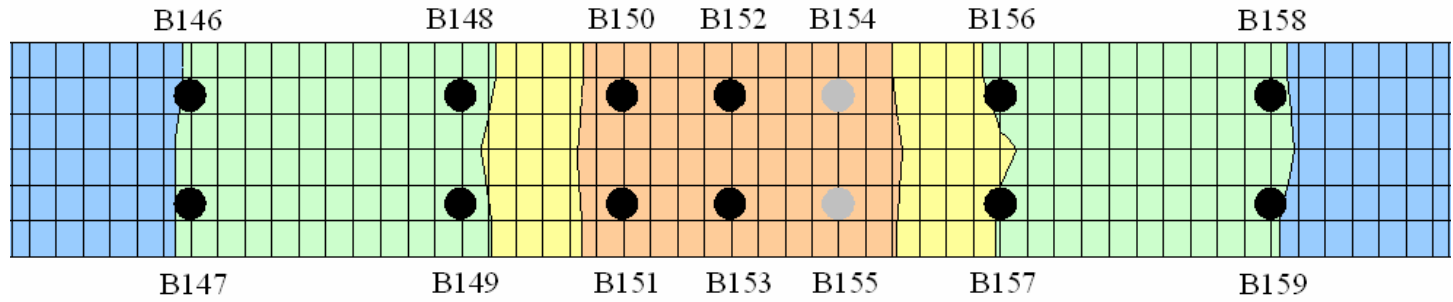


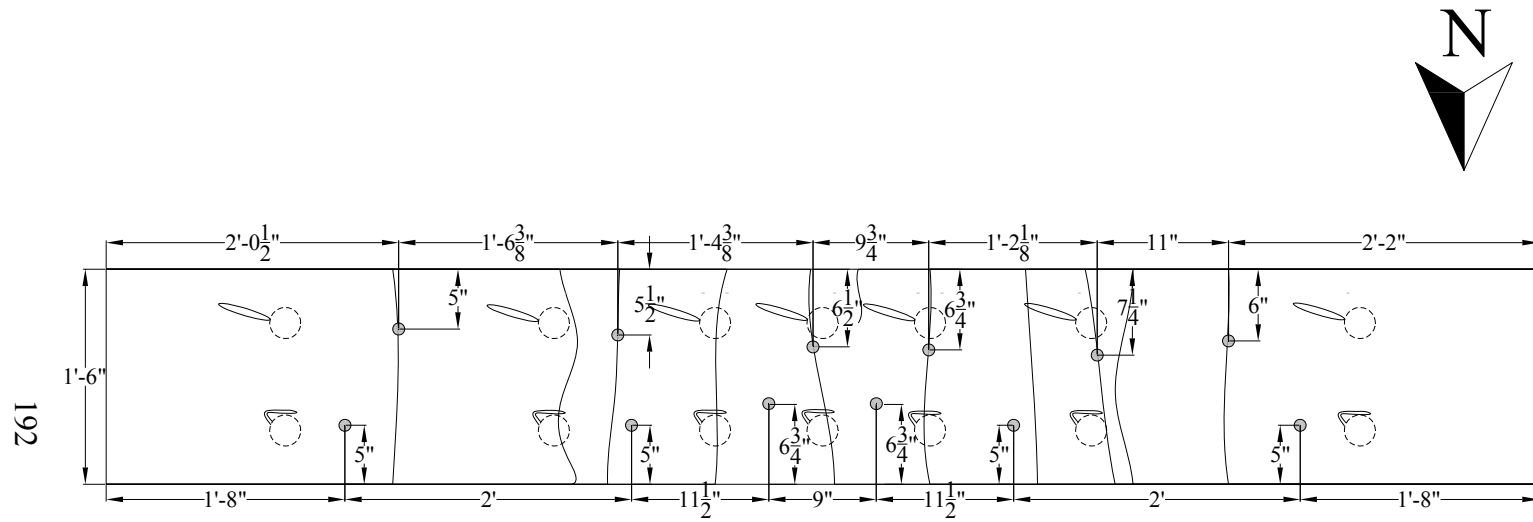
*Figure 5-43 Slab 4 Half-Cell Potential Distribution at the End of 12 Months of Testing*



In both Slabs 3 and 4, the correlation between the signals of the sensors and the indications of the half-cell potentials is weak. Two of the ten sensors in regions of high to severe corrosion risk in Slab 3 signaled the initiation of corrosion. In Slab 4, two of the six sensors located in regions of high to severe risk of corrosion signaled the initiation of corrosion. The duration of the tests, 12 months, was arbitrarily short. Had the tests of Slabs 3 and 4 continued for a longer period of time, the agreement between the signals of the sensors and indications from the half-cell potentials likely would have increased.

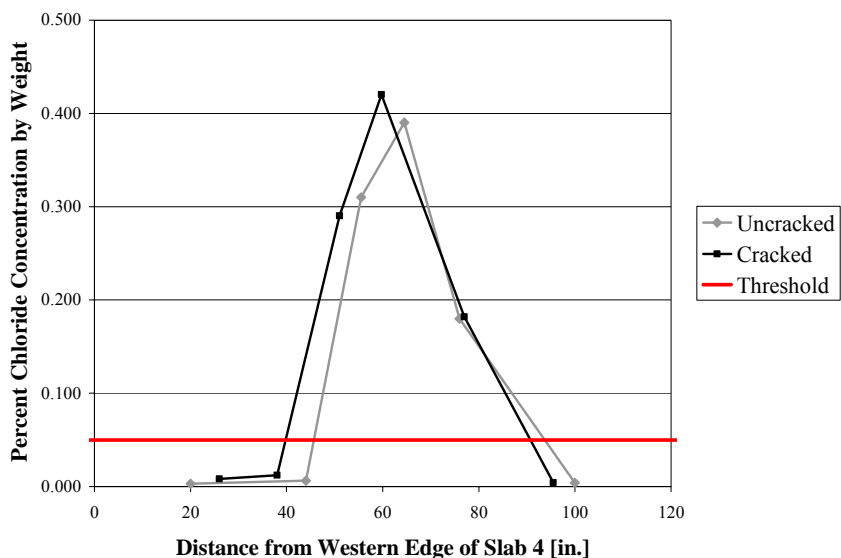
### **5.4.3 Chloride Concentration**

To determine the extent of chloride penetration into the concrete cover of Slab 4, samples of the concrete cover were taken from locations along the length of the specimen at the end of 12 months of testing. The samples were taken both from sound portions of the concrete cover and from within cracks in the concrete cover. These locations are shown in Figure 5-44 superimposed on the positions of the cracks and sensors. The acid-soluble chloride concentration by weight was determined by the James Instruments, Inc. chloride test system, which conforms to AASHTO T-260-94. The chloride samples were taken at a depth of 1 in. in the concrete cover, the nominal cover of the corrosion sensors.



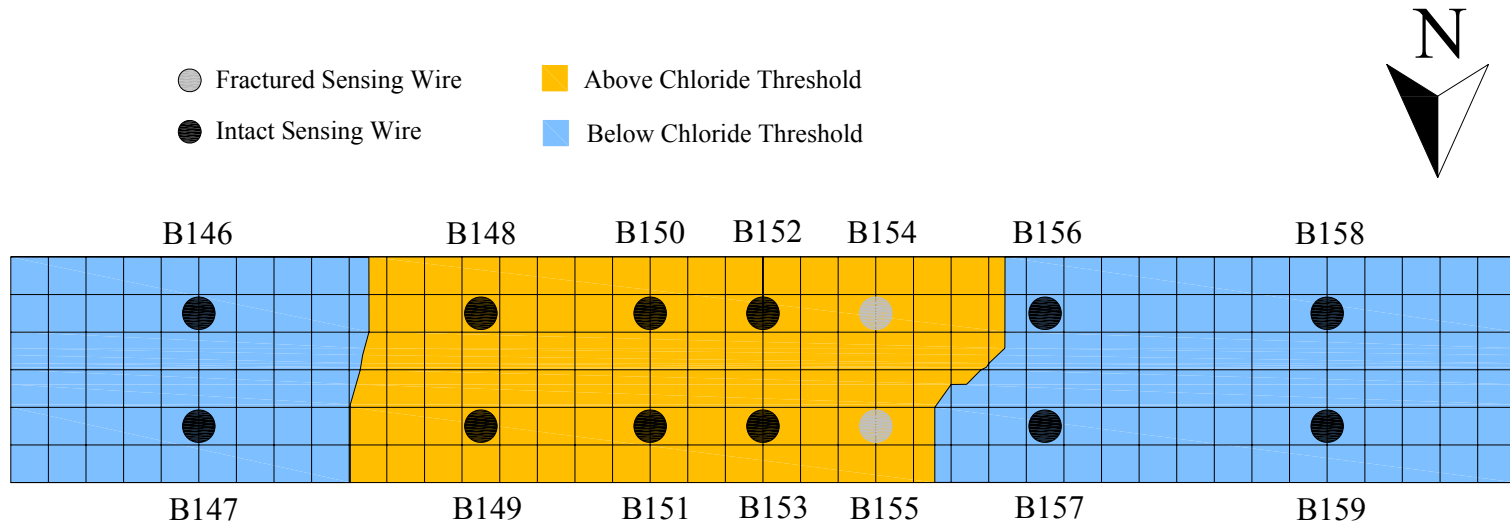
**Figure 5-44 Locations at which Chloride Concentration of Concrete Cover of Slab 4 Determined**

Figure 5-45 is a plot of the chloride concentration with respect to position on Slab 4. In terms of Figure 5-14, the coordinate 0 corresponds to the western edge of Slab 4. The chloride concentration of cracked concrete cover is plotted in black, while that of sound cover is plotted in gray. The chloride threshold value proposed by CEB is included in Figure 5-45. In contrast to Slabs 1 and 2, much of the concrete cover of Slab 4 reached or exceeded the chloride threshold value. As discussed in Section 5.3.3, the permeability of Slab 4 was likely significantly higher than that of Slabs 1 and 2 due to Slab 4 being subjected to poor curing. Therefore, chlorides were able to penetrate the concrete cover at a higher rate. There was, in addition, little difference in the chloride concentration of sound cover and cracked cover in Slab 4. The cracks in the concrete cover of Slab 4 were restricted to smaller widths than those in Slabs 1 and 2, causing a decrease in the rate of chloride ingress through cracks. This fact, coupled with the higher permeability of the concrete in Slab 4, caused the rate of chloride penetration to be comparable through sound and cracked concrete.



**Figure 5-45 Chloride Concentration of Slab 4**

The signals of the sensors were compared with the chloride concentration of the concrete cover by means of a contour plot, shown in Figure 5-46. The contour plot was developed by linearly interpolating among all measured values shown in Figure 5-44. That is, because the chloride concentration in sound cover was comparable to that in cracked cover, interpolation was performed among both types of values. Because corrosion initiation is associated with a threshold value in a chloride concentration test, only two colors — blue for below threshold and orange for above the threshold — were used. The grid spacing in the contour plot is 3 in. in both the vertical and horizontal directions. Sensors with intact sensing wires are colored black, while those with fractured sensing wires are colored gray. As in the case of the half-cell potentials, the correlation between the signals of the sensors and the indications of the chloride concentration test was weak. Only two of the eight sensors in the region above the chloride threshold signaled the initiation of corrosion. Again, testing was arbitrarily ended after 12 months. Had testing been allowed to continue, agreement between the signals of the sensors and the chloride test likely would have increased.



*Figure 5-46 Chloride Concentration of the Concrete Cover of Slab 4 at the End of 12 Months of Testing*

#### **5.4.4 Influence of Crack Path**

As was discussed in 5.4.3, the rates at which chlorides penetrated sound and cracked concrete cover in the case of Slab 4 were comparable. The cause of this uniform penetration was likely high permeability of the concrete relative the width of cracks in the concrete cover. The result of uniform penetration was that the paths of cracks less influenced which sensing wires corroded, signaling the initiation of corrosion.

Figure 5-47 shows maximum widths that cracks on the concrete cover of Slabs 3 and 4 reached during testing. The crack maps were recorded immediately before the specimens were unloaded on day 317 of testing. The paths of the cracks are superimposed over the positions of the sensors. Sensors with fractured sensing wires are labeled in red. In the Figure 5-47, cases in which cracks intersected the sensing wire of a sensor without causing it to fracture are evident. In addition, there is a case, sensor B138, in which the crack failed to intersect the sensing wire but the sensing wire fractured. Therefore, Figure 5-47 is consistent with the claim that the paths of cracks little influenced the reliability of the sensors at detecting initiation of corrosion.

While Figure 5-47 can be consistent or inconsistent with claims about the effect of crack path on sensor reliability, it can never be a basis for such claims. Knowledge of whether a crack intersects the sensing wire of a sensor can only be obtained by observation. But, to observe the sensing wire, the concrete around it must be removed, destroying the path of the crack in the concrete cover. Thus, a record like Figure 5-47 cannot itself serve as a basis for claims about the effect of crack path on sensor reliability. Rather, such claims are based on chloride concentration tests, as discussed in Section 5.4.4, since such tests determine the effect of cracks in the concrete cover on the rate of chloride ingress.

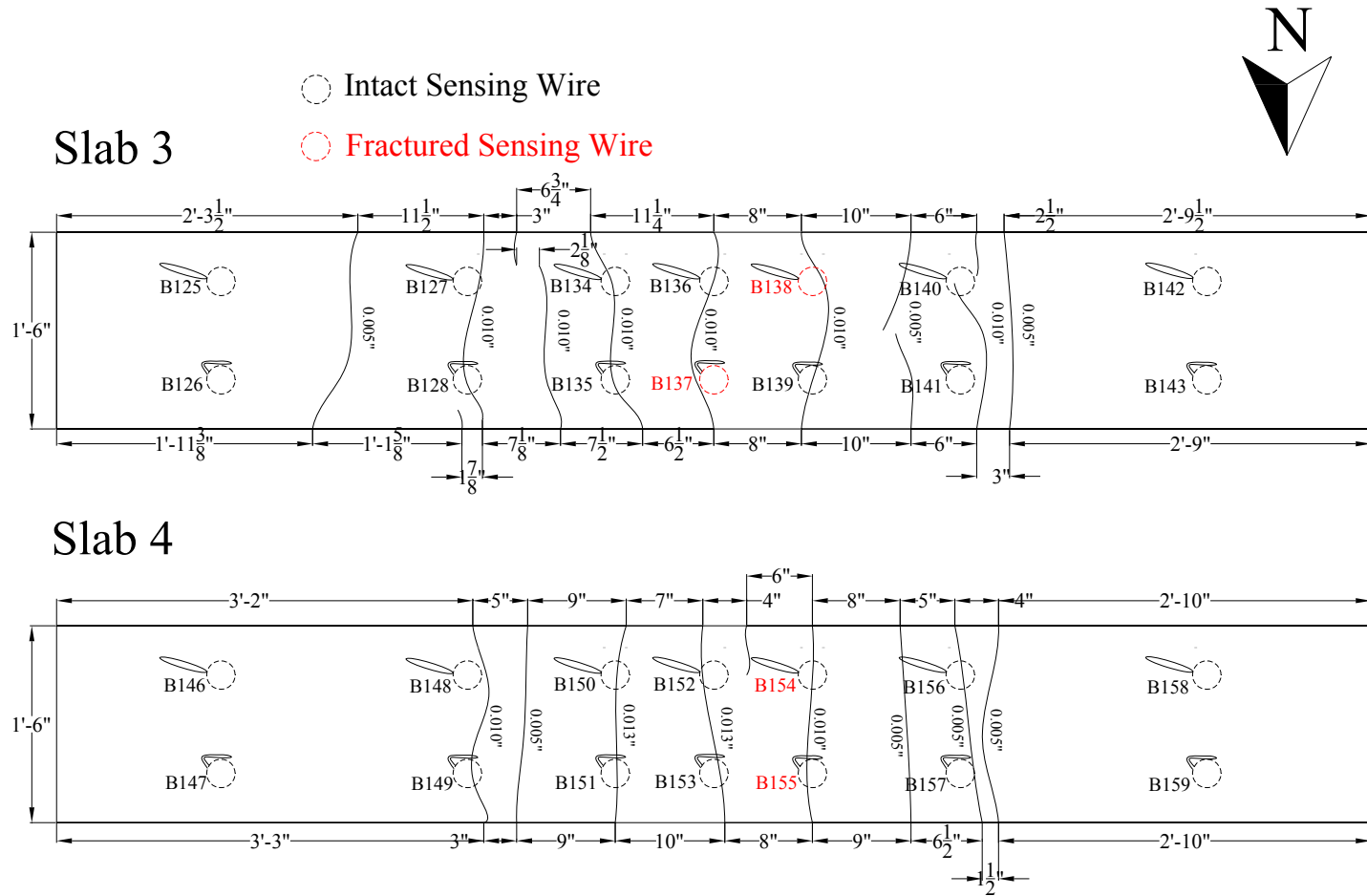


*Figure 5-47 Paths of Cracks in Specimens Superimposed on the Positions of the Sensors*

## 5.5 CONCLUSION

In summary, a set of coupled sensors was tested in sections of a reinforced concrete bridge deck. The sensors were arranged in the specimens to determine the tributary area over which the sensors detect initiation of corrosion of the reinforcement. The functioning of the sensors was assessed in terms of their measured responses and their reliability at detecting initiation of corrosion of the reinforcement.

The measured responses of sensors tested in Slabs 3 and 4 were found to exhibit relatively low variability when their sensing wires were intact and relatively high variability when their sensing wires were fractured. Greater quality control of the condition of the reader coil reduced the number of baseline shifts in the data of sensors tested in Slabs 3 and 4, decreasing the variability in the response of sensors with intact sensing wires.

There were two possible causes of the relatively high variability observed in the response of sensors with fractured sensing wires tested in Slabs 3 and 4. One possible cause was that the epoxy housing cracked, allowing moisture to reach the surface of the reference inductor. Changes in moisture on the surface of the inductor may have introduced variability into the response of the sensors. Another likely cause was the relatively high permeability of Slabs 3 and 4. The higher permeability of Slabs 3 and 4 increased the volume of moisture per unit volume of concrete in the specimens. The increased amount of moisture in the specimens allowed the internal environment of the concrete to participate in the response of the sensors with fractured sensing wires to a detectable degree. Because the moisture varied with the environmental cycles to which the specimens were subjected, the participation of the internal environment of the



concrete in the response of the sensors introduced variability into the response of the sensors.

The relatively high permeability of Slabs 3 and 4 permitted more uniform penetration of chlorides into the concrete cover of the specimens, compared to Slabs 1 and 2. This more uniform penetration likely caused uniform corrosion of the sensing wires of some of the sensors tested in Slabs 3 and 4. Uniform corrosion of the sensing wire was detectable in the response of these sensors by gradual decreases in the phase dips and pseudo-quality factors of the sensors.

Internal black corrosion likely caused deterioration of the reference circuits of two sensors. This result both proves the development of black corrosion to be characteristic of the epoxy housing itself and underscores that epoxy is an unacceptable material for the housing of the sensors.

A weak correlation was found among the response parameters of the sensors — resonant frequency, phase dip, and pseudo-quality factor — and the internal temperature of the concrete. Although a correlation existed, the dependence was weak. That is, for any given change in temperature, the change in the response parameters was small. Therefore, in the case of the corrosion sensors generally, the effect of temperature upon response can be neglected.

The reliability of the sensors at detecting the initiation of corrosion was assessed with respect to the observed condition of the reinforcement in the case of Slab 4. Compared to the steel reinforcement, the sensors tested in Slab 4 sent four erroneous signals, all false negatives. Examination of the locations where corrosion developed in the top layer of the reinforcement and where the sensing wires of the sensors were attached showed that the parameter  $d$ , which defines the tributary area of the coupled sensor, was less than a few inches. That is, electrically connecting the sensing wire of the coupled sensor to the reinforcement did not increase the area over which the sensor detected initiation of corrosion.

Rather, the coupled sensor functioned essentially as an isolated sensor, or point sensor.

The signals of the sensors tested in Slabs 3 and 4 were also compared with the half-cell potentials of the specimens. There was a lack of correlation between the indications of the half-cell potentials and the signals of the sensors. Sensors with fractured sensing wires were located in regions of highest corrosion risk, but few of the sensing wires of sensors in regions of highest risk fractured during 12 months of testing. In addition, the chloride concentration of the concrete cover of Slab 4 was determined, and the results were compared with the signals of the sensors tested in Slab 4. The signals of the sensors and the indications of the chloride test correlated poorly as well. Had the tests of Slabs 3 and 4 been of longer duration, the agreement between the signals of the sensors and the half-cell potentials and chloride concentration test likely would have increased.

In general, the functioning of the sensors was acceptable but not optimal. In the case of all sensors tested in Slab 4, the signal sent by the sensor was consistent with the physical state of the sensing wire. Thus, the sensors reliably signaled the state of their sensing wires. Furthermore, the response of the sensors correlated with the internal environment of the concrete. Sensors with uniformly corroding sensing wires signaled uniform corrosion in their response. The response parameters of the sensors also weakly correlated with temperature. All of these properties could potentially be exploited to obtain analog information about the internal environment of the concrete.

However, the sensors were not sufficiently reliable at detecting the initiation of corrosion. The number of false negatives signaled by the sensors was excessively high. It is the case that data from the tests only spans 12 months. Had the tests continued, the number of false negatives likely would have

decreased. However, a design for the sensor that is more responsive to initiation of corrosion over a tributary area associated with the sensor is necessary.

## **CHAPTER 6**

### **Black Corrosion within Epoxy Housing of Sensor**

#### **6.1 INTRODUCTION**

Black corrosion, mentioned in Section 5.3.5 as the likely cause of deterioration of reference circuits, was observed within the epoxy housing of the corrosion sensors tested in Slabs 1, 2, and 4. It is expected that black corrosion also developed in the housing of sensors tested in Slabs 3, but this possibility has not been verified by observation. Section 6.2 summarizes the observed instances of the black corrosion and the distributions of sensors with black corrosion in Slabs 1, 2, and 4. Two possible causes of black corrosion are discussed in Section 6.3: lack of passive layer on the segment of steel sensing wire within the epoxy and development of a differential aeration cell on the sensing wire.

#### **6.2 DEVELOPMENT OF BLACK CORROSION**

Black corrosion was observed within the epoxy housings of many of the sensors embedded beneath the salt-water reservoirs in Slabs 1, 2 and 4. Figure 6-1 provides an example of severe black corrosion within sensor B52, which was tested in Slab 2. Cracks in the epoxy housing, as shown in Figure 6-1, were observed in several sensors and likely increased the extent of black corrosion by providing a path of ingress into the circuitry of the sensors. The cause of the cracks was likely not the corrosion itself because, as noted by Broomfield (1997), black corrosion does not result in the development of expansive forces. Rather, likely causes of the cracking of the epoxy housings were imperfections in the

potting of the epoxy housing and differential thermal expansion between the epoxy and concrete.



***Figure 6-1 Black Corrosion in the Housing of Sensor B52***

Although almost entirely restricted to sensors embedded beneath the salt-water reservoirs, black corrosion was observed in one sensor embedded at the end of a slab, despite the fact that the area had low risk of corrosion. Figure 6-2 shows this sensor, A57, which was tested in Slab 2. As labeled, a trace of corrosion was observed on the steel wire inside the epoxy. No corrosion was observed on the sensing wires of other sensors embedded at the ends of Slabs 1 and 2. This fact was an indication that corrosion on the sensing wire within the epoxy of A57 developed during testing because the corrosion was apparently not characteristic of how the sensors were fabricated. Because the A57 was embedded at the end of Slab 2, the only source of moisture was the pore solution of the concrete. This source was possibly sufficient to facilitate the development of black corrosion. The formation of even a slight amount of corrosion on the sensing wire within the epoxy was not expected case since that portion of the wire was assumed to be sealed from the surrounding environment.

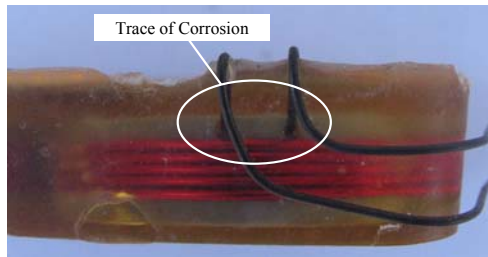


**Figure 6-2 Trace of Black Corrosion in the Housing of Sensor A57**

Figure 6-3 through Figure 6-5 identify the sensors that developed internal black corrosion. Again, except for the case of sensor A57, all sensors that developed black corrosion were exposed to chlorides, either regularly or irregularly.

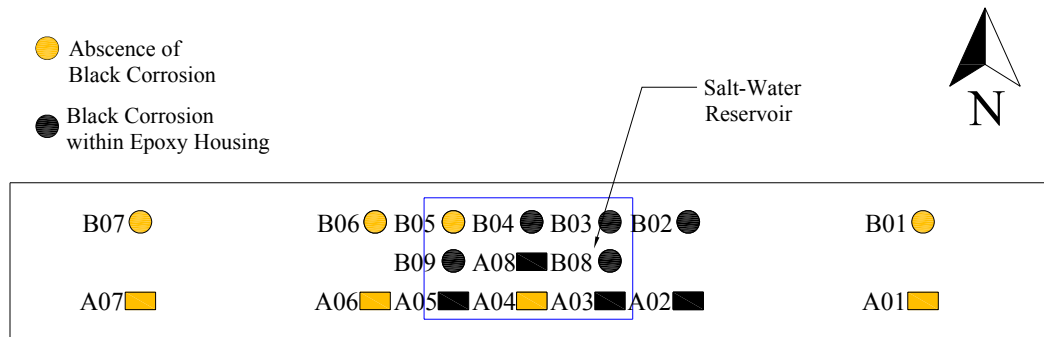


**Figure 6-3 Instances of Internal Black Corrosion in Slab 1**

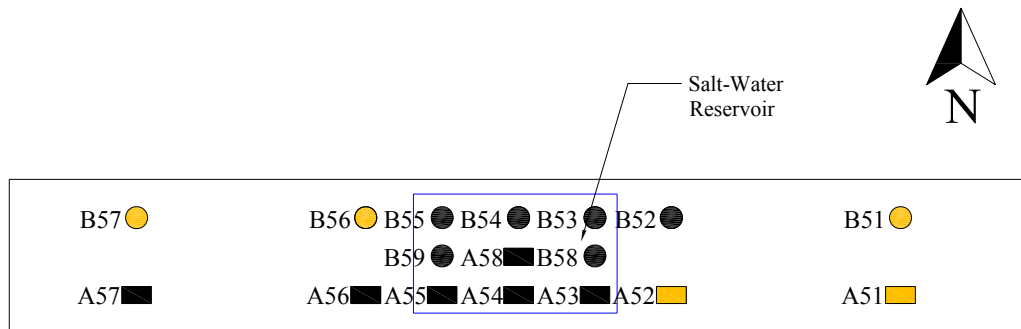


**Figure 6-4 Instances of Internal Black Corrosion in Slab 2**

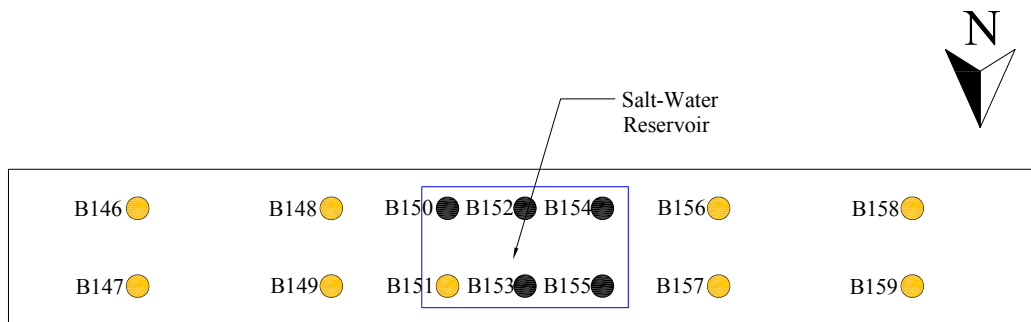


**Figure 6-5 Instances of Internal Black Corrosion in Slab 4**

The development of black corrosion within the housings of some sensors has considerable practical importance. First, as was mentioned in Section 5.3.5, internal black corrosion likely lead to the deterioration of the reference circuit of sensor B152, tested in Slab 4. Second, the possibility of the sensing wire corroding internally in the absence of corrosive agents, as in the case of A57, allows for the possibility of the sensor signaling a false positive. Third, even if black corrosion only developed in the presence of corrosive agents, its development decreases sensor reliability. Indeed, an essential requirement for reliable detection of initiation of corrosion in the steel reinforcement is that the sensing wire corrode at a rate similar to that of the surrounding steel

reinforcement. The development of a black corrosion within the epoxy housing implies that a portion of the sensing wire is corroding differently than the sensing wire exposed to the environmental conditions of the concrete. It should, nevertheless, be noted that the presence of corrosive agents in the concrete accelerated the formation of black corrosion. In that way, there were instances of sensing wires fracturing internally due to black corrosion which was accelerated by the presence of corrosive agents. Therefore, on the whole, the sensors functioned as designed even when black corrosion developed. However, the possibility of black corrosion is yet another indication that epoxy is an unsuitable material for the sensor housing. An alternative design for the housing of the sensors, tested in Slabs 5 and 6, is discussed in Section 7.2.

### **6.3 CAUSES OF BLACK CORROSION OF THE SENSING WIRE**

One possible cause of the black corrosion within the epoxy housing is failure of the sensing wire within the epoxy to develop a passive layer. The passive layer of steel embedded in concrete is known to form primarily during hydration of the concrete due to the high pH. The sensors were generally potted shortly before placing of the concrete in the specimens. Consequently, the epoxy was likely closely bonded to the steel. This bond prevented hydroxyls from reaching the surface of the sensing wire during hydration of the concrete. However, as noted in Section 3.4.5, the coefficient of thermal expansion of the epoxy housing and the steel were significantly different. The interior temperature of the building in which the Slabs 1, 2, and 4 were stored fluctuated from approximately 40 to 100 °F during testing. As illustrated in Figure 6-6, this temperature fluctuation likely caused the epoxy housing to separate from the steel, leaving a small cavity, or gap, along the length of the steel wire between the wire and the epoxy. As a result, corrosive agents were able to reach the sensing wire



within the epoxy, causing the wire to corrode. Because access to the cavity was constricted — the access point for chemicals was small relative the volume of the cavity itself — the environment within the cavity became depleted of oxygen, causing the corrosion to be dark in color.

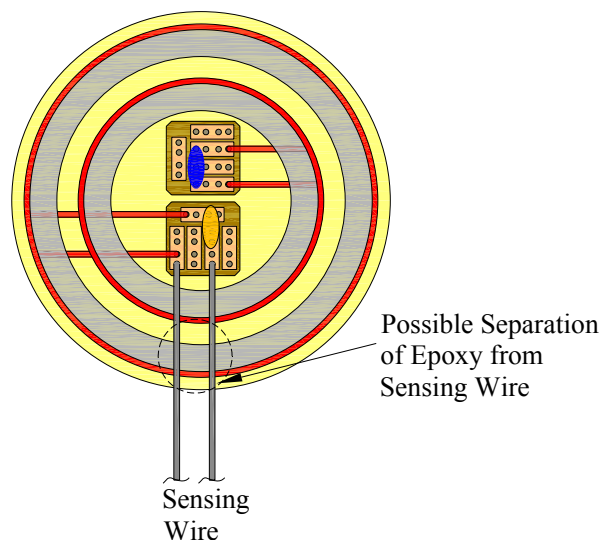


**Figure 6-6** *Development of Cavity along Sensing Wire*

A second possible cause of the black corrosion, differential aeration of the sensing wire, is described in terms of mixed potential theory, which is discussed below briefly. The discussion of mixed potential theory and differential aeration is based on Jones (1996). Because lack of a passive layer on a portion of the sensing wire and differential aeration of the sensing wire are not mutually exclusive, both of these causes could have been present in the development of black corrosion.

### **6.3.1 Mixed Potential Theory**

It is commonly known that when a metal is placed in a solution of ions, the metal develops a potential on its surface. For example, if iron is placed in a

solution of hydroxyls contaminated by chlorides, some equilibrium potential,  $E_a$ , will develop on the surface of the iron over time. Corresponding with this equilibrium potential is a current generated by the corroding iron,  $i_a$ . This electrochemical system is described by the following expression, where the loss of electrons from the iron sustains the potential  $E_a$  and the current  $i_a$ :



Reaction 6.1 is the anodic half-cell reaction of corrosion of steel reinforcement in concrete, described in Section 2.4.2.

If a positive potential is applied to the surface of the iron, the potential of the iron increases to some value  $E_1$ . Corresponding with the change in potential is a change in the current generated by the iron. The current after the potential has been applied is  $i_1$ . In contrast, if a negative potential is applied to the surface of the iron, the potential of the iron decreases to a value of  $E_2$ . Similarly, there is a corresponding change in the current generated by the iron, with the new value of current being  $i_2$ . This change in the potential and current of the iron due to an applied potential is called polarization. Polarization in the positive direction is called cathodic polarization, while polarization in the negative direction is called anodic polarization. The polarization curve of reaction 6.1, illustrated in Figure 6-7 with current on the log scale, is developed by repeated discrete polarizations in the cathodic and anodic directions.

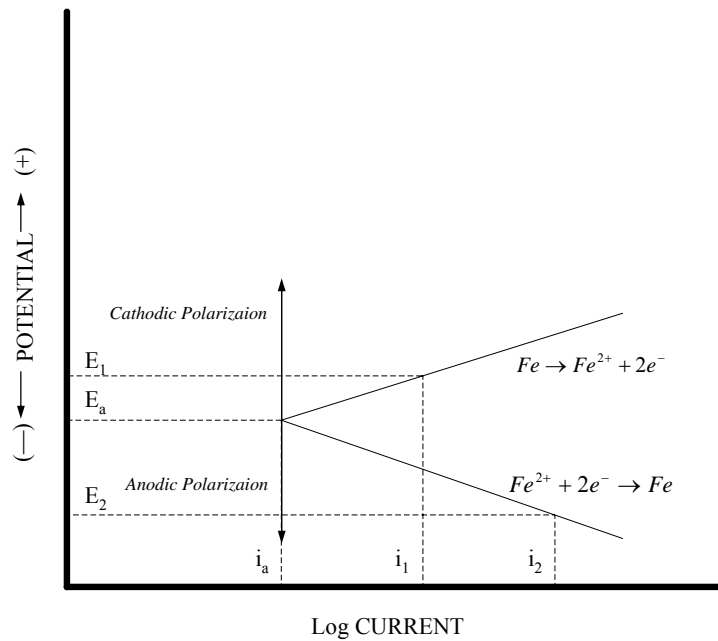


**Figure 6-7 Polarization Curve of Reaction  $Fe \rightarrow Fe^{2+} + 2e^{-}$**

As described in Section 2.4.2, the anodic half-cell reaction (reaction 6.1) requires a corresponding cathodic reaction to consume the electrons generated by the anodic reaction. For corrosion of steel in reinforced concrete, this cathodic reaction is described by reaction 6.2:



Because the cathodic reaction also occurs on the surface of the corroding steel, that reaction is subject to polarization, as shown in Figure 6-8, as in the case of the anodic half-cell reaction. The equilibrium potential,  $E_c$ , of reaction 6.2 is positive compared with the equilibrium potential of the anodic reaction.

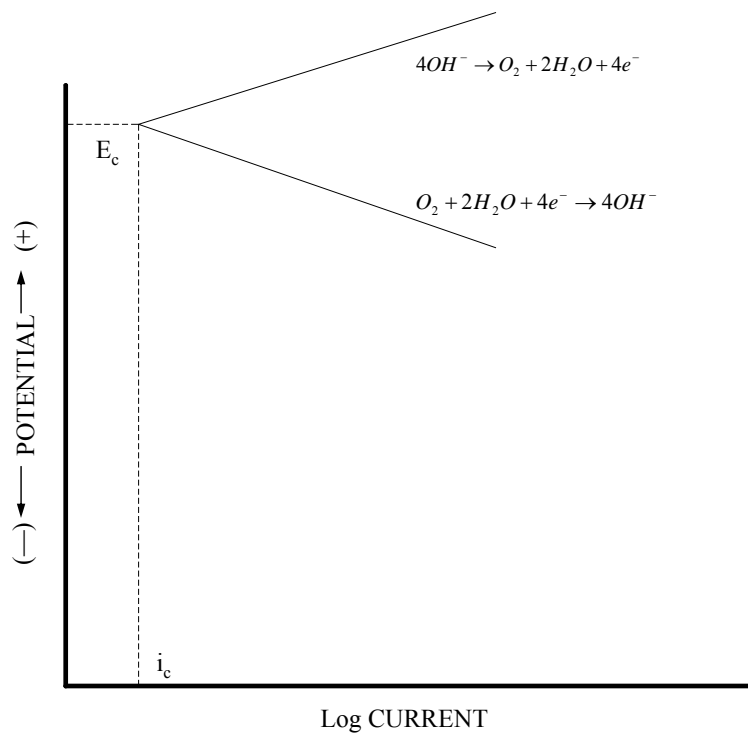


**Figure 6-8 Polarization Curve of Reaction  $O_2 + 2H_2O + 4e^- \rightarrow 4OH^-$**

In any corrosion cell, the same quantity of electrons that is generated by the anodic reaction is consumed by the cathodic reaction. Therefore, the anodic and cathodic reactions occur at the same rate. Equivalently, the currents of the two half-cell reactions must be equal. Consequently, the corrosion potential,  $E_{\text{corr}}$ , and corrosion current,  $i_{\text{corr}}$ , of a corrosion cell are determined by where the polarization curves of the anodic and cathodic reactions intersect, as shown in Figure 6-9. In this way, the polarization curves, which are developed empirically for a given reaction, can be used to estimate the corrosion potential and current of a given system. Such an estimate is based on mixed potential theory.

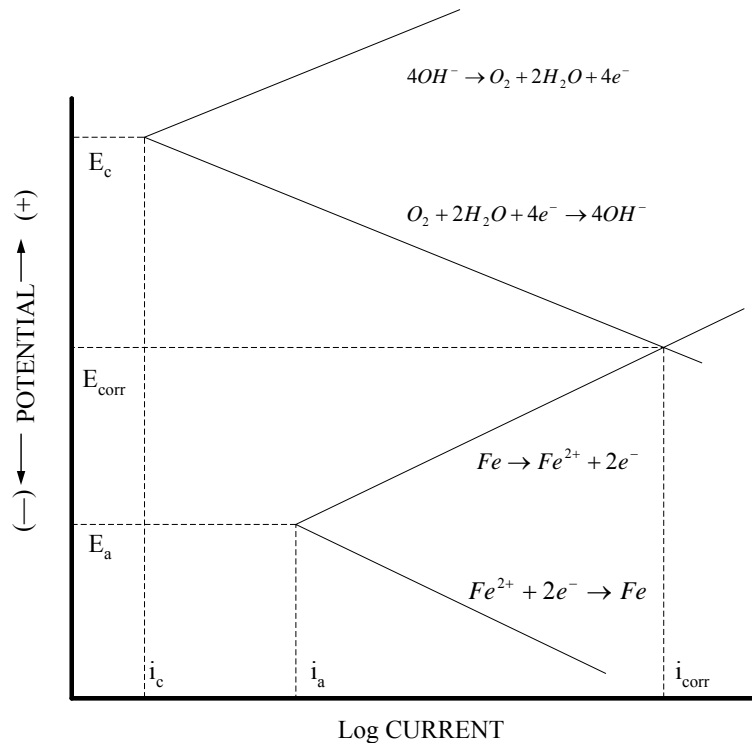


**Figure 6-9 Corrosion Potential and Current Defined by Anodic and Cathodic Polarization Curves**

### 6.3.2 Differential Aeration

The shape of the cathodic polarization curve depends on the concentration of the reactants. Specifically, the polarization curve of cathodic reaction 6.2 varies with the concentration of oxygen in the solution. As a result, the location at which the cathodic curve intersects the anodic curve, reaction 6.1, depends upon the concentration of oxygen in the solution. Because that intersection defines the corrosion potential and current, the potential and rate at which corrosion occurs also depend on the concentration of oxygen in the solution. As shown in Figure 6-10, the deaerated cathodic curve intersects the anodic curve at a more negative potential than does the aerated cathodic curve. Therefore, the

corrosion potential in a deaerated corrosion cell,  $E_{\text{corr,d}}$ , is more negative than the corrosion potential in an aerated corrosion cell,  $E_{\text{corr,a}}$ . The currents corresponding with these potentials are  $i_{\text{corr,d}}$  and  $i_{\text{corr,a}}$ , respectively.

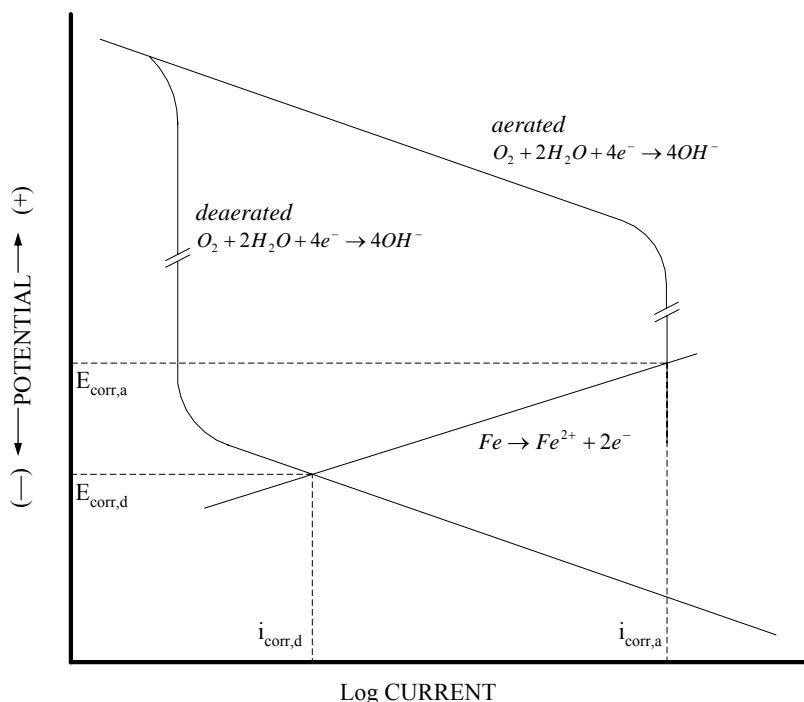


**Figure 6-10 Effect of Aeration on Corrosion Potential and Current (Jones 1996)**

If two rods of iron, chemically identical, are placed in portions of a saline solution separated by a diaphragm and the two rods are electrically connected, differential aeration of the two portions of the solution causes a potential difference to develop between the rods. A model of this differential aeration cell is shown in Figure 6-11. On one side, air is bubbled into the solution, aerating the cell. On the other side, either hydrogen or nitrogen gas is bubbled into the solution, deaerating the cell. As a result, the cathodic half-cell reactions combining with the respective anodic iron reactions are distinct, causing the

corrosion potentials of the two rods to be distinct. The rod in the deaerated solution serves as the anode of the rod in the aerated solution, and the rate of corrosion of the anode increases.

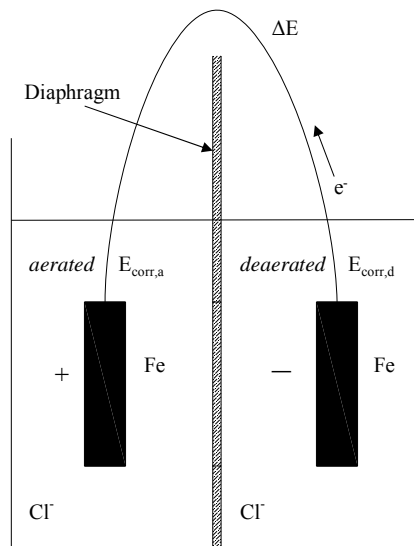


**Figure 6-11 Differential Aeration Cell**

The formation of a differential aeration cell on the sensing wire of the sensors possibly caused the internal black corrosion observed in the epoxy housings. The differences in coefficients of thermal expansion between the epoxy and steel likely caused a small cavity to develop along the length of the sensing wire, as illustrated in Figure 6-12. Because access to the cavity was constricted, the environment within the cavity became deaerated. As the environment around the sensing wire within the epoxy became deaerated, the portion of the wire within the epoxy became anodic compared with the portion of the sensing wire outside the epoxy. Consequently, the external portion of the wire drove corrosion of the internal portion of the wire. The black corrosion observed in the epoxy housings was characteristic of corrosion in low-oxygen environments.

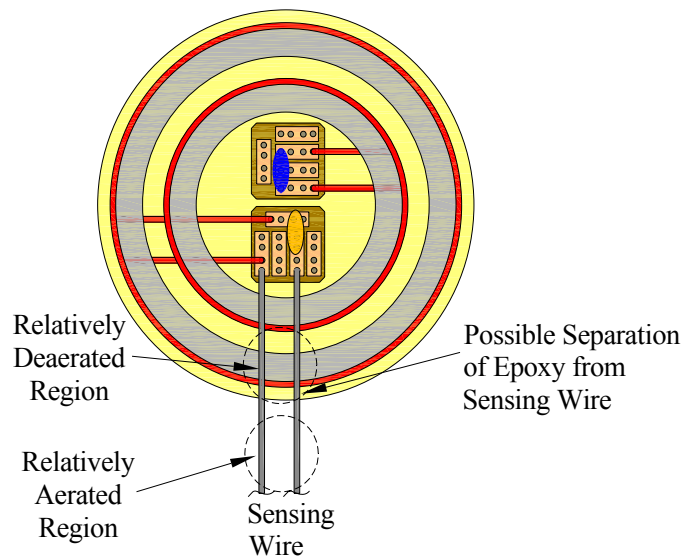


**Figure 6-12 Differential Aeration Cell on Sensing Wire**

The fact that, in several cases, the sensing wires of sensors tested in Slabs 1 and 2 fractured within the epoxy, rather than outside of the epoxy, is consistent with either lack of passive layer on the surface of the steel embedded within the epoxy or differential aeration of the sensing wire being the cause of the black corrosion. An example of a sensing wire that fractured within the epoxy was the sensing wire of B04, shown in Figure 6-13. B04 signaled a fractured sensing wire, but the sensing wire outside the epoxy was intact.



**Figure 6-13 Black Corrosion in B04**

In contrast to sensors tested in Slabs 1, 2 and 4, black corrosion did not develop in sensors tested in the prisms. Such was the case despite the fact that



cracks, pathways for the ingress of corrosive agents, developed in the epoxy housings of sensors tested in prisms subjected to extreme temperatures. Figure 6-14 is a photograph of a crack in the housing of sensor B23. Sensors embedded in the prisms were subjected either to extreme temperature fluctuations — room temperature to 230 °F or room temperature to -15 °F — or to minimal temperature fluctuations — constant room temperature. In the case of the former, the cavity around the steel wire in the epoxy was likely large enough to permit circulation of oxygen and thus avoid deaeration within the cavity. In the case of the latter, no cavity developed because the temperature fluctuations were minimal. It was the relatively moderate temperature fluctuations experienced by the sensors embedded in the slab sections that facilitated deaeration within the cavity and thus black corrosion.

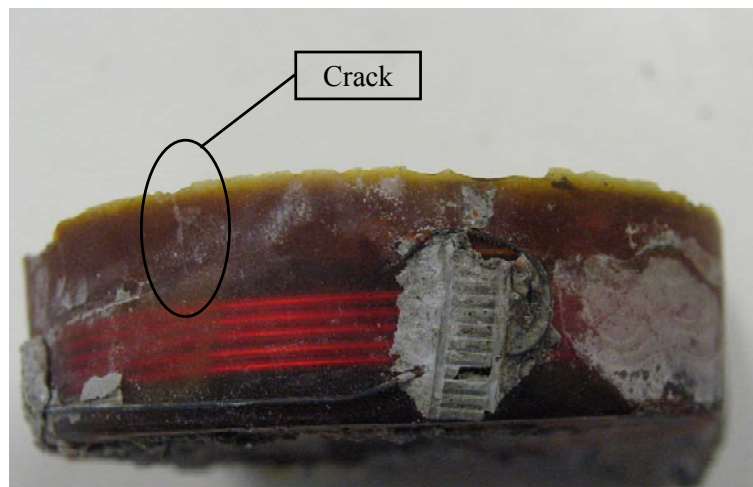


*Figure 6-14 Crack in the Housing of Sensor B23*

#### **6.4 CONCLUSION**

Black corrosion was observed within the epoxy housings of sensors tested in Slabs 1, 2, and 4. The development of black corrosion was problematic for

three reasons. Black corrosion likely caused the deterioration of reference circuits in some sensors. In one case, black corrosion developed in absence of corrosive agents, allowing for the possibility of a false positive. Finally, that black corrosion existed within the epoxy housing of the sensor indicates that a portion of the sensing wire was corroding differently than the remainder of the sensing wire, a condition that may reduce the reliability of the sensors.

Possible causes of black corrosion were lack of a passive layer on the surface of the sensing wire within the epoxy and differential aeration of the sensing wire. Differential thermal expansion of the epoxy and steel sensing wire allowed a small cavity to develop around the sensing wire within the epoxy. This cavity became deaerated over time, compared to the environment surrounding the external portion of the sensing wire. As a result, the corrosion that formed on the sensing wire within the epoxy was dark in color. The possible lack of a passive layer on the portion of the sensing wire within the epoxy caused that portion of the sensing wire to corrode preferentially. Furthermore, differential aeration of the sensing wire may have allowed a potential difference to develop between the internal and external portions of the sensing wire. The potential difference particularly facilitated corrosion of the internal portion of the sensing wire because the internal portion of the wire was anodic compared to the external portion.

## **CHAPTER 7**

# **Testing of Anodic Sensors in Reinforced Concrete Slab Sections**

### **7.1 INTRODUCTION**

The concept of the anodic sensor was tested using two metals for the sensing wire, zinc and aluminum, both of which are active compared with steel in the galvanic series. Both sets of sensors were tested in reinforced concrete slab sections. Tests are ongoing, but results from the first 14 weeks of testing are discussed in this chapter. The design of the experiment is described in Section 5.2. Section 5.3 discusses the measured response of both sets of sensors over the first 14 weeks of testing. Finally, Section 5.4 compares the measured sensor response with the measured half-cell potentials of the specimens. Section 5.4 also provides evidence, based on the total current circulating in the specimens, that the sensing wires served as sacrificial anodes to the steel reinforcement.

### **7.2 DESIGN OF THE EXPERIMENT**

The slab sections constructed to test the anodic sensors were 14-ft long, 18-in. wide, and 8-in. deep. Top and bottom plan views of the two specimens, Slabs 5 and 6, and a typical section of the specimens are shown in Figure 7-1 through Figure 7-5.

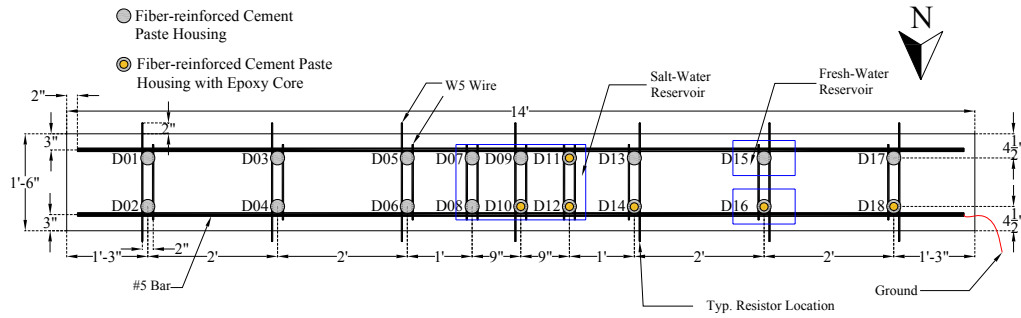


**Figure 7-1 Top Plan View of Slab 5**

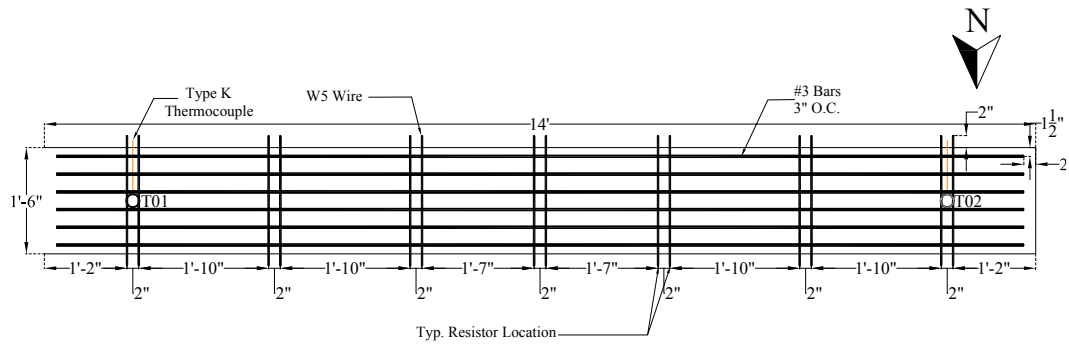


**Figure 7-2 Bottom Plan View of Slab 5**

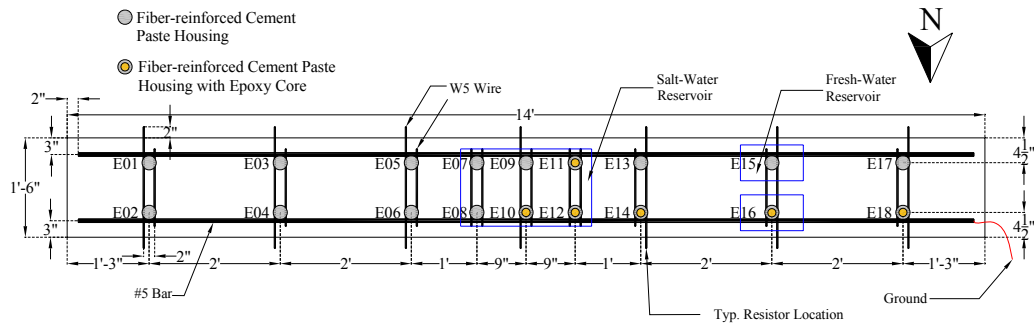


**Figure 7-3 Top Plan View of Slab 6**

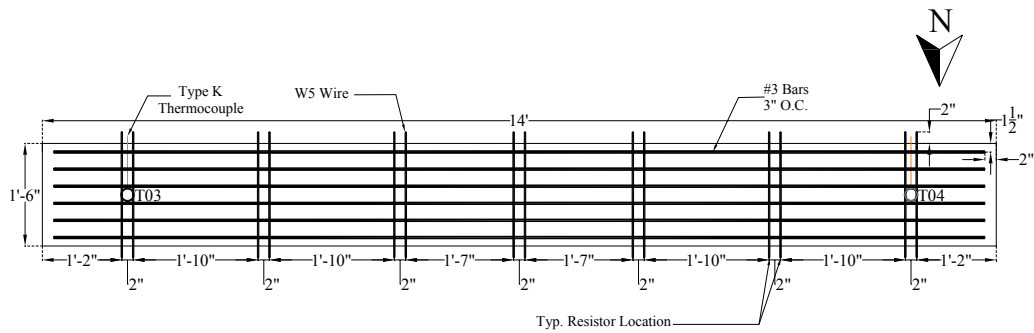


**Figure 7-4 Bottom Plan View of Slab 6**

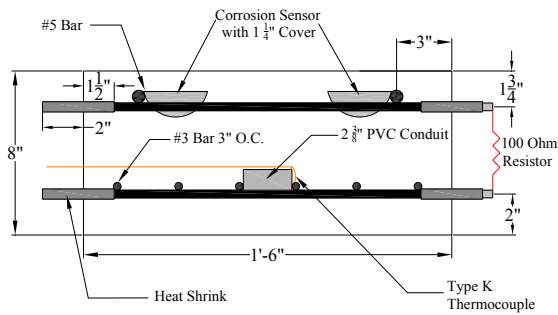


**Figure 7-5 Typical Section of Slabs 5 and 6**

All sensors tested in Slabs 5 and 6 had concentric geometry. The eighteen sensors tested in Slab 5 had 0.0393-in. (1 mm) diameter zinc sensing wires; they are labeled in Figure 7-1 as sensors D01 through D18. Similarly, sensors E01 through E18, shown in Figure 7-3, had 18-gage (0.0403-in. diameter) aluminum sensing wires. The chemical compositions of the sensing wires were determined by chemical analysis and are given in Table 7-1. From the table, the percentage of elements other than zinc in the zinc wire is so small that the wire may be regarded as pure zinc. The same holds for the aluminum wire. That is, neither of the types of wire should be regarded as an alloy.

**Table 7-1 Chemical Composition of Zinc and Aluminum Sensing Wire**

<b>Chemical Element</b>	<b>Zinc Wire</b>	<b>Aluminum Wire</b>
	<b>[% ]</b>	<b>[% ]</b>
<i>Copper</i>	0.010	0.05
<i>Cadmium</i>	<0.001	-
<i>Magnesium</i>	<0.005	<0.05
<i>Lead</i>	<0.002	<0.05
<i>Tin</i>	<0.001	<0.05
<i>Nickel</i>	<0.005	<0.05
<i>Iron</i>	<0.01	0.45
<i>Silicon</i>	-	0.06
<i>Titanium</i>	-	<0.05
<i>Manganese</i>	-	<0.05
<i>Chromium</i>	-	<0.05
<i>Other</i>	-	<0.15
<i>Zinc</i>	>99.85	<0.01
<i>Aluminum</i>	0.12	>98.93

The sensors embedded in a given specimen were nominally identical except for type of housing. As shown in Figure 7-1 and Figure 7-3, most of the sensors in each specimen had a fiber-reinforced cement paste housing, while several had a fiber-reinforced cement paste housing with an epoxy core. For brevity in subsequent sections, the types of housing are distinguished by whether or not they have an epoxy core. The fiber-reinforced cement paste housing was cement paste reinforced with polypropylene fibers. A sensor with such a housing is illustrated in Figure 7-6 and shown in Figure 7-7. The mold used had a convex

bottom in order to avoid trapping air below the sensor during placement of the concrete, as was observed in tests of sensors with concave bottoms, discussed in Section 4.4.5. The circuits — sensing and reference — of sensors with the fiber-reinforced cement paste housing were fabricated as described in Dickerson (2005). The only differences in the fabrication of the sensors tested in Slabs 5 and 6 was how the sensing wires were soldered to the sensing circuit and how the circuits were potted. Soldering of the sensing wires and potting of the sensors in fiber-reinforced cement paste is described in Appendix E.

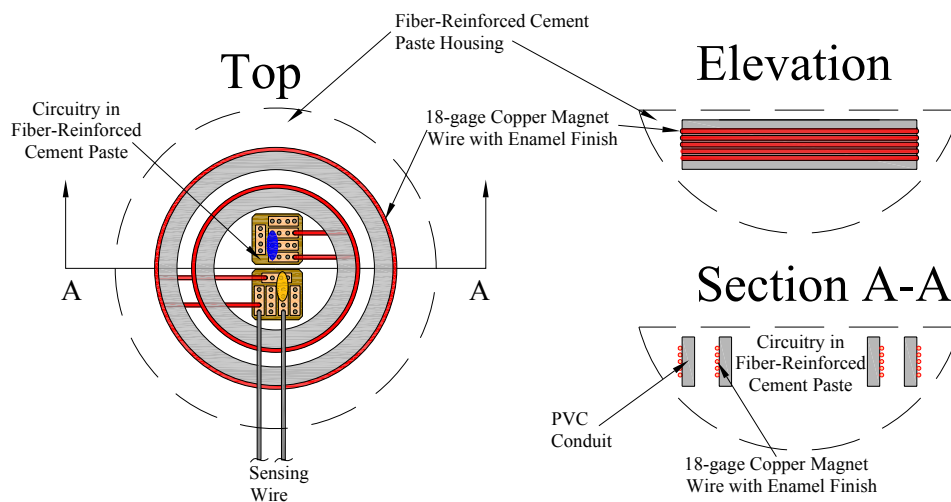


**Figure 7-6** *Illustration of Sensor with Fiber-Reinforced Cement Paste Housing*



**Figure 7-7** *Sensor with Fiber-Reinforced Cement Paste Housing*

Fiber-reinforced cement paste was used for the sensor housing for two reasons. First, fiber-reinforced cement paste is permeable, in contrast to epoxy. Therefore, all of the steel sensing wire, both what is within the housing and what is outside the housing, would become passivated at the time of hydration. Furthermore, the development of a differential aeration cell on the sensing wire due to the internal environment of the sensor housing being distinct from the internal environment of the concrete is unlikely. Second, the fiber-reinforced cement paste was found to have a coefficient of thermal expansion similar to that of concrete. Appendix E includes a discussion of tests that support this claim. Comparable coefficients of thermal expansion between the fiber-reinforced cement paste housing and concrete minimize the possibility of the cement paste housing cracking the concrete due to temperature changes. Extreme cases of epoxy housings causing concrete to crack were discussed in Section 3.4.5.

One potential difficulty with a cement paste housing was that both the sensing and reference circuits are exposed to the internal environment of the concrete, as compared with an epoxy housing. Specifically, from the onset of testing, the permeability of the fiber-reinforced cement paste would likely permit the pore solution and its contents to reach the circuits themselves. The epoxy housing allowed the internal environment of the concrete to reach the circuits but only after some period of time, the result being internal black corrosion which caused some circuits to deteriorate. Another possible difficulty was that the effect of the alkaline environment of the fiber-reinforced cement paste on the circuits was unknown. For that reason, several sensors, illustrated in Figure 7-8 and shown in Figure 7-9, were cast in fiber reinforced cement paste after the circuitry of both sensors — PC boards, exposed copper leads, and capacitors — had first been potted in marine epoxy. Although the epoxy was known to be a poor material for the housing of the sensor over a long period of time, it was used in



this case to initially protect the circuitry from the internal environment of the concrete and the cement paste itself.

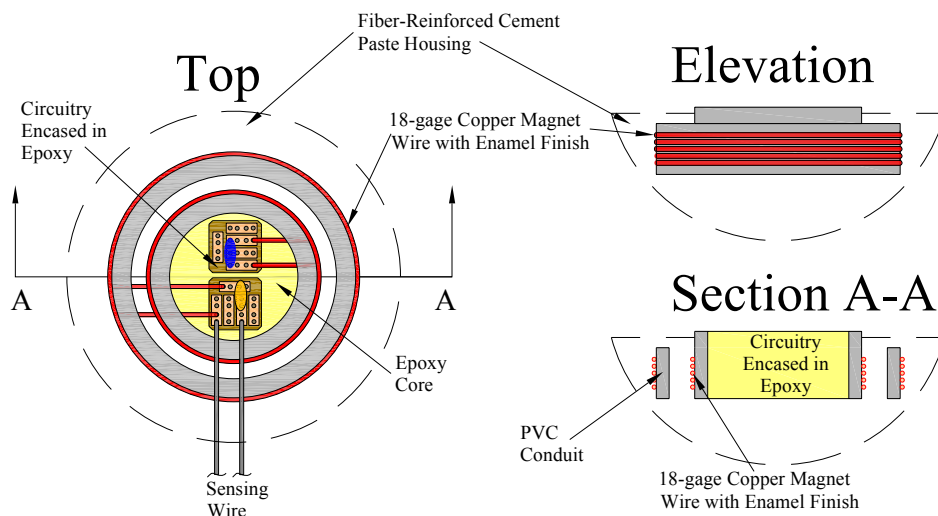


**Figure 7-8** *Illustration of Sensor with Fiber-Reinforced Cement Paste Housing with Epoxy Core*



**Figure 7-9** *Sensor with Fiber-Reinforced Cement Paste Housing with Epoxy Core*

The sensors were distributed along the length of the specimens on platforms composed of two lengths of W5 wire, identical to the platforms used in Slabs 3 and 4. One of the transverse bars extended from the concrete; the other was simply secured to the longitudinal reinforcement to support the sensor. With

this arrangement, the concrete cover over the sensors was nominally 1 1/4 ". Figure 7-10 is a photograph of the layout of the sensors and steel reinforcement. As was done in the case of Slabs 3 and 4, the sensing wires of different sensors were placed in the expected path of the cracks in the concrete cover and out of the expected path of the cracks, as shown in Figure 7-11 and Figure 7-12, respectively. The sensing wires were secured to the longitudinal reinforcement with steel tie wire in order to ensure electrochemical coupling between the sensing wire and steel reinforcement.



***Figure 7-10 Layout of Sensors and Steel Reinforcement***

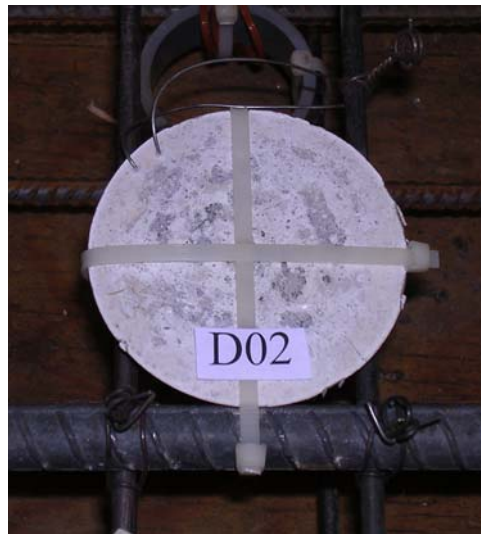


*Figure 7-11 Sensing Wire Placed in the Expected Path of the Crack*



*Figure 7-12 Sensing Wire Placed out of the Expected Path of the Crack*

The top and bottom layers of steel reinforcement of Slabs 5 and 6 were electrically connected in order to facilitate the development of macrocell corrosion. As in the case of Slabs 3 and 4, distributed along the lengths of Slabs 5 and 6 were sets of a single length of W5 wire extending out of the concrete from the top layer of reinforcement and two lengths of W5 wire extending out of the concrete from the bottom layer of reinforcement. As described in Section 5.2, the

portions of the transverse bars extending out of the concrete were wrapped in electroplating tape and then covered with heat shrink from their ends to 1 ½ in. into the concrete. On one side of a given set of transverse bars, the ends of the bars were threaded and stainless steel couplings were attached. The coupling of the top bar was connected to the coupling of the bottom bars using a 100-Ohm resistor and 18-gage copper magnet wire. The corrosion current circulating in the specimens was determined by measuring the voltage over the 100-Ohm resistor.

In contrast to Slabs 3 and 4, there were seven such sets of top and bottom transverse reinforcement, all of which were connected with a resistor in both Slabs 5 and 6. Slabs 5 and 6 had more sets of transverse reinforcement than Slabs 3 and 4 because their lengths were increased from 10 ft, the lengths of Slabs 3 and 4, to 14 ft. The lengths of Slabs 5 and 6 were increased to define the tributary area of the anodic sensors. The tributary area of the anodic sensors was expected to be larger than that of the coupled sensors because of the possibility of galvanic coupling developing between the sensing wires and the steel. Therefore, to define the tributary area of the anodic sensors empirically, the sensors were placed at greater distances from the salt-water reservoir. If the sensing wire of a sensor were attached some distance  $d_1$  from a point of corrosion and the sensing wire fractured, the parameter  $d$  defining the tributary area of the sensor would be greater than  $d_1$ . In contrast, if the sensing wire of a sensor were attached some distance  $d_2$  from a point of corrosion and the sensing wire failed to fracture, then  $d$  would be less than  $d_2$ .

To assess the contribution of the atmosphere to the internal corrosion of Slabs 5 and 6, a control specimen for each of the slab specimens was constructed and stored with Slabs 5 and 6. Plan views of the control specimens are shown in Figure 7-13 and Figure 7-14, respectively. The sections of the control specimens were identical to the sections of Slabs 5 and 6, shown in Figure 7-5. The control

specimen associated with Slab 5 contained a single sensor with a zinc sensing wire and fiber-reinforced cement paste housing. The sensor in the control specimen of Slab 6 had an aluminum sensing wire and fiber-reinforced cement paste housing. Incidentally, the top of the sensor in Figure 7-9 is not the top of sensor E20: it is the top of E18. E20 did not have an epoxy core but was included in Figure 7-9 because the bottom of its housing was properly cured. Appendix E discusses proper curing of the fiber-reinforced cement paste housing.

Corrosion current circulating in the control specimens was determined by measuring the potential difference over their resistors. Because the control specimens were not exposed to chlorides, the value of corrosion current circulating within them was regarded as an indication of the atmospheric contribution to the internal corrosion of Slabs 5 and 6.

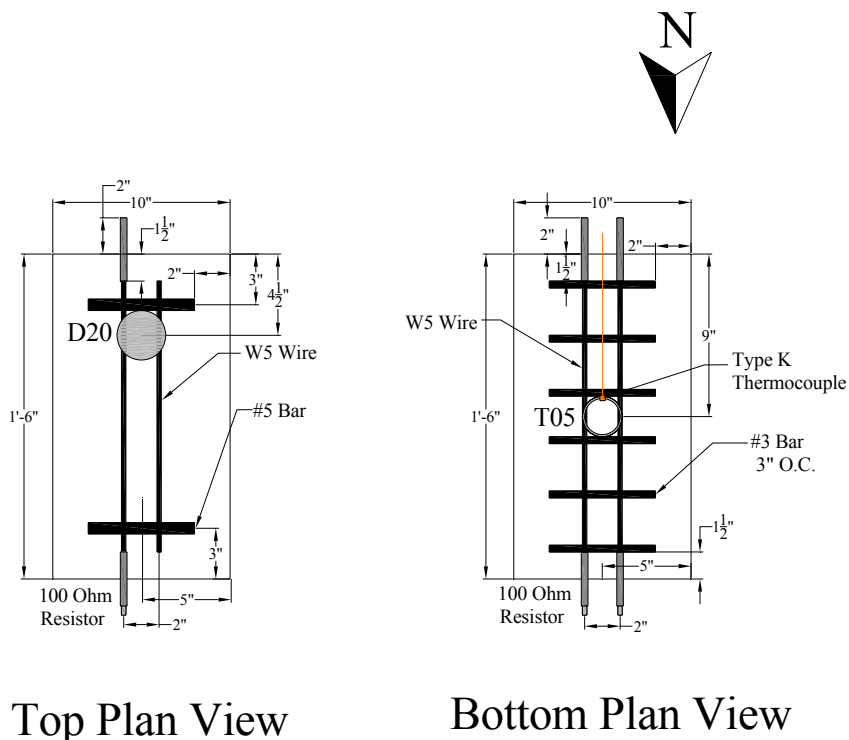


**Figure 7-13 Top and Bottom Plan Views of Slab 5 Control Specimen**

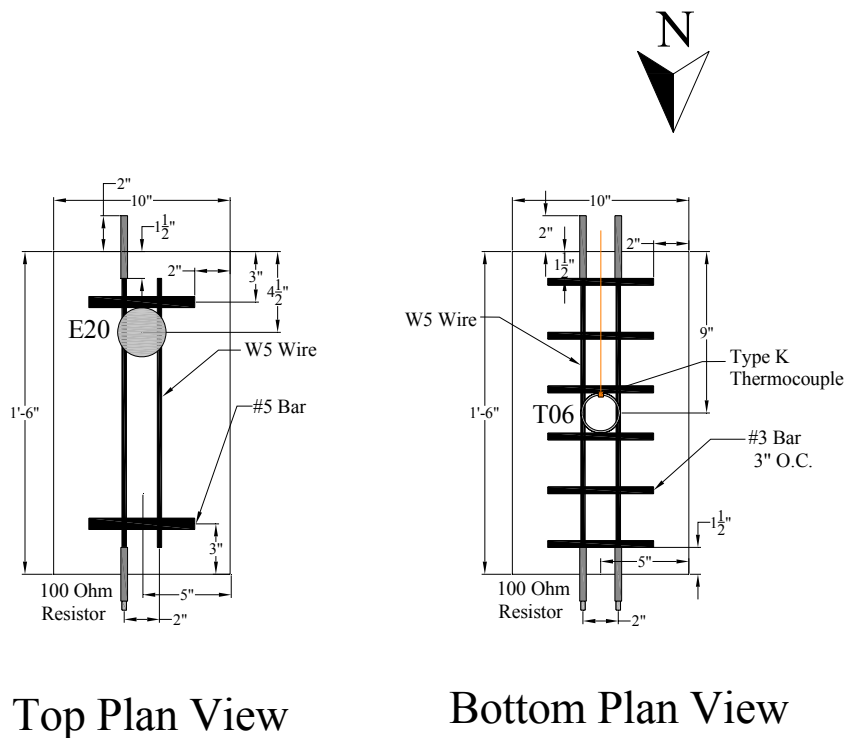


**Figure 7-14 Top and Bottom Plan Views of Slab 6 Control Specimen**

Type K thermocouples were included at the ends of Slabs 5 and 6 and within their associated control specimens to measure the internal temperature of the specimens. The end of the thermocouples, which sense the change in temperature, was placed 2 in. from the bottom surface of the specimens. The thermocouples were secured to the bottom layer of steel reinforcement by being wrapped around a 1-in. slice of  $2 \frac{3}{8}$  in. PVC conduit, which was secured to the reinforcement using plastic zip ties.

The concrete was placed 26 January 2007. The specimens were allowed to cure for four weeks and were draped with plastic to promote moist curing. Prior to the specimens being removed from the casting bed, the compressive strength of a concrete cylinder cast with the specimens was determined. The 18-day strength of the concrete was 3,200 psi. At the end of the curing period, the

specimens were loaded at their ends, as shown in Figure 7-15. The specimens were loaded until the maximum width of flexural cracks on their top surface was approximately 0.010 in. Crack maps of Slabs 5 and 6, recorded immediately after the specimens were loaded, are given in Figure 7-16 and Figure 7-17, respectively. Cracks smaller than 0.005 in. were not measured and thus were not included in the crack maps. The positions of the cracks in each specimen are superimposed over the positions of the sensors. In Figure 7-17, sensors with fractured sensing wires are red, while those with intact sensing wires are black.

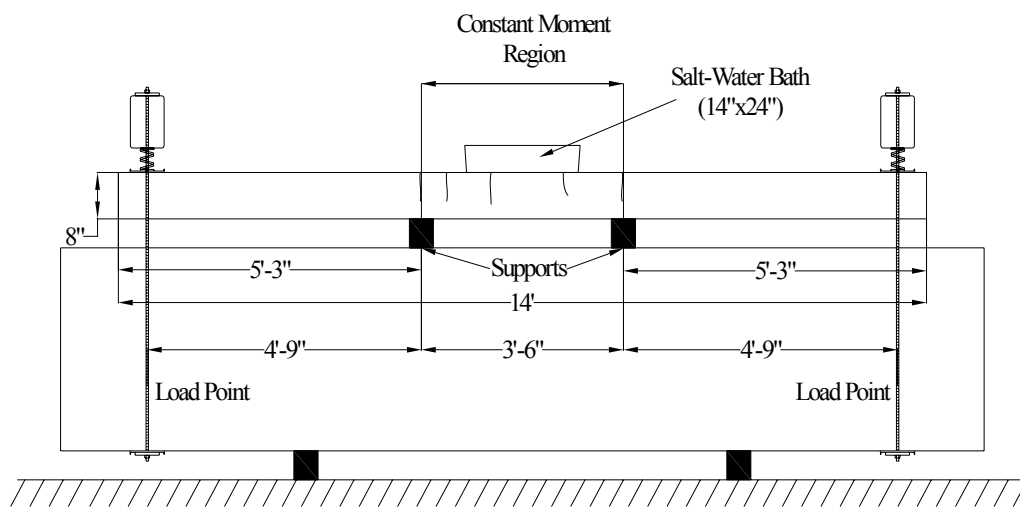


**Figure 7-15 Loaded Slab with Water Reservoir**

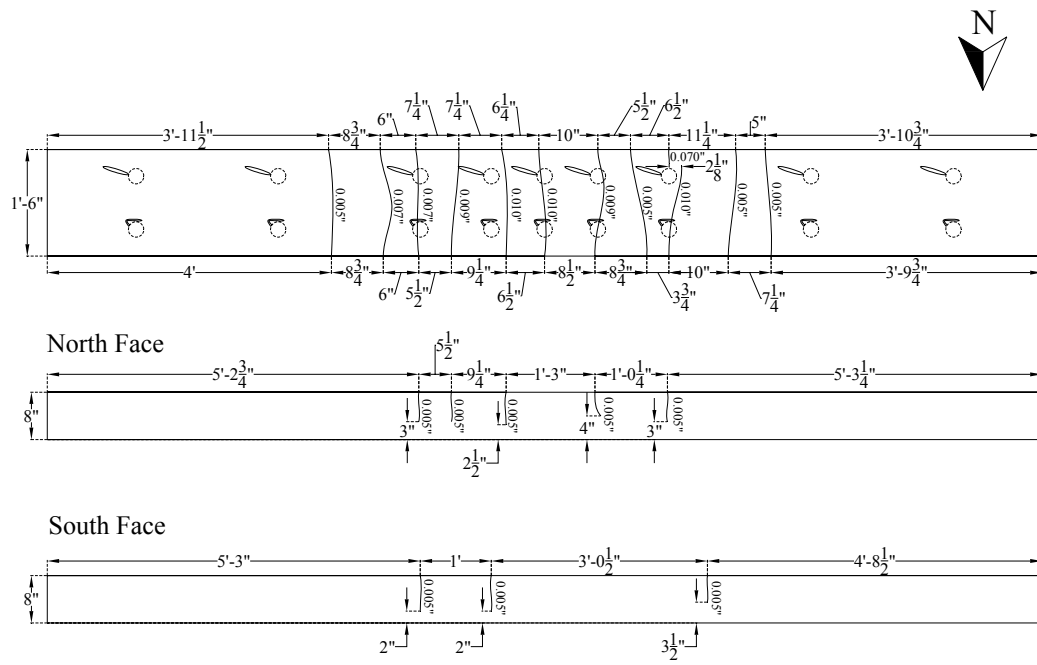


**Figure 7-16 Crack Map of Slab 5 Immediately after Loading**



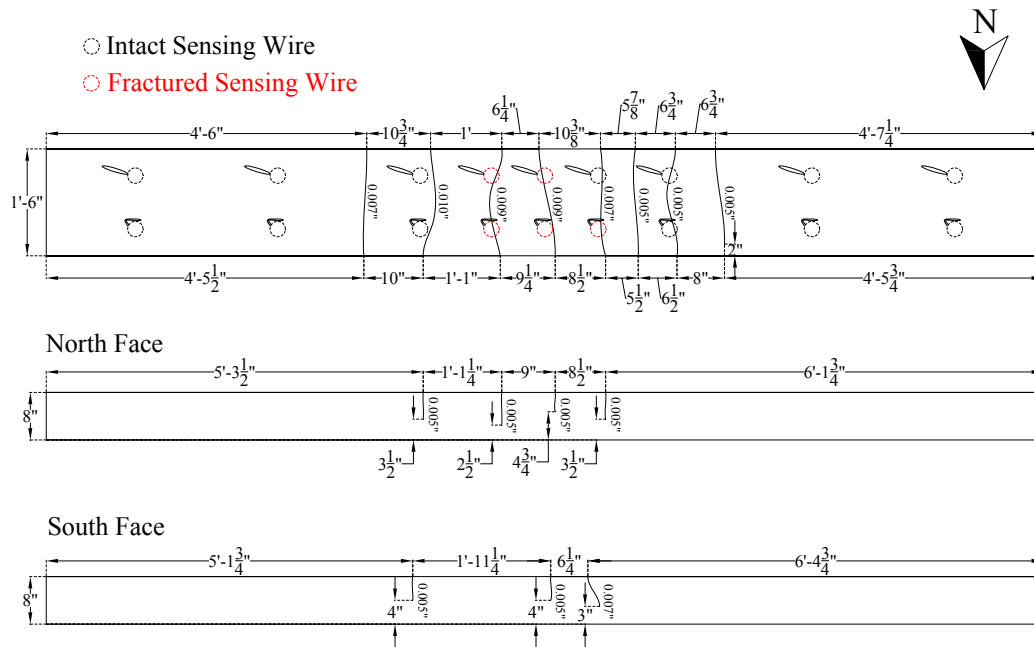


**Figure 7-17 Crack Map of Slab 6 Immediately after Loading**

After the specimens were loaded, salt-water reservoirs were fixed to the top surface of the specimens using the adhesive Sika 11FC. As discussed in Section 7.3.1, five of the six sensors with aluminum sensing wires embedded beneath the salt-water reservoir of Slab 6 signaled that their sensing wires had fractured after only 13 days of testing, the end of the first wet cycle. To determine whether the fracture of the sensing wires was due to moisture with chlorides or simply moisture, fresh-water reservoirs were placed above sensors E15 and E16 on day 29 of testing. The same was done in the case of D15 and D16 in Slab 5. The position of the salt-water and fresh-water reservoirs of Slabs 5 and 6 are shown in Figure 7-1 and Figure 7-3 and, respectively. The fresh-water wet and dry cycles corresponded in time with the salt-water wet and dry cycles.

These environmental cycles simulated extreme service conditions for a bridge deck.

Testing began 22 February 2007. The sensors were interrogated and the salt-water reservoirs filled with 3.5% NaCl by weight salt-water. The two-week wet cycle was followed by a two-week dry cycle, and the wet and dry cycles have continued for 14 weeks. The fresh-water cycles corresponded with the salt-water cycles once they began, after 29 days of testing. To control the exposure of the specimens to moisture and chlorides, the specimens have been stored indoors throughout testing. The temperature of the building was not controlled such that the specimens have been subjected to temperature fluctuations of over 30°F.

As was the case with Slabs 1 through 4, sensors were distributed along the length of Slabs 5 and 6 such that the sensors were exposed to varied conditions within the concrete. Because Slabs 5 and 6 were longer than Slabs 1 through 4, an additional 2 sensors per specimen were subjected to dry conditions. Because fresh-water reservoirs were placed over D15, D16, E15, and E16, these sensors were subjected to controlled moisture conditions without chlorides. Even though sensors D05, D06, D13, D14, E05, E06, E13, and E14, were located slightly closer to the salt-water reservoir than the transition sensors in Slabs 3 and 4, they likely still experienced transition conditions. The conditions to which the sensors were subjected are summarized in Table 7-2.

**Table 7-2 Moisture and Chloride Conditions of Sensors**

	<b>SLAB 5</b>	<b>SLAB 6</b>
<b>Ends of Slab</b> <i>(Dry Conditions)</i>	D01	E01
	D02	E02
	D03	E03
	D04	E04
	D17	E17
	D18	E18
<b>Beneath Fresh-Water Reservoirs</b> <i>(Controlled Moisture Conditions)</i>	D15	E15
	D16	E16
<b>Beneath Salt-Water Reservoir</b> <i>(Controlled Moisture and Chloride Conditions)</i>	D07	E07
	D08	E08
	D09	E09
	D10	E10
	D11	E11
	D12	E12
<b>Transition Regions</b> <i>(Varying Moisture and Chloride Conditions)</i>	D05	E05
	D06	E06

A Solartron SI 1260 Impedance/Gain-Phase Analyzer was used to interrogate the sensors. The reader coil was 4 in. in diameter, with five turns of 18-gage copper magnet wire. The reader coil was connected to the Solartron with a 3-ft coaxial cable. At the end of each environmental cycle, the sensors were interrogated and measurements were taken. The measurements included the static half-cell potentials of the specimens, the voltage over the resistors, and the internal temperature of the specimens at the locations of the thermocouples. The temperature and relative humidity of the air in which the specimens were stored was recorded before the half-cell potentials were taken. The static half-cell potentials were taken at locations shown in Figure 7-18. Interrogation and

measurement of the specimens are ongoing. Measurements of Slabs 5 and 6 not discussed in this chapter are reported in Appendix D.

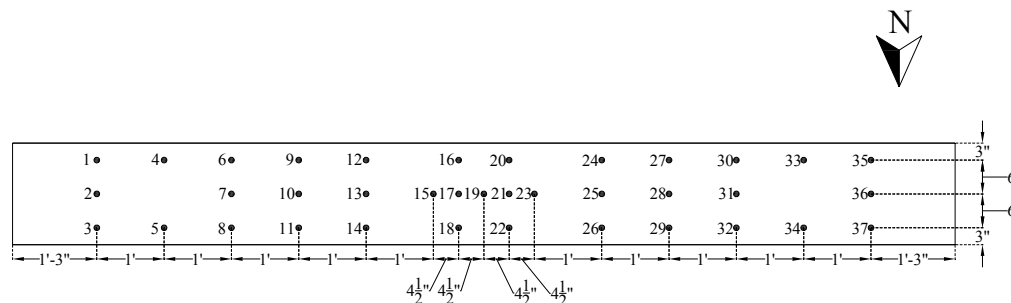


**Figure 7-18** Locations at which Half-Cell Potentials Taken in Slabs 5 and 6

### 7.3 MEASURED RESPONSE OF SENSORS

The measured responses of the sensors over the first 14 weeks of testing are discussed in this section. The data from sensors not discussed in this section are presented in Appendix D. While no sensor in Slab 5 signaled a fractured sensing wire, five of the eighteen sensors tested in Slab 6 signaled that their sensing wires had fractured. Section 7.3.1 describes the detected state of the sensors tested in Slabs 5 and 6. A statistical summary of the measured responses of sensors after 14 weeks of testing in Slabs 5 and 6 is given in Section 7.3.2. In no case did the phase dip at the sensing frequency reappear after the phase dip had disappeared due to the sensing wire fracturing. Thus, the internal environment of the concrete was not such that the environment completed the fractured sensing circuit with low enough resistance for a phase dip to appear at the sensing frequency. However, the internal environment of the concrete did influence the responses of the sensors, and this effect is assessed in Section 7.3.3. There were indications that the internal environment of the concrete was causing the reference

circuit of sensors without epoxy cores to decay with time. Section 7.3.4 discusses these indications.

### 7.3.1 State of the Sensing Wires after 14 Weeks of Testing

All sensors that signaled the initiation of corrosion were embedded beneath the salt-water reservoir in Slab 6. The sensors all had aluminum sensing wires, and the sensing wires all fractured between the first and second interrogations. That is, as shown in Figure 7-19, the sensing wires fractured on or before day 13 of testing. Figure 7-20 illustrates the position of sensors with fractured and intact sensing wires after 14 weeks of testing. The former are colored red, and the latter are colored gray.

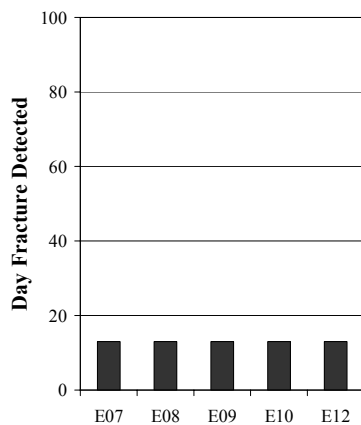


*Figure 7-19 Sensors with Fractured Sensing Wires after 14 Weeks of Testing*

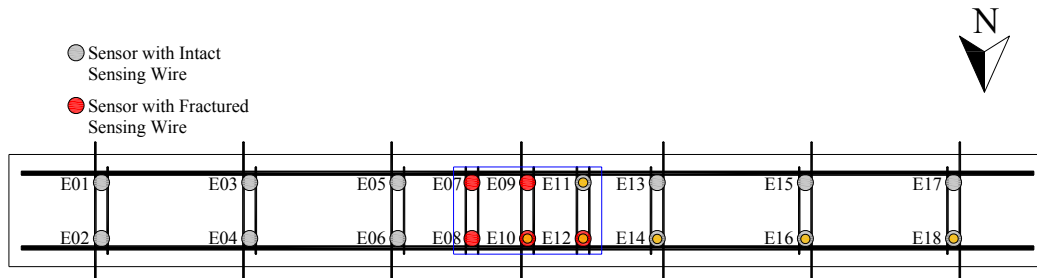


***Figure 7-20 Detected State of the Sensing Wires in Slab 6 after 14 Weeks of Testing***

All the sensing wires that fractured in Slab 6 were in the salt-water reservoir because that was the region of highest risk. Fracture of the sensing wires elsewhere in just 14 weeks of testing was unlikely because risk of corrosion decreased outside the salt-water reservoir. Fracture of all the aluminum sensing wires beneath the salt-water reservoir except one within the first two weeks of testing demonstrated that the sensors with aluminum sensing wires were highly responsive to the presence of moisture and chlorides in the concrete cover. However, the responsiveness of sensors with aluminum wires may result in their signaling false positives over long service periods. That is, the presence of agents other than chlorides, such as moisture and hydroxyls in the pore solution of the concrete, may cause corrosion of the aluminum sensing wire. Since day 29 of testing, sensors E15 and E16 have been exposed to wet cycles of fresh water. That the sensing wires of these two sensors have not fractured indicates that the sensing wires beneath the salt-water reservoir fractured due to the presence of chlorides. However, the cracks in the concrete cover above sensors E15 and E16 were smaller than 0.005 in. Consequently, the sensing wires of E15 and E16 may have fractured simply due to being exposed to moisture had the cracks on the concrete cover above the sensors been wider. Additional testing conducted to

assess the susceptibility of anodic sensors to signaling false positives is discussed in Chapter 8.

### 7.3.2 Summary of the Measured Response of the Sensors

A statistical summary of the responses of sensors during the first 14 weeks of testing in Slabs 5 and 6 is given in Table 7-3 through Table 7-7. The mean resonant frequency is denoted as  $f_0$ , mean phase dip as  $\phi$ , and mean pseudo-quality factor as  $\bar{Q}$ . Sensors with epoxy-core housings are shaded gray in the tables, while those without epoxy cores were left unshaded. As shown in the tables, the variability of the phase dips and pseudo-quality factors of the sensors was significant. In contrast to Slabs 1 through 4, the cause of this variability was not baseline shift. In fact, there were essentially no instances of baseline shift in the data of Slabs 5 and 6. An example is the response of sensors D18, shown in Figure 7-21. Rather, the cause of the variability in the response of sensors tested in Slabs 5 and 6 was likely changes in the moisture on the surface of the inductors of the sensors, as discussed in Section 7.3.3.

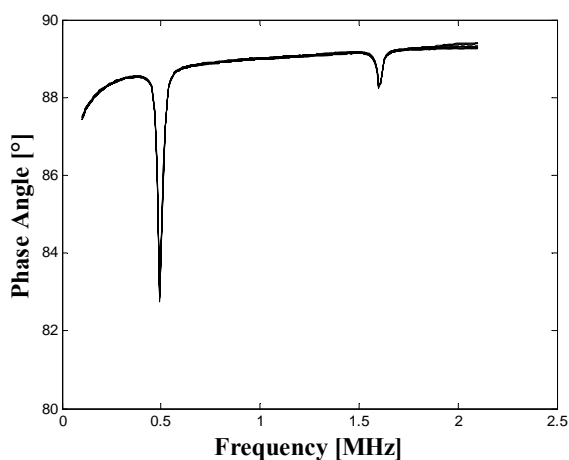


*Figure 7-21 Response of D18 over First 14 Weeks of Testing*

Another source of variability in the response of the reference circuit was likely the decay of the reference circuit with time. In fact, the pseudo-quality factors of many of the reference circuits tested in Slabs 5 and 6 decreased by 20% from their initial values over 14 weeks of testing. This effect and its likely causes are discussed in Section 7.3.4.



*Table 7-3 Statistical Summary of Sensors Tested in Slab 5 and Control*

Sensor	Sensing Circuit						Reference Circuit					
	$f_0$ [MHz]	COV [%]	$\phi$ [°]	COV [%]	$\bar{Q}$	COV [%]	$f_0$ [MHz]	COV [%]	$\phi$ [°]	COV [%]	$\bar{Q}$	COV [%]
<b>D01</b>	0.49	0.0	4.1	2.9	18.3	1.0	1.56	0.0	0.5	4.8	37.7	12.3
<b>D02</b>	0.49	0.0	4.5	3.6	20.6	2.2	1.55	0.0	0.7	4.6	44.2	7.8
<b>D03</b>	0.49	0.0	4.1	4.1	21.8	1.9	1.55	0.0	0.4	5.6	40.2	9.2
<b>D04</b>	0.49	0.0	3.9	4.2	22.0	1.8	1.56	0.0	0.4	5.1	42.3	8.4
<b>D05</b>	0.49	0.0	4.0	2.5	18.8	1.9	1.53	0.0	0.5	3.4	39.6	11.6
<b>D06</b>	0.49	0.0	3.7	2.3	22.8	3.1	1.56	0.1	0.4	5.2	40.4	14.1
<b>D07</b>	0.49	0.2	3.5	17.4	19.4	17.6	1.53	0.3	0.4	17.8	30.3	23.4
<b>D08</b>	0.49	0.2	3.6	17.5	19.8	18.7	1.56	0.2	0.4	20.6	30.3	24.9
<b>D09</b>	0.49	0.3	3.4	22.5	16.4	22.6	1.55	0.5	0.3	33.0	20.0	40.9
<b>D10</b>	0.49	0.4	5.1	14.5	22.9	15.0	1.59	0.2	0.7	9.9	44.9	10.1
<b>D11</b>	0.49	0.3	5.0	16.8	23.3	17.6	1.52	0.2	0.6	12.1	44.4	14.3
<b>D12</b>	0.49	0.3	5.6	15.9	25.7	14.7	1.57	0.2	0.6	14.5	45.6	15.5
<b>D13</b>	0.49	0.0	4.9	1.8	20.5	2.9	1.58	0.0	0.6	2.2	37.0	10.2
<b>D14</b>	0.49	0.0	5.1	2.6	21.8	1.7	1.55	0.0	0.8	1.9	56.2	5.9
<b>D15</b>	0.49	0.2	5.8	22.8	18.0	17.4	1.55	0.3	0.5	27.8	28.7	30.2
<b>D16</b>	0.49	0.1	5.9	18.4	21.7	8.0	1.56	0.1	0.9	17.3	47.5	7.6
<b>D17</b>	0.49	0.0	7.7	3.2	19.7	1.6	1.54	0.0	0.9	4.1	38.4	4.0
<b>D18</b>	0.49	0.0	6.2	1.8	18.5	0.5	1.60	0.0	1.0	2.8	53.1	3.4
<b>D20<sup>+</sup></b>	0.49	0.1	2.2	5.9	17.4	1.4	1.56	0.0	0.3	8.8	32.1	18.6

<sup>+</sup>Sensor embedded in control specimen; \*Shaded rows indicate sensors with epoxy cores

**Table 7-4 Statistical Summary of Sensors with Intact Sensing Wires Tested in Slab 6 and Control**

Sensor	Sensing Circuit						Reference Circuit					
	$f_0$ [MHz]	COV [%]	$\phi$ [°]	COV [%]	$\bar{Q}$	COV [%]	$f_0$ [MHz]	COV [%]	$\phi$ [°]	COV [%]	$\bar{Q}$	COV [%]
<b>E01</b>	0.49	0.0	6.6	3.3	20.2	1.9	1.57	0.0	0.7	5.4	39.3	4.5
<b>E02</b>	0.49	0.0	5.0	2.8	18.2	0.8	1.58	0.0	0.6	4.6	41.1	3.4
<b>E03</b>	0.49	0.0	4.7	4.3	19.9	1.9	1.56	0.0	0.5	5.2	39.7	6.0
<b>E04</b>	0.49	0.0	4.7	2.2	20.2	1.3	1.58	0.0	0.6	3.8	40.8	4.2
<b>E05</b>	0.49	0.1	6.0	3.9	20.8	2.1	1.56	0.0	0.6	4.5	38.5	5.9
<b>E06</b>	0.49	0.1	6.6	3.5	22.1	2.0	1.55	0.0	0.9	4.5	39.6	4.3
<b>E11</b>	0.49	0.2	7.4	11.7	23.2	11.4	1.58	0.2	0.7	10.3	43.2	11.5
<b>E13</b>	0.49	0.0	8.8	6.2	23.8	6.6	1.53	0.0	0.9	4.2	39.4	7.9
<b>E14</b>	0.49	0.0	6.4	3.7	24.2	3.3	1.57	0.0	0.9	3.1	49.1	3.1
<b>E15</b>	0.49	0.4	4.2	32.4	17.3	22.5	1.53	0.3	0.5	30.1	30.6	29.3
<b>E16</b>	0.49	0.1	4.7	17.2	19.1	7.2	1.57	0.2	0.7	19.7	45.3	12.2
<b>E17</b>	0.49	0.0	5.9	3.2	19.4	2.4	1.54	0.0	0.5	4.8	34.7	8.0
<b>E18</b>	0.49	0.0	6.3	3.0	20.4	1.8	1.55	0.0	0.9	3.1	50.1	4.0
<b>E20<sup>+</sup></b>	0.49	0.2	4.0	11.4	19.2	6.5	1.57	0.0	0.4	5.7	35.8	10.4

<sup>+</sup>Sensor embedded in control specimen; \*Shaded rows indicate sensors with epoxy cores

**Table 7-5 Mean Resonant Frequency of Sensors with Fractured Sensing Wires Tested in Slab 6**

Sensor	Sensing Circuit	Reference Circuit		
	<i>Intact</i>	<i>Intact</i>	<i>Fractured</i>	
	$f_0$ [MHz]	$f_0$ [MHz]	$f_0$ [MHz]	COV [%]
<b>E07</b>	0.49	1.56	1.40	0.6
<b>E08</b>	0.49	1.56	1.39	0.6
<b>E09</b>	0.49	1.54	1.38	0.5
<b>E10</b>	0.49	1.57	1.41	0.2
<b>E12</b>	0.49	1.55	1.40	0.3

**Table 7-6 Mean Phase Dip of Sensors with Fractured Sensing Wires Tested in Slab 6**

Sensor	Sensing Circuit	Reference Circuit		
	<i>Intact</i>	<i>Intact</i>	<i>Fractured</i>	
	$\phi$ [°]	$\phi$ [°]	$\phi$ [°]	COV [%]
<b>E07</b>	5.7	0.6	1.8	23.2
<b>E08</b>	4.9	0.7	1.7	31.6
<b>E09</b>	5.6	0.6	2.0	28.9
<b>E10</b>	4.4	0.8	2.0	14.4
<b>E12</b>	6.4	0.8	3.4	16.8

**Table 7-7 Mean Pseudo-Quality Factor of Sensors with Fractured Sensing Wires Tested in Slab 6**

Sensor	Sensing Circuit	Reference Circuit		
	<i>Intact</i>	<i>Intact</i>	<i>Fractured</i>	
	$\bar{Q}$	$\bar{Q}$	$\bar{Q}$	COV [%]
<b>E07</b>	23.0	40.8	14.8	24.0
<b>E08</b>	21.63	41.7	14.4	35.2
<b>E09</b>	22.4	44.6	17.2	31.9
<b>E10</b>	23.0	55.5	20.5	11.0
<b>E12</b>	26.0	50.8	28.7	15.0

### **7.3.3 Effect of Moisture on the Surface of the Sensor Inductors**

In almost all cases, the phase dips and pseudo-quality factors for the sensors oscillated between high and low values. For brevity, this oscillation of phase dips and pseudo-quality factors between high and low values is called cyclical response. The cyclical response of the sensors correlated with the moisture cycles of the concrete. That is, at the end of a wet cycle, the phase dips and pseudo-quality factors of the sensors were lower in value. At the end of a dry cycle, the phase dips and pseudo-quality factors of the sensors were higher in value. Evidently, the internal environment of the concrete influenced the response of the sensors. This cyclical quality was most apparent in the response of sensors embedded beneath the salt-water and fresh-water reservoirs. As shown in Figure 7-22, the response of sensor D11, which had an epoxy-core housing, illustrates this behavior. In the case of all sensors discussed in this chapter, contour lines were placed at the following values of phase angle: 80°, 82°, 84°, 86°, 88°, 88.9°, and 90°. Incidentally, the effect of temperature on the response of sensors tested in Slabs 5 and 6 was examined as in Section 5.3.6. As in the case of Slabs 3 and 4, the responses of sensors tested in Slabs 5 and 6 were not sensitive to changes in temperature and depend weakly on temperature. Therefore, the contribution of temperature variations to sensor response was neglected.

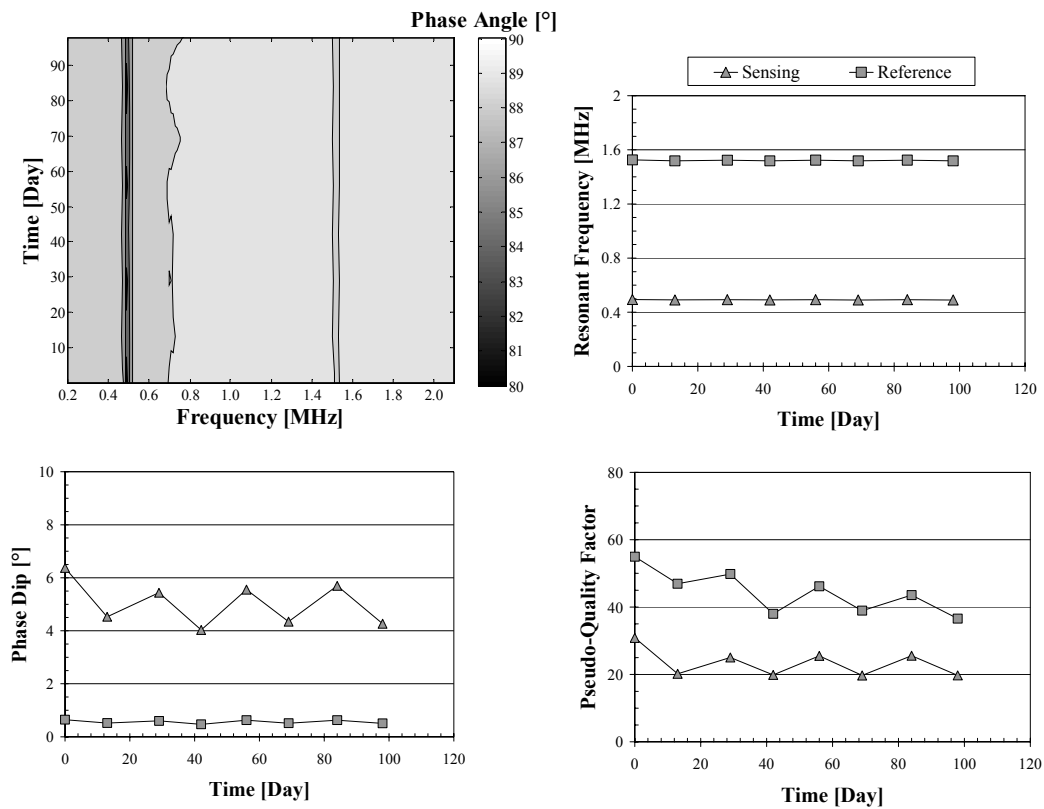


**Figure 7-22 Response of Sensor D11**

Because the housing of sensor D11 had an epoxy core, the only components of the circuitry exposed to the internal environment of the concrete by the permeable fiber-reinforced cement paste housing were the inductors for both the sensing and reference circuits. This condition is illustrated in Figure 7-8 and Figure 7-9. Sensors with intact sensing wires in Slabs 1 through 4 did not, on the whole, exhibit distinct cyclic response. In addition, the only way in which sensor D11 differed from sensors tested in Slabs 1 through 4 was that its inductors were exposed to moisture variations due to the permeability of the fiber-reinforced cement paste. Therefore, variability in the response of D11 was likely introduced by changes in the amount of moisture in contact with its inductors.

Plastic shrinkage cracks in the fiber-reinforced cement paste significantly increased the permeability of the sensor housings. Nearly all the housings for sensors embedded in Slabs 5 and 6 developed plastic shrinkage cracks prior to their being embedded in the specimens. An instance of severe cracks in the housing of a sensor, sensor E08, due to plastic shrinkage is shown in Figure 7-23. Control over the quality of sensor housing increased as more sensor housings were potted. As a result, the sensors with epoxy cores had fewer plastic shrinkage cracks than those without epoxy cores because they were the last set of sensors potted. As will be discussed in Appendix E, moist curing reduced the extent of plastic shrinkage cracks. Another factor that likely reduced the extent of plastic shrinkage cracks in the epoxy-core sensors was that they were potted 8 days prior to the placing of concrete in Slabs 5 and 6. In contrast, the sensors without epoxy cores were potted 14 to 22 days prior to placing of the concrete. Because the curing concrete was a source of moisture for the curing fiber-reinforced cement paste housings, a decrease in the time interval between potting of the housing and placing of the concrete likely decreased the extent of plastic shrinkage cracks.

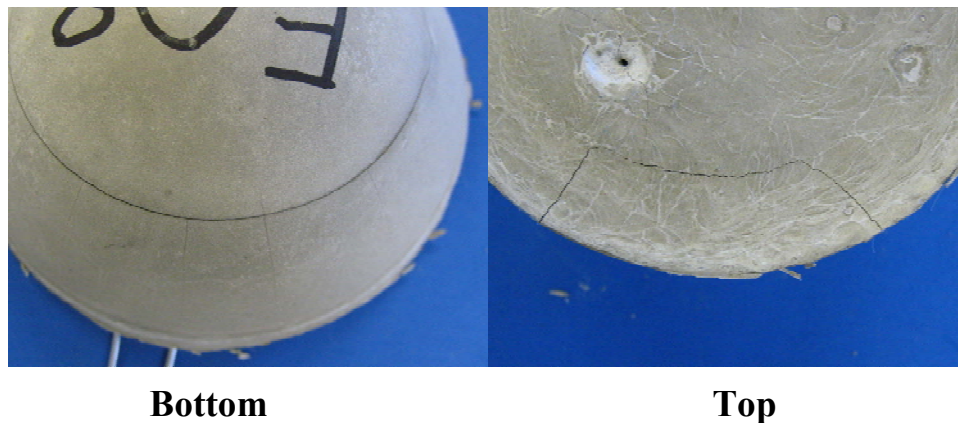


*Figure 7-23 Plastic Shrinkage Cracks in the Housing of E08*

The permeability of the sensor housings permitted moisture to reach the surface of the sensor inductors. Changes in the amount of moisture in contact with the inductors caused changes in the parasitic inductance on the coupled circuit of the reader coil and sensor. Parasitic inductance on the coupled circuit is in general due to the coupled circuit magnetically coupling with the environment around the circuit. Because such coupling consumes magnetic energy, parasitic inductance is manifested as a decrease in the phase dips and pseudo-quality factors of the sensor. Moisture in direct contact with the inductors increased the coupling of the reader coil and sensor to the surrounding environment. The larger the amount of moisture, the greater the coupling with the surrounding environment. Therefore, at the end of a wet cycle, more moisture adhered to the surface of the inductors, increasing parasitic inductance on the coupled circuit and decreasing the response parameters. In contrast, at the end of a dry cycle, less moisture adhered to the surface of the inductors, decreasing the parasitic inductance on the coupled circuit and increasing the response parameters. The effect of changes in moisture was amplified in the case of the reference circuit by influence from the sensing circuit through mutual inductance. Sensor D11, the response of which is shown in Figure 7-22, is an example of cyclic response being amplified in the case of the reference circuit.

The above conjecture was empirically verified with the following experiment. A single RLC circuit with the electrical components — capacitor and inductor — of a sensing circuit was placed in a dry container beside a threaded steel bar  $\frac{5}{8}$  in. in diameter and 4 in. in length. The experiment is shown in Figure 7-24. The circuit was interrogated, and the result, with response parameters, is shown in Figure 7-25, labeled “Dry.” The read range between the reader coil and sensor was 1 in. Then, the container was filled with a simulated concrete pore solution that had been contaminated with chlorides. The solution contained 1%

pulverized concrete and 3% salt by weight. The container was filled in such a way that only the inductor of the sensing circuit was in contact with the solution. That is, no other circuit component or exposed copper leads contacted the solution. This situation was identical, in exposure of the inductor, to that of sensors with an epoxy core. The circuit was interrogated a second time with the solution in the container, and the result, with response parameters, is shown in Figure 7-25, labeled “Wet.” The phase dip and pseudo-quality factor decreased significantly from the dry case to the wet case. Therefore, from the experiment, moisture in contact with the inductor of an RLC circuit increases the parasitic inductance associated with the circuit and reader coil. This effect, in turn, is likely amplified in the response of the reference circuit through mutual inductance.

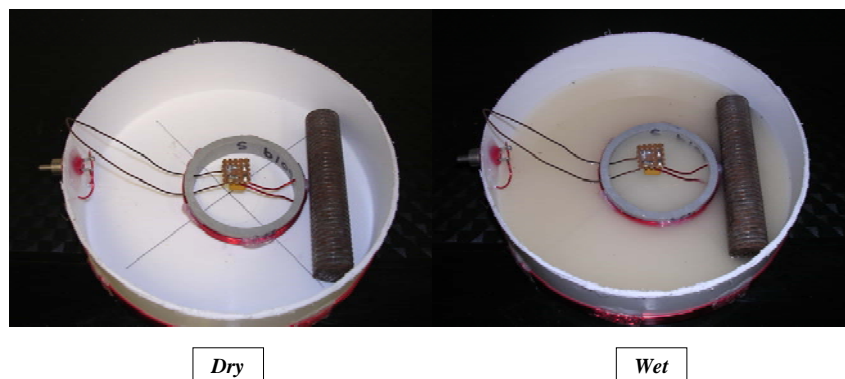


***Figure 7-24 Experiment Indicating Effect of Parasitic Inductance***



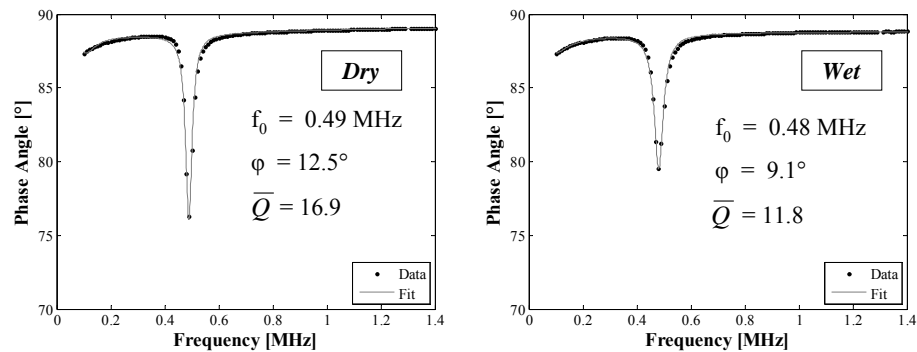


**Figure 7-25 Parasitic Inductance due to Moisture**

Exposure of the circuitry of the sensors, by the permeable cement paste housing, to significant changes in the moisture content of the concrete introduced additional variability into the phase dips and pseudo-quality factors of the reference circuits. The reference circuit was markedly sensitive to the effect of changes in moisture content because it was likely influenced by the sensing circuit through mutual inductance. The coefficients of variation of the phase dips and pseudo-quality factors of the reference circuits of epoxy-core sensors were lower than those of sensors without epoxy cores, all things being equal. Furthermore, because the sensors without epoxy cores were exposed to greater parasitic inductance in general, the mean phase dips and pseudo-quality factors of their reference circuits were lower than those of sensors with epoxy cores. These observations are illustrated in Figure 7-26 and Figure 7-27 by a comparison of the sensors embedded beneath the salt-water reservoirs in Slabs 5 and 6. It should be noted that all sensors with zinc sensing wires compared below had intact sensing wires, while the five sensors with aluminum sensing wire compared below had fractured sensing wires.

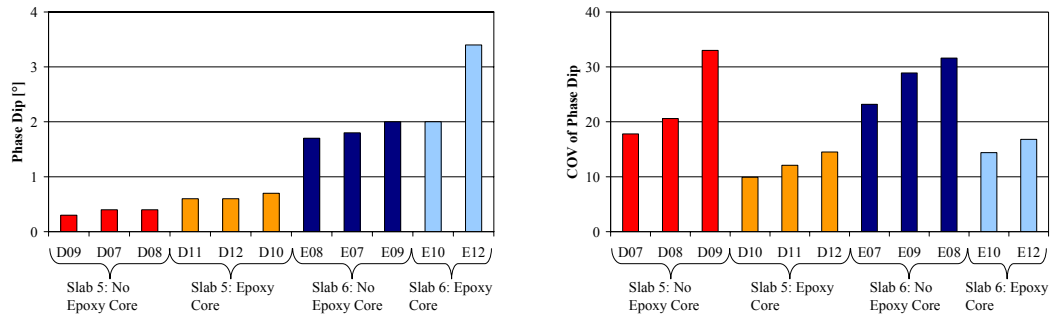


**Figure 7-26 Effect of Sensor Housing on Value and Variability of Reference Phase Dip**

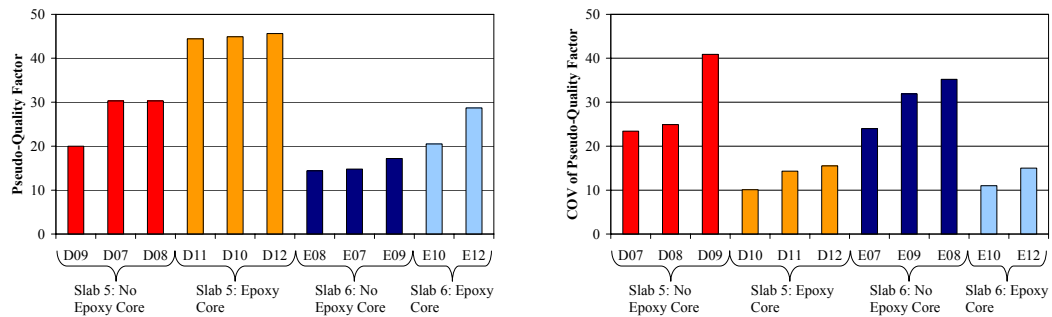


**Figure 7-27 Effect of Sensor Housing on Value and Variability of Reference Pseudo-Quality Factor**

Cyclical response of the sensors was also observed in sensors with fractured sensing wires. The response of sensor E07 is shown in Figure 7-28. This effect was likely due primarily to changes in the amount of moisture in contact with the inductor of the reference circuit. However, the sensing circuit of E07 may have continued to influence the response of the reference circuit. As was observed in the case of Slabs 3 and 4 and discussed in Section 5.3.3, the moisture within the pore structure of the concrete likely completed the sensing circuit, but the completed sensing circuit had high resistance. Consequently, a phase dip did not reappear at the sensing frequency. Once completed, the sensing

circuit influenced the reference circuit as if the sensing circuit were intact. The result was cyclic response of the reference circuit of sensors with fractured sensing wires. Such an effect may have been present in the response of E07 at the reference frequency. It should be emphasized that the cyclic response observed in Slabs 3 and 4 did not develop until after the sensing wire had fractured. In contrast, cyclic response in Slabs 5 and 6 was present in sensors prior to their sensing wires fracturing. This difference suggested different explanations for the cause of the cyclic response in Slabs 3 and 4 and Slabs 5 and 6.

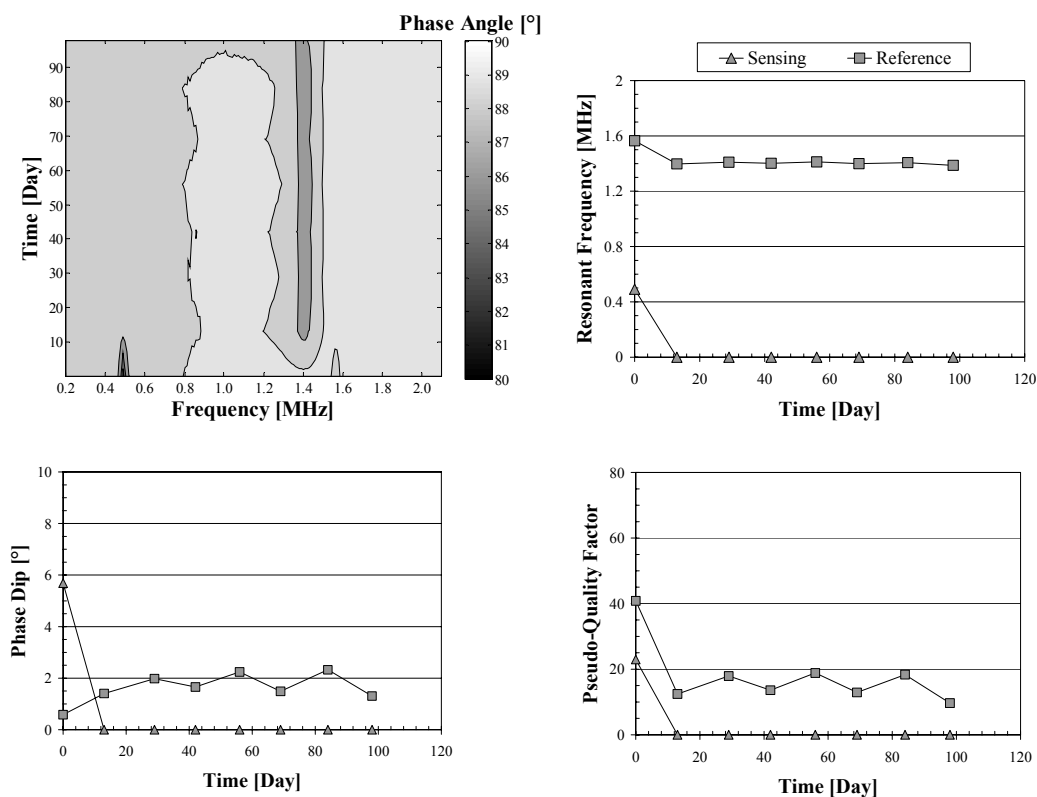


**Figure 7-28** Response of Sensor E07

### **7.3.4 Causes of the General Decrease in the Phase Dip and Pseudo-Quality Factors of the Reference Circuits**

In addition to varying with the moisture cycles of the specimens, pseudo-quality factors for the reference circuits of most sensors decreased with time. The response of D11, shown in Figure 7-22, typifies this trend. A decrease in the pseudo-quality factor of the reference circuit is significant because such a decrease has been an indication that the reference circuit was decaying with time. In Section 5.3.5, a precipitous decrease in the pseudo-quality factor of B152 was observed to correlate with the formation of black corrosion along the reference circuit within the epoxy housing. Furthermore, a decrease in the pseudo-quality factor of the reference circuit of B135 occurred before the phase dip at the reference frequency disappeared. The case of B152 and B135 support use of the reference pseudo-quality factor as a parameter characterizing the condition of the reference circuit.

Table 7-8 lists the change in the pseudo-quality factor of the reference circuit for all sensors in Slabs 5 and 6. The percent change is relative the value of the pseudo-quality factor on the second interrogation, and the change is from the value on the second interrogation to the value on the 14-week (last-reported) interrogation. The value on the last interrogation was compared with the value on the second interrogation because both of these interrogations occurred at the end of a wet cycle. Comparing the pseudo-quality factor of the reference circuit on the last interrogation to that on the first interrogation would have inflated the percent change because the specimens had not undergone a wet cycle prior to the first interrogation. In Table 7-8, a negative change represents a decrease in the pseudo-quality factor for the reference circuit, while a positive change represents an increase. Furthermore, gray shading indicates that the sensor had an epoxy-

core housing. Finally, italicization of the name of a sensor indicates that the sensing wire of the sensor had fractured.

**Table 7-8 Change in Reference Pseudo-Quality Factor of Sensors Tested in Slabs 5 and 6**

Sensor	Change in Reference $\bar{Q}$ [%]	Sensor	Change in Reference $\bar{Q}$ [%]
D01	-33	E01	-5
D02	-22	E02	-5
D03	-24	E03	-9
D04	-21	E04	-7
D05	-29	E05	-10
D06	-33	E06	-9
D07	-28	<i>E07*</i>	-23
D08	-22	<i>E08*</i>	-3
D09	-8	<i>E09*</i>	-10
D10	0	<i>E10*</i>	17
D11	-22	E11	-8
D12	-19	<i>E12*</i>	31
D13	-25	E13	-18
D14	-15	E14	-7
D15	-52	E15	-56
D16	-20	E16	-19
D17	-12	E17	-18
D18	-9	E18	-9
D20	-26	E20	-16

Notes: Shaded sensors represent sensors with epoxy cores.

\*Sensors with fractured sensing wires.

Several observations can be made from Table 7-8. First, all sensors, with the exception of D10, E10, and E12 experienced decreases in the pseudo-quality factors for the reference circuit during 14 weeks of testing. In many cases, this decrease was significant: the value of the pseudo-quality factor decreased by 20% or more for 15 sensors. The possibility of the fiber-reinforced cement paste housing causing corrosion of the circuitry suggests that in order to assess possible causes of decrease of the reference pseudo-quality factor, sensors should be

distinguished by type of housing — fiber-reinforced cement paste with or without epoxy core.

#### ***7.3.4.1 Sensors with Epoxy-Core Housings***

There were two likely causes of the decrease of the reference pseudo-quality factor in sensors with epoxy-core housings and intact sensing wires. As shown in Figure 7-8 and Figure 7-9, all of the circuit components of a sensor with an epoxy-core housing were materially separated from the alkaline environment of the concrete. Even though the inductors were exposed to the alkaline environment, they were materially isolated because the copper magnet wire used to fabricate the inductors had an intact finish. Thus, the inductors could not chemically react with environment around them. Rather, the inductors only interacted with their surrounding environment by magnetic coupling. Furthermore, a testing period of 14 weeks was likely too short a period for black corrosion to develop within the epoxy core. Indeed, sensors B152 and B135, discussed in Section 5.3.5, did not indicate the presence of damage due to internal black corrosion until after nearly a year of testing. Therefore, decay of the circuitry of the sensor due to chemical reaction with the surrounding environment was likely not a cause of the decrease in the reference pseudo-quality factor of sensors with epoxy-cores housings.

With decay of the circuitry eliminated as a possible cause, the decrease in the phase dip and pseudo-quality factor of the reference circuit was due either to gradual corrosion of the sensing wire or increasing moisture content of the environment around the sensing circuit. In the case of the former, gradual corrosion of the sensing wire would increase the resistance of the sensing wire. If the corrosion were gradual enough, it would likely have little detectable effect on the response of the sensing circuit but be detectable in the response of the

reference circuit. Slight changes in the condition of the sensing circuit have been undetectable in the response of the sensing circuit but detectable in the response of the reference circuit. An example is the response of sensor B155 discussed in Section 5.3.3. In contrast, increasing the moisture content of the concrete around the inductors would increase the parasitic inductance. If the increases were gradual enough, the effect in the response of the sensor would be observed at the reference frequency more readily than at the sensing frequency. However, increasing moisture content likely was not the cause of the decrease in the reference pseudo-quality factor. If it were the cause, some decrease in the reference pseudo-quality factor of sensors with epoxy-core housings and fractured sensing wires would be expected, but there was no such decrease. Indeed, effects due to the change in the moisture content of the concrete on the response of an epoxy-core sensor were observed whether or not the sensing wire was intact. For example, the response of sensor E12, as shown in Figure 7-29, was cyclical in correlation with changes in moisture content of the concrete. E12 both had an epoxy-core housing and a fractured sensing wire.

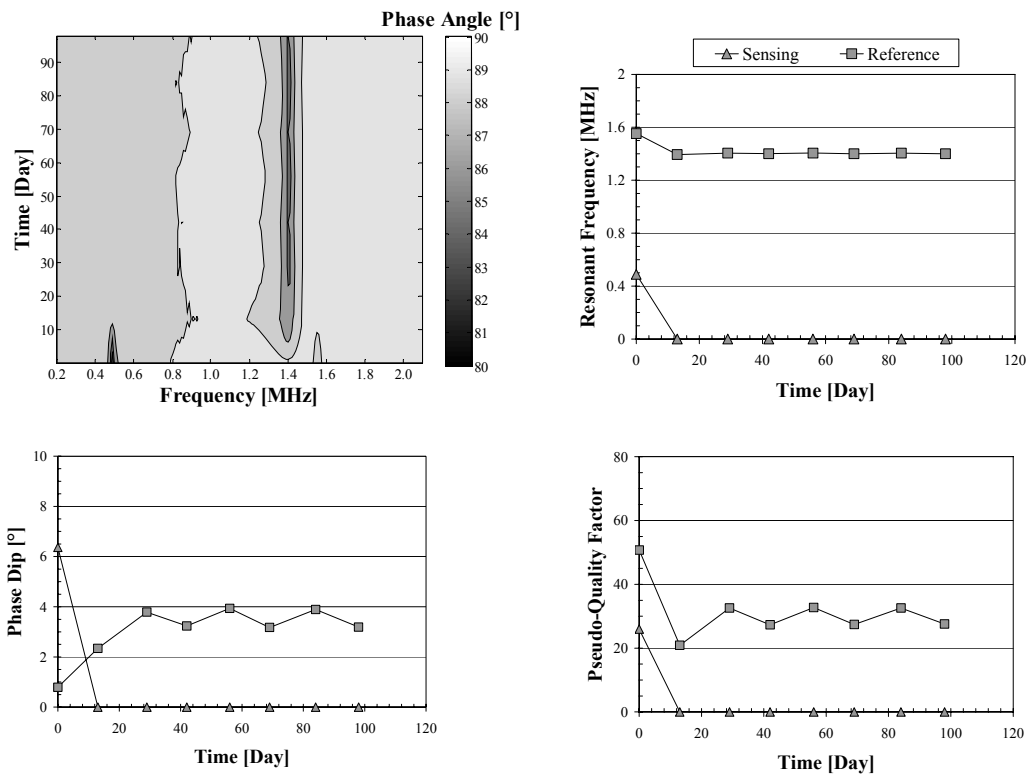


**Figure 7-29 Response of Sensor E12**

With decay of the circuitry of the sensor and increasing moisture content of the concrete excluded, the likely cause of the decrease in the pseudo-quality factor of the reference circuit of sensors with epoxy-core housings was gradual corrosion of the sensing wire. This conclusion can be reinforced with a brief statement of the argument. The reference pseudo-quality factors of sensors with epoxy cores decreased unless the sensing wire was fractured. In fact, no sensor with an epoxy core and fractured sensing wire exhibited a decrease in the reference pseudo-quality factor. The only difference between sensors with decreasing pseudo-quality factors and those without was the state of their sensing wires. Therefore, the decrease was likely caused by changes in the intact sensing circuit. These changes were manifest in the response of the reference circuit through mutual inductance. Because the only plausible way in which the sensing



circuit could change with time was corrosion of the sensing wire, corrosion of the sensing wire caused a decrease in the reference pseudo-quality factor by adding to the resistance of the reference circuit through mutual inductance. Because the corrosion was gradual, it was not yet detectable in the response of the sensing circuit. Though uniform corrosion of the sensing wires seems to be the most likely cause of the gradual decrease of the reference pseudo-quality factor, additional testing is required to firmly support that conclusion.

#### ***7.3.4.2 Sensors without Epoxy-Core Housings***

Sensors with fiber-reinforced cement paste housings having intact sensing wires also exhibited a decrease in the pseudo-quality factor at the reference frequency. For example, the pseudo-quality factor of the reference circuit of D06, which was in the transition region of the slab, decreased 33% from the second interrogation to the 14-week interrogation. The response of D06 is shown in Figure 7-30.

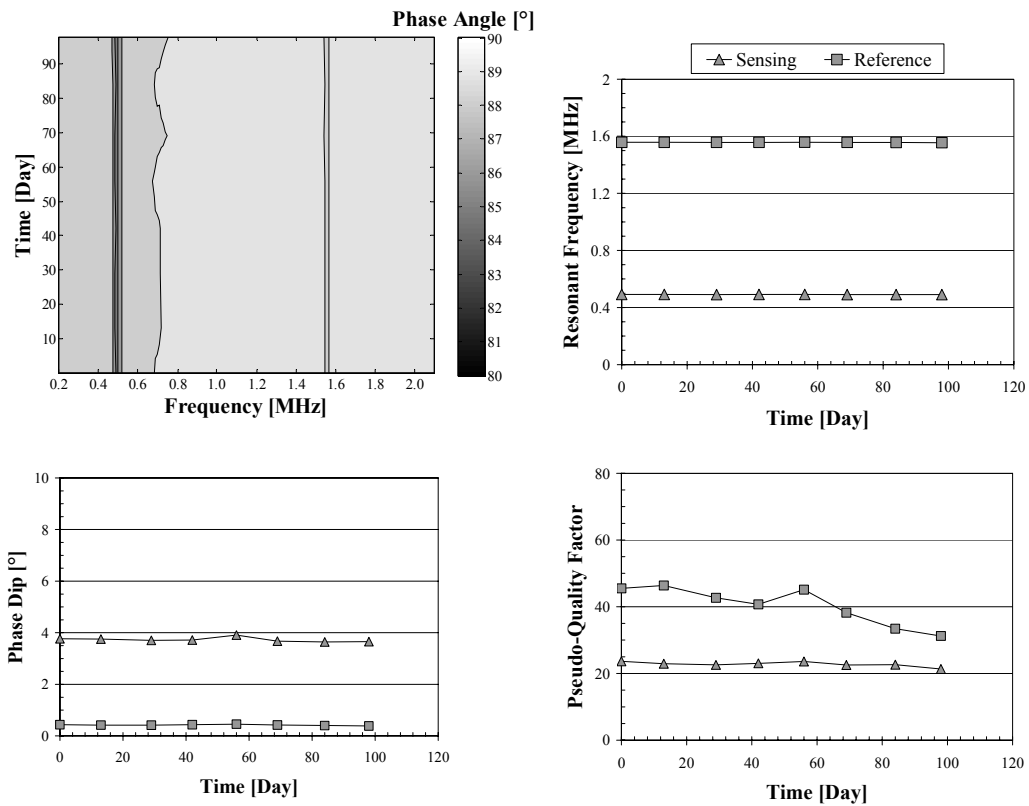


**Figure 7-30 Response of D06**

In contrast to sensors with an epoxy core, the circuitry of sensors without an epoxy-core was exposed to the internal environment of the concrete through the permeable housing. Consequently, an additional possible cause of the gradual decrease in the reference pseudo-quality factor of sensors without an epoxy core was decay of the circuitry of the sensor. Two other possible causes were gradual corrosion of the sensing wire and increasing moisture content of the concrete around the sensor. Again, increasing moisture content of the concrete was an unlikely cause because there was no decrease in the reference pseudo-quality factors of sensors with epoxy-core housings and fractured sensing wires. Furthermore, the decrease in the pseudo-quality factor of the reference circuit of D06 and other sensors without epoxy-core housings was too rapid to be caused

simply by corrosion of the sensing wire, without a detectable change in the response of the sensing circuit. Indeed, the response of D06 was similar to that of B152, discussed in Section 5.3.5, the reference circuit of which decayed due to internal black corrosion. Therefore, the pseudo-quality factor of sensors with intact sensing wires but without epoxy-core housings was most likely due to decay of the circuitry of the sensors. With such a housing, the copper leads of the circuit are exposed to the alkaline environment of the fiber-reinforced cement paste housing and concrete, possibly an aggressive environment for the copper.

Decay of the circuitry was also the likely cause of decrease in the reference pseudo-quality factor of sensors with fractured sensing wires. The only difference between sensors E07, the response of which is shown in Figure 7-28, and E12, the response of which is shown in Figure 7-29, is that the housing of the former lacks an epoxy core, while that of the latter includes an epoxy core. However, the reference pseudo-quality factor of E07 decreased with time whereas that of E12 actually increased with time. Therefore, the most likely cause of the decrease in the reference pseudo-quality factor of E07, and other sensors of its class, was that the circuitry of the sensor was exposed to the alkaline environment of the cement paste and concrete. In that case, the reference circuit of E07 was decaying much like that of D06.

#### **7.4 SENSOR RESPONSE, HALF-CELL POTENTIALS, AND CORROSION CURRENT**

Because testing of Slabs 5 and 6 is ongoing, the response of the sensors could only be compared with the measured half-cell potentials taken during the first 14 weeks of testing. This comparison is discussed in Section 7.4.1. At the conclusion of testing, when the specimens are autopsied, the signals of the sensors will additionally be compared with the observed condition of the reinforcement and the chloride concentration of the concrete cover. Section 7.4.2 describes the

distribution of current in Slabs 5 and 6 and compares the total current circulating in the specimens to the total current in Slabs 3 and 4.

#### **7.4.1 Half-Cell Potentials**

The half-cell potentials of Slabs 5 and 6 were obtained with a standard calomel electrode (SCE), in units of millivolts. Values on the SCE scale were converted to the copper-copper-sulfate electrode (CSE) scale to determine risk of corrosion in terms of ASTM C876. Inferences about risk of corrosion in the case of Slabs 5 and 6 were less certain than in the case of Slabs 1 through 4 because Slabs 5 and 6 included metals other than steel. That is, the zinc and aluminum sensing wires and parts of the copper circuitry of the sensors were in electrical contact with the steel reinforcement. It is possible that these metals influenced the potential of the steel at any given location.

As in the case of Slabs 1 through 4, potentials at points equidistant from the center of the salt-water reservoir were averaged and plotted with respect to time as a single data series. From Figure 7-18, there were eight series of data for each specimen: 69", 57", 45", 33", 21", 9", 4.5", and center. The result for Slabs 5 and 6 are shown in Figure 7-31 and Figure 7-32, respectively. In the case of Slab 5, the half-cell potentials within the salt-water reservoir indicated severe risk of corrosion whereas those in the transition areas, data series 21", reached high risk of corrosion. Elsewhere on Slab 5, the risk of corrosion was intermediate. In the case of Slab 6, half-cell potentials within the salt-water reservoir indicated severe risk of corrosion. Potentials in the transition areas, again data series 21", indicated high risk of corrosion. In contrast to Slab 5, the half-cell potentials of Slab 6 a distance of 33" from the center of the salt-water reservoir reached the high risk of corrosion. Elsewhere in Slab 6, the risk of corrosion was intermediate. Again, because the estimates of corrosion risk given in ASTM

C876 do not take account of galvanic effects, these estimates of corrosion risk given for Slabs 5 and 6 should to be considered to be approximate.

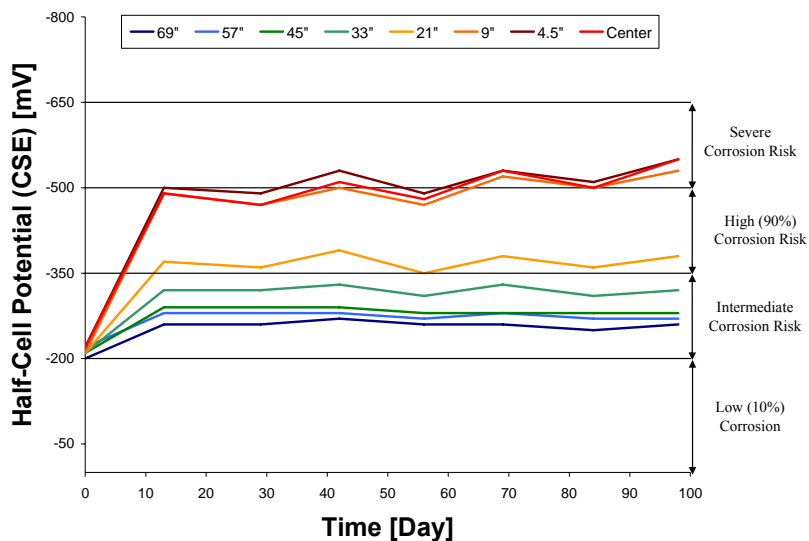


*Figure 7-31 Half-Cell Potentials of Slab 5 with Respect to Time*

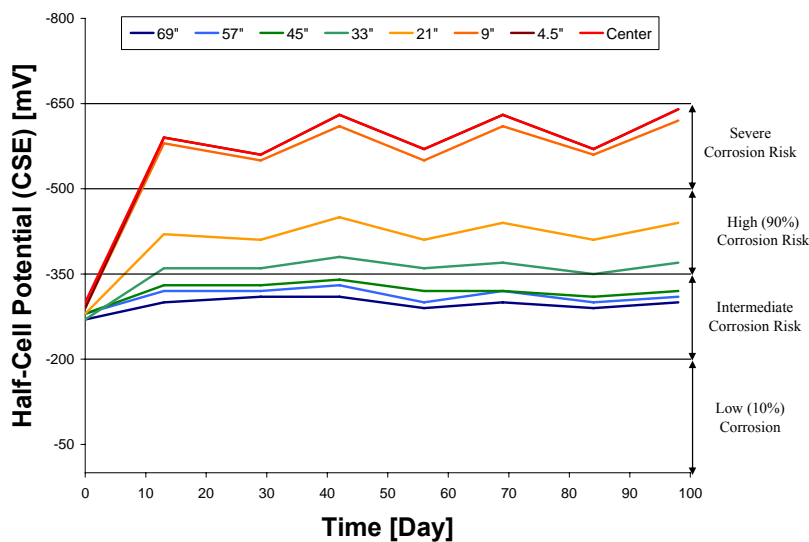


*Figure 7-32 Half-Cell Potentials of Slab 6 with Respect to Time*

In order to compare the risk of corrosion indicated by the half-cell potentials taken from Slabs 5 and 6 with the signals of the sensors, contour plots of the half-cell potentials were developed. The contour plots were obtained by linearly interpolating among the measured values shown in Figure 7-18. The half-cell potentials converged over time to two distinct values associated with the environmental cycles to which the specimens were subjected, with the potentials at the end of a wet cycle being higher than those at the end of a dry cycle. Consequently, two contour plots were developed for each specimen, one corresponding to the end of the last wet cycle, the other corresponding to the end of the last dry cycle. These contour plots are shown in Figure 7-33 through Figure 7-36. The half-cell potentials of Slabs 6 at the end of the environmental cycle during which the sensors in Slab 6 fractured is shown in Figure 7-37. The gridlines on the plots were spaced 3 in. apart, both in the vertical and horizontal directions. The positions of sensors tested in Slabs 5 and 6 were superimposed on the contour plots to illustrate risk of corrosion near the sensors. The sensors with aluminum sensing wires, tested in Slab 6, were highly responsive in that five of the six sensors in the region of severe corrosion risk signaled that their sensing wires had fractured. That is, the signals of sensors with aluminum sensing wires embedded beneath the salt-water reservoir correlated with conclusions drawn from the distribution of half-cell potentials in Slab 6. However, the aluminum sensing wires may have fractured simply due to the presence of significant moisture in the concrete cover. Significant corrosion could not have developed after 13 days. Despite that fact, the half-cell potentials indicated high to severe risk of corrosion near the salt-water reservoir of Slab 6 after only 13 days of exposure to salt-water, as shown in Figure 7-37. No sensors with aluminum sensing wires in the region of high corrosion risk have signaled initiation of corrosion. Furthermore, in no case did the sensors with zinc sensing wire signal

that corrosion had initiated. Because testing has only been conducted for 14 weeks, these results were not conclusive. With additional time for testing, the signals of the sensors will likely further correlate with the distribution of half-cell potentials in the specimens.

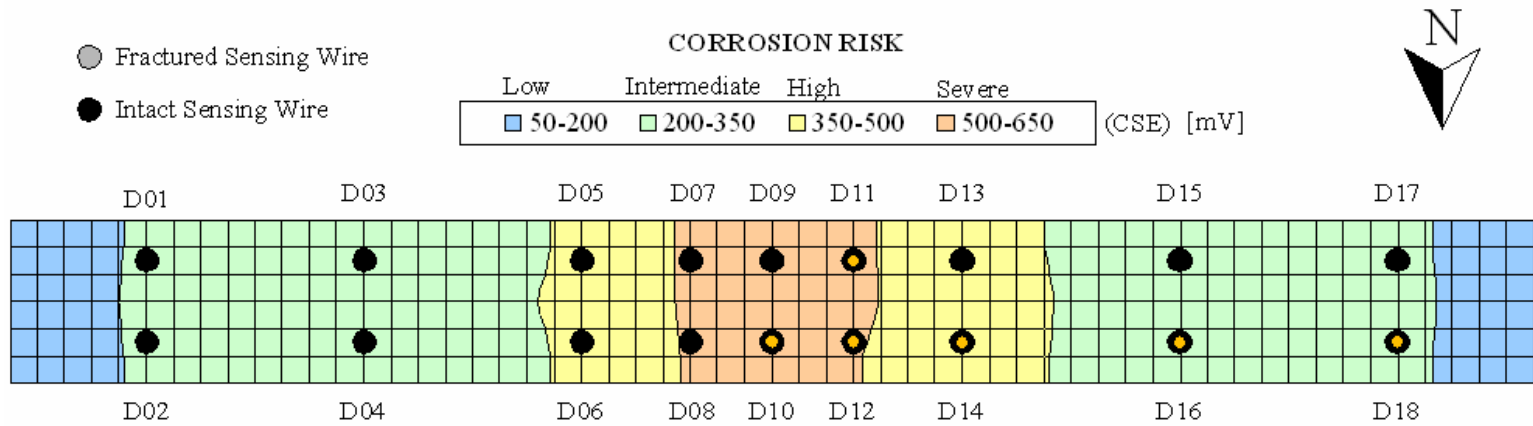


*Figure 7-33 Slab 5 Half-Cell Potential Distribution at 14 Weeks: End of Wet Cycle*

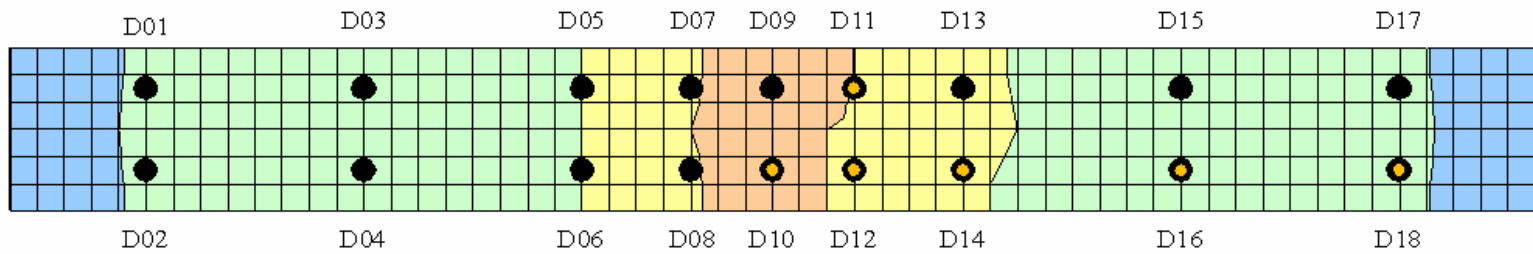


*Figure 7-34 Slab 5 Half-Cell Potential Distribution at 12 Weeks: End of Dry Cycle*



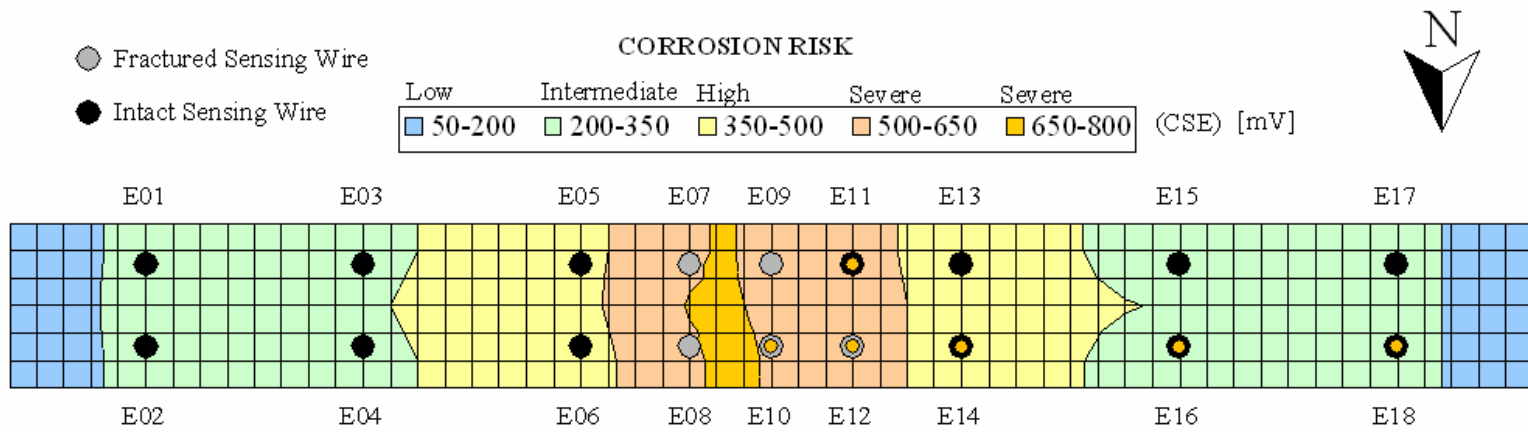


**Figure 7-35 Slab 6 Half-Cell Potential Distribution at 14 Weeks: End of Wet Cycle**

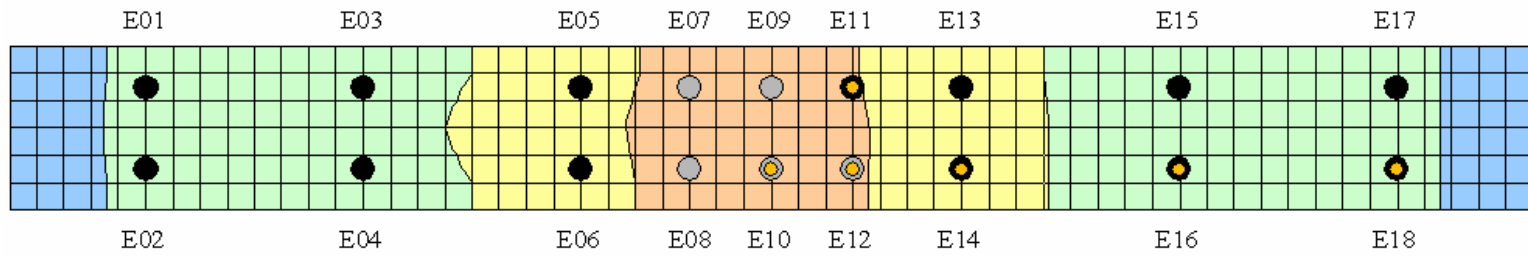


**Figure 7-36 Slab 6 Half-Cell Potential Distribution at 12 Weeks: End of Dry Cycle**

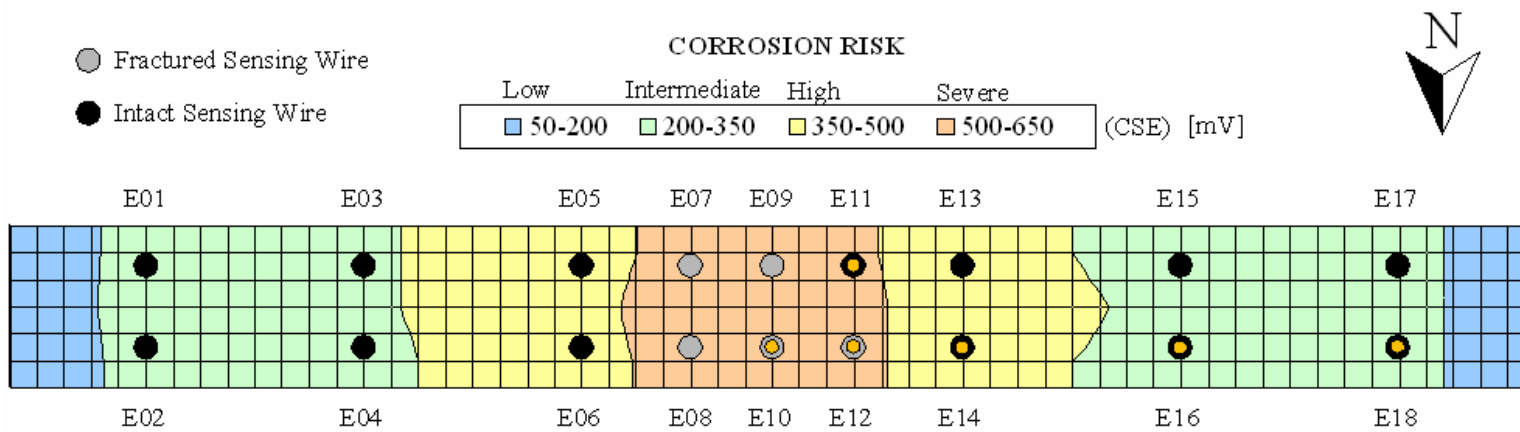


**Figure 7-37 Slab 6 Half-Cell Potential Distribution at 13 days: End of Wet Cycle**

#### 7.4.2 Current Circulation in Slabs 5 and 6

The current circulating in Slabs 5 and 6 was expressed as four distinct data series: 69", 45", 21", and Center. Currents measured at transverse reinforcement equidistant from the center of the salt-water reservoir were averaged to develop these data series. The results for Slabs 5 and 6, when the current was plotted with respect to time, are shown in Figure 7-38 and Figure 7-39, respectively. As was the case with Slabs 3 and 4, the current was equal across all resistors, and consequently, there is only one distinct curve in the figures. The direction of the current remained constant throughout the first 14 weeks of testing, with the top layer of reinforcement being negative relative the bottom layer. The current circulating in the control specimens of Slabs 5 and 6 was small compared the current circulating in Slabs 5 and 6. Thus, the contribution of the atmosphere to the internal corrosion of Slabs 5 and 6 was likely negligible.

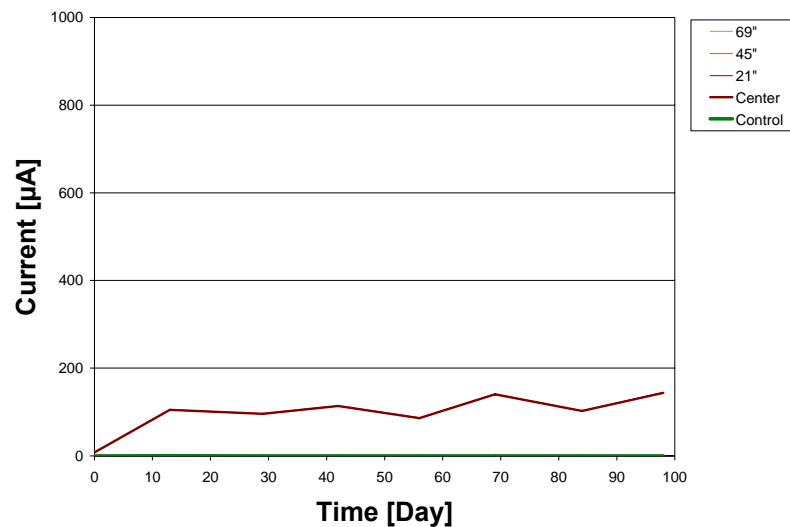


*Figure 7-38 Current in Slab 5 with Respect to Time*

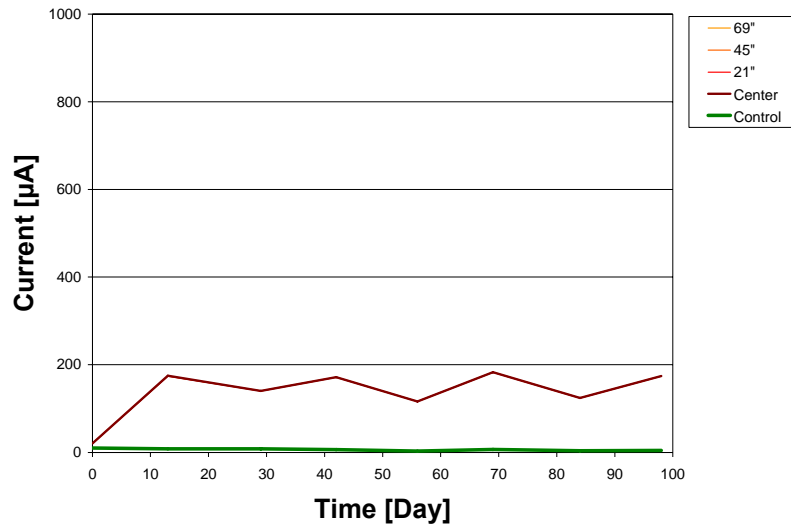


**Figure 7-39 Current in Slab 6 with Respect to time**

In order to access the extent to which the sensing wires — zinc in Slab 5 and aluminum in Slab 6 — served as sacrificial anodes to the steel reinforcement, the total current circulating in Slabs 5 and 6 over the first 14 weeks of testing was compared to the total current circulating in Slabs 3 and 4 during their first 14 weeks of testing. The total current for a given specimen was obtained by summing the current crossing over all the resistors of the specimen. The resulting total current was the proper basis of comparison among the specimens because Slabs 3 and 4 had a different number pathways from the top layer of reinforcement than did Slabs 5 and 6. The former had five pathways, while the latter had seven. What is important for corrosion of Slabs 3 through 6 is the total quantity of charged particles circulating in the system, not simply the quantity of charged particles passing through any local pathway. The total current of Slabs 3 through 6 is plotted with respect to time in Figure 7-40. Both Slabs 3 and 4 had sensors with steel sensing wires, but the two specimens were distinguished, as discussed in Section 5.2, by how many resistors connected the top and bottom

layers of reinforcement. Slab 3 had only one resistor connected, in the middle of the specimen, through the first 14 weeks of testing, whereas Slab 4 had all five resistors connected. Because the resistors of Slabs 3 and 4 were connected after 28 days of testing, the current curves of Slabs 3 and 4 begin on day 42. Current measurements were taken at the end of each environmental cycle.

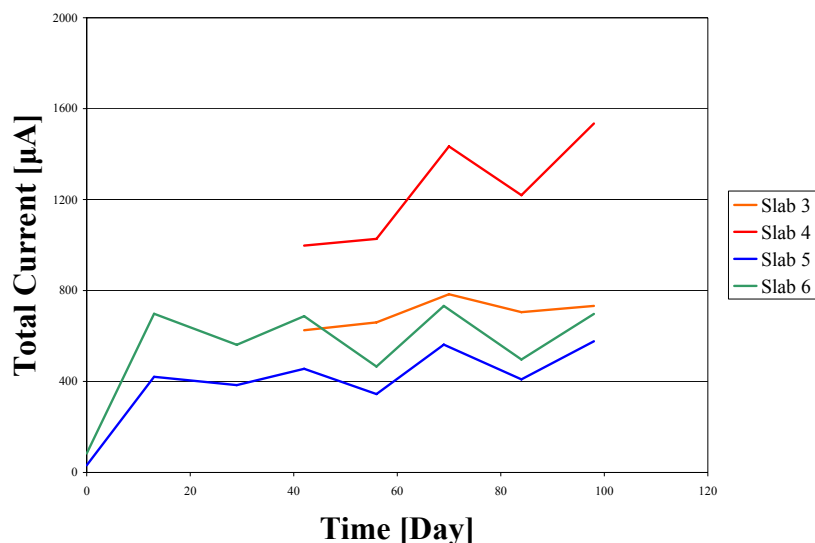


**Figure 7-40 Total Current in Specimens with Steel, Aluminum, and Zinc Sensing Wires**

The total corrosion current circulating in Slab 4 was much greater than that of the other specimens. Slab 4 contained no metal that was active compared with the steel reinforcement. Furthermore, there were multiple pathways for current flow in Slab 4, in contrast to Slab 3, which only had one pathway from the top layer of reinforcement to the bottom layer. However, despite the fact that Slabs 5 and 6 had multiple pathways for the circulation of corrosion current, the total corrosion current of both specimens was less than that of Slab 3. This result is an indication, but by no means proof, that the sensing wires of Slabs 5 and 6 were serving as sacrificial anodes to the steel reinforcement to which they were

attached. That is, because the aluminum and zinc sensing wires of sensors embedded in Slabs 5 and 6 have a negative potential relative the steel reinforcement, they were suppressing corrosion current from the steel reinforcement. The fact that less current circulated in Slab 5 than Slab 6 indicates that the zinc sensing wires were more effectively suppressing the corrosion current of the steel. It is the case that five of the six sensing wires in Slab 6 have fractured, likely thereby reducing the effect of the aluminum sensing wires on the steel reinforcement. However, there remains an indication that the zinc sensing wires coupled galvanically with the steel more readily than did the aluminum, a fact which may result in the sensors with zinc sensing wire having a larger tributary area than sensors with aluminum sensing wires. Additional testing is required to settle this matter.

## **7.5 CONCLUSION**

Anodic sensors, one set with zinc sensing wires, another with aluminum, were tested in reinforced concrete slab sections. The sensors were arranged in order to obtain insight into the tributary area over which the sensors detect initiation of corrosion. The functioning of the sensors was assessed by their measured response and by the degree to which their signals correlated with the half-cell potentials of the specimens.

Sensors with aluminum sensing wires were found to be highly responsive to the presence of moisture and chlorides in the concrete cover of the specimens. In fact, at the end of the first, two-week wet cycle, five of the six sensors with aluminum sensing wires embedded beneath the salt-water reservoir of a specimen signaled the initiation of corrosion. The responsiveness of the sensors with aluminum sensing wires raises the possibility that the sensors are susceptible to signaling false positives. Additional testing in Chapter 8 assesses this possibility.

After 14 weeks of testing, no sensors with zinc sensing wires have signaled the initiation of corrosion, but testing is ongoing.

Two observations were made about the response of sensors tested in Slabs 5 and 6. First, the internal environment of the concrete of the specimens introduced variability into the response of sensors tested within them. This result was likely due to the fact that the fiber-reinforced cement paste housings used for sensors tested in Slabs 5 and 6 were permeable. The permeability of the housings was greatly increased by the development of plastic shrinkage cracks. In all cases, the inductors of both the sensing and reference circuits were exposed by the permeable sensor housing to changes in the moisture content of the concrete. Consequently, parasitic inductance on the coupled circuit of the sensor and reader coil changed with environmental cycles. This regular change in the moisture content of the concrete thereby increased the coefficients of variation of the response parameters of sensor tested in Slabs 5 and 6. The more exposed the circuitry of the sensor was, the greater the introduced variability. As a result, sensors with cement paste housings that lacked an epoxy core responded with greater variability, especially at the reference frequency.

Second, the pseudo-quality factors of the reference circuits were observed to decrease with time in most cases. The sensors with an epoxy-core housing and fractured sensing wires did not exhibit this trend. The most likely cause of the decrease in the reference pseudo-quality factor of sensors with epoxy-core housings and intact sensing wires was gradual corrosion of the sensing wire. In contrast, decay of the copper circuitry of the sensor was the most likely cause of the decrease in the pseudo-quality factor in the case of sensors without epoxy-core housings. The housing of such sensors was entirely fiber-reinforced cement paste. Apparently, the alkaline environment of the fiber-reinforced cement paste

housing and of surrounding concrete was chemically aggressive to the exposed circuitry.

The signals of sensors with aluminum sensing wires correlated fairly well with risk of corrosion implied by the half-cell potentials of the slab section. All the sensors in areas of severe risk of corrosion, except one, signaled the initiation of corrosion, while those in areas of high risk have yet to signal initiation of corrosion. Because no sensor with zinc sensing wire has signaled that corrosion has initiated, the signals of the sensors with zinc sensor wire have not correlated with half-cell potential. Indeed, there are areas of both high and severe risk of corrosion the slab section containing the sensors with zinc sensing wire. However, because testing has only been conducted for 14 weeks, these results were inconclusive.

The total corrosion current in the slab sections with zinc and aluminum sensing wire was less than that with steel sensing wire. This fact is an indication that the zinc and aluminum are serving as sacrificial anodes to the top layer of reinforcement, suppressing the total corrosion current. In that event, the anodic sensors may have a nontrivial tributary area, in contrast to the coupled sensors. As discussed in Section 5.4.1, the tributary area of the coupled sensors was essentially zero.



## **CHAPTER 8**

# **Susceptibility of Anodic Sensors to False Positive Readings**

### **8.1 INTRODUCTION**

As discussed in Section 2.4.3, the sensing wire of the anodic sensor was chosen to be galvanically active compared with steel in an attempt to increase the tributary area over which the sensor detects initiation of corrosion. However, this galvanic activity of the sensing wire compared with the steel potentially renders the anodic sensor susceptible to false positive readings, signaling that corrosion has initiated when it, in fact, has not. Even chemically passive steel corrodes at a detectable rate, although that rate is orders of magnitude less than the corrosion rate of chemically active steel. Furthermore, the sensing wire of an anodic sensor, in practice, would be coupled with a surface area of steel much larger than the surface area of the sensing wire. The result would be a large cathode-to-anode ratio, which also increases the rate of corrosion of the sensing wire, or anode. Therefore, even though chemically passive steel corrodes at a low rate, the greater area of the steel could increase any corrosion of the sensing wire at a high enough rate for the sensing wire to fracture within the service life of the sensor. Because such a fracture would occur in the absence of corrosive agents penetrating the concrete cover, fracture of the sensing wire would cause the sensor to signal a false positive.

Two separate experiments were conducted to assess the susceptibility of anodic sensors to false positive readings. In the first experiment, two anodic sensors, one with a zinc sensing wire and one with an aluminum sensing wire, were embedded in an 8-ft by 21-ft section of a bridge deck. The specimen was

not exposed to corrosive agents; therefore, it may be assumed that the embedded reinforcement remained passive. The sensors were periodically interrogated to determine the state of the sensing wire. In addition, the large-scale of the specimen permitted observations to be made about the influence of the sensors on the durability of a typical bridge deck. The design and results of this experiment are described in Section 8.2.

The second experiment was a galvanic corrosion test. Zinc and aluminum sensing wires were each coupled with a set of steel mats in a simulated concrete pore solution. The total surface area of the steel mats was equal to the area of the top steel reinforcement in an 8-ft by 8-ft section of bridge deck. The sensing wires were observed to determine whether they corroded at an appreciable rate. In an attempt to determine the actual rates of corrosion, zinc and aluminum rods were attached to two other sets of steel mats. The currents flowing between the rods and the steel were measured to determine trends in the corrosion rates of the rods. Section 8.3 describes this experiment and discusses the results.

## **8.2 ANODIC SENSORS TESTED IN A LARGE AREA OF BRIDGE DECK**

Two anodic sensors were embedded in a section of a bridge deck with a standard steel layout. The design of the experiment is described in Section 8.2.1. Section 8.2.2 assesses the response of the sensors. Finally, the effect of the sensors on the durability of the structure is described in Section 8.2.3.

### **8.2.1 Design of the Experiment**

The test specimen was constructed using 4-in. prestressed concrete panels and a 4-in. cast-in-place topping slab. The reinforcement in the topping slab is shown in Figure 8-1. The test specimen was subjected to fatigue loads as part of

an independent research project, discussed in Agnew (2007). The two anodic sensors, D19 with a 0.0393-in. (1-mm) diameter zinc sensing wire and E19 with a 18-gage (0.0403-in diameter) aluminum sensing wire, were placed within the specimen in the regions that were not damaged by the fatigue loads. The sensors had fiber-reinforced cement paste housings. At the conclusion of the fatigue tests, no cracks were observed in the vicinity of the sensors.

As shown in Figure 8-2 and Figure 8-3, the sensors were placed on platforms of two #5 bars, which were wired to the top layer of steel reinforcement. The sensors were placed on the platforms to reduce the cover to 1 in. so that the response of the sensors was detectable. The sensing wires were connected to the steel reinforcement with mild steel wire.

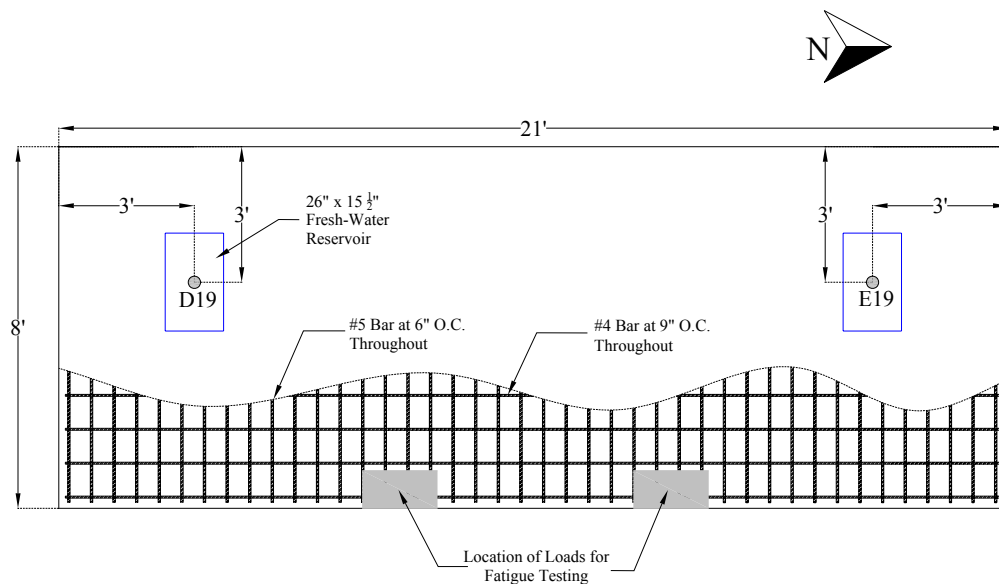


**Figure 8-1 Plan View of Tributary Area of Bridge Deck**

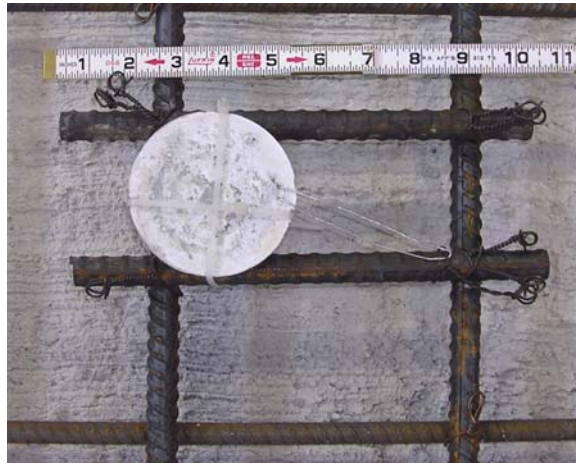


***Figure 8-2 Sensor D19***

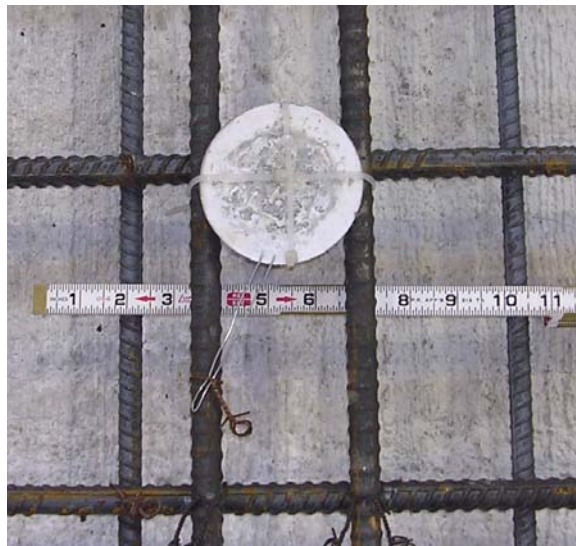


***Figure 8-3 Sensor E19***

Concrete was placed on 9 November 2006. Figure 8-4 is a photograph of fresh concrete being poured over a sensor. After one week of curing, interrogation of the sensors began and has continued for 29 weeks, on two-week intervals. A Solartron Impedance/Gain-Phase Analyzer was used to interrogate the sensors. The reader coil was 4 in. in diameter with five turns of 18-gage copper magnet wire. Interrogation of the sensors is ongoing. Initially, the

specimen was stored inside and was exposed to no moisture. After approximately nine weeks of testing, the specimen was moved outside, where it was exposed to rain. Furthermore, after 11 weeks of testing, a reservoir containing fresh water was attached to the top surface of the bridge deck, above the sensors. Thereafter, the concrete above the sensors was subjected to wet and dry cycles on two-week intervals. The fresh-water reservoirs were added to the bridge deck because moisture in the pore structure of the concrete is essential to the formation of a galvanic cell between the sensing wire and steel reinforcement. However, a galvanic cell could potentially form even in dry service conditions because there is always residual moisture in the pore structure of concrete.



*Figure 8-4 Placing of Concrete*

### **8.2.2 Measured Response of the Sensors**

Over 29 weeks of testing, the sensing wires of both sensors remained intact. The responses of D19 and E19 are shown in Figure 8-5 and Figure 8-6, respectively. Due to the constraints of the testing arrangement, a 6-ft coaxial

cable was used to connect the reader coil to the impedance analyzer for the first 9 weeks of testing. Thereafter, change in the testing arrangement permitted use of a 3-ft cable. Because the 3-ft cable provided a baseline that changed in phase angle less over the frequency domain of interrogation, it was used in place of the 6-ft cable after 9 weeks of testing. The change in baseline due to the change in cable prevented a contour plot from being developed for the response of the sensors. Therefore, a plot of their responses in the plane of phase angle and frequency is provided in place of the contour plot.

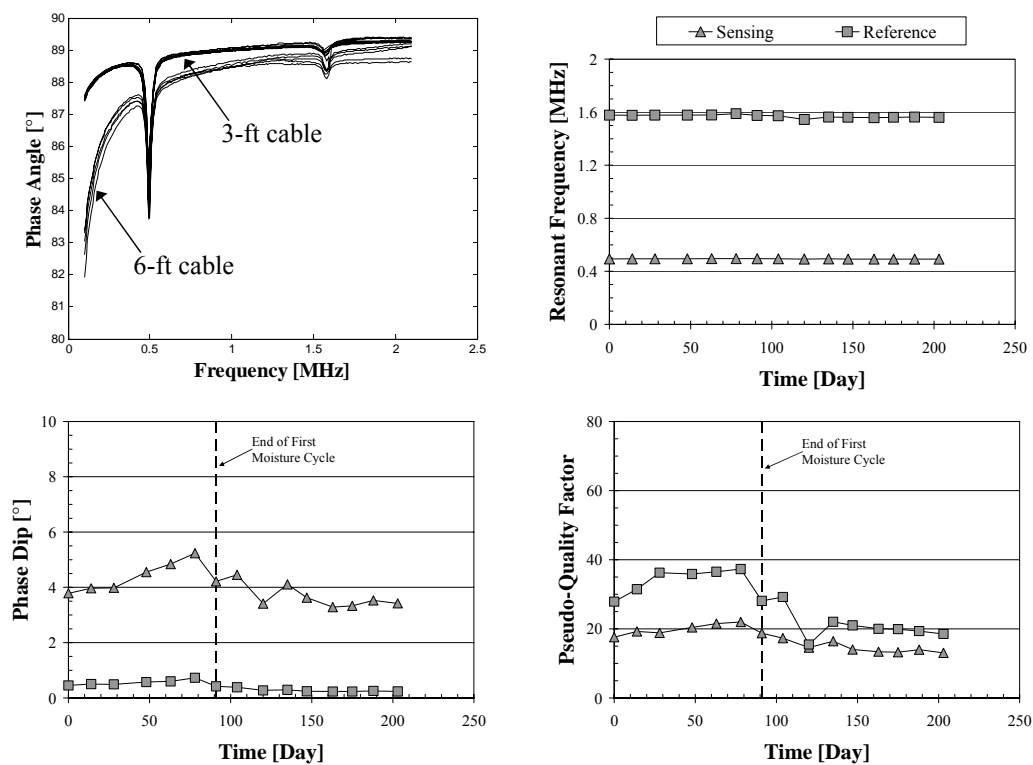


**Figure 8-5 Response of Sensor D19**

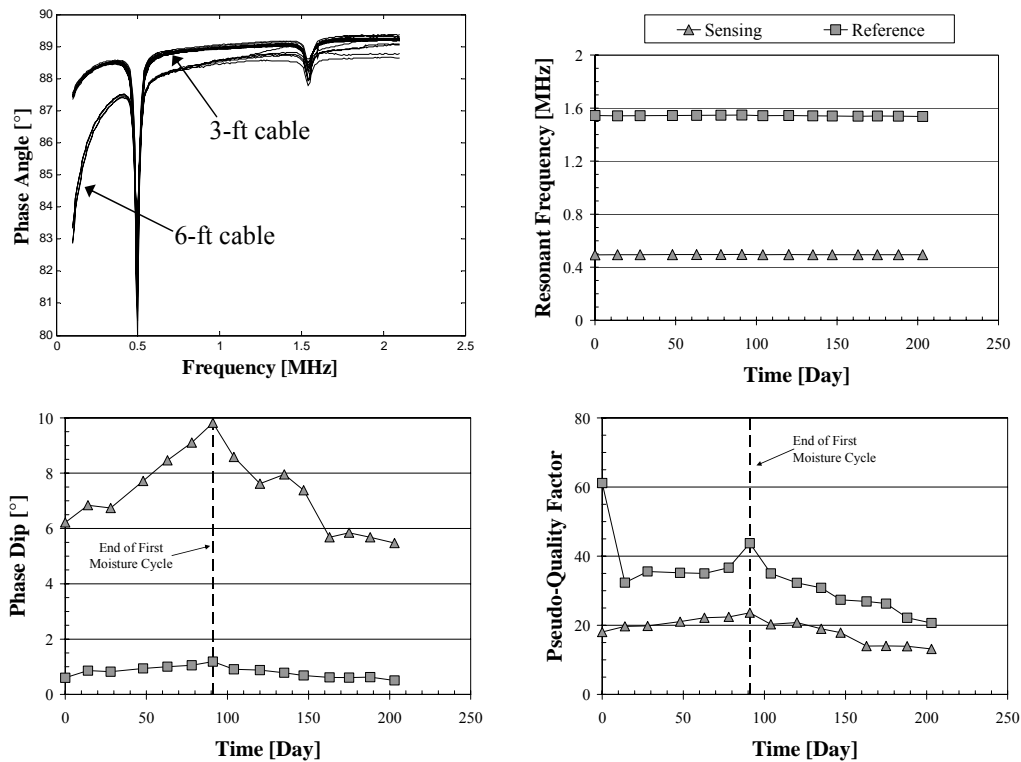


**Figure 8-6 Response of Sensor E19**

From the figures, it is clear that the sensing wires of D19 and E19 remained intact throughout the first 29 weeks of testing. Therefore, neither the zinc nor aluminum sensing wire was highly susceptible to galvanic corrosion when coupled with a large area of passive steel reinforcement. However, 29 weeks of testing was only a small fraction of the required design life of the sensor, which must be comparable to the design life of the structure in which it is embedded. The possibility remains that, over many years of service, the zinc and aluminum sensing wires would corrode simply by being coupled with a large area of passive steel.

Table 8-1 summarizes the responses of sensors D19 and E19 statistically. In the table, the mean resonant frequency is symbolized as  $f_0$ , the mean phase dip

as  $\phi$ , and the means pseudo-quality factor as  $\bar{Q}$ . The table includes the coefficients of variation for each of these parameters.

**Table 8-1 Statistical Summary of Response of D19 and E19**

Sensor		$f_0$ [MHz]	COV [%]	$\phi$ [°]	COV [%]	$\bar{Q}$	COV [%]
<b>D19</b>	<i>Sensing Circuit</i>	0.49	0.3	4.0	14.8	16.9	18.4
	<i>Reference Circuit</i>	1.57	0.7	0.4	40.6	26.6	28.6
<b>E19</b>	<i>Sensing Circuit</i>	0.49	0.1	7.3	18.6	18.7	18.3
	<i>Reference Circuit</i>	1.54	0.2	0.8	24.3	33.4	29.1

There were indications in the response of both sensors that the sensing and reference circuits were decaying with time. The sensing phase dips of both sensors steadily increased until after the end of the first moisture cycle, noted in Figure 8-5 and Figure 8-6. The phase dip of E19 increased after the first moisture cycle but decreased thereafter. The sensing phase dip of D19 began to decrease immediately after the first moisture cycle. A similar trend was evident in the phase dip of the reference circuit, but not as pronounced. In addition, after the end of the first moisture cycle, the pseudo-quality factors of both circuits began to decrease.

The trends in the phase dips and pseudo-quality factors of sensors D19 and E19 were distinct from those observed in the sensors tested in Slab 5 and 6. The circuits of the sensors D19 and E19 were clearly decaying with time, but the causes — whether corrosion of the sensing wire, changes in the moisture content of the concrete, or decay of the circuitry — cannot be determined. Uncertainty was introduced by three conditions. First, the moisture cycles of the specimens could not be controlled because the specimens were stored outside. Second, only one sensor with each material of sensing wire was embedded in the specimen.



Consequently, comparisons cannot be made among the responses of sensors. Third, the change in baseline due to change in coaxial cable likely introduced variability into the response parameters returned by the curve-fitting algorithm. Therefore, no conclusions about the causes of variability in the response of the sensors can be drawn. Nevertheless, the fact that the sensing wires remained intact throughout the 29 weeks of testing indicated that the anodic sensors were not highly susceptible to false positive readings. However, the fact that the circuits are decaying with time indicated that, if tested over a longer period, the sensors may signal false positives.

### **8.2.3 Effect of the Embedded Sensor on the Durability of the Structure**

Full-scale reinforced concrete structures in which corrosion sensors might be embedded are exposed to significant variations in temperature. Furthermore, concrete structures exhibit plastic shrinkage as they cure. The possibility arises that sensors embedded in a full-scale structure would cause cracking of the concrete around them. To assess this possibility, the concrete cover of the bridge deck section discussed in Section 8.2.1 was monitored to determine whether cracks formed in the cover of the concrete near the sensors. Despite the structure being exposed to significant temperature variation and undergoing plastic shrinkage as it cured, no cracks were observed in the cover near the sensors.

A set of six sensors was embedded in the deck of the full-scale bridge shown in Figure 8-7 and Figure 8-8. The responses of the sensors B160 through B165 are reported in Appendix F. Again, although the bridge deck has been exposed to wide ranges of temperature and exhibited plastic shrinkage, no cracks were observed in the bridge deck near the sensors.



**Figure 8-7 Sensors Embedded in Full-Scale Bridge Deck**

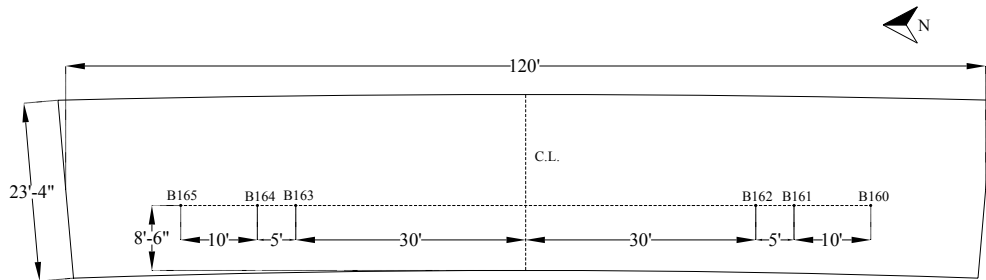


**Figure 8-8 Plan View of Full-Scale Bridge Deck and Position of Sensors**

### **8.3 GALVANIC CORROSION EXPERIMENT**

In order to determine differences in how zinc and aluminum sensing wires corrode when coupled to a large area of passive steel, zinc and aluminum sensing wires were connected to a set of steel mats and immersed in a simulated pore solution. The sensing wires were monitored over a period of time to determine if they were corroding. In addition, zinc and aluminum bars were coupled with separate sets of steel mats, and the current flowing between the bars and mats was monitored. These data were used to estimate trends in corrosion rates. Section 8.3.1 describes the design of the experiment, and results are discussed in Section 8.3.2.

### **8.3.1 Design of the Galvanic Experiment**

The galvanic corrosion experiments, in both the cases of the sensing wire and bar, are illustrated in Figure 8-9. Four, 55-gallon barrels were filled with a simulated pore solution of saturated calcium hydroxide (1.85 g of calcium hydroxide per liter of tap water). The pore solution was continuously aerated, but the temperature of the solution was not controlled. A 10-in. segment of zinc wire and a zinc bar (12-in. long and 1-in. diameter) were placed in separate solutions and each connected to a set of steel mats with 18-gage copper magnet wire. An identical test was performed using an aluminum sensing wire and bar of identical dimensions. Both the zinc and aluminum sensing wires were nominally identical to the sensing wires used to construct the sensors tested in Slabs 5 and 6. The steel mats collectively had the surface area of an 8-ft by 8-ft section of the top layer of steel from a standard bridge deck layout (#5 bars spaced at 6 in. on center in the longitudinal direction and #4 bars spaced at 9 in. on center in the transverse direction). The steel mats were composed entirely of #3 bars. Seven mats were placed in each barrel. Six of the seven mats had seventeen, 32-in. long longitudinal bars, wired to 15-in. long transverse bars. A 31-in. diagonal brace was included for stability. The seventh mat had eight longitudinal bars instead of seventeen. The two types of mats are pictured in Figure 8-10.

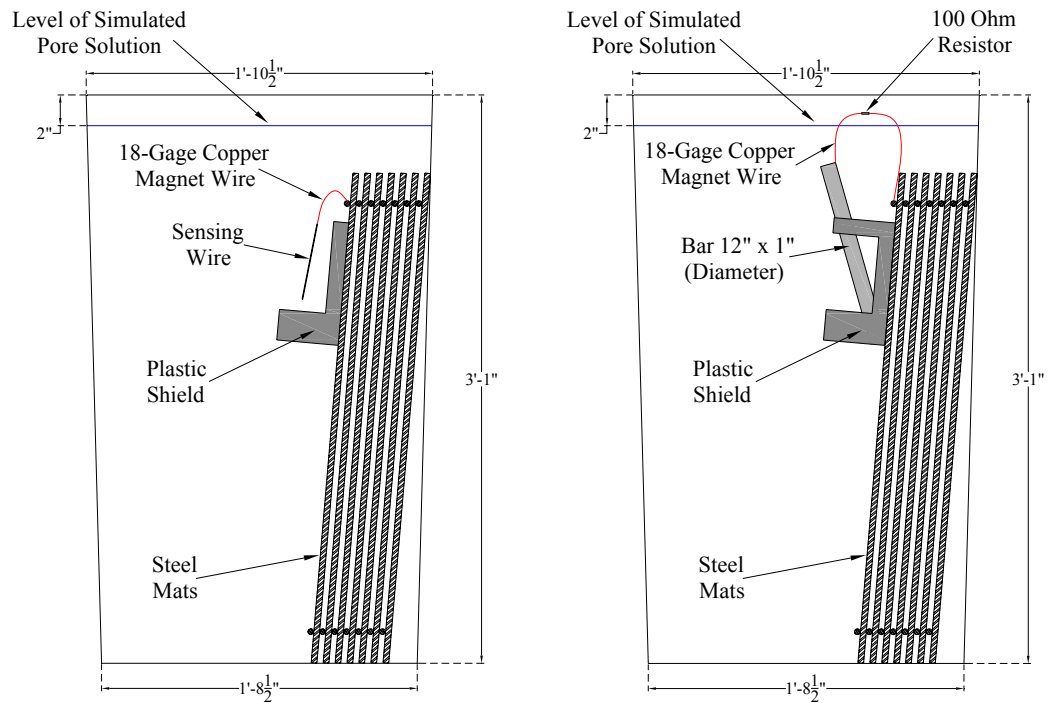


**Figure 8-9 Galvanic Corrosion Experiment for Sensing Wire and Bar**

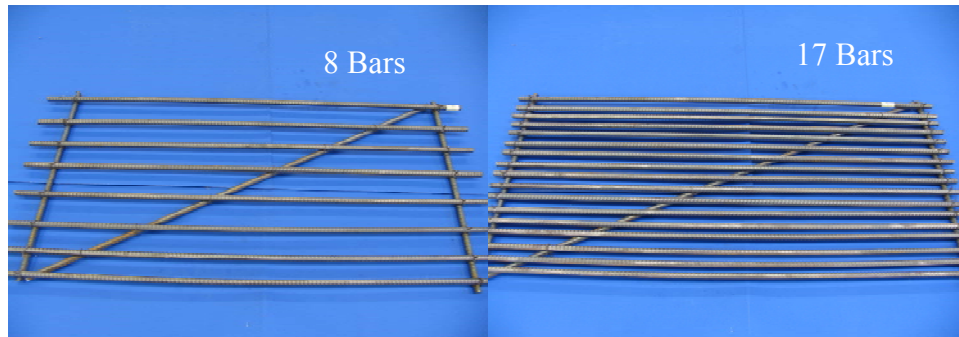


**Figure 8-10 Steel Mats with Eight and Seventeen Bars**

Other than being connected to the steel by copper magnet wire, the sensing wires and bars were electrically isolated from the steel by plastic shields fabricated from concrete cylinder molds. These shields were supported by the extreme steel mats with plastic zip ties. The magnet wire was connected to the

sensing wire and steel wire wrapped around the extreme steel mat by steel clips to which the magnet wire was screwed. These connections are shown in Figure 8-11. The connection of the sensing wire to the steel was intended to model the way in which the sensing wire of an anodic sensors would be connected to steel reinforcement in service conditions.

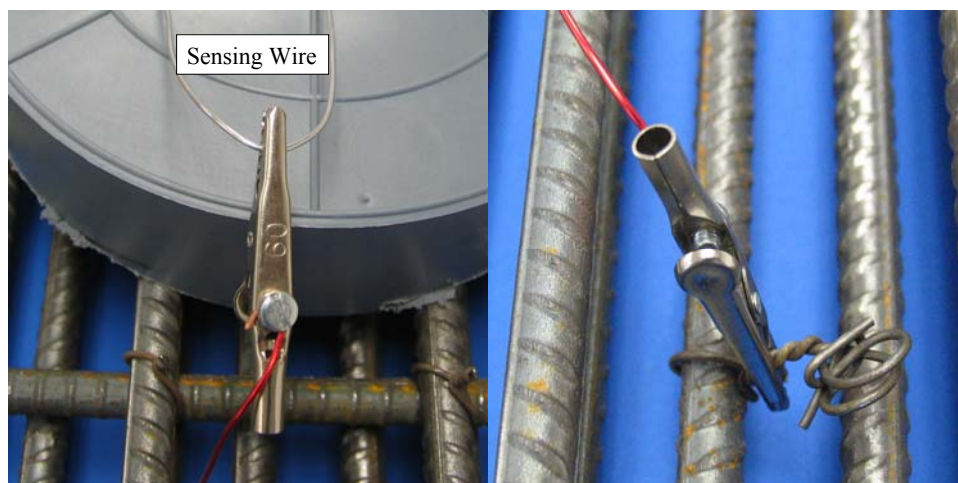


**Figure 8-11 Connection of Magnet Wire to Sensing Wire and Steel Mat**

The magnet wire was connected to the zinc and aluminum bars and extreme steel mat with copper clips that had been soldered to the magnet wire, as shown in Figure 8-12. Unlike the copper magnet wire, the copper clips did not have an enamel finish. Therefore, because their copper was exposed, they likely affected the galvanic cell that developed between the bars and steel. However, because the surface area of the clips was much less than that of both the bars and mats, the effect of the clips on the galvanic cell was assumed to be small. In order to determine the corrosion current flowing from the bars to the steel mats, a 100-Ohm resistor was included in the length of the copper magnet wire and the voltage drop over the resistor was measured.

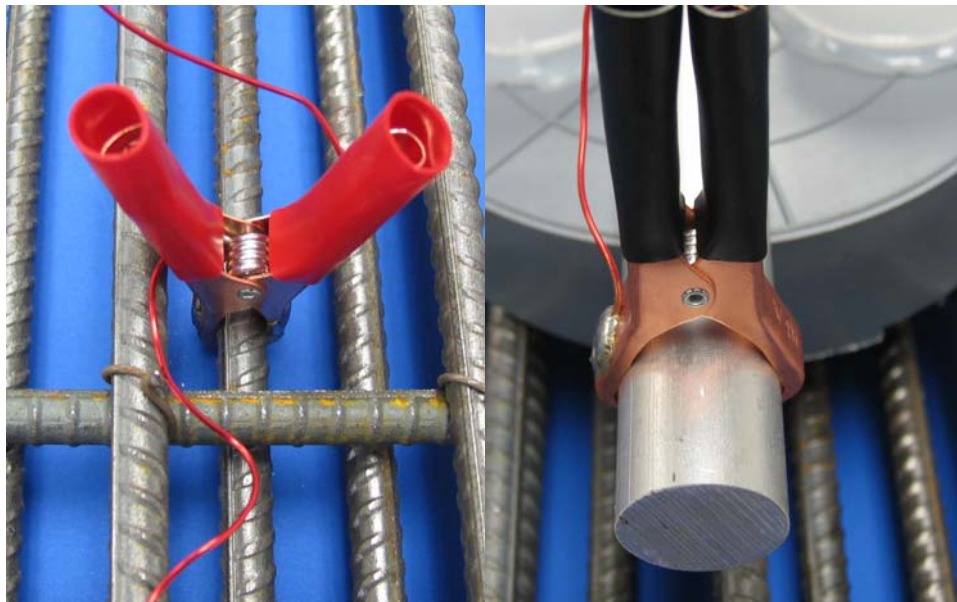


***Figure 8-12 Connection of Magnet Wire to Bar and Steel Mat***

Testing began 19 October 2006 and continued for 124 days. To initiate testing, the sensing wires and bars were immersed in the simulated pore solution. After one week of immersion, the sensing wires were observed to determine if there was any indication of corrosion. The voltage over the resistors was measured in the case of the bars. Furthermore, the wires and bars were weighed and compared with their initial weights. A standard calomel electrode was used to determine the potential of the steel mats with which the zinc and aluminum bars were coupled. Finally, the temperature, pH, and dissolved oxygen content of the simulated pore solution were measured. After two, one-week monitoring intervals the experiment was monitored every two weeks for the duration of the test.

### **8.3.2 Results from the Galvanic Experiment**

Several complications developed with the experiment. First, the containers initially used for the simulated pore solution developed leaks. After one week of testing, the containers were replaced. While the new containers were being procured, the sensing wires, bars, and steel mats were stored in air, a period of one week. Testing resumed, with the first monitoring of resumed testing being after one week. Thereafter, monitoring occurred every two weeks.

Second, in order for the cathode-to-anode ratio to represent service conditions, a large area of steel was required for the experiment. Immersion of the steel in a simulated pore solution, in turn, required a large volume of solution. A consequence of the scale of the experiment was that quality control of the simulated pore solution was difficult. The calcium hydroxide tended to precipitate out of solution, even though the solution was continuously aerated. As a result, the pH of the solution varied, at times dropping to low values. That fact reduced the likelihood that any significant conclusions could be drawn from the experiment.

Third, although the weights of the wires and bars were expected to decrease with time throughout the experiment, in most cases the weights increased. This result was due to corrosion products chemically adhering to the surface of the specimens. Because the corrosion products could only be removed by specialized chemical means, which were beyond the scope of this research, little information could be obtained about the corrosion rates of the wires and bars from their changes in weight. Data collected the galvanic experiment and not discussed in this section are given in Appendix G.

Despite these complications, several dominant trends were evident. As shown in Figure 8-13, the current flowing between the aluminum bar and steel mats initially was very large, indicative of a high corrosion rate. Thereafter, the current decreased to a low values, despite changes in pH. The cause of this decrease in current was likely the formation of a thick layer of aluminum hydroxide on the surface of the bar, which functioned as a passive layer, preventing further reaction between the aluminum and the pore solution. This passive layer is shown in Figure 8-14. Because the aluminum bar had a 1-in. diameter, the passive layer was able to form without causing the specimen to fracture. In contrast, the aluminum sensing wire, shown in Figure 8-15, fractured after only 67 days of testing. The passive layer penetrated to the center of the sensing wire, causing the wire to fracture. The pH of the solution containing the aluminum wire, shown in Figure 8-16, remained above 12.4, during the 67 days.

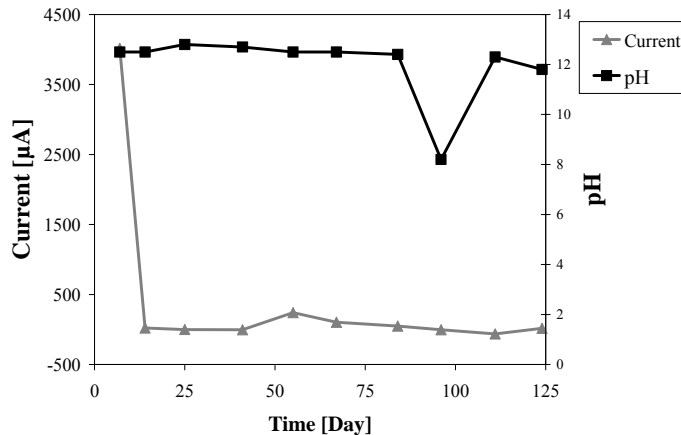


**Figure 8-13** *Current and pH in the Case of Aluminum Bar*



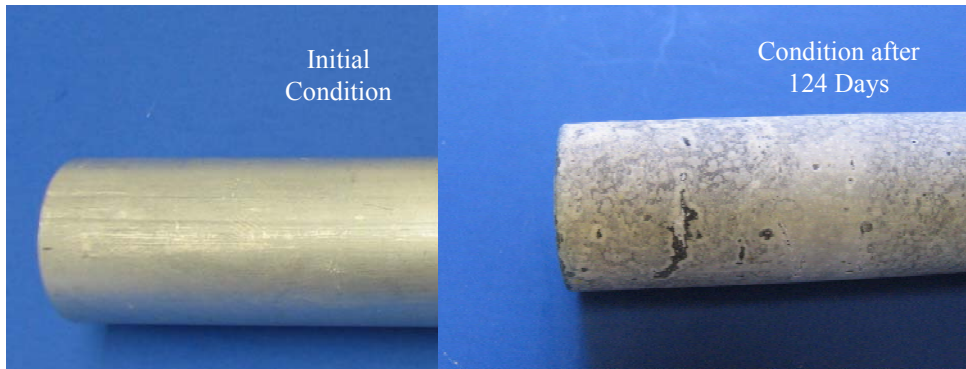


**Figure 8-14** *Passive Layer on Surface of Aluminum Bar*

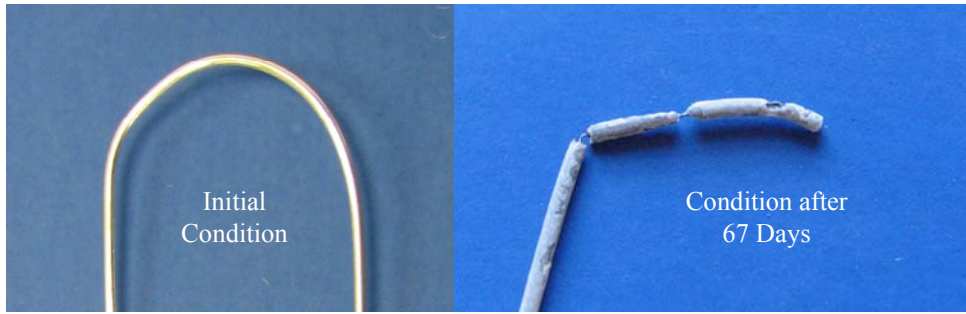


**Figure 8-15** *Initial and Fractured Condition of Aluminum Sensing Wire*

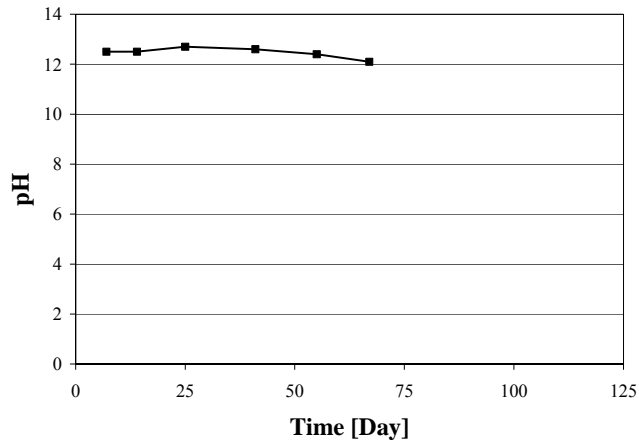


**Figure 8-16** *pH of Solution Containing Aluminum Wire*

As in the case of the aluminum bar, the current between the zinc bar and steel was initially high but decreased with time, as shown in Figure 8-17. As with the aluminum, the zinc likely formed a passive layer of zinc hydroxide, shown in Figure 8-18. In contrast to the aluminum bar, the current between the zinc bar and steel increased when the pH decreased. The pH of the solution containing the zinc wire remained at relatively high values, as shown in Figure 8-19. The relatively high values of pH likely sustained a passive layer on the zinc wire, such that it did not fracture after 124 days of testing. The initial and final conditions of the zinc sensing wire are shown in Figure 8-20.

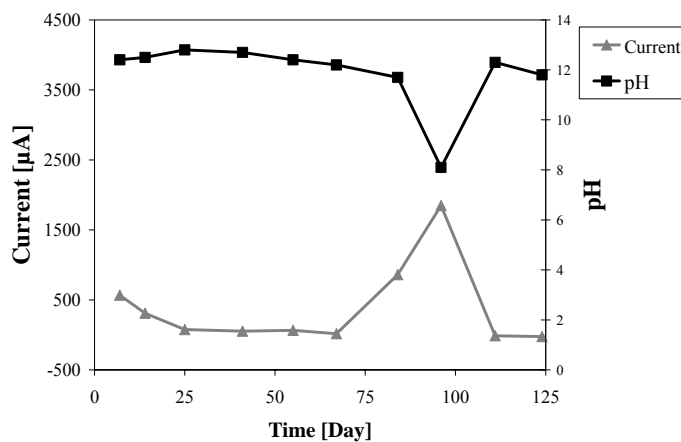


**Figure 8-17** *Current and pH in the Case of Zinc Bar*

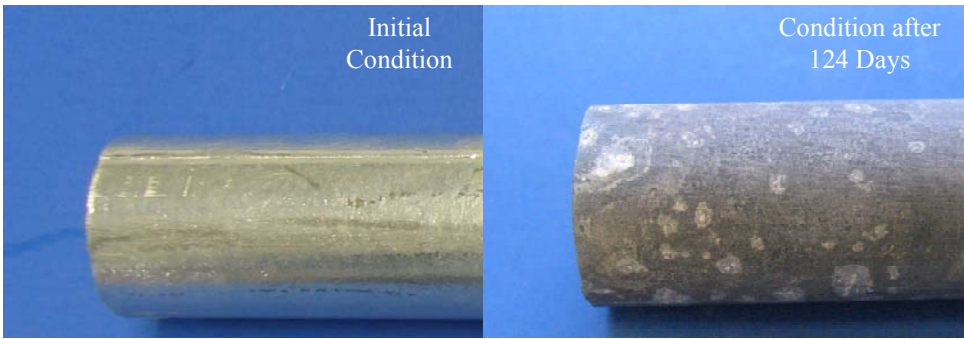


**Figure 8-18** *Passive Layer on Surface of Zinc Bar*

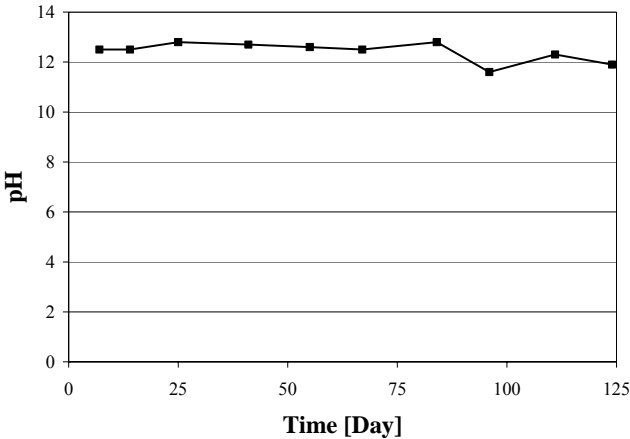


**Figure 8-19** *pH of Solution Containing Zinc Wire*

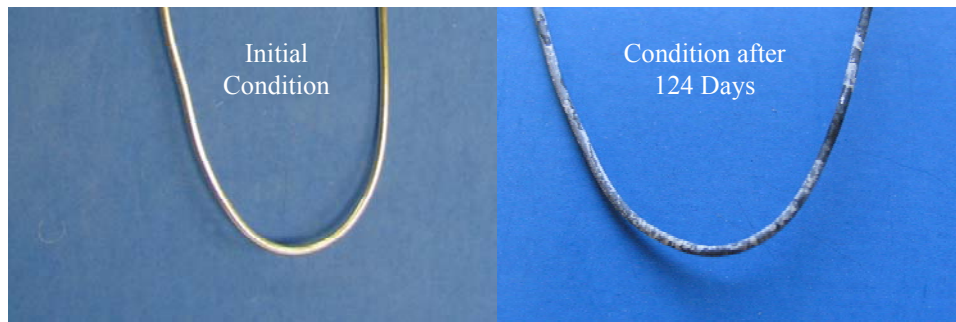


***Figure 8-20 Intact Zinc Sensing Wire Initially and after 124 Days of Testing***

#### **8.4 CONCLUSION**

In summary, the anodic sensors do not appear to be highly susceptible to false positive readings when their sensing wires are coupled with a large area of passive steel. Over 29 weeks of testing, the sensing wires embedded in an uncracked section of concrete bridge deck remained intact. However, their responses indicated that the circuits of the sensors were decaying with time, leaving open the possibility that, given enough time, the sensors would signal a false positive or fail to respond at the reference frequency. Examination of the bridge deck section and a full-scale bridge deck in which corrosion sensors were embedded showed that, in service conditions, the sensors did not cause cracks in the concrete cover.

Difficulty with quality control of the simulated pore solution in the galvanic corrosion experiment limited the conclusions that could be drawn from the experiment. However, differences on how aluminum and zinc behaved when coupled with steel in a pore solution were evident. Aluminum initially reacted at a very high rate with the pore solution, thereby developing a passive layer that made it unresponsive to changes in pH. This initial rapid reaction likely caused

fracture of the aluminum sensing wire. Zinc similarly reacted at a moderately high rate when first exposed to the simulated pore solution. Thereafter, the zinc developed a passive layer that reduced the rate of corrosion. In contrast to the aluminum, however, the passive layer of the zinc was sensitive to changes in the pH. Specifically, a drop in pH correlated with an increase in the amount of current flowing from the zinc bar to the steel mats. Because the pH remained high in the case of the zinc wire, the wire remained intact throughout the 124 days of testing.

# CHAPTER 9

## Conclusions

### 9.1 SUMMARY

The passive, wireless corrosion sensor is intended to detect initiation of corrosion in a reinforced concrete structure. That application of the sensor requires that it be economical, reliable, and durable. This chapter assesses the degree to which sensors tested over the course of this research meet these requirements.

The economy of the tested sensors was evident from the onset of the research. Each sensor was fabricated for less than \$1.50 in materials, and additional refinement of the fabrication process would dramatically decrease this cost of fabrication. The costs of installing and maintaining the sensors were strictly labor costs.

Extensive testing was required to assess the reliability and durability of the sensors. The three types of sensors — isolated, coupled, and anodic — were subjected to several different tests. Isolated sensors of both concentric and coplanar geometries were tested in small-scale specimens, concrete prisms, and two large-scale specimens, reinforced concrete slab sections. Both the concrete prisms and slab sections were subjected to long-term environmental testing. Coupled sensors were tested in two additional reinforced concrete slab sections, which were also subjected to long-term testing. Testing of one of the specimens containing coupled sensors is ongoing. Finally, anodic sensors were tested in two additional slab sections, which continue to undergo moisture cycles of salt-water.

Testing of the sensors in the concrete prisms and six reinforced concrete slab sections permitted assessment of the reliability of the sensors. The reliability of the sensors was assessed in terms of how accurately the sensors detected the initiation of corrosion in a reinforced concrete structure and how sensitive the response of the sensors was to the surrounding environment. In no case did a sensor return a false positive reading. Concentric sensors with small-gage sensing wire were highly reliable at detecting the initiation of corrosion. Only one concentric sensor with small-gage sensing wire returned an erroneous signal, a false negative. However, a larger number of sensors tested in other specimens returned false negative readings. Electrically connecting the sensing wire to the steel reinforcement, as done in the case of the coupled sensor, did not reduce the number of erroneous signals. Tests with sensing wires galvanically active compared with steel, characteristic of anodic sensors are ongoing. It is the case completed tests were terminated after a relatively short duration. Had the tests been allowed to continue, the number of false negatives likely would have decreased.

In all tests, cracks in the cover of the concrete decreased the reliability of the sensors by increasing the number of false negatives. Cracks allowed for nonuniform penetration of corrosive agents to the steel reinforcement. In multiple cases, a crack formed near the sensing wire of a sensor but did not intersect the wire. As a result, corrosion developed on steel reinforcement near the sensor, but the sensor did not signal the initiation of corrosion.

All sensors clearly signaled whether or not their sensing wires were intact. In that respect, the response of the sensors was unambiguous. The sensors provided binary information about whether or not the corrosion threshold had been reached. However, variability in the phase dips and pseudo-quality factors

of the sensors was observed, and this variability complicated efforts to extract analog information about the physical state of the circuits composing the sensor.

In all cases, the source of that variability was the environment in which the sensors were tested. The sensitivity of the sensors to the environment depended on their design and the state of their sensing wires. In no case did the response of sensors tested in dry conditions exhibit significant variability. In addition, the response of sensors with epoxy housings and intact sensing wires was not sensitive to changes in the moisture content of the concrete. Despite that fact, baseline shift of the reader coil, due to moisture on its surface, increased the variability of sensors with epoxy housings. Better quality control of the reader coil eventually eliminated instances of baseline shift. Variability attributed to changes in the moisture content of the concrete was observed in the response of sensors with epoxy housings, once the sensing wires had fractured.

The response of sensors with fiber-reinforced cement paste housings was significantly influenced by changes in the moisture content of the concrete, independent of whether the sensing wires had fractured. The fiber-reinforced cement paste housings were permeable, allowing moisture, to reach the inductors of the sensors. Changes in moisture on the surface of the inductors introduced variability into the response of the sensors. The response of all sensors was practically independent of temperature fluctuations to which the sensors would be subjected in service conditions.

Long-term testing of the sensors also allowed for assessment of their durability. Sensors with epoxy housings that were not exposed to moisture cycles were highly durable. In no case did the circuitry or epoxy housings of sensors tested in dry conditions decay with time. In contrast, both sensors with epoxy housings and fiber-reinforced cement paste housings decayed with time if exposed to moisture cycles. Several sensors with epoxy housings developed



internal black corrosion which damaged the reference circuits of the sensors in some cases. The circuitry of sensors with fiber-reinforced cement paste housings likely corroded when exposed to moisture and the alkaline environment of the cement paste housing and concrete. This decay of the reference circuits introduced variability into the response of the sensors.

The epoxy housings of the sensors had a negative effect on the durability of the specimens in which the sensors were embedded. Sensors with epoxy housings were potted in molds with concave bottoms. Air voids developed beneath the sensors during casting of the concrete. Corrosive agents, in turn, collected in these air voids, above the transverse reinforcement on which the sensors were placed. The result was accelerated corrosion of the transverse reinforcement. Sensors with fiber-reinforced cement paste housings were potted in molds with convex bottoms to correct this deficiency. Finally, sensors were embedded in full-scale structures and in no case caused cracks in the concrete around them. This result indicated that the sensors did not have a negative effect on the quality of the concrete in which they were embedded.

In summation, the sensors were economical to fabricate and maintain. All sensors unambiguously signaled the state of their sensing wires. Some classes of the sensors functioned with acceptable reliability as threshold sensors. However, variability in the response of the sensors prevented the extraction of analog information from the response. Finally, the durability of the sensors was insufficient for service conditions within a reinforced concrete structure.

## **9.2 RECOMMENDATIONS**

As indicated above, the primary problem with sensors tested over the course of this research was their housing. Although the epoxy housing initially protected the circuits from the environment in which the sensor was embedded,

corrosive agents eventually reached the circuitry, causing the circuitry to deteriorate. The problems encountered with the epoxy housing suggested that a permeable housing be developed. However, the permeable fiber-reinforced cement paste housing rendered the response of the sensor dependent on changes in the surrounding environment. Furthermore, the circuitry of the sensor deteriorated when exposed to the alkaline environment of the cement paste and concrete. The causes of this deterioration are not fully understood and should be further studied.

The initial effectiveness of the epoxy housing suggests that an epoxy housing with a coefficient of thermal expansion comparable to that of steel may be effective. If there is no differential thermal expansion between the epoxy and steel, the possibility of internal black corrosion would likely be eliminated. Attempts to improve the sensor housing should follow this approach.

An abiding deficiency of the sensors is their limited read range. Either the current approach to interrogating the sensors must be optimized or some other approach to interrogation must be developed. The present read range of the sensors is likely less than 2 in., far less than is required for use of the sensors in full-scale structures.

The threshold signal of the corrosion sensor is unambiguous: either the sensing wire is intact or fractured. To date, variability in the response of the sensor has prevented it from being used as an analog sensor. As variability is reduced and controlled, the possibility of using the sensor as an analog sensor improves. The pseudo-quality factor of the circuits composing the sensor has proven to be a useful parameter. In fact, the pseudo-quality factor better reflected the physical state of the circuits than did the phase dip. Because the pseudo-quality factor could potentially be used to extract analog information from the

response of a given sensor, that parameter would be critical for any analog application of the sensor.

## APPENDIX A

### Concrete Prism Sensor Monitoring Results

Results from monitoring concrete prisms with embedded sensors are presented in this appendix. The initial weights of the prisms are shown in Table A-1. Changes in the moisture content of the prisms, at the time of interrogation, are shown in Table A-2 and Table A-3. The changes in moisture content are relative the initial weights of the prisms.

*Table A-1 Initial Weights of Concrete Prisms*

Prism	Initial Weight Measured 10 Jan 2005 (g)
A21	1412.1
A22	1409.1
A23	1428.3
A24	1455.2
A25	1411.9
A26	1384.6
A27	1368.4
A28	1414.2
A29	1416.9
A30	1417.6
B19	1416.3
B20	1396.5
B21	1406.2
B22	1418.5
B23	1420.6
B24	1414.7
B25	1405.2
B26	1415.9
B27	1422.0
B28	1417.5
B29	1405.2
B30	1422.1

**Table A-2 Change in Moisture Content of Concrete Prisms with Time (17 Jan to 09 May 2005)**

Prism	17-Jan	24-Jan	31-Jan	07-Feb	14-Feb	21-Feb	28-Feb	07-Mar	21-Mar	28-Mar	04-Apr	11-Apr	18-Apr	25-Apr	02-May	09-May
A21	-0.5%	-0.2%	-0.2%	-0.1%	-0.1%	0.0%	-0.1%	0.0%	-0.1%	0.0%	-0.1%	0.0%	0.0%	0.0%	0.0%	0.0%
A22	-0.6%	-0.3%	-0.1%	-0.1%	-0.1%	-0.1%	0.0%	0.0%	-0.1%	-0.1%	0.0%	0.0%	0.0%	0.0%	0.0%	0.0%
A23*	1.7%	-5.3%	5.7%	-5.3%	5.7%	-5.2%	5.5%	-5.0%	5.4%	-5.1%	5.3%	-5.2%	5.4%	-4.7%	4.9%	-1.7%
A24*	1.7%	-5.4%	5.6%	-5.4%	5.8%	-5.4%	5.6%	-5.2%	5.6%	-5.2%	5.4%	-5.4%	5.7%	-5.1%	5.4%	-2.4%
A25	1.7%	-5.8%	6.2%	-5.7%	6.0%	-5.5%	5.8%	-5.3%	5.7%	-5.1%	5.3%	-5.1%	5.4%	-5.1%	5.3%	-1.6%
A26	1.8%	-5.8%	6.2%	-5.6%	6.0%	-5.5%	5.8%	-5.3%	5.7%	-5.2%	5.4%	-	-	-	-	-
A27	1.8%	-1.5%	1.4%	-1.2%	1.2%	-1.1%	1.1%	-1.0%	1.1%	-1.0%	1.1%	-0.9%	0.9%	2.4%	-2.3%	-0.7%
A28	1.8%	-1.4%	1.4%	-1.2%	1.2%	-1.1%	1.1%	-1.0%	1.1%	-1.0%	1.0%	-0.9%	0.9%	0.9%	-0.9%	-0.8%
A29	1.7%	-1.3%	1.2%	-1.1%	1.1%	-0.9%	0.9%	-0.8%	0.9%	-	-	-	-	-	-	-
A30	1.7%	-1.2%	1.2%	-1.1%	1.0%	-0.9%	0.9%	-0.8%	0.9%	-0.9%	-	-	-	-	-	-
B19	-0.5%	-4.0%	0.4%	-0.4%	0.4%	-0.4%	0.4%	-0.4%	0.5%	-0.4%	0.3%	-0.4%	0.4%	-0.4%	0.4%	0.2%
B20	-0.6%	0.0%	-0.3%	0.1%	-0.2%	0.0%	0.0%	0.0%	-0.1%	0.0%	0.0%	0.1%	-0.1%	0.1%	-0.1%	0.0%
B21	-0.6%	-0.2%	-0.2%	-0.1%	-0.1%	0.0%	-0.1%	0.0%	-0.1%	0.0%	-0.1%	0.0%	0.0%	0.0%	0.0%	0.0%
B22	-0.6%	-0.3%	-0.1%	-0.1%	-0.1%	-0.1%	0.0%	0.0%	-0.1%	0.0%	0.0%	0.0%	0.0%	0.0%	0.0%	0.0%
B23*	1.4%	-5.1%	5.6%	-5.3%	5.7%	-5.2%	5.5%	-5.0%	5.5%	-5.2%	5.3%	-5.4%	5.6%	-4.8%	5.1%	-1.9%
B24*	1.5%	-5.3%	5.6%	-5.3%	5.7%	-5.3%	5.5%	-5.2%	5.5%	-5.1%	5.3%	-5.3%	5.6%	-5.0%	5.2%	-2.2%
B25	1.4%	-5.7%	6.2%	-5.7%	6.1%	-5.5%	5.9%	-5.4%	5.8%	-5.1%	5.3%	-	-	-	-	-
B26	1.5%	-5.7%	6.2%	-5.7%	6.0%	-5.4%	5.8%	-5.3%	5.7%	-5.0%	5.2%	-5.1%	5.3%	-5.0%	5.3%	-1.5%
B27	1.7%	-1.4%	1.4%	-1.2%	1.2%	-1.1%	1.1%	-1.0%	1.1%	-1.0%	1.0%	-0.9%	0.9%	-0.9%	0.9%	-0.8%
B28	1.6%	-1.4%	1.4%	-1.2%	1.2%	-1.1%	1.1%	-1.0%	1.1%	-1.0%	1.0%	-0.9%	0.9%	-0.9%	0.9%	-0.8%
B29	1.5%	-1.2%	1.3%	-1.1%	1.1%	-1.0%	1.0%	-0.9%	1.0%	-0.9%	0.9%	-0.8%	0.8%	-0.8%	0.9%	-0.7%
B30	1.6%	-1.2%	1.3%	-1.1%	1.1%	-1.0%	1.0%	-0.8%	1.0%	-0.9%	0.9%	-	-	-	-	-

\* Moisture content change of prisms between oven cycles and freezer cycles was negligible

**Table A-3 Change in Moisture Content of Concrete Prisms with Time  
(09 May to 12 Jul 2005)**

Prism	16-May	24-May	31-May	06-Jun	13-Jun	21-Jun	28-Jun	05-Jul	12-Jul
A21	0.0%	0.0%	0.0%	0.1%	0.0%	-0.6%	0.6%	0.0%	0.0%
A22	0.0%	0.0%	0.0%	0.0%	0.0%	0.2%	-0.2%	0.0%	0.0%
A23*	1.8%	-4.9%	5.1%	-4.7%	4.9%	-5.1%	5.4%	-4.9%	5.1%
A24*	2.7%	-5.3%	5.5%	-5.1%	5.4%	-4.7%	4.9%	-5.4%	5.7%
A25	1.8%	-5.3%	5.5%	-4.9%	5.2%	-5.0%	5.3%	-5.0%	5.2%
A27	0.9%	-0.8%	0.8%	-0.7%	0.7%	-0.7%	0.7%	-0.7%	0.7%
A28	0.9%	-0.8%	0.8%	-0.7%	0.7%	-0.8%	0.8%	-0.7%	0.7%
B19	0.1%	-0.7%	0.5%	-0.4%	0.5%	-0.5%	0.4%	-0.4%	0.4%
B20	0.0%	0.1%	0.0%	0.1%	0.0%	0.7%	-0.7%	0.1%	-0.1%
B21	0.0%	0.0%	0.0%	0.0%	0.0%	0.0%	0.0%	0.0%	0.0%
B22	0.0%	0.0%	0.0%	0.0%	0.1%	0.0%	0.0%	0.0%	0.0%
B23*	2.0%	-5.1%	5.2%	-4.8%	5.0%	-4.8%	5.0%	-4.8%	5.1%
B24*	2.5%	-5.1%	5.3%	-4.9%	5.2%	-5.1%	5.4%	-5.1%	5.4%
B26	1.7%	-5.2%	5.5%	-4.9%	5.2%	-5.0%	5.3%	-5.0%	5.3%
B27	0.9%	-0.8%	0.8%	-0.7%	0.7%	-0.7%	0.7%	-0.7%	0.7%
B28	0.9%	-0.8%	0.8%	-0.7%	0.7%	-0.7%	0.8%	-0.7%	0.7%
B29	0.8%	-0.8%	0.8%	-0.7%	0.7%	-0.7%	0.7%	-0.6%	0.7%

\* Moisture content change of prisms between oven cycles and freezer cycles was negligible

The responses of sensors tested in the concrete prisms are presented below. The responses of sensors that were discussed in Chapter 3 are omitted from this appendix. Sensors A23, A29, A30, B25, and B30 were autopsied by Dickerson (2005) prior to the conclusion of the environmental tests. The remaining sensors were autopsied after 183 days of testing. The contour lines for the contour plots of all coplanar sensors with the exception of sensor A26 were set at 80°, 82°, 84°, 86°, 88.3°, and 90°. The contour lines of the A26 contour plot were set at 80°, 82°, 84°, 86°, 88.4°, 88.8°, and 90°. Finally, the contour lines for the contour plots of the concentric sensors were set at 80°, 82°, 84°, 86°, 87°, 88.1°, and 90°.

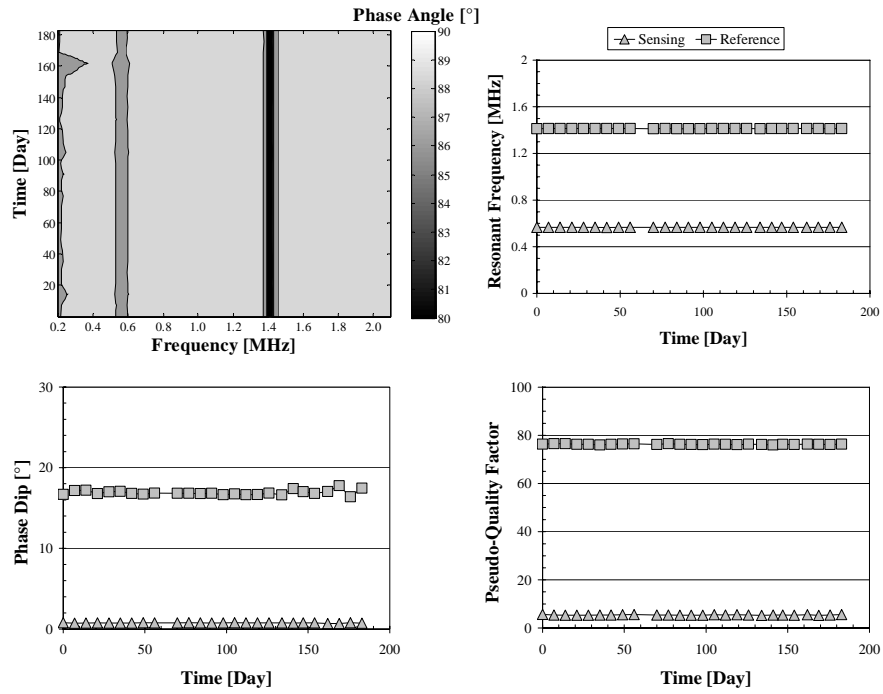


*Figure A-1 Response of Sensor A21*

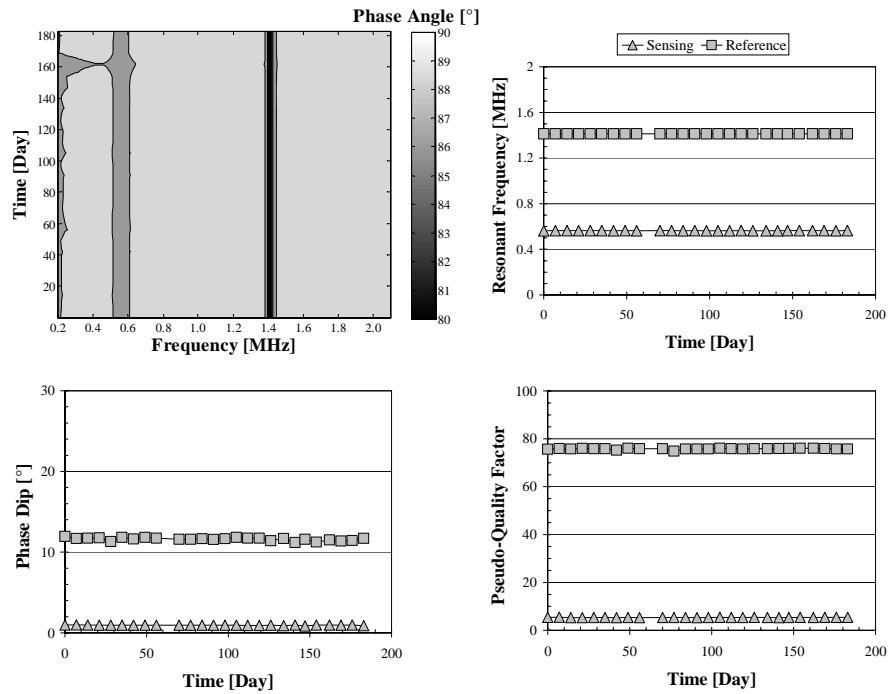


*Figure A-2 Response of Sensor A22*

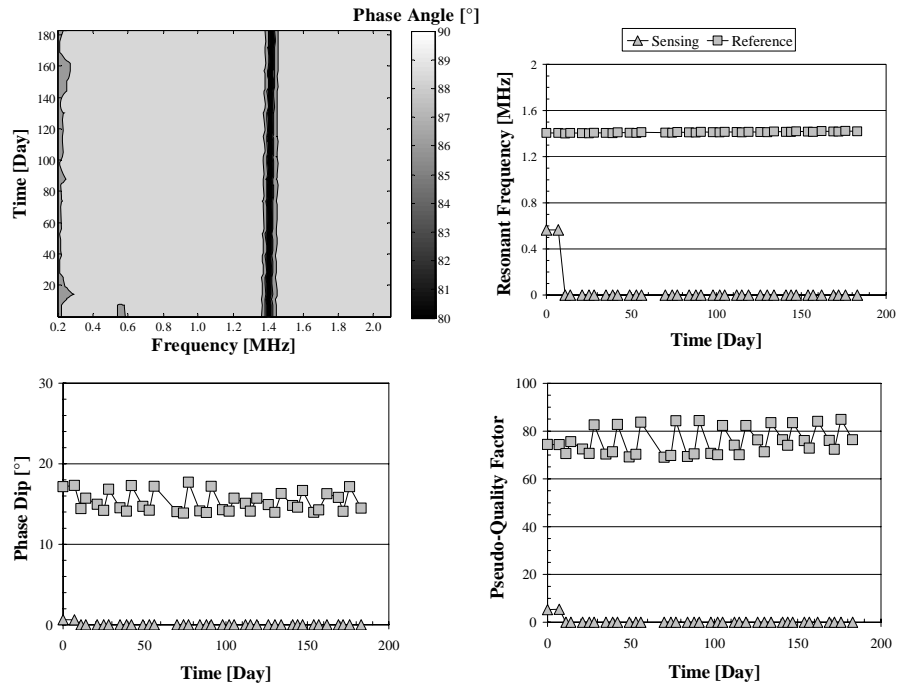


**Figure A-3 Response of Sensor A23**

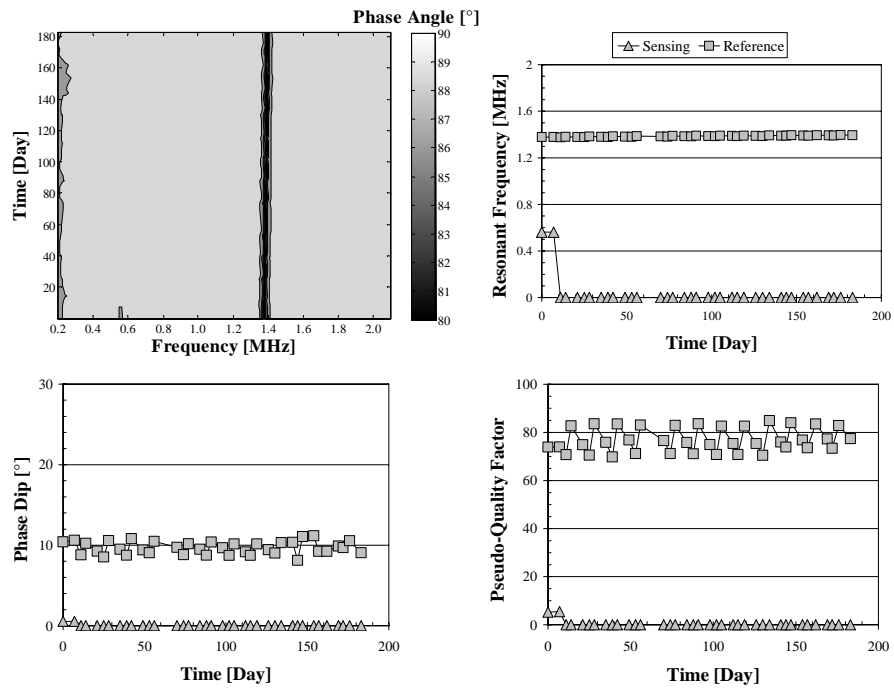


**Figure A-4 Response of Sensor A24**



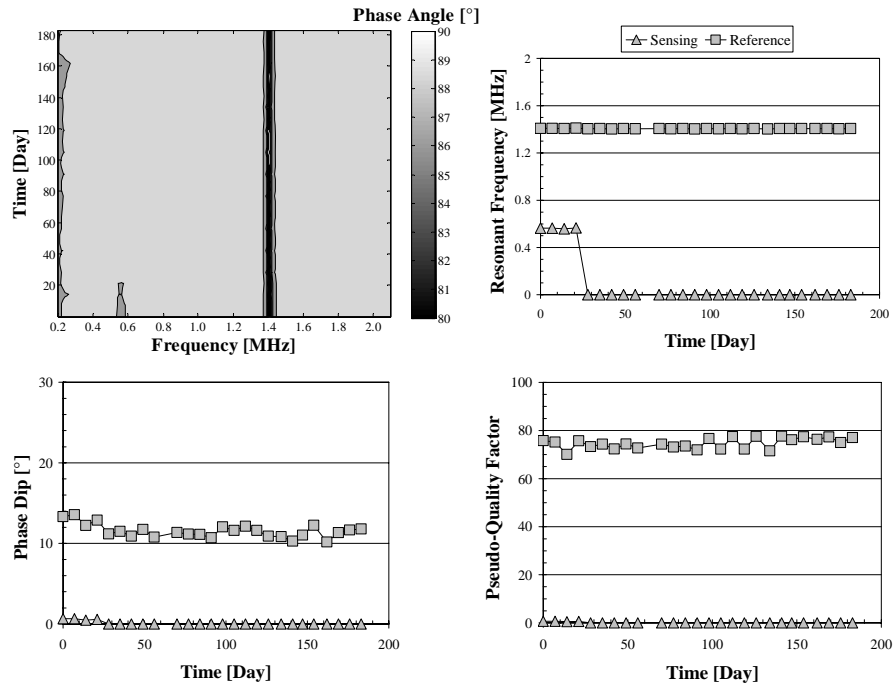


**Figure A-5 Response of Sensor A25**

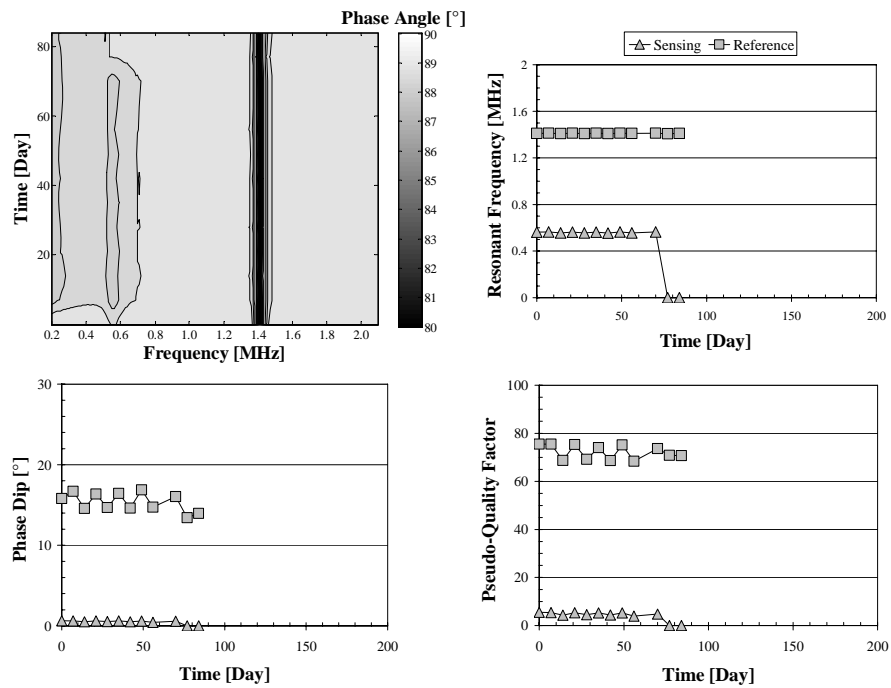


**Figure A-6 Response of Sensor A26**

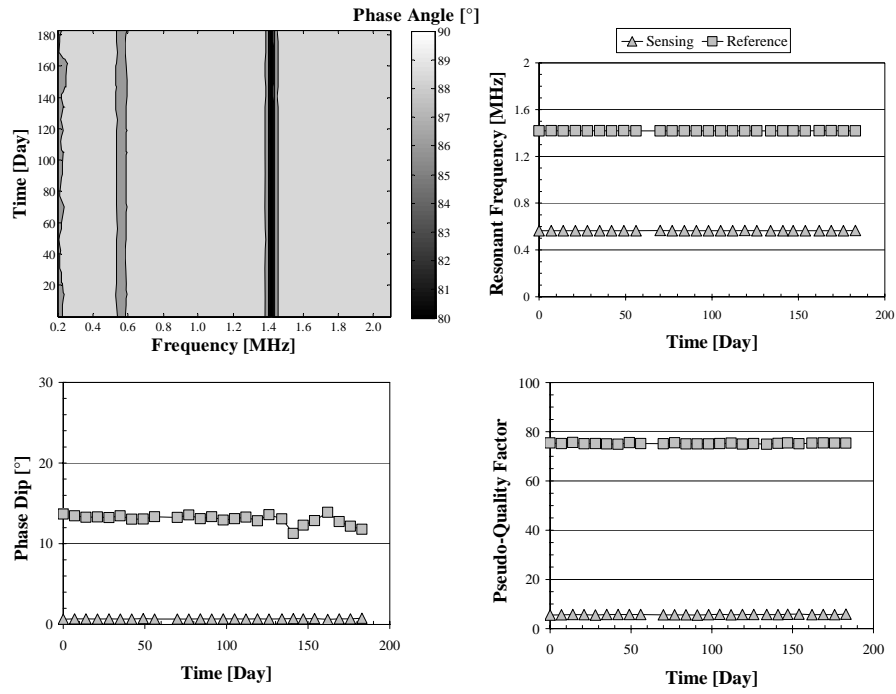


**Figure A-7 Response of Sensor A28**

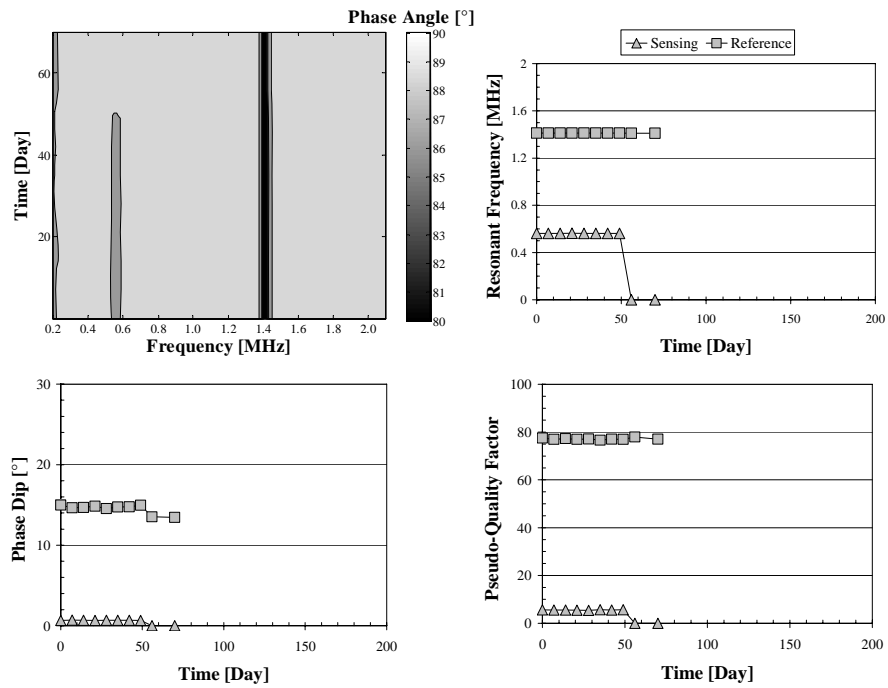


**Figure A-8 Response of Sensor A29**

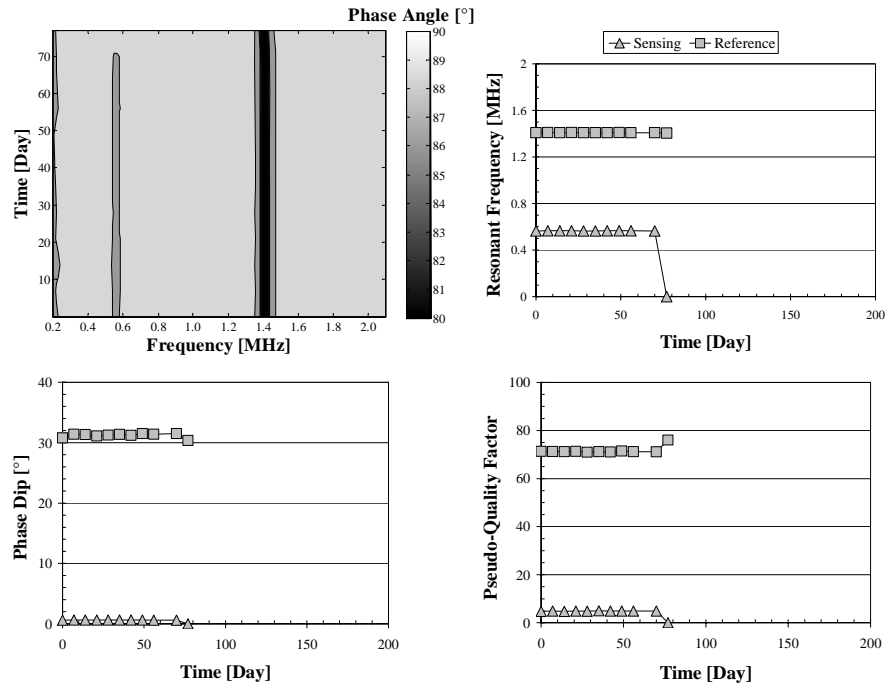


**Figure A-9 Response of Sensor A30**

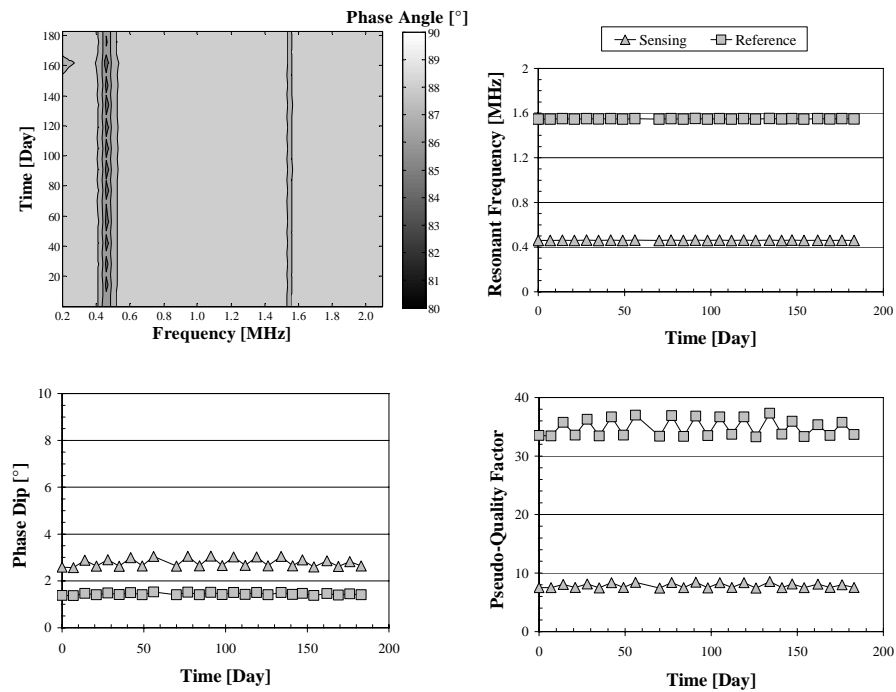


**Figure A-10 Response of Sensor B20**

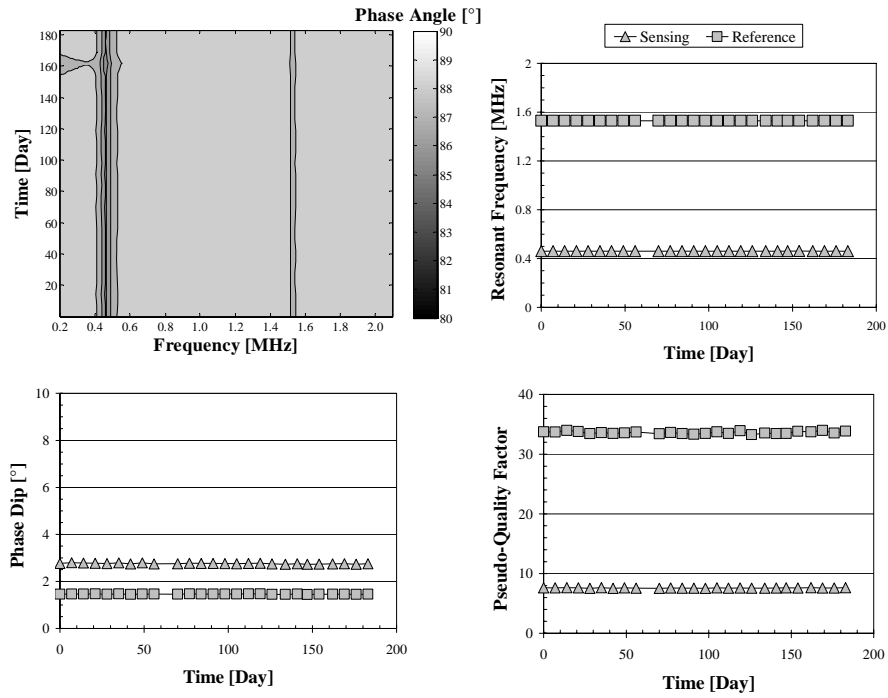


**Figure A-11 Response of Sensor B21**

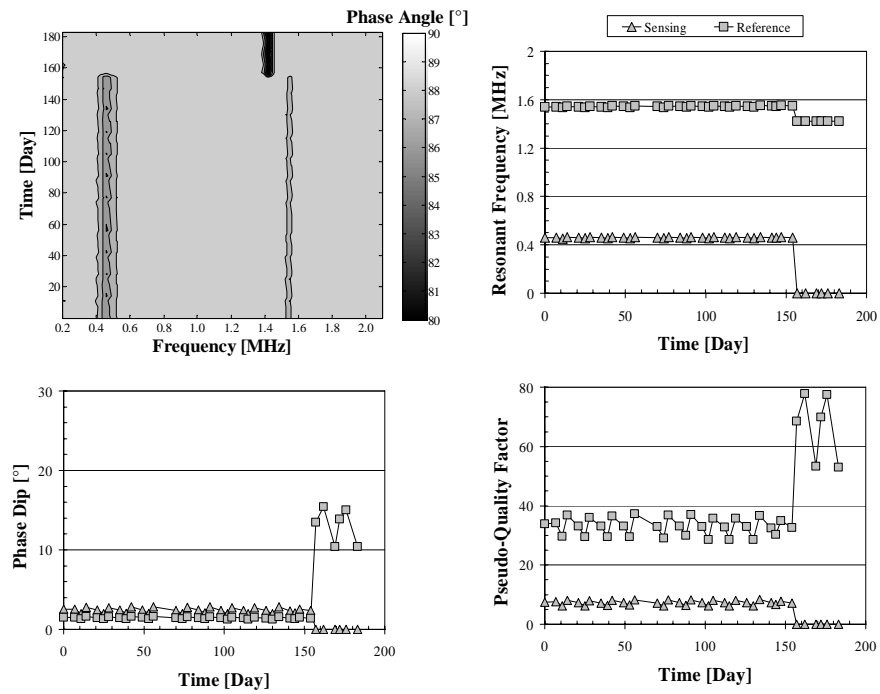


**Figure A-12 Response of Sensor B24**

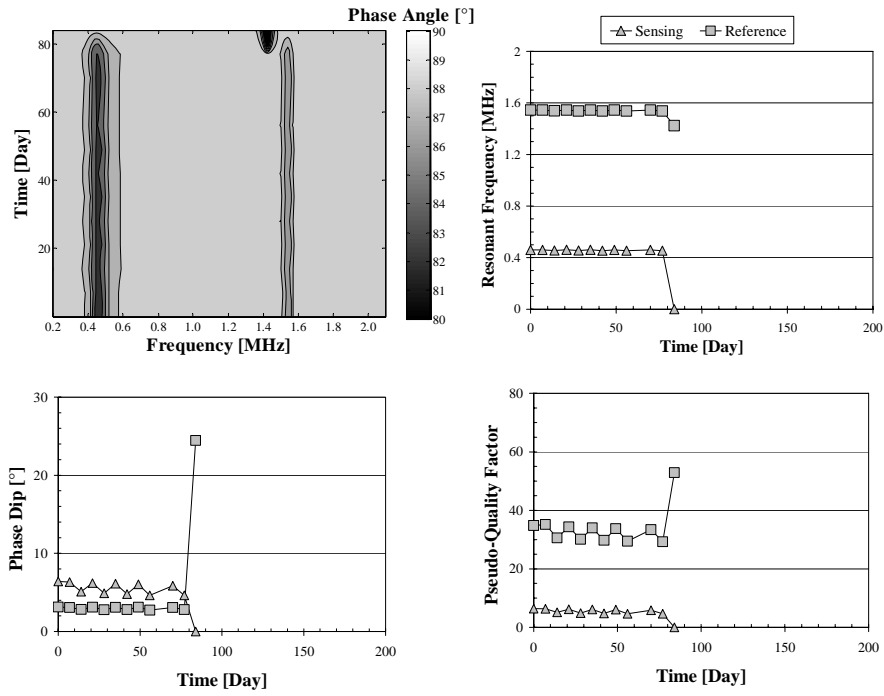


**Figure A-13 Response of Sensor B25**

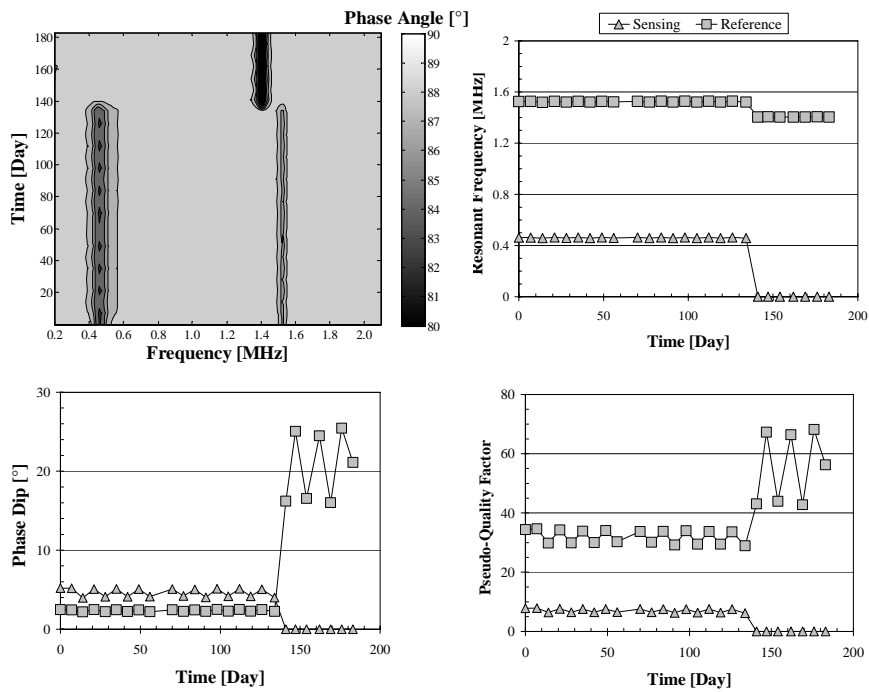


**Figure A-14 Response of Sensor B26**

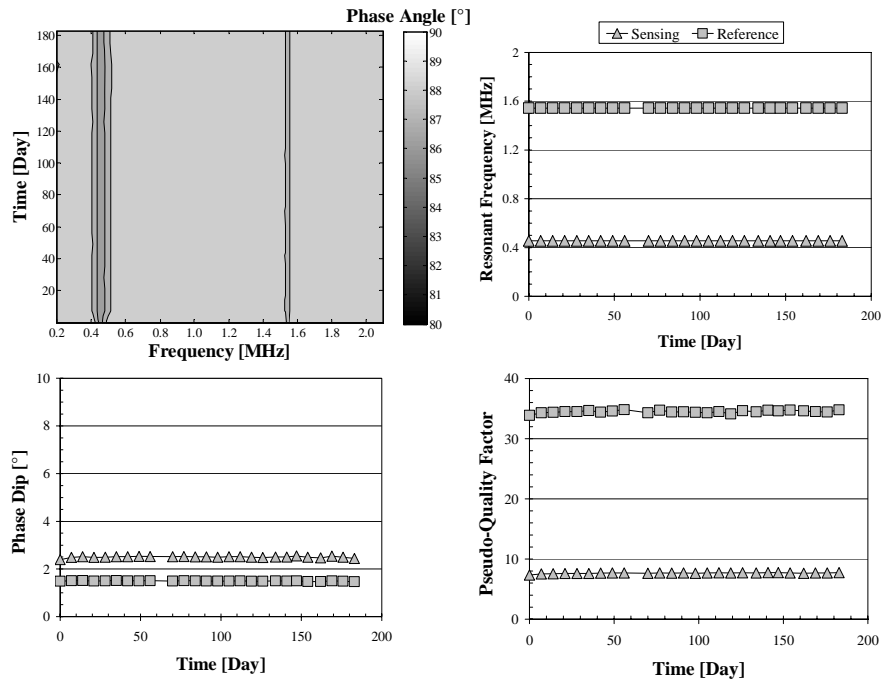


**Figure A-15 Response of Sensor B28**

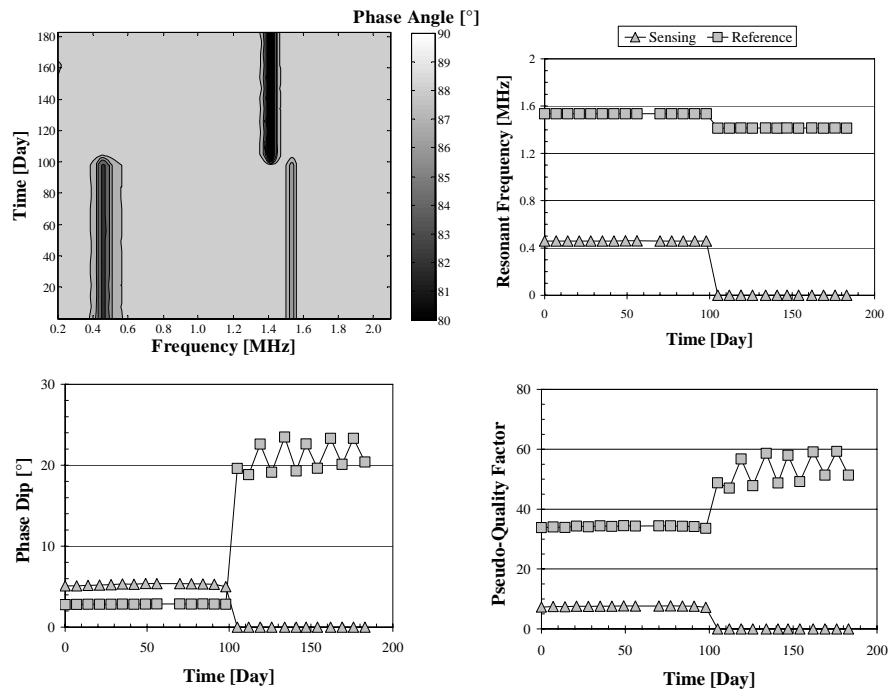


**Figure A-16 Response of Sensor B29**

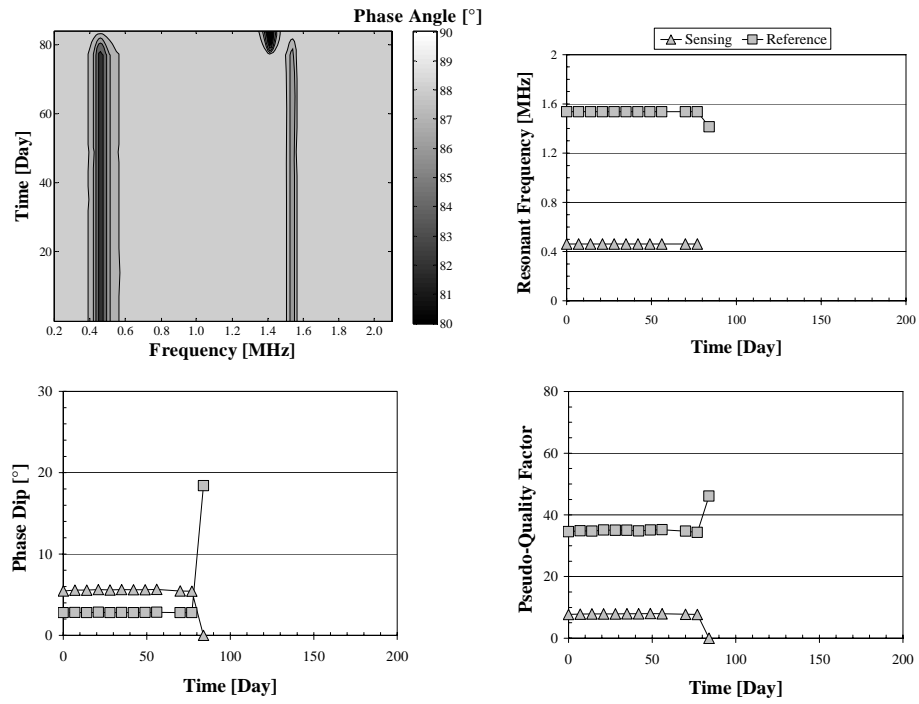


*Figure A-17 Response of Sensor B30*

## APPENDIX B

### Monitoring Results for Slabs 1 and 2

Results from monitoring Slabs 1 and 2 are reported in this appendix. Figure B-1 shows the temperature of the air in which Slabs 1 and 2 were stored over 511 days of testing. The air temperature was recorded immediately before half-cell potentials of the specimens were taken.

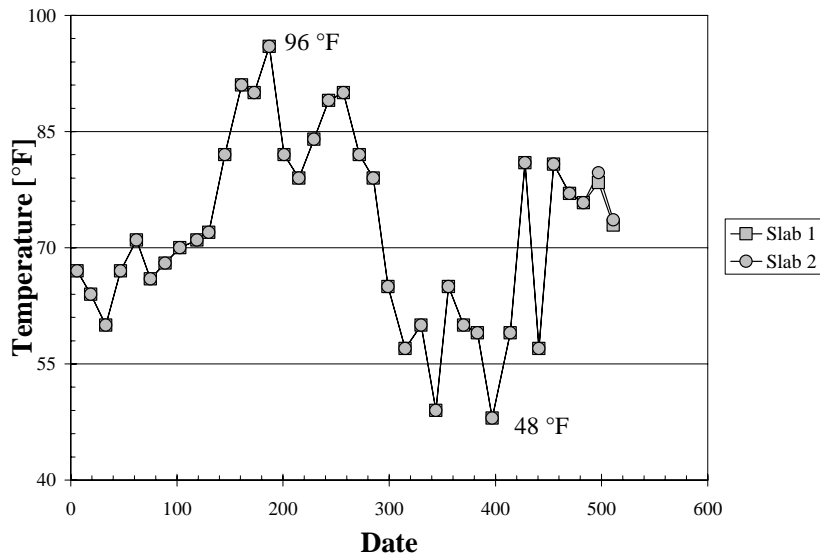


*Figure B-1 Temperature of Air in which Slabs 1 and 2 Stored*

In some cases, the responses of sensors tested in Slabs 1 and 2 were edited because of the presence of spurious values. Unpredictable baseline shift of the reader coil caused the curve-fitting algorithm to return spurious values periodically. There were two types of spurious values, and each was handled differently. The first type was caused by a fictitious phase dip in the curve-fit baseline and was observed only in the case of sensors with fractured sensing wires. A fictitious phase dip, labeled in Figure B-2, is evident in the response of sensor B08 on day 441. A detail in the figure shows the fictitious phase dip in the curve-fit baseline. Distortion of the curve-fit baseline due to baseline shift in the



measured impedance data caused the fictitious phase dip to develop. The algorithm then returned the resonant frequency, phase dip, and pseudo-quality factor of that fictitious phase dip as if the fictitious phase dip were the phase dip of the sensing circuit. Such phase dips were readily identified as fictitious by examination of the impedance data. Consequently, when the curve-fitting algorithm returned apparently spurious values for the response parameters of the sensing circuit, such values could readily be proven spurious. Spurious values for the parameters of the sensing circuit were replaced with values of zero once the impedance data were examined to verify that there was no phase dip at the sensing frequency. Values of zero that replaced the spurious values for the response parameters are colored white in the responses of the sensors below.

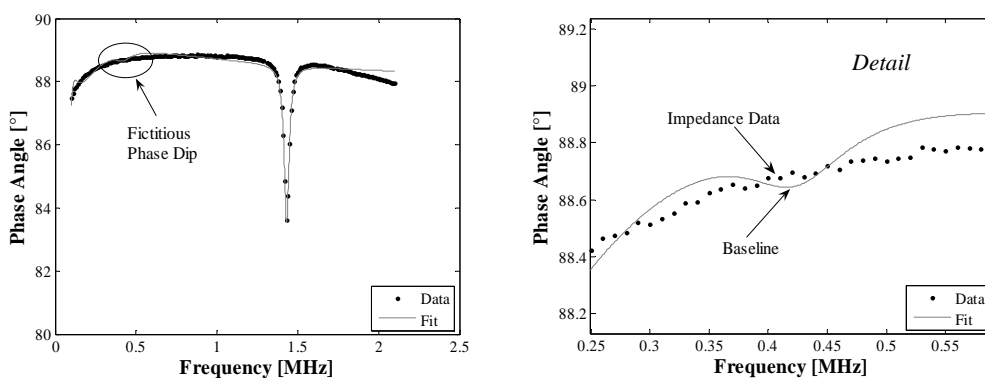


**Figure B-2 Fictitious Phase Dip in Response of B08**

The other type of spurious value was simply a miscalculation by the curve-fitting algorithm due to baseline shift. In that case, the baseline shift in the impedance data was so distorted that the algorithm calculated a value for a given response parameter that clearly did not correspond with the physical state of the circuit. Such values were not reported. A given value was not reported if two conditions were satisfied, and these conditions were the following. First, the value of the given response parameter was significantly different from the values near it without any trends indicating such significant change in the circuit. That is, a value for a given response parameter that was in significant discontinuity

with the values around it was deemed suspect. An example is shown in Figure B-3, a plot of the pseudo-quality factors of sensor B54. The second condition was that some distortion in the measured baseline of the impedance data be observed, serving as the probable cause for the miscalculation by the curve-fitting algorithm. Figure B-4 shows the baseline shift observed in the response of B54 on the day (day 441) when the spurious value for the referenced pseudo-quality factor was returned by the algorithm.

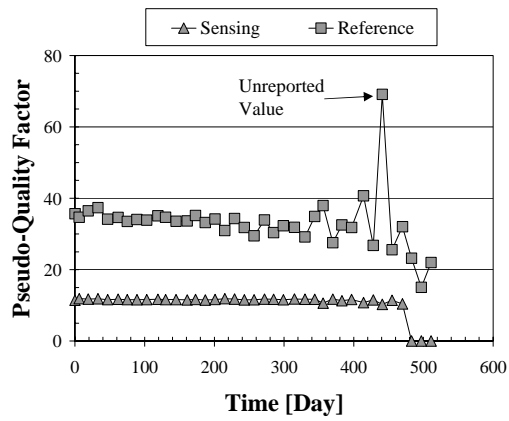


**Figure B-3 Unreported Value of Reference Pseudo-Quality Factor of B54**

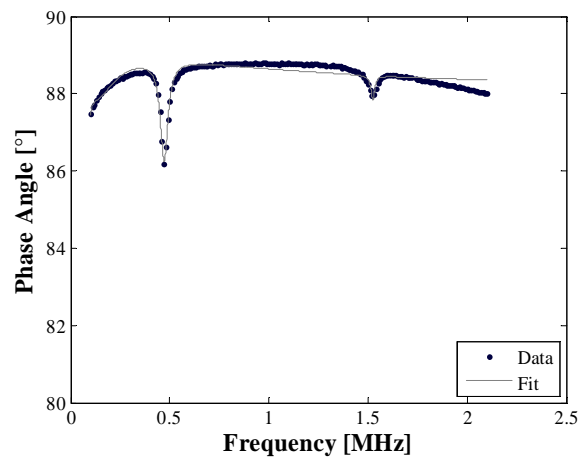


**Figure B-4 Baseline Shift in the Response of B54**

The responses of sensors tested in Slabs 1 and 2 are presented below. The responses of sensors that were discussed in Chapter 4 are omitted from this appendix. The small phase dip of the coplanar sensing circuit rendered the development of contour plots for the coplanar sensors impossible. In one case, sensor A06, the response parameters of the sensing circuit could not be determined by the curve-fitting algorithm. Therefore, the contour plot of each coplanar sensor was replaced with the response of the sensor in the plane of phase angle and frequency. Data from all the interrogations of a given coplanar sensor are plotted in that plane. The elevations of the contour lines for each contour plot of the sensors are given in Table B-1.

***Table B-1 Elevation of Contour Lines for Contour Plots of Concentric Sensors***

<b>Sensor</b>	<b>Elevations of Contour Lines [°]</b>
B02	80, 82, 84, 86, 88, 88.7, 90
B03	80, 82, 84, 86, 88, 88.8, 89.1, 90
B04	80, 82, 84, 86, 88, 88.3, 88.97, 90
B06	80, 82, 84, 86, 88.1, 88.9, 90
B07	80, 82, 84, 86, 88, 88.7, 90
B08	80, 82, 84, 86, 88, 88.9, 90
B09	80, 82, 84, 86, 88.4, 89, 90
B51	80, 82, 84, 86, 88, 88.8, 90
B52	80, 82, 84, 86, 88, 88.8, 90
B53	80, 84, 85, 86, 87, 88, 88.6, 90
B54	80, 84, 85, 86, 87, 88, 88.2, 88.6, 90
B55	80, 82, 84, 86, 88, 88.7, 90
B56	80, 84, 85, 86, 87, 88.6, 90
B58	80, 82, 84, 86, 88, 88.8, 90
B59	80, 84, 85, 86, 87.8, 88.2, 90

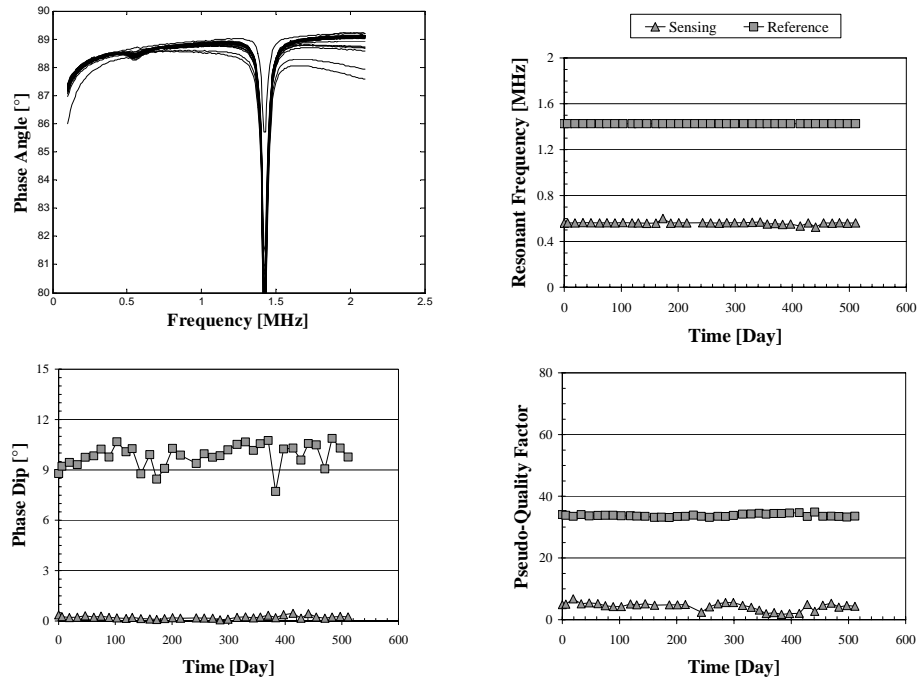


*Figure B-5 Response of Sensor A01*

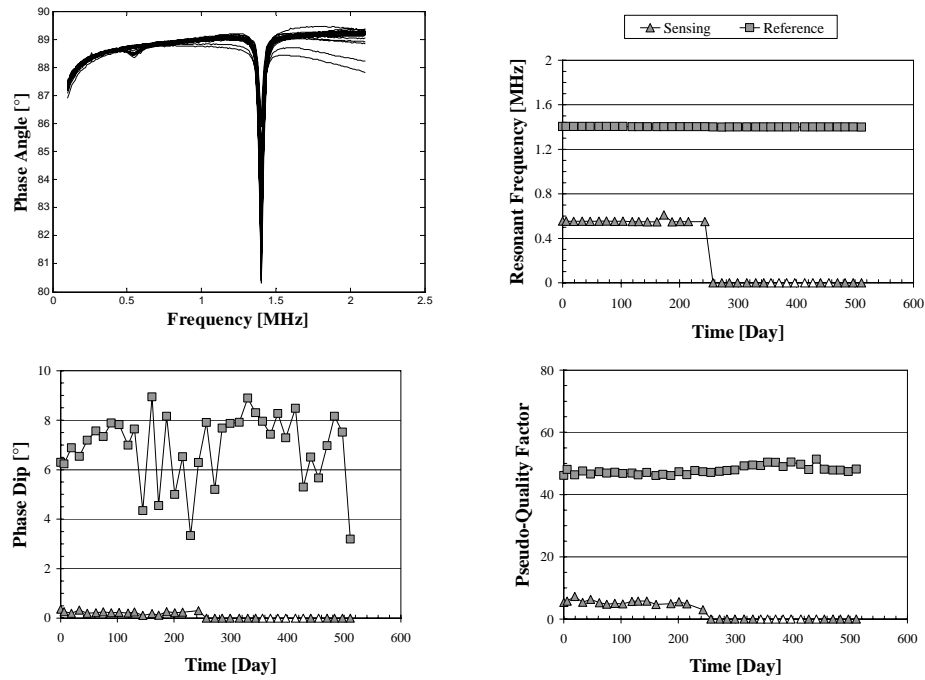


*Figure B-6 Response of Sensor A02*

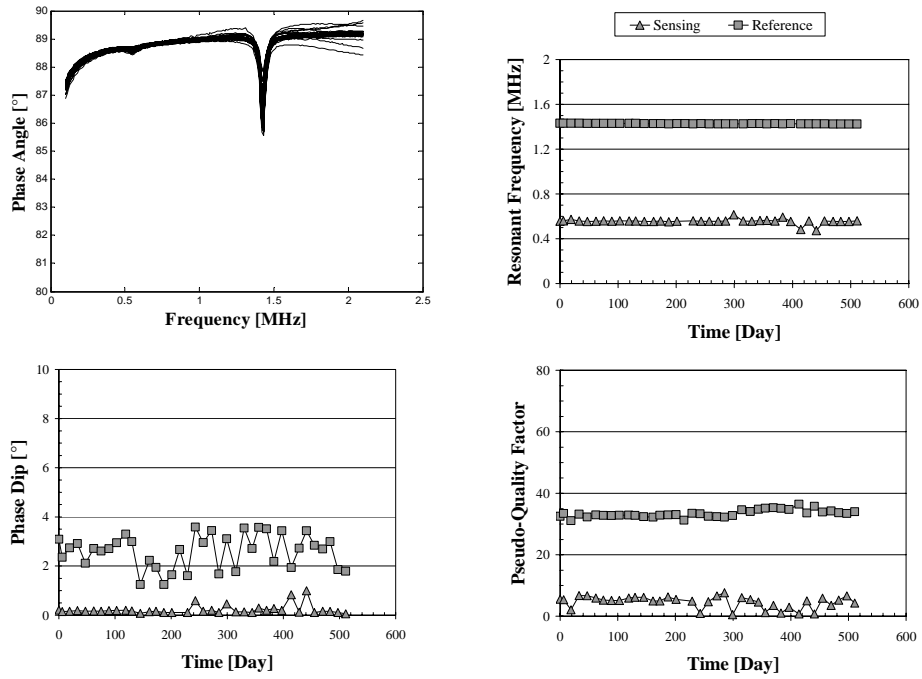


**Figure B-7 Response of Sensor A03**

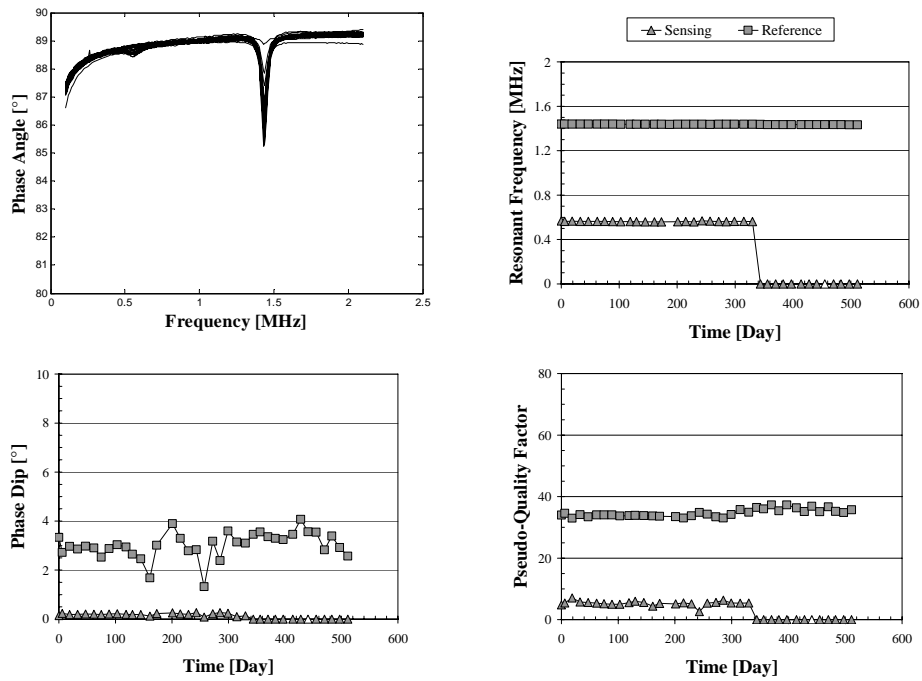


**Figure B-8 Response of Sensor A04**

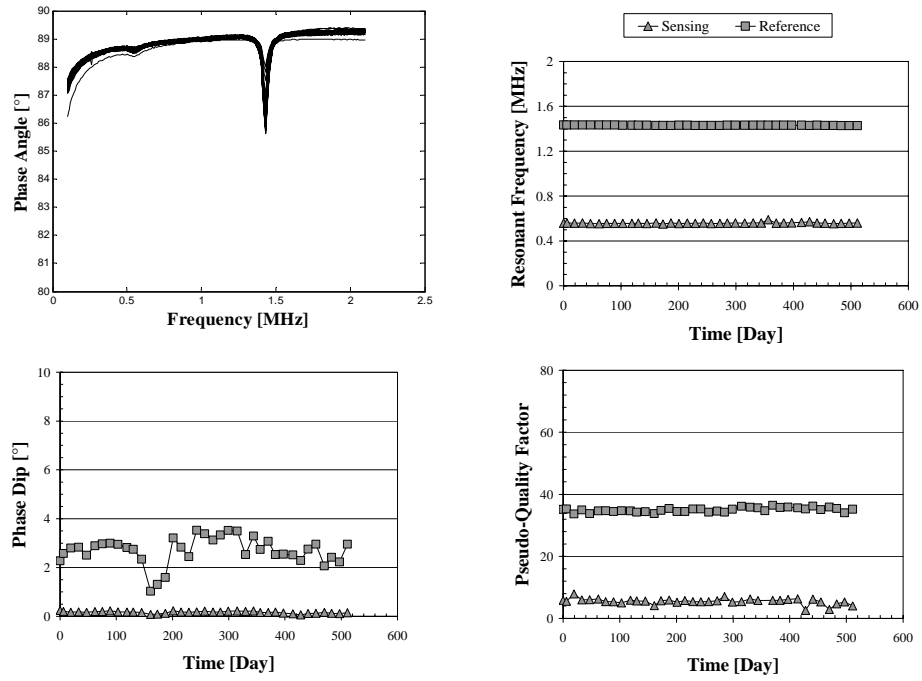


*Figure B-9 Response of Sensor A05*

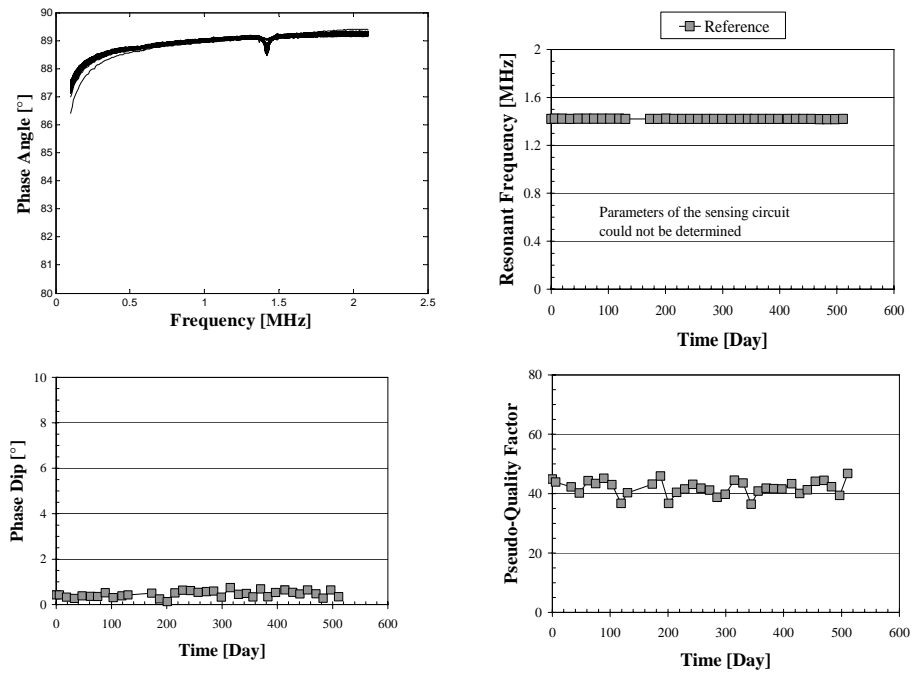


*Figure B-10 Response of Sensor A06*

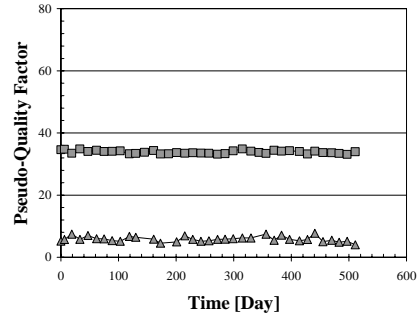
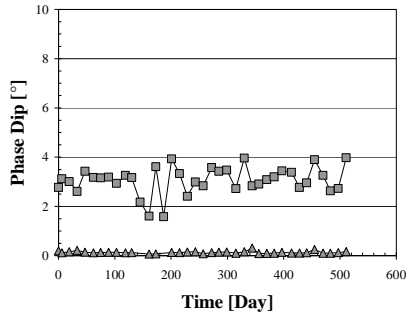
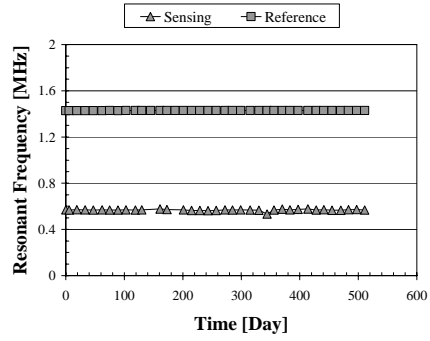
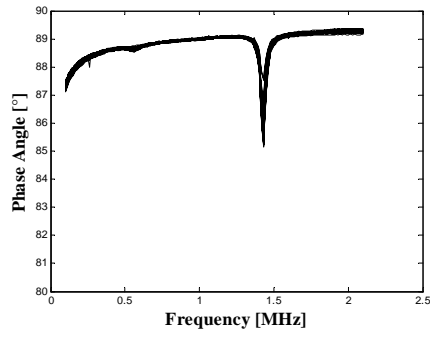


*Figure B-11 Response of Sensor A07*

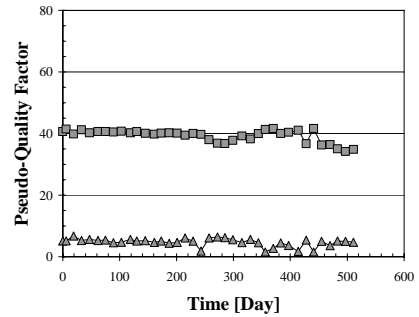
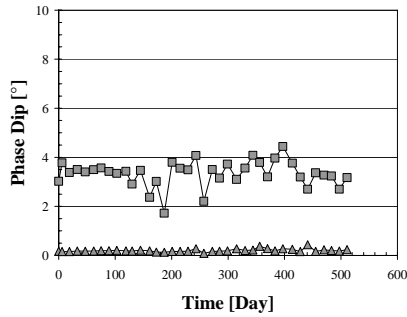
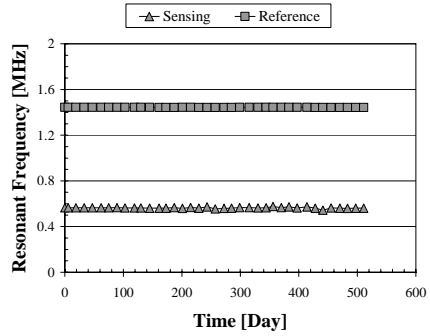
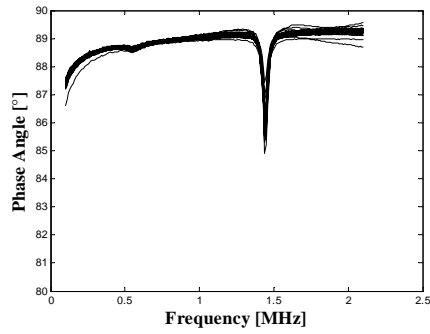


*Figure B-12 Response of Sensor A08*

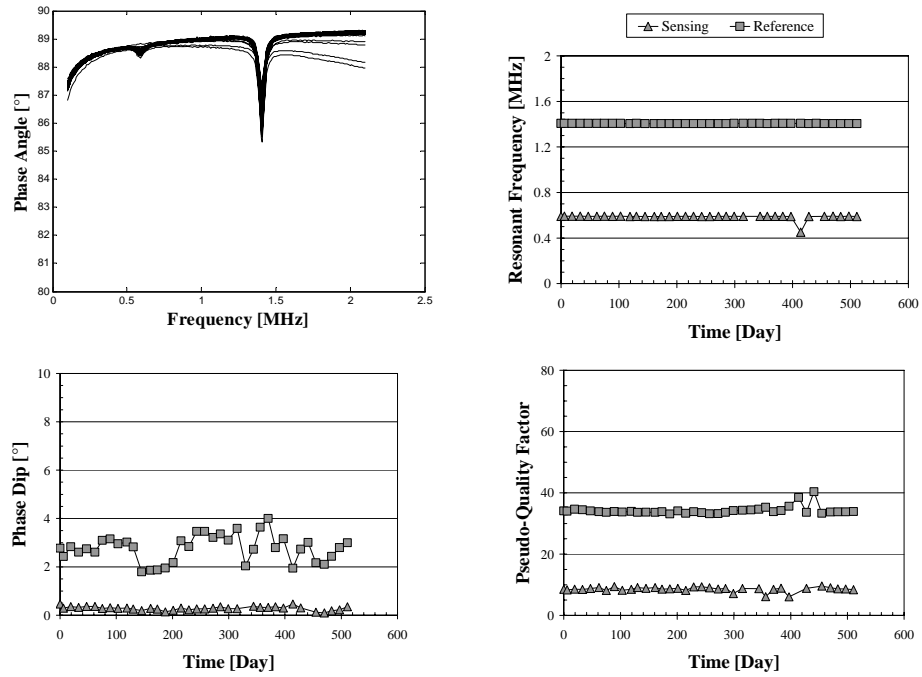


*Figure B-13 Response of Sensor A51*

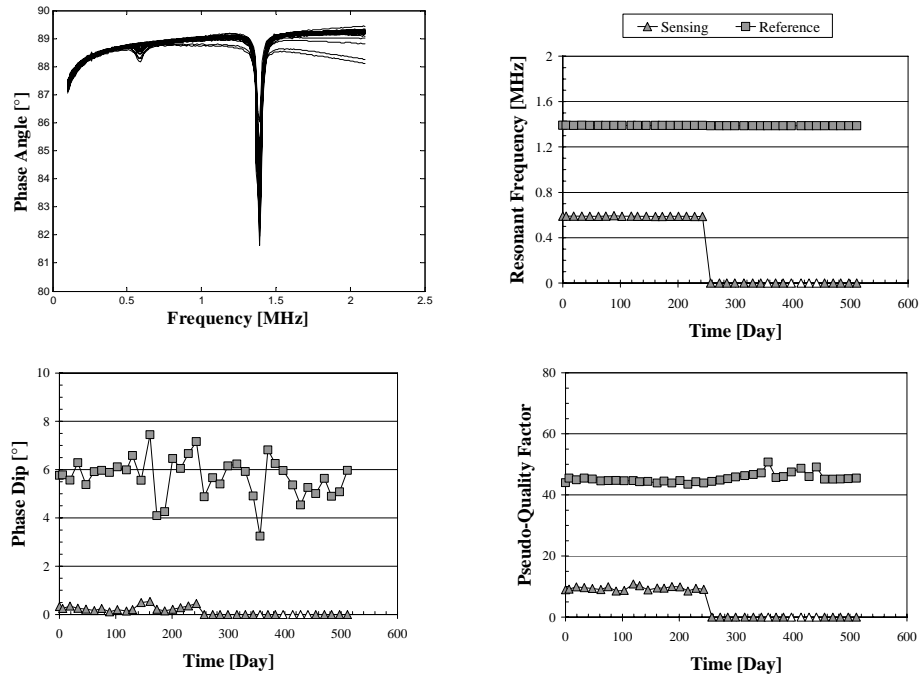


*Figure B-14 Response of Sensor A52*



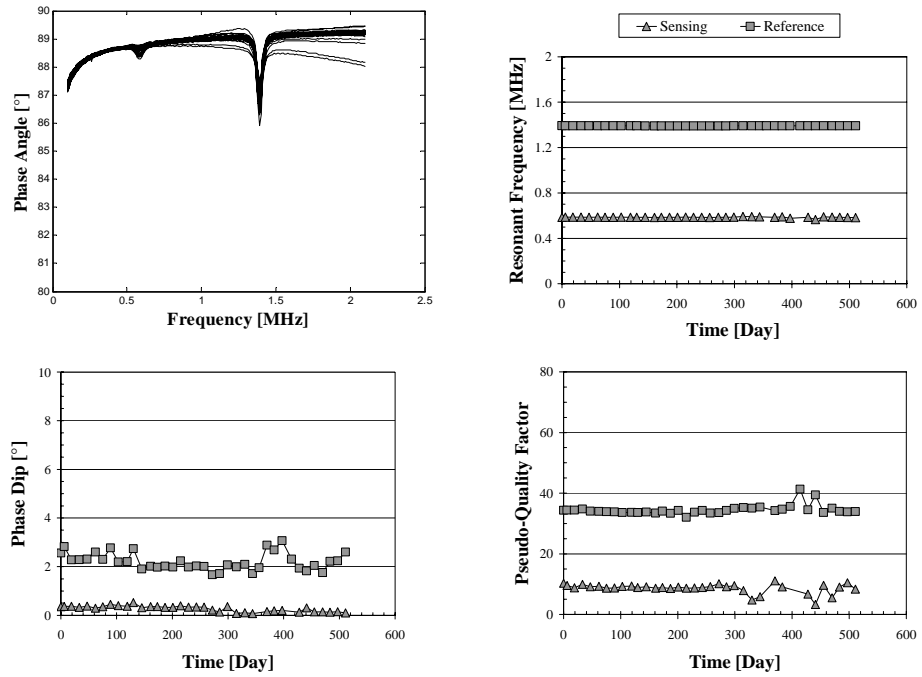


*Figure B-15 Response of Sensor A53*

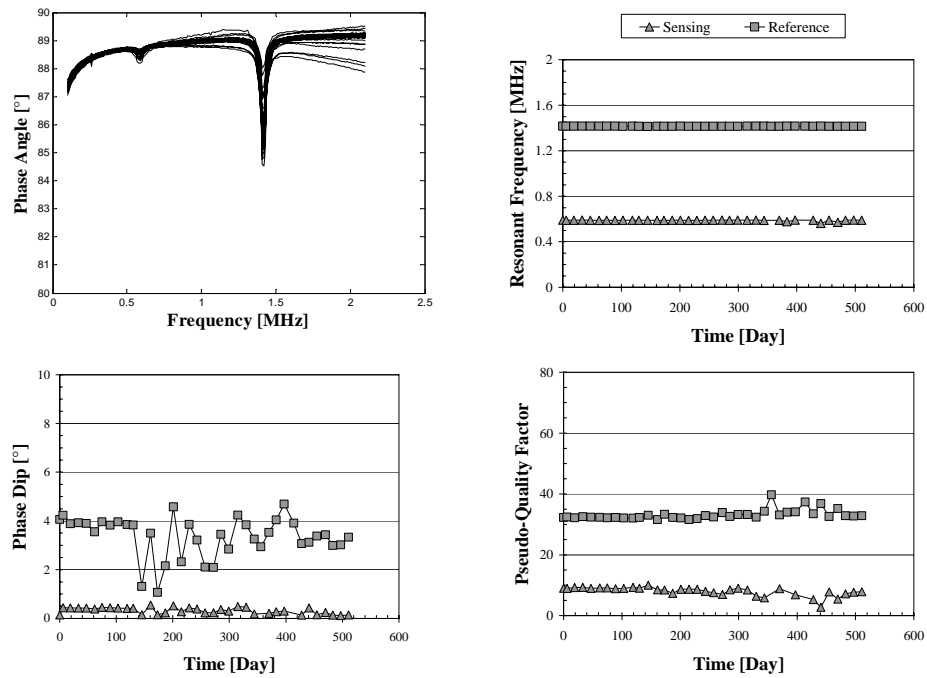


*Figure B-16 Response of Sensor A54*

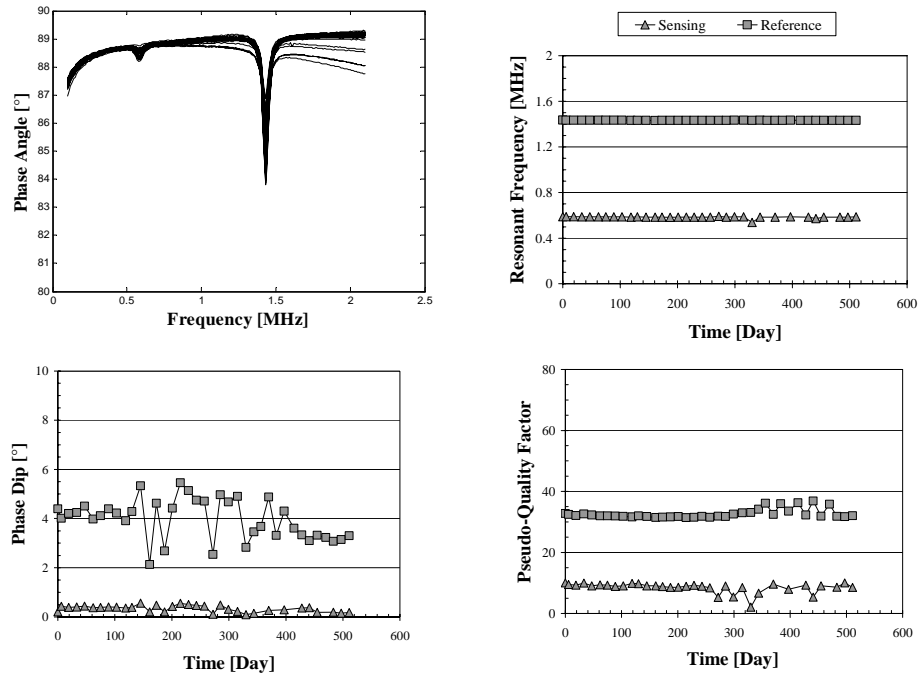


*Figure B-17 Response of Sensor A55*

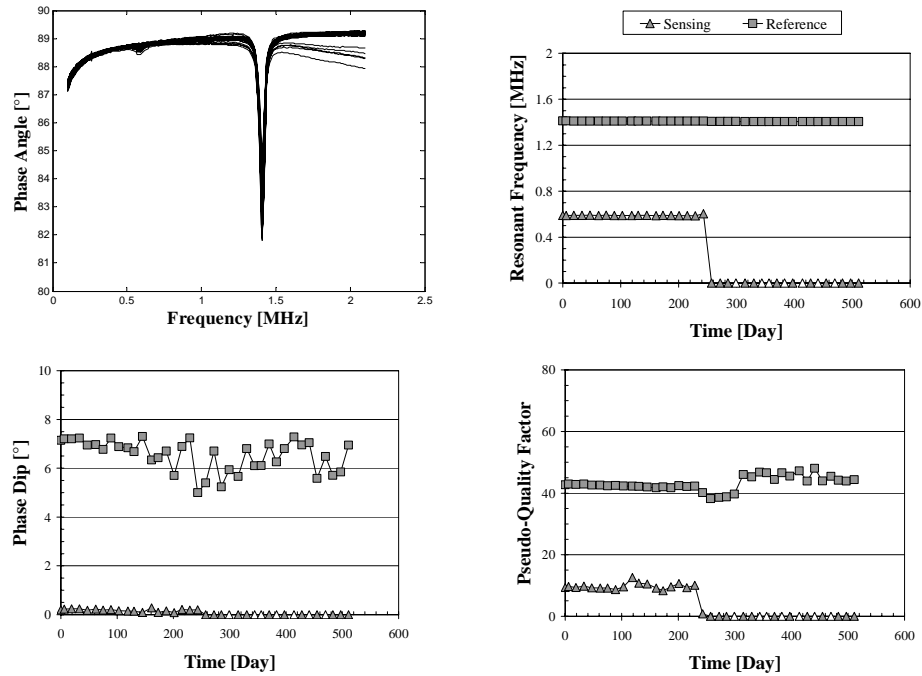


*Figure B-18 Response of Sensor A56*

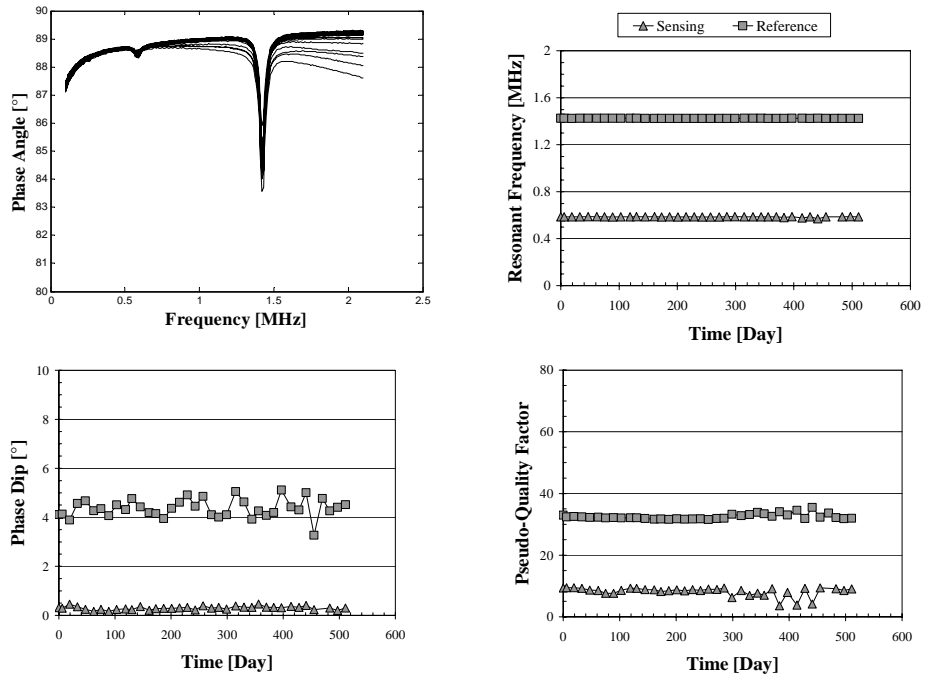


**Figure B-19 Response of Sensor A57**

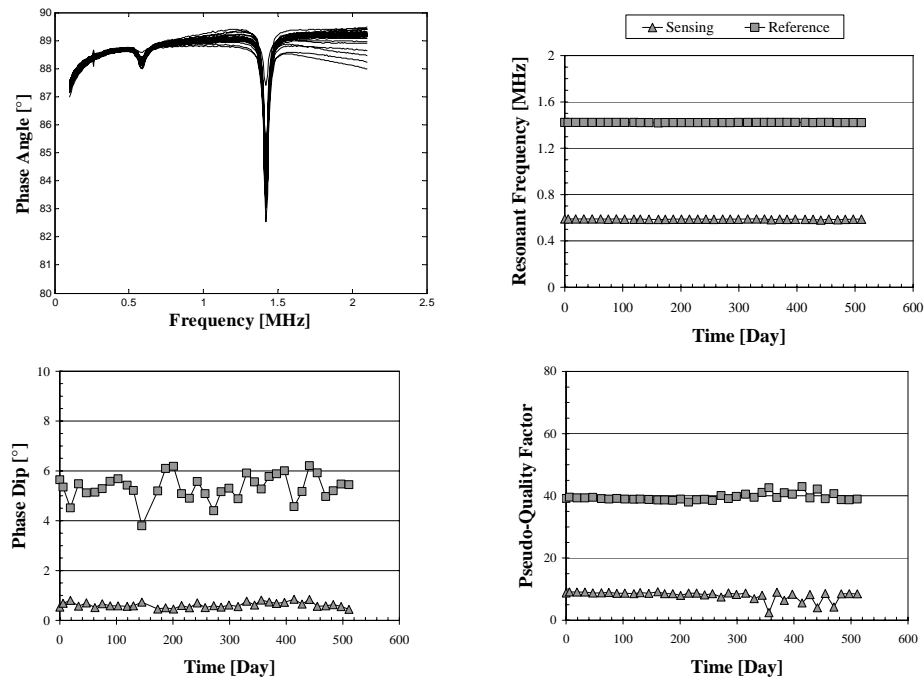


**Figure B-20 Response of Sensor A58**

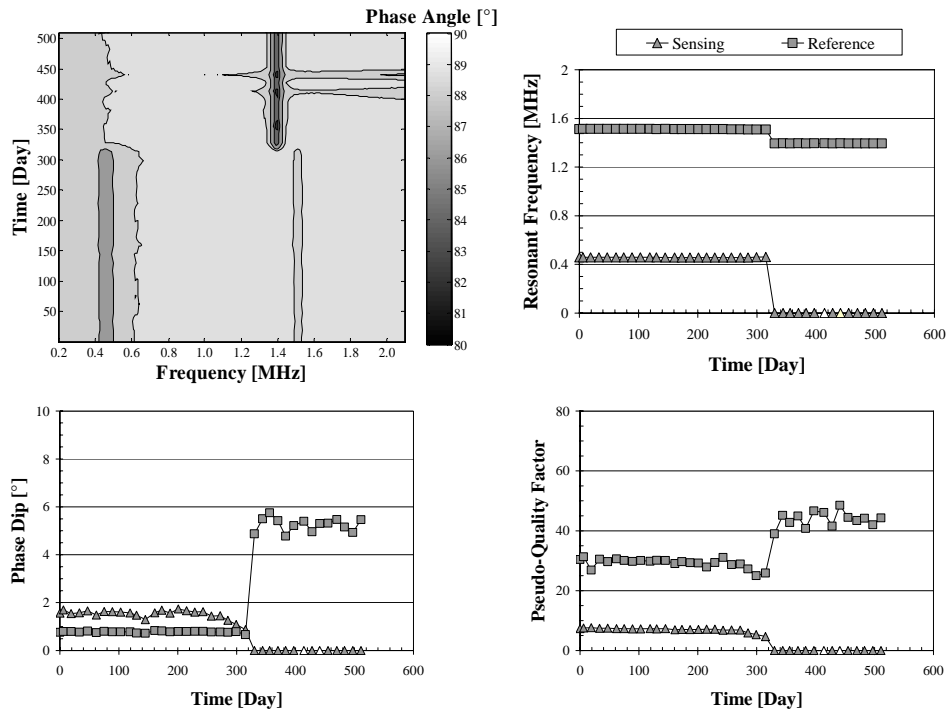


**Figure B-21 Response of Sensor B02**

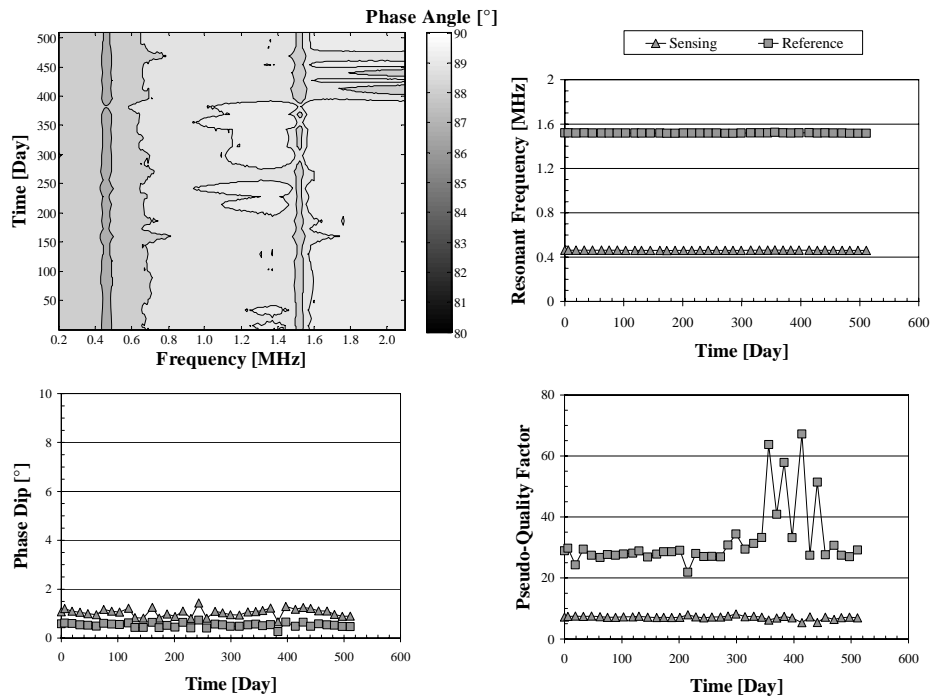


**Figure B-22 Response of Sensor B03**

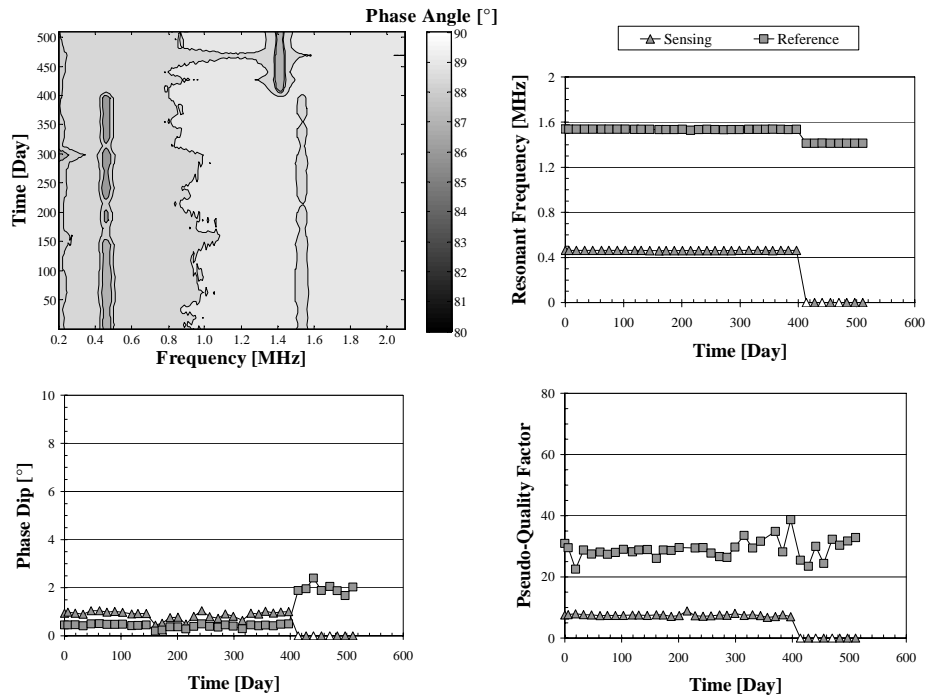


*Figure B-23 Response of B04*

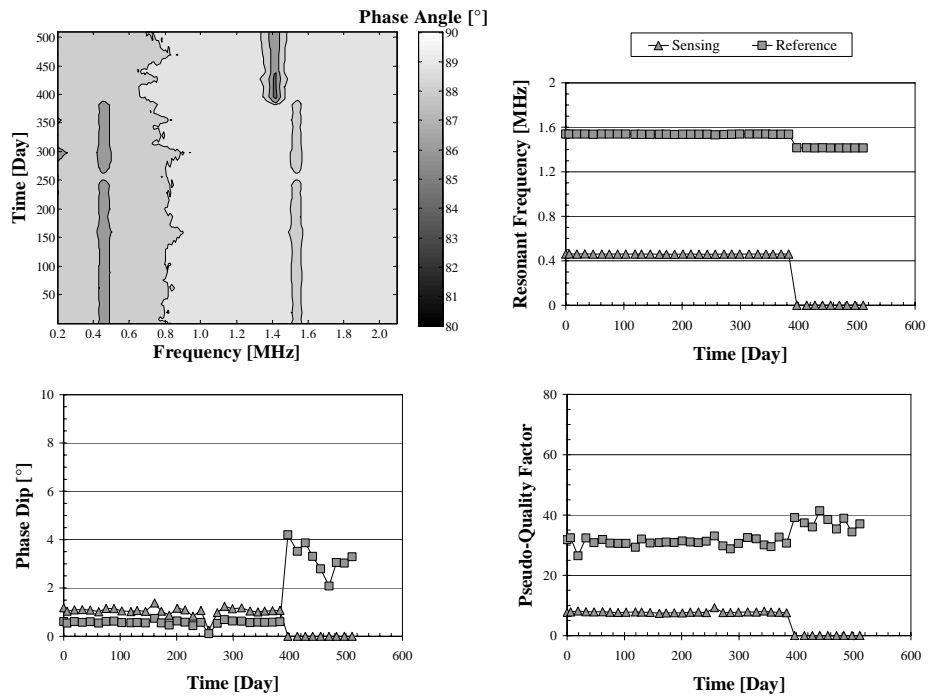


*Figure B-24 Response of Sensor B06*

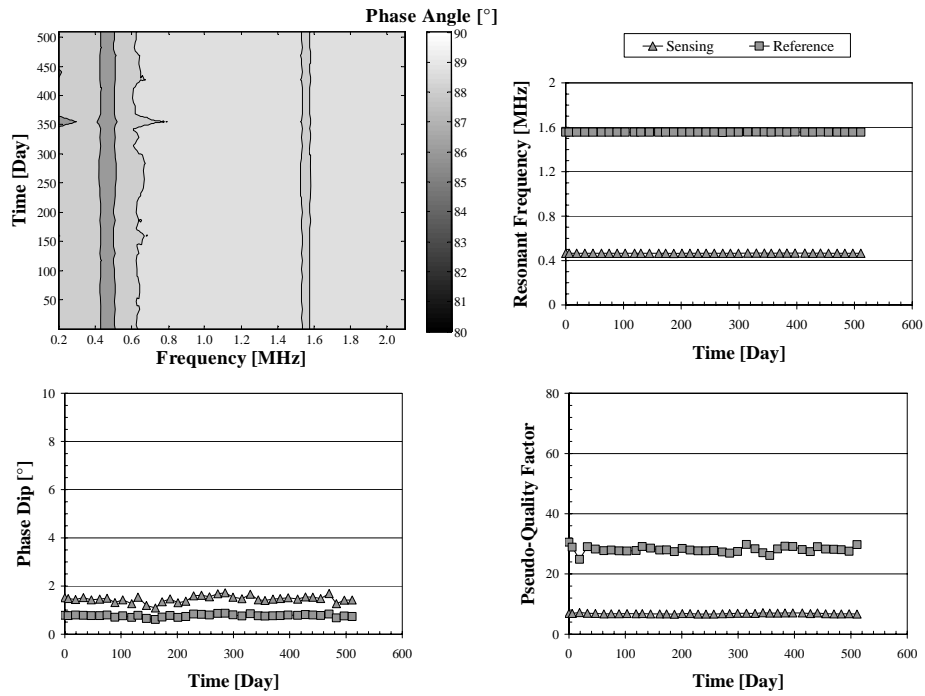


**Figure B-25 Response of Sensor B07**

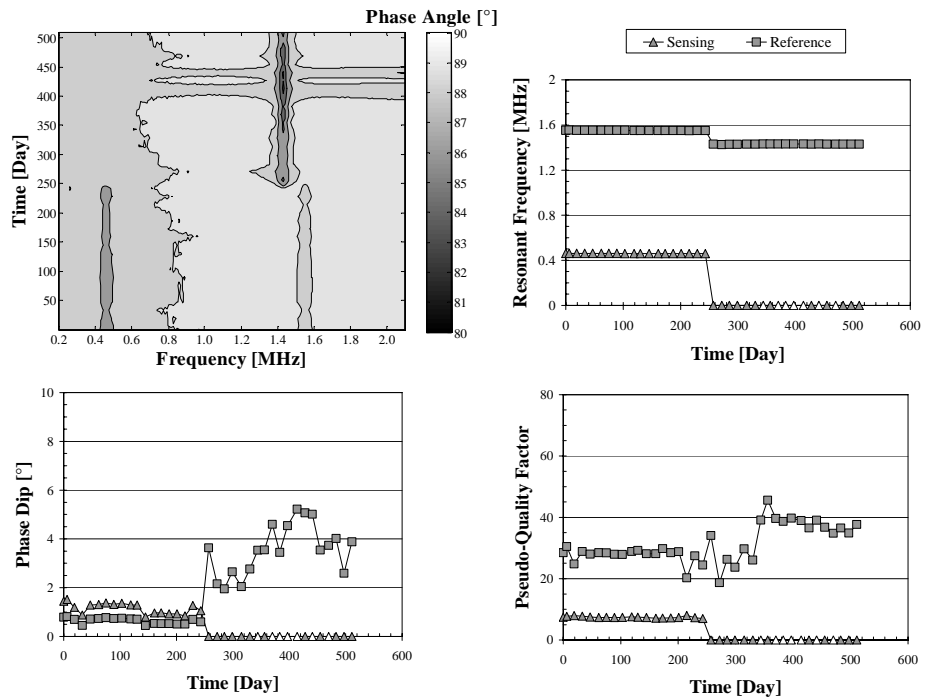


**Figure B-26 Response of Sensor B08**

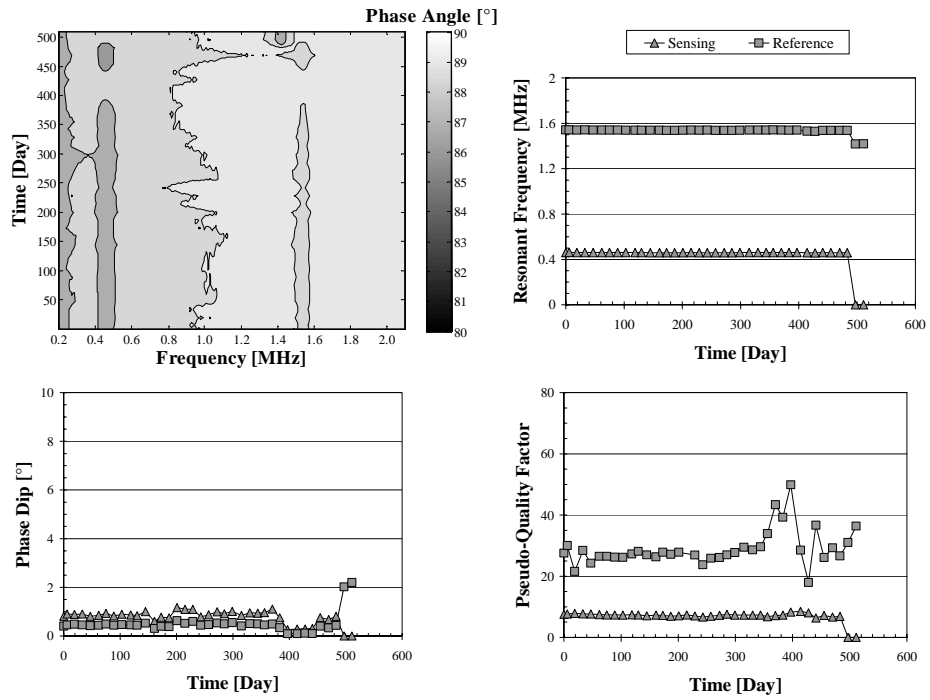


**Figure B-27 Response of Sensor B09**

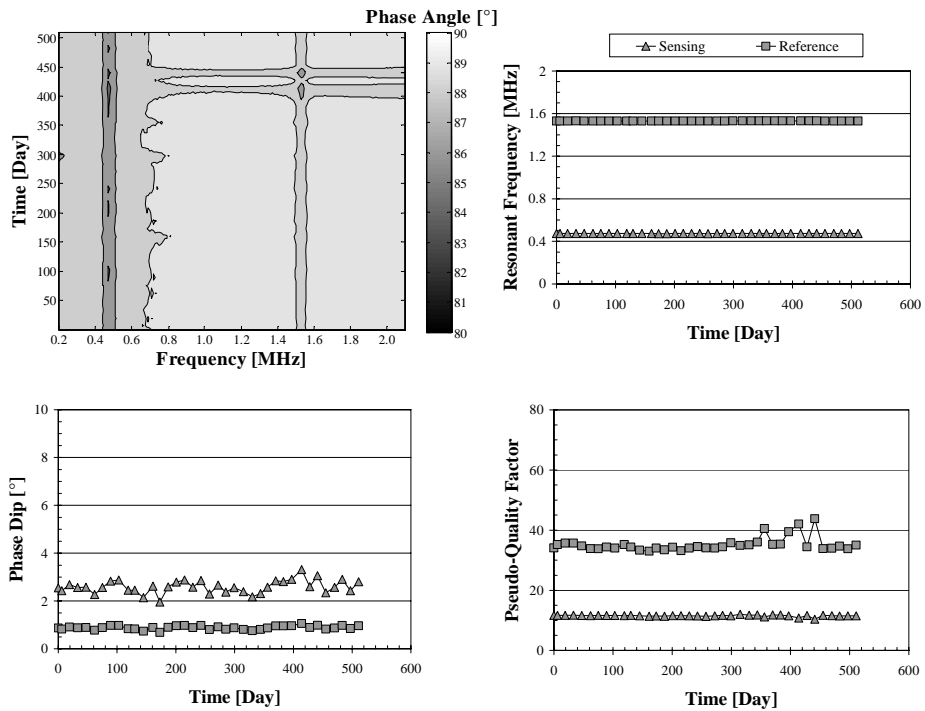


**Figure B-28 Response of Sensor B51**

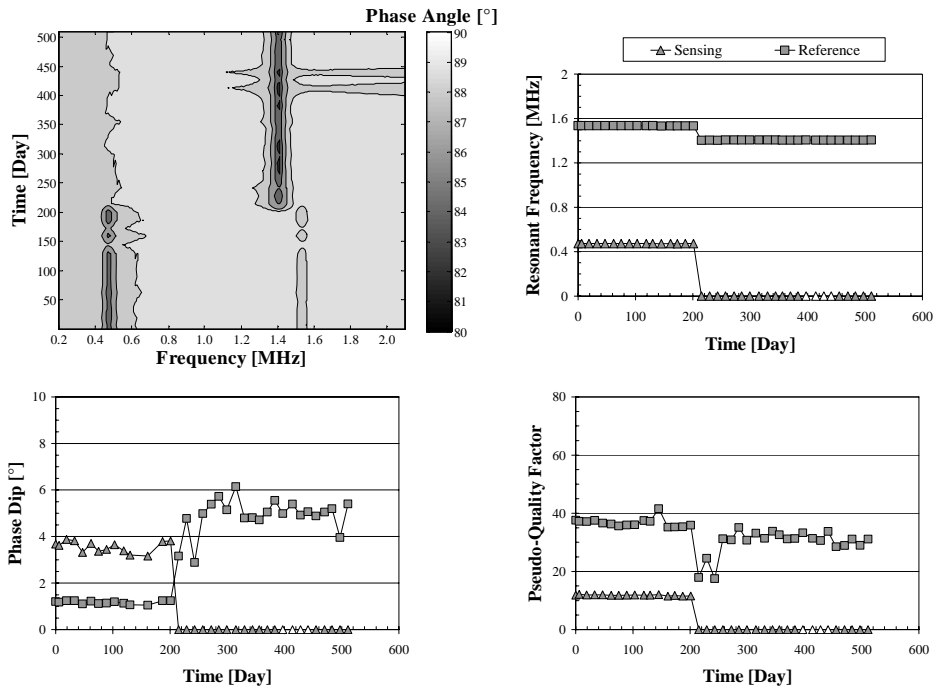


**Figure B-29 Response of Sensor B52**

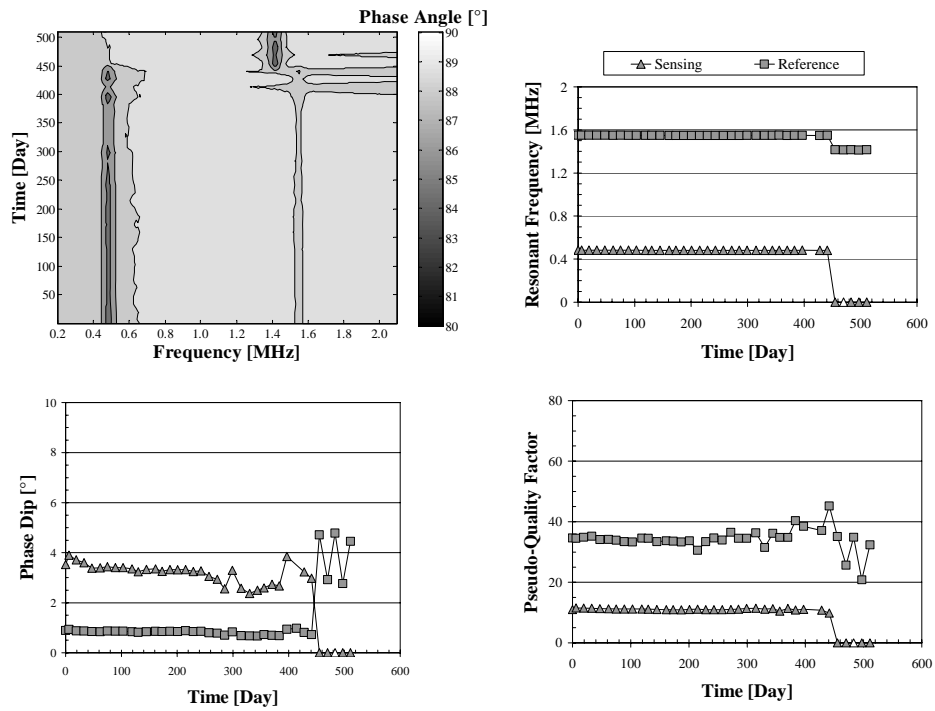


**Figure B-30 Response of Sensor B53**



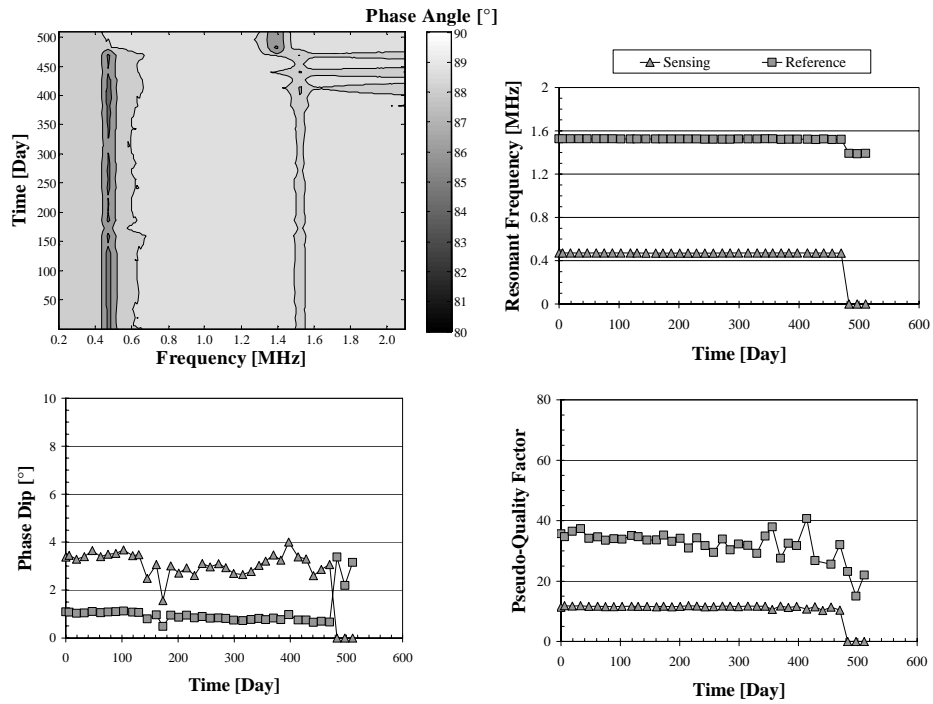


**Figure B-31 Response of Sensor B54**

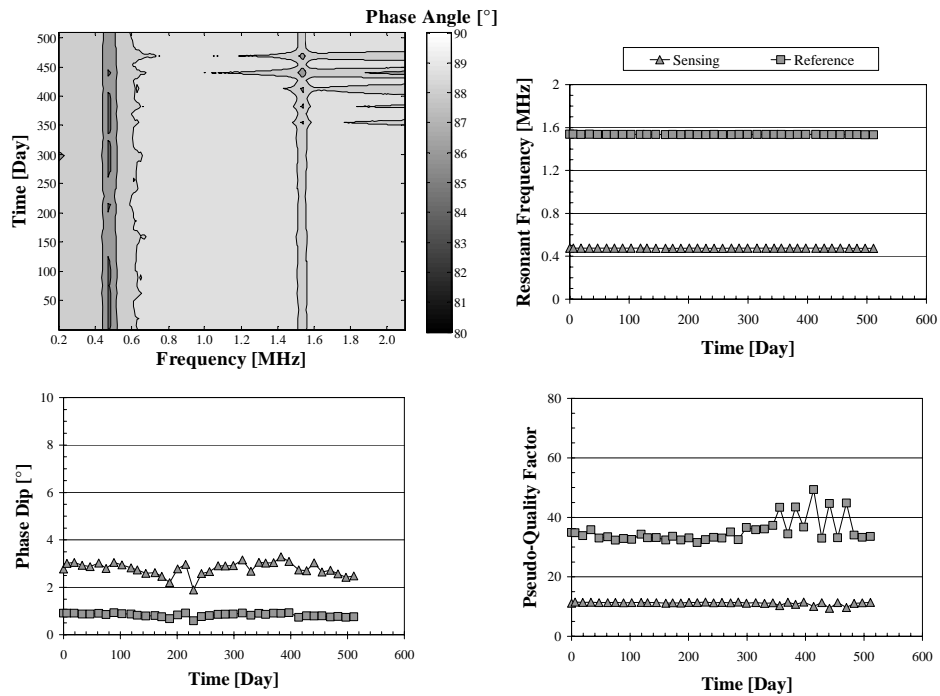


**Figure B-32 Response of Sensor B55**

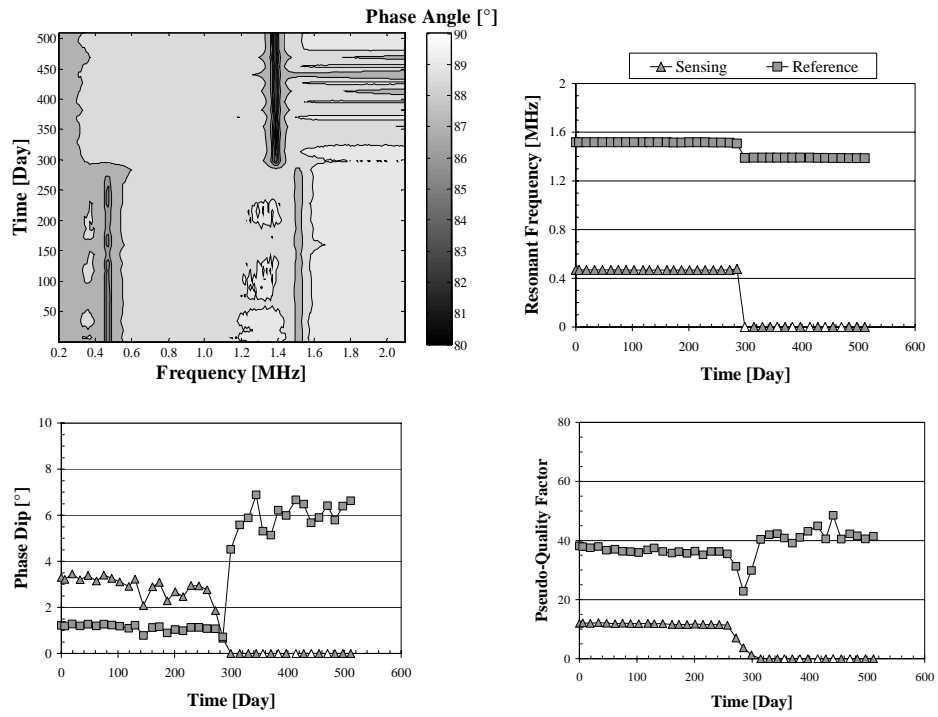


**Figure B-33 Response of Sensor B56**

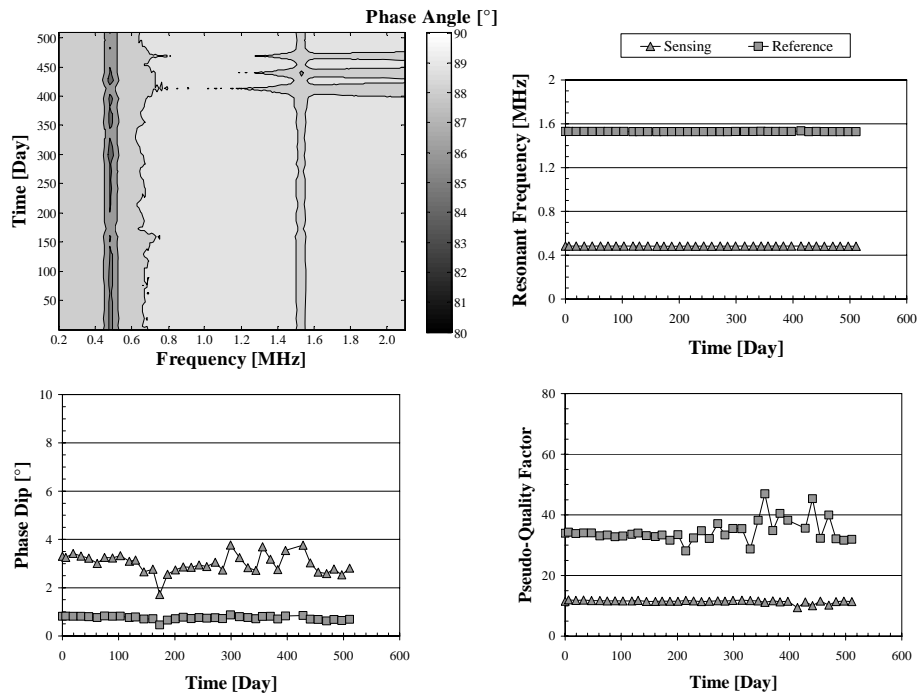


**Figure B-34 Response of Sensor B58**

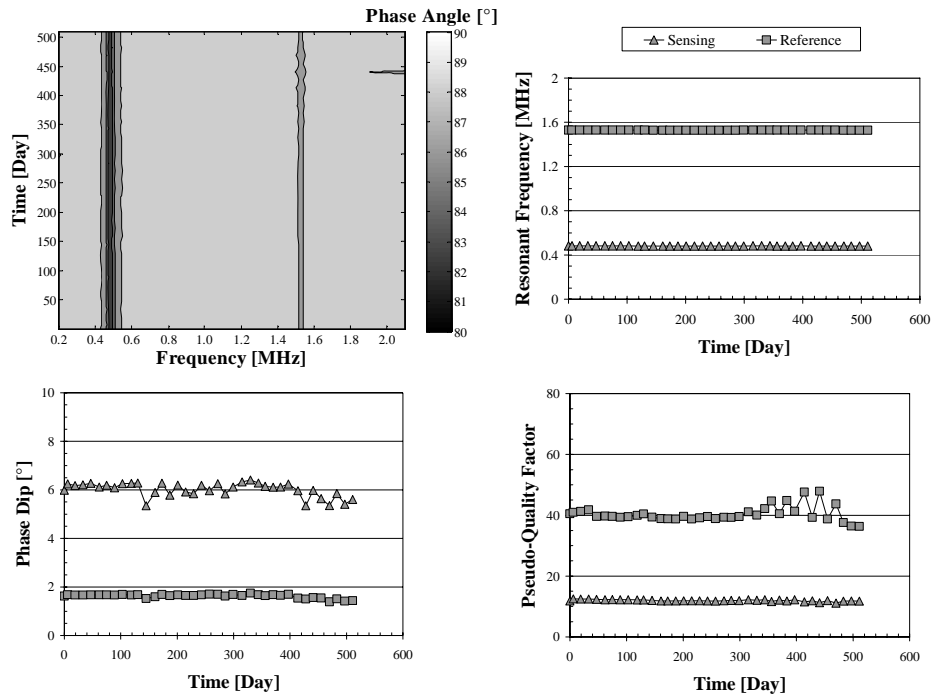


*Figure B-35 Response of Sensor B59*

## APPENDIX C

### Monitoring Results for Slabs 3 and 4

Figure C-1 shows the relative humidity of the air in which Slabs 3 and 4 were stored. The relative humidity was recorded immediately before half-cell measurements were taken for each specimen, beginning on day 126 of testing. The reported values are the averages of those two values.

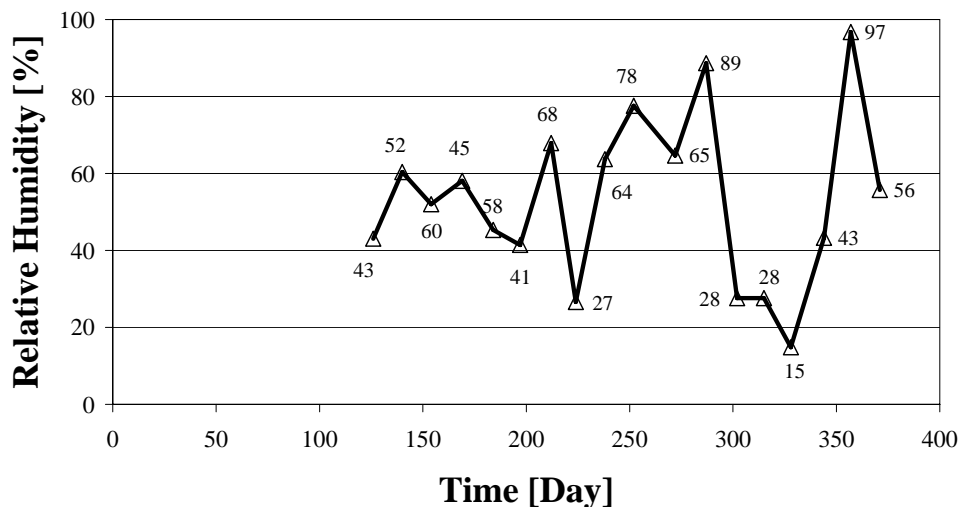


*Figure C-1 Relative Humidity of Air*

The responses of sensors tested in Slabs 3 and 4 and their control specimen, after 371 days of testing, are presented below. The responses of sensors that were discussed in Chapter 5 are omitted from this appendix. Slab 4 has been autopsied, while testing of Slab 3 and the control specimen is ongoing. The elevations of contour lines in the contour plots are given in Table C-1. In some cases, the responses of the sensors were edited due to the curve-fitting algorithm returning spurious values for the response parameters — resonant

frequency, phase dip, and pseudo-quality factor. The editing of the responses followed the conventions described in Appendix B.

**Table C-1 Elevation of Contour Lines for Contour Plots**

<b>Sensor</b>	<b>Elevations of Contour Lines [°]</b>
B125	80, 82, 84, 86, 88, 88.95, 90
B126	80, 82, 84, 86, 88.5, 90
B127	80, 82, 84, 86, 88, 88.7, 90
B128	
B136	80, 82, 84, 86, 88, 88.4, 90
B137	80, 82, 84, 86, 88, 88.6, 90
B138	
B139	
B140	80, 82, 84, 86, 88, 88.8, 90
B141	80, 82, 84, 86, 88, 88.6, 90
B142	
B143	
B146	
B147	
B149	
B150	
B151	
B153	
B156	
B157	
B158	
B159	
B144*	

\*Tested in control specimen.

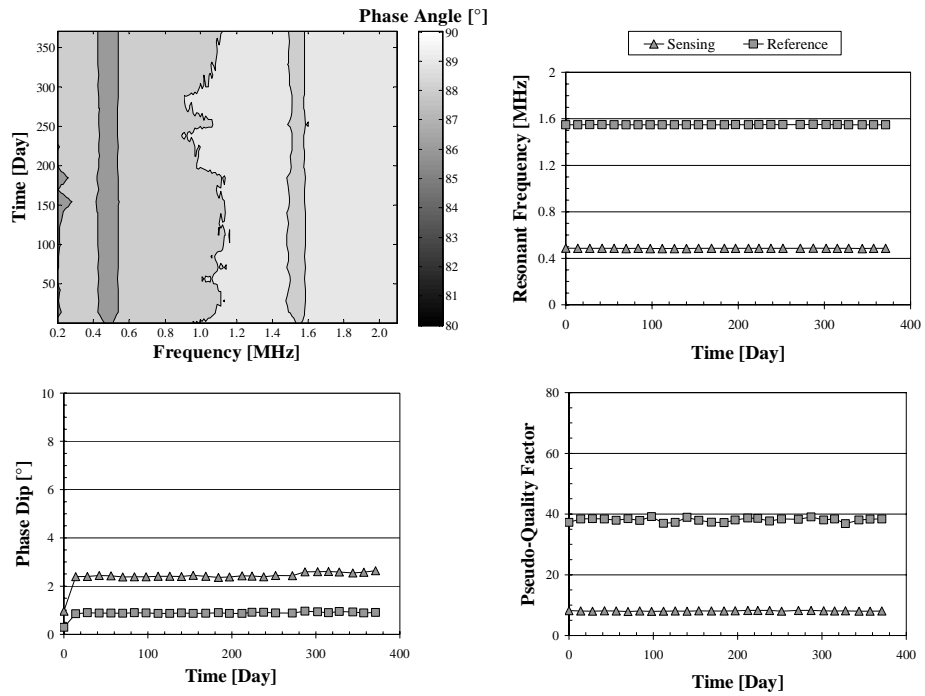


**Figure C-2 Response of Sensor B125**

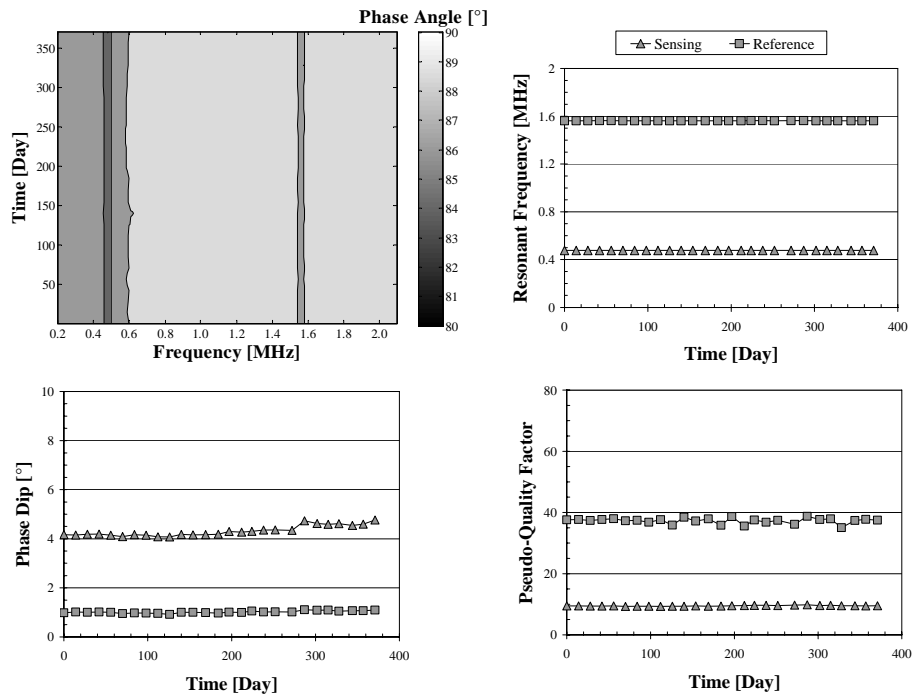


**Figure C-3 Response of Sensor B126**

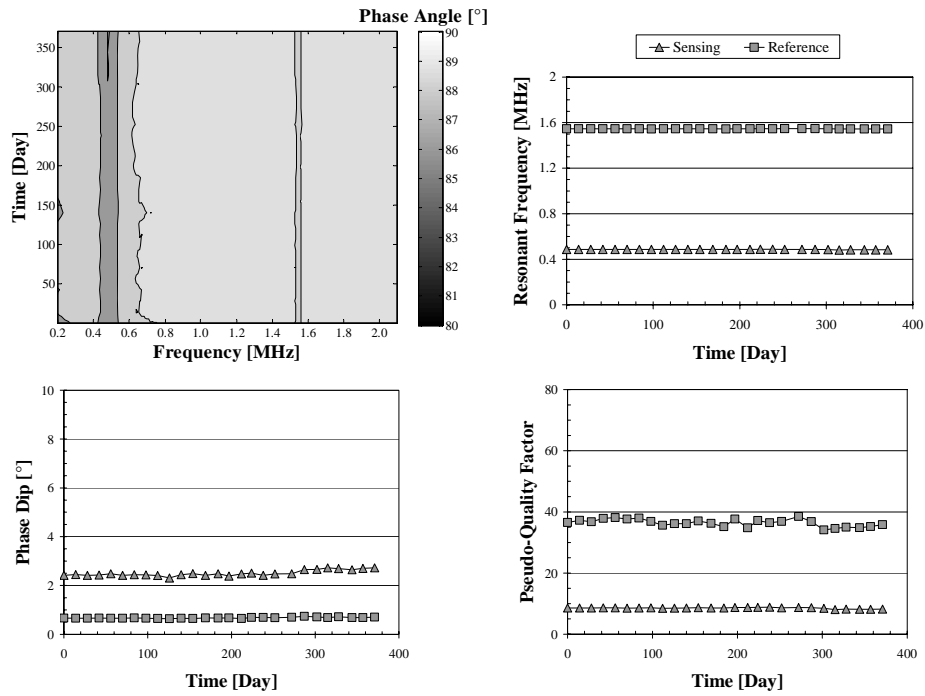


**Figure C-4 Response of Sensor B127**

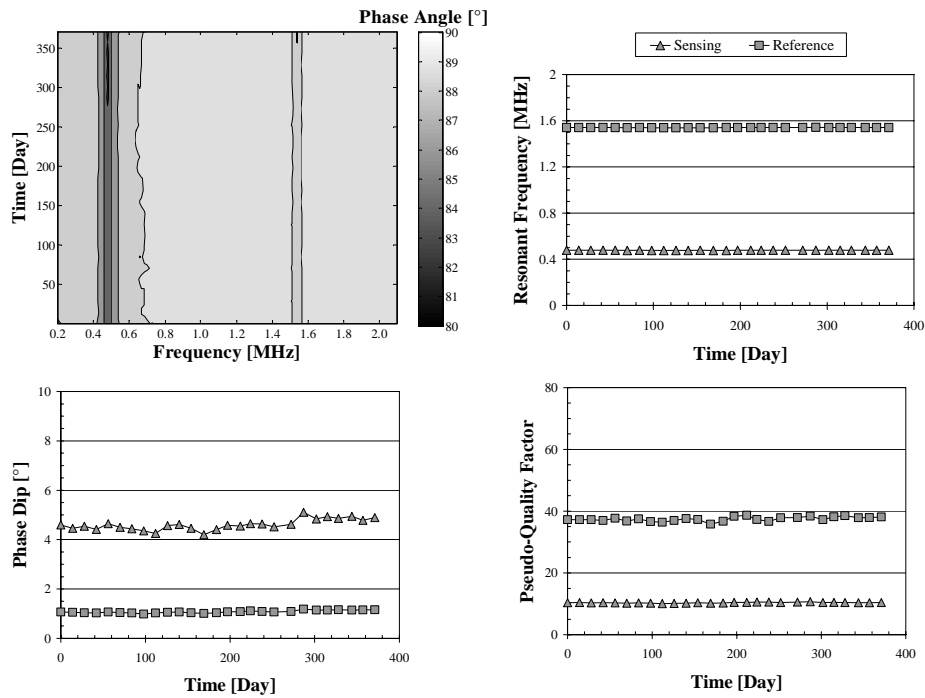


**Figure C-5 Response of Sensor B128**

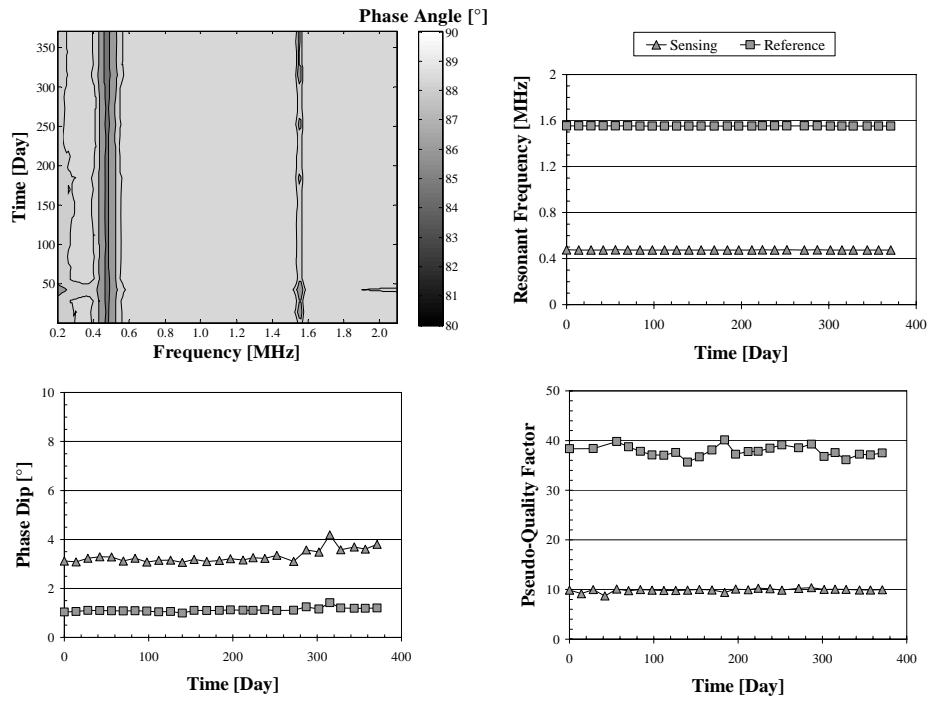


**Figure C-6 Response of Sensor B136**

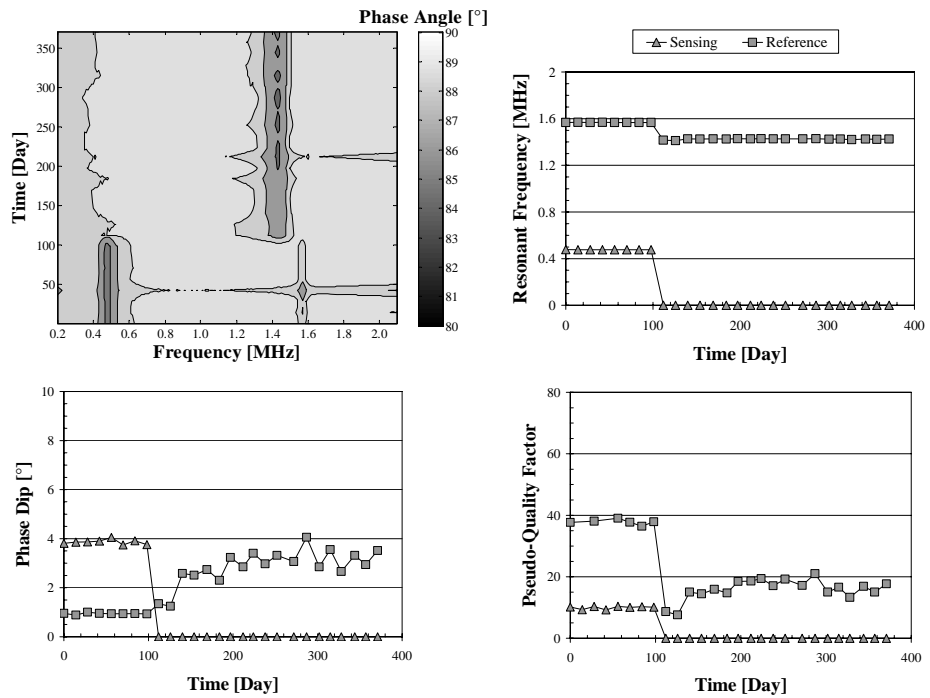


**Figure C-7 Response of Sensor B137**



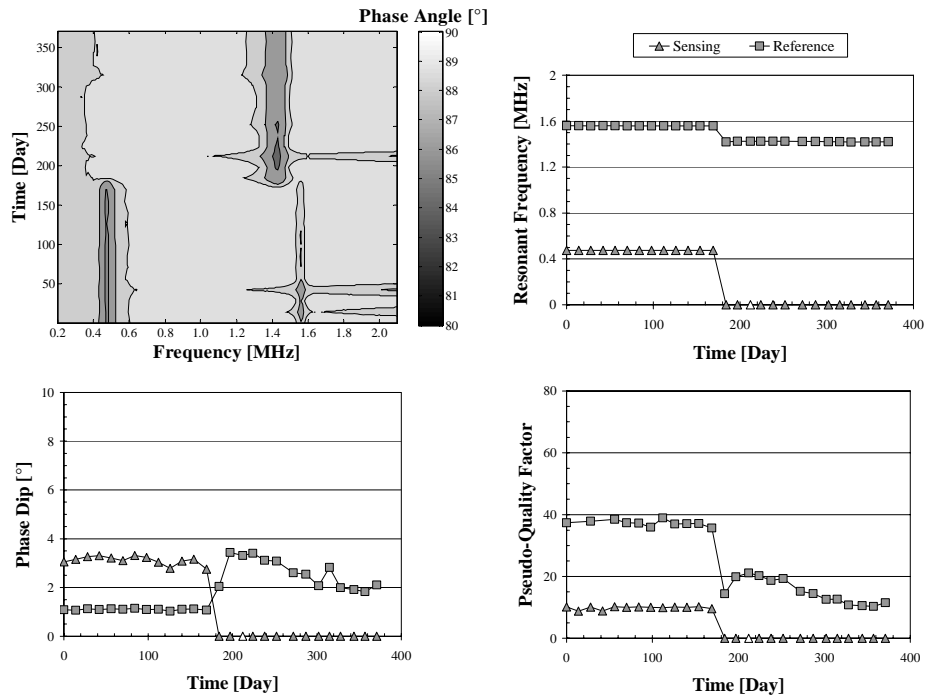


**Figure C-8 Response of Sensor B138**

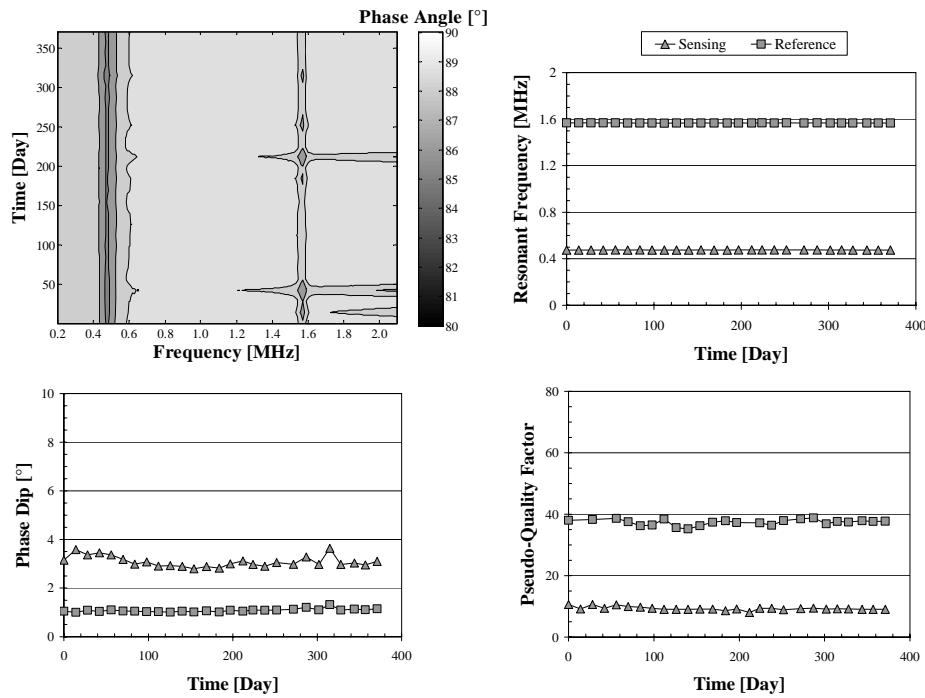


**Figure C-9 Response of Sensor B139**

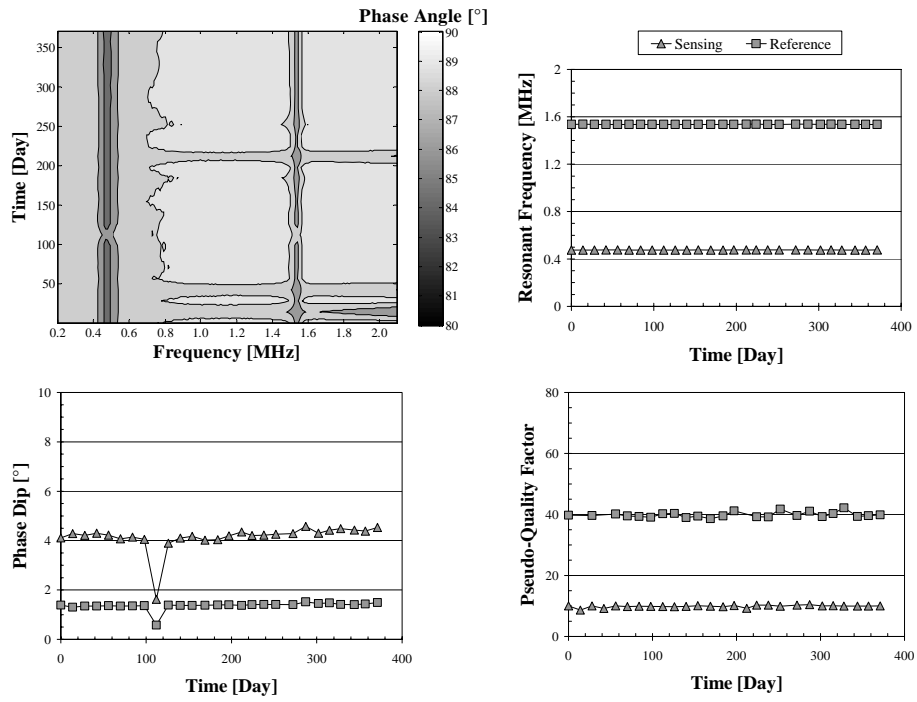


*Figure C-10 Response of Sensor B140*

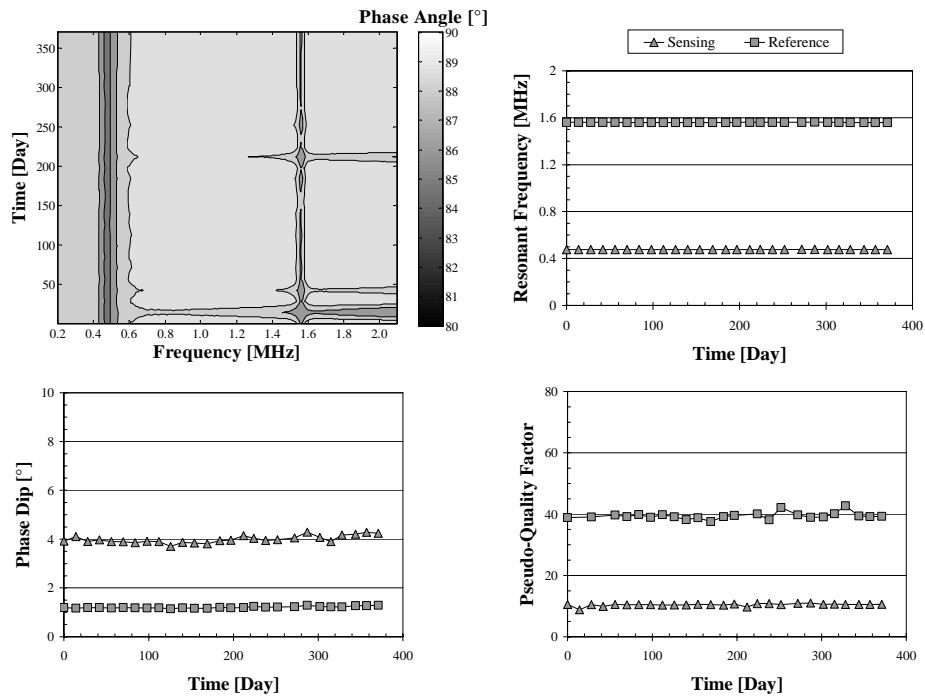


*Figure C-11 Response of Sensor B141*

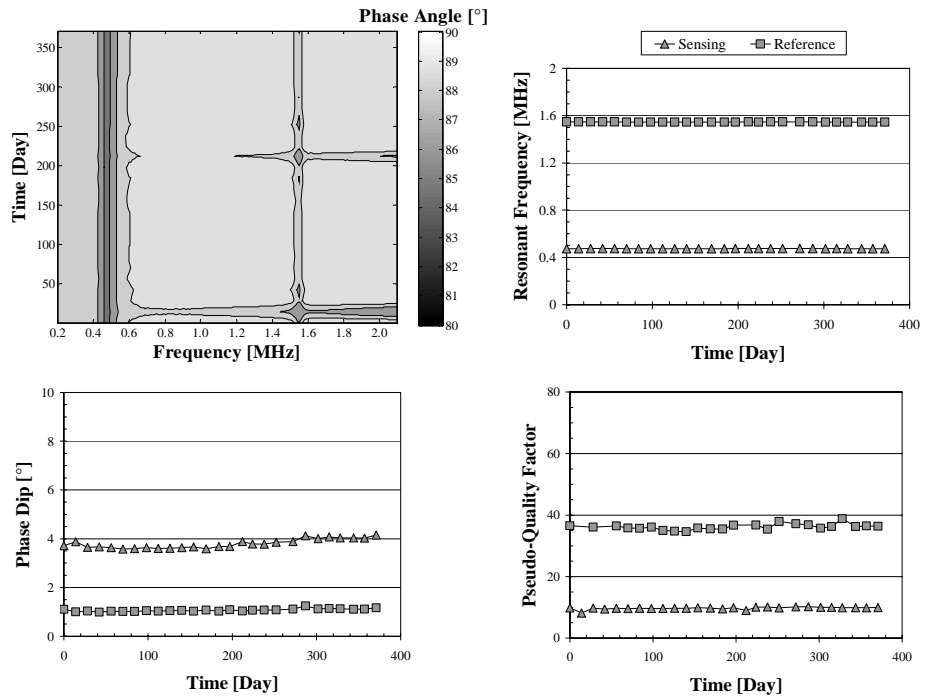


*Figure C-12 Response of Sensor B142*

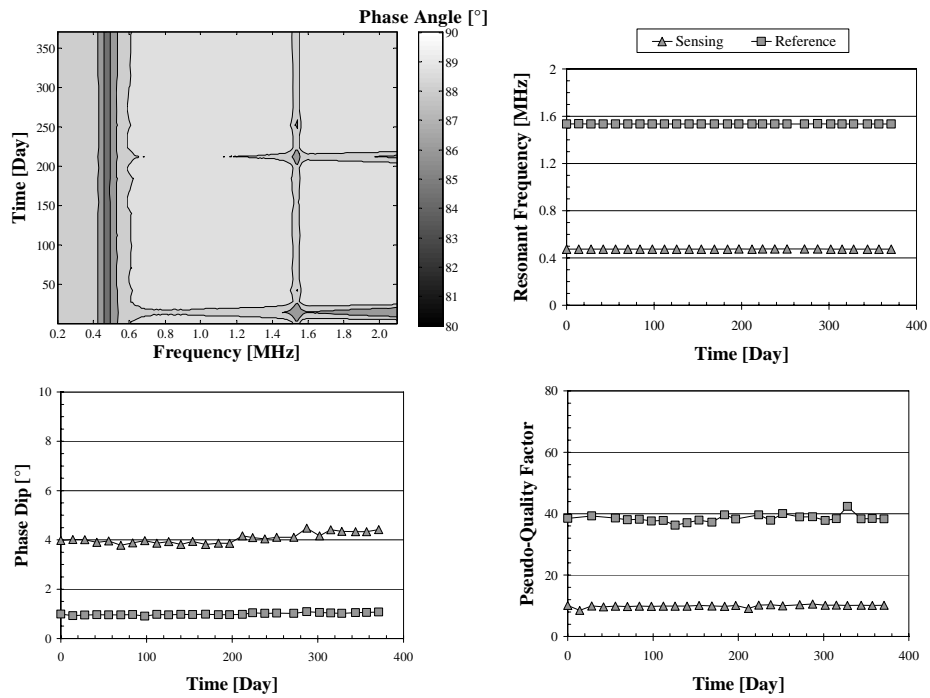


*Figure C-13 Response of Sensor B143*

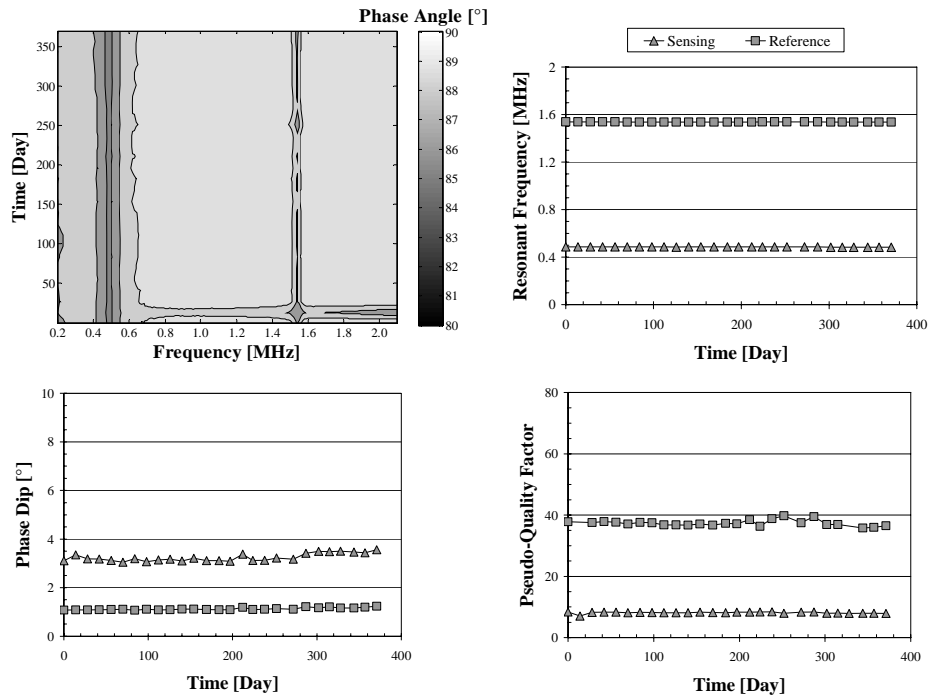


*Figure C-14 Response of Sensor B146*

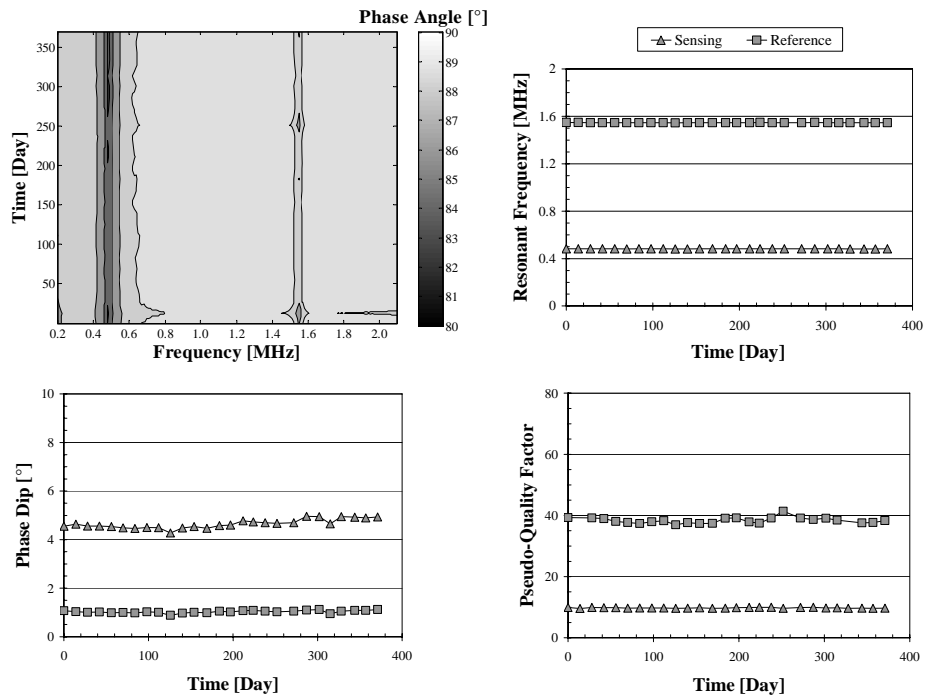


*Figure C-15 Response of Sensor B147*

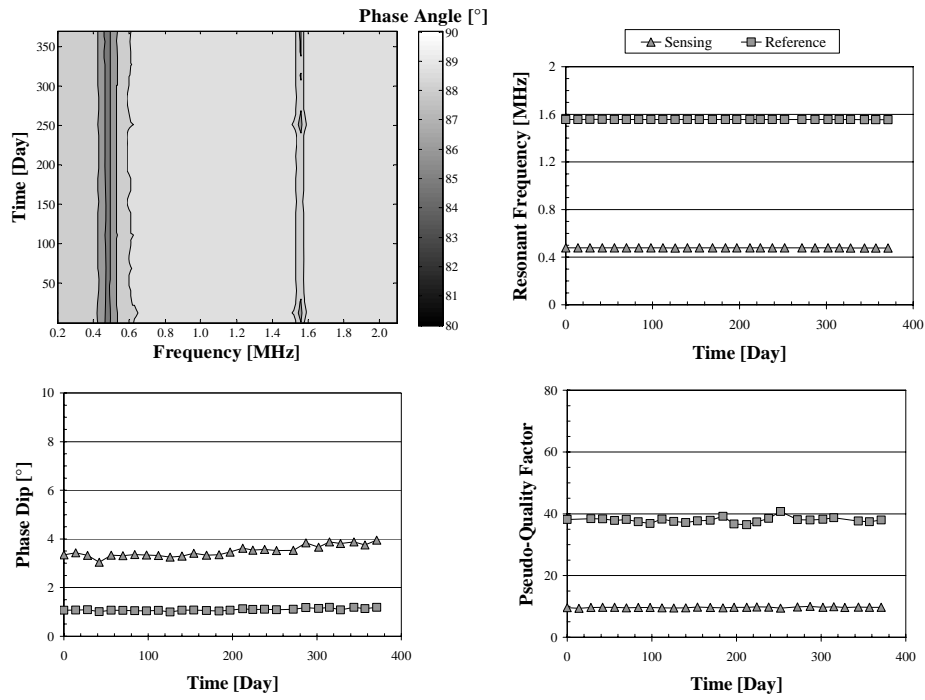


*Figure C-16 Response of Sensor B149*

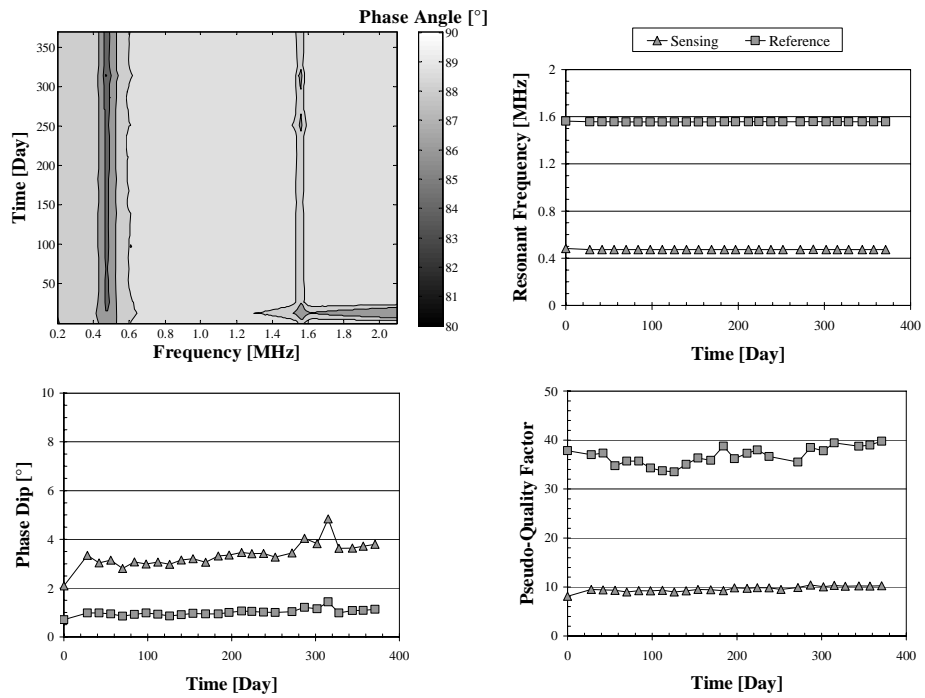


*Figure C-17 Response of Sensor B150*

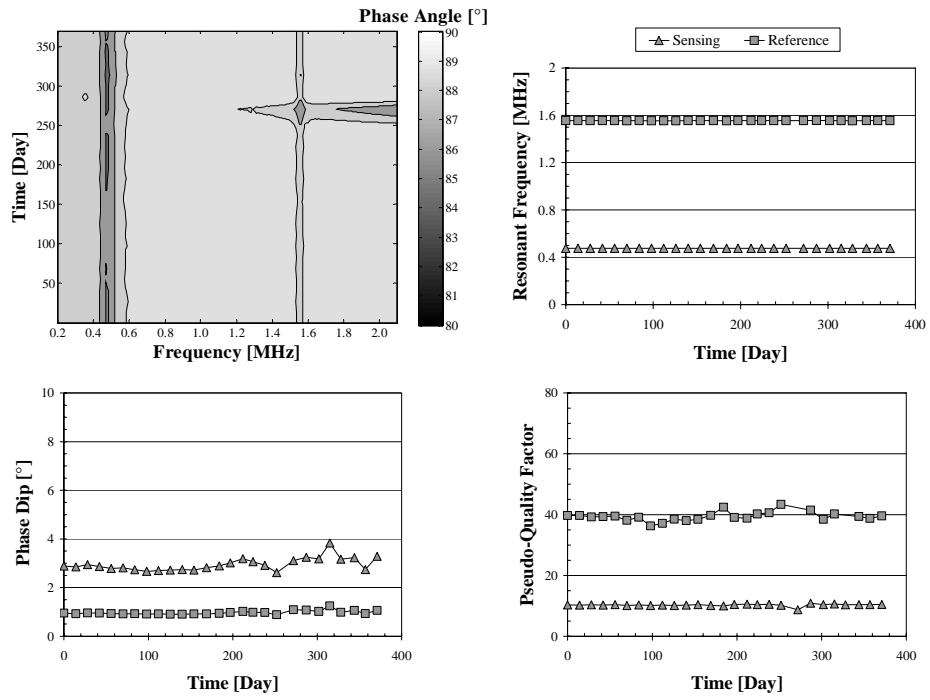


*Figure C-18 Response of Sensor B151*

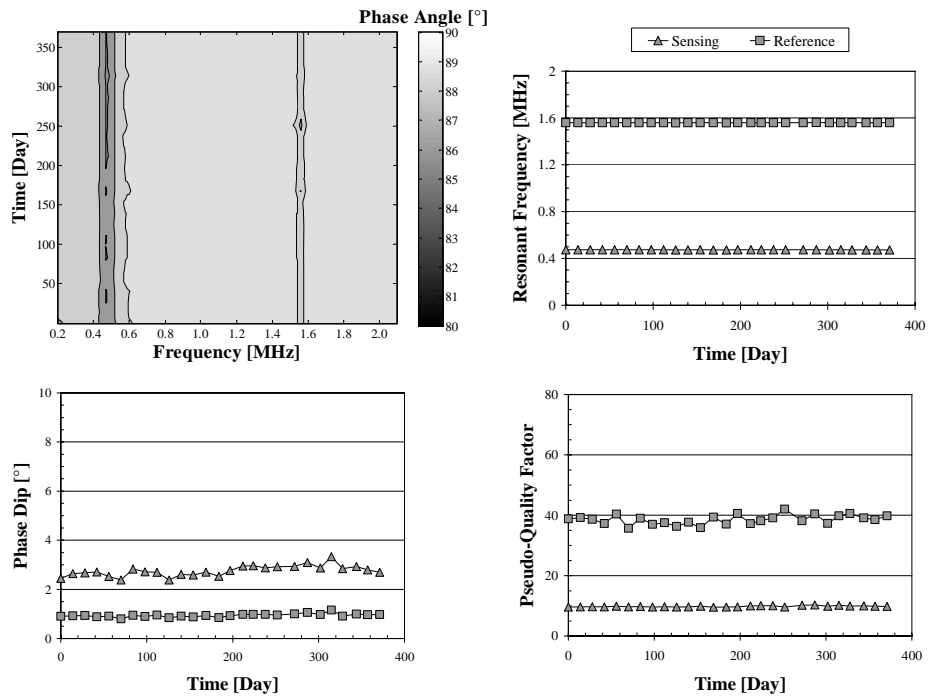


*Figure C-19 Response of Sensor B153*

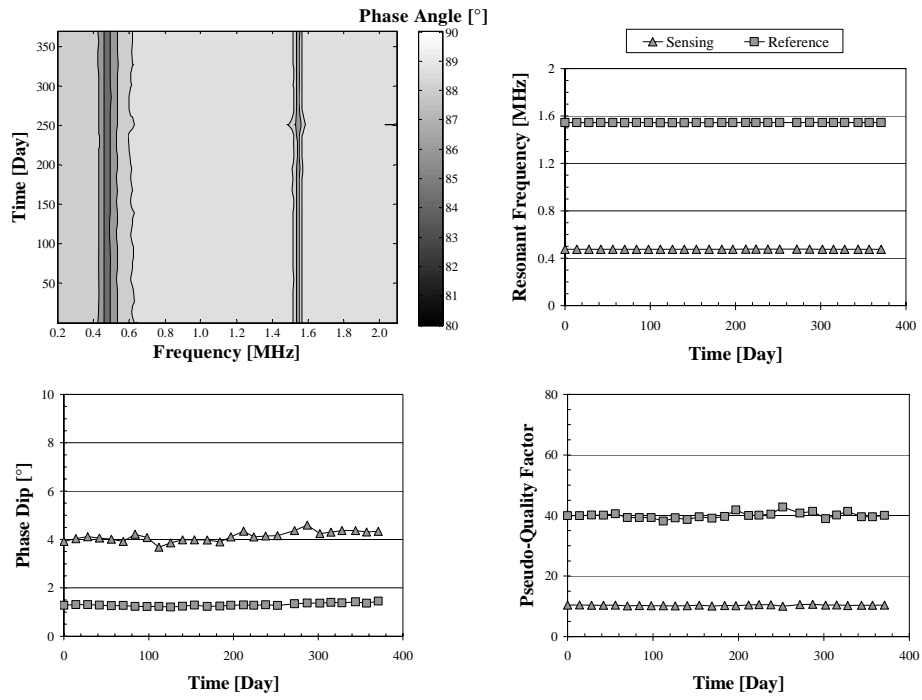


*Figure C-20 Response of Sensor B156*

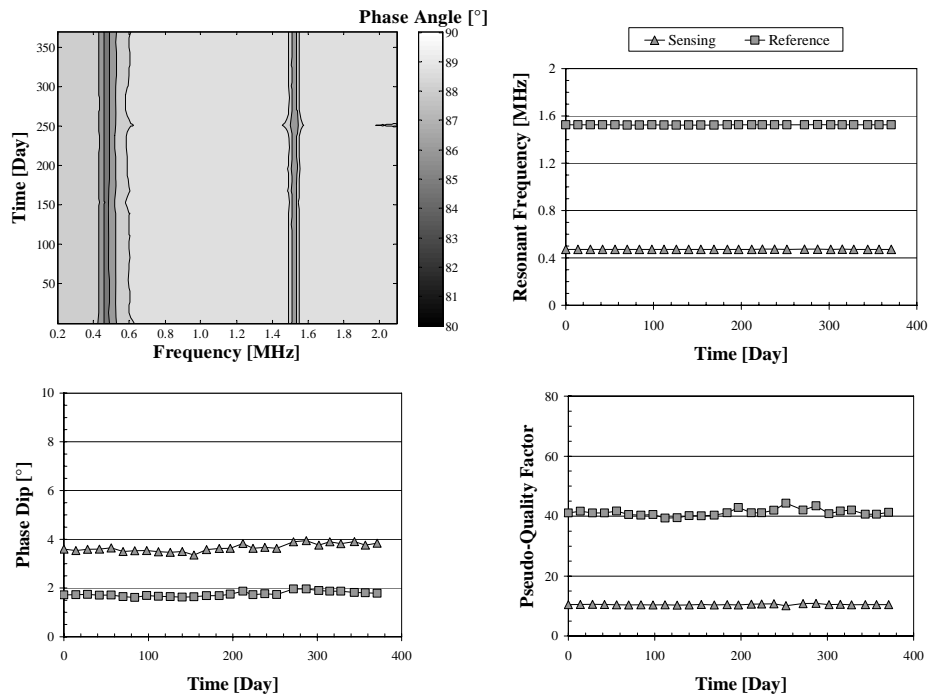


*Figure C-21 Response of Sensor B157*

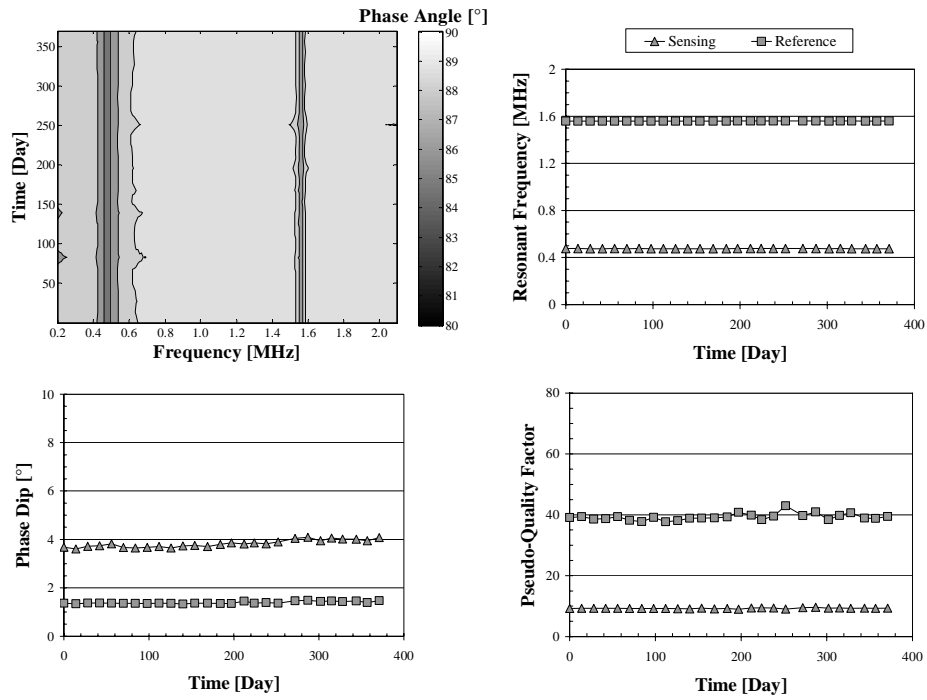


*Figure C-22 Response of Sensor B158*

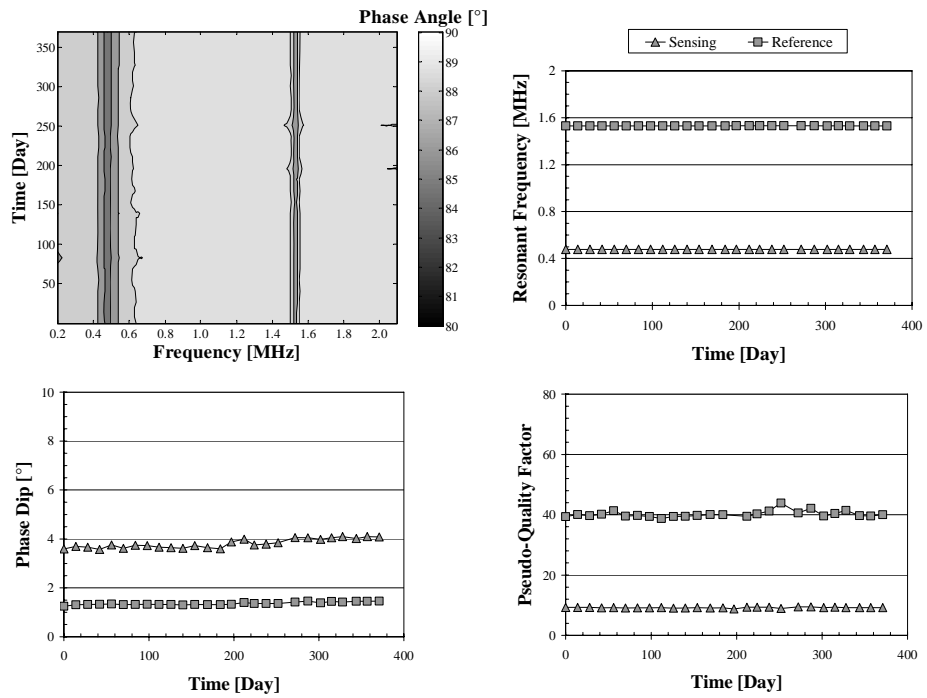


*Figure C-23 Response of Sensor B159*



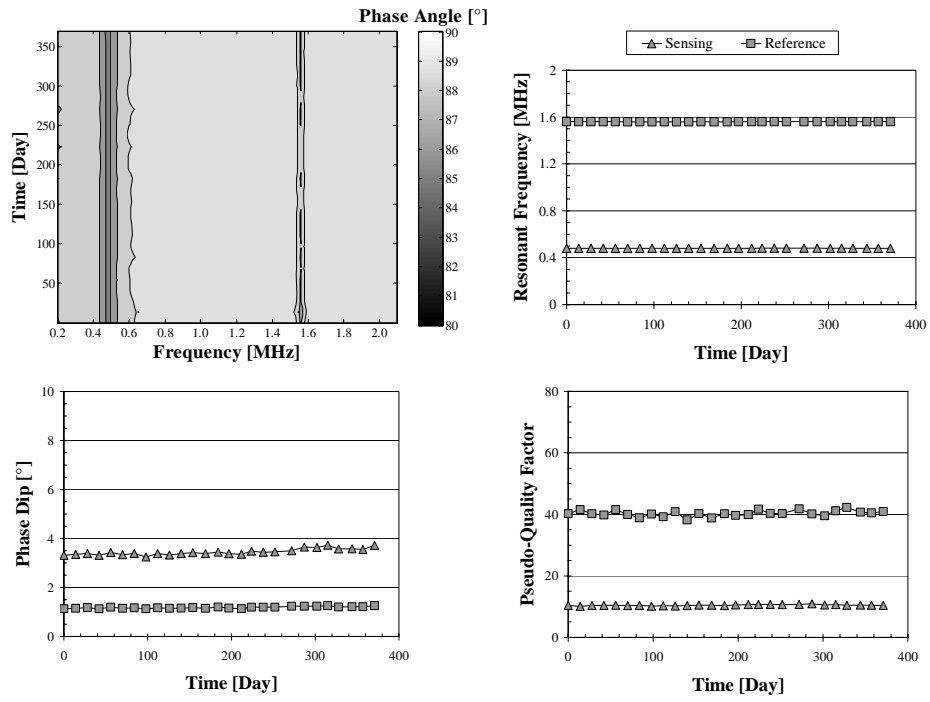


**Figure C-24 Response of Sensor B144 (Control Specimen)**

## APPENDIX D

### Monitoring Results for Slabs 5 and 6

Results from monitoring Slabs 5 and 6 are reported in this appendix. Figure D-1 shows the temperature of the interior of the Slabs 5 and 6, determined using the embedded thermocouples, and the temperature of the air in which the specimens were stored. The air temperature, which is shown by the data labels, is the average of the two air temperatures taken immediately before half-cell potentials of each specimen were measured. Figure D-2 shows the relative humidity of the air in which Slabs 5 and 6 were stored. The relative humidity was recorded immediately before half-cell measurements were taken for each specimen. The reported values are the averages of those two values.

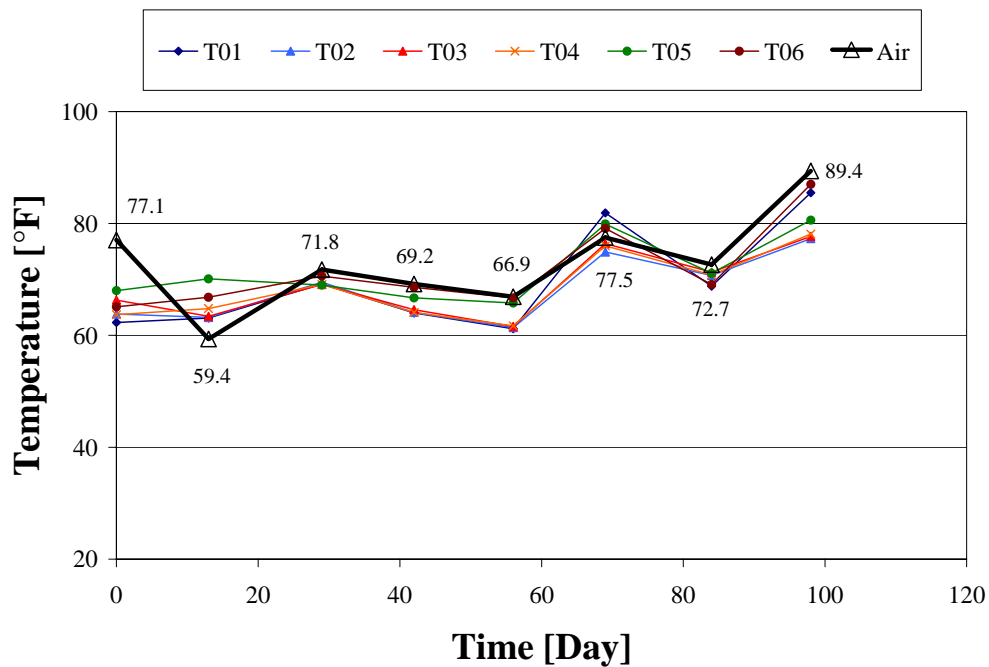


*Figure D-1 Temperature Measured by Thermocouples Compared with Air Temperature*

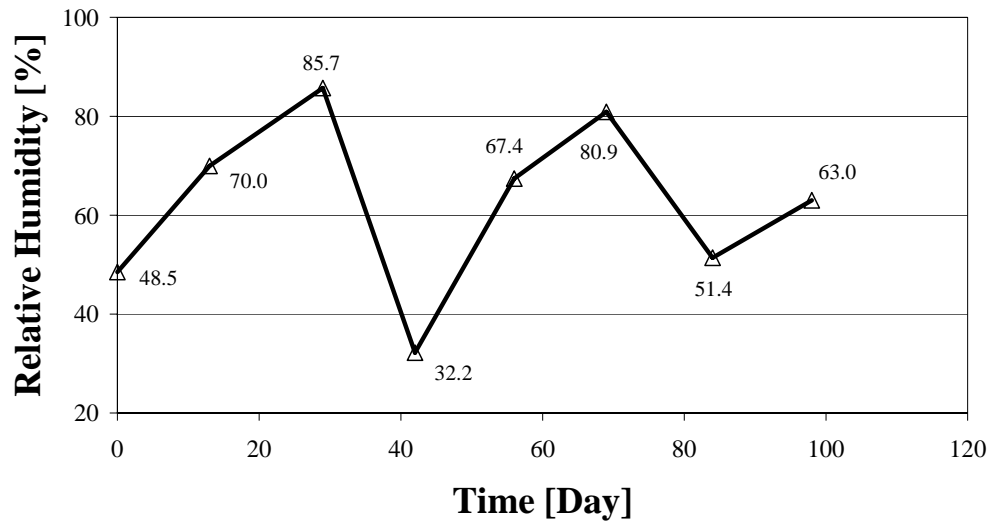


*Figure D-2 Relative Humidity of Air*

The 14-week measured responses of all sensors tested in Slabs 5 and 6 are given below. Furthermore, the responses of sensors tested in control specimens, sensors D20 and E20, are provided. Testing of all specimens is ongoing. The responses of sensors that were discussed in Chapter 7 are omitted from this appendix. In no case did the responses of the sensors require editing. The elevations of contour lines for the contour plots of each sensor are given in Table D-1.

**Table D-1 Elevation of Contour Lines for Contour Plots**

<b>Sensor</b>	<b>Elevations of Contour Lines [°]</b>
D01	80, 82, 84, 86, 88, 88.9, 90
D02	
D03	
D04	
D05	
D07	80, 82, 84, 86, 88, 88.95, 90
D08	
D09	80, 82, 84, 86, 88, 89, 90
D10	
D11	
D12	
D13	
D14	
D15	
D16	
D17	
D18	
E01	80,82,84,86,88,89,90
E02	
E03	
E04	
E05	
E06	
E08	80, 82, 84, 86, 88, 88.9, 90
E09	
E10	
E11	
E12	
E13	80, 82, 84, 86, 88, 89, 90
E14	
E15	
E16	
E17	
E18	
D20*	80, 82, 84, 86, 88, 89.1, 90
E20*	80, 82, 84, 86, 88, 89, 90

\*Sensors embedded in control specimens

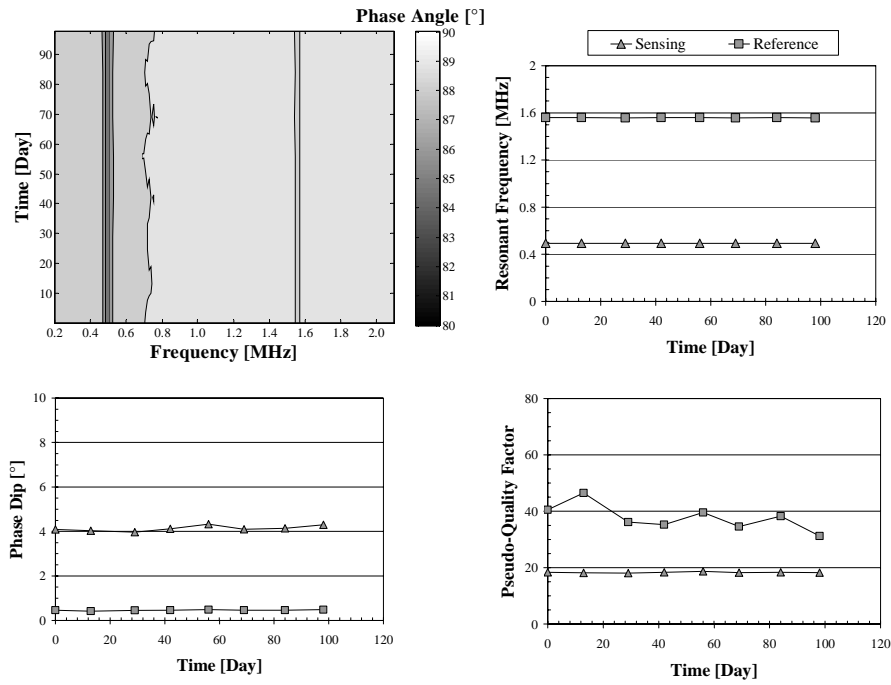


**Figure D-3 Response of Sensor D01**

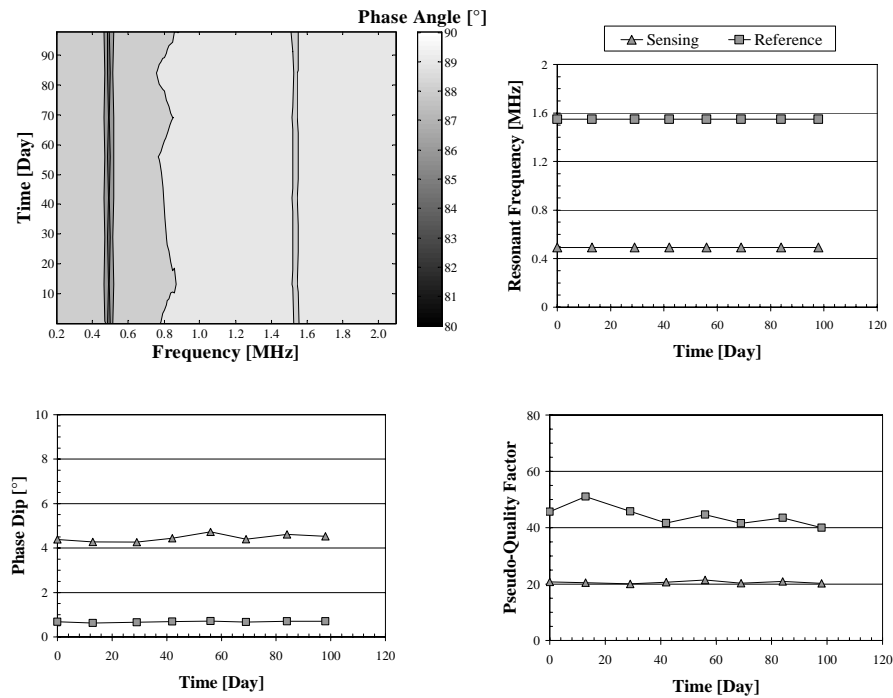


**Figure D-4 Response of Sensor D02**

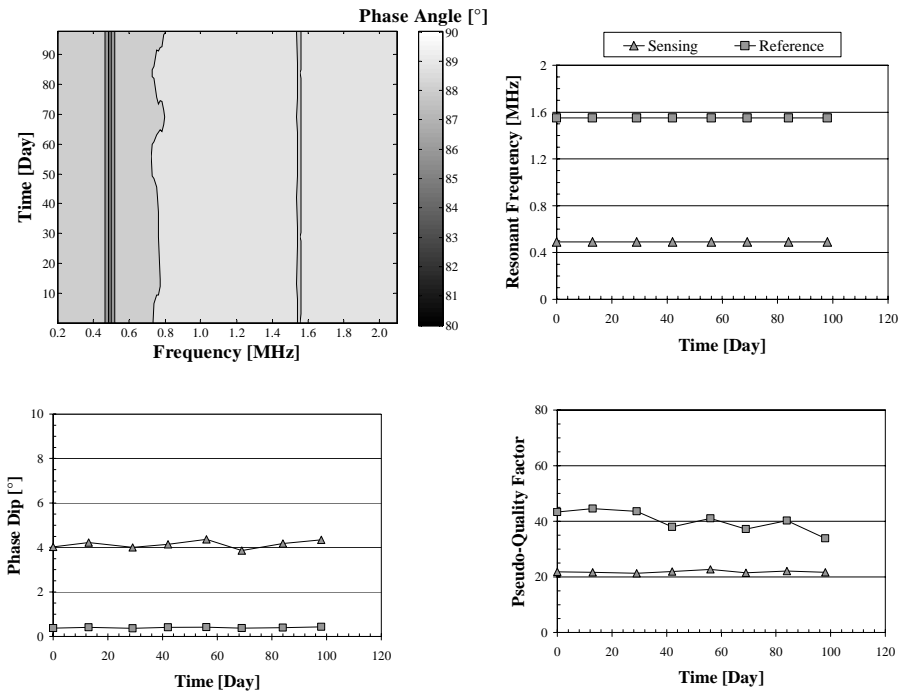


**Figure D-5 Response of Sensor D03**

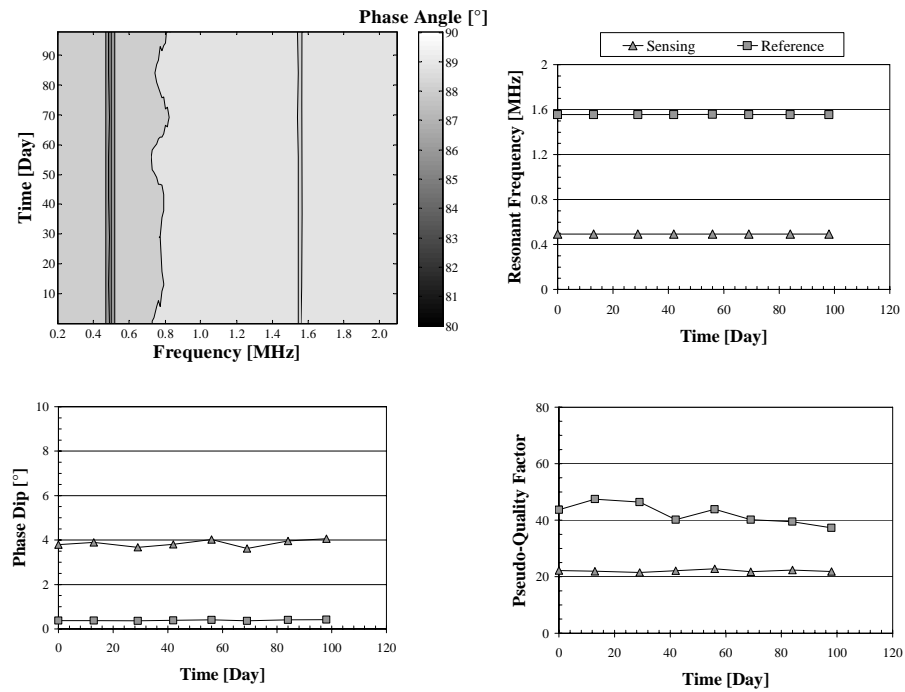


**Figure D-6 Response of Sensor D04**

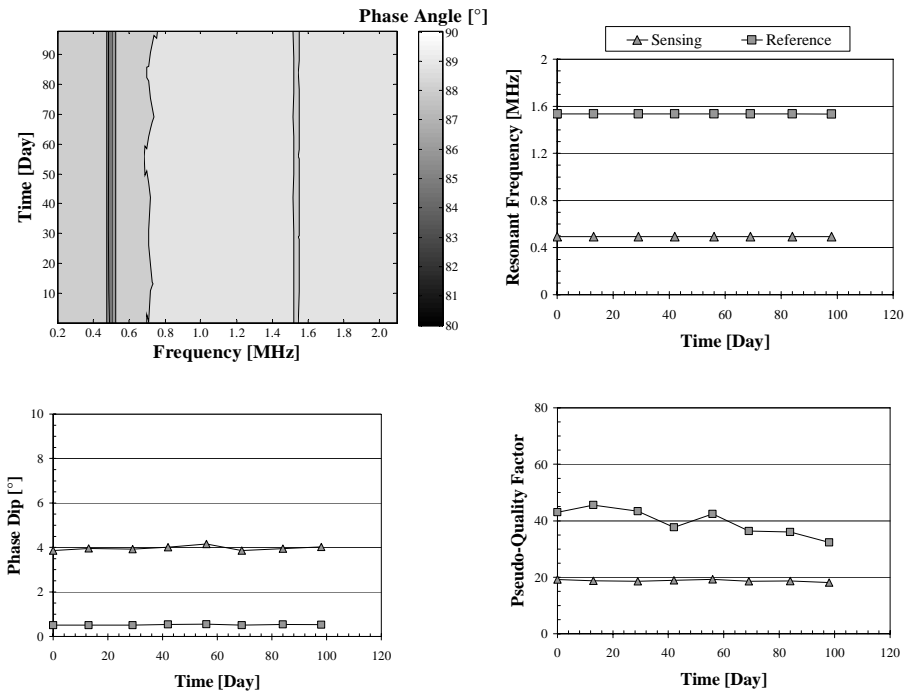


*Figure D-7 Response of Sensor D05*

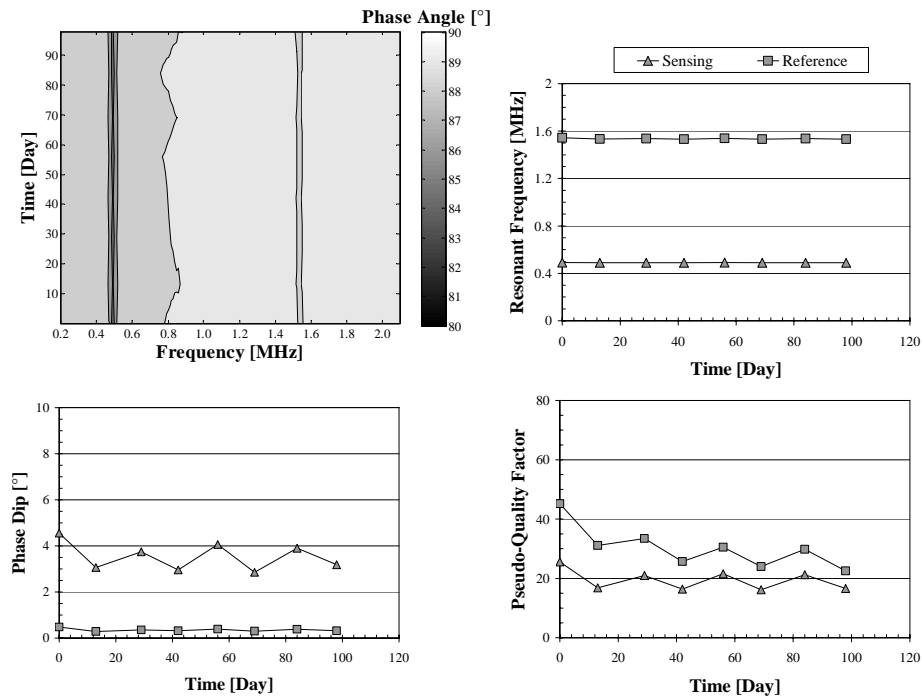


*Figure D-8 Response of Sensor D07*

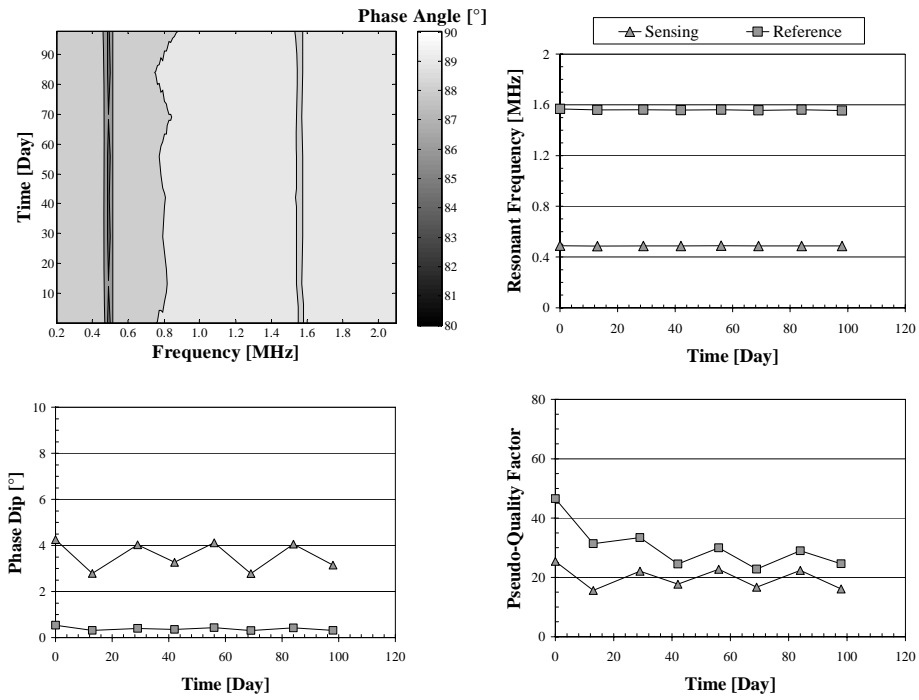


Figure D-9 Response of Sensor D08

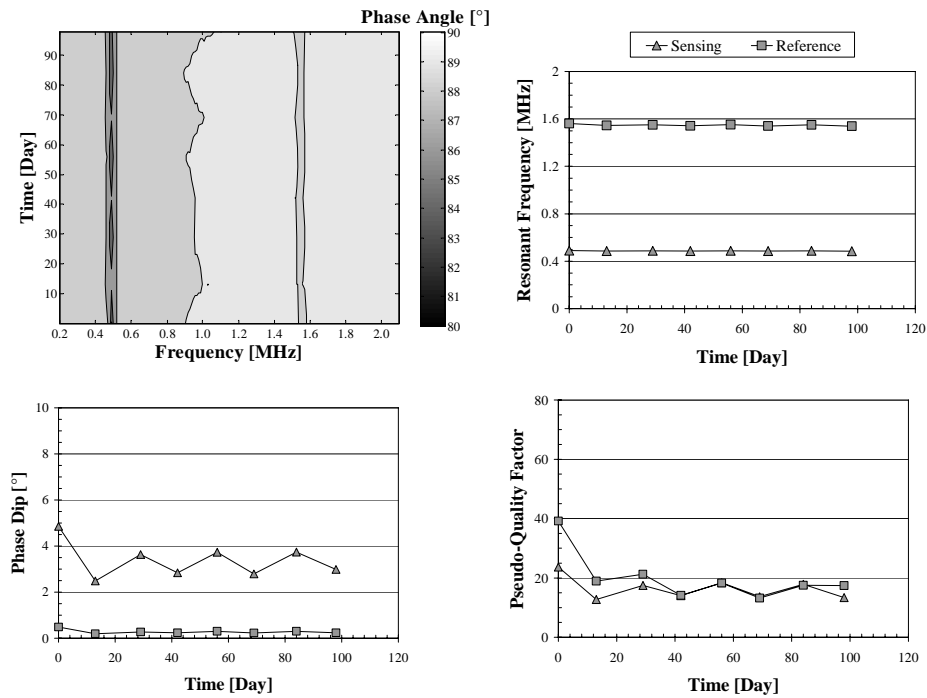
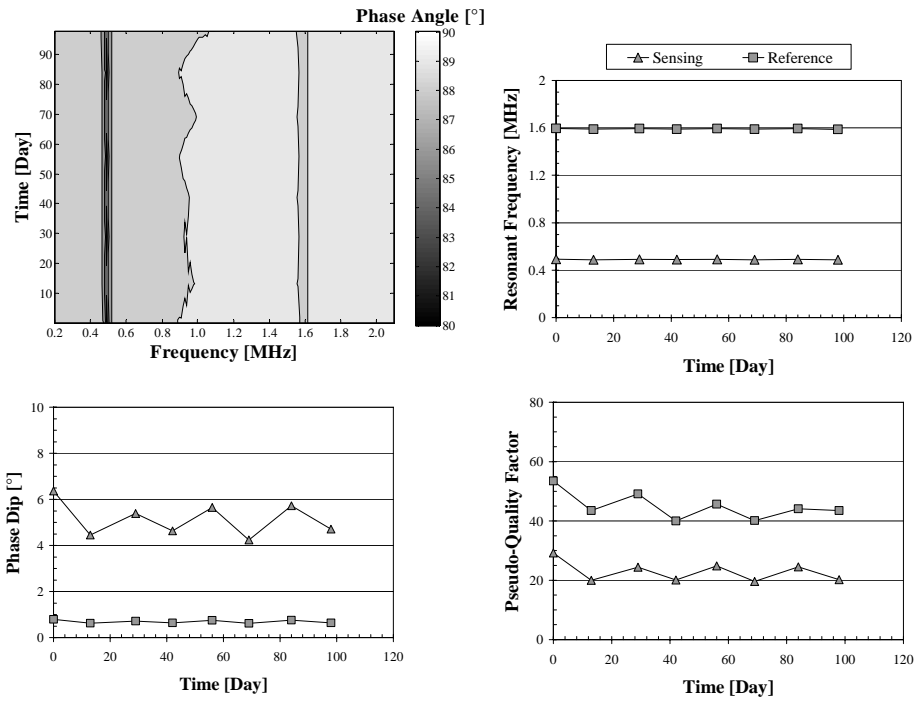
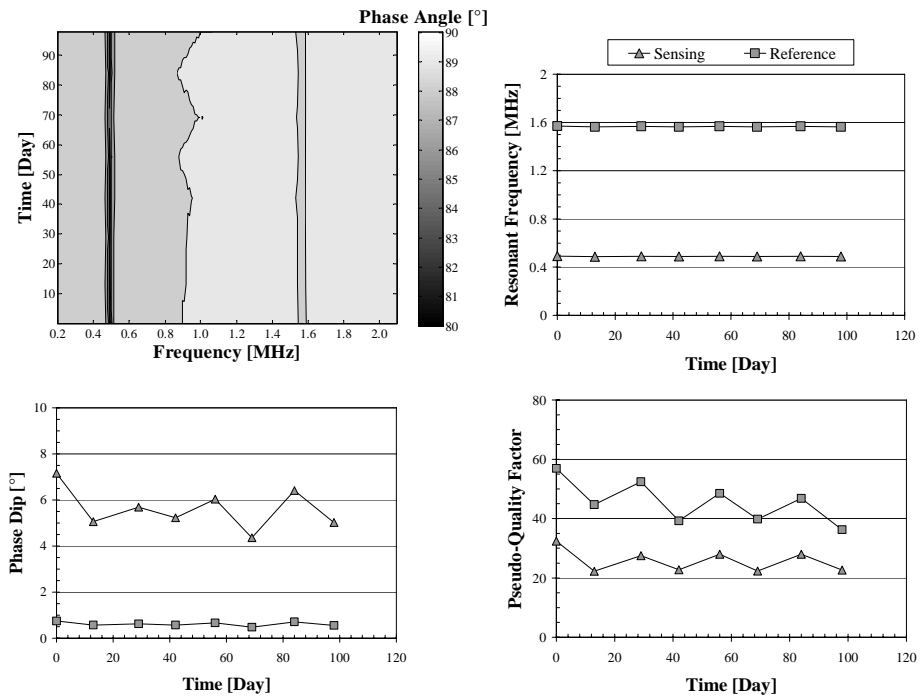


Figure D-10 Response of Sensor D09





**Figure D-11 Response of Sensor D10**



**Figure D-12 Response of Sensor D12**

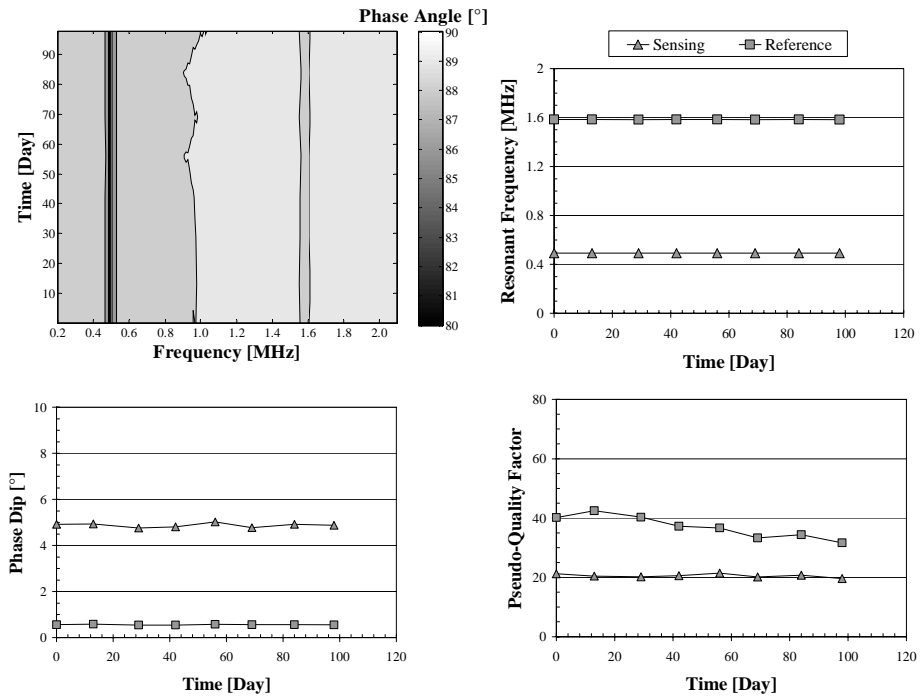


**Figure D-13 Response of Sensor D13**

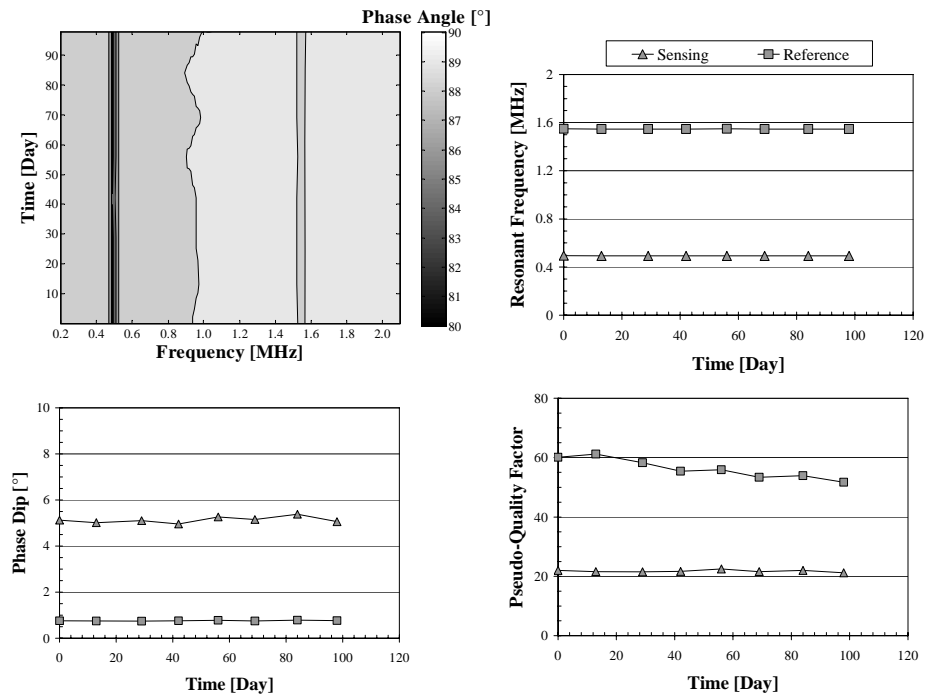


**Figure D-14 Response of Sensor D14**

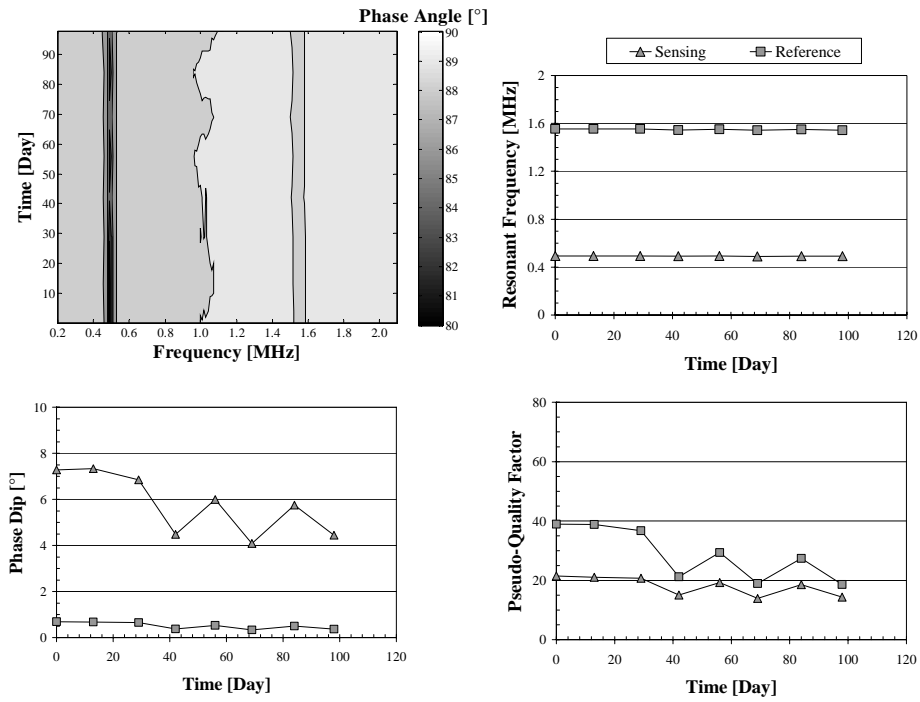


**Figure D-15 Response of Sensor D15**

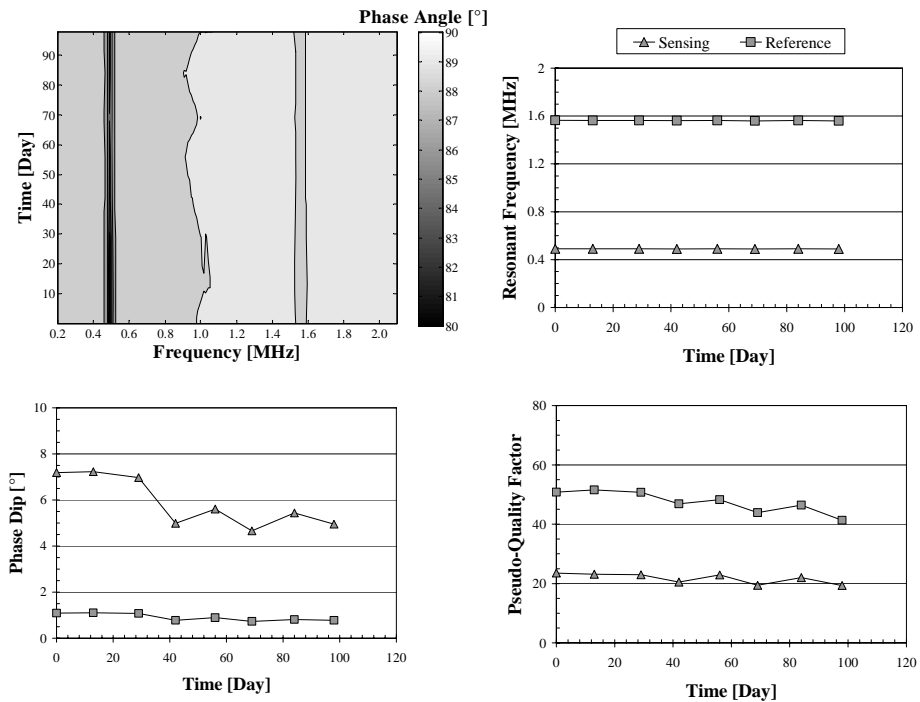


**Figure D-16 Response of Sensor D16**

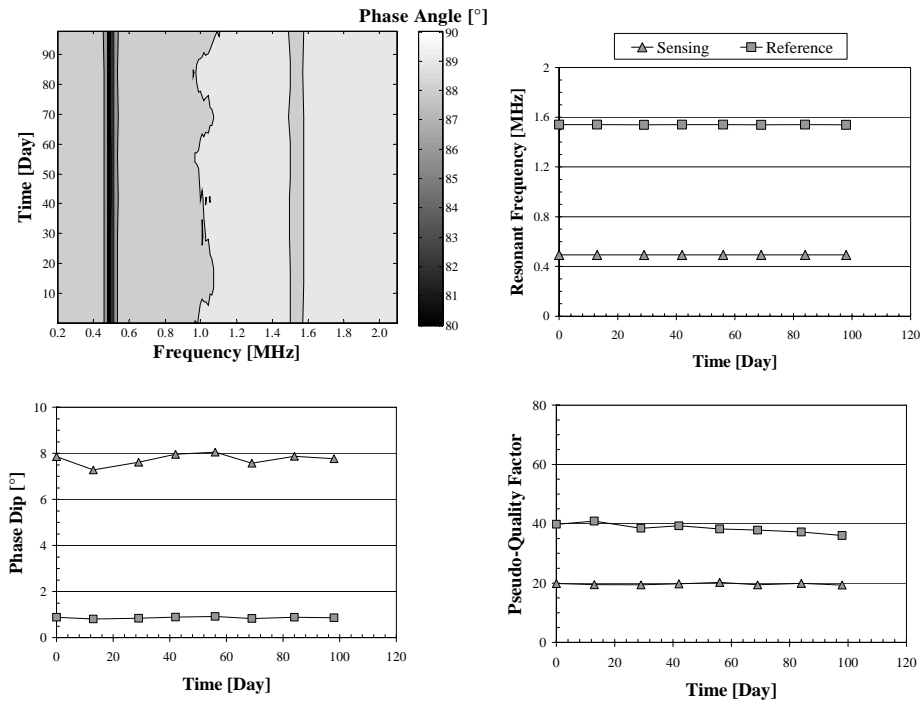


**Figure D-17 Response of Sensor D17**

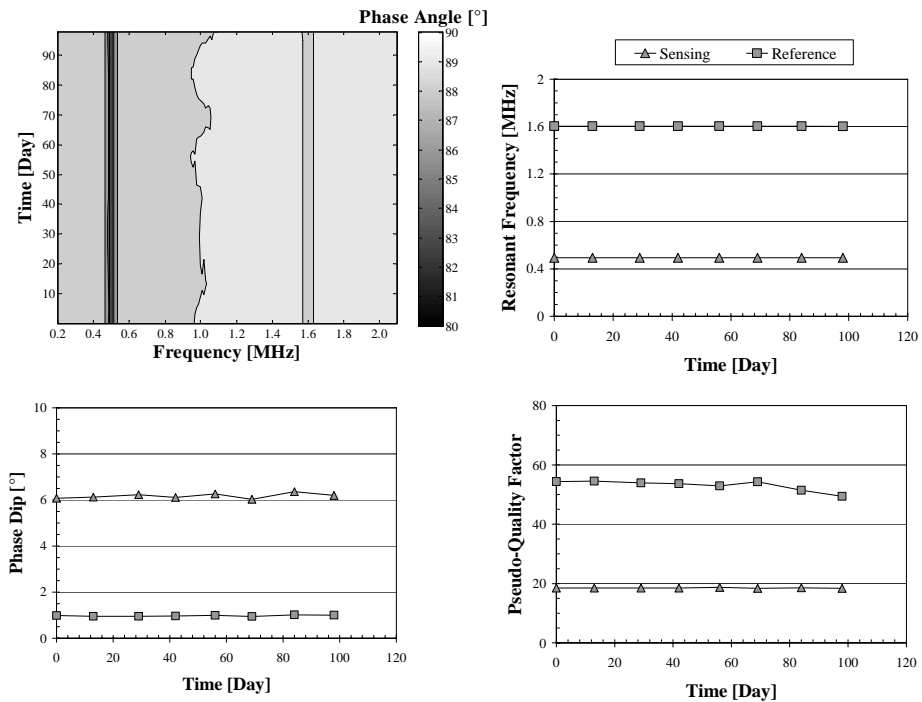


**Figure D-18 Response of Sensor D18**

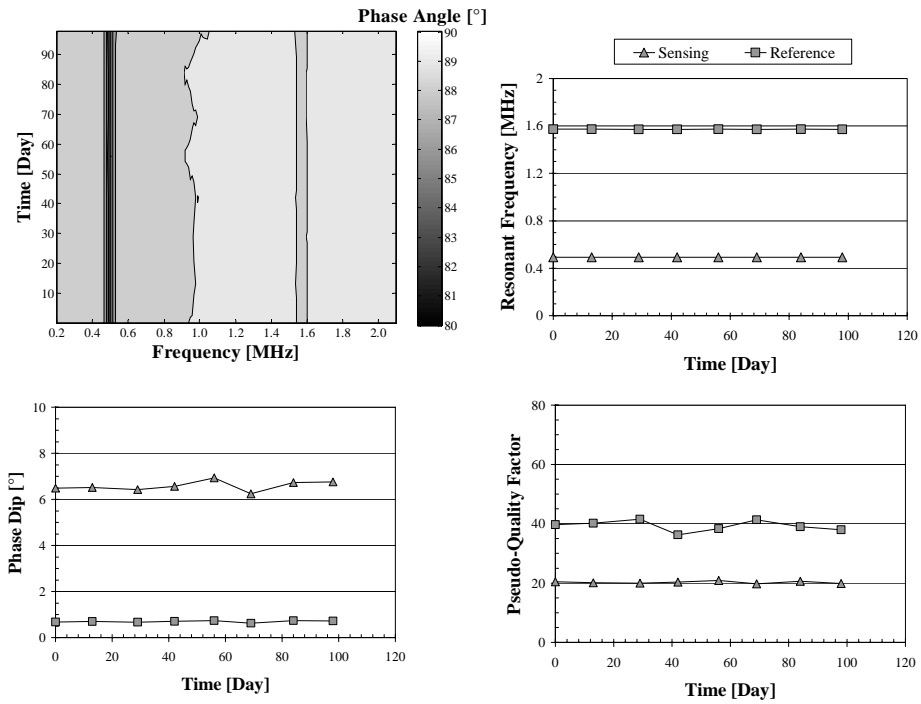


**Figure D-19 Response of Sensor E01**

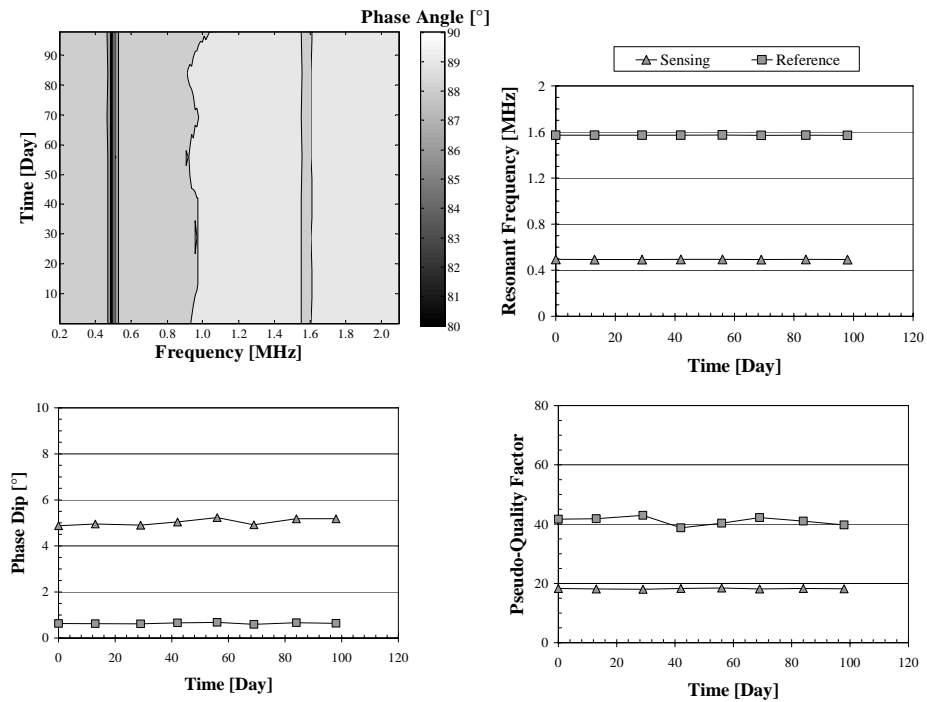


**Figure D-20 Response of Sensor E02**

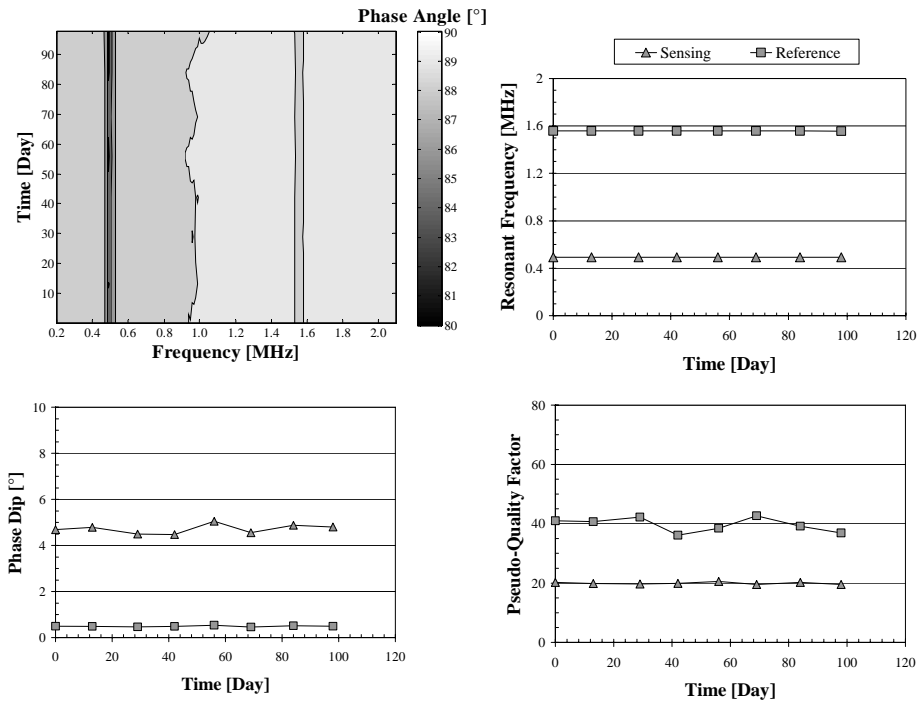


**Figure D-21 Response of Sensor E03**

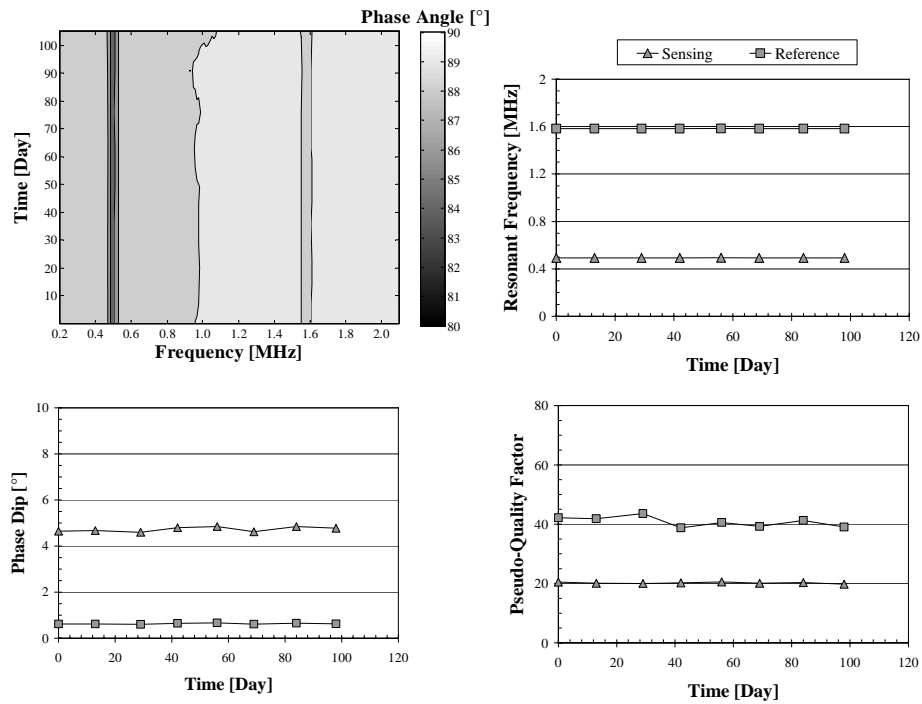


**Figure D-22 Response of Sensor E04**

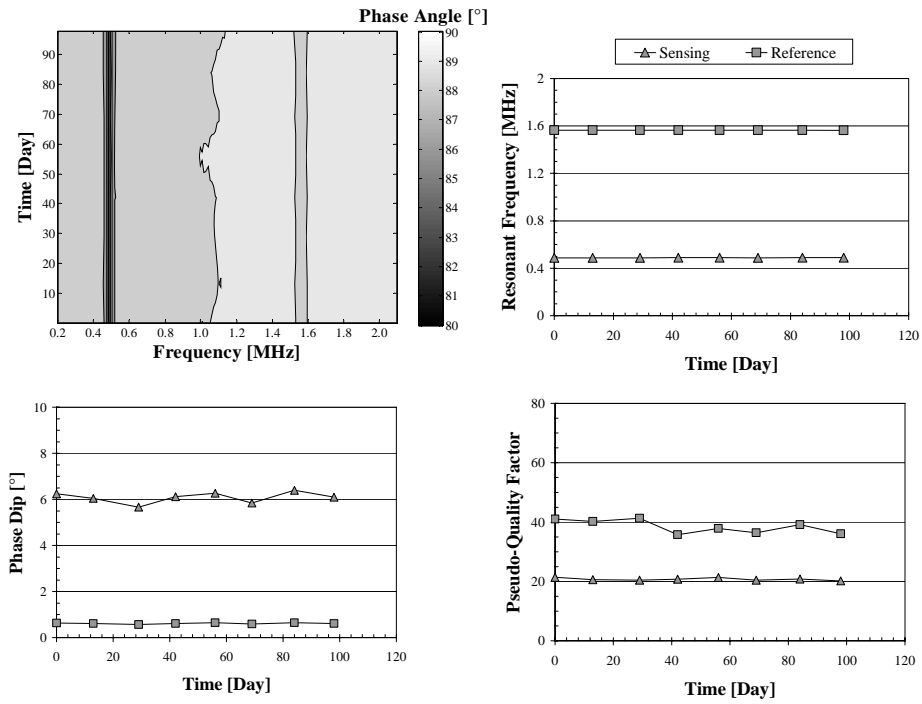


**Figure D-23 Response of Sensor E05**

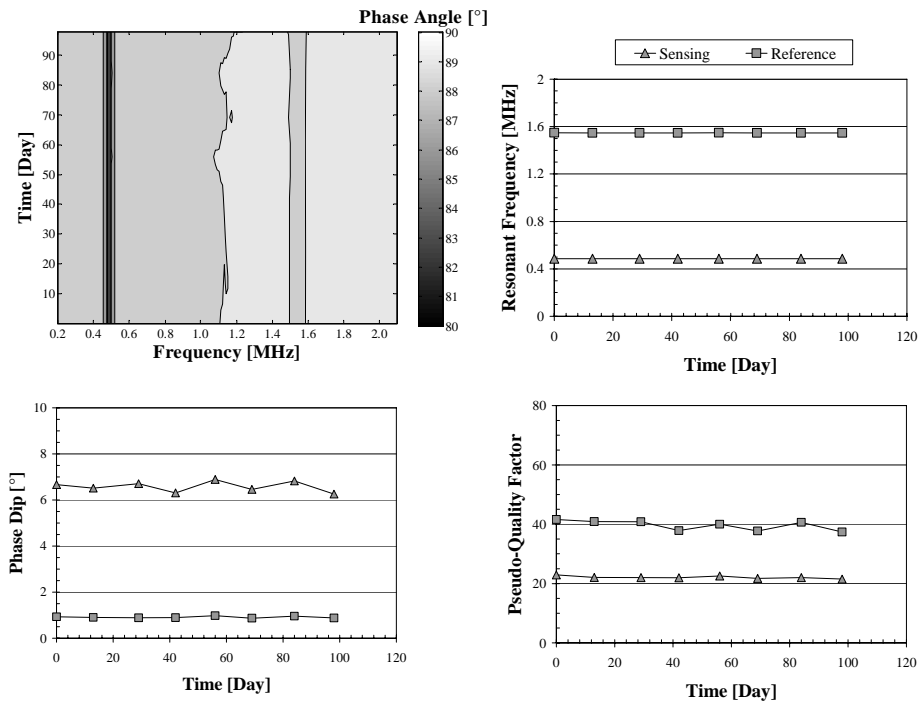


**Figure D-24 Response of Sensor E06**

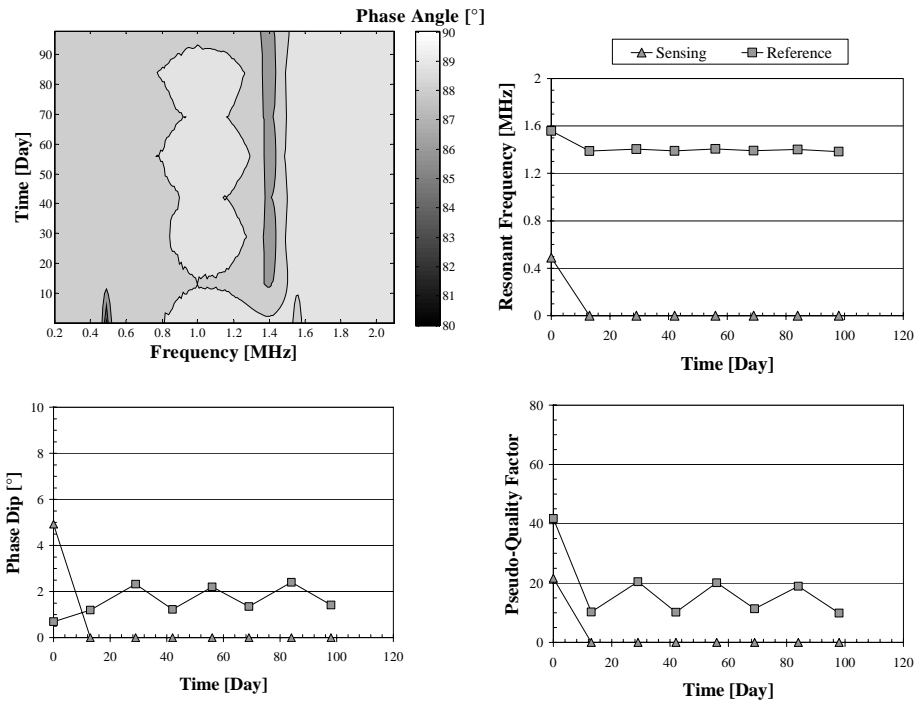


**Figure D-25 Response of Sensor E08**

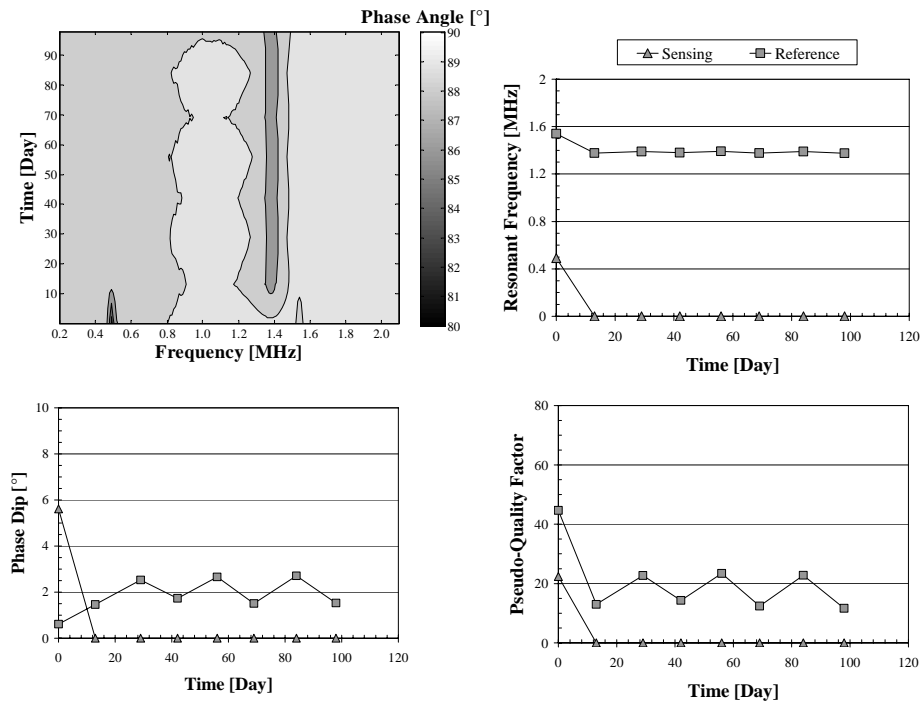


**Figure D-26 Response of Sensor E09**



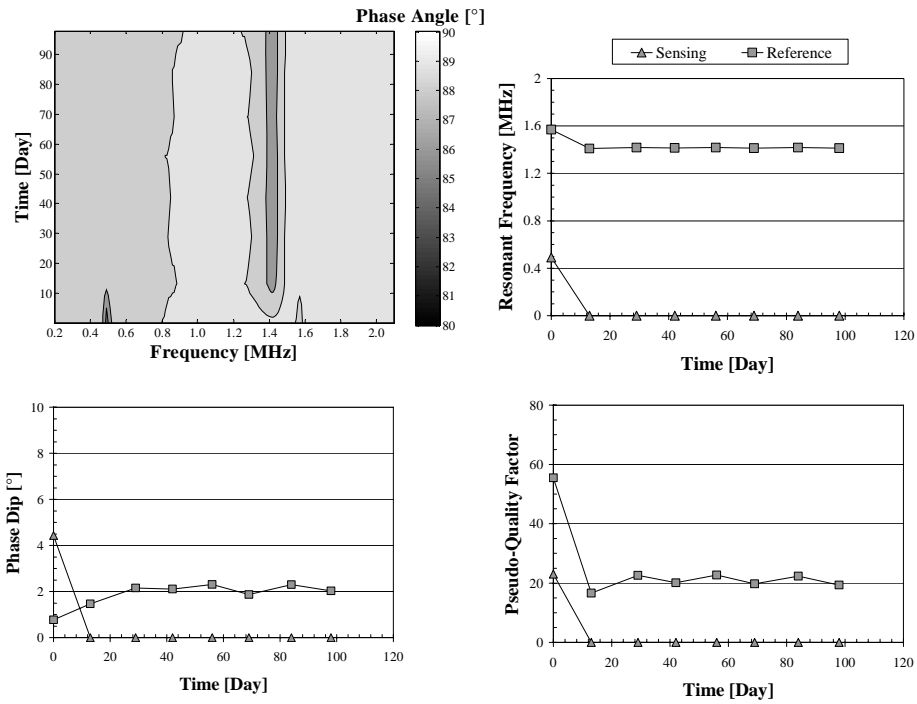


**Figure D-27 Response of Sensor E10**

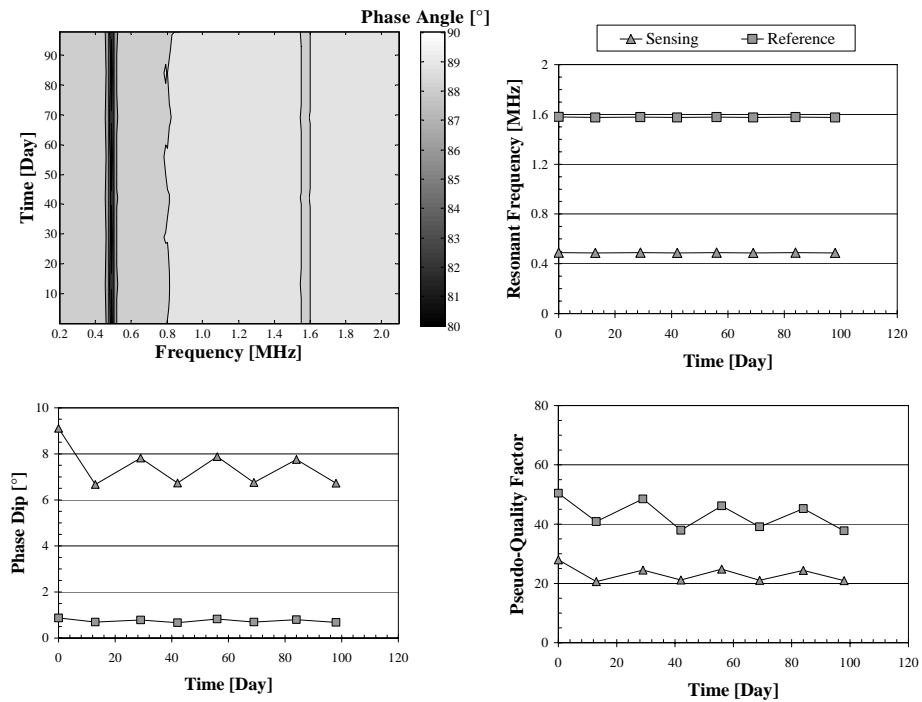


**Figure D-28 Response of Sensor E11**

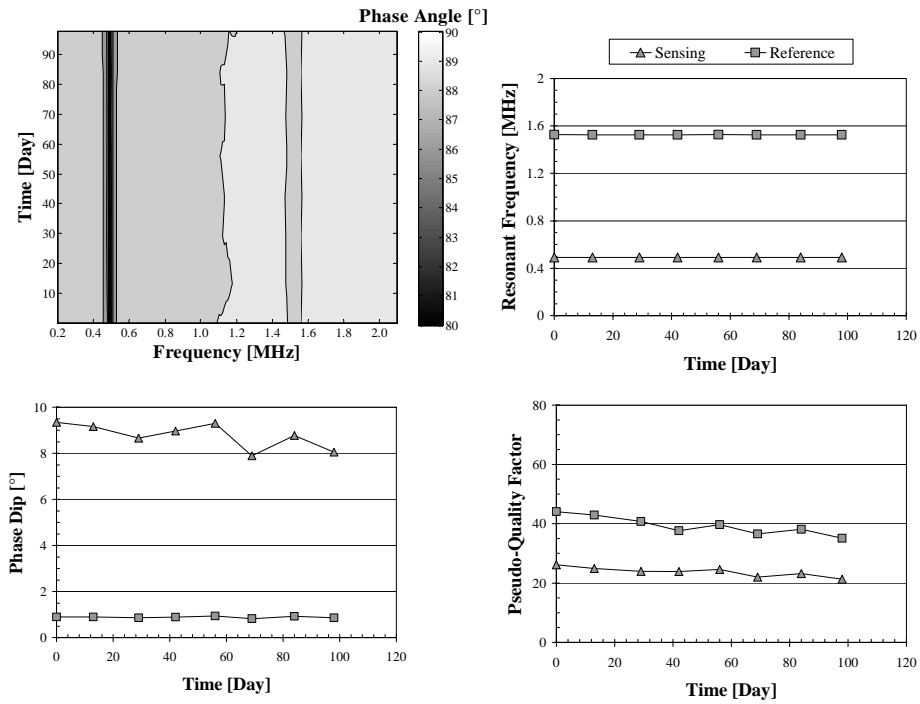


**Figure D-29 Response of Sensor E13**

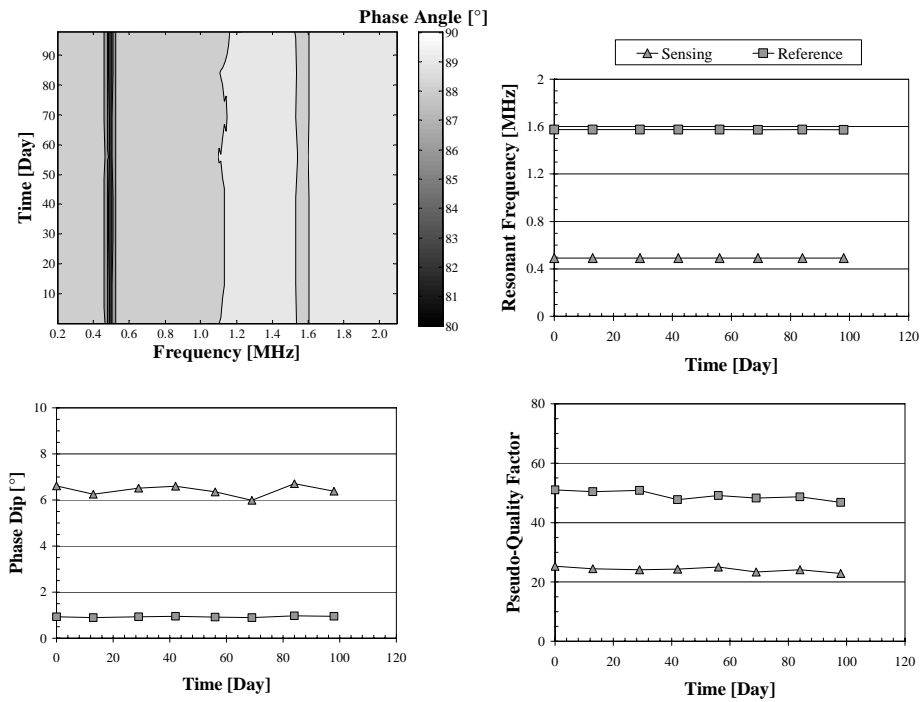


**Figure D-30 Response of Sensor E14**

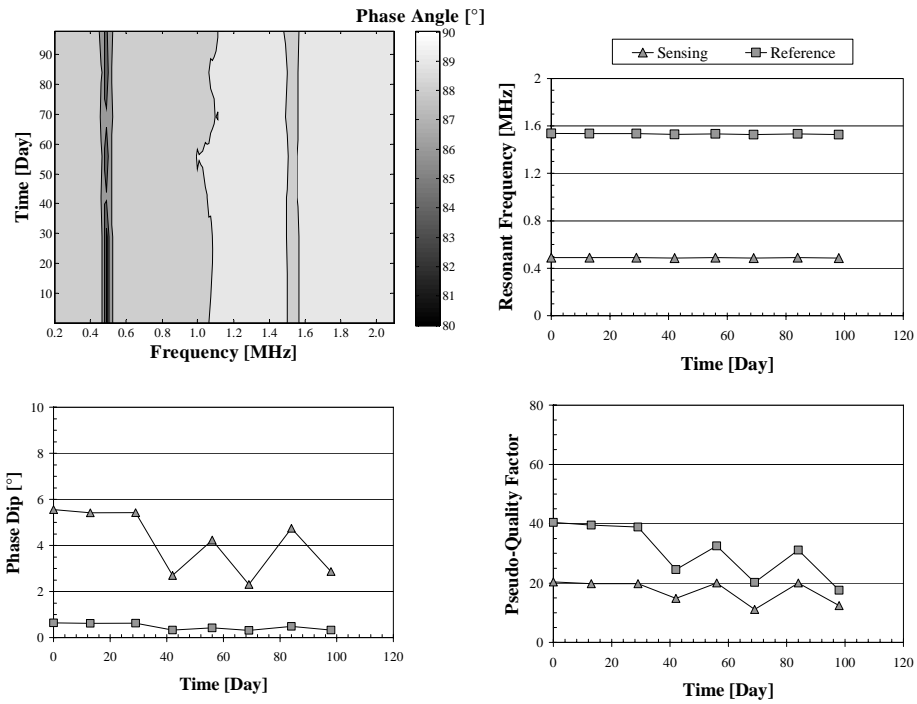


**Figure D-31 Response of Sensor E15**

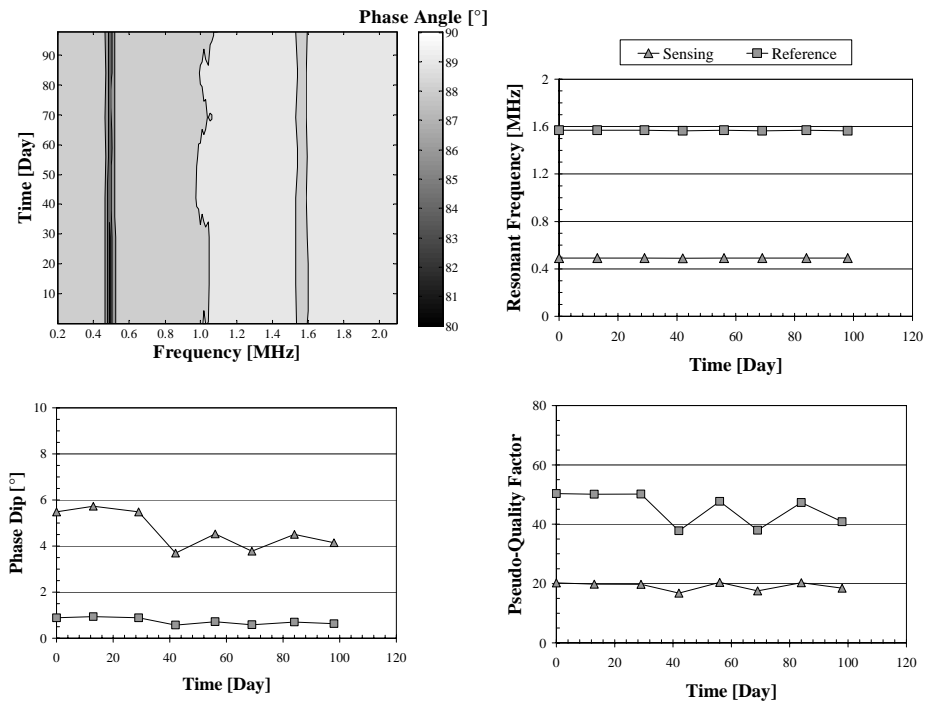


**Figure D-32 Response of Sensor E16**

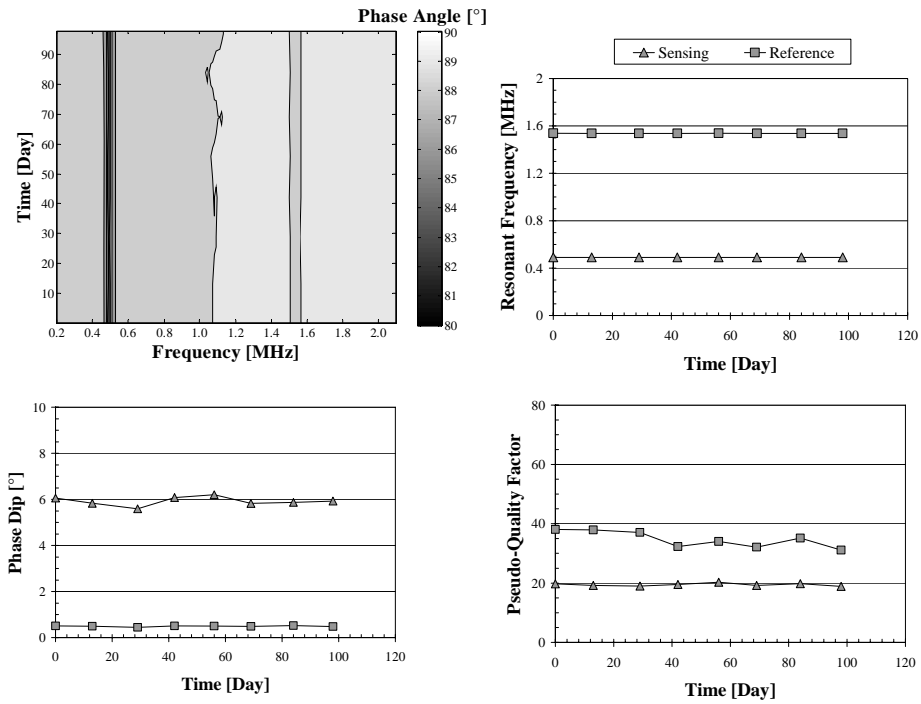


**Figure D-33 Response of Sensor E17**

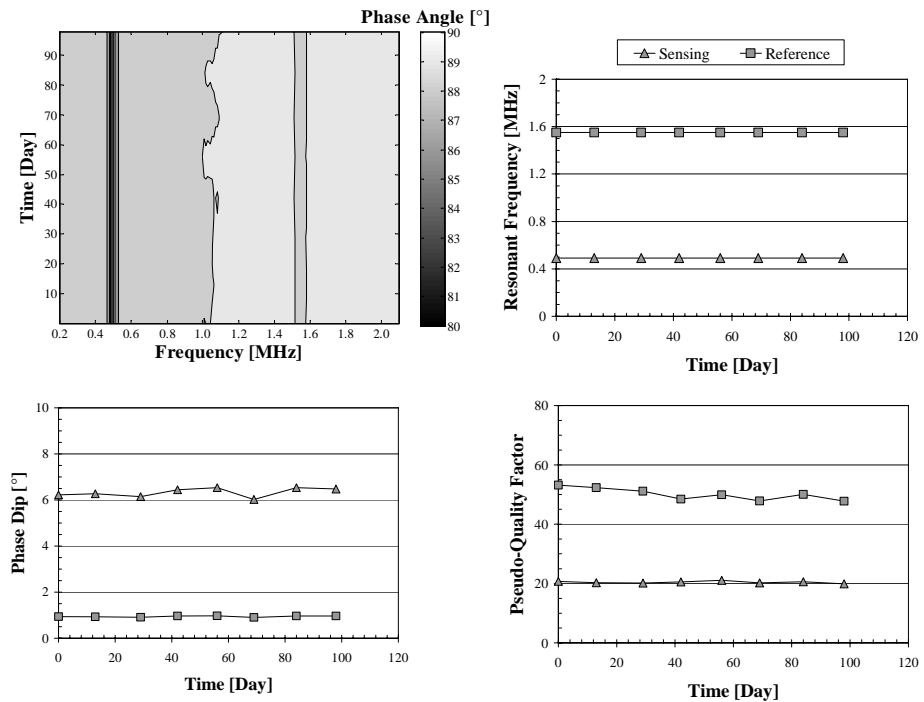


**Figure D-34 Response of Sensor E18**

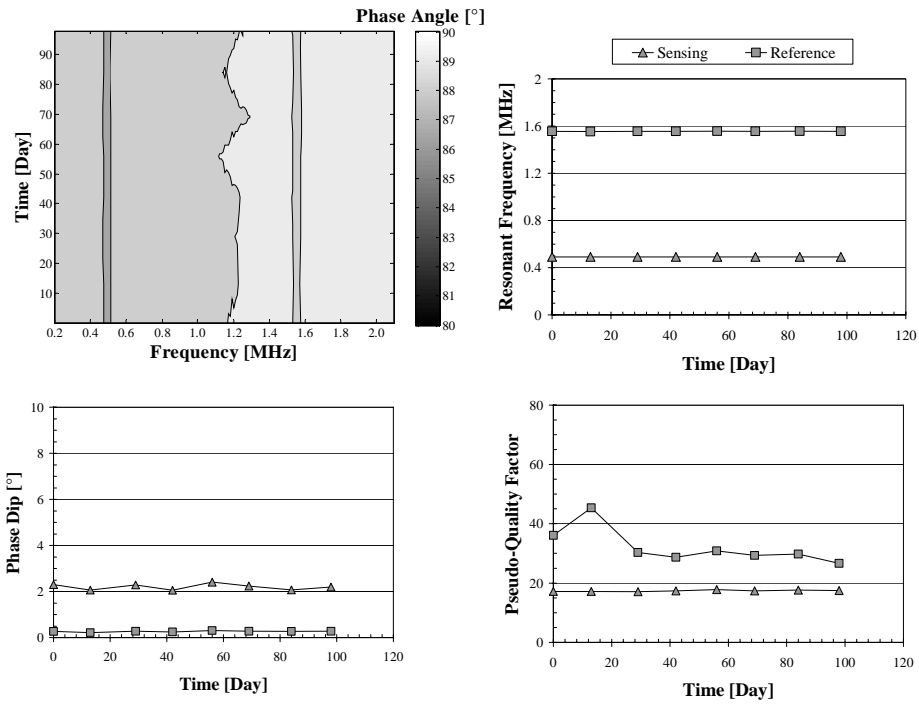


**Figure D-35 Response of Sensor D20 (Control Specimen)**

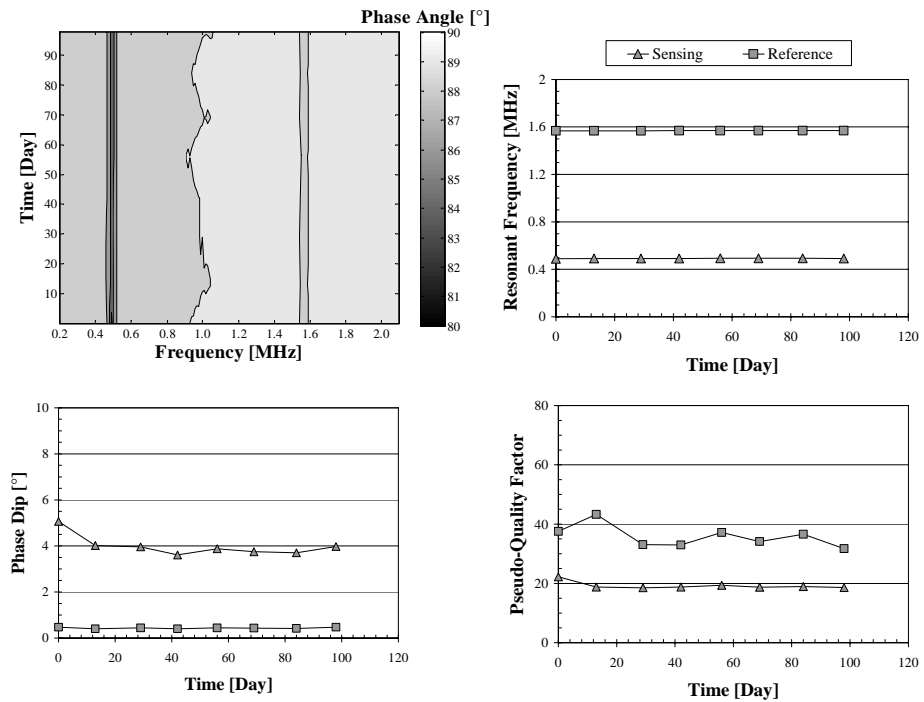


**Figure D-36 Response of Sensor E20 (Control Specimen)**

## **APPENDIX E**

### **Fiber-Reinforced Cement Paste Sensor Housing**

All sensors tested in Slabs 5 and 6 were fabricated as described in Dickerson (2005) but with two exceptions. First, the aluminum sensing wires of sensors tested in Slabs 6 required Solder-It™ Aluminum solder paste as a flux. Ideally, a soldering iron with an output of 120 Watts would be used to solder the aluminum wires. However, the aluminum sensing wires of sensors tested in Slab 6 were successfully soldered using two, 60-Watt soldering irons simultaneously.

The second difference was that a fiber-reinforced cement paste housing was used for the sensors. These sensor housings were fabricated using the following procedure. As was mentioned in Chapter 7, most sensor housings tested in Slabs 5 and 6 were not cured in moist conditions, although moist curing is important to reduce the extent of plastic shrinkage cracking in the housing.

The fiber-reinforced cement paste itself is composed of cement paste and ¼-in. long polypropylene fibers, which are used to stabilize stucco. The potting material is produced by mixing cement, water, polypropylene fibers, and a polycarboxylate-based high-range water reducer, ASTM type F. These components are shown in Figure E-1, and the amounts of each component to be combined for the potting material are shown in Table E-1. The water reducer is added to the mixture in order to decrease its viscosity. Low viscosity is essential to the potting material encompassing all the circuitry of the sensor.



***Figure E-1 Components of Fiber-Reinforced Cement Paste Housing***

***Table E-1 Amounts of Components Combined to Make Fiber-Reinforced Cement Paste Housing***

<b>Component</b>	<b>Amount</b>
Cement	1361 g
Water	545 g
Fibers	5.3 g
Superplasticizer	4 mL

The components were combined in two steps. First, the cement was gradually added to the water, and the resulting mixture was stirred with a plastic spatula. Second, the fibers and superplasticizer were added to the mixture. The superplasticizer lowered the viscosity of the cement paste sufficiently for the mixture to be stirred with a mortar paddle attached to an electric drill, as shown in Figure E-2.



***Figure E-2 Mortar Paddle Used to Stir the Mixture***

Once the mixture was homogenous, it was poured into a mold in which a sensor had been placed. Common kitchen ladles with the handles removed were used as molds to produce sensors with convex bottoms. Figure E-3 is a photograph of such a mold. The mold was stabilized for pouring by being placed on a stand made from a plastic cup. As shown in Figure E-4, the low viscosity of the mixture permitted it to be poured readily. The sensing wire was bent upward to prevent the wire from being covered with potting material.



***Figure E-3 Mold with Convex Bottom***





***Figure E-4 Mixture Poured into Mold Containing Sensor***

After the mold has been filled with potting material, it was vibrated by hand to remove any air voids from beneath the sensor. The fresh housing was then covered with plastic to facilitate moist curing, as shown in Figure E-5. Once the housing has hardened sufficiently to be removed from the mold, it was submerged in water for one week for continued moist curing.

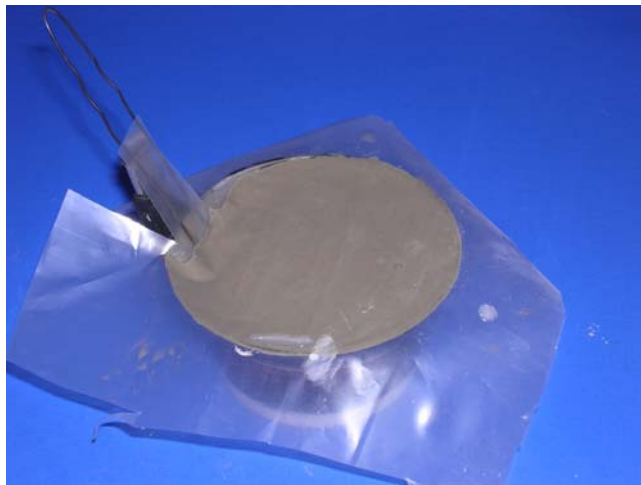


***Figure E-5 Moist Curing of Sensor Housing***

Sensors with epoxy cores were potted using the same steps above. However, prior to the sensor being potted in fiber-reinforced cement paste, the

circuitry of the sensor was potted in epoxy. The PVC slice used to fabricate the reference inductor was used as a mold for the epoxy core. In order for the epoxy core to extend slightly beyond the surface of the fiber-reinforced cement paste, a  $\frac{3}{4}$ -in. thick PVC slice was used for the reference inductor. A  $\frac{1}{2}$ -in. thick PVC slice was used by Dickerson (2005). Otherwise, sensors with epoxy cores were fabricated as described in Dickerson (2005). As shown in Figure E-6, the additional  $\frac{1}{4}$  in. of thickness extends beyond the top of the sensing inductor.

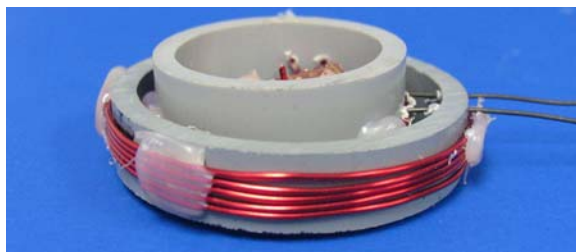


***Figure E-6 PVC Slice of Reference Inductor Extending beyond Top of Sensing Inductor***

For the purposes of potting the epoxy core, the sensor was placed upside down on a smooth, level surface. As shown in Figure E-7, a bead of hot glue was placed around the line of contact between the reference inductor and surface. The hot glue sealed the top edge of the reference inductor in order that low-viscosity Bondo™ marine epoxy could be poured over the circuitry of the sensor through the bottom of the reference inductor, as shown in Figure E-8. The epoxy was poured into the reference inductor until it was level with the bottom of the reference inductor. After the epoxy had cured for 24 hours, the fiber-reinforced cement paste housing was cast as described above. The level of the fresh fiber-reinforced cement paste should remain below the top of the epoxy core for the epoxy core to remain visible on the top of the sensor, as shown in Figure E-9.

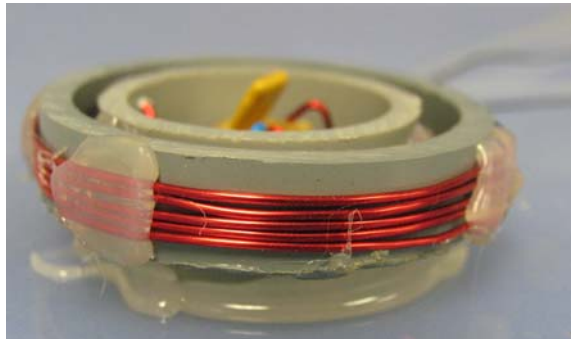


*Figure E-7 Bead of Hot Glue around Reference Inductor*

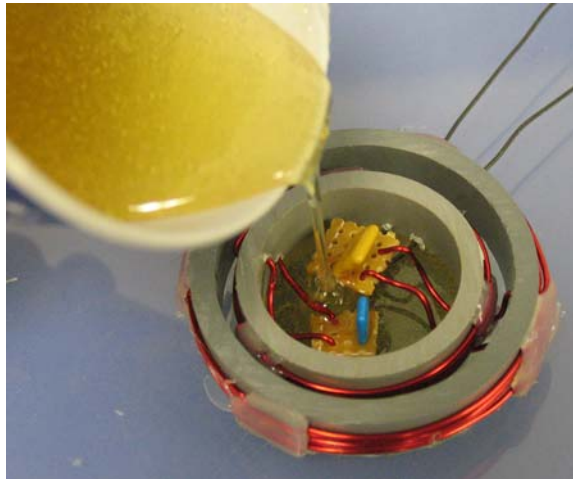


*Figure E-8 Epoxy Poured through Bottom of Reference Inductor*



*Figure E-9 Epoxy Core Visible on Top of Sensor*

As was observed in Chapter 3, differential thermal expansion of the epoxy housing and the concrete caused complications in the functioning of the sensor. Therefore, the following brief experiment was conducted to determine whether the coefficient of thermal expansion of the fiber-reinforced cement paste housing was comparable to that of concrete. Six fiber-reinforced cement paste discs, as shown in Figure E-10, were potted. The discs had a 2½-in. diameter and a 1-in. thickness. Each of the six discs was cast in a concrete prism having a 6-in. diameter and a 3½-in. height. A prism is shown in Figure E-11.



*Figure E-10 Fiber-Reinforced Cement Paste Discs*



*Figure E-11 Concrete Prism*

The prisms, with embedded discs, were subjected to extreme thermal cycles. One thermal cycle consisted of the prisms being placed in an oven at 210 °F for one week and then stored in air for two weeks. The prisms underwent four such thermal cycles. At the end of the cycles, the prisms were examined, and no cracks were observed on their surface. Therefore, the coefficient of thermal expansion of the fiber-reinforced cement paste was concluded be comparable to that of concrete.

## APPENDIX F

### Responses of Sensors Embedded in a Full-Scale Bridge Deck

The responses of sensors B160 through B165, which were embedded in the full-scale bridge deck, are reported in this appendix. The responses of the sensors are shown in the plane of phase angle and frequency. The sensing wires of B160 through B165 were 21-gage (0.0285-in. diameter) AISI-ASE 1006 with a total length of 40 in. Once doubled-over, the sensing wire extended from the housing of the epoxy approximately 19 in. The interrogation labeled “8/1” in the responses was taken on 1 August 2006, before the sensors were embedded in the bridge deck. The concrete for the bridge deck was placed 17 August 2006. After the sensors were embedded in the bridge deck, they could only be interrogated with a 30-ft coaxial cable. The baseline of the 30-ft cable differed significantly from the baseline than a 3-ft cable, as is evident in the responses of the sensors. Interrogations of the sensors with the 30-ft cable took place on 19 September 2006 and 7 December 2006.

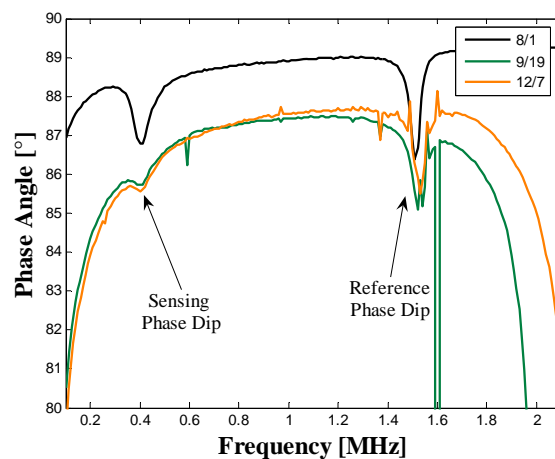


*Figure F-1 Response of B160*

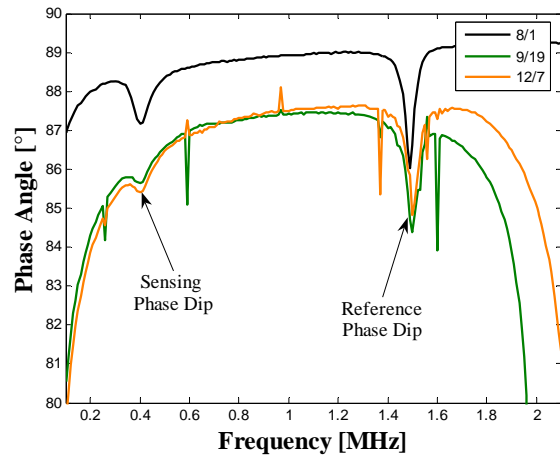


**Figure F-2 Response of B161**

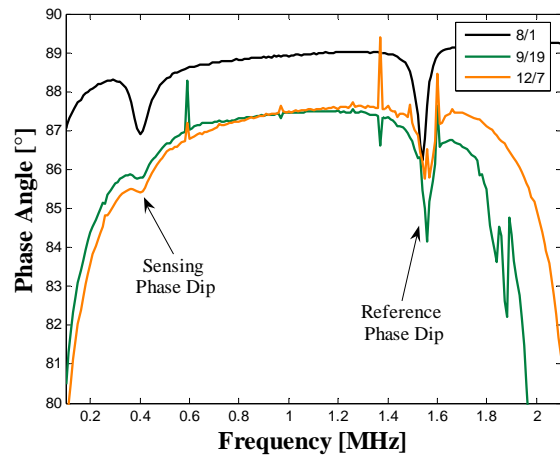


**Figure F-3 Response of B162**

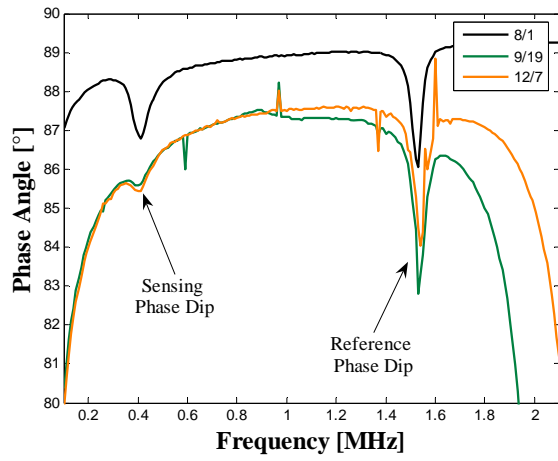


**Figure F-4 Response of B163**

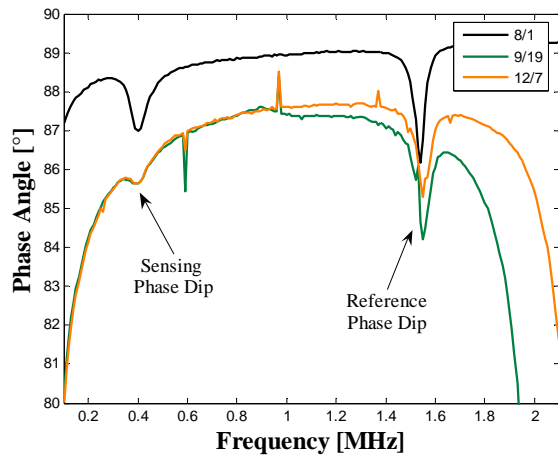


**Figure F-5 Response of B164**



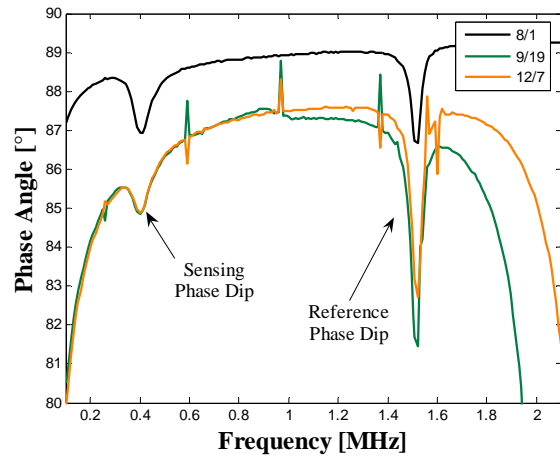


**Figure F-6 Response of B165**

## APPENDIX G

### Galvanic Corrosion Test Results

Results from the galvanic corrosion test are reported in this appendix. These results include the weights of the zinc sensing wire and bar and aluminum sensing wire and bar. Furthermore, the temperatures and dissolved oxygen content of the simulated pore solutions in which the specimens were tested are presented here. In the plots pertaining to the pore solutions, each pore solution is identified by the specimen that the solution contained. For example, the solution containing the zinc sensing wire was identified as “Zn Wire.” The half-cell potentials of the steel mats with which the bars were coupled are also reported. The potentials were taken with a standard calomel electrode.

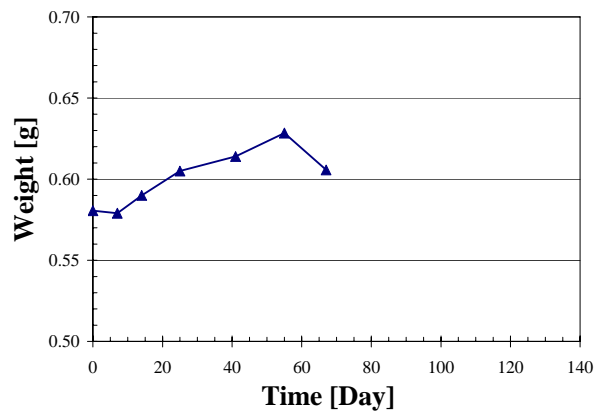


*Figure G-1 Weight of Aluminum Wire*

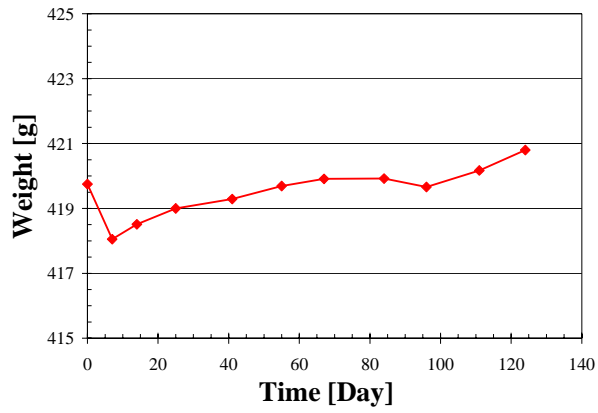


*Figure G-2 Weight of Aluminum Bar*

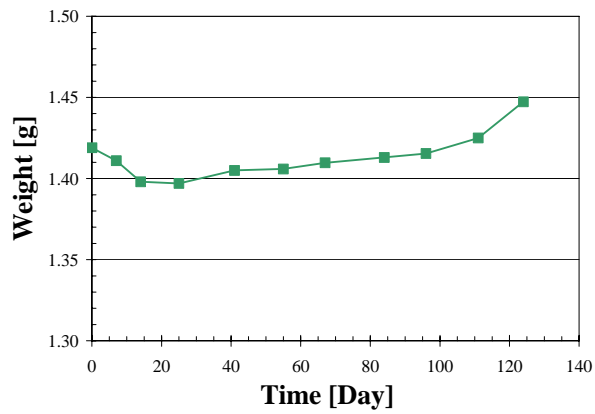


*Figure G-3 Weight of Zinc Wire*

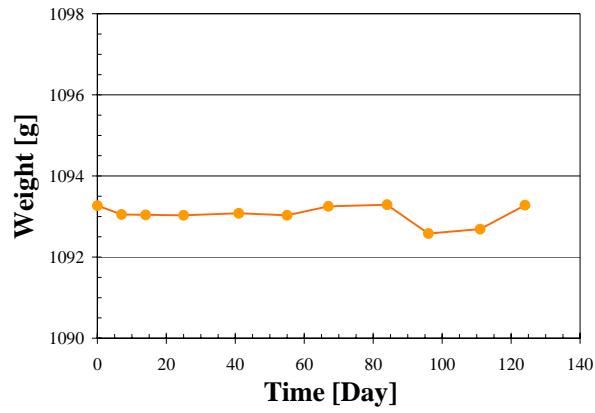


*Figure G-4 Weight of Zinc Bar*

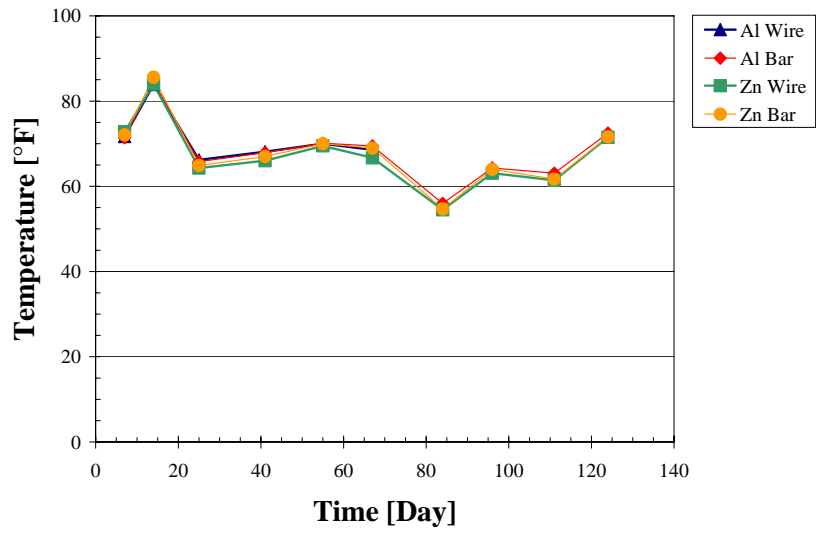


*Figure G-5 Temperature of Simulated Pore Solutions*

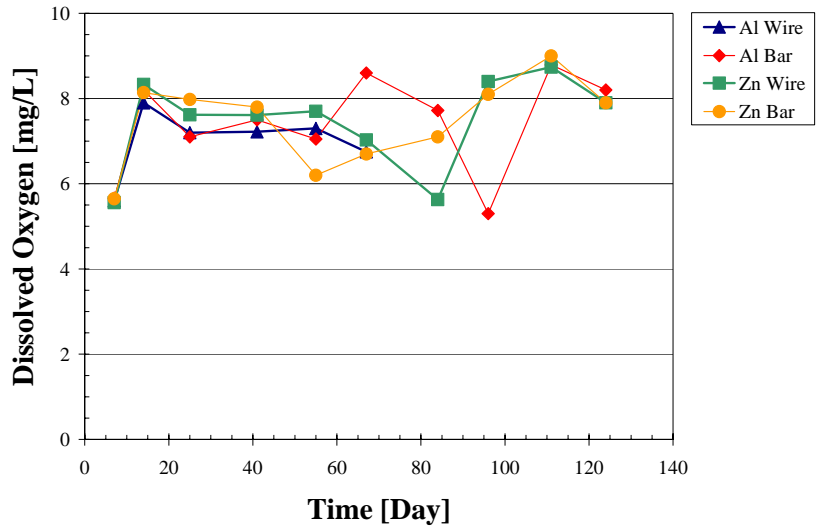


*Figure G-6 Dissolved Oxygen Content of Simulated Pore Solutions*

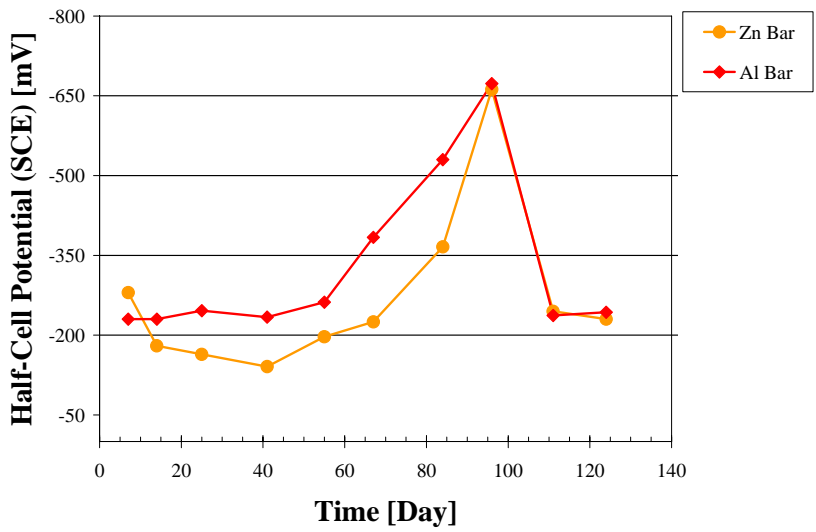


*Figure G-7 Half-Cell Potentials of Steel Mats Coupled with Bars*

## References

1. AASTO T260-94 (1994). "Standard Method of Sampling and Testing for Total Chloride Ion in Concrete and Concrete Raw Materials." American Association of State Highway Transportation Officers, Washington, DC.
2. Agnew, Lewis (2007). "Evaluation of Fatigue Behavior of Bridge Decks with Precast Panels at Expansion Joints." M.S. Thesis, Dept. of Civil, Architectural, and Environmental Engineering, University of Texas at Austin.
3. Andringa, Matthew M. (2003). "Development of a Passive Wireless Analog Resistance Sensor." M. S. Thesis, Dept. of Electrical and Computer Engineering, University of Texas at Austin.
4. Andringa, Matthew M (2005). Collaborative work between Andringa and the author.
5. Andringa, Matthew M. (2006). "Unpowered Wireless Sensors for Structural Health Monitoring." Ph.D. Dissertation, Dept. of Electrical and Computer Engineering, University of Texas at Austin.
6. ASTM C 876 (1999). "Standard Test Method for Half-Cell Potentials of Uncoated Reinforcing Steel in Concrete." American Society for Testing and Materials, West Conshohocken, PA.
7. ASTM G 109 (1992). "Standard Test Method for Determining the Effects of Chemical Admixtures on the Corrosion of Embedded Steel Reinforcement in Concrete Exposed to Chloride Environments." American Society for Testing and Materials, West Conshohocken, PA.
8. Bertolini, Luca; Elsener, Bernhard; Pedferri, Pietro; Polder, Rob (2004). "Corrosion of Steel in Concrete: Prevention, Diagnosis, Repair." Wiley-Vch Verlag GmbH & Co. KGaA, Weinheim, Germany.
9. Bertolini, Luca; Gastaldi, Matteo; Pedferri, MariaPia; Redealli, Elena (2002). "Prevention of Steel Corrosion in Concrete Exposed to Seawater with Submerged Sacrificial Anodes." Corrosion Science, vol. no. 44, 1497-1513.

10. Broomfield, John P. (1997). "Corrosion of Steel in Concrete: Understanding, Investigation and Repair." E & FN Spon, 2-6 Boundary Row, London SE1 8HN, UK.
11. Dickerson, Nathan P. (2005). "Wireless Corrosion Sensors for Reinforced Concrete Structures." M.S. Thesis, Dept. of Civil, Architectural, and Environmental Engineering, University of Texas at Austin.
12. Jones, Denny A. (1996). "Principles and Prevention of Corrosion," 2<sup>nd</sup> ed. Prentice Hall, Inc., Upper Saddle River, NJ.
13. West, Jeffrey (1999). "Durability Design of Post Tensioned Bridge Substructures." Ph.D. Dissertation, Dept. of Civil, Architectural, and Environmental Engineering, University of Texas at Austin.
14. Tullmin, M. (2006). [www.corrosion-club.com](http://www.corrosion-club.com)
15. Transportation Research Board (1991). "Highway Deicing: Comparing Salt and Calcium Magnesium Acetate." Special Report 235, National Research Council, Washington D. C.

## VITA

John Mark Howard Puryear was born on April 30, 1981 in Houston, Texas to Michael R. and Joanne E. Puryear, the fourth of seven children. After a brief sojourn to Oklahoma, the Puryear family settled north of Angleton, Texas, where John was raised. John was homeschooled along with his siblings through high school. After a year at Brazosport Community College, John obtained a Bachelor of Science in Mathematics and Philosophy from Wheaton College in Wheaton, Illinois. After graduation, John worked as a house framer for two years at Porter Bluff Construction in Scurry, Texas. In August of 2004, John began coursework in civil engineering at the University of Texas at Austin. After completing undergraduate prerequisites in civil engineering, John began work as a research assistant at Ferguson Structural Laboratory under the supervision of Dr. Sharon L. Wood. John graduated in August of 2007 with a Master of Science in Civil Engineering and accepted a position with Protection Engineering Consulting in Spring Branch, Texas.

## Publications

Dickerson, N.P., Andringa, M.M., Puryear, J.M., Wood, S.L., and Neikirk, D.P. "Wireless Threshold Sensors for Detecting Corrosion in Reinforced Concrete Structures." *Sensors and Smart Structures Technologies for Civil, Mechanical, and Aerospace Systems*, International Society for Optical Engineering, San Diego, California, February 2006.

Andringa, M.M., Puryear, J.M., Neikirk, D.P., and Wood, S.L. "Low-Cost Wireless Corrosion and Conductivity Sensors." *Sensors and Smart Structures Technologies for Civil, Mechanical, and Aerospace Systems*, International Society for Optical Engineering, San Diego, California, February 2006.

Permanent Address: 510 Windmill Breeze

Bulverde, Texas 78163

United States of America

This thesis was typed by the author.